A BROADBAND MAGNETOTELLURIC STUDY

IN THE NORTH ENGLAND HIGH HEAT FLOW REGION

by

Martin NOVAK

Thesis presented for the degree of Doctor of Philosophy of the University of Edinburgh in the Faculty of Science.

1981

ABSTRACT

The application of the magnetotelluric method to geoelectric exploration is described in this thesis, utilising the natural field variations in the frequency band 1/1000 - 1000 Hz. These broadband measurements are made over a region in north east England where above average heat flow values have been detected.

The area, which is extensively mineralised, is known to be underlain by a granite batholith (the Weardale granite) and has been the subject of many detailed studies, particularly with respect to these (related) features.

In this thesis the geological and geophysical features of these studies are examined, the significance of conductivity measurements is reviewed, supported by a number of reference tables, and the theory of the magnetotelluric method is outlined for the interested reader. The technical details of the audio-magnetotelluric system - assembled for the first time in the U.K. - are presented, and its subsequent calibration and field trials described. From the system calibration, both the amplitude and phase responses are used in the computer-based data analysis, to fully utilise the capabilities of the instrumentation and to produce, as far as possible, reliable station results.

The introduction of a minicomputer to the acquisition and preliminary processing of data, mainly with respect to the conventional MT method, is described.

The single station data results from the seven broadband stations are presented followed by those from the twenty stations where only the AMT measurements exist. The rotated major and rotated minor impedance estimates, azimuthal angle of the rotation, skew factors and a simple resistivity - depth representation are shown and discussed. The real and imaginary induction vectors are included in the case of the conventional MT station data results.

A one-dimensional interpretation is made of selected station data and the validity of this is examined with respect to data showing a two or three-dimensional response. The inclusion of the phase data in the derivation of many-layered models is demonstrated to be an integral part of the modelling process. The information derived from these models - the number of layers chosen to satisfy the data as best as possible - is compared with the existing geological and geophysical information to derive a compatible model for the study area. The depth to the granite at the shallowest point, in particular, is easily determined and shows remarkable agreement with the data derived from the nearby Rookhope borehole.

An areal interpretation of the short period AMT data results is made, based on a one-dimensional inversion of data from representative stations. This is shown to map the general features of the area including the presence of the granite, base of the Northumberland trough and the transitions associated with the main faults bounding the Alston block. The geological and geophysical implications of a number of very low-resistivity regions, as well as the features above, are discussed.

This work examines the viability of the AMT technique in the U.K. Even without improvements, to alleviate the problems caused by industrial noise, the method is capable of defining lateral conductivity variations and detecting prominent resistive bodies or localised conductive regions. It is shown that the station spacing, which was too great in the short period part of this study, needs to be carefully chosen.

On account of the inadequate station spacing of the AMT soundings, the lack of data in the frequency range 10 - 10^{-1} Hz and the fact that so far only one-dimensional modelling has been attempted, no consideration has yet been given to the relationship between the results of this study and the known high heat flow reported in the study region.

Based on the work, some suggestions are made about (i) the future development of the technique, (ii) additional modelling - two dimensional - of existing data and (iii) further field-work in northern England.

ACKNOWLEDGEMENTS

I respectfully acknowledge the help of Dr Rosemary Hutton, my supervisor, who has kept a watchful eye over my progress from my early years as an undergraduate student. Through her thoughtful planning she has initiated this project and my involvement with it and ensured that I obtained a complete geophysical education from the work.

I express my gratitude to the Geophysics Department of Edinburgh University for providing the place and the facilities for my research. I wish to thank the members of the Department for their friendly and helpful attitude. In particular, I would like to mention Reid Fowler, who, after achieving much progress with the initial preparatory work, had to return to Canada before seeing the results of his work. It is through working closely with him that I have gained much of my knowledge of modern electronics. My gratitude is extended to Graham Dawes for the many hours of enlightening and invaluable conversations and also for his companionship. I also wish to mention Drs Bruce Hobbs and David Summers for their assistance and stimulating conversations regarding some of the theoretical aspects of this work.

The help of Ian MacDonald in the initial stages of the fieldwork and Stuart Becker in the latter, is duly appreciated. I would like to thank Charles Fife of the Global Seismology Unit of the I.G.S. for his assistance during the many late sessions of digitising of the raw data. My thanks go again to Graham Dawes for making available many of the computer programmes used in the course of this research and for his help with the numerous computer related problems.

I am pleased to acknowledge the kind invitation of Drs Harry Dosso and Wolf Nienaber to work on the analogue scale model induction problem at the Department of Physics of the University of Victoria, B.C., Canada.

I wish to thank the many people, who gave permission for the instruments to be situated on their land. It is through their generosity that the fieldwork was made possible.

The financial support for this research was by a Natural Environment Research Council grant and I express my gratitude for their support.

Finally, I extend my fondest thanks to my wife Elaine, who remained my closest companion throughout, typed and proof-read the complete text and gave me support during the difficult closing stages. I am grateful to her, again to Dr Hutton and to my new colleagues at British Gypsum who all gave their help and support in getting the work completed.

CONTENTS

INDEX TO FIGURES

LIST OF TABLES

CHAPTER 1

INTRODUCTION

In this thesis the magnetotelluric method of induction will be applied, in an investigation of the crustal structure in a well studied region of the U.K. The work will describe the development of existing instrumentation into the audio-frequency range and, subsequently, its use in this area.

1.1 The technique

In magnetotelluric studies, the term 'magneto' refers to the naturally occuring magnetic fields at the Earth's surface. The existence of such natural large scale fields conforms with observations of (telluric) earth currents induced in the cables of the British telegraph system by Barlow in 1847. Combined observations of the magnetic and telluric fields were made by Airy (1868) and later, Schuster (1889) performed the first separation of the internal and the external parts of the observed magnetic field. Today the character and the structure of the magnetic field around the Earth is extremely well defined from long term ground observatory measurements, (Wienert, 1970) and geomagnetic satellite observations, (Kahle et al., 1969). The origins of the various periodic and transient fluctuations which this field displays can, in the main, be attributed to the interplay between the impinging solar emissions and the natural magnetic field of the Earth, (Orr, 1973). The resultant electromagnetic fields are propagated with some attenuation towards the Earth. A particular part of the electromagnetic spectrum observed

at the Earth's surface has its source mechanism in a space between it and the ionosphere where electromagnetic waves behave in a manner not dissimilar to that of guided waves. At the Earth's surface these electromagnetic waves can appear as plane waves with an extremely wide frequency spectrum.

These waves diffuse, as described by the Faraday-Henry law, into the Earth's surface where they generate electric fields and attenuate as a result. The induced electric currents have associated magnetic fields according to the Biot-Savart law. These secondary magnetic fields appear with the primary magnetic fields at the surface and are superimposed on them.

It is these variations, in two horizontal directions, together with those of the telluric field that provide the basis for the magnetotelluric (MT) technique.

An example of the magnetic and electric field amplitude spectrum detectable at the surface of the Earth has been analysed by Serson (1973) and can be seen in figure 1.1(b). Variations occur at higher frequencies (Keller and Frischknecht,1966), figure 1.1(a) and as high as 100 kHz. Of partiuclar interest are the fluctuations of period 1 hour or less up to those of a frequency of a few thousand Hertz.

In magnetotelluric studies field variations of periods greater than 1 second are considered to be of the

Figure 1.1a Typical spectrum of amplitudes of electromagnetic noise in the extremely low frequency (ELF) range. (From Keller and Frischknecht 1966)

Figure 1.1b Amplitudes of natural variations in the horizontal geomagnetic field useful in induction research (A) and corresponding amplitudes in the earth-electric field, computed for a model earth of uniform resistivity 20 ohm-m (B).
(From Serson 1973)

Figure 1.1c Average natural field in Garchy, France

Figure 1.1

(a)

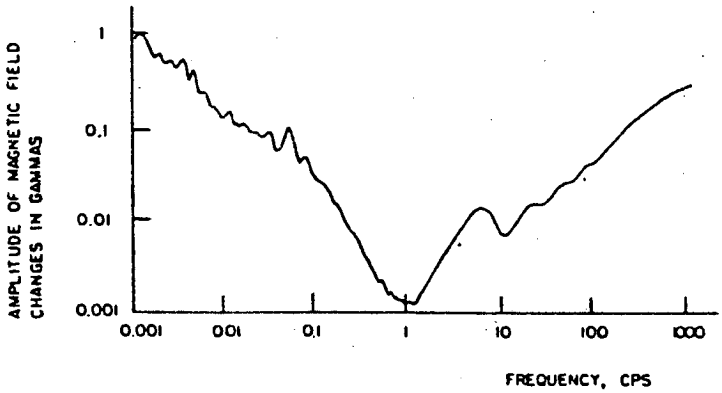

(b)

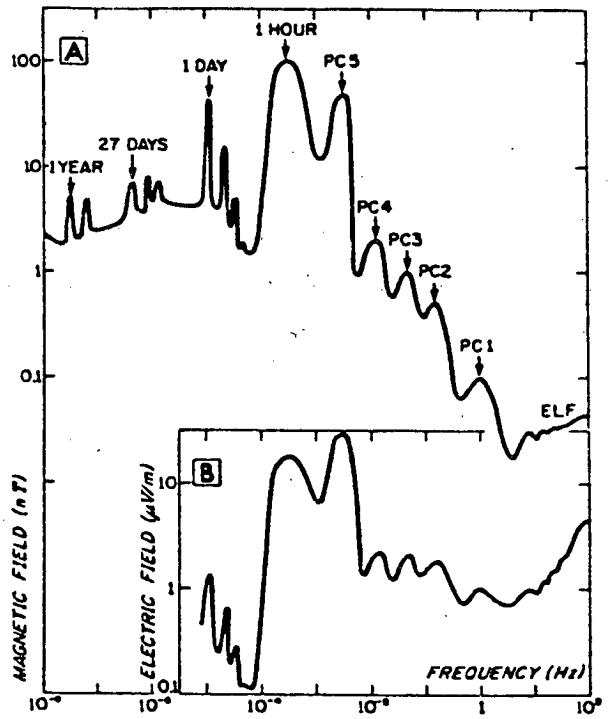

(c)

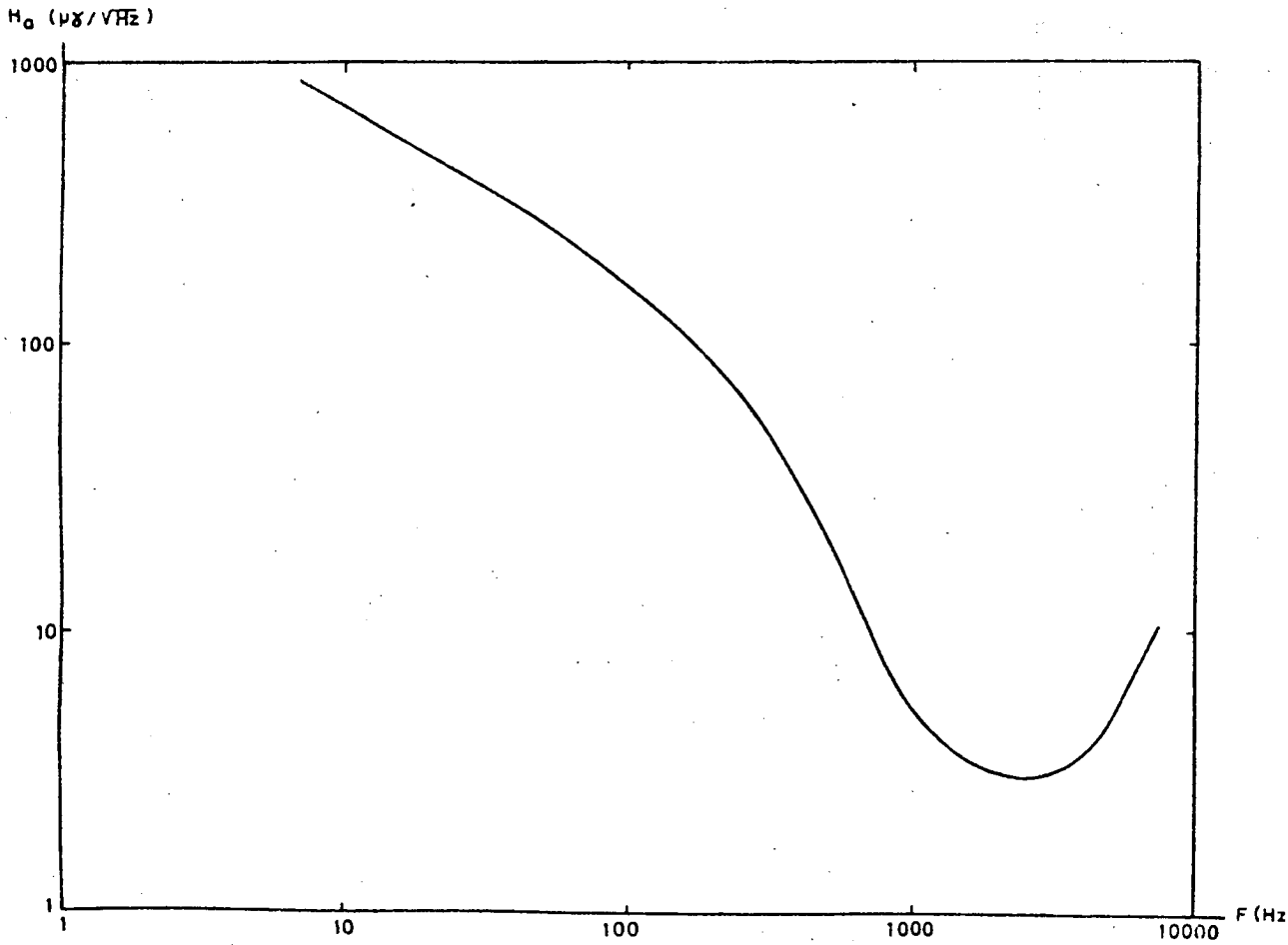

long period type. In this period range MT soundings will often be called 'conventional', largely to distinguish them from the higher audio frequency magnetotelluric soundings (AMT). These latter fluctuations of period less than 1 second and up to some 20 kHz lie in the audio frequency range of the spectrum. The fluctuations observed in this part of the EM spectrum are referred to as extremly low frequency fluctuations (ELF). Their propagation will be discussed in a future chapter, but at this stage it is sufficient to note that their power has been observed to peak at several distinct frequencies, particularly at 8, 14 and 760 Hz (Telford, 1977). The association with electric storm activity is known, with much of the power delivered at these and higher frequencies originating during lightning discharges.

The extension of the frequency spectrum of the magnetotelluric method in this work extends the type of source activity, to include these geo-electric effects. The application of this extension forms a major contribution to this thesis.

The proposed extension would cover the frequency range 1 Hz - 1 kHz enabling measurements to be made in this range in addition to the 1/1000 Hz - 1/10 Hz spectrum covered by the existing equipment. The combined equipment would enable the Edinburgh group to make broadband magnetotelluric measurements from frequencies as low as 10^{-3} Hz (1000 sec) up to 1000 Hz in the audio-frequency range. The penetration into the surface of the Earth of

Figure 1.2 Generalised skin depths for the period range 10,000 seconds to 10,000 Hz, indicating the extent of the possible coverage of the broadband instrumentation (solid lines)

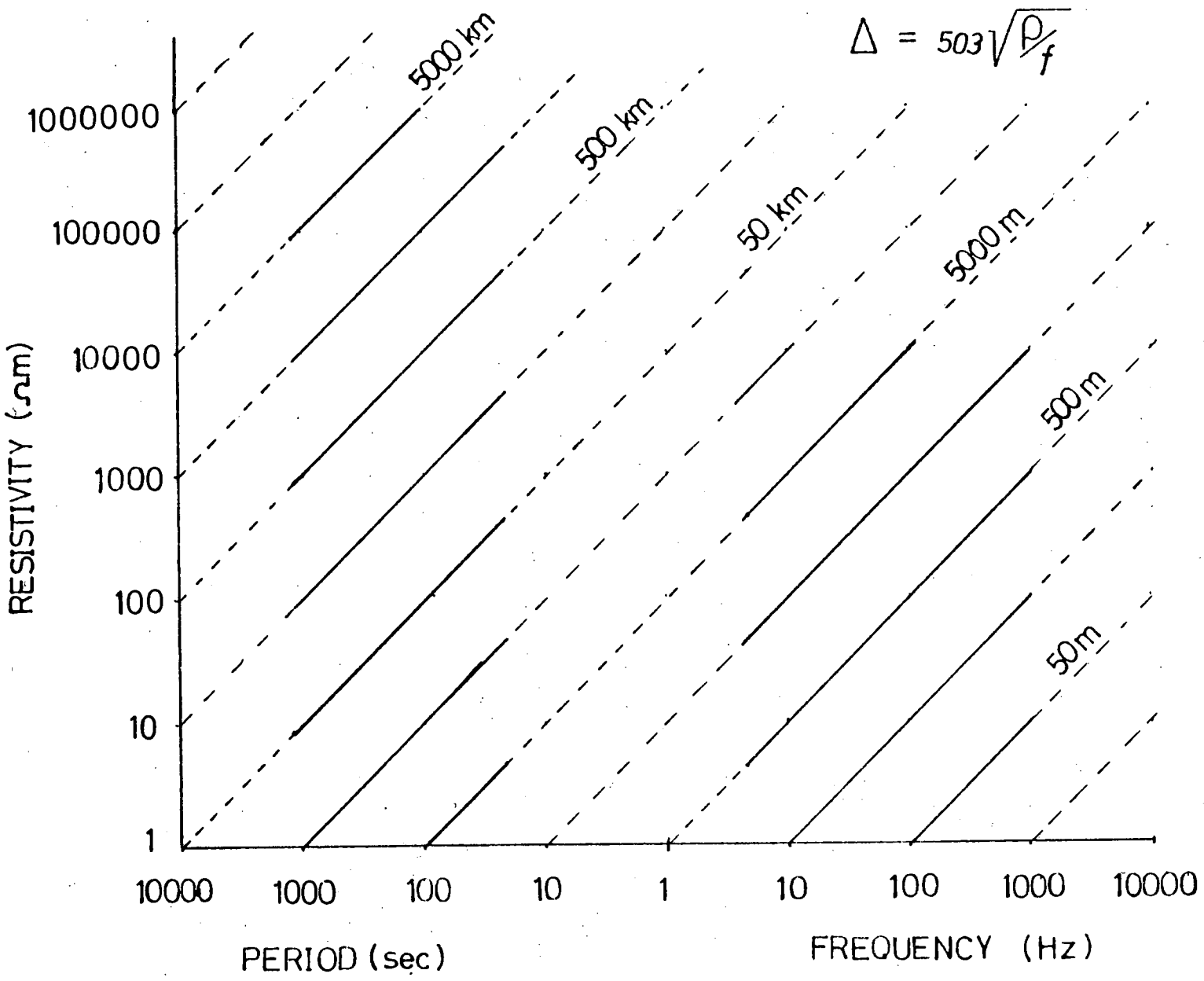
$\Delta = 503\sqrt{\rho/f}$
5000 km
500 km
50 km
5000 m
500 m
50 m
RESISTIVITY (Ωm)
1000000
100000
10000
1000
100
10
1
10000
1000
100
10
1
10
100
1000
10000
PERIOD (sec)
FREQUENCY (Hz)

Figure 1.2

the signals in this range is generalised in figure 1.2 and will provide increased resolution of the surface values of conductivity. This is particularly valuable in determining the correct values of conductivity at the greater depths of penetration.

1.2 The study area

The area chosen for the investigation - the region of the Weardale, in N.E. England - was distinguished by a number of features. Possibly the most unusual and revealing was the high heat flow measured at a number of locations. These establish the area as one of two in the UK with heat flow values of more than 60 mW m^2. The other lies in S.W. England roughly encompassing the granite masses of Devon and Cornwall. See figure 1.3. The survey region is likewise in possession of a granitic mass although it does not outcrop.

The previous geological and geophysical work carried out in this region is summarised in table 1.1. The geology has been well studied particularly with respect to the large concentrations of lead, zinc, fluorine and barium deposits, which have been extensively mined for hundreds of years. A complete review of the Northern Pennine orefield is given by Dunham (1948). More recently

Figure 1.3a Heat flow values contoured at 45, 60 and 75 mWm^{-2}. The two belts of higher heat flow are delineated here by the 60 mWm^{-2} isopleth.

Figure 1.3b Provinces of high heat flow in central and southern Britain (a). Heat flow in shaded areas exceeds 60 mWm^{-2} indicated by dashed lines in (b), which also records the spatial occurrence of some important centres of hydrothermal mineralisation in England and Wales. (From Brown et al, 1980)

Figure 1.3

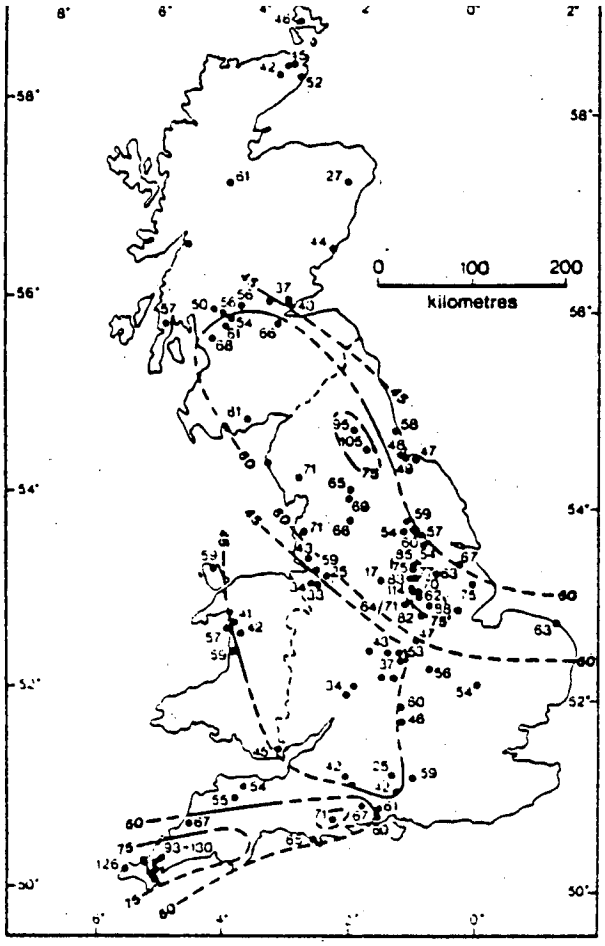
0 100 200
kilometres

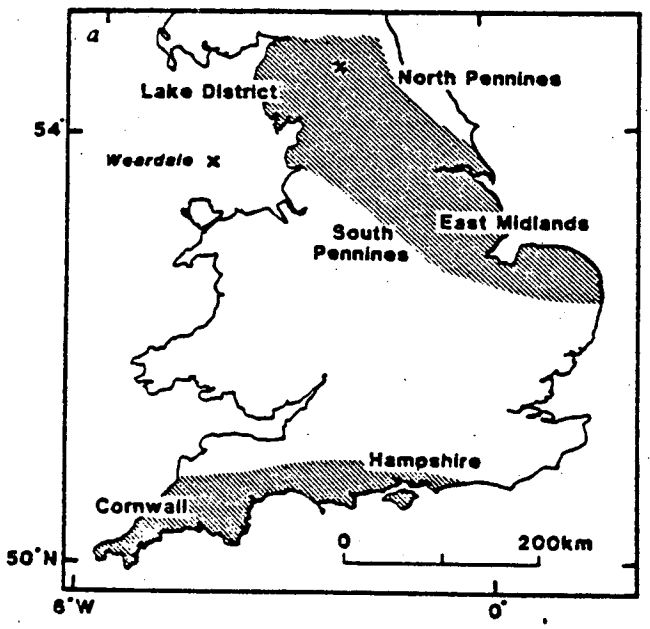
a
Lake District
North Pennines
Weardale
South Pennines
East Midlands
Hampshire
Cornwall
0 200km
54°
50°N
6°W
0°

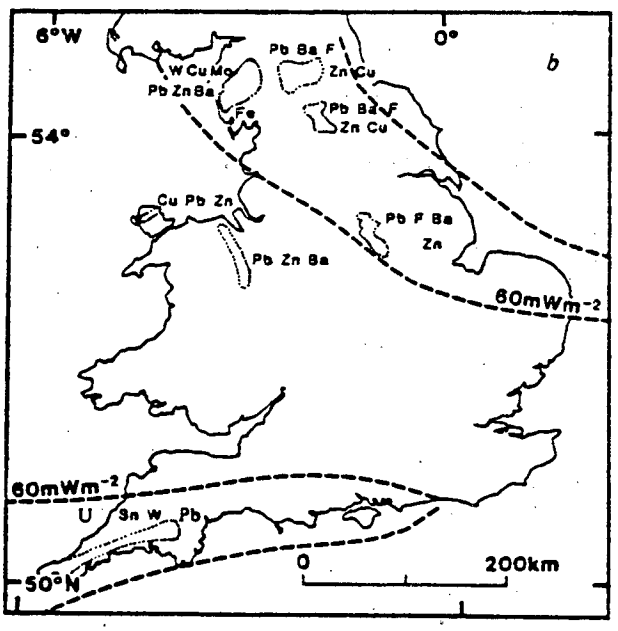
b
6°W
0°
54°
50°N
Pb Ba F
W Cu Mo
Pb Zn Ba
Zn Cu
Pb Ba F
Zn Cu
Cu Pb Zn
Pb F Ba
Zn
Pb Zn Ba
60mWm⁻²
60mWm⁻²
U Sn W Pb
0 200km

Brown et al.(1980) has examined the connection between the Caledonian granite and hypogene (Dunham,1931) mineralisation. The region is dominated by Carboniferous sediments dipping from the Pennine faults in the west, where they are relatively thin, to the east, where they reach somewhat greater depths. In the east extensive coal measures form a part of the structure, surfacing as the Durham and other coal fields.

The Carboniferous succession lies unconformably on a basement of folded lower Palaeozoic shales at depths ranging from 300 - 1000 m.

To the north and south and clearly divided from it by hinge and fault lines, lie deep sedimentary basins. To the north and separated by the Stublick and Ninety Fathom faults is the Northumberland trough. To the south and on the down-throw side of the Butterknowle, Lunedale and Staindrop fault system, lies the Stainmore trough. These lower Carboniferous sedimentary basins reach maximum depths of approximately 3 km.

Thus an area bound on three sides by fault lines and extending out towards the North Sea on the fourth is located. It is a stable block named the Alston block and is intruded by a major Caledonian batholith of Devonian age.

Details of the surface geology are given in publications of the Institute of Geological Sciences,

A SUMMARY OF GEOPHYSICAL WORK

IN THE REGION OF THE WEARDALE GRANITE

GEOLOGY	Mineralisation	K C DUNHAM	(1948)
GRAVITY	Regional Survey	M H P BOTT + D MASON-SMITH a.	(1957)
MAGNETICS	Regional Survey	M H P BOTT + D MASON-SMITH b.	(1957)
BORING	Rookhope	K C DUNHAM et al	(1965)
HEAT FLOW	Woodland, Rookhope	M H P BOTT et al	(1972)
SEISMIC	LISPB(γ section)	D BAMFORD et al	(1978)
RESISTIVITY	Rookhope	G M HABBERJAM + C THANASSOULAS	(1979)
MT	Northumberland Basin	A G JONES	(1977)
GDS	Regional Profile	D BEAMISH	(1981)

(MacGregor and MacGregor, 1948), (Eastwood, 1953)

The area is notable for a number of intrusions. The most important of these is a quartz dolerite sill called the Whin sill intruded into the carboniferous successions. Its depth within the limestone strata is variable throughout the 400 square kilometers it covers and it is found to outcrop in the region of Teesdale in the south-east and to reach a depth of 400 m in the west. A number of igneous dykes have also been mapped. Possibly the two most important of these are the one associated with the Ninety Fathom fault and that associated with the Lunedale fault. This latter intrusion is thought to be connected with the Great Whin sill.

Much of the accurate information regarding geological features described above was determined from a number of boreholes. These are situated in the area as shown in figure 1.4. Probably the most documented of these was one drilled at Rookhope for the University of Durham (Dunham et al.,1961,1965) to investigate an earlier prediction of a granite under the Pennines and of mineralisation at depth. The granite was originally postulated to explain a negative gravity anomaly detected in a study over the Alston block, although its presence was suggested by drawing a comparison with the mineralisation associated with the Cornish granites, (Hospers and Wilmore,1953). The anomaly, figure 1.4, which covers an area of some 20 x 50 km is elongated in an ENE direction and reaches a minimum value of 23.6 mgal. Assuming that it was caused

Figure 1.4 The geological features of the study area, showing Bouguer isogals at 5 mgal intervals. The extent of the mineralisation (within the dotted line), the limit of the Permian and Triasic cover (speckled area) and the position of the exposed Lower Palaeozoic basement (dashed area) have also been included. The positions of the main faults and boreholes are indicated. (Ro - Rookhope, Wo - Woodland, Cr - Crook, Bu - Burtree Pasture, Ra - Rampgill shaft, Co - Cowgreen mine, Cf - Cross Fell outcrop)

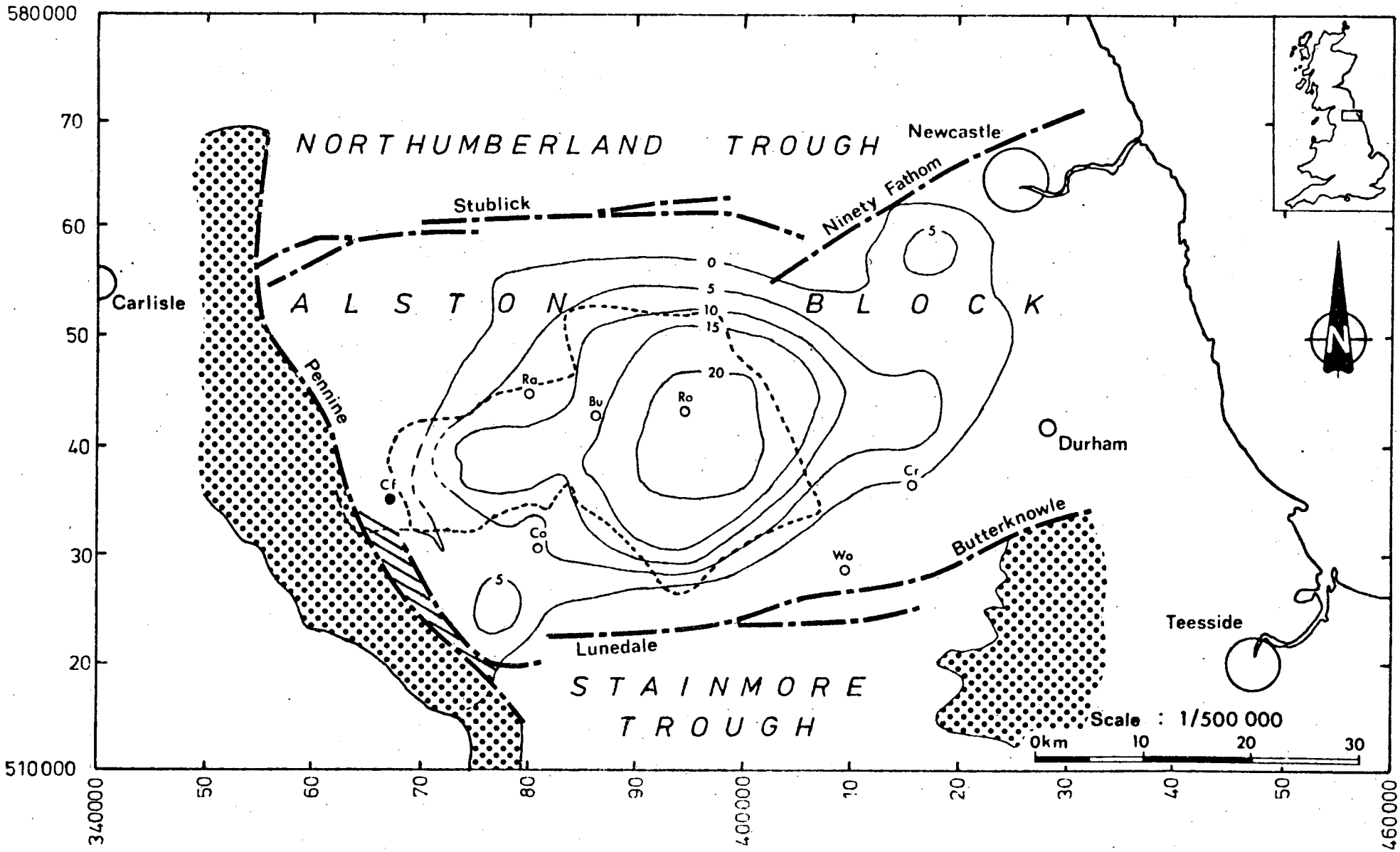
580000
70
60
50
40
30
20
510000
340000
50
60
70
80
90
400000
10
20
30
40
50
460000
NORTHUMBERLAND TROUGH
Newcastle
Ninety Fathom
Stublick
Carlisle
ALSTON BLOCK
0
5
10
15
20
5
Ra
Bu
Ro
Cr
Cf
Co
Wo
Pennine
Durham
Butterknowle
Teesside
Lunedale
STAINMORE TROUGH
N
Scale : 1/500 000
0km
10
20
30

Figure 1.4

by a low density granite, the anomaly was interpreted to obtain its lateral extent. The probable vertical extent was given as approximately 9 km and the presence of 5 granitic cupolas extending towards the surface was also suggested. A ground magnetic survey (Bott and Mason-Smith,1957b) gave results consistent with the existence of a granite. The anomaly was attributed to the lower magnetisation of the granite in relation to the surrounding country rock. The borehole finally confirmed its existence and proved the granite to be of pre-carboniferous origin (Dunham,1961). The exact age (Dodson and Moorbath,1961) has been revised to approximately 400 my (Fitch and Miller,1965,Holland and Lambert,1970), bringing it in line with other known granites in the U.K. Now called the Weardale granite it is located at exactly 390 metres below the surface at the site of the Rookhope bore.

An interesting feature of this borehole was that the mineralisation was found to extend well into the granite with an age given as 300 m.y. - postdating the emplacement of the granite by 100 m.y. It is consequently of hypogene origin, suggesting a mechanism by which the granitic cupolas enabled the flow of brines to reach the surface from a source placed somewhere beneath the top of these cupolas. The Great Limestone and the Great and Little Whin Sill have also been accurately mapped. Bott (1972) made heat flow measurements in the Rookhope borehole during and after drilling and a value of 2.19 μcal $cm^{-2}s^{-1}$ was reported. This high value was explained, in part at least, by the high observed radioactivity of the Weardale

Granite. Heat flow contributing to the surface value from depths greater than the estimated base of the Granite was necessarily suggested to be greater than that at the neighbouring North Yorkshire. The heat flow value of 2.19 μcal cm^{-2} s^{-1} has been revised recently by Richardson and Oxburgh (1978) and a value of 2.28 μcal cm^{-2} s^{-1} is now accepted. Empirical calculations based on these values suggest a vertical extent of 16 km for this and the many granites found in the U.K.

The vertical field magnetic survey described by Bott and Mason-Smith (1957b) also determined the Great Whin sill to be highly magnetised and outlined the presence of a marginal feature in the region of Blanchland. Situated on the northern flank of the Alston block it is explained as either a basic intrusion or a concentration of magnetic minerals.

A stratigraphical borehole situated at Woodland in the south of the Alston block, but beyond the margin of the Weardale granite provided more information. Drilled between January and September 1962 under the supervision of the IGS the hole penetrated 464 metres of carboniferous strata terminating at a depth of 484 metres in the Whin sill (Mills et al. ,1968). The unusually high value of 2.29 μcal $cm^{-2}s^{-1}$ - revised to 2.49 μcal cm^{-2} s^{-1} - reported for the heat flow at Woodland by Bott and Johnston (1968) is thought to be caused by rising hydrothermal water.

The region has been the centre of other geophysical

work. Habberjam and Thanassoulas (1979) have made a number of studies using the D.C. resistivity technique. The centre of one such resistivity array was located near the site of the Rookhope borehole. At this site they report acceptable agreement between their values and the resistivities suggested by the resistivity log carried out in the borehole. The best fit of the resistivity data was produced by a model suggesting a somewhat different structure. The other resistivity array was centered in the north east of the survey area in the region of the Wark forest.

In chapter 6, a comparison is presented of the D.C. resistivity data of Habberjam and Thanassoulas (1979) and selected AMT results.

Magnetotelluric measurements were made by Jones (1977) at sites further to the north of the area and extending as far south as Towhouse in the Northumberland basin. One other station was Newcastleton some 35 km to the NW. Jones suggested that the response observed at Towhouse was representative of the Northumberland basin region. At that time he had no other stations with which to support this observation. It was intended in this study to provide these stations by extending the same profile further to the south.

More recently the results of the LISPB project (Bamford et al.,1978) have yielded useful information about the seismic velocity interfaces to depths

corresponding to the upper mantle.

1.3 Electromagnetic induction studies - with special reference to high heat flow regions.

Since the development of the magnetotelluric method by Cagniard (1953) - Tikhonov (1950) in the USSR -, electromagnetic methods have been used increasingly as a valuable means for estimating the conductivity distributions within the Earth. On a global scale Price (1973) gives a comprehensive review of the geomagnetic deep sounding method. With special reference to the nature and the dimensions of the source field, Wait (1954), Price (1962) have further studied the induction method. Rikitake (1966) reviewed particularly useful concepts of the induction method. The very long period geomagnetic variations have been used to derive conductivity models of the inner Earth by Lahiri and Price (1939), Rikitake (1950), McDonald (1957), Yukutake (1959) and Banks (1969) using long period geomagnetic data collected at international observatories. The pertinent induction theory has been reviewed by Rikitake (1973) and the extension to multilayered media is described by Weaver (1973) for the magnetic induction method, and by Price (1962), Wait (1962), Srivastava (1965) and Schmucker (1970) for the magnetotelluric method. The comprehensive work by Keller and Frischknecht (1966) provides a useful reference to this day. Fournier (1966) has published an important bibliography of papers on electromagnetic induction, particularly with respect to magnetotelluric studies. The consideration of lateral inhomogeneities has

been the subject of a review by Jones (1973). Induction in semi-infinite conductors with a plane boundary has been examined in an excellent clasical paper by Price (1950) and investigated by d'Erceville and Kunetz (1962). Jones and Price (1970) have gone on to consider the boundary conditions at an interface prior to developing two-dimensional modelling algorithms, (Jones and Pascoe,1971). More recently (Brewitt-Taylor and Weaver,1976) have developed a solution to two-dimensional induction problems using the method of finite differences. Later, Jones and Pascoe (1972) and in a review, Hewson-Browne and Kendall (1976) have examined the three-dimensional problem. The effect of the presence of a land-ocean boundary on induction studies has been examined by Schmucker (1964) and the development of geomagnetic vectors to represent the anomalous vertical field was seen by Parkinson (1959,1962,1964).

The coast effect has been studied on a scaled model by Dosso (1973) particularly with respect to two-dimensional effects. A review of techniques and theoretical solutions for electromagnetic induction in the oceans was given by Ashour (1973) and , with an emphasis on instrumentation, by Filloux (1973). Turning to shallower studies, particularly of crustal conductivity anomalies, Edwards (1976) describes the method used in obtaining electrical conductivity information in the uppermost 20 km. Serson (1973) and later Mosnier (1980) present a review of long period geomagnetic and geoelectric field detection instrumentation, with a

reference to the Gough and Reitzel (1967) three-componenet magnetometer and the Bobrov (1971) five-component field station. The Fluxgate magnetometer is described by Trigg et al. (1971). In recent years geomagnetic studies have advanced tremendously, benefiting from the use of improved instrumentation, computer analysis and associated advances in interpretation techniques. The application of cored induction coils in the detection of geomagnetic variations has progressed from early studies in 1949 to the more recent and widely quoted work of Vozoff (1972). The application of high permeability coils for the detection of rapid oscillations of the magnetic field is now widely spread. Vozoff (1972) has also overcome the problems of digital recording and describes, in this standard literature, its application to magnetotelluric sounding in a shallow crust environment. The method of shallow magnetotelluric probing has been applied consistently by Keller (1971) and with increasing incidence by many other workers. (e.g. Benderitter et al, 1978. in Finland)

The conductivity anomaly mapping associated with tectonically active regions has recently been reviewed by Hutton (1976), while others have examined the relation of other geophysical parameters to electrical conductivity. Banks and Ottey (1974), Beamish (1976) and Rooney (1976) have all carried out geomagnetic investigations in the Rift Valley of Kenya. Stegena (1976) presents a particularly useful review of electrical conductivity studies in geothermally active regions. The centres for geothermal research have all been in the

likely areas of U.S.A, U.S.S.R., Japan, Iceland, Turkey, and New Zealand to name but a few. Most of the available literature comes from authors working from the west. Keller (1980) particularly, has been closely involved in the exploration of vapour dominated reservoirs such as 'The Geysers' in California, reporting on the successful application of AMT sounding and other resistivity mapping techniques. The area of Larderello, in Italy, also containing high tamperature steam, has been the site of much scientific reasearch and is currently the subject of comparative studies by Berktold et al.(1981) and Fischer et al.(1981). Other areas of study include the 'Broadlands' geothermal region in New Zealand from where Risk et al. (1970) report of a D.C. resistivity survey and Whiteford (1975) reports of an AMT study in which resistivities of 2 to 12 ohm-m are mapped. In Iceland Hermance and Grillot (1970) have correlated their MT results with other geophysical techniques to examine their inter-dependence at depth. Particularly relevant studies have been performed by Leary and Phiney (1974) whose results from an MT traverse across the 'Yellowstone' geothermal region, U.S.A., established the method to be of extreme use in thermally active regions. Audio Magnetotelluric soundings have been reported in detail by Hoover et al. (1976) from a study in Long Valley, California. Their 8 Hz apparent resistivity map for the area is shown in figure 1.5. Similar work has been carried out by Strangway et al. (1973) who also reviews the appropriate equipment. Many studies (Long and Kaufmann, 1980) and recently (Ander,1981) have been performed in

Figure 1.5 Apparent resistivity (ohm-m) map (8 Hz), Long Valley, California. (From Hoover et al, 1976)

Figure 1.5

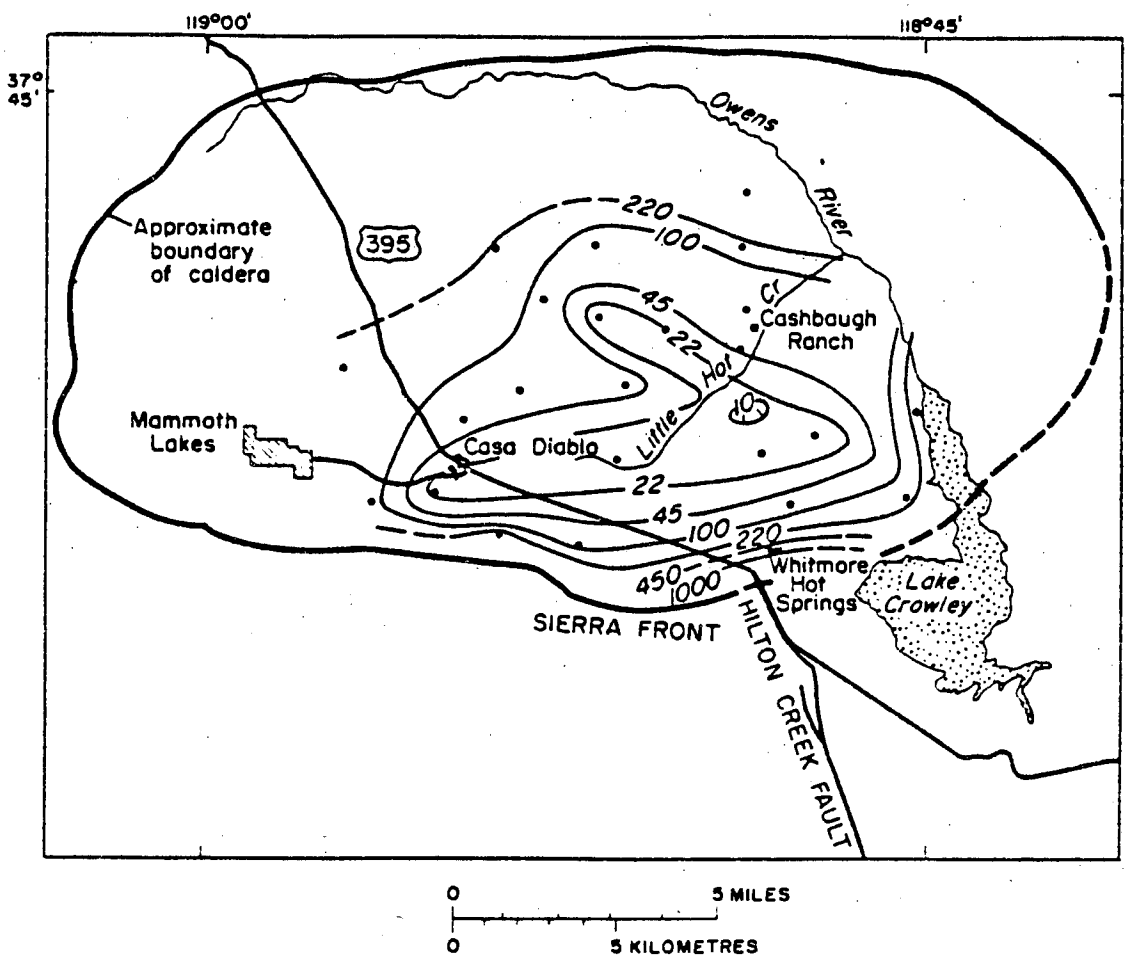
119°00'
118°45'
37°
45'
Owens
River
Approximate
boundary
of caldera
395
220
100
45
22
Hot
Cashbaugh
Ranch
Creek
Mammoth
Lakes
Casa Diablo
Little
22
45
100
220
450
1000
Whitmore
Hot
Springs
Lake
Crowley
SIERRA FRONT
HILTON CREEK FAULT
0
5 MILES
0
5 KILOMETRES

prospective geothermal areas and the interested reader is advised to refer to proceedings of such conferences as The San Francisco Geothermal Conference and to the large amount of information awaiting publication.

1.4 The purpose of the work

The following itemised sections describe the six main aims of this work.

(a) To extend the function of the existing MT equipment into the frequency range 1Hz - 1 kHz.

(b) To evaluate the assembled equipment and use it to survey a geophysically well mapped area.

(c) To make suitable modifications to existing data processing computer programmes and execute these on the new data.

(d) To provide increased resolution of the shallow conductivity structure and derive a broadband conductivity profile at a number of sites.

(e) To make a special study at the site of the Rookhope boring.

(f) To use the AMT data in an attempt to make an areal interpretation of the shallow crustal conductivity structure of the region.

1.5 Anticipated problems

In this section a brief introduction to the forward planning of the project is given. The problems listed are only examples of all the problems which were considered at the beginning, as well as throughout the course of the project.

To detect signals in the extended frequency range, natural signal strengths have first to be determined. The typical average signal strengths are well determined, but allowances have to be made for variations in this level. The unnatural signal content is more difficult to predict and consequently estimations of the signal-to-noise ratio are likely to vary between stations. The inclusion of notch filters, to diminish the most common of noise contributions, namely that of the 50 Hz electricity mains supply, is an important aspect of the design of the system. The natural harmonics of 50 Hz such as 150 Hz, 250 Hz etc. usually occur at decreasing power levels and the extent to which further notch filters must be included in the electronics has to be determined.

A suitable power supply for the complete system has to be established. The general aspects associated with the use of a portable generator in the field to supply this power must be considered, paying particular attention to the likelyhood of generating additional unnatural noise.

It was noted that the need for too rapid replacement of computer 'hardware' and 'software' can seriously hinder the planned progress. This condition was constantly checked, so as not to allow existing items to be superseded before they had been thoroughly used.

CHAPTER 2

THEORY AND INSTRUMENTATION PERTINENT TO MT STUDIES

2.1 General

The Magnetotelluric (MT) method is one means by which the electrical conductivity distribution within the Earth's crust and mantle can be inferred. The natural magnetic and electric field variations, measured at the Earth's surface, provide the origin for this task. The derived conductivity structure may then be related to naturally occurring rock structures through our knowledge of the electrical properties of rocks.

As with other geophysical techniques the outcome is a model which represents, by a limited number of parameters, the structure within the real Earth. The derived parameters must:

(a). be consistent, within our criteria, with the measured data and

(b). lie within the range of geophysically possible values.

The models satisfying the above conditions are then regarded as representing the actual conductivity of the Earth. This is permissible even though the Earth and particularly the geological structure of the crust is an immensely complex quantity.

In considering the MT method, it is convenient, as with other geophysical methods, to reduce the problem to a form in which it can be realistically solved. Thus in MT studies the magnetic and electric variations at the Earth's surface are considered to include the response of the conducting Earth to an external inducing magnetic field. The problem can then be expressed in terms of basic electromagnetic theory and the response of the Earth can finally be represented by a measure, often used in electrical conductivity measurements, called the impedance.

To show how the impedance can be calculated for a particular conductivity distribution within the Earth, we must consult the solutions of Maxwell's equations of electromagnetism.

2.2 The basis of the magnetotelluric method.

2.2.1 Basic theory

The propagation and attenuation of electromagnetic waves in a medium are best understood by developing the electromagnetic theory from Maxwell's equations.

Firstly, the relationships between the electric and magnetic field vectors can be expressed by their time derivatives as:

$$\underline{\nabla} \times \underline{E} = -\partial \underline{B}/\partial t \qquad 2.1$$

$$\nabla \times \underline{H} = \underline{J} + \partial \underline{D}/\partial t \qquad 2.2$$

where:

$\underline{J}$ = current density (A/m^2)

$\underline{E}$ = electric field intensity (V/m)

$\underline{B}$ = magnetic flux density ($weber/m^2$)

$\underline{H}$ = magnetic field intensity (ampere-turns/m)

$\underline{D}$ = electric displacement (C/m^2).

Equation 2.1 simply states that an electric field exists in the region of a time-varying magnetic field. The emf. thus induced is proportional to the negative rate of the change of the magnetic flux. Equation 2.2 states that a magnetic field is generated when a current flow exists in space and that this field is proportional to the total current present. In the equation $\underline{J}$ and $\partial \underline{D}/\partial t$ represent the conduction and displacement current flow respectively. The relationship of the electric and magnetic vectors for a typical plane electromagnetic wave is shown schematically in figure 2.1.

From equation 2.1 by applying the vector identity

$$\nabla . \nabla \times \underline{A} = 0 \quad \text{Unit vector } \underline{A}$$

we can derive the equation

$$\nabla . \underline{B} = 0 \qquad 2.3$$

Figure 2.1 The E and H vectors for a plane electromagnetic wave travelling in the positive direction along the z-axis. (a) The variation of E and H with z at a particular moment. The two vectors are in phase, but perpendicualr to each other. (b) The corresponding lines of force as seen when looking down on the xz-plane. The lines represent the electric field. The dots represent magnetic lines of force coming out of the paper, and the crosses represent magnetic lines of force going into the paper. The vector E x H gives the direction of propagation.
(From Lorrain and Corson, 1970)

Figure 2.1

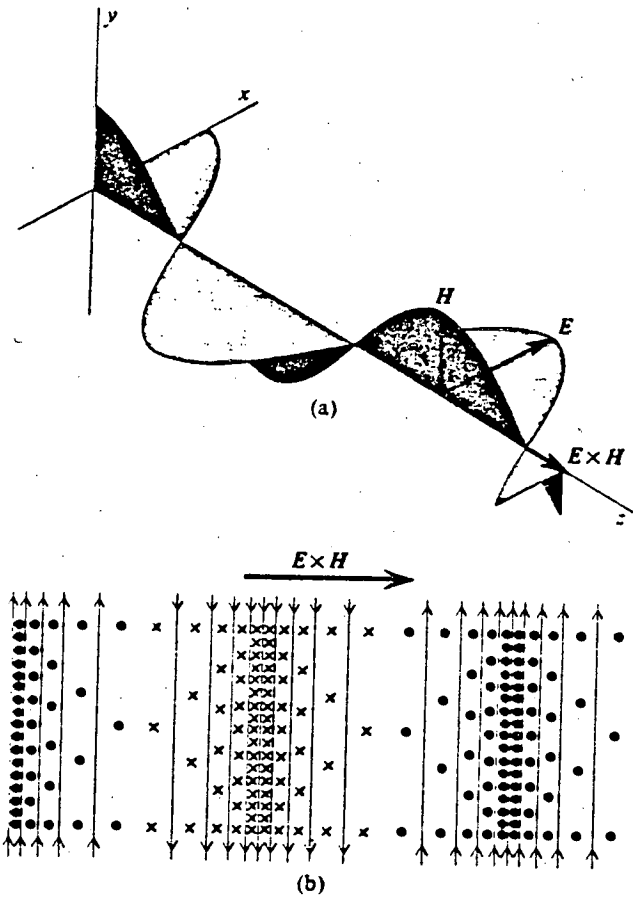

which merely states that magnetic flux never diverges from a point source but forms closed loops. Further in any conducting medium where charge does not accumulate during current flow, the same identity, applied to the equation 2.2, gives

$$\nabla \cdot \underline{D} = 0 \qquad 2.4$$

Introducing the following relationships

$$\underline{D} = \varepsilon \underline{E} \quad \underline{B} = \mu \underline{H} \quad \underline{J} = \sigma \underline{E} \qquad 2.5$$

where ε, μ and σ are respectively the permittivity (farads/m), permeability (henrys/m) and conductivity (mhos/m) of the medium, the equations 2.1 and 2.2 reduce - for sinusoidal variations as $E(t) = E_o \exp(jwt)$ and $H(t) = H_o \exp(jwt)$ - to

$$\nabla^2 \underline{E} = jw\mu\sigma \underline{E} - w^2 \varepsilon \mu \underline{E} \qquad 2.6$$

$$\nabla^2 \underline{H} = jw\mu\sigma \underline{H} - w^2 \varepsilon \mu \underline{H} \qquad 2.7$$

These equations represent the propagation of electric and magnetic field vectors in an isotropic homogeneous medium.

We must now return to the case of the Earth. Even in its most simple form we must consider the presence of an interface and the effect it will have on these equations. At each interface σ, ε and μ may be expected to change

and some conditions are therefore necessary to govern the behaviour of all electromagnetic fields crossing such an interface. The following quantities - by being continuous with respect to the interface - provide the necessary conditions:

1. The tangential component of the electric field.
2. The tangential component of the magnetic field.
3. The normal component of the current density.
4. The normal component of the magnetic flux.

These have been summarised in figure 2.2.

Two further conditions governing the behaviour of the field at opposite distances away from the interface require to be satisfied. One concerns the origin of the field and the second requires the field to be finite as it approaches infinity.

In considering the condition of finiteness at infinity first, it will be shown that the equations of wave propagation reduce to the diffusion equation whose solutions naturally satisfy the condition.

In considering the possible values of σ , ε and μ in the Earth we find that σ may vary between 10^{-5}mho/m in granite, for example, to 10^{3} mho/m in regions of high conductivity. The dielectic constant ε assumes a value of the order of $9\times\varepsilon_0$ but can reach $80\times\varepsilon_0$ in water. The permeability μ is typically very close to μ_0 and can therefore be assumed to equal $4\pi \times 10^{-7}$H/m throughout.

Figure 2.2 The boundary conditions at the interface of two media, using the Gaussian surface, (a) and the Closed Path (b) representation. Upper (a) and (b) refers to electrostatic fields, showing $D_n - D_n = 0$ and $E_t - E_t = 0$ respectively. The displacement currents are assumed to be negligible in MT theory. Lower (a) and (b) refer to $\underline{B}$ and $\underline{H}$ fields respectively, demonstrating that $B_n = B_n$ and $H_t = H_t$.

Figure 2.2

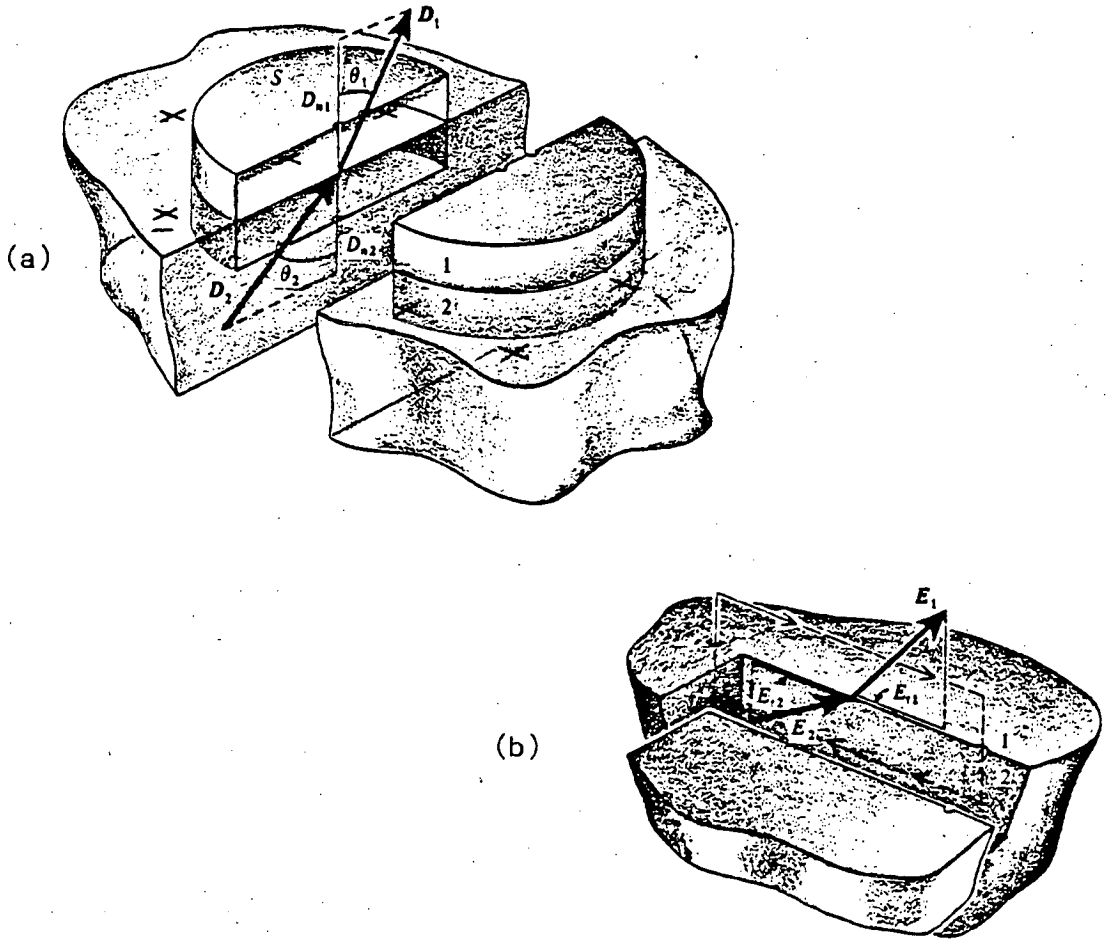
(a)
D_1
θ_1
D_{n1}
S
D_{n2}
D_2
θ_2
1
2
(b)
E_1
E_{t1}
E_{t2}
E_2
1
2

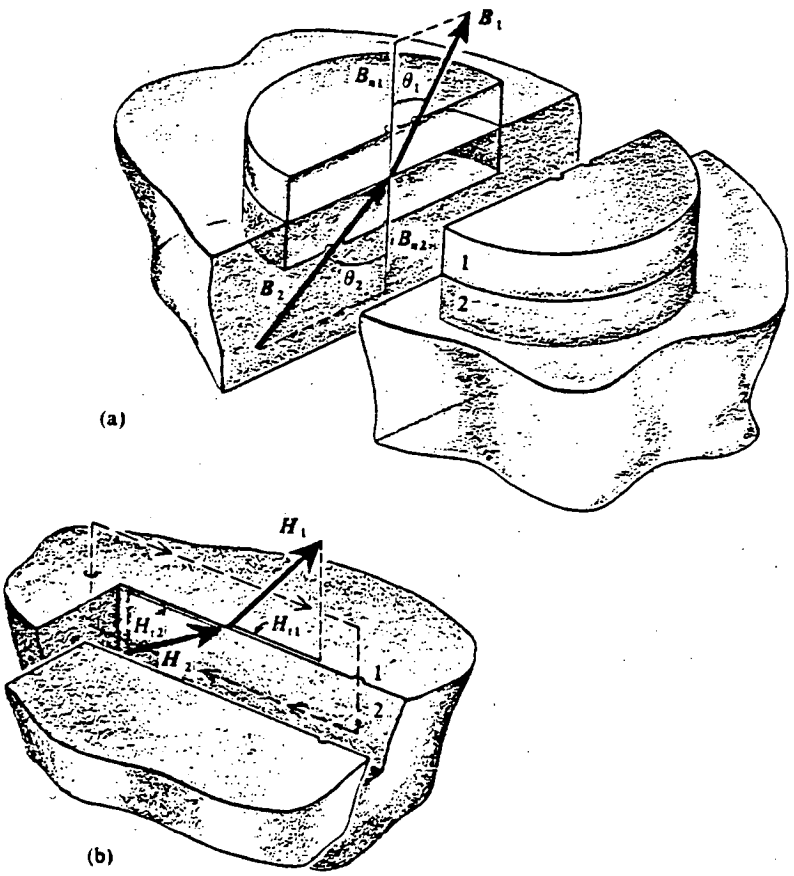
B_1
B_{n1}
θ_1
B_{n2}
B_2
θ_2
1
2
(a)
H_1
H_{t1}
H_{t2}
H_2
1
2
(b)

These values substituted in equations 2.6 and 2.7 give the amplitudes of the conduction and displacement currents for the maximum frequency of 1000 Hz as:

$$\nabla^2 \underline{E} \simeq 8x j\underline{E} - 4x10^{-9}\,\underline{E}$$ for conductive regions and

$$\nabla^2 \underline{E} \simeq 8x10^{-8}\, j\underline{E} - 4x10^{-9}\,\underline{E}$$ for highly resistive regions.

By comparing the relative magnitudes of the real and imaginary parts, we may conclude that the real part, which corresponds to the displacement current, is in both cases, negligible. This we now take to be the case.

Finally in air and in poorly conducting rocks

$$\nabla^2 \underline{E} \simeq 0, \qquad \nabla^2 \underline{H} \simeq 0$$

Conversely, in well conducting materials the equations of motion reduce to

$$\nabla^2 \underline{E} = jw\mu\sigma\underline{E}$$

and $$\nabla^2 \underline{H} = jw\mu\sigma\underline{H}$$

These equations are then the vector diffusion equations.

The solutions to these equations, for a plane wave propagating along the z axis and finite at $Z = \infty$, take the form

$$H = H_0 e^{-az} \cos (wt - az) \qquad 2.8$$

where $a = \sqrt{w\mu\sigma/2}$. This is an equation of a sinusodial wave with a phase shift, decaying exponentially with propagation distance.

The depth at which the amplitude of the field is reduced to 1/e of its original value is given by the skin depth:

$$\delta = 503\sqrt{(\rho/f)} \text{ metres} \qquad 2.9$$

This is a fundamental result in the natural diffusion of currents in conductive media and we shall be returning to it later. In the above treatment, the reader will note that the first of the two further conditions namely that concerning the origin of the field, has been implied in the form of a polarised plane wave. Such a plane wave will have a wavelength given by:

$$\lambda = c/f \text{ metres}$$

To examine what happens to the magnetic field - equation 2.8 - as it diffuses into the Earth, we note that in accordance with equation 2.2 it will have associated with it a conduction current. This current will be at right angles to the field and takes the form

$$J = -\partial H/\partial z = \sqrt{2a}H_0 e^{-az}\cos(wt - az + \pi/4)$$

with

$$a = \sqrt{w\mu\sigma/2}$$

The equation contains the inducing magnetic field amplitude H_0 and the exponential decay term e^{-az}. The current will therefore exhibit a skin depth effect. Also the term

$$\sqrt{\sigma\mu w/2}$$

relates the induced current to the magnetic field. Together with a phase difference it governs the characteristics of this induced electric field. These electric currents, in propagating through the Earth, cause yet another magnetic field to exist. In accordance with our original equations of electromagnetics (2.2), the field produced by a current flow will be radial around the flow and proportional to the total current present. This magnetic field is the secondary magnetic field which is again observable at the surface.

The magnitudes of the electric and magnetic fields measured at the surface therefore consist of a superposition of inducing and induced fields. This relationship is determined by this term $\sqrt{w\mu\sigma/2}$ where, σ represents the conductivity of rock.

The sources of the magnetic variations which we are considering are located outside the Earth and correlated with such phenomena as magnetic substorm activity, pulsation phenomena and atmospherics. Other recognised types of magnetic activity are 'bays' and 'magnetic storms'. Between the Ionosphere and the Earth's surface, the magnetic variations are propagated as EM waves and can be detected at very large distances from their source with only slight attenuation. For the period range 1000 seconds to 1 kHz , the wavelength, given by the equation above, is 3×10^8 km to 300 km. When applied to the MT case, Wait (1954) and Price (1962) have argued that the electromagnetic plane wave approach may not at these wavelengths be an adequate representation of the possibly complex structure of the variations and, therefore, produce misleading results. Srivastave (1965) considers the plane wave approach to be adequate for fluctuations of periods less than 1000 seconds.

For the audio frequency part of the spectrum the sources of signal are primarily lightning discharges (sferics) - associated with worldwide thunderstorm activity. An additional source is, of course, man-made noise. The energy of these sources is converted to electromagnetic

fields which propagate within the Ionosphere-Earth interspace. Over large distances these magnetic fluctuations, being transverse electric and magnetic waves, show distortion through the effects of attenuation and dispersion. Unless these waves travel unbounded and in a vacuum, they will be attenuated through their contact with the conducting Earth (Joule losses) and dispersed. This would be the case for any electromagnetic wave of many frequencies travelling in air. The attenuation effect was already observed in equation 2.8 where 'a' was the imaginary part of the complex wave number (k) such that 1/a defined the attenuation distance.

Dispersion of the wave and early attenuation of the high frequency content of the wave produces distinctively different wave forms between near and far sources. The effect is such that thunderstorm activity within some 100 km of a measuring station can be recognised. At these small source distances the integrity of the above implication is in any case questionable.

2.2.2 Resistivity of rocks

In the last section we saw how the conductivity of a medium influenced the propagation of electromagnetic waves in that medium and particularly how the properties of the medium govern the surface magnetic and electric fields.

Table 2.1 (from Telford et al 1976)

Mineral	Permeability	Mineral	Permeability
Magnetite	5	Rutile	1·0000035
Pyrrhotite	2·55	Calcite	0·999987
Ilmenite	1·55	Quartz	0·999985
Hematite	1·05	Hornblende	1·00015
Pyrite	1·0015		

Rock, mineral	Dielectric const.	Rock, mineral	Dielectric const.
Galena	18	Gypsum	5–11·5
Sphalerite	7·9–69·7	Beryl	5·5–7·8
Corundum	11–13·2	Biotite	4·7–9·3
Cassiterite	23	Epidote	7·6–15·4
Hematite	25	Orthoclase feldspar	3–5·8
Rutile	31–170	Plagioclase feldspar	5·4–7·1
Fluorite	6·2–6·8	Quartz	4·2–5
Calcite	7·8–8·5	Zircon	8·6–12
Apatite	7·4–11·7	Granite (dry)	4·8–18·9
Barite	7–12·2	Gabbro	8·5–40
Peridotite	8·6	Diorite	6·0
Norite	61	Serpentine	6·6
Quartz porphyry	14–49·3	Gneiss	8·5
Diabase	10·5–34·5	Sandstone (dry to moist)	4·7–12
Trap	18·9–39·8	Packed sand (dry to moist)	2·9–105
Dacite	6·8–8·2	Soil (dry to moist)	3·9–29·4
Obsidian	5·8–10·4	Basalt	12
Sulphur	3·6–4·7	Clays (dry to moist)	7–43
Rock salt	5·6	Petroleum	2·07–2·14
Anthracite	5·6–6·3	Water (20°C)	80·36
		Ice	3–4·3

Table 2.2 (from Telford et al 1976)

Mineral	Formula	Resistivity (Ωm)	
		Range	Average
Argentite	Ag_2S	2×10^{-3}–10^{4}	$1{\cdot}7 \times 10^{-3}$
Bismuthinite	Bi_2S_3	18–570	
Covellite	CuS	3×10^{-7}–8×10^{-5}	2×10^{-5}
Chalcocite	Cu_2S	3×10^{-5}–0·6	10^{-4}
Chalcopyrite	$CuFeS_2$	$1{\cdot}2 \times 10^{-5}$–0·3	4×10^{-3}
Bornite	Cu_5FeS_4	$2{\cdot}5 \times 10^{-5}$–0·5	3×10^{-3}
Marcasite	FeS_2	10^{-3}–3·5	5×10^{-2}
Pyrite	FeS_2	$2{\cdot}9 \times 10^{-5}$–1·5	3×10^{-1}
Pyrrhotite	Fe_nS_m	$6{\cdot}5 \times 10^{-6}$–5×10^{-2}	10^{-4}
Cinnabar	HgS		2×10^{7}
Molybdenite	MoS_2	10^{-3}–10^{6}	10
Galena	PbS	3×10^{-5}–3×10^{2}	2×10^{-3}
Millerite	NiS		3×10^{-7}
Stannite	Cu_2FeSnS_2	10^{-3}–6×10^{3}	
Stibnite	Sb_2S_3	10^{5}–10^{12}	5×10^{6}
Sphalerite	ZnS	1·5–10^{7}	10^{2}
Cobaltite	CoAsS	$3{\cdot}5 \times 10^{-4}$–10^{-1}	
Smaltite	$CoAs_2$		5×10^{-5}
Arsenopyrite	FeAsS	2×10^{-5}–15	10^{-3}
Niccolite	NiAs	10^{-7}–2×10^{-3}	2×10^{-5}
Sylvanite	$AgAuTe_4$	4×10^{-6}–2×10^{-5}	
Bauxite	$Al_2O_3.nH_2O$	2×10^{2}–6×10^{3}	
Braunite	Mn_2O_3	0·16–1·2	
Cuprite	Cu_2O	10^{-3}–300	30
Chromite	$FeCr_2O_4$	1–10^{6}	
Specularite	Fe_2O_3		6×10^{-3}
Hematite	Fe_2O_3	$3{\cdot}5 \times 10^{-3}$–10^{7}	
Limonite	$2Fe_2O_3.3H_2O$	10^{3}–10^{7}	
Magnetite	Fe_3O_4	5×10^{-5}–$5{\cdot}7 \times 10^{3}$	
Ilmenite	$FeTiO_3$	10^{-3}–50	
Wolframite	Fe, Mn, WO_4	10–10^{5}	
Manganite	MnO(OH)	10^{-2}–0·3	
Pyrolusite	MnO_2	5×10^{-3}–10	
Quartz	SiO_2	4×10^{10}–2×10^{14}	
Cassiterite	SnO_2	4×10^{-4}–10^{4}	0·2
Rutile	TiO_2	30–1000	500
Uraninite (Pitchblende)	UO_2	1–200	
Anhydrite	$CaSO_4$		10^{9}
Calcite	$CaCO_3$		2×10^{12}
Fluorite	CaF_2		8×10^{13}
Siderite	$Fe_2(CO_3)_3$		70
Rock salt	NaCl	30–10^{13}	
Sylvite	KCl	10^{11}–10^{12}	
Diamond	C	10–10^{14}	
Serpentine		2×10^{2}–3×10^{3}	
Hornblende		2×10^{2}–10^{6}	
Mica		9×10^{2}–10^{14}	
Biotite		2×10^{2}–10^{6}	
Phlogopite		10^{11}–10^{12}	
Bitum. coal		0·6–10^{5}	
Coals (various)		10–10^{11}	
Anthracite		10^{-3}–2×10^{5}	
Lignite		9–200	
Fire clay			30
Meteoric waters		30–10^{3}	
Surface waters (ign. rocks)		0·1–3×10^{3}	
Surface waters (sediments)		10–100	
Soil waters			100
Natural waters (ign. rocks)		0·5–150	9
Natural waters (sediments)		1–100	3
Sea water			0·2
Saline waters, 3%			0·15
Saline waters, 20%			0·05

In the case of the Earth the medium is a rock or a mineral whose electromagnetic characteristics are described, in part, by the parameters μ, ε and σ. We also know that for material within the Earth, there are other important parameters which govern its electrical behaviour, such as the presence of pore fluids.

The three parameters μ, ε and σ all show some variation from one rock type to another. In comparison to the measurement of conductivity, which shows variations over 24 decades (table 2.2), the measurement of magnetic permeability and permittivity is only of very minor significance in MT prospecting. Although the variation in μ, due, in part, to the small concentrations of magnetite in rock (table 2.1), can be observed and used in this type of work (Orr and Kao, 1980), its effect on conductivity measurements is small and is consequently often ignored.

Most rocks are generally poor conductors, having conductivity values between 1 Mho/m and 10^{-7} Mho/m. Were it not for the fluids contained in pores within the rock structure, the resistivities of most rocks would be considerably higher. The governing conduction process is electrolytic, where the rock conductivity is governed by the mobility, concentration and degree of dissociation of the ions in the solvent, which in turn bear a relationship to the porosity of the rock, the

Table 2.3 (from Telford et al 1976)

Rock type	Resistivity range (Ωm)
Consolidated shales	20–2×10^3
Argillites	10–8×10^2
Conglomerates	2×10^3–10^4
Sandstones	1–$6{\cdot}4 \times 10^8$
Limestones	50–10^7
Dolomite	$3{\cdot}5 \times 10^2$–5×10^3
Unconsolidated wet clay	20
Marls	3–70
Clays	1–100
Alluvium and sands	10–800
Oil sands	4–800

Rock type	Resistivity range (Ωm)
Granite	3×10^2–10^6
Granite porphyry	$4{\cdot}5 \times 10^3$ (wet)–$1{\cdot}3 \times 10^6$ (dry)
Feldspar porphyry	4×10^3 (wet)
Albite	3×10^2 (wet)–$3{\cdot}3 \times 10^3$ (dry)
Syenite	10^2–10^6
Diorite	10^4–10^5
Diorite porphyry	$1{\cdot}9 \times 10^3$ (wet)–$2{\cdot}8 \times 10^4$ (dry)
Porphyrite	10–5×10^4 (wet)–$3{\cdot}3 \times 10^3$ (dry)
Carbonatized porphyry	$2{\cdot}5 \times 10^3$ (wet)–6×10^4 (dry)
Quartz porphyry	3×10^2–9×10^5
Quartz diorite	2×10^4–2×10^6 (wet)–$1{\cdot}8 \times 10^5$ (dry)
Porphyry (various)	60–10^4
Dacite	2×10^4 (wet)
Andesite	$4{\cdot}5 \times 10^4$ (wet)–$1{\cdot}7 \times 10^2$ (dry)
Diabase porphyry	10^3 (wet)–$1{\cdot}7 \times 10^5$ (dry)
Diabase (various)	20–5×10^7
Lavas	10^2–5×10^4
Gabbro	10^3–10^6
Basalt	10–$1{\cdot}3 \times 10^7$ (dry)
Olivine norite	10^3–6×10^4 (wet)
Peridotite	3×10^3 (wet)–$6{\cdot}5 \times 10^3$ (dry)
Hornfels	8×10^3 (wet)–6×10^7 (dry)
Schists (calcareous and mica)	20–10^4
Tuffs	2×10^3 (wet)–10^5 (dry)
Graphite schist	10–10^2
Slates (various)	6×10^2–4×10^7
Gneiss (various)	$6{\cdot}8 \times 10^4$ (wet)–3×10^6 (dry)
Marble	10^2–$2{\cdot}5 \times 10^8$ (dry)
Skarn	$2{\cdot}5 \times 10^2$ (wet)–$2{\cdot}5 \times 10^8$ (dry)
Quartzites (various)	10–2×10^8

Table 2.4 (from Keller and Frischknecht 1966)

Age	Marine sedimentary rocks	Terrestrial sedimentary rocks	Extrusive rocks (basalt, rhyolite)	Intrusive rocks (granite, gabbro)	Chemical precipitates (limestone, salt)
Quaternary and Tertiary ages	1–10	15–50	10–200	500–2000	50–5000
Mesozoic	5–20	25–100	20–500	500–2000	100–10,000
Carboniferous Paleozoic	10–40	50–300	50–1000	1000–5000	200–100,000
Early Paleozoic	40–200	100–500	100–2000	1000–5000	10,000–100,000
Precambrian	100–2000	300–5000	200–5000	5000–20,000	10,000–100,000

values in Ohm-metres

(from Telford et al 1976)

Rock	% H_2O	$\rho(\Omega m)$	Rock	% H_2O	$\rho(\Omega m)$
Siltstone	0·54	$1·5 \times 10^4$	Pyrophyllite	0·76	6×10^6
Siltstone	0·44	$8·4 \times 10^6$	Pyrophyllite	0·72	5×10^7
Siltstone	0·38	$5·6 \times 10^6$	Pyrophyllite	0·7	2×10^8
Coarse grain SS	0·39	$9·6 \times 10^5$	Pyrophyllite	0	10^{11}
Coarse grain SS	0·18	10^8	Granite	0·31	$4·4 \times 10^3$
Medium grain SS	1·0	$4·2 \times 10^3$	Granite	0·19	$1·8 \times 10^6$
Medium grain SS	1·67	$3·2 \times 10^6$	Granite	0·06	$1·3 \times 10^8$
Medium grain SS	0·1	$1·4 \times 10^6$	Granite	0	10^{10}
Graywacke SS	1·16	$4·7 \times 10^3$	Diorite	0·02	$5·8 \times 10^5$
Graywacke SS	0·45	$5·8 \times 10^4$	Diorite	0	6×10^5
Arkosic SS	1·26	10^3	Basalt	0·95	4×10^4
Arkosic SS	1·0	$1·4 \times 10^3$	Basalt	0·49	9×10^5
Organic limestone	11	$0·6 \times 10^3$	Basalt	0·26	3×10^7
Dolomite	2	$5·3 \times 10^3$	Basalt	0	$1·3 \times 10^9$
Dolomite	1·3	6×10^3	Olivine-pyrox.	0·028	2×10^4
Dolomite	0·96	8×10^3	Olivine-pyrox.	0·014	4×10^5
Peridotite	0·1	3×10^3	Olivine-pyrox.	0	$5·6 \times 10^7$
Peridotite	0·03	2×10^4			
Peridotite	0·016	10^6			
Peridotite	0	$1·8 \times 10^7$			

Table 2.5 (from Telford et al 1976)

Element	Resistivity (Ωm)		Element	Resistivity (Ωm)	
	Range	Average		Range	Average
Antimony		4.5×10^{-7}	Molybdenum		5.7×10^{-8}
Arsenic		2.2×10^{-7}	Nickel		7.8×10^{-8}
Bismuth		1.2×10^{-6}	Platinum		10^{-7}
Copper		1.7×10^{-8}	Silver		1.6×10^{-8}
Gold		2.4×10^{-8}	Sulphur	10^{7}–10^{16}	10^{14}
Graphite	5×10^{-7}–10	10^{-3}	Tellurium	10^{-4}–2×10^{-3}	10^{-3}
Iron		10^{-7}	Tin		1.1×10^{-7}
Lead		2.2×10^{-7}	Uranium		3×10^{-7}
Mercury		9.6×10^{-7}	Zinc		5.8×10^{-8}

Ore	Other minerals	Gangue	ρ(Ωm)
Pyrite			
18%	2% (chalco)	80%	300
40	20%	40	130
60	5% (ZnS) + 15%	20	0·9
75	10% (ZnS) + 5%	10	0·14
95	5% (ZnS)		1·0
95		5	7·0
Pyrrhotite			
41%		59%	2.2×10^{-4}
58		42	2.3×10^{-4}
79		21	1.4×10^{-3}
82		18	8.5×10^{-3}
95		5	1.4×10^{-6}
SbS_2 in quartz			4×10^{3}–3×10^{7}
FeAsS 60%	FeS 20%	20% SiO_2	0·39
FeAsS	—		1×10^{-4}–1×10^{-2}
$CuFeS_4$			3×10^{-3}
Cu_5FeS_4		60% SiO_2	7×10^{-2}
Cu_5FeS_4 40%			2×10^{4}
Fe, Mn, WO_4 80%	CoAsS		10^{3}–10^{7}
Fe, Mn, WO_4			7×10^{-2}
PbS, massive			0·8
PbS, near massive			10^{-2}–3
PbS 50–80%			0·1–300
Fe_2O_3, massive			2.5×10^{3}
Iron			
Fe_3O_4 60%			45
Fe_3O_4 from contact met.			0·5–10^{3}
Diss. brown iron oxide			8×10^{2}–3×10^{5}
75% brown iron oxide		25%	2×10^{4}–8×10^{5}
Fe_2O_3 fine grained			2.5×10^{3}
Fe_3O_4			5×10^{3}–8×10^{3}
Fe_3O_4 in pegmatite			7×10^{3}–2×10^{5}
Zinc			
30%	5% PbS, 15% FeS	50%	0·75
70%	3% chalco, 17% PbS, 10% FeS		20
80	10% PbS, 10% FeS		1.7×10^{3}
80	2% chalco, 1% PbS, 2% FeS	15%	1·3
90	5% PbS	5%	130

prevalent pressure (Duba, 1976), and the salinity of the fluid. The relation has been represented empirically and is of fundamental significance. It gives the basis for a major part of the effects on the conductivity distributions, observed in the course of this thesis and is given in terms of the bulk conductivity by Archies' law, (Archie, 1942)

$$\sigma_r = \sigma_p \eta^m$$

where σ_r is the overall conductivity of the rock, σ_p the conductivity of the fluid, η the porosity and m is taken as 1-2, (Keller and Frischknecht, 1966). The conductivity of porous rock, encountered at crustal depths, is thus determined by the structure and volume of the immanent pore spaces, as well as by the nature of the fluid contained within them (Stanley et al, 1977). This structure of the interstices of the rock is also responsible for much of the effects of rock resistivity anisotropy - the difference in the freedom of current flow in different directions.

At greater depths laboratory measurements have shown (Brace, 1971) that the temperature is of importance, particularly if coupled with the presence of water, either in the free state, or as water of hydration. In these cases, partial melting has been shown to be possible in the lower crust. At upper mantle depths semi-conduction becomes dominant and mineral conductivity

increases with temperature (Kittel, 1953). Further discussion with references to much of the experimental evidence, can be found in an excellent review by Shankland (1975).

For the purposes of shallow crustal investigations, rock types can be grouped according to their resistivities. This is shown in table 2.3. Igneous rocks, in general, have highest resistivity while metamorphic rocks are more conductive. Sedimentary rocks show the lowest resistivity. Further, both the age of the rock and lithology will vary the resistivity of rock, possibly through their effects on the porosity of the rock (table 2.4 (a)). Small variations in the amounts of water present and of its salinity will cause very large resistivity fluctuations in the rock. These effects were summarised by Telford et al (1976) and are presented in table 2.4 (b). A compilation of resistivity values for common elements and ores is provided in table 2.5.

2.2.3 Magnetotelluric application

The wave equations derived in section 2.2.1 for the basic case will now be applied to the MT case. To do this, certain simplifying assumptions have to be made, some of which have already been justified above.

For the wave motion the frequencies of interest are low enough to make the displacement currents negligible. This was shown to be the case in section 2.1. Next, the source field is a plane electromagnetic wave of infinite wave length. This enables all variations $\partial / \partial x$ and $\partial / \partial y$

in the horizontal plane to be made equal to zero. Again, for the highest frequency used in this study, this assumption is valid. The field is considered to consist of a superposition of periodic variations only.

The theory satisfying these conditions alone is sufficient to produce the basic magnetotelluric equations (Schmucker,1970). However in considering these equations it will be evident that two further conditions have been assumed. Namely, that the Earth is planar rather than spherical (Summers,1981) and also that it is isotropic and stratified.

Consider a magnetic vector

$$H = H_0 e^{-az} \cos (wt - az)$$

corresponding to the solution derived in 2.8. We may express its components in the x and y directions as:

$$Hx = (H_0 \cos \theta) e^{-az} \cos (wt - az)$$

$$Hy = (H_0 \sin \theta) e^{-az} \cos (wt - az)$$

Applying Maxwell's equation 2.2 and satisfying the required conditions, the induced electric currents in the directions x and y will be $\sqrt{2}a/\sigma$ times the orthogonal magnetic component and will lead it by $\pi/4$ degrees.

The squares of the ratios of the resulting orthogonal

electric and magnetic amplitudes $|Ex/Hy|^2$ and $|Ey/Hx|^2$ are equal and take the value

$$2(a/\sigma)^2 \qquad \text{where } a = \sqrt{w\mu\sigma/2}$$

The ratio E/H of the orthogonal components will be seen to contain all the information necessary to obtain our estimate of the resistivity of the Earth at all periods. Termed the impedance and denoted by Z, it represents the Earth's response to an unit electromagnetic impulse. For a one-dimensional structure, in which σ varies only with depth z, the apparent resistivity ρ_a will be given by

$$\rho_a = 1/\sigma = 1\omega\mu|E/H|^2$$

In practical terms $\mu = \mu_0 = 4\pi \times 10^{-7}$ H/m as we have seen, E and H take units mV/km and gammas respectively and the equation for apparent resistivity takes the form

$$\rho_a = 0.2\ T|E/H|^2 \text{ Ohm m} \qquad 2.10$$

This is the Cagniard's expression for apparent resistivity and states that the amplitudes of the orthogonal electric and magnetic field components measured at the Earth's surface at different frequencies can be used directly to determine the variation of resistivity with depth.

It is convenient here to introduce the concept of the impedance tensor. It provides for a fuller representation of the observed parameters by retaining the complex (as opposed to scalar) representation throughout.

If the Earth is assumed to have a response denoted by the response functions: Za , Zb , Zc , Zd , then the resulting fields E(t) and N(t) measured at the surface will be given by the convolution of these response functions with the magnetic fields H'(t) and D'(t).

$$N'(t) = \int Za(t - \tau)H'(t)dt + \int Zb(t - \tau)D'(t)dt$$

$$E'(t) = \int Zc(t - \tau)H'(t)dt + \int Zd(t - \tau)D'(t)dt$$

In the frequency domain the relationships transform to:

$$N = ZxxH + ZxyD \qquad 2.11$$

$$E = ZyxH + ZyyD \qquad 2.12$$

The components Zxx, Zxy, Zyx , Zyy are the elements of $\underline{\underline{Z}}$ the impedance tensor and represent the Fourier transforms of Za ,Zb ,Zc ,Zd. In tensor notation the electric field response $\underline{E}$ is given by

$$\underline{E} = \underline{\underline{Z}}\,\underline{H} \qquad 2.13$$

In the Cagniard case, where the Earth is

one-dimensional the electric field components are related only to their respective orthogonal magnetic field components and the elements:

$$Zxx = Zyy = 0$$

and $$Zxy = -Zyx$$

The Cagniard apparent resistivity ρ_a and phase ϕ_a is then defined by the scalar relation

$$\rho_a = 0.2\ T|Zxy|^2$$

and $$\phi_a = \arg(Zxy)$$

where the scalar element Zxy can also be Zyx.

Response of an n layer 1/2 space

In the case of a simple n layered 1/2 space the wave equations derived above must hold for each of the n layers. If, as they must, the boundary conditions are satisfied at each interface, the analytic solution for the surface impedance can be represented by a recursion relation as follows:

$$Z(0) = \frac{iw\mu}{\theta_1} \coth\left[\theta_1 h_1 + \coth^{-1}\left(\frac{\theta_1}{\theta_2}\coth^{-1}\left[\theta_2 h_2 + \ldots \ldots \coth^{-1}\frac{\theta_{n-1}}{\theta_n}\right]\right)\ldots\right)\right]$$

where $$\theta_i = \left(\frac{w\mu_i\sigma_i}{2}\right)^{\frac{1}{2}} + i\left(\frac{w\mu_i\sigma_i}{2}\right)^{\frac{1}{2}}$$

Z(0) is the impedance of an n layered structure at the Earth's surface. Also h_i and σ_i are the depth and

Figure 2.3a Apparent resistivity calculated from magneto-telluric measurements over a two-layer earth.

Figure 2.3b Phase retardation of the magnetic component of a magnetotelluric field observed over a layered earth consisting of a single overburden layer and a uniform substratum.
(From Keller and Frischknecht, 1966)

Figure 2.3

(a)

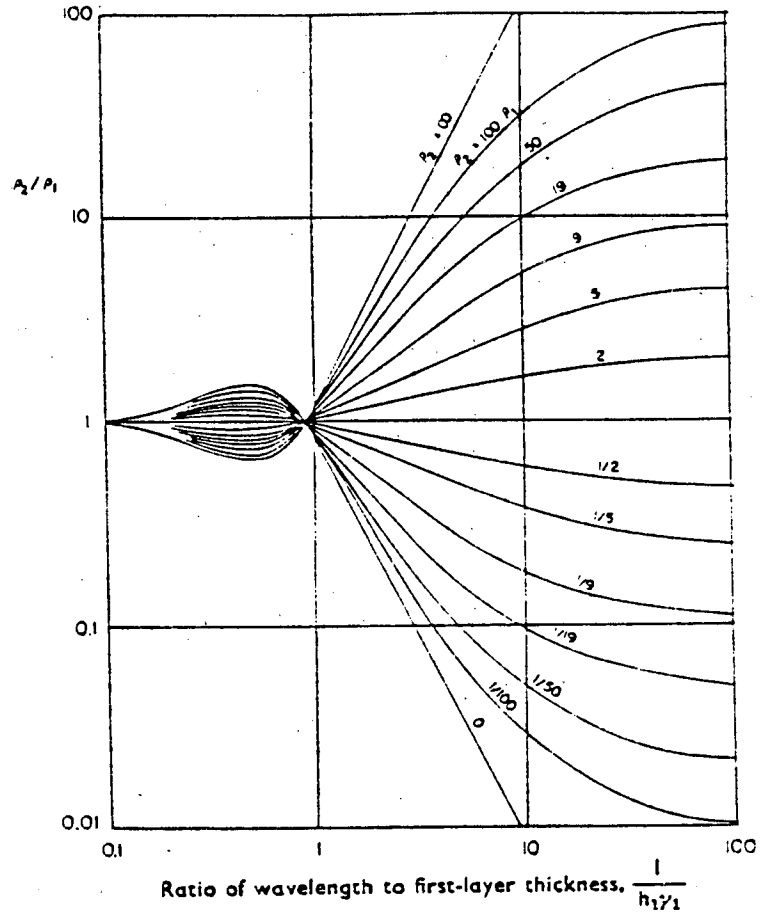
100
10
1
0.1
0.01
A_2/A_1
$\rho_2 = \infty$
$\rho_2 = 100\,\rho_1$
50
19
9
5
2
1/2
1/5
1/9
1/19
1/50
1/100
0
0.1
1
10
100
Ratio of wavelength to first-layer thickness, $\frac{l}{h_1\gamma_1}$

(b)

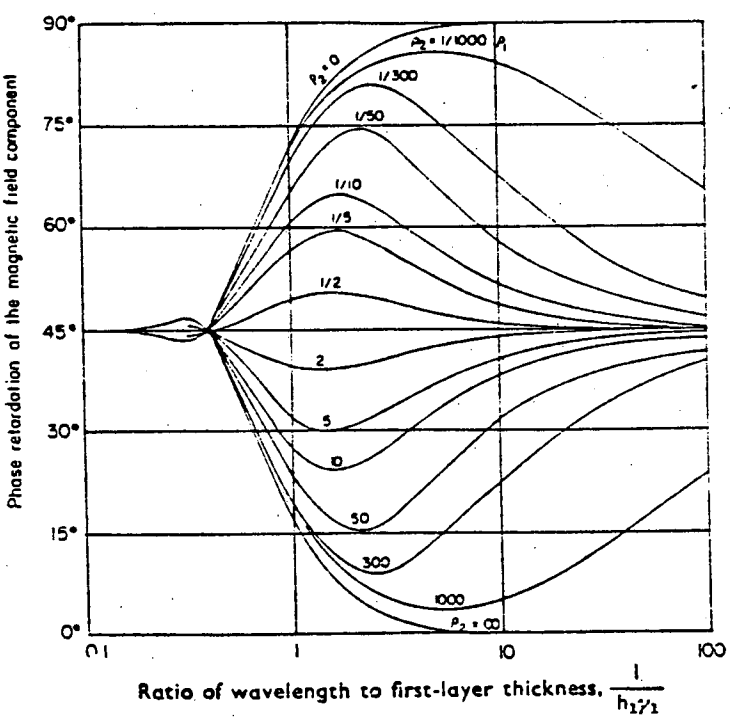
90°
75°
60°
45°
30°
15°
0°
Phase retardation of the magnetic field component
$\rho_2 = 1/1000\,\rho_1$
$\rho_2 = 0$
1/300
1/50
1/10
1/5
1/2
2
5
10
50
300
1000
$\rho_2 = \infty$
0.1
1
10
100
Ratio of wavelength to first-layer thickness, $\frac{l}{h_1\gamma_1}$

conductivity of the ith layer. This recursion equation is utilised to produce such master curves as in figure 2.3 or to generate the responses of test models in one-dimensional inversion schemes as is described in chapter 6.

2.3 The two- and three-dimensional response

When dealing with a complex structure such as the Earth's crust, it is necessary to consider the solutions to the induction problem in a two-and three-dimensional Earth.

In the last section the analytical solutions for $\underline{E}$ and $\underline{H}$ were obtained for a medium where σ was only a function of Z. In a two-dimensional case, by definition, σ is a function of one other component, say, y. In the three-dimensional case σ is a function of x, y and z.

The criterion for two-dimensionality is usually expressed in terms of a structure whose dimensions extend in one direction to infinity. In real terms, this distance need only be of the order of a few skin depths. In this situation the MT impedances are very different to those of the one-dimensional case. Treating the structure mathematically becomes rather cumbersome as all the field components are coupled to each other.

Commonly, therefore, the simplifications described in the preceding sections are invoked and one finds that the case of the two-dimensional structure is separated into

two distinct modes. These correspond to the E polaristion and H polaristion cases where, respectively, the E and H fields are polarised parallel to the strike of the structure.

In this case the Maxwell's equations for the electric and magnetic components in the Cartesian system reduce from 2.1 and 2.2 to

$$\underline{H} = \frac{1}{\mu_o w} \left(\underline{y} \frac{\partial E}{\partial z} - \underline{z} \frac{\partial E}{\partial y} \right)$$

$$\underline{E} = \frac{1}{\sigma} \left(\underline{y} \frac{\partial H}{\partial z} - \underline{z} \frac{\partial H}{\partial z} \right)$$

where $\underline{E}$ = Ex for the E polarisation field and $\underline{H}$ = Hx for the H polarisation field. The terms x, y and z are the unit vectors along the axes of the Cartesian coordinates. These equations do not lend themselves to an analytical solution. Numerical procedures have been devised by various authors, to calculate two-dimensional responses. In essence these involve the use of a mesh of grid points throughout the area of the conducting space. The fields are then calculated by finite differences or by finite element methods and are subject to continuity conditions at all boundary surfaces.

Under the simplifications the equations above, corresponding to the two modes, give the impedances in parallel and perpendicular notation as:

$Z_{||} = Ex/Hy$ for the E polarisation

case and

$Z_{\perp} = Ey/Hx$ for the H polarisation case.

This decoupling of the solutions holds only for the case, where the directions of Ex and Ey are parallel and perpendicular to the independent axes. In such a case Zxx and Zyy are equal to zero

$$Z_{\perp} = Zxy$$

$$Z_{\parallel} = Zyx$$

and the two modes are completely independent of each other. For any other direction of the measuring axes the elements Ex and Ey will each depend on both of the elements Hx and Hy.

To observe the character of this relationship the equation 2.13 is best expressed in matrix form thus:

$$\begin{pmatrix} Ex \\ Ey \end{pmatrix} = \begin{pmatrix} Zxx & Zxy \\ Zyx & Zyy \end{pmatrix} \begin{pmatrix} Hx \\ Hy \end{pmatrix}$$

Applying a rotation through an angle theta, the new elements E'x and E'y will be given by:

$$\begin{pmatrix} E'x \\ E'y \end{pmatrix} = R \begin{pmatrix} Zxx & Zxy \\ Zxy & Zyy \end{pmatrix} R^T \begin{pmatrix} H'x \\ H'y \end{pmatrix}$$

where $$R = \begin{pmatrix} \cos\theta & \sin\theta \\ -\sin\theta & \cos\theta \end{pmatrix}$$

and is the rotation matrix. The impedance tensor at the new direction is given by:

$$\underline{\underline{Z}}'(\theta) = \underline{\underline{R}}\,\underline{\underline{Z}}\,\underline{\underline{R}}^T \qquad 2.14$$

In a theoretical two-dimensional case, the angle can be found such that the measuring axes correspond with the strike direction and $Z'xx = Z'yy = 0$. This angle corresponds to $Z'xy$ being maximised, or minimised. The direction then defined by θ is the principal direction.

In practice the impedances $Z'xx$ and $Z'yy$ never vanish. This is shown for station data showing a two and three-dimensional response in figure 2.4. Furthermore the direction of strike is often unknown. It is necessary, therefore, to devise a means by which the rotation could be performed and such an orientation found at which a response was most like a two-dimensional response. This orientation, it is hoped, will be the same as that defined by the strike.

By expanding equation 2.14 we can relate the rotated tensor to its unrotated value.

Figure 2.4 Response of tensor elements under rotation for a two-dimensional and three-dimensional site. (From Mbipom, 1980)

COMPLEX : SITE

STATION 12

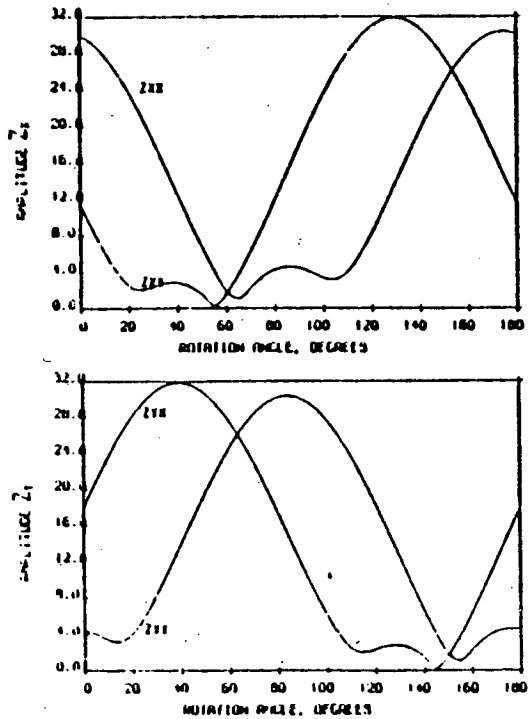

TWO-DIMENSIONAL SITE

STATION 14

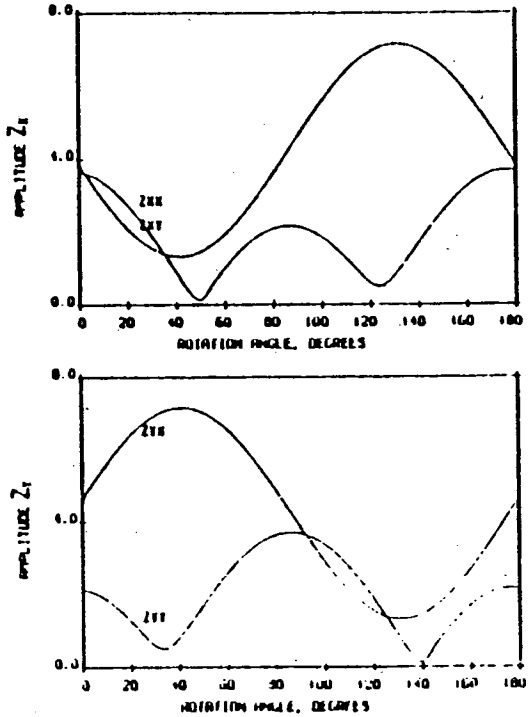

Figure 2.4

Most workers have chosen to maximise

$|Z'xy(\theta)|$ (Everett and Hyndman, 1967) or

$|Z'xy(\theta)|^2 + |Z'yx(\theta)|^2$ (Swift, 1967)

where the moduli are chosen because the impedances are complex. The latter can be represented analytically as:

$$\tan 4\theta = \frac{(Zxx - Zyy)(Zxy + Zyx)^* + (Zxx - Zyy)^*(Zxy + Zyx)}{|Zxx - Zyy|^2 - |Zxy + Zyx|^2} \qquad 2.15$$

The resulting value of θ yields components Zxy and Zyx which can be used to calculate $\rho_\perp$ and $\rho_{||}$ using equation 2.10. Either $\rho_\perp$ or $\rho_{||}$ is calculated depending on which side of a discontinuity measurements are made. On the resistive side $\rho_\perp$ is greater than $\rho_{||}$ and the maximum value of ρ_{xy} or ρ_{yx} can then be associated with $\rho_\perp$. The converse is true on the conductive side.

In many geophysical applications it is suitable to represent the problem by a two-dimensional approximation. Jones and Vozoff (1978) have shown that in a three-dimensional situation equation 2.15 still defines the gross two-dimensional strike of the feature. The case of the three-dimensional structure does not allow a simple form to be constructed and analytical solutions are not possible. Most workers have either chosen to use analogue laboratory models to imply the practical responses

(Dosso ,1966, 1973) or have used approximations to solve three-dimensional induction problems (Brewitt-Taylor and Weaver ,1976). In general it is shown that even simple three-dimensional conductivity structures confined to the surface layers can have a considerable effect on the electric and magnetic fields at depth. It is therefore necessary, to determine the dimensionality of a structure; particularly to separate the one- and two-dimensional structures from those having three-dimensional features. The most frequently used parameter is the skew.

$$\text{skew} = \left| Zxx+Zyy/\ Zxy-Zyx \right|$$

From equations 2.23 it can be seen to be independent of the angle theta. For the true one and two-dimensional case the skew is equal to zero. For real data from one-dimensional structures the diagonal elements can only be expected to approximate to zero because of noise. The skew will similarly only approximate to zero. For the two-dimensional case the same is true for an orientation in the strike direction. It is possible however for the skew to be large in the two dimensional case, when

$$Zxy - Zyx \simeq 0$$

In general the three-dimensional case will produce a complex variation in $|Zxy|$ and $|Zyx|$ with rotation and Zxx and Zyy will not be small. With the exception of

$|Zxy| >> |Zyx|$ or vice-versa the skew over a

three-dimensional structure will be high. The value commonly chosen to limit low skew values is 0.4.

It is necessary also to consider other parameters when assessing the degree of two-dimensionality. The variations of ρ max and ρ min over the frequency band indicate the degree of anisotropy. The character of the azimuth of the major impedance also provides useful information.

In GDS studies when the vertical magnetic field component is also measured it can be used to provide - together with the horizontal magnetic components H and D - some extra information about the conductivity structure. In the one-dimensional situation there is of course no vertical magnetic field. In the two-dimensional case a relationship between the three magnetic components Hx, Hy and Hz is found. This relationship becomes complex by the anomalous nature of the structure. If, however, an adjacent station exists, where the measurements of the magnetic components are considered to be normal, then the equations describing the relationship between the magnetic components can be solved. In practice the relationship can be reduced to the single station equation:

$$Hz = AHx + BHy + e$$

where e is the noise term representing the residual part of Hz that does not correlate with the horizontal field. This is admissible when the following simplifying assumptions are made.

(a) The normal inducing vertical field is negligible with respect to Hz.

(b) The anomalous horizontal fields are also negligible with respect to the inducing horizontal fields.

(c) There is no correlation between the inducing vertical field and the inducing horizontal fields.

These assumptions were considered adequate for studies in mid-latitudes (Banks ,1973). In the equation above, A and B are the frequency dependent single station transfer functions. They represent complex quantities and their values can be evaluated from cross spectral estimates in the frequency domain of the calculation. These estimates are best determined from a weighted mean of estimates of transfer functions obtained from individual records, as discussed by Beamish (1979).

The equation separates into the real and imaginary expressions. These are determined from the complex values of A and B as

$$|R| = (Ar^2 + Br^2)^{1/2} \qquad \theta_r = \tan^{-1} Br/Ar$$

$$|I| = (Ai^2 + Bi^2)^{1/2} \qquad \theta_i = \tan^{-1} Bi/Ai$$

Ar ,Ai ,Br and Bi are those real and imaginary parts of A and B.

These equations represent two vectors (R,θr) and (I,θi), which are consequently known as the real and imaginary induction vectors. They are usually plotted as solid and broken lines, emanating from a particular station. When reversed (Parkinson,1962), the real arrow points towards current concentrations while the imaginary vector, tends to be large when surface conductors are present. This representation provides, at a glance, a useful indication of the anomalous field content in the area.

2.4 Development of the AMT system

To supplement and extend the instrumentation already in use, the system capable of making measurements of the electric and magnetic field variations in the frequency range 1 Hz to 1000 Hz, was developed by the group, with the author's assistance. The system was based on that assembled by a group in Neuchatel (Fischer et. al,1980) and it bears many of their design features.

The construction and calibration carried out in the Edinburgh Geophysics Department and the subsequent field trials are described in detail below.

2.4.1 Construction of the instrumentation

A block diagram of the system is shown in figure 2.5. It comprises telluric lines with electrodes, high permeability core induction coils, power supplies and amplifiers with 50 Hz and 150 Hz notch filters. Analogue

Figure 2.5 AMT system block diagram

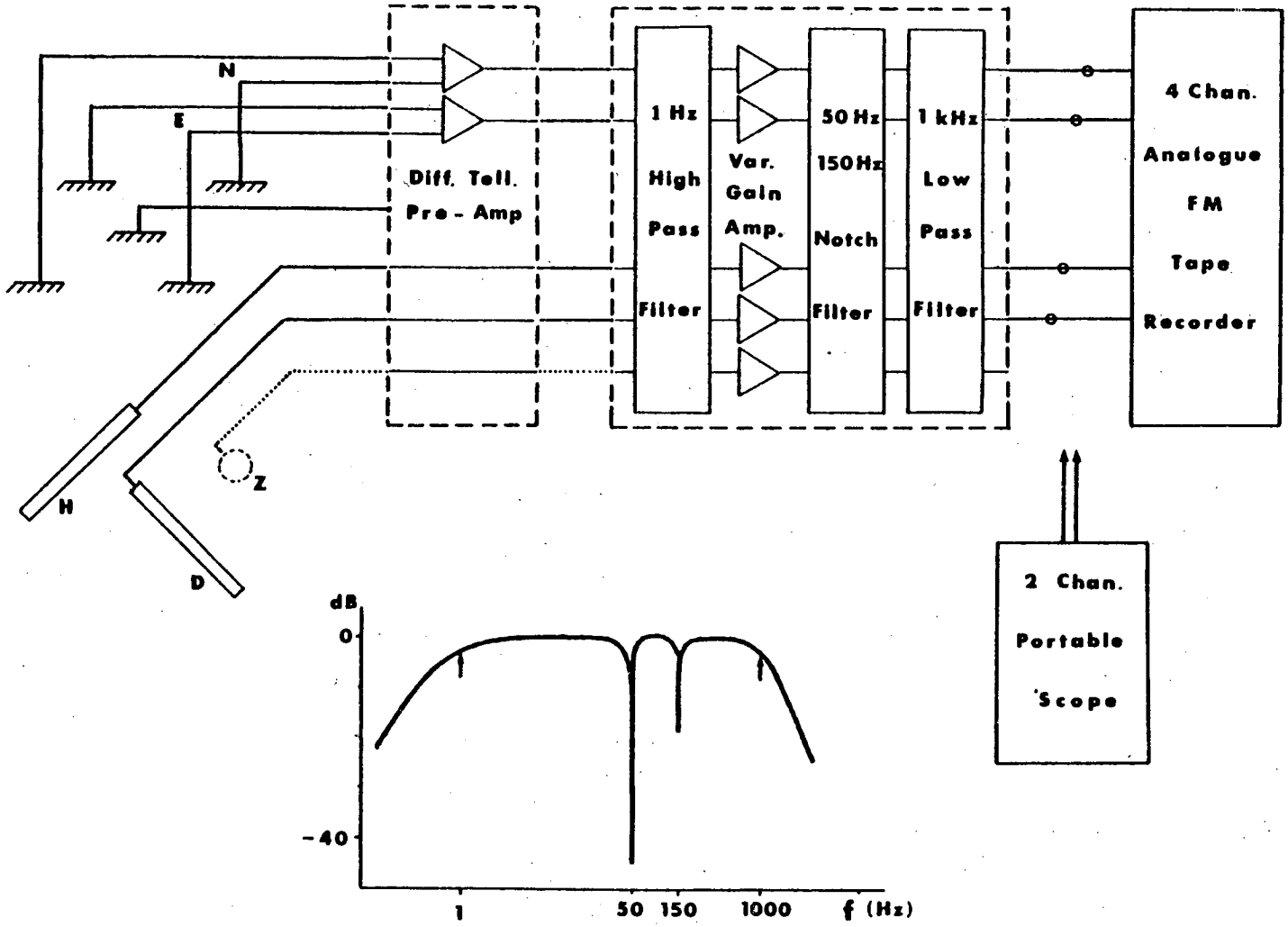
N
E
H
Z
D
Diff. Tell.
Pre - Amp
1 Hz
High
Pass
Filter
Var.
Gain
Amp.
50 Hz
150 Hz
Notch
Filter
1 kHz
Low
Pass
Filter
4 Chan.
Analogue
FM
Tape
Recorder
2 Chan.
Portable
Scope
dB
0
-40
1
50
150
1000
f (Hz)

Figure 2.5

signals are retained on a magnetic tape recorder, capable of handling 4 channels simultaneously.

The instrumentation was designed to make use of readily obtainable commercial equipment, to fit a limited budget and to be operational in a given time interval. It was anticipated that in the future a more advanced version would be constructed, based largely on the requirements highlighted by the use of the present instrumentation.

Experience has shown that simplicity of operation can be achieved through good design without the need to sacrifice any essential capabilities. Furthermore, experience has shown that simple well constructed instrumentation is often most suitable for outdoor operation.

The purpose of the telluric measurements was to obtain a record of the surface electric field over a suitable length of time. To measure the potential gradient in a given direction it is necessary to measure the voltage difference between two electrodes in contact with the ground and separated by a known distance.

The surface electric field is then directly related to the potential gradient by

$$\underline{E} = -\nabla V$$

V is the electric scalar potential at any

point on the surface and has the units Volt/metre.

In compliance with the requirements derived in section 2.2.3 regarding tensor analysis, the electric field was monitored in two directions perpendicular to each other.

Unlike the long period MT instrumentation the electrode configuration adopted was always the cross array. The electrodes were of stainless steel in the form of a stake, 63 cm long and 2.5 cm in diameter. They were tapered at one end and had a 4 mm dia. hole drilled close to the other end, to receive a standard 4 mm (banana) plug.

Problems associated with chemical potentials were regarded to be of negligible significance in the frequency range 1 Hz - 1 kHz. Other long period effects, such as those caused by temperature fluctuations were considered to be also negligible. The telluric lines consisted of high-quality 3-core rubber-sleeved domestic cable, cut to 26 metres in length. Separate wire loops were attached 1/2 metre from each end to act as guides for the spacing between electrodes.

A centre electrode provided a common Earth for the entire system. At this electrode and connected to it by an earthing strap, was situated the junction box. To improve the signal-to-noise ratio during the subsequent electronic stages, the signal was amplified with two

differential input amplifiers with fixed gains of 20. These pre-amplifiers were housed in the junction box together with the individual voltage regulators for both the telluric pre-amplifiers and the magnetic coils. The relevant circuit diagrams are shown in Fig 2.6. (See Appendix 1. for a note regarding the input impedance of the circuit.

Induction coils are generally preferred in audio-frequency magnetic field sensing, since their sensitivity rises with increasing frequency. It is common to incorporate high permeability cores to provide compactness and portability.

The induction coils used in the construction of the AMT equipment were designed and built by Societe E.C.A of France. They incorporate a feedback system in which the electromotive force generated by the primary detection coil is amplified and the current is used to drive a secondary coil. This coil, wound in antiphase with respect to the primary coil, is in turn used to null the field acting on the primary coil. The feedback current is monitored and gives the required output. Calibration of the coils carried out by the manufacturer revealed a constant sensitivity of 50 mV/γ between 8 Hz and 370 Hz.

For field use, spiked aluminium collars were made and fitted to the coils. These were later modified to break the loop formed by the circular conducting collar. Plastic half-cylindrical shields were acquired to shield the detectors from the adverse effects of the sun and rain. In addition to eliminating spurious effects caused

Figure 2.6 **Telluric pre-amplifier circuit diagram, with power supply.** The satisfactory operation of the amplifier has come into question, as the impedance of the input passive-filter network is too low. A correction for this effect is given in Appendix 1.

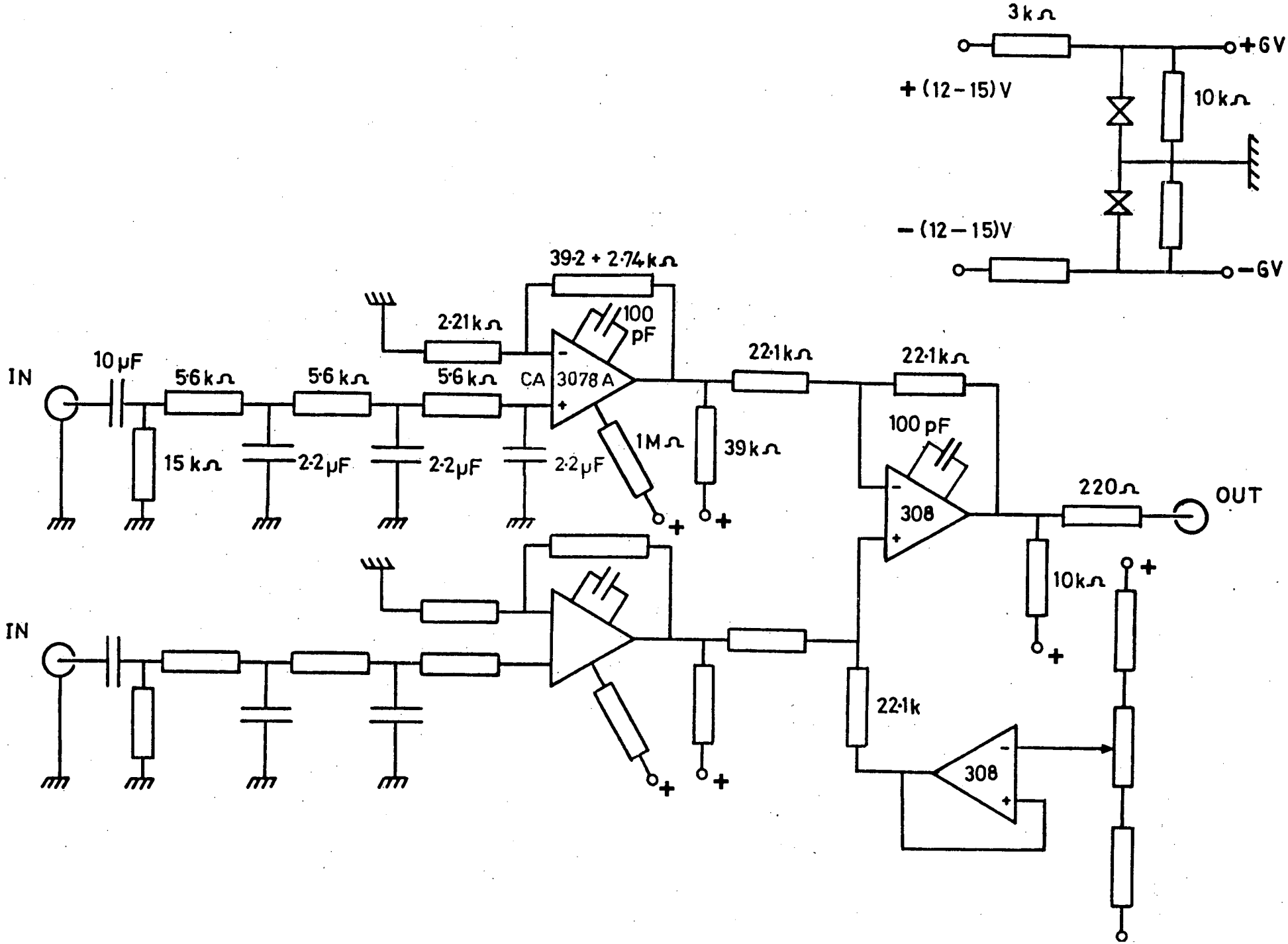
3 kΩ
+6V
+ (12 – 15) V
10 kΩ
– (12 – 15)V
–6V
39·2 + 2·74 kΩ
100 pF
2·21 kΩ
IN
10 μF
5·6 kΩ
5·6 kΩ
5·6 kΩ
CA 3078 A
22·1 kΩ
22·1 kΩ
15 kΩ
2·2 μF
2·2 μF
2·2 μF
1M Ω
39 kΩ
100 pF
308
220Ω
OUT
10kΩ
IN
22·1k
308

Figure 2.6

by temperature variation these shields protected the sensors from the vibrational effects caused by wind and rain. The junction box was connected to the main amplifier stage via a 50 metre individually shielded coaxial signal cable - a sufficient distance away to reduce anomalous effects to a minimum. A second 50 meter cable carried the necessary power supply to the junction box. Five identical amplifiers were assembled, each separately regulated and with gains variable from 24 to 4800 in approximate steps of factor of two. Each amplifier had a passband of 1 Hz to 1 kHz with tunable notch filters at 50 Hz and 150 Hz. The circuit diagram of the amplifier stage is shown in figure 2.7.

Attenuation provided by the notch filters was over 40 dB and 20 dB respectively for the 50 and 150 Hz notch filters. The bandpass filters had - 3 dB cut-off points at 1 Hz and 1 kHz and attenuation of the order of 9 dB/oct and 18 dB/oct respectively.

The gain variations and phase shifts associated with the filter characteristics of the amplifiers were observed and are discussed in the next section. It is evident, though, that if these responses are the same for all four channels their effects should be self compensating when only ratios of the measured quantities are considered.

Power requirements of the complete system were fulfilled in two parts. For the entire amplifying system, including the electronic circuitry of the induction coils,

Figure 2.7 AMT system circuit diagram

a. First stage amplification and high pass filter
b. 50 Hz (150 Hz) notch filter
c. 100 Hz/1000 Hz low pass filter
d. 2nd stage amplification
e. Final stage
f. Overload detection

(a)

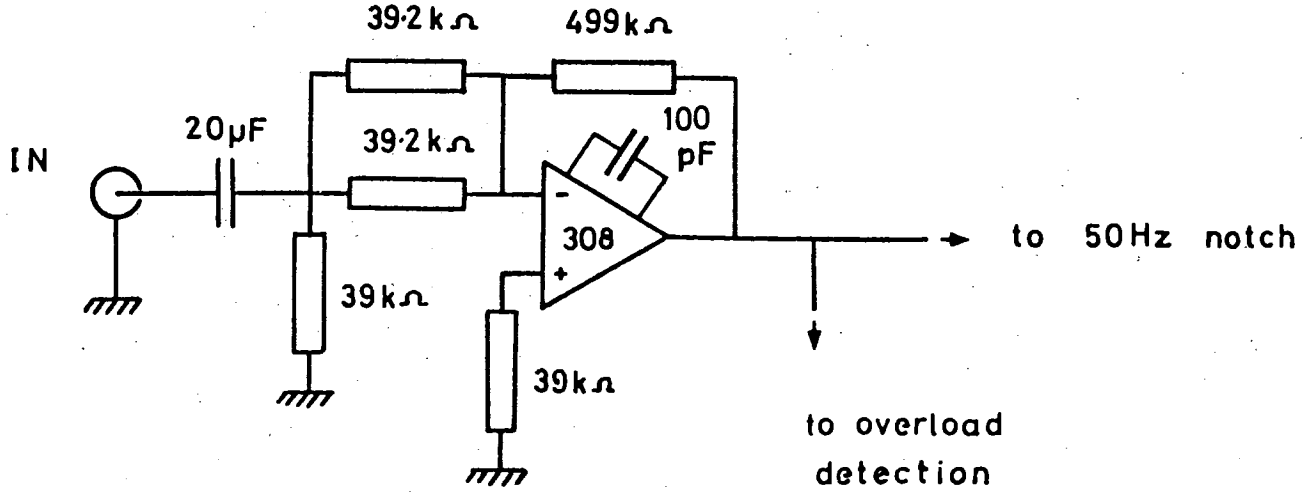
39·2 kΩ
499 kΩ
IN
20 μF
39·2 kΩ
100 pF
308
to 50 Hz notch
39 kΩ
39 kΩ
to overload detection

Figure 2.7 a.

(b)

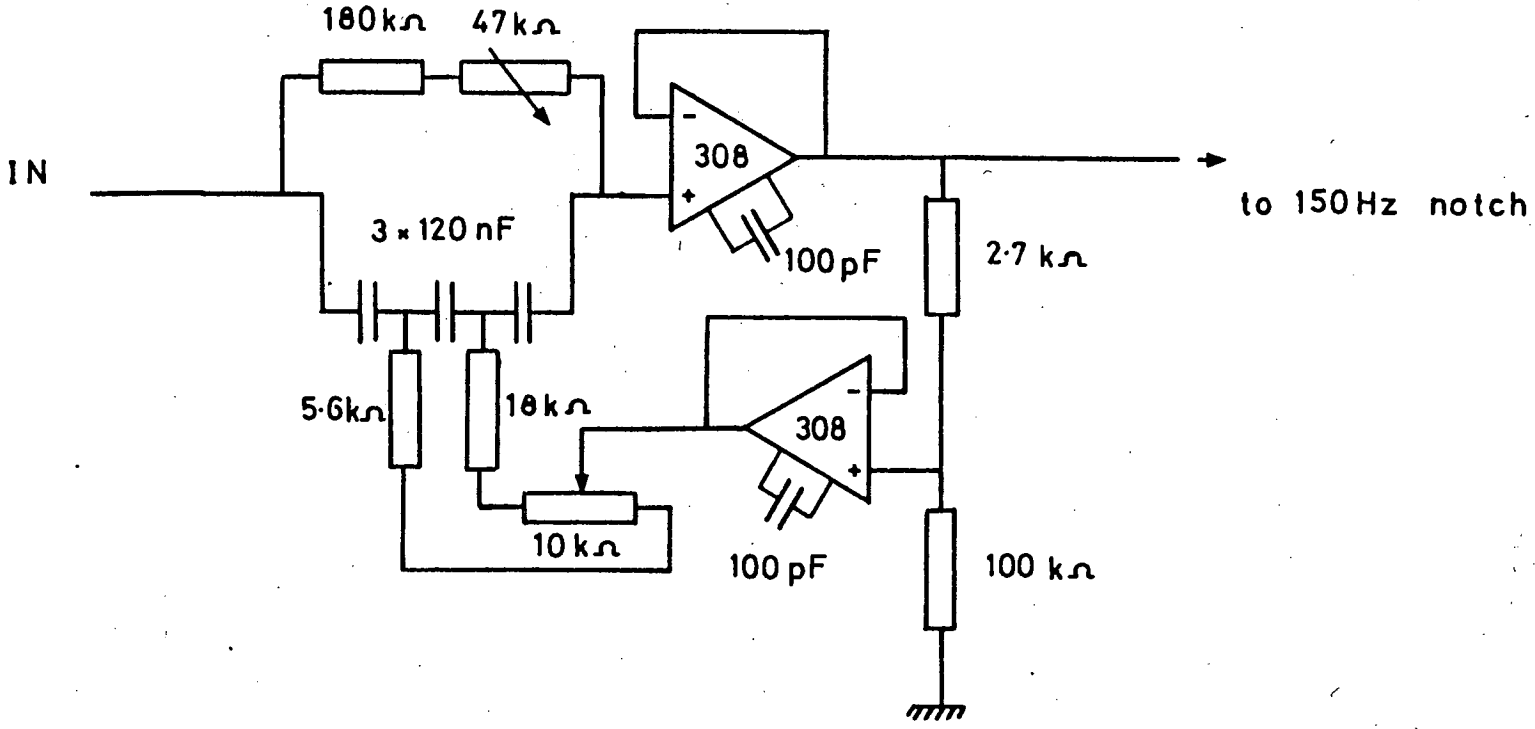
180kΩ
47kΩ
IN
3 × 120 nF
308
100pF
to 150Hz notch
2·7 kΩ
5·6kΩ
18kΩ
308
10kΩ
100 pF
100 kΩ

Figure 2.7 b.

(c)

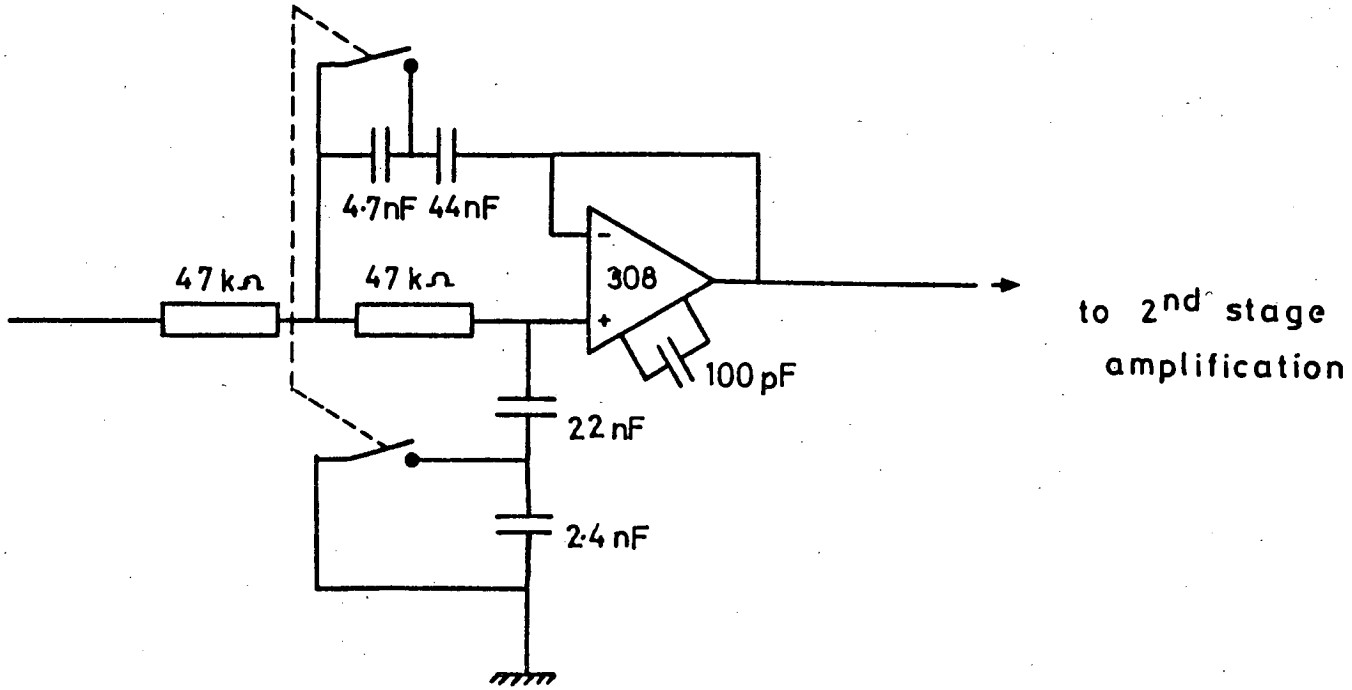
4·7nF
44nF
47 kΩ
47 kΩ
308
100 pF
2·2 nF
2·4 nF
to 2nd stage
amplification

Figure 2.7 c.

(d)

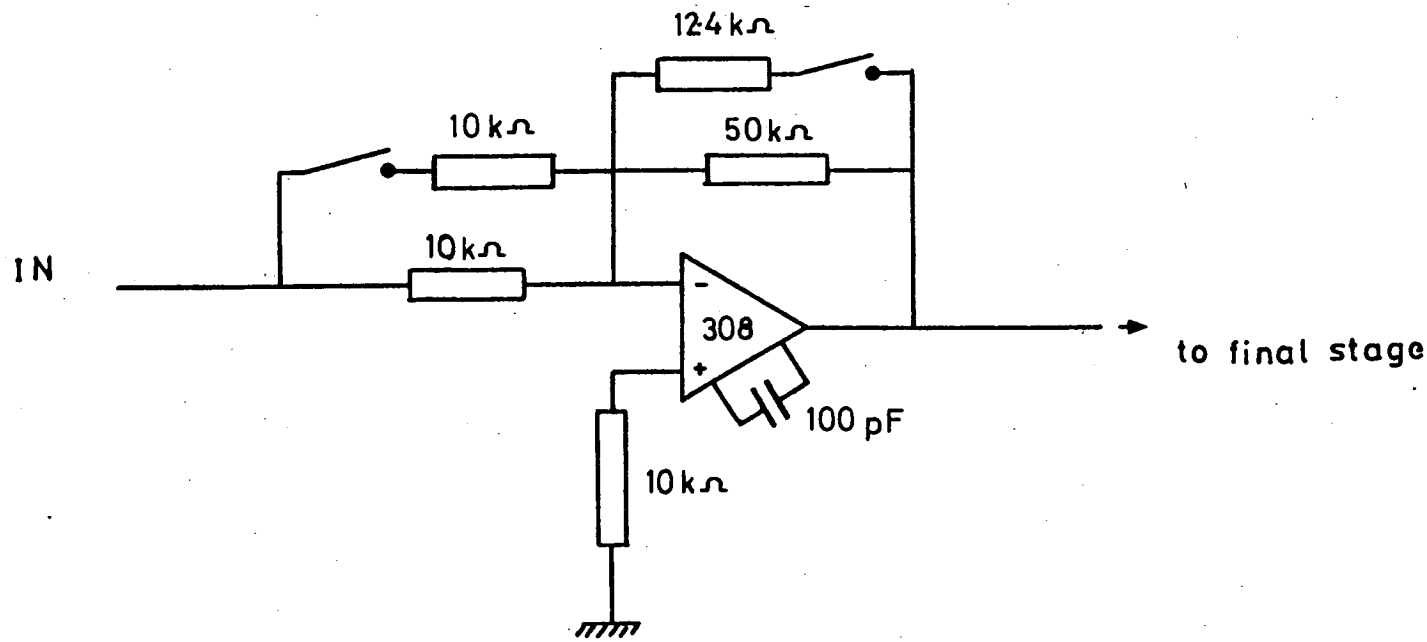

Figure 2.7 d.

(e)

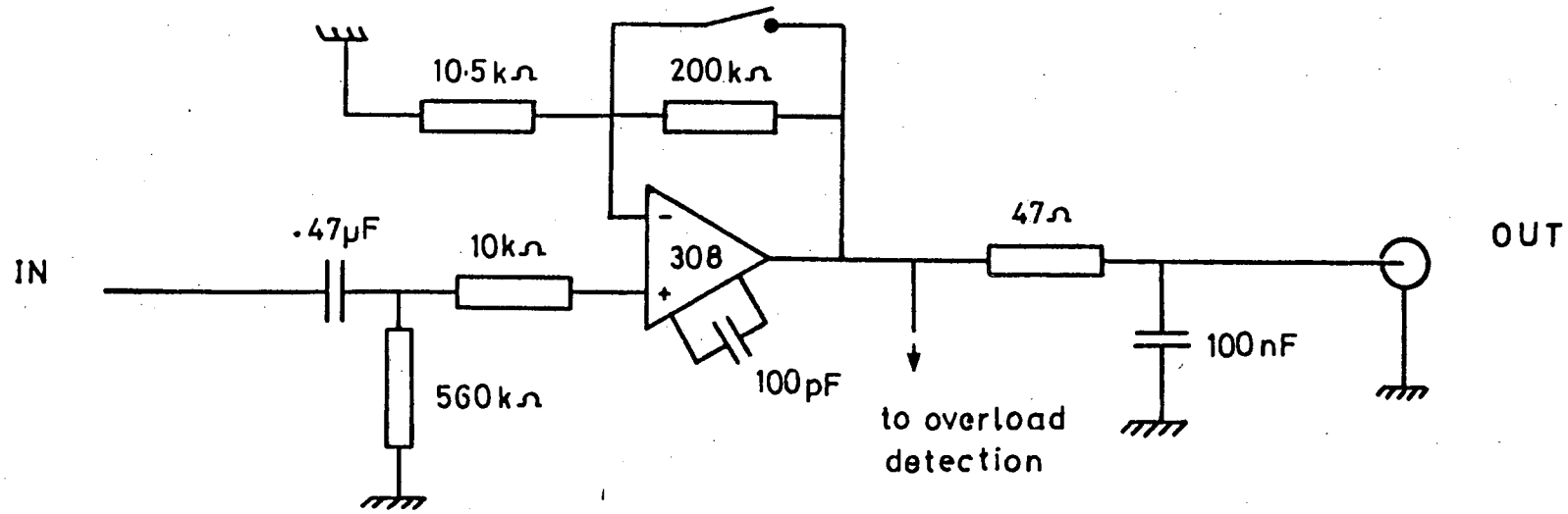
10·5kΩ
200kΩ
IN
·47μF
10kΩ
308
47Ω
OUT
560kΩ
100pF
to overload
detection
100nF

Figure 2.7 e.

(f)

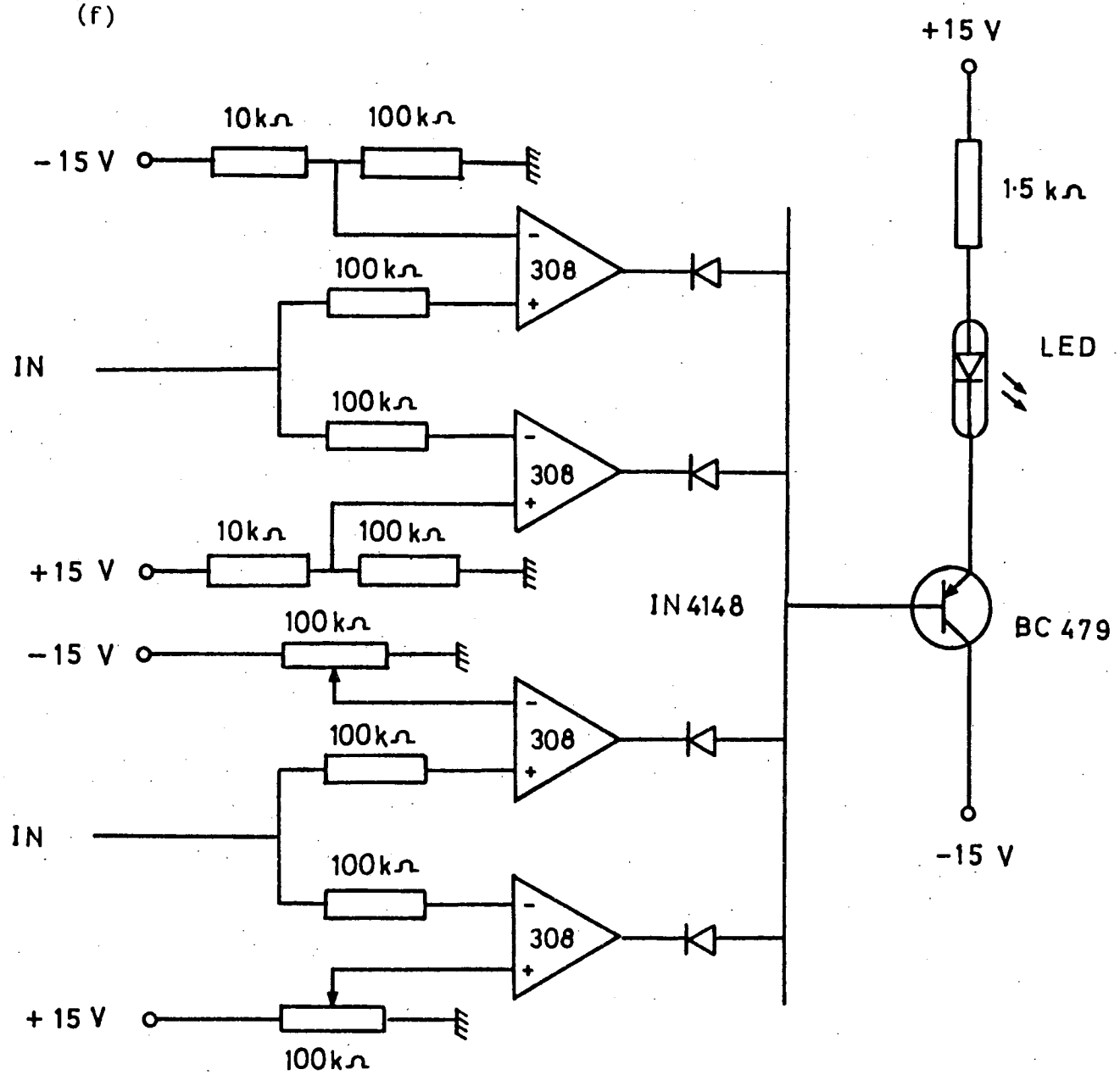
+15 V
10kΩ
100kΩ
-15 V
308
100kΩ
IN
100kΩ
308
10kΩ
100kΩ
+15 V
IN4148
100kΩ
-15 V
308
100kΩ
IN
100kΩ
308
+15 V
100kΩ
1·5 kΩ
LED
BC 479
-15 V

Figure 2.7 f.

four 12 V 5.7 A-Hr sealed rechargeable lead-acid batteries were used. These could provide several days' use before recharging was necessary. For the analogue tape recorder two further 12 V 60 A-Hr lead acid batteries were employed. These provided a minimum of 40 days' use at a current rating of 3.5 Amps.

2.4.2 Calibration

Each stage and unit of the operational AMT instrumentation shown in Fig 2.5 was calibrated in turn.

All except the induction coils were calibrated in the departmental laboratories. The facilities of the required type were not available and instead the manufacturer's specifications were used. An opportunity to perform the calibration arose only after the field work had been completed.

Observations of the differences between units of the same stage revealed that amplifier # 1 showed more instrument noise than the other four. As such it could provide a backup function in the present four component arangement. The position of the adjustable notch filters was critical as it could introduce considerable differences into the individual response curves. Typically the differences between units were very small.

The complete calibration curve for the amplifier units is shown in Fig 2.8. It shows the high and low pass filter responses and the effects of the 50 Hz and 150 Hz

Figure 2.8 Calibration curves of the amplification stage

a. Amplitude

b. Phase

(a)

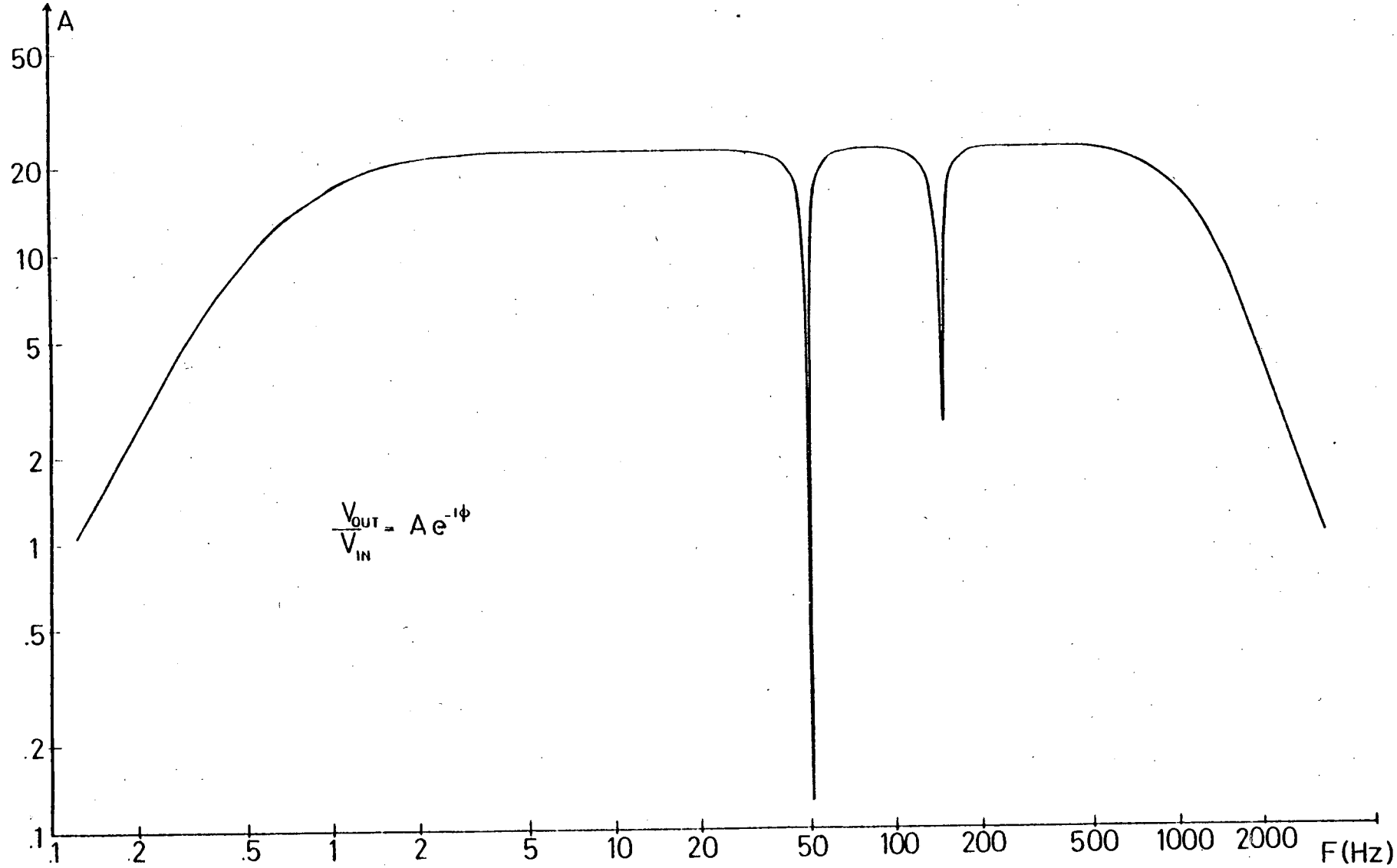
A
50
20
10
5
2
1
.5
.2
.1
$\frac{V_{OUT}}{V_{IN}} = A e^{-i\phi}$
.1
.2
.5
1
2
5
10
20
50
100
200
500
1000
2000
F(Hz)

Figure 2.8 a.

(b)

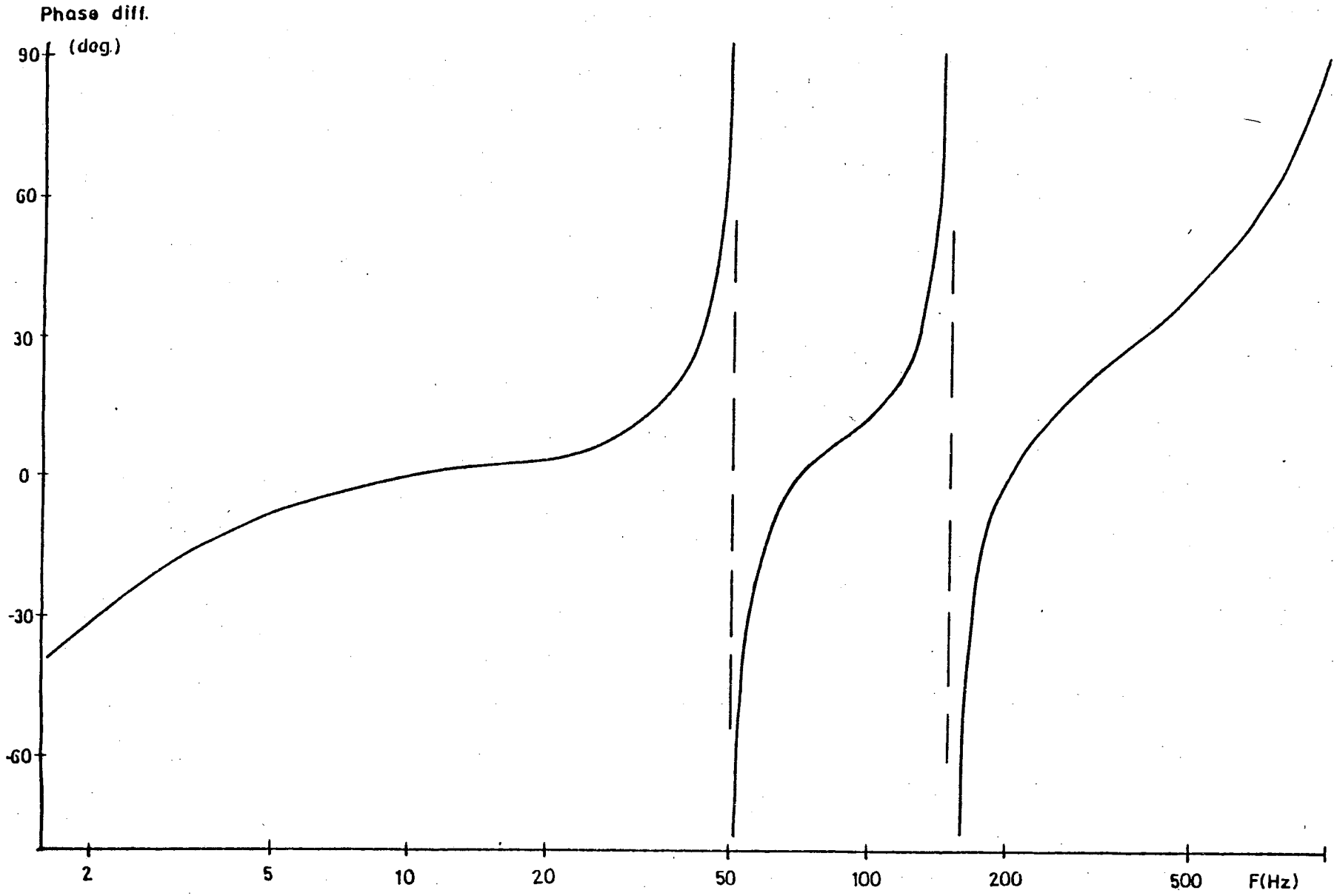

Figure 2.8 b.

notch filters.

The telluric pre-ampifier calibration curve is shown in Fig 2.9. It shows the gain of 19.6 to be uniform over the range 5 Hz to 600 Hz. The -3 dB ponts occur at 0.8 Hz and 3000 Hz with a 6 dB/oct characteristic decay in the gain thereafter.

The mean calibration curve for the three induction coils is plotted in Fig 2.10 The data were those supplied by the manufacturer.

It is evident that the magnitude of the non-uniformity of the responses outside 8 Hz and 400 Hz is such that corrections for the responses for those parts of the spectrum would need to be applied, for the AMT measurements to be meaningful. This was indeed done and is fully described in section 4.2.1.

2.4.3 Field trials

It was expected that the main limitations were most likely to be caused by excessive noise. It was essential at an early stage to establish the viability of magnetotelluric measurement in the audio frequency range in the U.K. To this aim the two magnetic and two electric components were monitored in turn, as soon as the system was completed. Magnetic field variations were found to be of the order of 10^{-2} to $10^{-9}\gamma$ in amplitude, which when fully amplified produced an amplitude of 2.4 - 24 Volts at the

Figure 2.9 Calibration curves of the telluric pre-amplifier stage

a. Amplitude
b. Phase

(a)

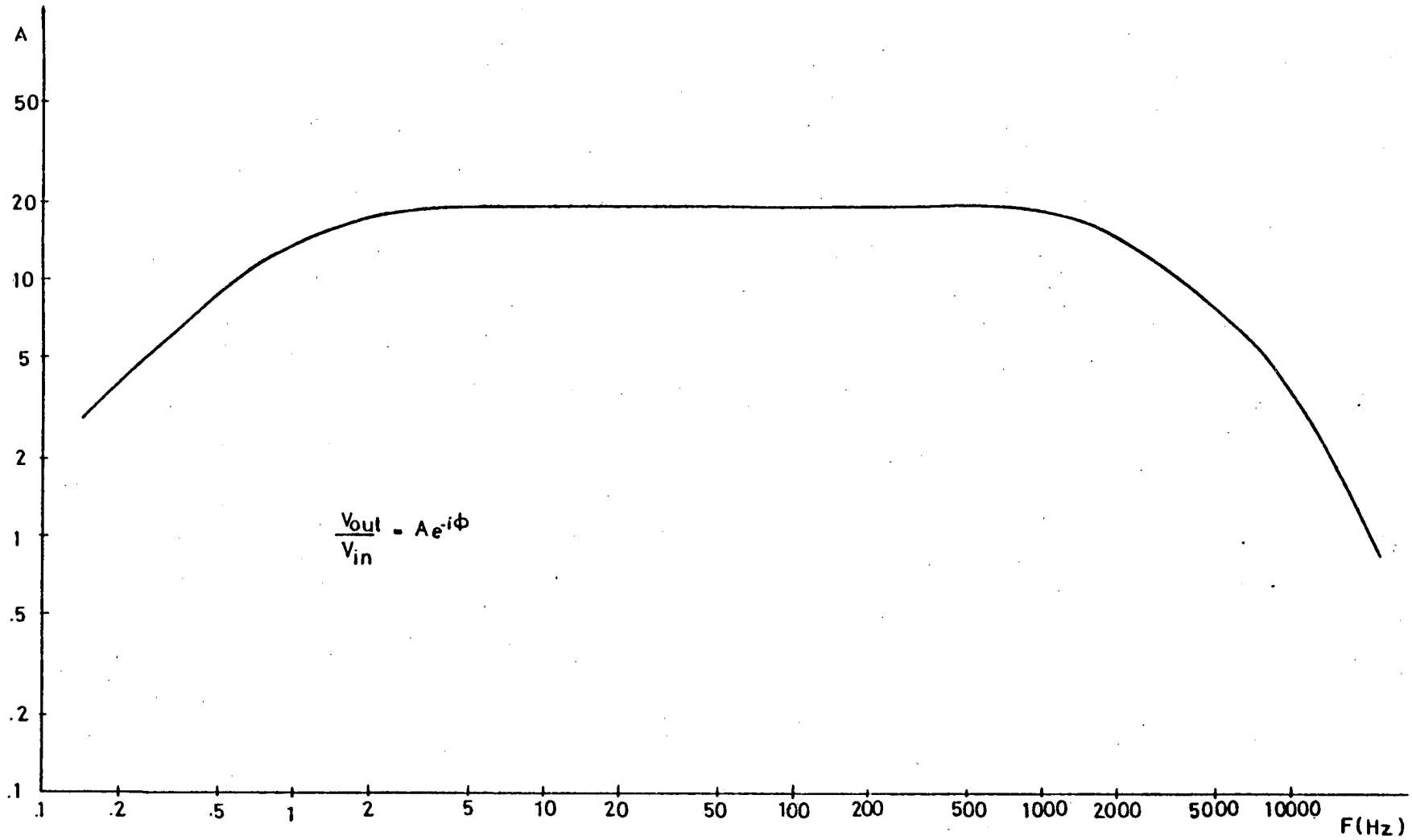
A
50
20
10
5
2
1
.5
.2
.1
$\frac{V_{out}}{V_{in}} = Ae^{-i\phi}$
.1
.2
.5
1
2
5
10
20
50
100
200
500
1000
2000
5000
10000
F(Hz)

Figure 2.9 a.

(b)

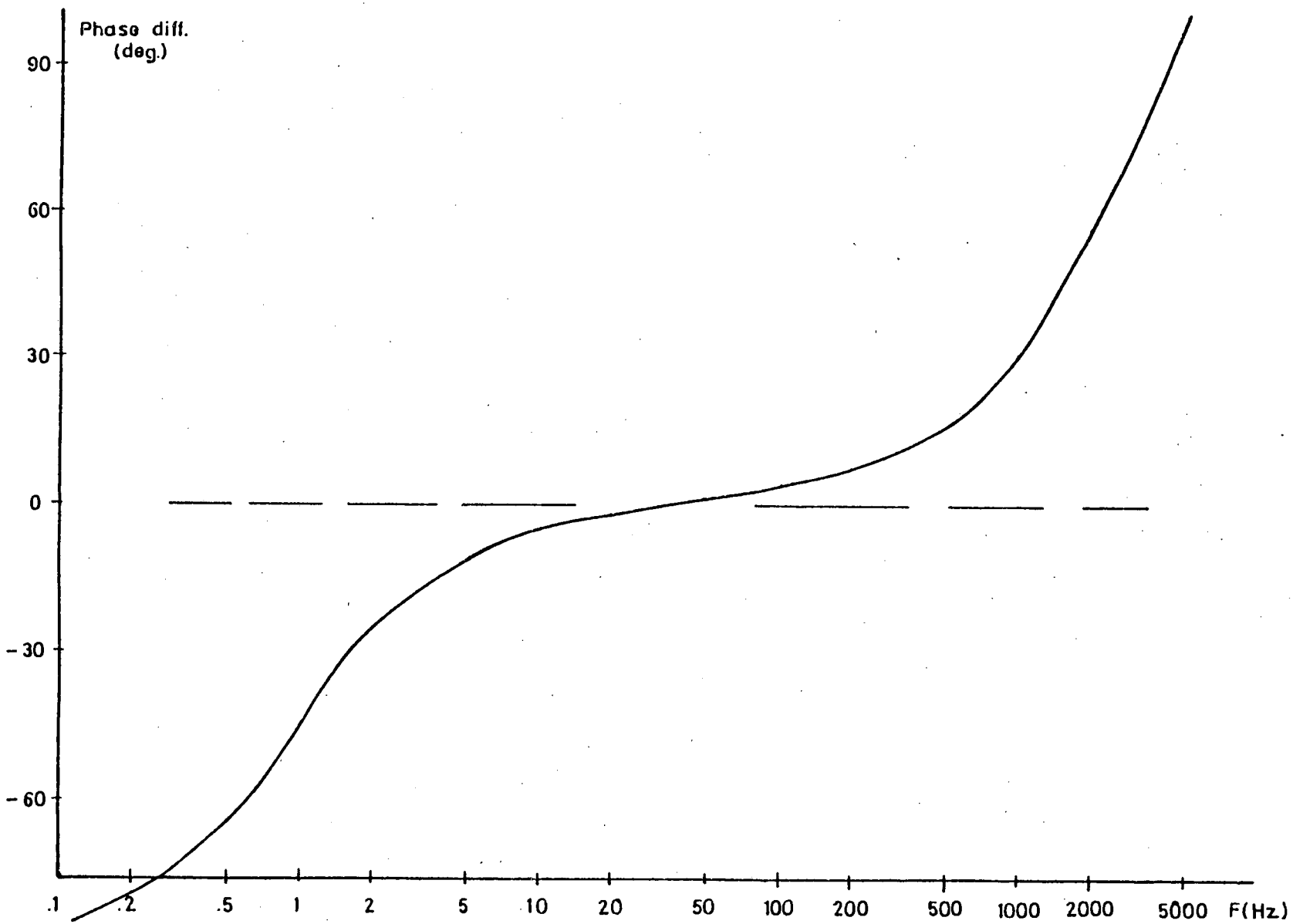
Phase diff.
(deg.)
90
60
30
0
-30
-60
.1
.2
.5
1
2
5
10
20
50
100
200
500
1000
2000
5000
F(Hz)

Figure 2.9 b.

output stage. Wide variations in signal strength of several orders of magnitude were observed at irregular intervals of 1 second to one day. It could be expected that similar variations occur at intervals greater than 1 day and hence may influence the measurements made at the same site at different times. The natural activity observed within a time of 1 hour was considered suitable for making a representative sounding from any site.

Noise signal with a regular appearance could be detected at many stations. Generally its frequency was confined to one of 50, 150 or 250 Hz. On a few occasions the notch filters were not capable of sufficiently eliminating this signal.

The telluric signals showed similar features to those observed in the magnetic components. Signal strengths were of the order of 10 mV/km and did not show such a pronounced drop in signal strength with increasing frequency as the magnetic components. This could be attributed to the proportionality of the rate of change of the magnetic field to the telluric field.

Noise measurements made at full gain with sensors lying in opposite directions gave indications of the amount of residual and instrumental noise. These were greater than the 0.1 Volt observed in all channels with the inputs shorted to ground. The limitation to measurements of only four independent components, imposed by the use of the particular magnetic tape recorder, resulted in the

Figure 2.10 Calibration curves of the induction coils

a. Amplitude
b. Phase

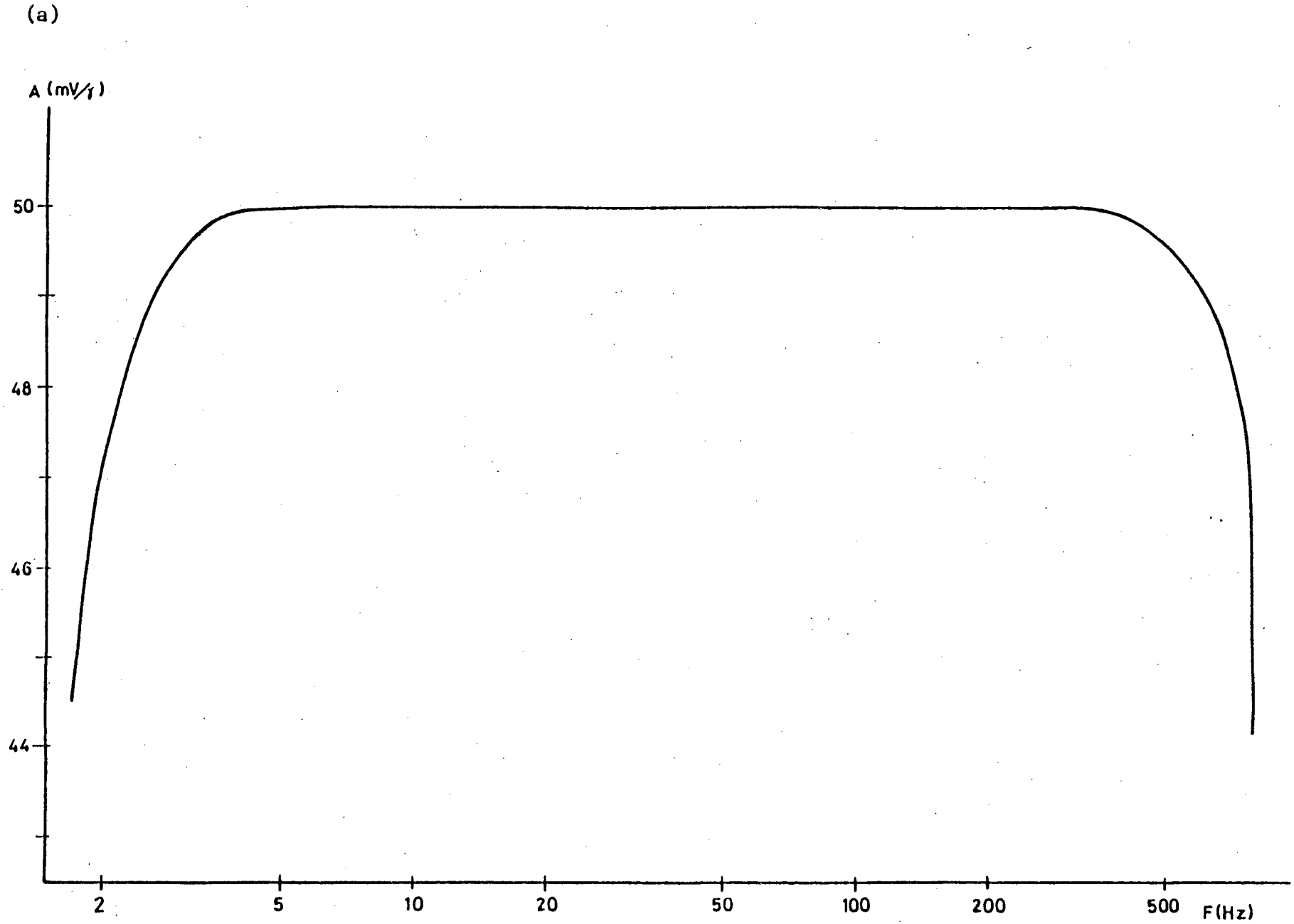

Figure 2.10 a.

(b)

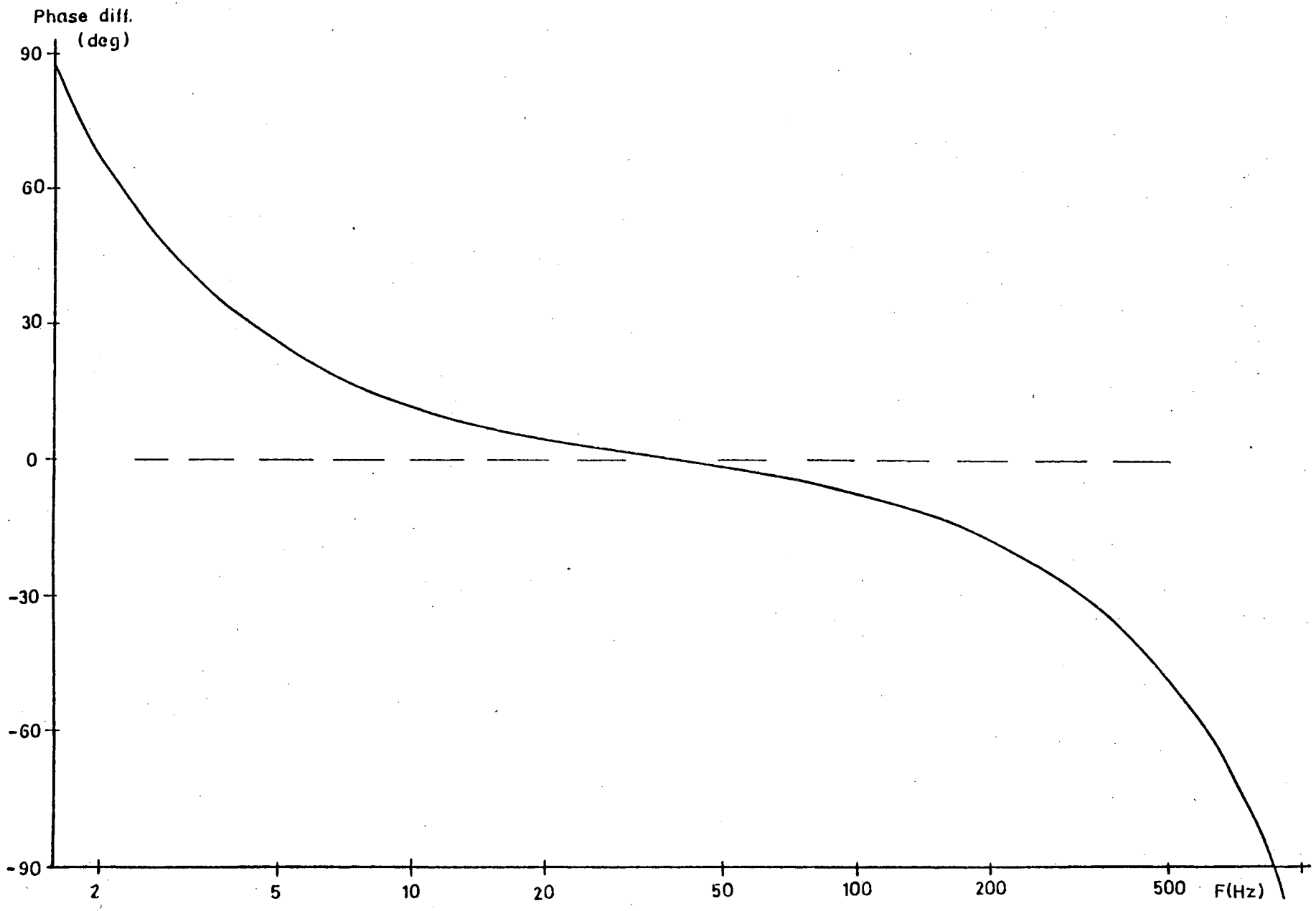

Figure 2.10 b.

omission of the measurement of the vertical magnetic field at all sites in this study.

It was found that to accurately set the notch filters in the absence of 50 Hz and 150 Hz noise, a field precission oscillator was most useful. Conversely, when such spurious signals were present, the tuning of all notch filter settings was assumed to eliminate possible inter-amplifier differences in the regions of the notch filter 'troughs'.

CHAPTER 3

DATA ACQUISITION

In this chapter the operations involved in making a magnetotelluric sounding will be discussed. Attention will be paid to the criteria for individual site selection, to the equipment installation procedure and to the method of data recording. Finally a summary of all station particulars will be given.

The procedures relevant to MT site operation, described by Mbipom (1980), were followed in this study. In this account, a detailed description is therefore limited to the AMT method only. Additionally, the application of a DIGITAL EQUIPMENT CORPORATION MINC-11 (Modular INstrument Computer) minicomputer to the processing of MT data during the field operation itself is discussed.

A complete description of the instrumentation has been given in the preceeding chapter. The author feels it appropriate to note here that a complete check of the correct functioning of all the equipment is absolutely necessary before each fieldwork session. While prior calibration of the equipment is also desirable, facilities for the calibration of the induction coils were not available in Edinburgh. Calibration was thus limited to the remainder of the equipment. Colleagues visiting Garchy, France, in late 1980 were however able to check

the specifications supplied by the manufacturer of the coils.

Finally it is essential to ensure that all batteries are fully charged, particularly in the case of the portable oscilliscope which requires charging for 14 hours, for 4 hours continuous operation.

3.1 Choice of recording sites.

In view of the different observational times demanded, fewer MT than AMT sites were planned. Geomagnetic Deep Soundings (GDS) were also undertaken in this region, by the department and colleagues, as a contribution to the U.K. Deep Geology Programme (Beamish,1981).

3.1.1 MT and AMT station distribution.

Since 1974, several traverses of MT soundings have been undertaken in Scotland and north England (Jones,1977,Mbipom,1980,Ingham,1981). At the start of 1979 the station Towhouse marked the extent of the profile coverage to the south. It was natural to overlap and extend the line of the existing profile southwards. The area covered by this proposed extension forms the north east corner of England.

On the basis of the known geophysical features of the region outlined in chapter 1, it was decided to undertake the fieldwork in two basic stages:

1. (1979) A line of stations across the Weardale region, approximately in the direction of previous traverses, and

2. (1980) A grid of stations over the entire extent of the area.

In the former case both MT and AMT measurements were made at each station. The density of the stations along the profile was determined by the time available. A total traverse length of 80 km. provided for an interstation spacing of some 10 km. For such separation, the data from the MT sites could be expected to show supporting features of the deep structure in the area. Short period ,AMT, measurements only were made in the second stage. Again the size of the grid and the density of its stations were determined by the time available, with most sites located along the available roads at approximately 6 km intervals.

The results from the first stage were interpreted prior to the second stage of fieldwork, and any information derived from the initial work was used to select, more advantageously, the sites for the subsequent work. As a result, additional stations were located where the response from neighbouring stations suggested an interface position. Where well defined station models provided good agreement with known geology, less stations could be located. The total number of AMT stations was determined as work progressed, but was initially

based on logistic experience gained during field trials.

The fieldwork involving the long period soundings was planned in a similar manner. It was assisted, by contrast to previous work of this type, by the in-field data processing capability of the MINC computer and was, therefore, expected to progress as new results and daily events developed.

Both the MT and AMT work progressed according to the initial plan during 1979. By 1980 all data from the MT sites had been partially processed. The results of the AMT work at a number of key sites had also been interpreted. Prior to the 1980 fieldwork, there were indications that the outcome of the second leg of the fieldwork might provide some more definite information about a number of features of the area. Care was thus taken in choosing the site locations for the 1980 AMT soundings so that their distribution was favourable for examination of the following questions:

1. Using the magnetotelluric method, is it possible to detect the granite and utilise the higher resolution of the AMT measurements to delineate its extent?

2. Knowing the position of the major fault systems to the north and south of the granite, is it possible, using the method, to resolve the features associated with these faults?

3. Are there any regions of low-resistivity which might be reasonably assumed to correlate with the high temperature measurements recorded in the region?

As a maximum of 20 soundings was considered logistically feasible for this AMT survey, it was decided the objectives could best be achieved by undertaking 3 extra traverses across the region, one to the east and two to the west of the 1979 traverse. The number of stations per line was governed by (i) the postulated extent of the granite, from gravity interpretation, (ii) the known positions of the faults and (iii) the location of built-up areas e.g. near Newcastle in the north-east and Darlington in the south-east.

To examine the probable lateral variations in conductivity across the two faults to the north and south of the Alston block, 6 stations were located in the fault regions, 2 on each side of each fault and 2 over it. In addition, the 1979 MT/AMT traverse was extended to the south by 3 sites.

The actual site distribution was finalised after a visit to the region and is shown in figure 3.1.

3.1.2. Site selection

A suitable site for occupation by the AMT equipment had to satisfy a number of criteria. Firstly, permission for access had to be granted. In general land owners were most forthcoming in this respect. Secondly, the land had to be accessible by Land Rover and accommodate the spread of the telluric lines. Both of these requirements were generally easily satisfied. Thereafter, the slope of the land had to be limited to 10 degrees (representing some

Figure 3.1 Station distribution map, showing AMT stations (crosses) and MT stations (diamonds). The postulated extent of the Weardale granite and the raised cupolas have been outlined, based on the gravitational survey interpretation of Bott and Mason-Smith (1957). The stations marked by the diamonds and crosses formed the main profile. At these stations the MT and AMT measurements were combined to produce broadband station results. The numbers refer to the station code. All station codes are compiled with coordinates in table 3.2 after page 65.

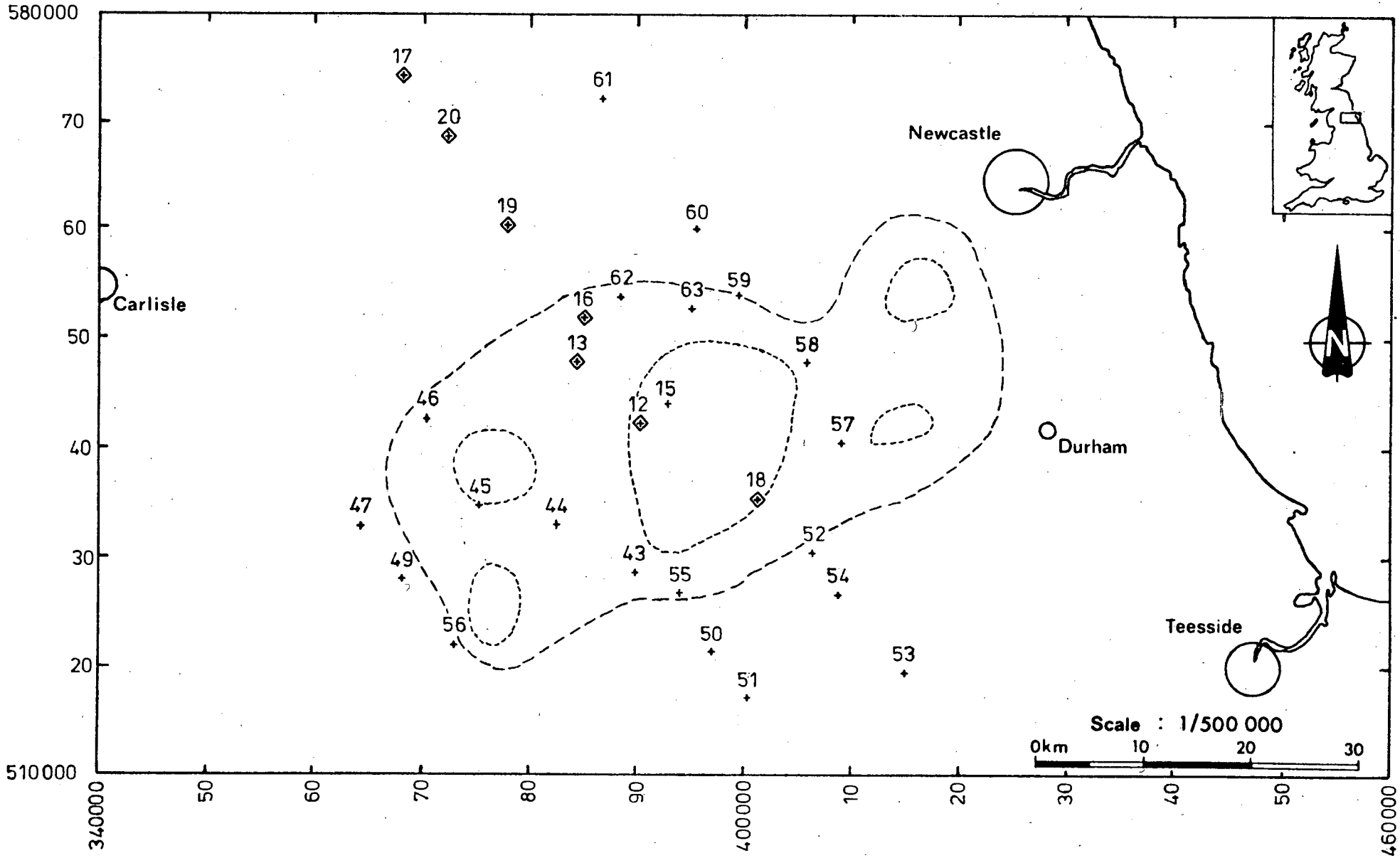
580000
70
60
50
40
30
20
510000
340000
50
60
70
80
90
400000
10
20
30
40
50
460000
Carlisle
Newcastle
Durham
Teesside
17
61
20
19
60
62
63
59
16
13
58
46
15
12
57
45
18
47
44
52
49
43
55
54
56
50
53
51
N
Scale : 1/500 000
0km
10
20
30

Figure 3.1

1.5 percent error in the measured signal) and the ground cover had to support the magnetic sensors adequately. The best base was found to be compacted earth on a good rock base. On many occasions the base was peat or water saturated soil which promoted vibration of the magnetic sensors. This effect was particularly evident in strong wind. An example of recorded signals showing uncorrelated fluctuations in the two magnetic components is shown in figure 3.2. There is no supporting evidence for ground vibration caused by adjacent trees or long grass, but vibrations originating from footfalls etc. could be detected on certain surfaces. Wind could also be correlated to magnetic noise, an effect reduced by the use of wind shields. There were minimal problems with electrode penetration, although on rocky or hard ground the electrodes had to be inserted away from the vertical.

Finally an important condition, required of all sites, was that the recorded signal be corrupted as little as possible by industrial noise. During field trials it was found that noise free sites could be located in remote enough areas, e.g. away from houses, power lines, railways etc. This is consistent with the dissipation of E-M fields and the distribution of noise sources in general.

In practice, it was difficult to find any definite pattern between common sources of noise and their effect at a distance. These are often subject to variations such as load (which is dependent on time of day) and other unseen factors.

Figure 3.2 Four component AMT signal trace showing wind-caused low period fluctuations in the magnetic channels only. The time scale (1 second = 13 cm) shows an underlying vibration in the H component of frequency 20 Hz (wind/ground vibration) and a superimposed pulsation of frequency 4 Hz (buffeting).

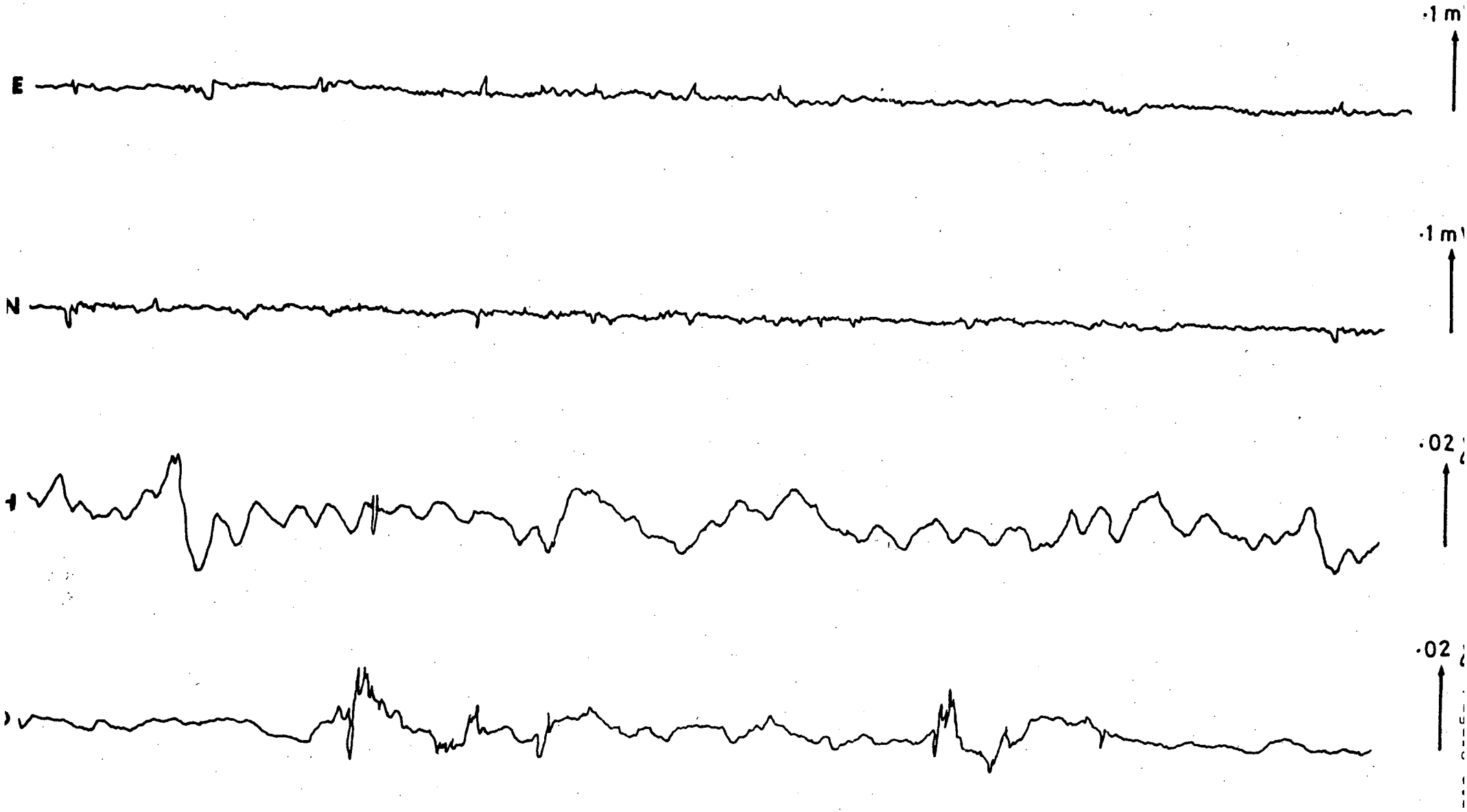
E
·1 m
N
·1 m
·02
·02

As a rough guide therefore, measurements of the electric and magnetic fields were made at one of the sites in directions parallel and perpendicular to a 3 phase 1100 Volt overhead line at two distances: close (20 m) and far (400 m). The amplitude of the dominant frequency decreased by a factor of 4 between the two sites. The N/S telluric line was generally most succeptible to noise. The noise at the far site constituted some 20 per cent of the total signal amplitude. This level of noise was typically encountered at many of the stations degraded by this form of manmade electrical contamination.

As a norm stations were not selected within 3 km of 12000 V cables (supported by pylons) and within 400 m of 1100 V cables and individual dwellings.

It is evident that the relationship between the distance from a power carrier and the effect on the magnetic and telluric fields is not simple. It does not behave as a simple case of a wire current and as such, can not easily be modelled. The resultant noise must be considered to be a superposition of all the contributions from the total array of sources. Despite these problems, most of the sites selected for the 1980 fieldwork were close to their planned positions, with only one site having to be excluded.

The requirements for the MT site selection differed from those described by Mbipom (1980) in that mains power supply was no longer necessary at each site. This change had been possible, because the 'Watanabe' recorder, used

Figure 3.3 Station log form

Figure 3.3

A.M.T. Log.

CODE

DATE

SITE NAME

TIME

COORDINATES

OPERATOR

DESCRIPTION

PERMISSION FROM:

WEATHER

sun light wind

cloud heavy rain

GROUND CONDITION

arid dry moist

waterlogged wet damp

SURFACE ON SITE

flat undulating sloping

trees long grass

clay soil sand gravel

ELECTRODES: CONFIGURATION

CONTACT	N/S	E/W
AMPS		
VOLTS		
OHMS		

RECORDING		COMP.	COLOUR	AMP ✱	GAIN	TAPE CH.	SENS.	
TAPE I.D.		E			x2 x5 x20			
TAPE SPEED		N			x2 x5 x20			
START		H			x2 x5 x20			
TIME	COUNT	D			x2 x5 x20			

STOP

TIME | COUNT

COMMENTS

to monitor the signals during recording, was no longer used. The recorded signals were, instead, analysed at the end of each day. A caravan was used, as in earlier studies, to house all equipment required at each site.

3.2 Station preparation

The operational procedure used at an AMT site is given here in detail. Generally it presented few problems. A station log, an example of which is given in figure 3.3 was always kept.

The preparation procedure for an MT site remained unchanged using an 'L' shape configuration for the telluric lines, typically 100m in length and lead electrodes. Magnetic component recording was made by suspended magnet type magnetometers, (Jolivet,1966) which, with age, were becoming increasingly unreliable. A marked improvement in operating an MT site was achieved by eliminating the need for mains power. A generator was run at each site to facilitate the operation of the 'Watanabe' recorder for approximately 1/2 hr. The functioning of the equipment before the recording could thus be checked. After the site was satisfactorily erected the station was fully operational and independent, using rechargable batteries. After about 24 hrs. of recording, on a digital cassette at a logging period of 5 seconds, cassettes were removed for inspection and replaced bynew cassettes.

3.2.1 Telluric channels

Starting with the centre electrode, the 5 electrodes were located in the ground at distances pre-set by the

loops in the cables. On no occasion was it necessary to stray from the magnetic north/south and east/west alignments of the electrodes. In this way no correction had to be applied at any station for effects caused by rotation or separation of electrodes. The accuracy of all magnetic grid directions was kept to less than 2 deg., representing a maximum of 0.06 per cent error. Colour coding of all the connections greatly aided operations.

It was desirable too, at each station, to make resistance, current and voltage measurements between the two pairs of electrodes. These were noted on the log sheet and they served as an additional check on the satellite electrode connections.

3.2.2 Magnetic channels

The magnetic sensors, each with a 12 m connecting cable, were also all colour coded for simplicity. These were positioned in the magnetic N and E directions and levelled using a specially made spirit level. As with the telluric lines no corrections for rotation had to be made during subsequent processing.

Signal and power were transmitted via two 50 m cables between a junction box situated close to the earth electrode and the amplifiers mounted in the Land Rover. It was often necessary to place the junction box in a plastic bucket to shield it from ground water.

For the system description the reader is referred to

Chapter 2. The connections between the amplifier bank and the RACAL STORE-4 analogue tape recorder were all again aided by colour coding for each component recorded. Gains in each channel were adjusted to limit overloading, which was indicated by lights in the face of each amplifier bank. Each component was then in turn displayed on a dual-channel battery-operated oscilloscope and analysed for noise.

The notch filters were adjusted to minimise the contribution of any 50 and 150 Hz. signal present. In many of the noisy stations, spikes which could not be filtered out, were evident. If, as was sometimes the case, the noise distortion was too severe , the installation was moved to a new site. After entering all the relevant details in the station log, particularly the gains of all channels, the equipment was ready for recording.

3.3 Recording

Unlike signals with periods greater than 10 seconds, AMT signals can only be recorded digitally with advanced electronic circuitry. At the time of the 1979-1980 fieldwork this was not available. Recording was thus made in analogue form on a RACAL store-4 tape recorder on loan from the IGS Global seismology unit. This was a four channel Frequency Modulated (FM) analogue recorder, capable of securing signals in the frequency range 0 -20000 Hz or 0 - 2500 Hz at 7.5 in/sec to -1dB. It had a signal-to-noise ratio of 48 dB and flutter at 7.5 in/sec

of less than 0.35% peak-to-peak for the bandwidth 0.2 Hz to 1250 Hz. This figure improves at higher recording speeds. The tape drive mechanism is capable of maintaining the speed to $\pm$ 0.2% a small enough error affecting all channels simultaneously. The dynamic skew (the inter-channel time displacement error) is $\pm$ 6 micro-seconds at 7.5 in/sec, which represents an error of $\pm$ 6 degrees between channel 1 and 4 at 1000 Hz. This is approximately a 2% error. The start time is given as 1 second maximum. At a recording speed of 7.5 in/sec the recording of 12 stations per one reel of 1/4 inch tape of 2400 feet was possible. The tape records had then to be digitised later as described in chapter 4. The advantage of AMT over longer period MT recording is the short duration of event required for analyses. For the longest periods of 1 sec and a total requirement of 10 events, only some 20 seconds of signal recording were required. Initially however, ten times this amount was recorded to provide enough choice of events. This was quickly reduced to 3 minutes, comprising six 30 second intervals, from each of which a file of length 22.5 sec. could be digitised. The distribution of events was typically such that 5 separate events of up to 1 second duration could be selected from each file. The selection of events is discussed in the next chapter. For a summary of the above sequence, see table 3.1.

It is the case with sferics that there is always a storm present somewhere around the globe. It is also the characteristic of AMT recording that many stations can be surveyed in a short period of time. Consequently it was not

REDUCTION OF AMT RAW DATA - SUMMARY

Step	Signal Length	No of Selected Sections	Length of Each Section	Cummulative No of Separate Records	Total time record
1	Infinite	1 - Site recording session	½ hour	1	½ hour
2	½ hour	6 - Intervals	30 sec	6	3 min
3	30 sec	1 - Digitisation	22.5 sec	6	2 min 15 sec
4	22.5 sec	5 - Events	< 1 sec	30	< 30 sec
	The total time record derived from a ½ hour recording session was < 30 sec				
	AVERAGING OF SINGLE EVENTS - SUMMARY				
5	< 30 sec	10 - Best events	< 1 sec	10	< 10 sec
6	< 10 sec	1 - Averaging result	-	1	-

Table 3.1

practical to set up a station and record for say one hour, or until enough events containing large amplitude signals had been captured. Although the signal to noise ratio would have been improved with a longer recording period the advantages in terms of of tape and time requirements of a total recording interval of 3 minutes were preferred.

It was noted that previously used magnetic tapes were liable to acquire dirt and cause serious distortions to the signal. To rectify this, the magnetic tape and the magnetic head were cleaned periodically.

Recorded data were immediately replayed on the oscilloscope to check for spurious effects. In a few cases this resulted in a re-recording. Using an auxiliary microphone connected to the fourth channel, each station was given a voice track label for easy recognition.

The microphone, which could also serve as a loud-speaker during the recording and playback enabled the component on channel 4 to be monitored aurally as well as visually. This lent itself to a preliminary location of events for use during event selection, a feature which could have been improved by the use of a quality loudspeaker or headphones. Finally, it was found that suitable natural signals were available for monitoring at all times. When the signal was weak, higher amplification was needed to compensate for this loss and a reduction in the signal-to-noise was experienced. Nevertheless, a

total recording time of approximately 3 minuted, secured in most cases over a half hour period, was rarely exceeded in any of the fieldwork sessions.

In contrast to the recording of AMT signals, those of frequency less than 1Hz could be performed at much slower sampling rates (Mbioom,1980). Consequenty, a N.E.R.C Geologger, with a standard digital type cassette was used for recording the longer period data. This logger was capable of recording 8 channels simultaneously, at a typical digitising interval of 5 seconds and at the same time allowing the three magnetic channels to be duplicated at a more sensitive setting.

The power requirements of the MINC computer were not satisfied by the available small portable generator and consequently the use of the minicomputer had to be restricted to locations with a mains power supply.

3.4 Summary of stations and data collected

Data from all stations were recorded in two separate sessions. First 7 MT and 17 AMT stations were recorded during 1979 followed by 20 AMT stations in 1980. The stations best divide into three groups:-

(a) Those lying on a single profile across the survey area. This comprised 7 MT stations with an AMT measurement at each

(b) A coarse AMT grid over the extent of the area

(c) A fine AMT grid over an area near Spadeadam for comparison with a DC resistivity survey made in the area. (Habberjam, personal communication)

The position and designation of the stations described by sections (a) and (b) are illustrated in a map in figure 3.4 and tabulated with their respective map references in table 3.1.

The amount of data recorded at each MT site varied between 3 and 10 days. This represented a considerably smaller quantity than that which would be necessary if processing had not been possible after the recording of each cassette.

As described above the amount of data recorded at each AMT site was fixed with the exception of a number of 'noisy' sites showing contamination of the data. There the amount was limited to 45 seconds or 1/4 of the usual time. It was maintained that, rather than recording more data to acquire large amplitude events and thus improve the signal-to-noise ratio, only a token data set should be recorded. If this did not provide reliable data on processing, the site could then be excluded in the final analysis, without much loss of time and recording space.

There were no problems with noise contamination of any of the MT data and therefore there was no need to locate alternative recording sites. This greatly increased the speed of operation.

Figure 3.4 AMT station designation map showing the station code as in table 3.2 and the line of stations, which make up the main profile.

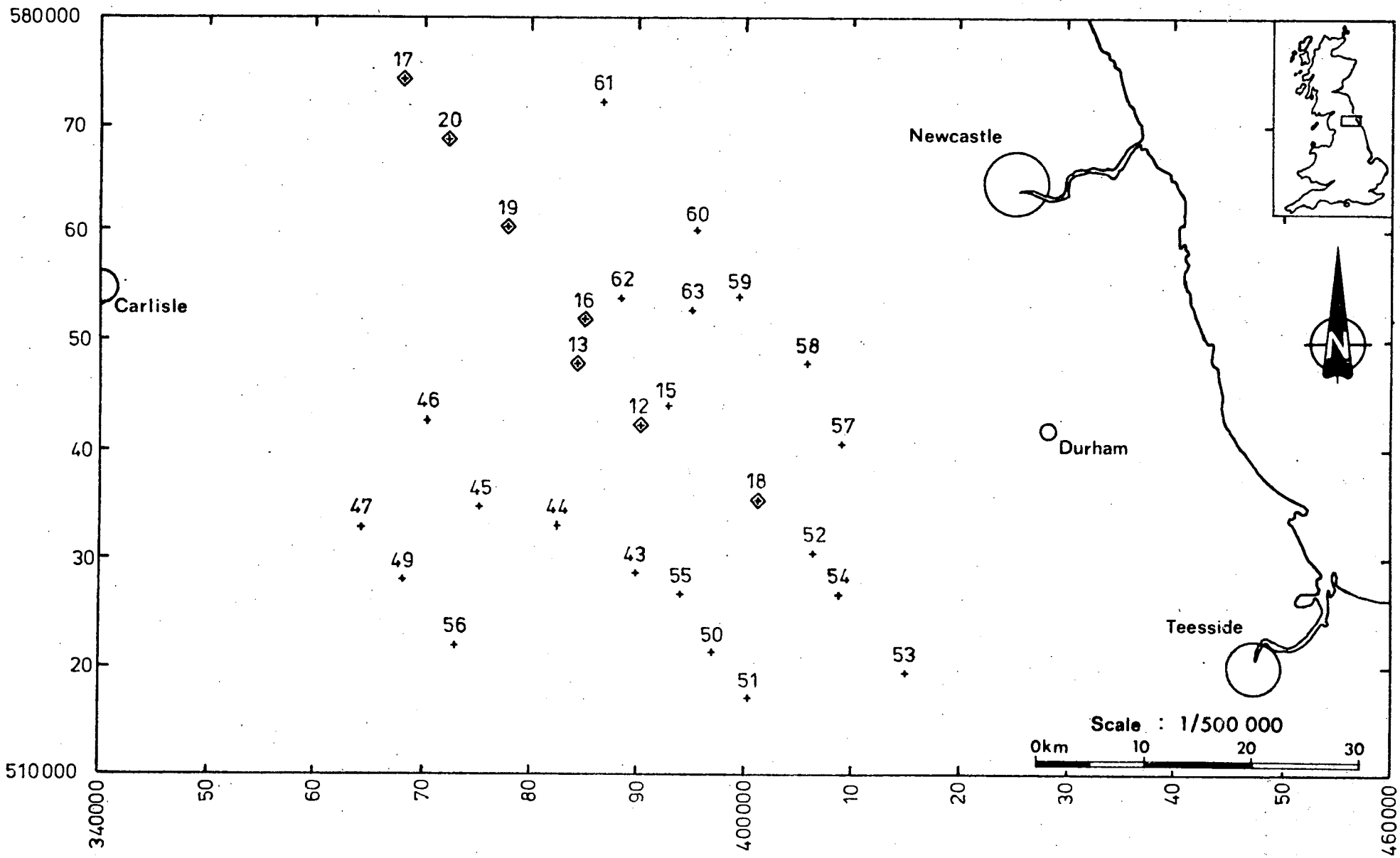
580000
70
60
50
40
30
20
510000
340000
50
60
70
80
90
400000
10
20
30
40
50
460000
17
61
20
19
60
62
63
59
16
13
58
46
15
12
57
45
18
47
44
52
49
43
55
54
56
50
53
51
Carlisle
Newcastle
Durham
Teesside
N
Scale : 1/500 000
0km
10
20
30

Figure 3.4

AMT data were more succeptible to noise. Of the 37 stations 20 showed definite contamination by noise, with more than one channel being affected at about half of those 20.

The N/S electrode line was the most frequently contaminated by noise. 8 stations showing contamination by 50Hz noise or spike formation. The E/W telluric component showed contamination at 7 stations. 50 Hz noise or spike contamination was observed in the magnetic components on only two occasions. In both cases only the D component was affected.

100 Hz contamination was evident at 5 stations and it usually affected all channels simultaneously. 150 Hz contamination was observed at only 2 stations.

Higher frequency contamination, e.g. 300, 600 and 1000 Hz., was present at 7 stations with more than one of these frequencies present at 3 of the 7 sites. The E/W telluric line here seemed to suffer most and the noise usually had a spike formation.

Contamination by frequencies lower than 50 Hz was found to be of two types. At 5 stations a spurious 3 Hz. signal was detected on the H and D component traces. This correlated directly with high wind and a peat ground cover. Secondly frequencies of 10 - 30 Hz appearing mostly as regular series of spikes, sometimes alternating in polarity, were observed on the telluric channels or on

COMPILATION OF STATION PARTICULARS

Table 3.2

AMT Station Code	MT Code	Station Name	Coordinates	
(D) 12	921	Rookhope I	E390250	N542400
(D) 13	920	Swinhope Shield	E384400	N548000
(D) 15		Rookhope II	E392950	N544100
(D) 16	923	Sinderhope Shield	E385000	N552000
(D) 17	927	Lampert	E368100	N574400
(D) 18	925	Hill End	E401200	N535475
(D) 19	296	Whitfield	E377880	N560490
(D) 20	924	Edges Green	E372330	N568670
(I) 43		Ash Hill	E389800	N528900
(I) 44		Harwood	E382500	N533250
(I) 45		Tyne Head	E375300	N535000
(I) 46		Leadgate	E370350	N542800
(I) 47		Bank Hall	E364250	N533000
(I) 49		Knock Pike	E368050	N528350
(I) 50		Romaldkirk Moor	E397000	N521600
(I) 51		Lartington	E400350	N517300
(D) 52		Hamsterly Forest	E406400	N530600
(D) 53		Raby Castle	E415000	N519600
(D) 54		Woodland	E408800	N526800
(I) 55		Middleton in Teesdale	E394000	N527000
(I) 56		Murton	E373050	N522150
(I) 57		Towlaw	E409000	N540650
(I) 58		Healey Field	E405750	N548000

Table 3.2 cont.

AMT Station Code	Station Name	Coordinates	
(I) 59	Derwent Reservoir	E399450	N554125
(I) 60	Linnel Wood	E395400	N560150
(I) 61	Uppertown	E386600	N572200
(I) 62	Hexhamshire Common	E388500	N553900
(I) 63	Blanchland Moor	E395000	N552800

all channels simultaneously. These seemed to be originating from a nearby transmitter

This summary is based on observations at stations where recordings were made and excludes those stations rejected on the basis of noise contamination. There were about 5 stations where recording was prevented by noise.

3.5 Conclusion

The data quality was at times seriously degraded by industrial noise contamination. This was particularly the case in the AMT soundings. However some improvement in the data quality was noticed in the more remote areas. Data quality decreased as built-up areas were approached. This was most clearly shown at a site near Sheffield - not connected with the work of this study - where noise contamination was so severe and high in amplitude, that a signal was clearly detected on an oscilloscope without the need for any amplification.

The contamination problem is likely to increase as the NEB policy of mains earthing is implemented, and power consumption increases. It is desirable for future studies, therefore, that a much improved system for detecting and eliminating un-natural signal be devised. This is likely to consist of improved notch filter application, selective bandpass filtering and digital filtering techniques. Further improvement to both the MT and the AMT systems could be made in the data recording and processing functions. It would also be advantageous

if both systems were capable of producing preliminary results, in the field, to permit the appraisal of station data. Selective recording of data would also allow for a reduction in the overall quantity of data. These improvements have since been undertaken (Dawes,1981) incorporating a microprocessor-based on-line event selection and digital processing technique, with a means for displaying and recording the selected results.

CHAPTER 4

DATA ANALYSIS

Data processing has benefited greatly from the increasing influence of modern computers. To make use of these benefits, the raw data of this study were converted to digital form as soon as possible.

In this chapter the main stages of data processing will be described. The digitisation and the main stages of data transcription and event selection will be explained, although certain stages of the AMT data transcription are considered to be of a temporary nature. The modifications made to the existing MT and GDS programmes for the processing of the AMT data will also be described in detail.

4.1 Data transcription

The MT digital recording procedure has been described fully by Mbipom (1980). Field variations of periods greater than 10 seconds are easily sampled with equipment such as the NERC logger. (Valiant,1976). For complete processing to take place, the data had also to be transcribed to the format of the Edinburgh Multi-Access System (EMAS). To do this, cassettes were either:

1. Loaded at the Edinburgh Regional Computing Centre (ERCC) to be read under the supervision of the operator and directly passed to their ICL 2980 mainframe computer.

or:

2. Read, utilising the capability of the MINC minicomputer to interface with a NERC cassette reader, with the data being stored on floppy disc. In this case the data were passed to the EMAS ICL 2980 computer in a further operation.

It soon became apparent that option 1 could not be used successfully. Errors in reading caused cassettes to be off-loaded by the operator. As a result, only a part of the tape was ever read.

Option 2 had the advantage of being operated by the author. Tapes which caused most errors in reading, could be left to be read at a later time. As such reading errors became quite disruptive at times, a short description of the problems and how they were dealt with is given here.

The majority of errors encountered during reading could be attributed to dirt entering the critical space between the magnetic tape and the magnetic reading head. In the case of many of the digital cassetes, which had been used before, the contamination was acquired when the tape was most exposed, such as during loading and unloading. As a rule, each tape itself was cleaned before reading with the correct proprietory cleaning products. From time to time the magnetic tape head was also cleaned. Any remaining errors were probably acquired during

recording.

Generally, to avoid data contamination by particles of dirt, it was necessary to:

1. Always keep cassettes in supplied boxes when not in use.

2. Replace the sealed covers to the loggers as soon as cassettes were loaded.

3. Clean tape heads regularly preferably after each cassette was removed.

These steps should alleviate the necessity to clean the tape itself - a practice probably harmful to the fine magnetic coating.

Some cassettes had the additional disadvantage of allowing the internal pad, used to guide the magnetic tape past the magnetic head during recording and playback, to spring away.

After reading, data were reduced to zero origin as necessary, and cleaned by applying the relevant programmes before they were stored on floppy disc. To achieve a time saving of some 15 hours per station it was decided to make the event selection on the MINC minicomputer and pass the selected events only. Event selection is described fully in section 4.1.2. The appropriate programmes for the above operations and for the data transfer from the MINC

minicomputer to the EMAS computer were developed by G. Dawes.

4.1.1 AMT data preparation, (digitisation)

Raw data recorded using the AMT equipment were subject to a more lengthy transcription process, including (a separate) digitisation, analogue playback, tape analysis, tape conversion and again tape analysis. Further, the data were always 'alias filtered' before the digitisation process.

Data transcription was accomplished through the facilities of the Institute of Geological Sciences (IGS) located on the University campus. A PDP-11 computer at the Global Seismology unit was used to control all the functions in the transcription process. Selected raw analogue data contained on 1/4" magnetic tape were replayed through 24 db/oct bandpass filters set to 1Hz and 1kHz. Simultaneously 2 channels were viewed on a twin-trace oscilloscope. Although this method of selecting sections of the raw record for digitisation was satisfactory, a better method of pre-selection was found with the use of a DIGITAL twin-trace osciloscope acquired by the group in 1980. This enabled one to store and view parts of the record in effective slow motion.

The 1 kHz low-pass filter effectively acted as an 'alias' filter for the following digitisation. This was performed at 2048 Hz using a 11 bit A/D converter accepting a $\pm$2.5 V input.

The digitisation rate was chosen making use of a simple algorithm to satisfy the following conditions:

(a) To enable a multiple of the fundamental digitising frequency to fall exactly on the frequencies: 50 Hz 150 Hz 250 Hz etc.

(b) To fix the Nyquist frequency above the maximum frequencies of 1000 Hz and 100 Hz corresponding to the fast and slow digitisation rates.

(c) To limit the amount of digitised data to a reasonable level.

As digitisation rates of 4 channels were limited to 3500 c/s and as only whole digitising frequencies were available at the IGS, this digitisation rate was set at 2048 samples per second. As a result, data sets of 2049 points produced individual power estimates at every whole frequency starting at 1 Hz.

The digital output was temporarily stored on standard 1/2" magnetic tape at a density of 800 bpi. A tape analysis could then be performed with outprinting to a line printer. The data were read from the tape and reproduced on paper in analogue form for subsequent inspection during event selection (section 4.1.2.). The writing was performed with a 24 channel JET PEN RECORDER whose function enables the frequencies used in the AMT recording to be reproduced satisfactorily.

To satisfy the tape reading requirements of the ERCC the digitised data were transcribed to 1600 bpi and labelled, again on a standard 1/2" magnetic tape. This function was also tested with a tape analysis. Finally the tapes were mounted at the ERCC and their contents transfered to immediate store on request.

The complete series of processes described above proved to be time consuming, particularly when seen in relation to the time spent in the field. It was inevitable that, with so many transformations, data corruption became a problem.

The steps described represent a temporary stage in the transcription of AMT data. Although this was intended to be the case it did not become apparent that such a weak link would be introduced into a generally well functioning method.

4.1.2 Event selection

An event is a data set, considered suitable for inclusion in the subsequent analysis. By including a number of such events in the final analysis, the quality of the response estimates and the subsequent interpretation should improve. The factors considered in deciding how an event is selected are essentially the same for both the MT and the AMT method. The selection of events, for the long period MT analysis, using the programme 'Select' (Dawes, 1980), has been described by Mbipom (1980). The refinements to this scheme, associated with the use of

the MINC minicomputer for the selection of MT data are listed in a later section.

The digitised AMT record was used to select events for subsequent processing. Extensive use was always made of the 4 track jet-pen records obtained during digitisation (section 4.1.1). These were scrutinised one file at a time, noting suitable bursts of energy above the ambient level of signal. The signal was expected to register to the same degree on all four channels, without overloading. The traces were also examined for signs of obvious instrumental malfunction, such as is shown in figure 4.2 (b). When the duration of such contamination was less than 1/100 second it was detected with the aid of the graphic facility of the computer, at a later stage. The paper records were used to time the duration of each event as well as its position within the digitised record. The analogue charts, such as those shown in figure 4.2 (a) often showed signals contaminated by large amplitude unnatural (periodic) noise. Considerable caution was required in the selection of possible event sections from such records. It was necessary to look down the length of the record, with the eye close to the paper to locate possible event positions. For data of such poor quality, only a limited number of data sections could be found for further examination.

The data sections obtained in the manner desribed above were then viewed on the Tectronics screen using the programme 'Select' (Dawes, 1980). The structure of the

signals was first viewed in the time domain expanding, if necessary, the time scale to inspect individual digitised points. The presence of data contamination, as small as one sampling point, could then be detected. Secondly, the data sections were transformed to the frequency domain, when further checks were made on the suitability of the data for event selection. The similarity in frequency content between the four channels and the occurrence of a 'natural' frequency spectrum were always examined. The absence of these features was often caused by secondary signal sources such as vibration of the magnetic sensors due to wind, footfalls, or man-made noise. In all these cases, the signal sequence was adjusted in length to exclude the inappropriate section, or rejected altogether.

At this stage, there were often up to fifteen sections of data which satisfied the above tests. These acceptable events were separated from the digitised data files and were subjected to the single event processing procedure. They were introduced to the processing programme in their pre-transformed form, as time series of length of 1 second and not less than 1/10 second in duration. In general such events always started and finished with the signal at zero amplitude and with a total of 2^n points (n = integer) up to the maximum of 2048 points per event.

Figure 4.1 Example of an event (1 second = 13 cm)

Figure 4.1

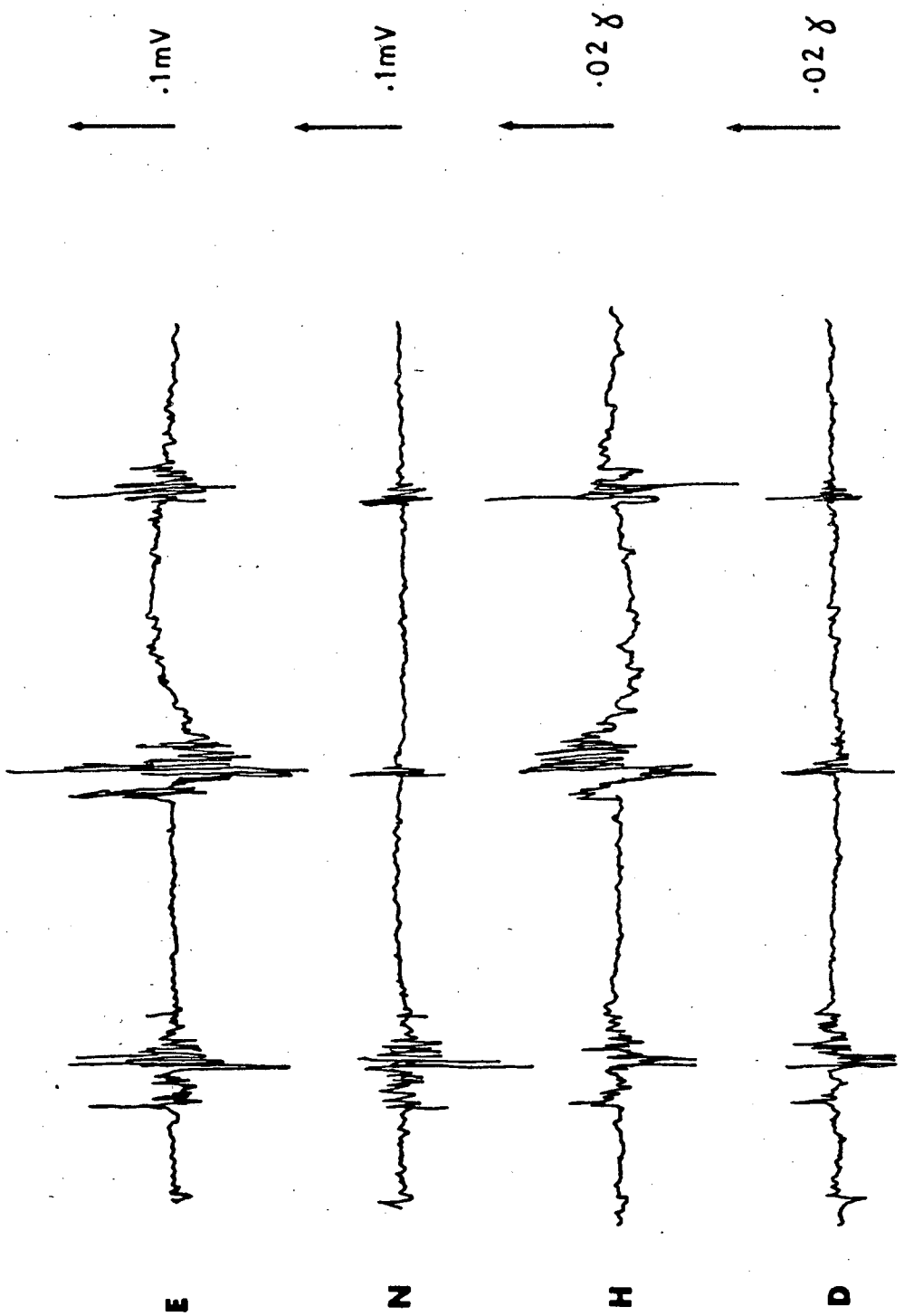

A typical event section taken from the AMT data record is shown in figure 4.1. It shows the two telluric channels E and N above the magnetic channels D and H. The data set contains an energy burst typically originating from a lightning discharge. Apart from this, the data are free from noise contamination. A section of the data record showing typical noise contamination is shown in figure 4.2. It shows a spike pair occuring at 50 times/sec. Any sine wave, 50 Hz in frequency has been removed by the notch filter in the amplifier circuit. The data are still grossly degraded. A data section showing the effects caused by particles of dirt on the recording tape is shown in figure 4.2(b).

Let us now consider the process of selection of events from the long period MT data records. The steps of this sequence are well established and have been fully documented (Mbipom, 1980). In this work it differed only in the application of the MINC computer, both in the field and in the laboratory. The normal and preferred procedure was to select and process events in the field, so that a day to day assessment of the fieldwork progress could be made. On return to the Department, upon the completion of the field session, the process was repeated with new events and more comprehensive processing on the main University computer. The following desription applies to second (in the lab.) selection of events, which provided more reliable response estimates.

Figure 4.2 a. AMT signal showing contamination by spike-like noise at 50 Hz frequency

b. Typical contamination of signal by dirt adhering to tape
(1 second = 13 cm)

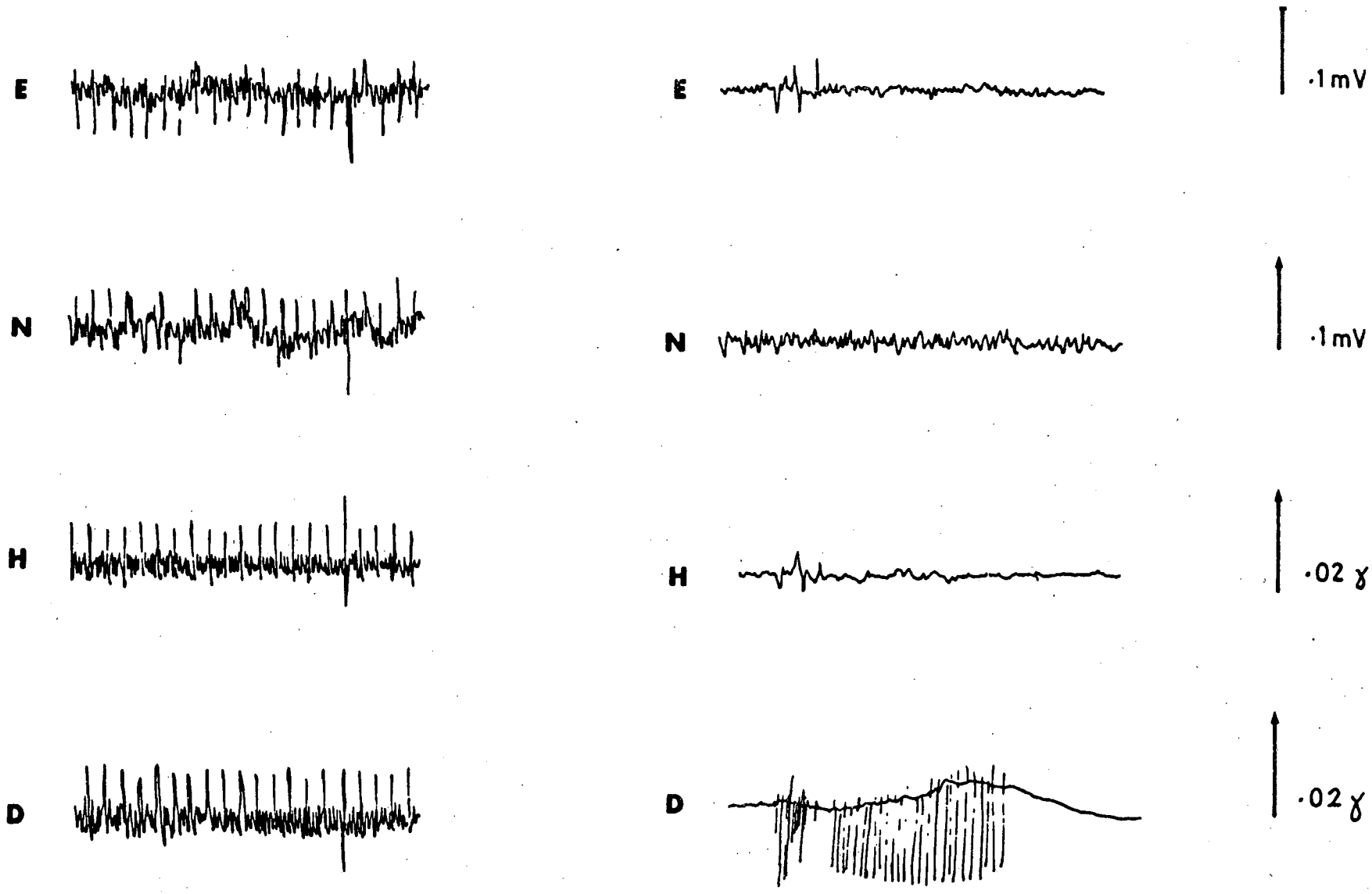

(a) (b)

Figure 4.2

Data from each recorded cassette were viewed in 8 hour sections, one channel at a time, to locate unsuitable sections in the recording. The most common cause for such data, was the malfunctioning of the three magnetic sensors during recording in the field. Similarly, sections containing reading errors, detected by viewing the analogue output during the magnetic cassette reading process, were also avoided. Suitable record sections were re-examined at much smaller time intervals, to inspect for the presence of detectable noise, such as 'switching' (a phenomenon most probably caused by nearby electrical machinery). From the remaining acceptable data record, up to 20 events were selected. These were 20 minutes to 2 hours and 40 minutes in duration, to utilise the 2048 points of the Fourier Transform during later processing. If enough data were available, some consideration was paid to obtaining some data sections with obvious short as well as long period fluctuations and some from different times of the day. The resulting distribution of selected events in any 24 hours was not noted to be biased towards a particular time of day.

The validity of both selection procedures was examined by a comparison of results obtained from a number of randomly selected events and the same number of events selected as described above. In each case, the predicted coherency estimates, evaluated during the single event processing, were used in the comparison.

The results showed, that as many as 4 times the number of estimates could be accepted during the analysis, if the selection of events was correctly carried out.

If, in the future, a fixed event selection procedure was to be constructed to act automatically during processing, it would, clearly, need to be based on the criteria implemented in the desribed manual procedure. However, the following observations based on actual data selection, some, more easily interpreted in mathematical terms, than others, are suggested for future development.

(a) Signal amplitudes of zero, or FSD may be produced by malfunctioning of part of the instrumentation. Such unacceptable data could be detected by examination of the signal amplitudes of the temporal record.

(b) Large and rapid changes in the amplitude accompany discontinuities in data record sections, including, in particular, the occurence of single or multiple data spikes. Data containing these characteristics must also be excluded, preferably in the time domain, where they can be detected by the rapid change in amplitude. Once transformed to the frequency domain such data produce exceptionally un-natural looking power spectra. When processed, such events produce low and wildly fluctuating predicted power coherency levels.

(c) Spurious data are the most difficult to detect, especially as they may not contain the features noted in (a) or (b) above. It is likely that the detection of such features would not be accomplished easily, with, possibly, the exception of the same analysis of the predicted power spectral coherency levels.

4.2 Single event processing

The acceptable events selected from the MT and AMT data records were processed using the single event analysis programme 'MAG' (Rooney,1976). This programme, also described by Jones (1978), was modified to accommodate the extended frequency spectrum of this work. The following, standard, operations were performed by the programme:

1. Long period and linear trends were removed, using a D.C. offset and least squares line fit respectively.

2. A Cosine taper was applied to the first and last 10% of the data record to reduce the power leakage from the side-lobes, created by the application of the box-car transform. Such box-car, or viewing, window was necessary to allow the Fourier transformation to be performed on a finite time series. The Fourier transform s(t) is given as

$$S(f) = \int_{+\infty}^{-\infty} s(t)\ \exp(-i\omega t)dt$$

3. The total number of points of the time series was

extended as a requirement of the Fast Fourier Transformation (FFT) algorithm, of Cooley and Tukey (1965), to a power of 2.

4. The FFT was applied by the subroutine RHARM in the processing programme, to each component in turn, using the above algorithm.

5. The auto- and cross-spectral estimates were calculated for each component of the transformed event and smoothed (Bendat and Piersol, 1971. p191) by averaging 8 adjoining estimates. Included in the modifications to the programme are the changes to the first 4 of these band averaged estimates.

6. The estimated coherency between the adjacent channels H and D, and N and E was calculated, followed by the coherency estimate between the measured Z, E and N fields and those calculated from the H and D fields. The technique of predicting power spectra was used to effectively establish a measure of the quality of the data.

7. The transfer function estimates, derived from the impedance tensor relationship were used to obtain apparent resistivity and phase values in two perpendicular directions given by the azimuthal rotation.

All parameters required for a single event analysis can be derived from the transfer function estimates. It can be seen that prior to the Fourier transformation, accepted forms of data handling were used. This was followed by determination of a measure of quality of the original data, based on the power spectral estimates. Thereafter, smoothing of the data to produce a reliable measure of the result with an indication of the error, was used to generate log(T) distributed estimates with standard deviation error bars.

An excellent analysis of windowing techniques and their effects on the data has been given by Harris (1978). It is possoble that, in view of Harris' results, certain parts of the processing programme 'MAG' may, in the future, require some revision.

4.2.1 Instrumental response corrections

Let us first examine the requirements for the correction of the instrument response. As seen in Chapter 2, each of the main stages namely, the magnetic coils, the telluric pre-amplifier and the instrument amplifiers with their notch filters, had a particular amplitude and phase response. Further, an inherent response of the digitisation process, in the form of the digitisation interval or slew rate was present. The question of aliasing and the S/N level of the magnetic coils are separate problems. To be able to correct for the 'responses' each had to be known for the whole frequency

bandwidth of the instrument. The relevant curves determined during construction of the instrumentation, were shown in figures 2.8-2.10. Next, each response had to be represented as some function of frequency. The way this was done depended on the shape of the curve. Most of the curves (or section of curves) were represented by an nth degree polynomial. The least value of 'n' which produced a satisfactory fit was chosen.

It is noted that no correction for amplifier gains and phases, figure 2.8, need be applied. Theoretically there are no relative amplitude or phase differences between individual channels. In practice, however, there are very small difference in both. Furthermore the amplitudes and phases in the vicinity of the 50 and 150 Hz notch filters vary abruptly and particular care needs to be exercised in working with these filters and with the data derived at and near these frequencies.

The corrections required were for responses of the following items: coil gain, coil phase, pre-amplifier gain, pre-amplifier phase and digitisation interval.

Coil Gain - The calibration curves supplied by Societe ECA show a flat response of 50 mV/Y between 4 and 480 Hz figure 2.10. It can be seen that the gain drops to 90 percent of its maximum value outside 1.7 and 800 Hz. In fact, at the low frequency end, the error is reduced to 2.5 percent by 3 Hz and is less than 1 percent above 4 Hz. In view of the small number of estimates at these low

frequencies it was not considered necessary to include this drop-off in gain, in the correction. At the high frequencies the gain begins to drop from about 400 Hz. The effect of this is to produce values of E/H enhanced by a factor of 1.2 at 780 Hz and by a factor of 1.7 at 1000 Hz. A straight line fit of the curve over the frequency range 480 - 1000 Hz was made and is shown in figure 4.3. This line cuts the response curve at 300, 530 and 900 Hz, where no difference in the E/H value results, and causes values, alternatively greater and smaller at 475, 700 and 1000 Hz of 1.2%, 2% and 2.1% (maximum) respectively. The total error inflicted by the fall-off in gain above 480 Hz considerably reduced. The equation of the line is:

$$X=4.747740602\times10^{-4}\ x(\text{frequency})+0.77210819$$

where 'frequency' is 'all frequencies over 480 Hz'. The application of this correction effectively extended the gain of 50 mV/Y to 1000 Hz. The correction was applied in the frequency domain by multiplying the Fourier coefficients, corresponding to the magnetic components by 'X' above. Reprocessing with the correction produced (a) a lowering of the resistivity values as expected and (b) a small change in the phase values. Both these effects were evident, naturally, at periods of 480 Hz to 1000 Hz only.

Coil Phase - The phase specifications for the 3 coils D16, D17, D18 were supplied by ECA. The two coils D16, D17 were used for the H and D magnetic directions respectively. Their phase response curves differed

Figure 4.3 Coil response between 100 and 1000 Hz showing the interpolated curves and the straight line fit. The supplied coil sensitivity data for the three induction coils were used to draw the curves. The line applies to frequencies between 480 Hz and 1 kHz, and its equation is given on p. 83.

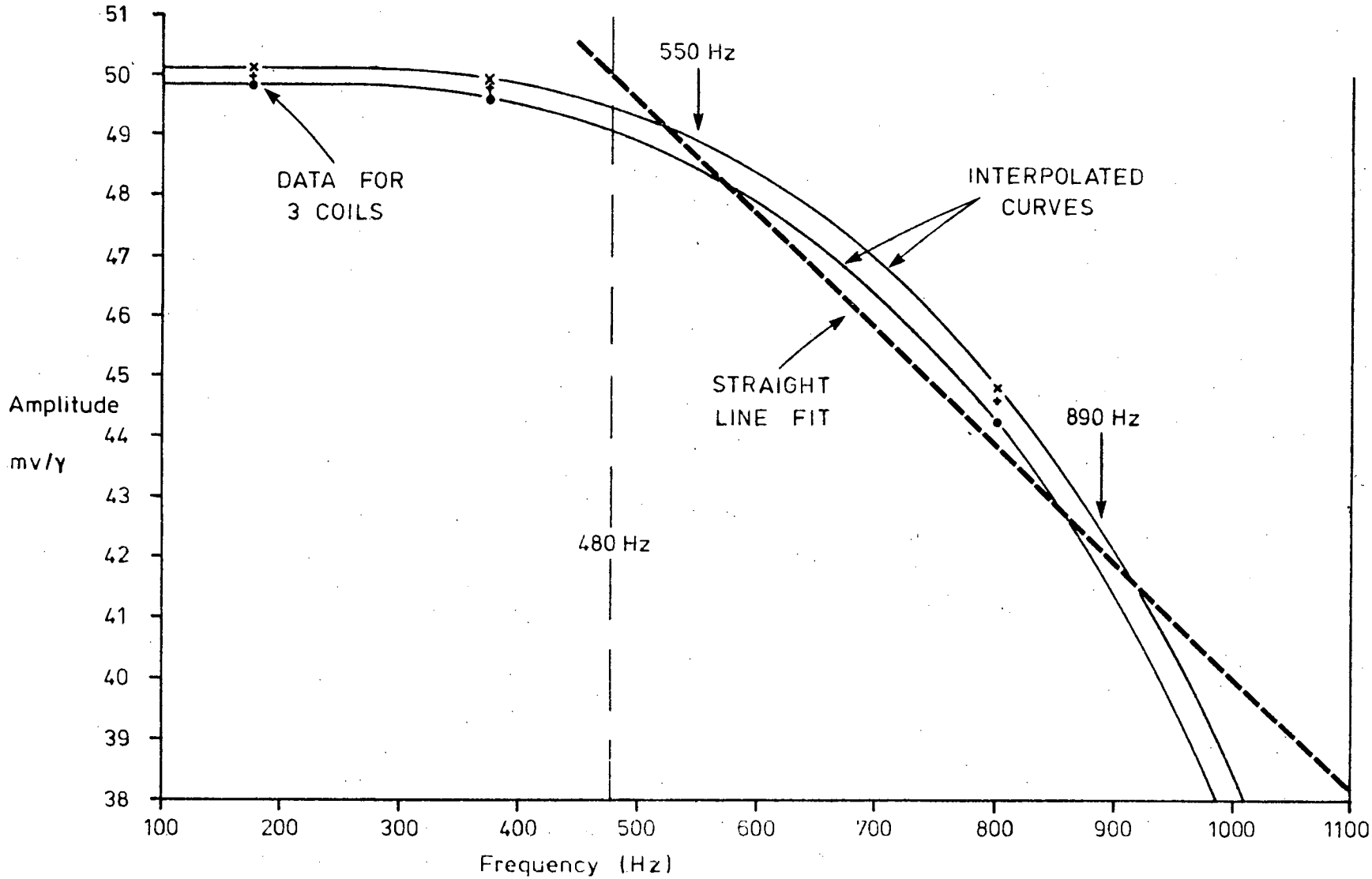
51
50
49
48
47
46
45
44
43
42
41
40
39
38
Amplitude
mv/γ
100
200
300
400
500
600
700
800
900
1000
1100
Frequency (Hz)
550 Hz
480 Hz
890 Hz
DATA FOR
3 COILS
INTERPOLATED
CURVES
STRAIGHT
LINE FIT

Figure 4.3

slightly so the mean was calculated (see figure 2.10). The resultant line was fitted with curves of varying degree using a computer programme written specifically for this purpose by the author. The 6th and the 8th degree polynomial produced the best approximations.

This 6th degree polynomial was used to represent the phase variation of the coils. The coefficients derived were as follows:

$$Y=2.64857x(X)^6 -18.25731x(X)^5 +41.12540x(X)^4$$
$$-0.83823x(X)^3 -137.18803x(X)^2 +219.17506x(X)-118.27004$$

The phase was then given by 'Y' where X is the log (frequency) to the base 10. To avoid using uncorrected data, the correction was applied to the appropriate Fourier transform coefficients immediately after their calculation. Data processed with the correction showed a considerable rotation in the phase, in accordance with the response model. The whole range of the instrument bandwidth was corrected for the response of the coil phase to within 2 percent.

Pre-amplifier Gain - The measured gain response of the two telluric pre-amplifiers was used to construct a single curve which could be used to approximate the response of both amplifiers. This mean curve was shown in figure 2.9. From this curve it can be seen that, at the two frequencies 1.7 Hz and 800 Hz, the amplitude has decreased to 85 and 96 per cent of its maximum value respectively.

It was therefore argued that no correction for the non-uniformity of the gain of the telluric pre-amplifiers was necessary. The gain of this stage of amplification was therefore taken to be 20. The resultant error was calculated to be zero between 6 Hz and 600 Hz, 3 percent between 4 Hz and 770 Hz rising to 32 and 6 percent at 1 Hz and 1 kHz respectively.

Pre-amplifier Phase. The phase response of the telluric pre-amplifiers was shown in figure 2.9. The mean response was again constructed and modelled using curves of varying degree. A 6th degree polynomial was chosen to represent the response, the equation of this polynomial curve is given by

$$\text{phase}=0.77575x(X)^6 - 5.83943x(X)^5 + 14.53647x(X)^4 - 3.04110x(X)^3 - 44.19104x(X)^2 + 77.39580x(X) - 45.37742$$

and satisfies the fit to 1 percent for the complete bandwidth of 1 Hz - 1 kHz. The equation was incorporated into the processing programme in the same way as that for the coils.

Digitisation interval - Typically the error introduced here was in the form of a phase shift between adjacent components and was caused by the finite time delay inherent in the sampling of adjacent channels. A value of 70 μs $\pm$5 μs was determined, using a sine wave input. The phase shift observed between the channels over 900 averaged occasions was used to determine this value accurately.

The order in which the channels were digitised was E-N-H-D-(Z). To implement this correction the formed pairs DE DN DH HE HN were assigned a delay equivalent to n times 70 μs, where n was the number of channel transitions between the individual elements of the pair. The pair EN was assigned a value of -70 μs. Between the most distant channels (eg. D and E) it amounts to 210 μs. This corresponds to a phase delay of 75.6 degrees at 1000 Hz.

As before, the corrections were applied at the first possibility in the processing programme, namely before the calculation of the complex cross-spectra from the elements mentioned. The correction was of the form $\exp(i\phi)$, where ϕ is the phase delay between two channels. It can be shown that the coherencies are independent of this delay.

In subsequent trials, using data from two stations, the expected change in the impedance phase values was observed. It is unlikely that impedance phase values would have been of significant use, in their uncorrected state.

4.2.2 Band averaging

The discrete frequency power spectral estimates, produced following the Fourier transformation, were band averaged to obtain a reliable measure of the results. By the principle of band averaging, smoothing of the results and a measure of the variance of the data in the averaged band, were achieved.

The band averaging methods followed in this work have been described in relation to long period MT data by Jones (1977) and were used in much the same form by Mbipom (1980) and Ingham (1981). In the scheme, 8 successive frequency estimates were averaged in each band, while the first and last 4 power estimates were disregarded to further improve the quality of results. Standard text shows, that the variance of the averaged data within each band decreases, as the number of degrees of freedom increases and that in order to produce meaningful error estimates, the number of degrees of freedom must be constant throughout the complete frequency spectrum. In this work, these principles did not take full advantage of the improved low frequency characteristics of the AMT instrumentation. The results from the third to the thirtieth estimate of a 1 second long event, were acceptable, but were only used, in the above averaging, to produce 4 band averaged estimates. By, partially, departing from these standard principles, and reducing the number of discrete power estimates in each band, in the low frequency part of the spectrum, a greater number of distinct band averaged results was derived.

In the first 8 bands 1,2,3,4,5,6,7 and 8 estimates were averaged, respectively, followed by 8 in the subsequent bands, ending with 4 as before. The first band average, now taken over only one estimate, was again ignored. The mean of the first of these bands was located at 2.5 Hz and that of the eighth at 25 Hz.

The result was to provide twice the number of smoothed estimates below 30 Hz. This can be clearly seen in many of the AMT station results.

In the approach of calculating the band averages, the modifications described above were not intended as an improvement in the general quality of resultant data. Rather, by reducing the reliability of the final results and of the associated errors, greater control was exercised over the limited number of discrete estimates in the part of the spectrum between 1 Hz and 30 Hz.

Although the modified band averaging approach was also applied in the processing of the long period MT data, most results remained largely unaffected, due to lack of acceptable estimates in the extreme of the long period part of the spectrum.

4.3 Station data averaging and acceptance criteria

The methods of averaging of single event MT data were fully described by Rooney (1976). In this work, they were applied to both MT and AMT measurements. The purpose was to increase the confidence of the station results and to provide response estimates evenly distributed on a logarithmic (period) scale. The following steps were undertaken in the averaging algorithm.

1. The results of the single event analysis were read for each event, as unrotated transfer function estimates.

2. Only the transfer function estimates with a predicted coherency greater than 0.9, in the E and N directions and 0.8 in the Z direction, were accepted.

3. The estimates were tested for an acceptable level of signal.

4. The estimates were averaged to produce equispaced estimates on a log (T) scale and to determine the variance of the result at each representative point.

5. The results were plotted as rotated apparent resistivity and phase, azimuth of rotation, skew and number of estimates.

The error bar calculated for each quantity represented one standard deviation about each average. The number of averaged estimates in each decade of period was chosen as 8 although further smoothing could be achieved by reducing this to 6.

The level of signal, tested in step 3 above, was calculated as a signal-to-noise ratio. In the case of the long period MT data the random noise component had been substantially reduced as a result of the use of the NERC Geologger (Mbipom, 1980). The highest level of random noise of the AMT equipment was found to be generated by the 2 induction coil sensors. The random noise

component, introduced through the digitisation process in the long period MT data, was negligible in the AMT data.

Figure 4.4 shows the average power of the magnetic field at Garchy in the frequency range 1 - 1000 Hz. Included in the diagram is the curve, representing the minimum power required to register an output from the coils. Above 370 Hz., where the two curves cross, the signal will consist of instrumental noise only. The exact magnetic field signal strength was determined at a number of sites. It was found that this level could vary by up to two orders of magnitude which shows, from figure 4.4, that the coils did provide an acceptable level of signal up to a maximum frequency of 1.5 kHz, during times of large magnetic field strength, but that at times of low field strength this frequency limit was at approximately 270 Hz.

To establish, accurately, the level of signal during each event and, consequently, whether power spectral estimates were acceptable for inclusion in the analysis, the signal level and the random noise component were determined at a number of carefully chosen events. The peak power was found to occur, on average, at 10 Hz. By 500 Hz the level had reduced to approximately 0.0003 % of the maximum level, thereafter remaining constant up to 1000 Hz. This constant level was the level of the random noise. Allowing for the effects of band averaging

Figure 4.4 Coil sensitivity (dashed line) - showing resonance at 90 Hz - plotted against the average natural field in Garchy.
At approximately 500 Hz the signal becomes insufficient to produce an output from the coils.

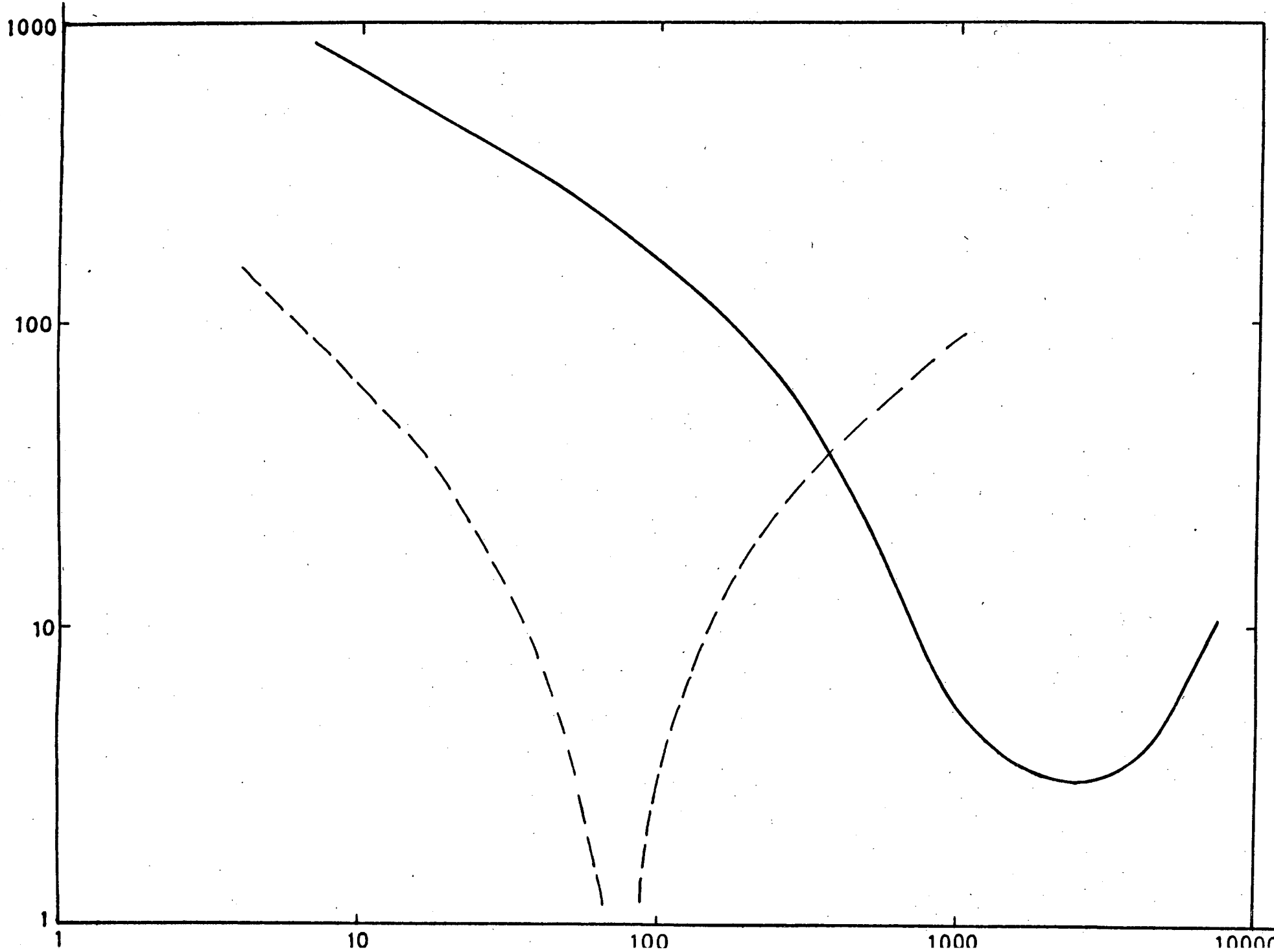

Figure 4.4

which increase the noise content by $\sqrt{n}$ against an increase of n of the signal (n=number of degrees of freedom), the random noise and the signal-to-noise were determined as follows.

$$\text{Power} = (\text{Ampitude})^2/\text{Hz}$$

$$\frac{\text{Signal}}{8} \times \text{Hz} = \text{Ampitude}^2, \quad \frac{100\%}{8} \times 10 = A^2, \quad A = 11.2 \text{ gamma}$$

$$\frac{\text{Noise}}{\sqrt{8}} \times \text{Hz} = \text{Amplitude}^2, \quad \frac{0.0003\%}{\sqrt{8}} \times 500 = A^2, \quad A = 0.23 \text{ gamma}$$

$$\text{Noise percent} \quad \frac{0.23}{11.2} \times 100 = 2\ \%$$

Thus for an error in the output of 2 percent - equivalent to the random noise contribution - the power level ratio of signal to noise would then be roughly 10000/4.

The figures for the magnetic component, read for a particular event, showed a typical maximum power of $1 \times 10^{-5} \gamma^2/\text{Hz}$. At this level a signal to noise ratio of unity would occur when the power level was $4 \times 10^{-9} \gamma^2/\text{Hz}$. Summing over 8 adjacent frequencies would produce a signal power of $8 \times 4 \times 10^{-9} \gamma^2/\text{Hz}$ and a noise power level of $\sqrt{8} \times 4 \times 10^{-9} \gamma^2/\text{Hz}$. For the S/N ratio to exceed unity the limit for acceptance of a particular bandwidth was set to $\sqrt{8} \times 4 \times 10^{-9}$. In line with accepted procedure the signal noise ratio of frequency bands on

either side of the band had to exceed S/N/2 for the band to be accepted. Tests carried out on data from selected sites, showed that frequency bands rejected on the basis of the signal to noise ratio above, commonly displayed predicted coherencies in the telluric component of less than 0.85.

After making independent tests, this value was subsequently used in averaging of all the AMT station data.

The results of the above work had shown, that the correct selection of events was important, in order to derive a sufficiently high signal-to-noise ratio and to produce much improved station results.

CHAPTER 5

RESULTS

A presentation of the results from the magnetotelluric soundings is made in this chapter. The results from stations along the main profile, at which both MT and AMT measurements were made, are presented together as broadband data. The results from selected AMT stations are then presented separately. For each site the variation with frequency of the following parameters is presented and discussed in the text.

Figure (a) Maximum and minimum apparent resistivities and phases.

Figure (b) Azimuth, skew and number of discrete frequency estimates, averaged in each plotted result. Also shown in figure (b) is a first approximation apparent resistivity - depth plot, calculated for each value in the rotated, and perpendicularly oriented, ρ max and ρ min results plotted in (a).

The apparent resistivity and phase results were discussed and derived in section 2.3. They represent the results at each site, following the rotation of the impedance tensor into the direction of the geological strike. The angle of the rotation, calculated for each averaged result

was given by the azimuth of rotation. This is shown in the 1st plot in (b). The skew parameter is a measure of the dimensionality of the data, defined in section 2.3, and was similarly calculated for each averaged result shown in (a). The averaging of individual power spectral estimates, following the FFT of the raw, time dependent record, was discussed in section 4.2.2. Above 30 Hz, the acceptable discrete estimates were band averaged in groups of 8 and the mean result was further averaged to provide evenly spaced results on a log (T) scale. The number of discrete estimates in each value plotted in (a) and (b) is plotted separately in figure (b) and labeled NU. A first approximation inversion scheme, based on a 2 layer model approximation (Schmucker, 1970) was used to calculate the result shown in figure (b). In the approximation

$$Z_o = i\omega\mu \left(h + \frac{1}{2}\delta_2 - i\frac{1}{2}\delta_2 \right)$$

$$C(\omega) = \frac{1}{i\omega\mu} Z(\omega)$$

$$C(\omega) = h + \frac{1}{2}\delta_2 - i\frac{1}{2}\delta_2$$

$$h = Re(C) - Im(C) = \frac{1}{\omega u}\left(Im(Z_o) - Re(Z_o)\right) \quad \text{and}$$

$$\rho_2 = 2\omega u \left(Im(C)\right)^2 = \frac{2}{\omega\mu}\left(Re(Z_o)\right)^2$$

The depth to the perfect substitute conductor h^* :

$$h^* = h + \frac{1}{2}\delta_2 = Re(C) = \frac{1}{\omega\mu} Im(Z_o)$$

The substitution is valid only if the conductivity increases with depth and has only a limited application in the interpretation of the results.

5.1 Broadband results

The results from the MT and the AMT measurements at each site were united, so as to be able to discuss each parameter as a function of the complete bandwidth. The dicussion of the results from the seven sites along the main traverse, is made in two parts. The stations in these groups show similar behaviour, although, as will be seen in chapter 6, important differences exist between stations in the group LAM, EDG, WHI and SIN. These were the 4 northern stations in the main traverse. The remaining three broadband stations SWI, ROO and HIL formed the southern extent of the traverse and although stations SIN and SWI were only 5 km apart their response curves showed positive differences.

The magnetic results, available only for the measurements corresponding to the long period MT range, are also presented and discussed.

5.1.1 The traverse to the north

The following stations are considered in this group: LAMPERT (LAM), EDGES GREEN (EDG), WHITFIELD (WHI), SINDERHOPE SHIELD (SIN). Their long period resistivity results show very similar responses, as can be seen in figures 5.1-5.4.

The maximum apparent resistivity (ρ_a) curves all have a magnitude of about 100 ohm-m in the high frequency band (f=10-1000Hz), rising to about 200 ohm-m in the low frequency band (f=1/10-1/1000Hz). The corresponding phase curves, (ϕ_a) show a rise from about 20 degrees - 60 degrees in the high frequency band and a decrease of 50 degrees - 20 degrees, typically, in the low frequency band. The (ϕ_a) values for station SIN show considerable scatter, as the data at this station were degraded by noise. The minimum ρ_a and ϕ_a curves show more scatter and a greater variation between stations. Station WHI has particularly well defined results. The azimuth of the major impedance in the high frequency band is dissimilar between stations but shows a distinctive trend in the low frequency band. There, it is well defined at all stations and shows a variation with frequency no greater than 10 degrees. The typical values are 50 degrees E of N for the most Northern station, rotating clockwise to about 80 degrees E of N for the next two stations and has a value of 95 degrees E of N (=85 degrees W of N) at the fourth

Figure 5.1 - 5.7 Broadband results from the seven stations where MT and AMT measurements were made.

a. MT rotated major and minor apparent resistivites and phases
b. MT azimuthal rotation angles, skew factors, number of estimates and a resistivity-depth plot.
c. AMT as in (a)
d. AMT as in (b)

Figure 5.1 Station Lampert

(a)

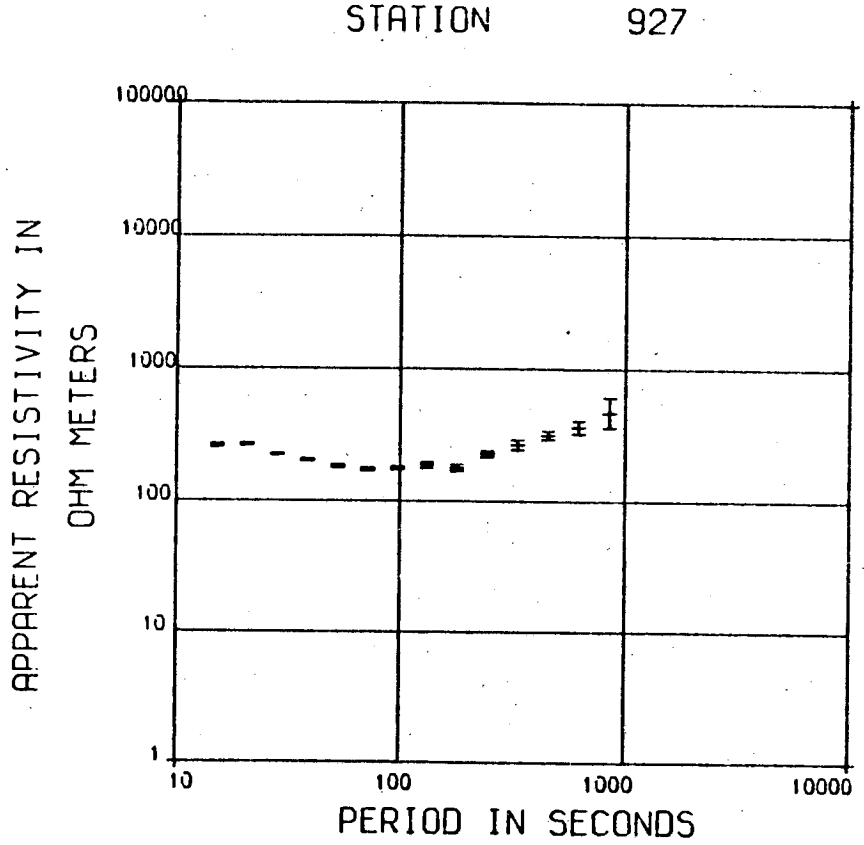
STATION 927
APPARENT RESISTIVITY IN OHM METERS
100000
10000
1000
100
10
1
10
100
1000
10000
PERIOD IN SECONDS

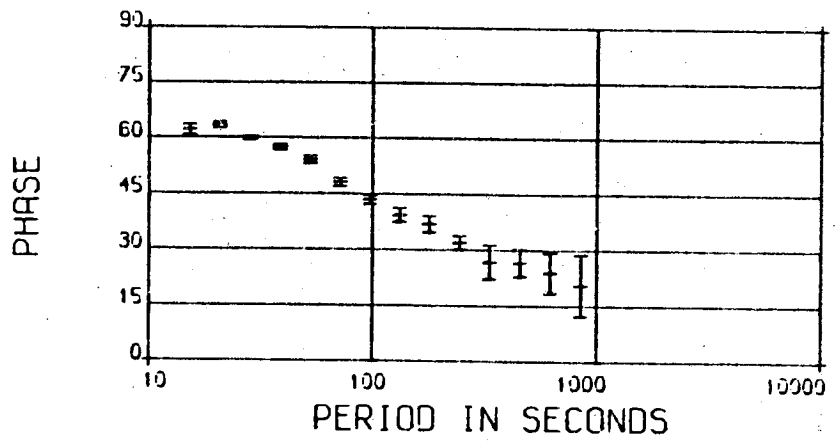
PHASE
90
75
60
45
30
15
0
10
100
1000
10000
PERIOD IN SECONDS

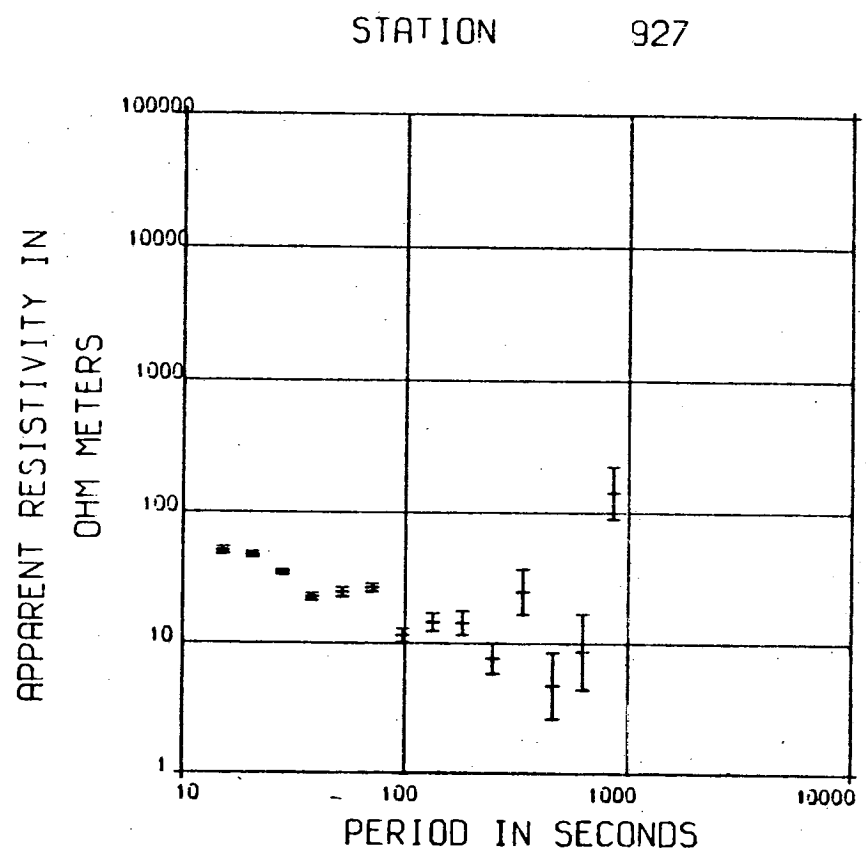
STATION 927
APPARENT RESISTIVITY IN OHM METERS
100000
10000
1000
100
10
1
10
100
1000
10000
PERIOD IN SECONDS

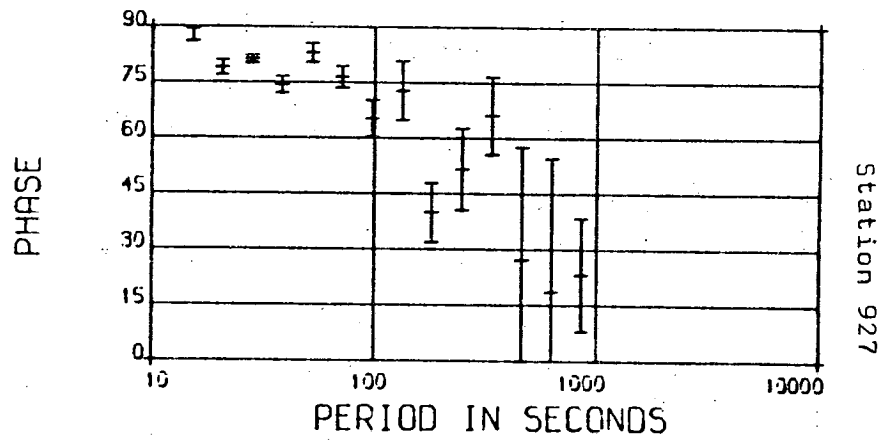
PHASE
90
75
60
45
30
15
0
10
100
1000
10000
PERIOD IN SECONDS
Station 927

STATION 927

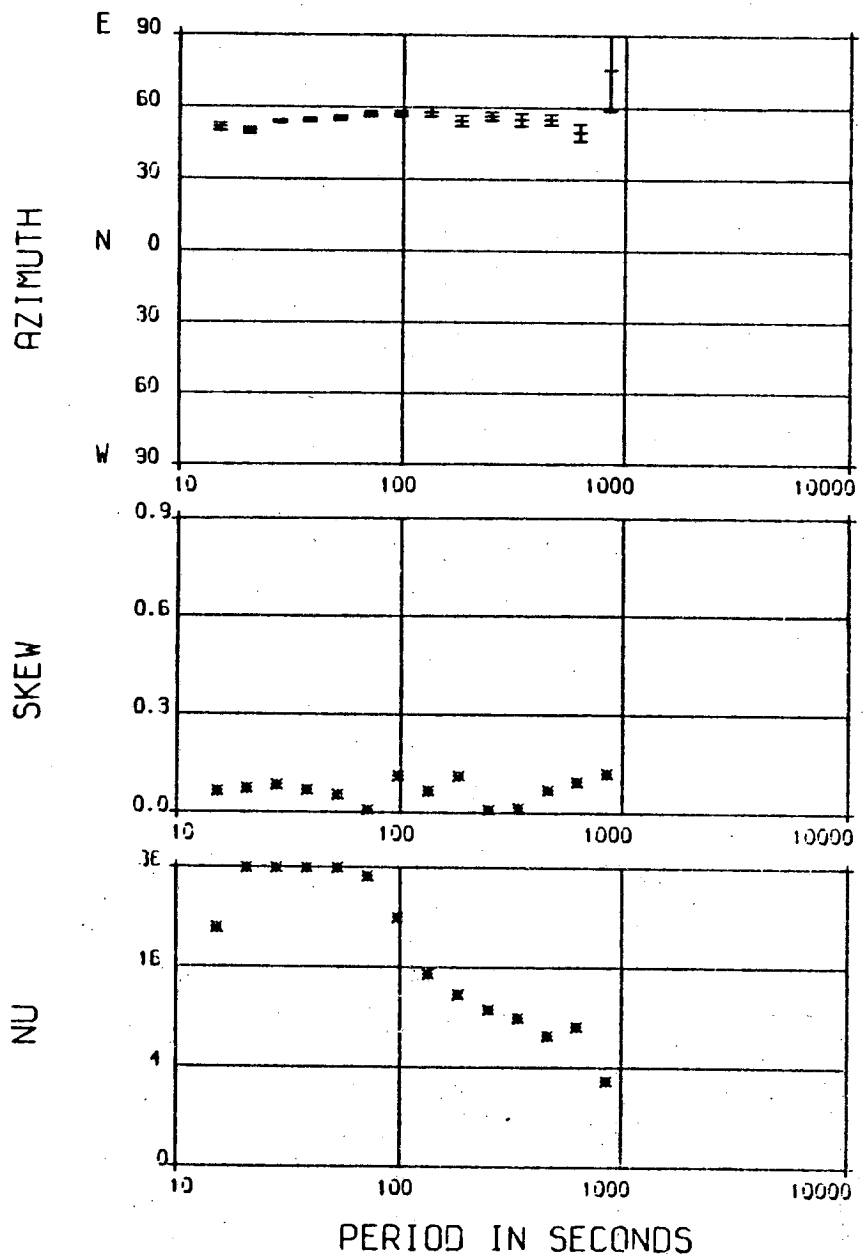

(b)

STATION 927

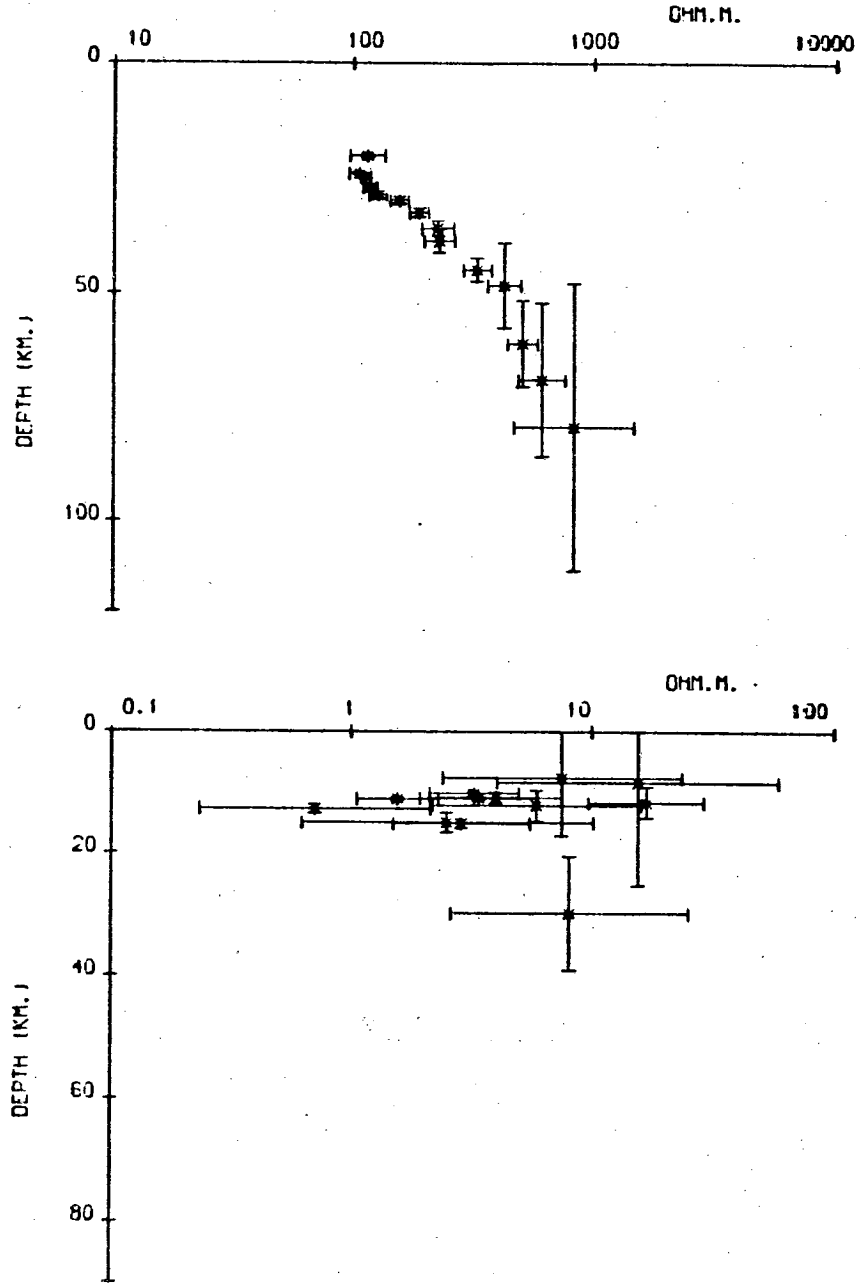

Station 927

(c)

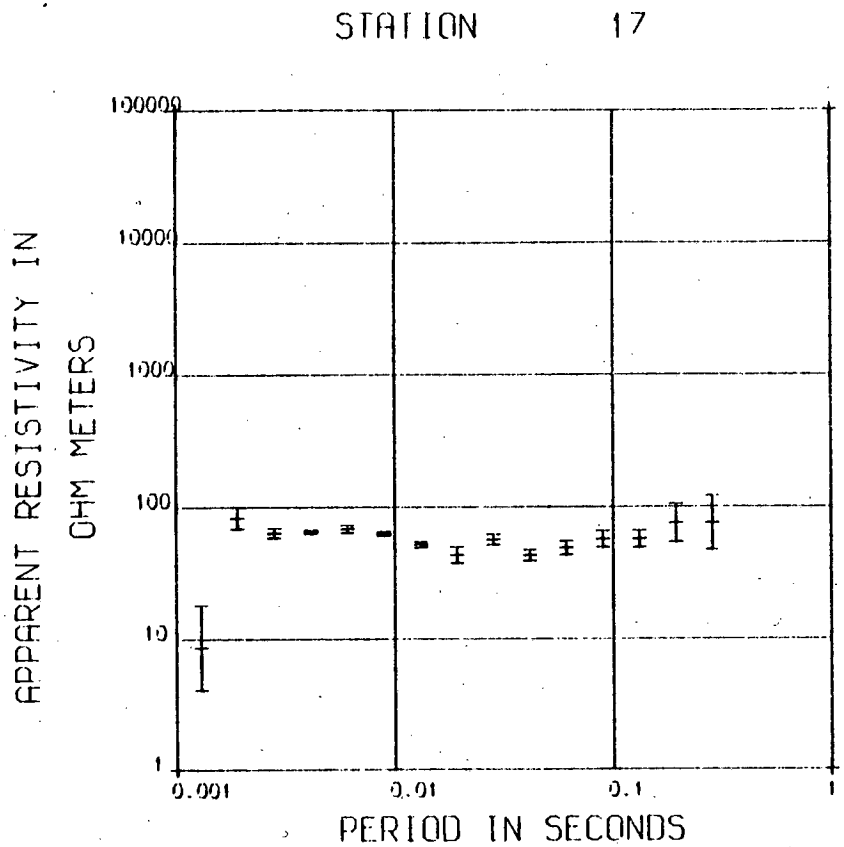
STATION 17
APPARENT RESISTIVITY IN OHM METERS
100000
10000
1000
100
10
1
0.001
0.01
0.1
1
PERIOD IN SECONDS

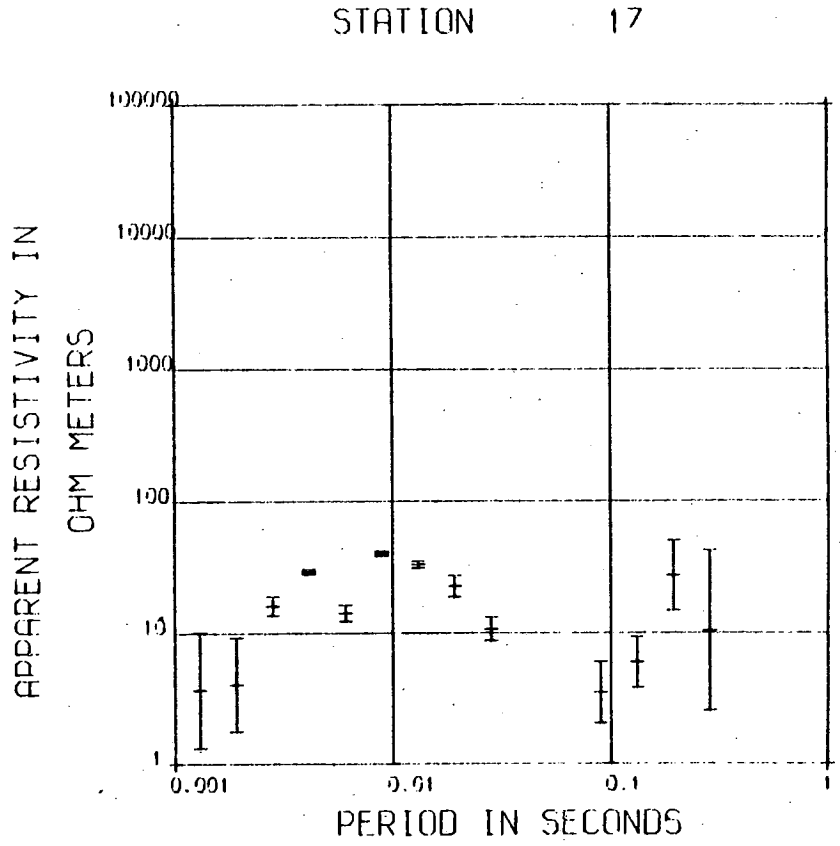
STATION 17
APPARENT RESISTIVITY IN OHM METERS
100000
10000
1000
100
10
1
0.001
0.01
0.1
1
PERIOD IN SECONDS

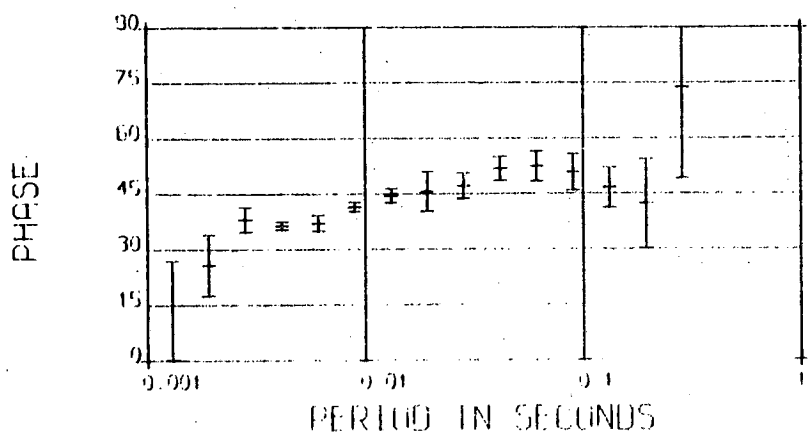
PHASE
90
75
60
45
30
15
0
0.001
0.01
0.1
1
PERIOD IN SECONDS

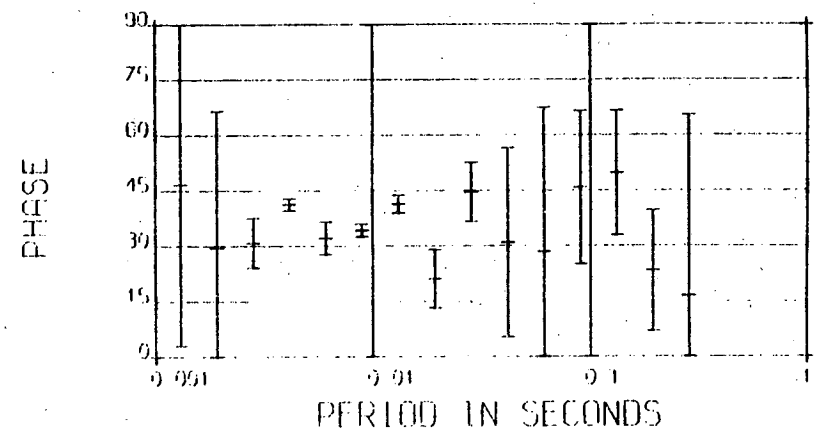
PHASE
90
75
60
45
30
15
0
0.001
0.01
0.1
1
PERIOD IN SECONDS

Station 17

(d)

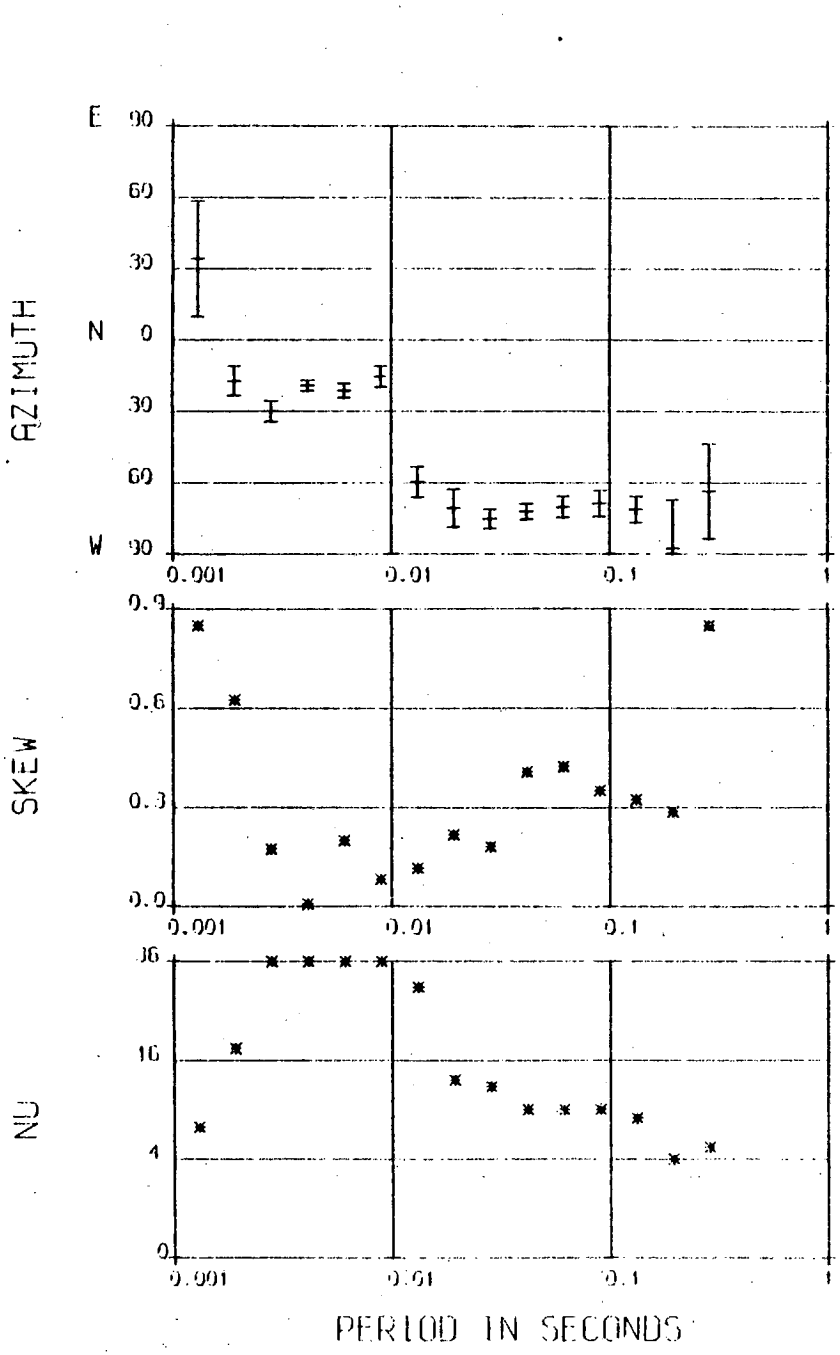
STATION 17
AZIMUTH
E 90
60
30
N 0
30
60
W 90
0.001
0.01
0.1
1
SKEW
0.9
0.6
0.3
0.0
NU
16
10
4
0
PERIOD IN SECONDS

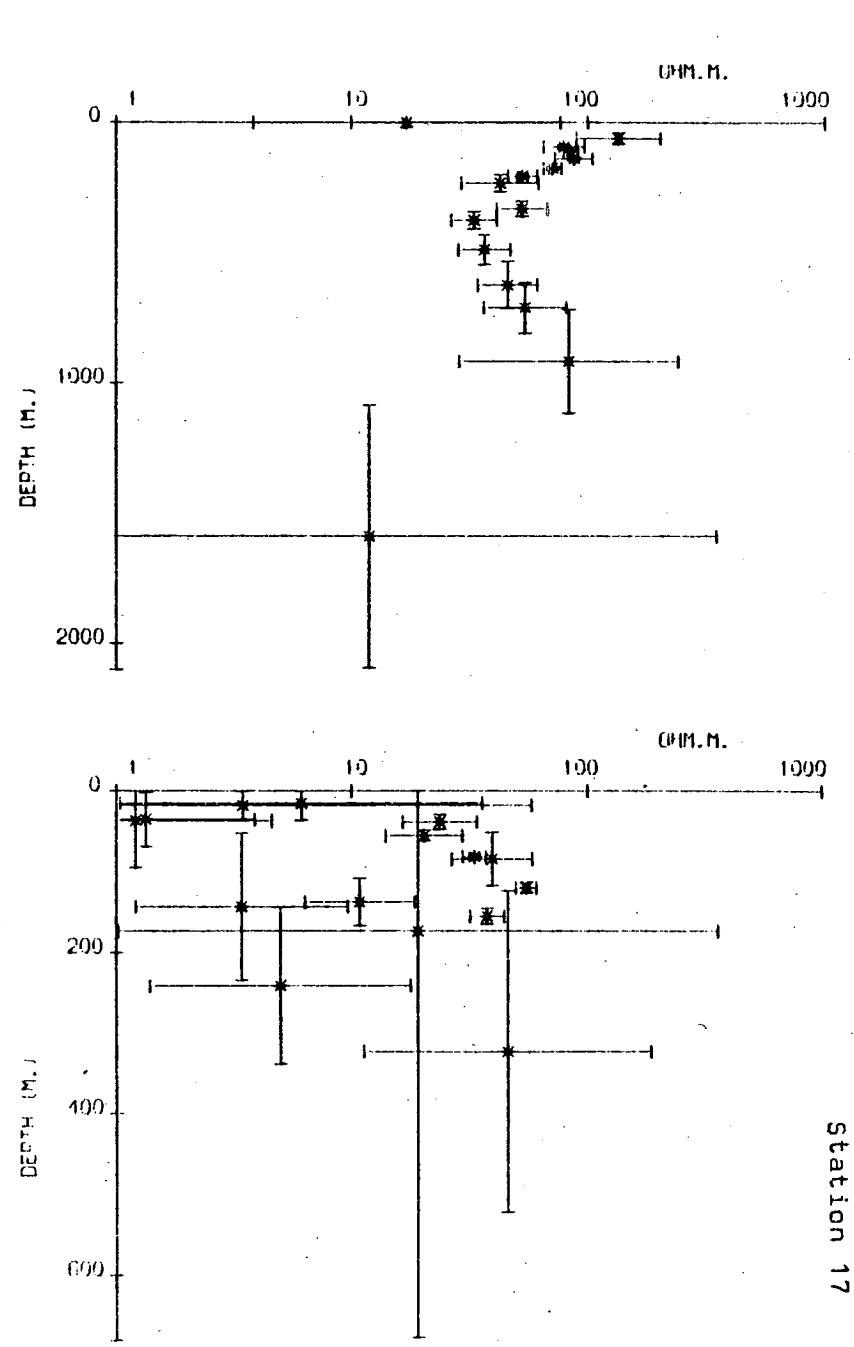
STATION 17
OHM.M.
1
10
100
1000
0
1000
2000
DEPTH (M.)
OHM.M.
1
10
100
1000
0
200
400
600
DEPTH (M.)
Station 17

Figure 5.2 Station Edges Green

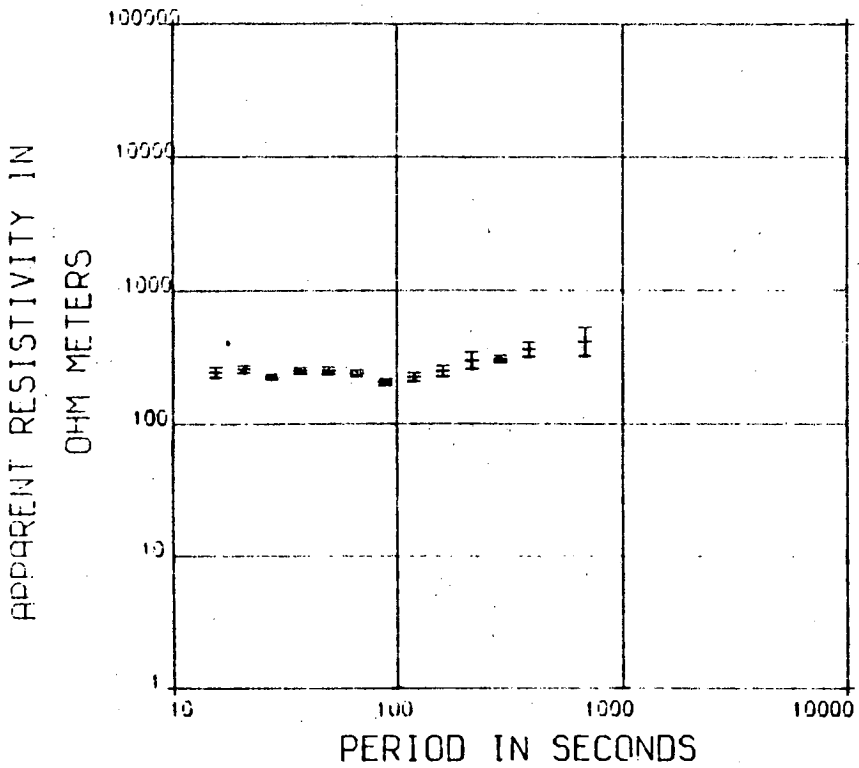
STATION 924
APPARENT RESISTIVITY IN OHM METERS
100000
10000
1000
100
10
1
10
100
1000
10000
PERIOD IN SECONDS

(a)

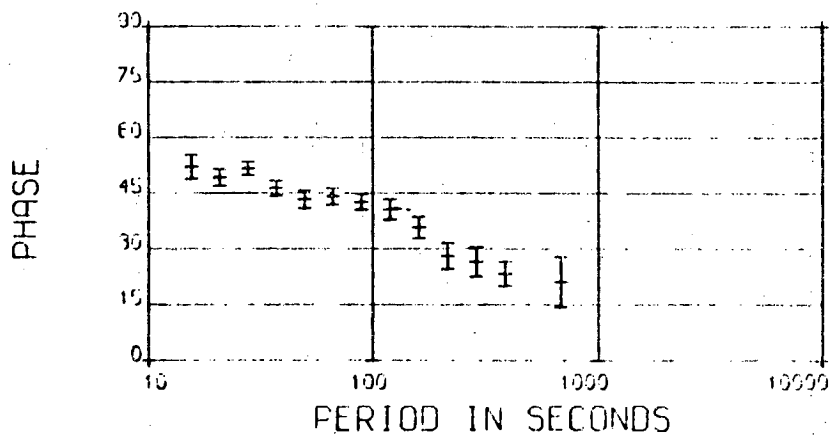
PHASE
90
75
60
45
30
15
0
10
100
1000
10000
PERIOD IN SECONDS

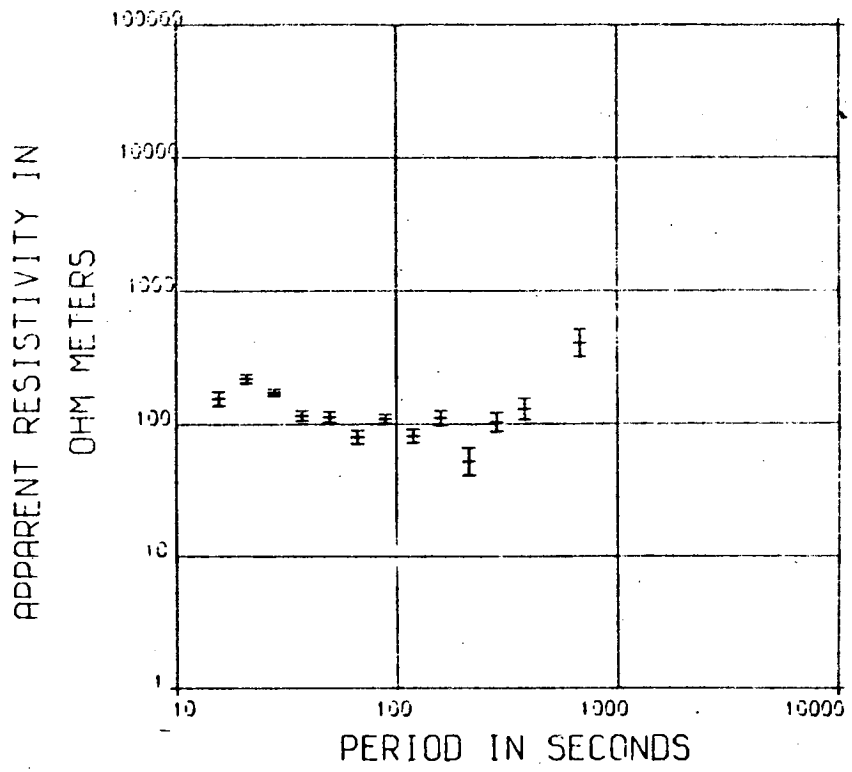
STATION 924
APPARENT RESISTIVITY IN OHM METERS
100000
10000
1000
100
10
1
10
100
1000
10000
PERIOD IN SECONDS

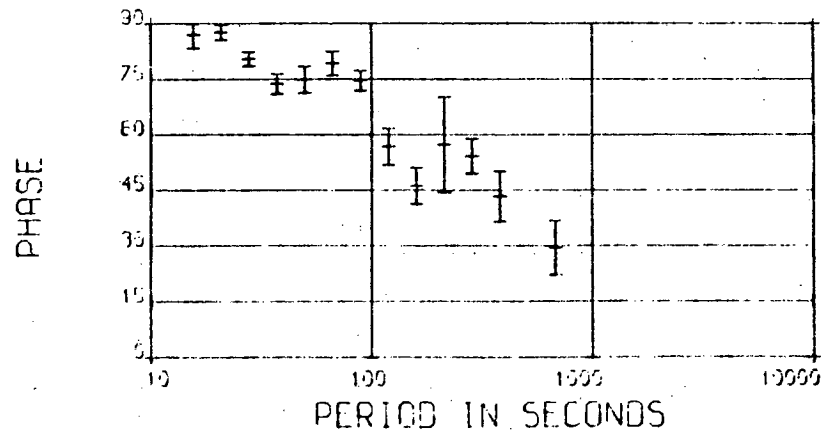
PHASE
90
75
60
45
30
15
0
10
100
1000
10000
PERIOD IN SECONDS
Station 924

(b)

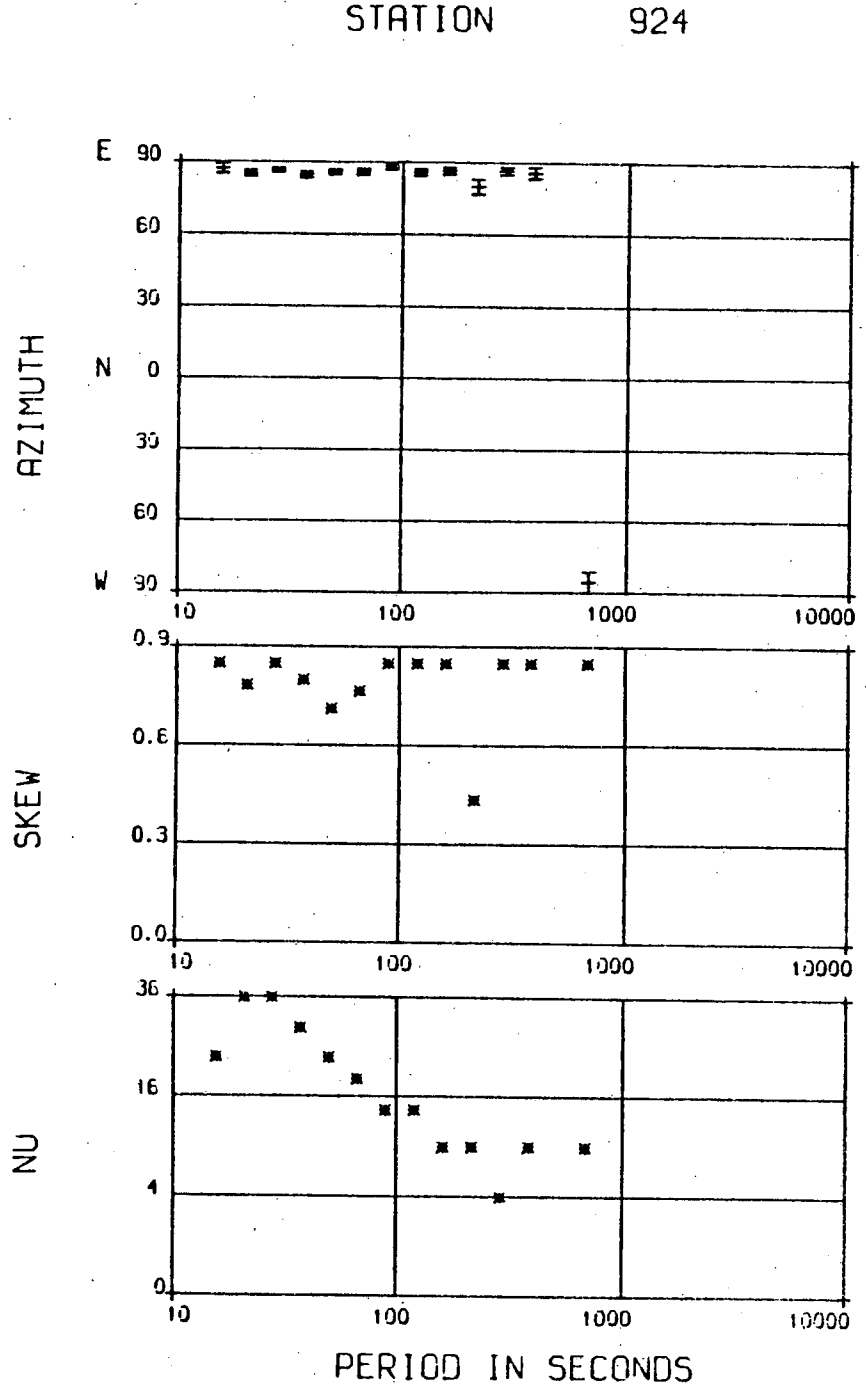
STATION 924
AZIMUTH
E 90
60
30
N 0
30
60
W 90
10
100
1000
10000
SKEW
0.9
0.6
0.3
0.0
NU
36
16
4
0
PERIOD IN SECONDS

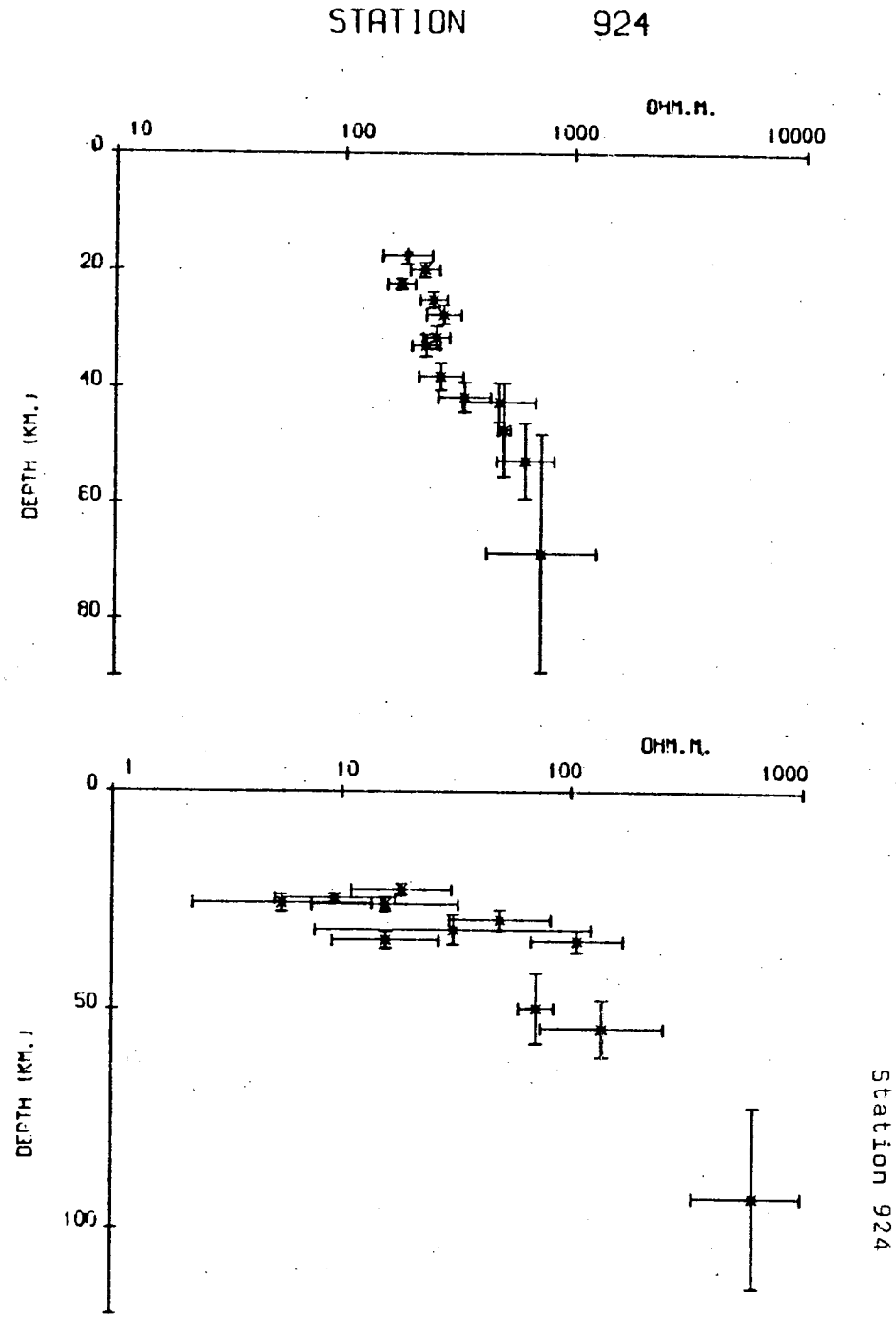
STATION 924
OHM.M.
10
100
1000
10000
0
20
40
60
80
DEPTH (KM.)
OHM.M.
1
10
100
1000
0
50
100
DEPTH (KM.)
Station 924

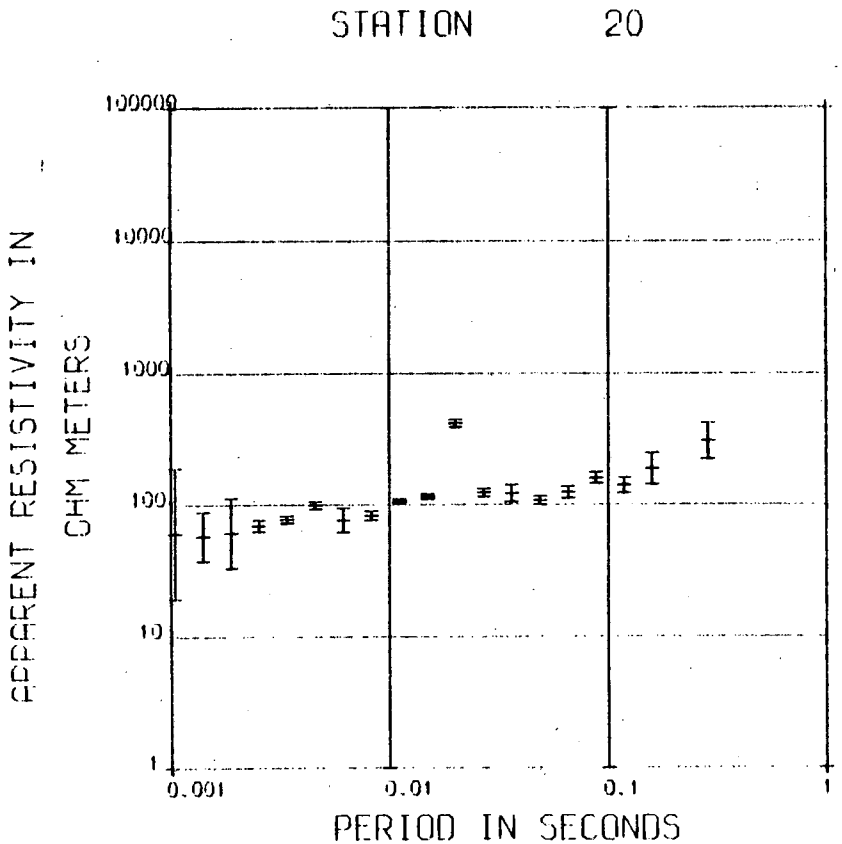
STATION 20
APPARENT RESISTIVITY IN OHM METERS
100000
10000
1000
100
10
1
0.001
0.01
0.1
1
PERIOD IN SECONDS

(c)

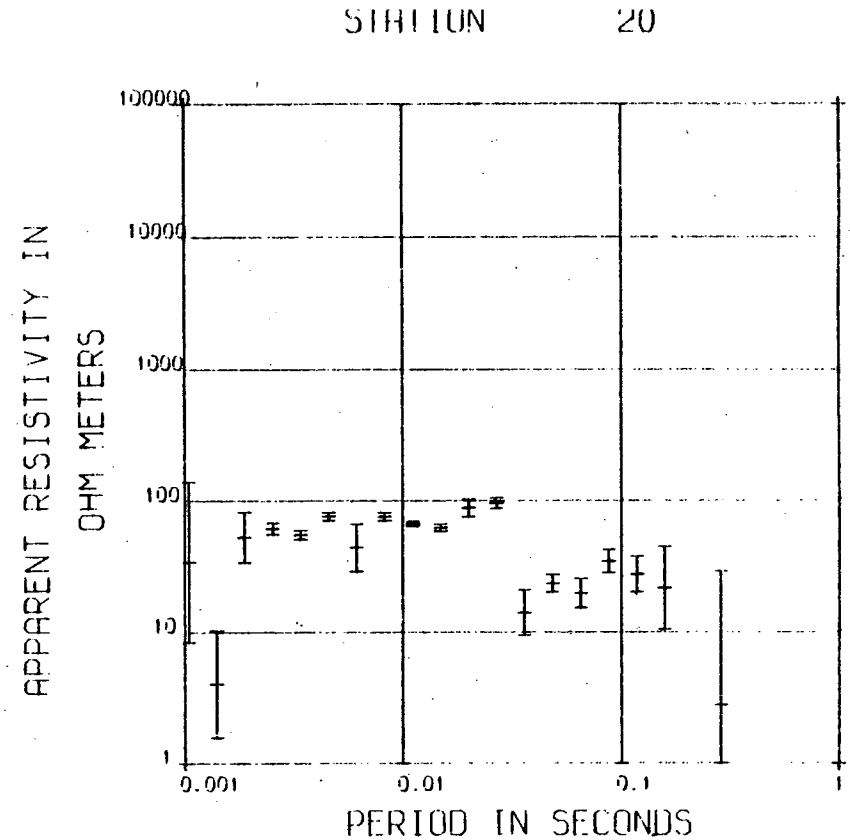
STATION 20
APPARENT RESISTIVITY IN OHM METERS
100000
10000
1000
100
10
1
0.001
0.01
0.1
1
PERIOD IN SECONDS

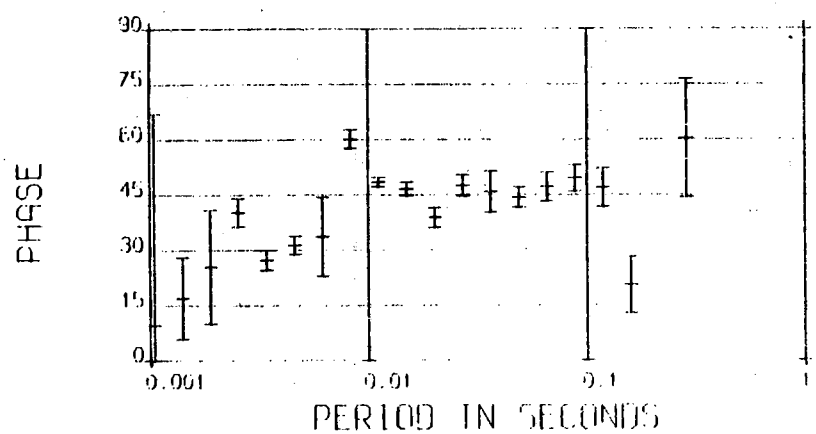
PHASE
90
75
60
45
30
15
0
0.001
0.01
0.1
1
PERIOD IN SECONDS

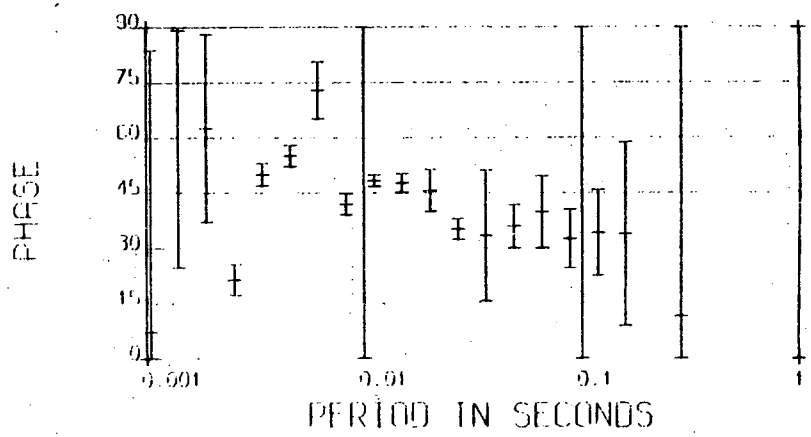
PHASE
90
75
60
45
30
15
0
0.001
0.01
0.1
1
PERIOD IN SECONDS

Station 20

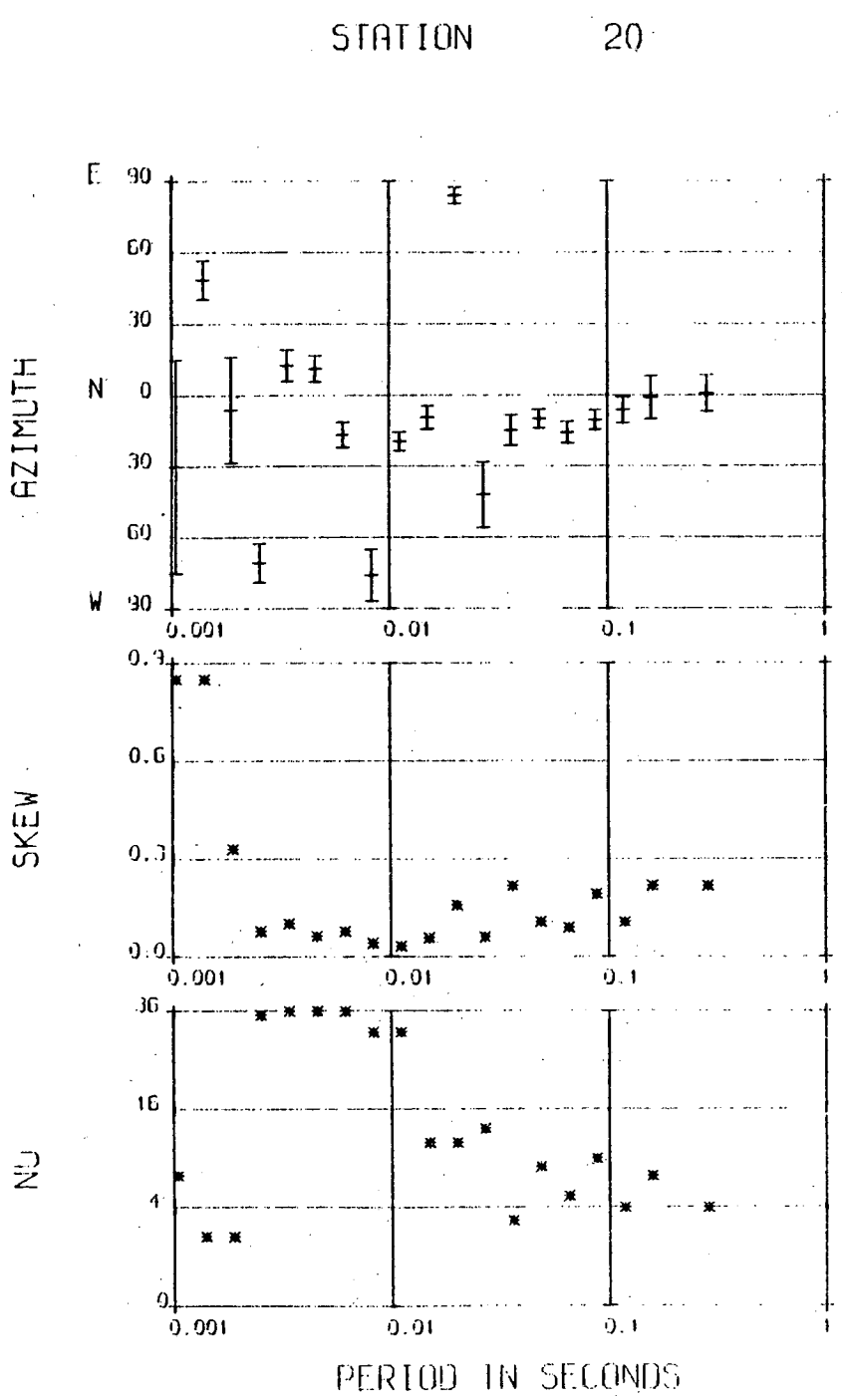
STATION 20
AZIMUTH
E 90
60
30
N 0
30
60
W 90
0.001
0.01
0.1
1
SKEW
0.9
0.6
0.3
0.0
NU
30
15
4
0
PERIOD IN SECONDS

(d)

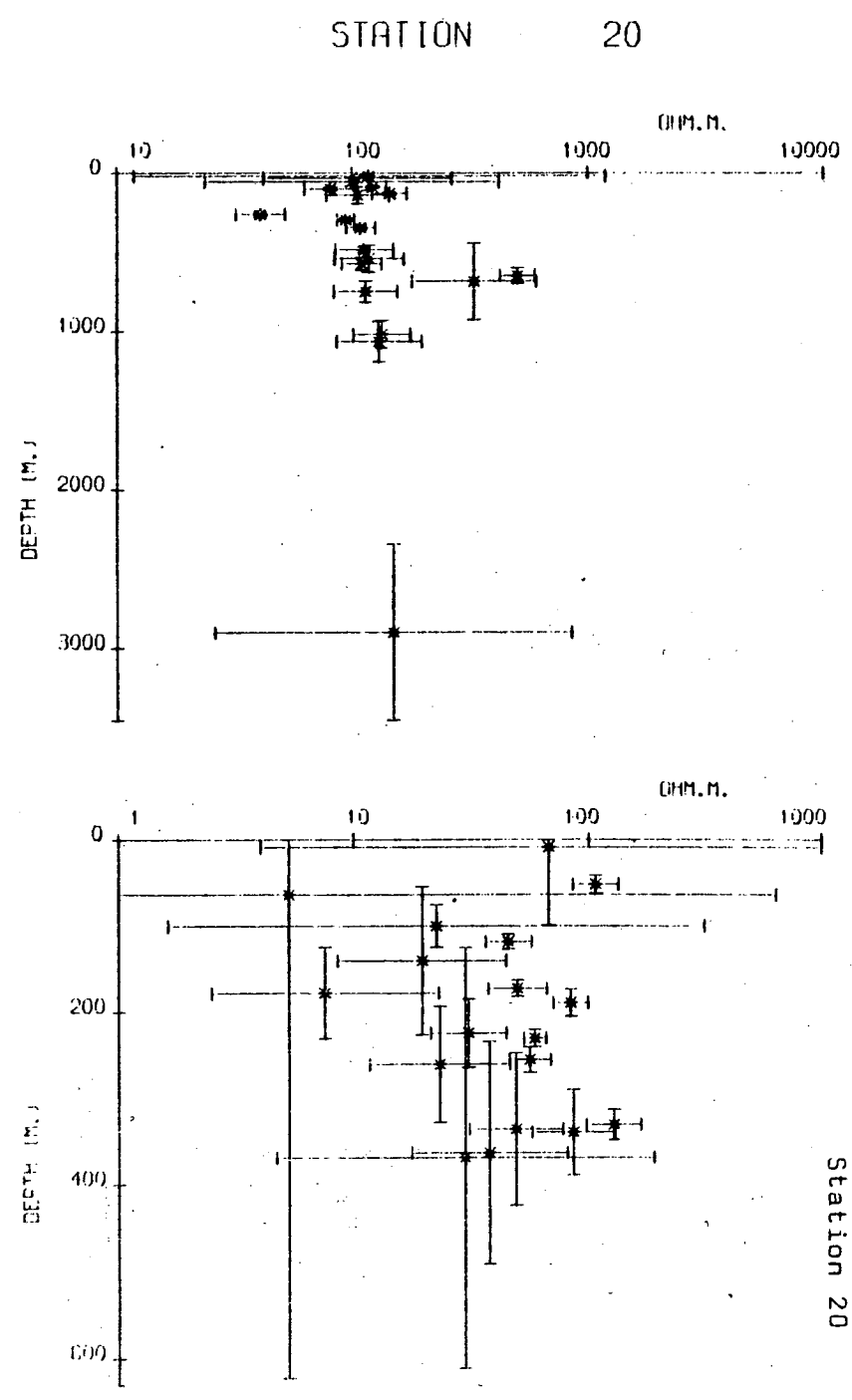
STATION 20
OHM.M.
10
100
1000
10000
0
1000
2000
3000
DEPTH (M.)
OHM.M.
1
10
100
1000
0
200
400
600
DEPTH (M.)
Station 20

Figure 5.3 Station Whitfield

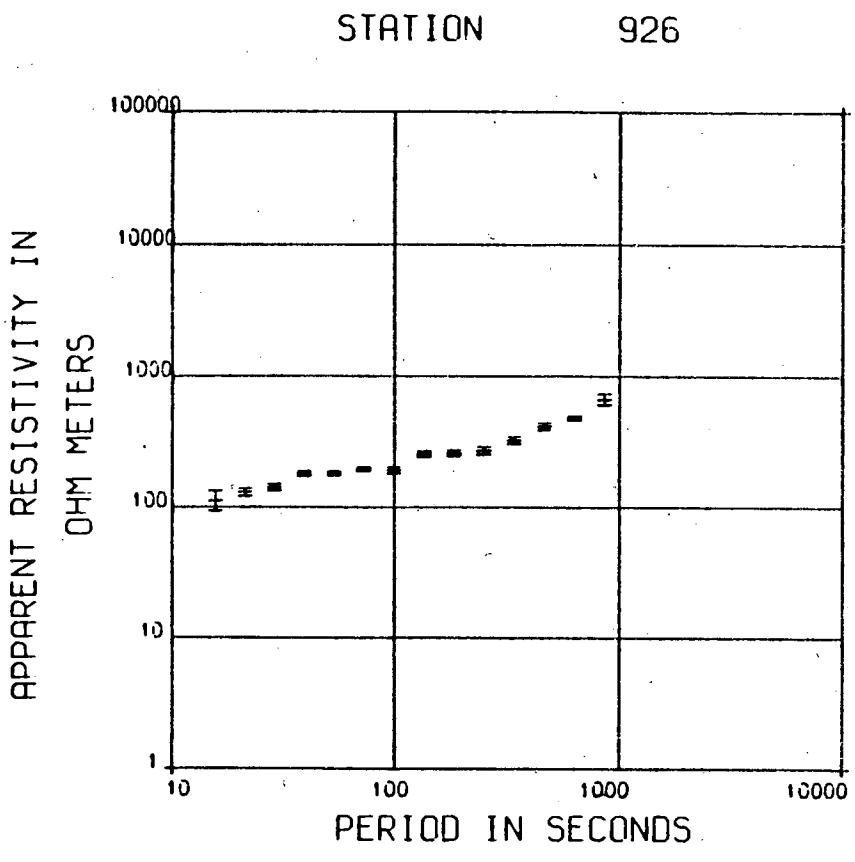

(a)

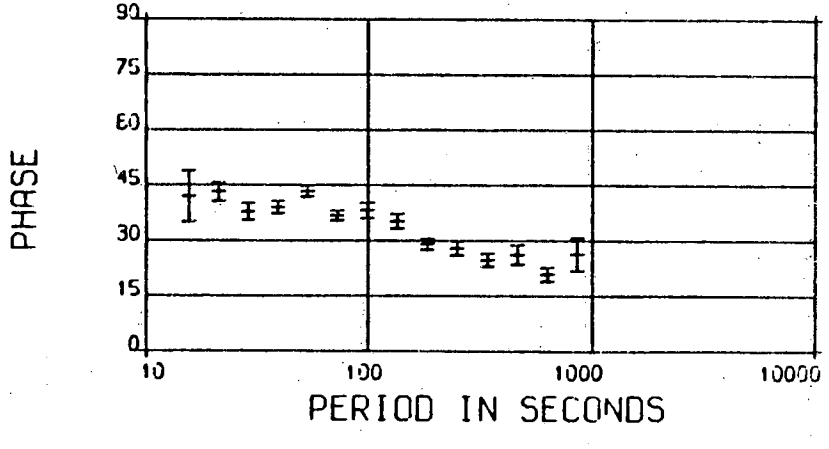

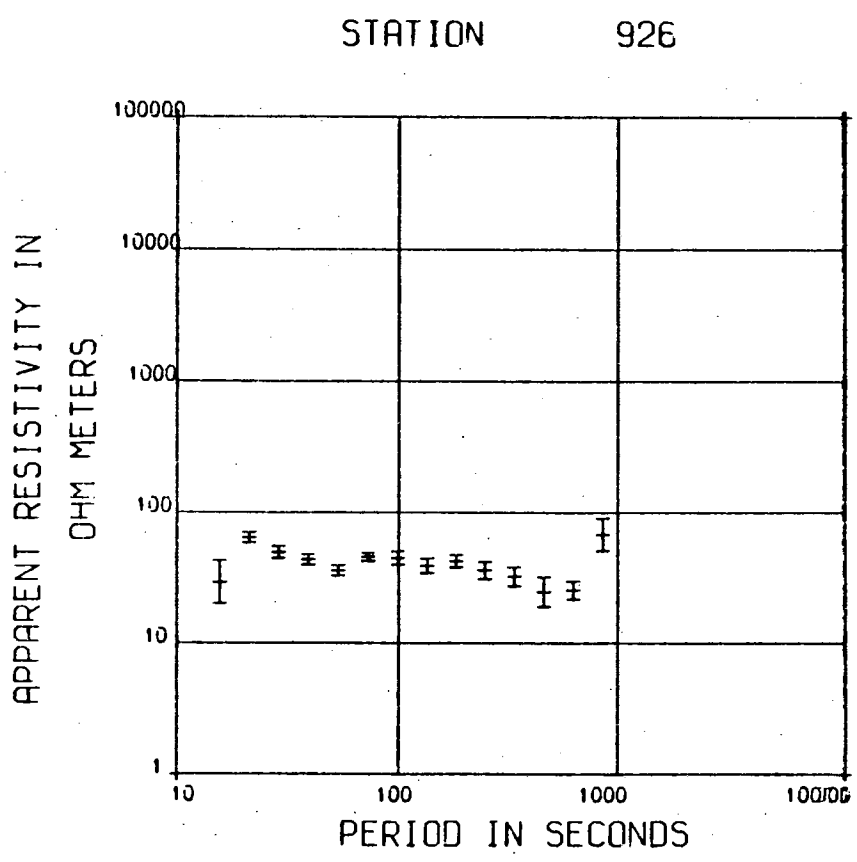

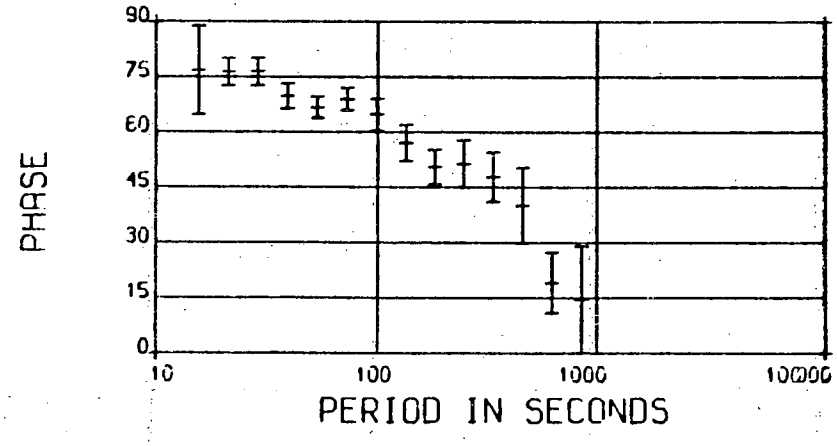

Station 926

(b)

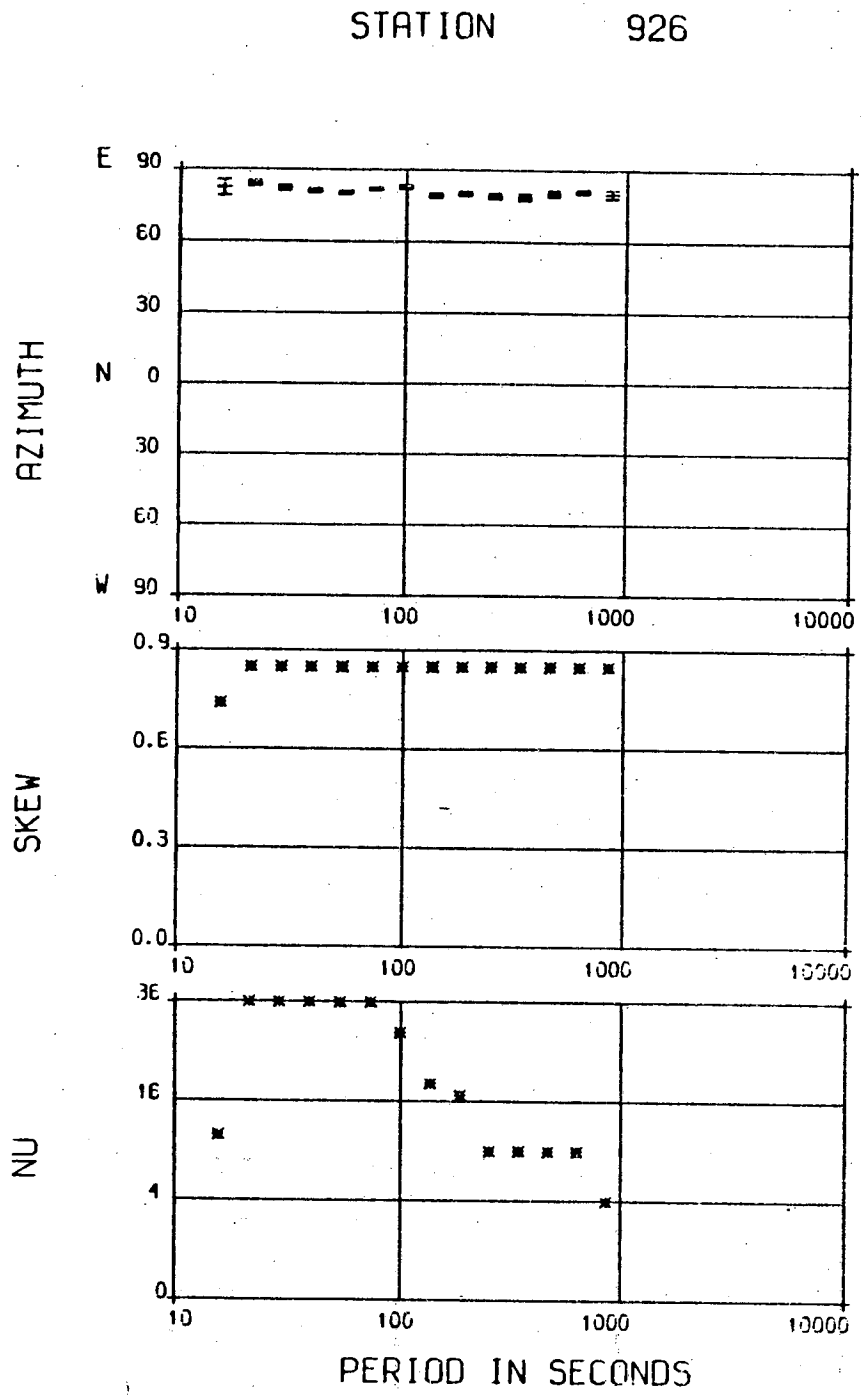

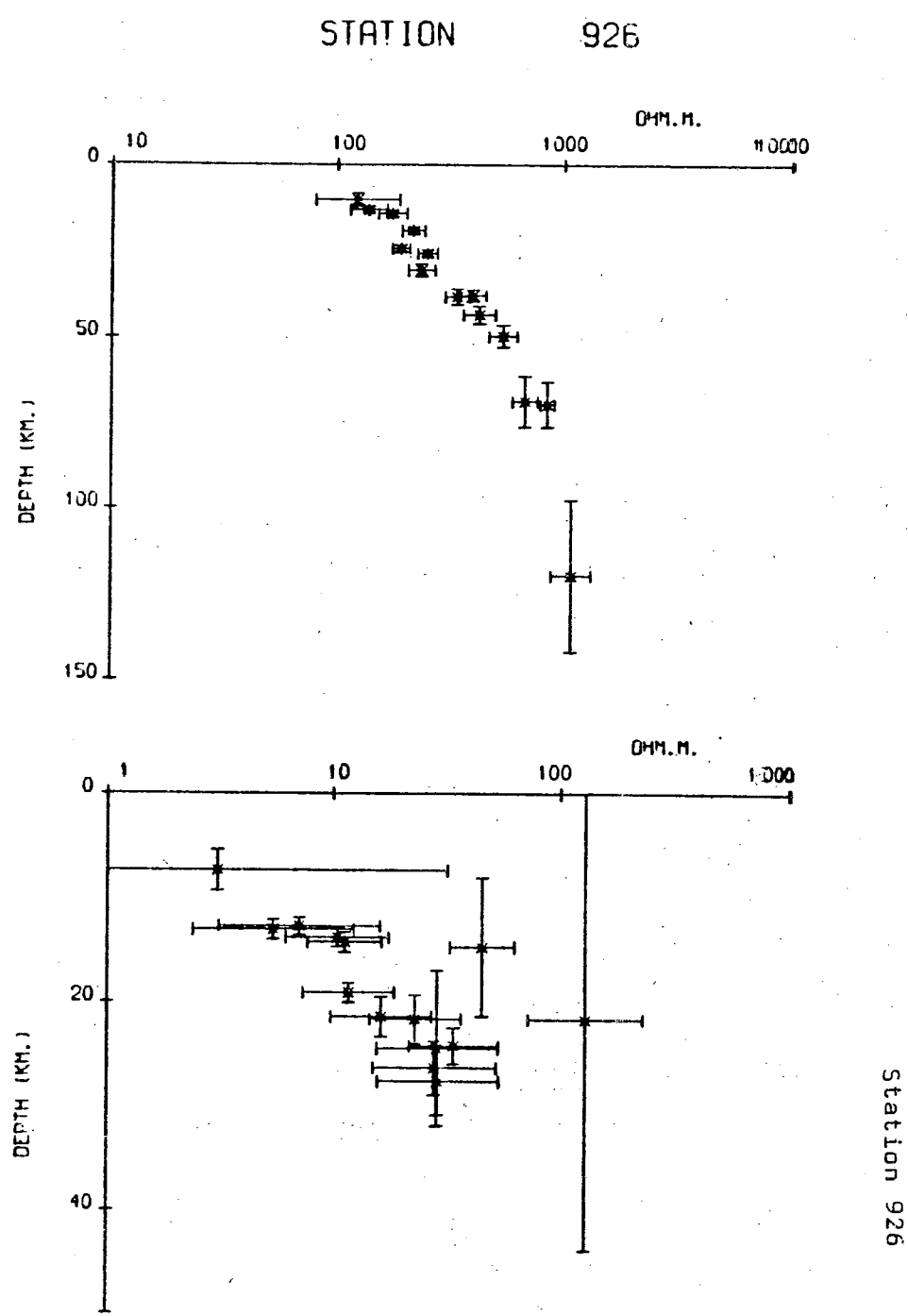

Station 926

STATION 19

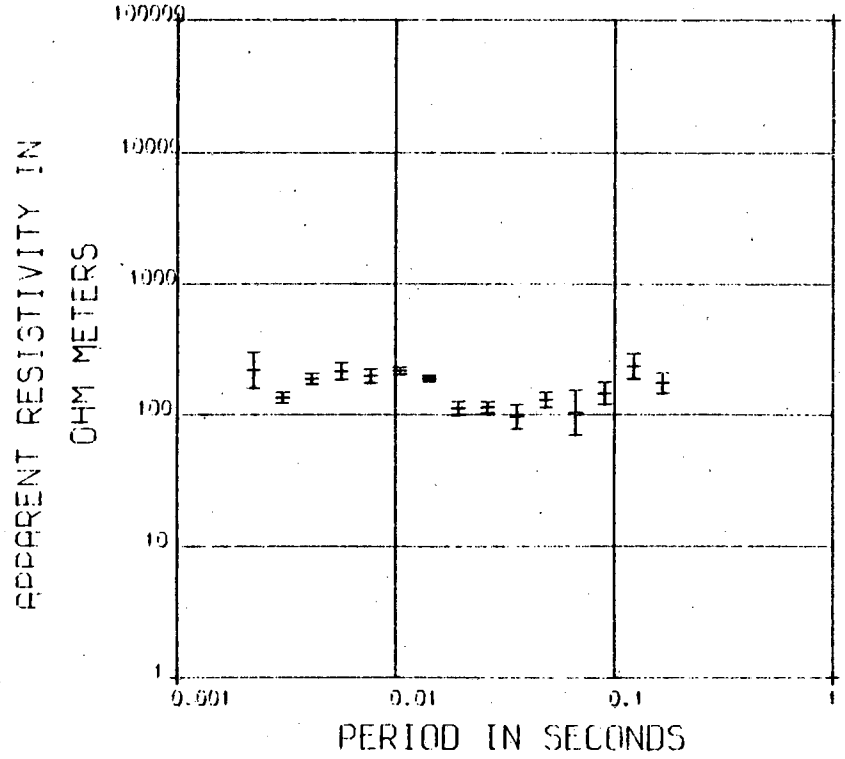

(c)

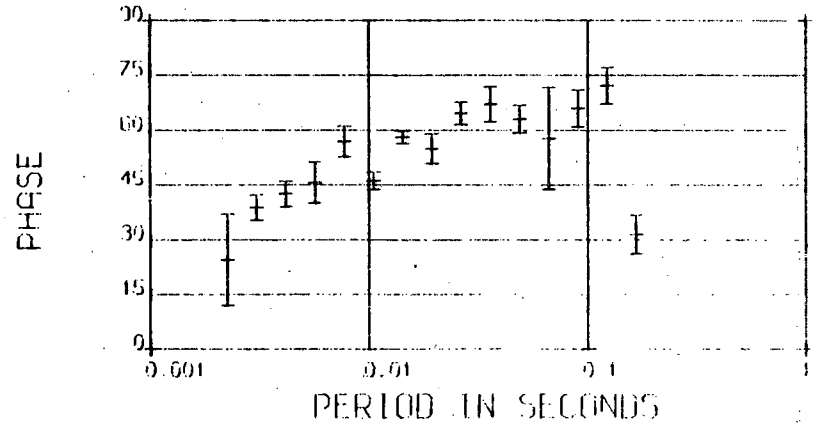

STATION 19

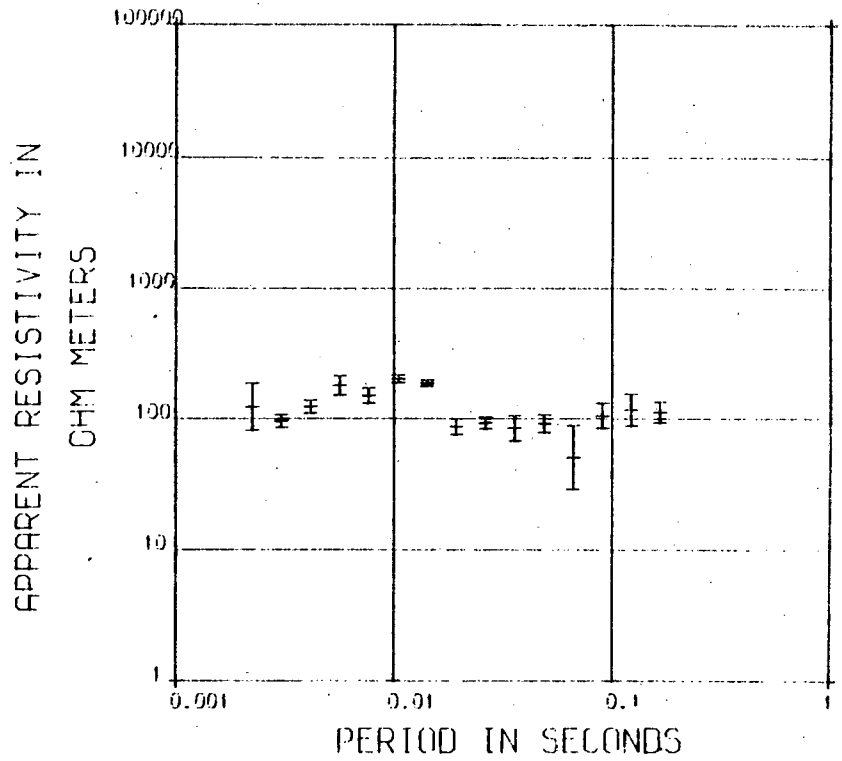

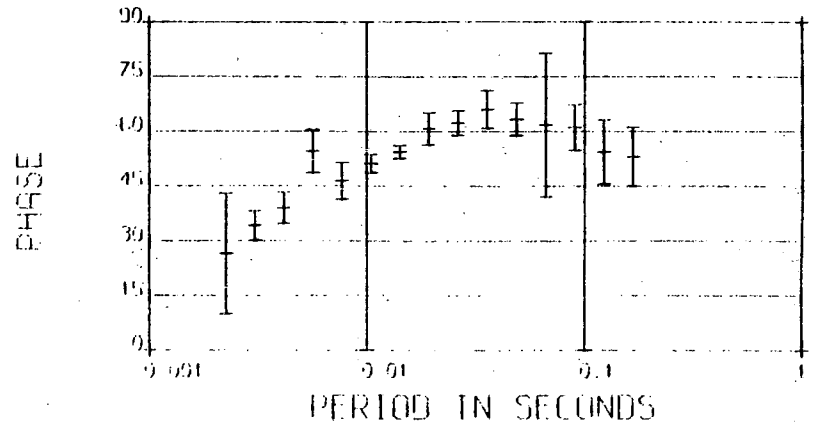

Station 19

STATION 19

(d)

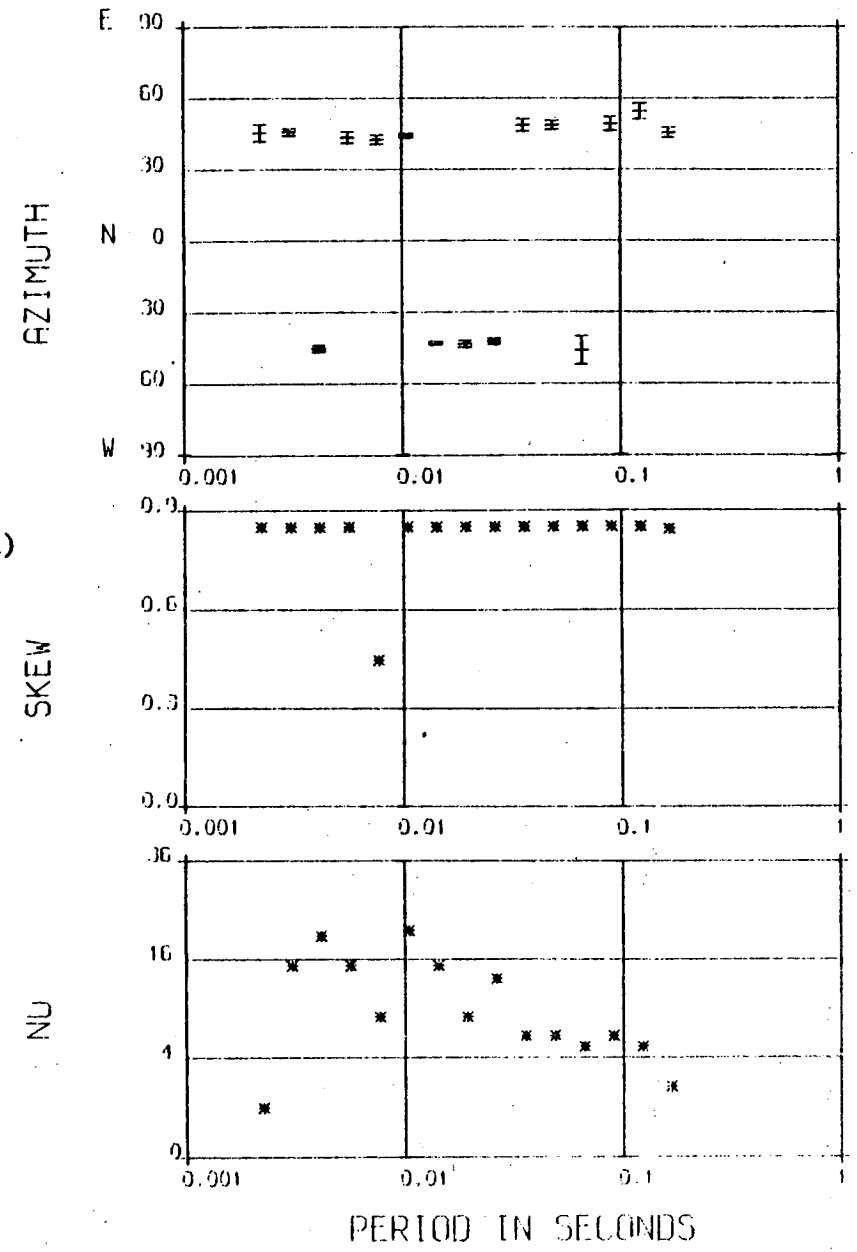

STATION 19

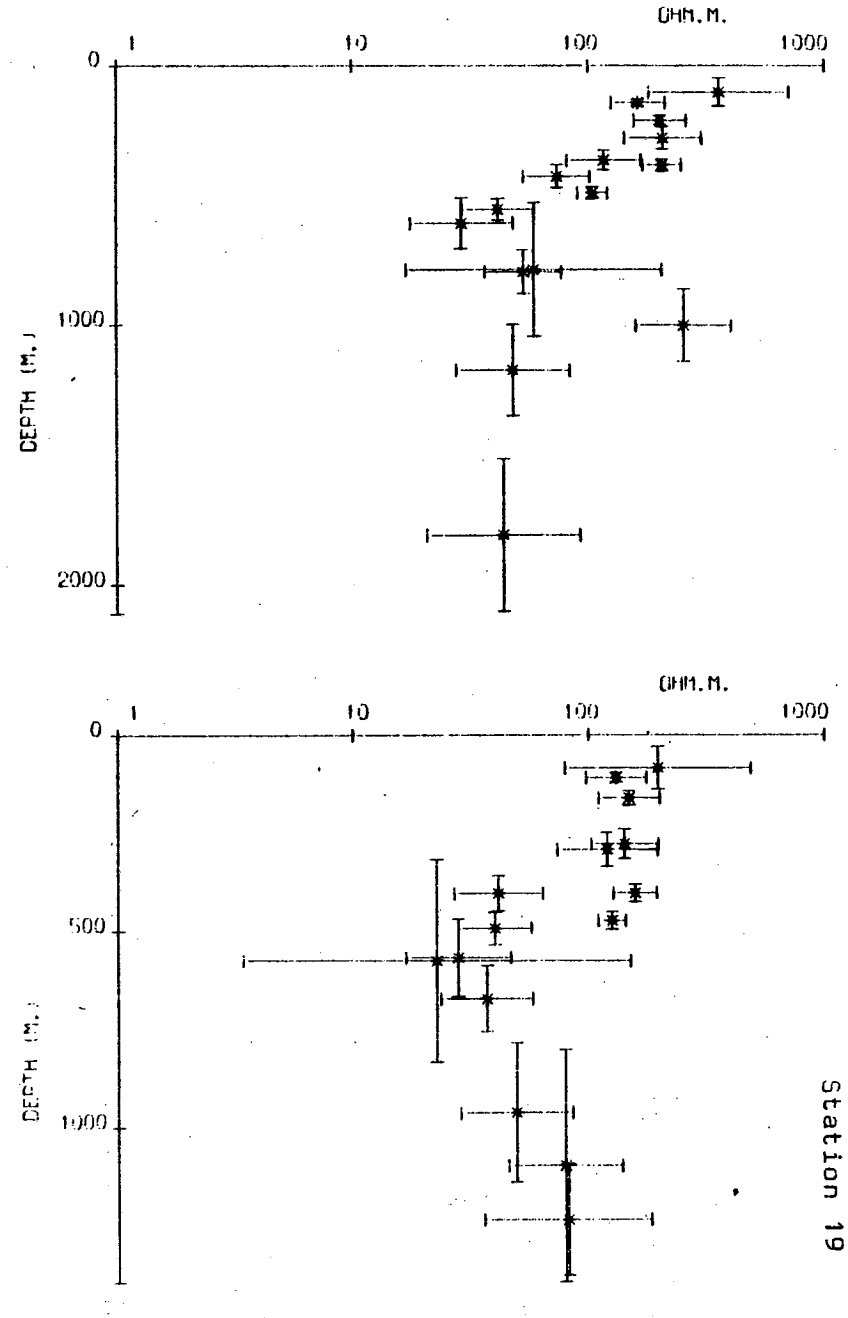

Figure 5.4 Station Sinderhope Shield

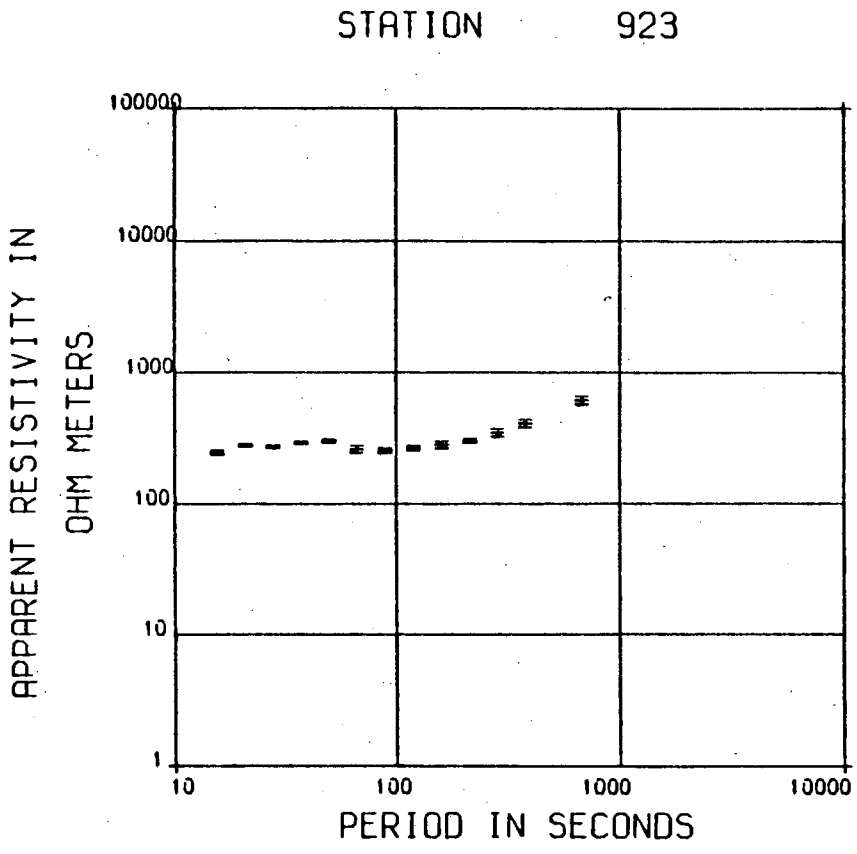

(a)

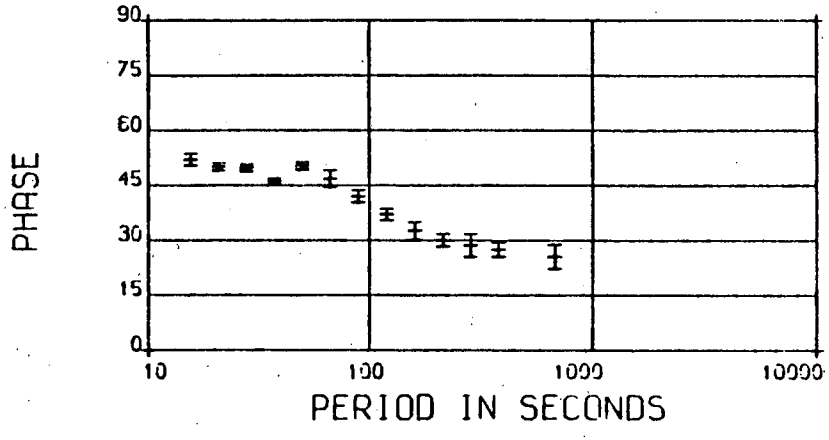

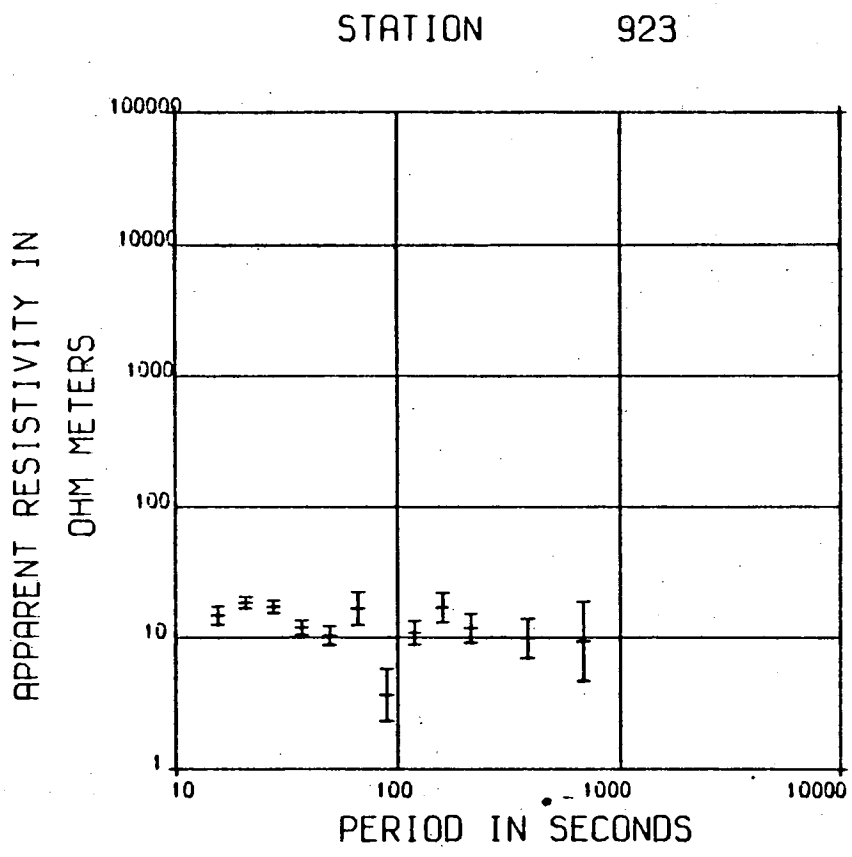

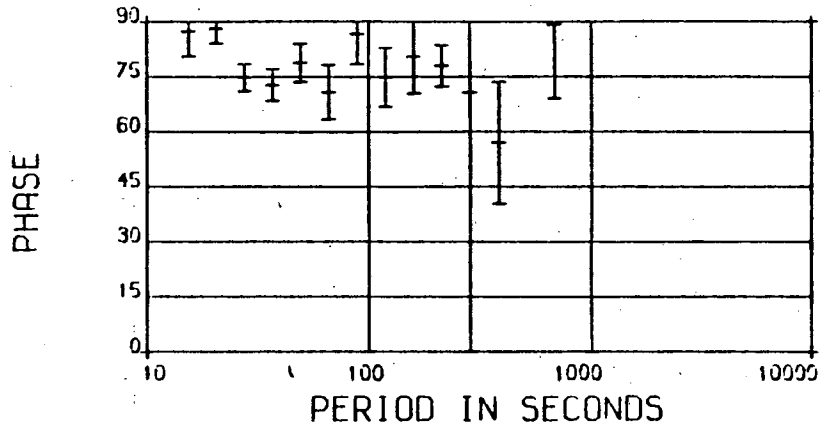

Station 923

(b)

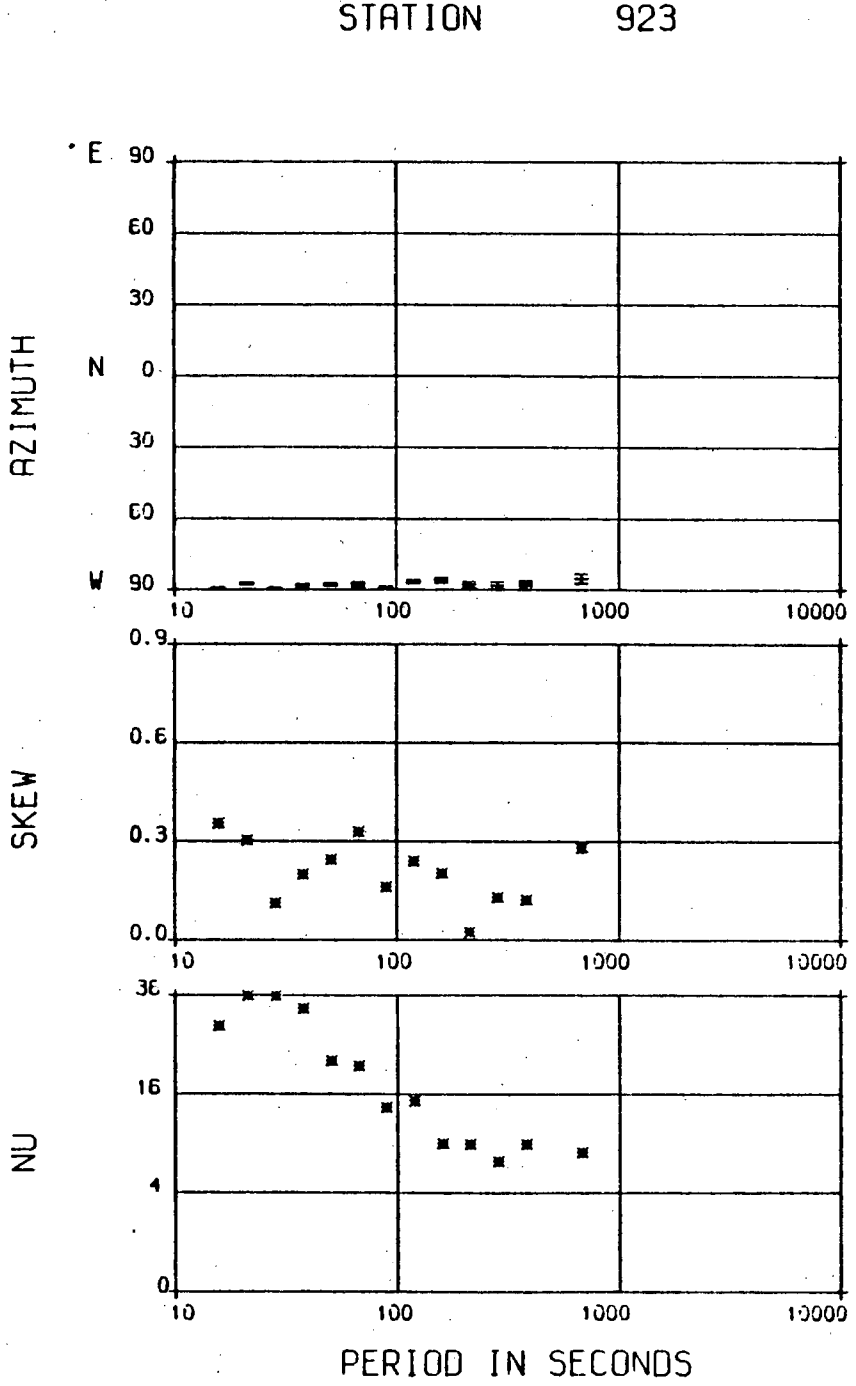
STATION 923
AZIMUTH
E 90
60
30
N 0
30
60
W 90
10
100
1000
10000
SKEW
0.9
0.6
0.3
0.0
NU
36
16
4
0
PERIOD IN SECONDS

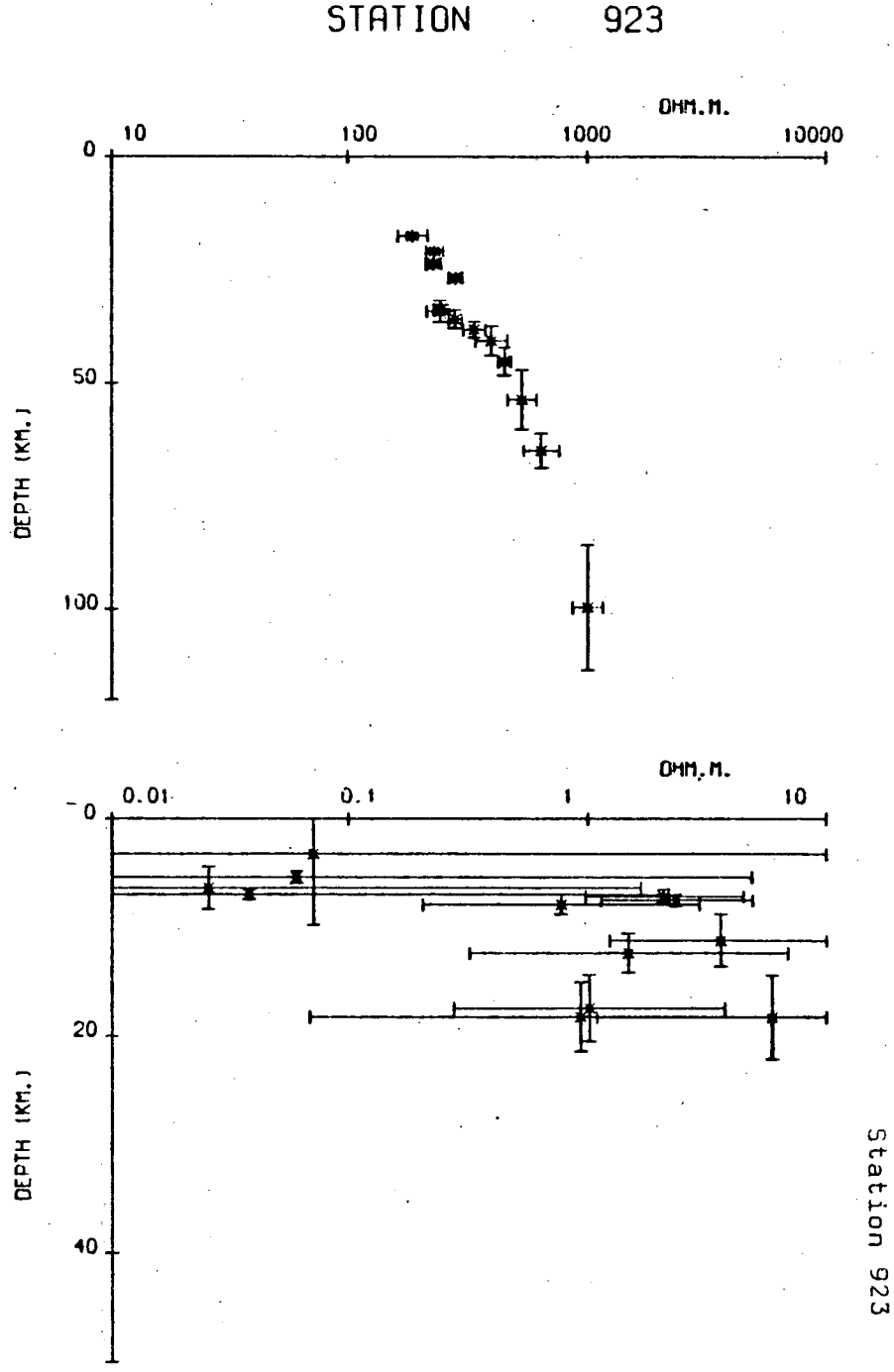
STATION 923
OHM.M.
10
100
1000
10000
0
50
100
DEPTH (KM.)
OHM.M.
0.01
0.1
1
10
0
20
40
DEPTH (KM.)
Station 923

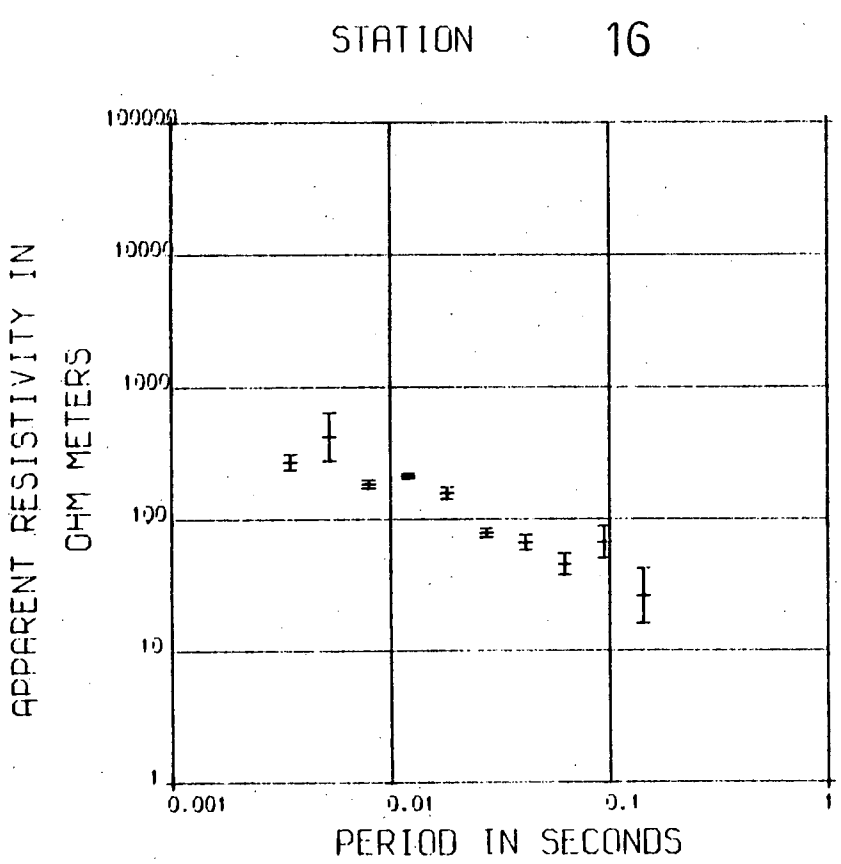
STATION 16
APPARENT RESISTIVITY IN OHM METERS
100000
10000
1000
100
10
1
0.001
0.01
0.1
1
PERIOD IN SECONDS

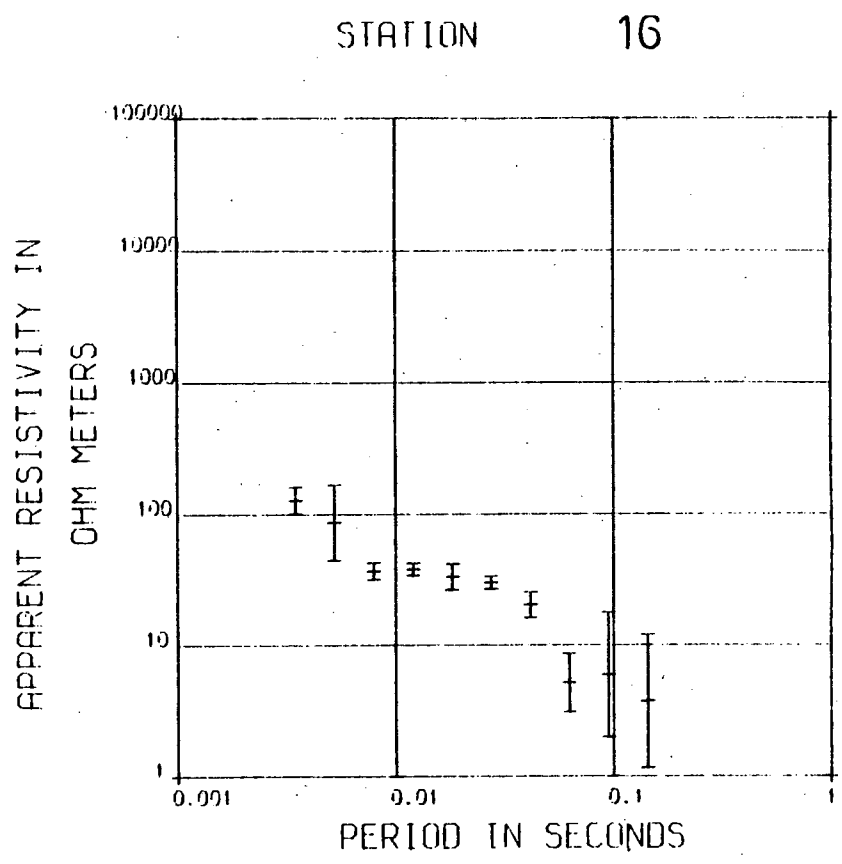
STATION 16
APPARENT RESISTIVITY IN OHM METERS
100000
10000
1000
100
10
1
0.001
0.01
0.1
1
PERIOD IN SECONDS

(c)

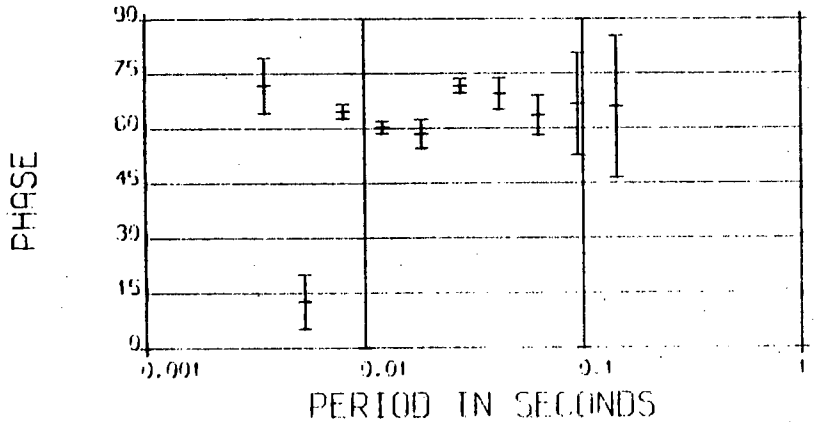
PHASE
90
75
60
45
30
15
0
0.001
0.01
0.1
1
PERIOD IN SECONDS

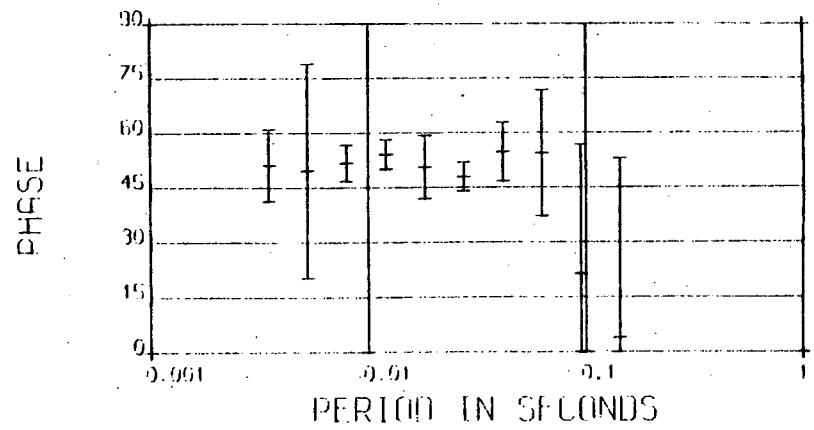
PHASE
90
75
60
45
30
15
0
0.001
0.01
0.1
1
PERIOD IN SECONDS

STATION 16

(d)

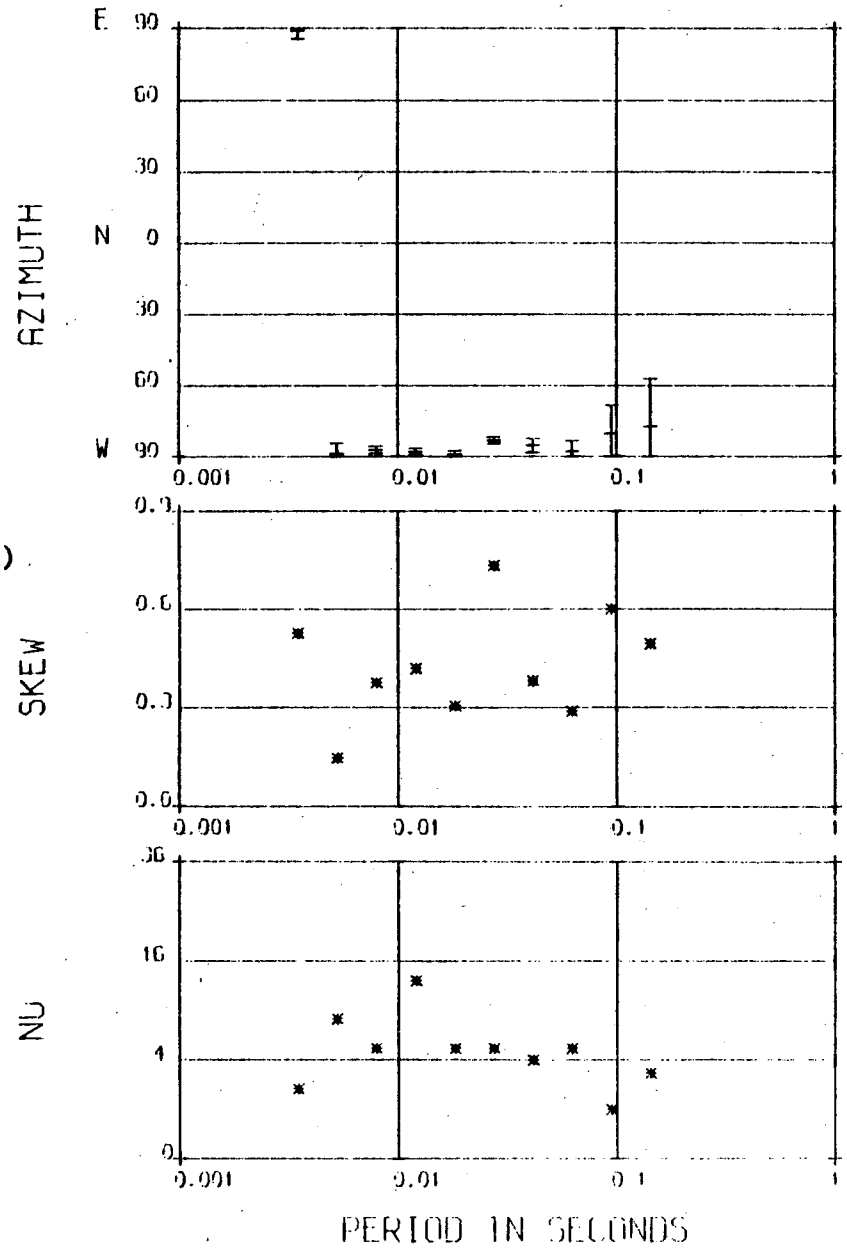

STATION 16

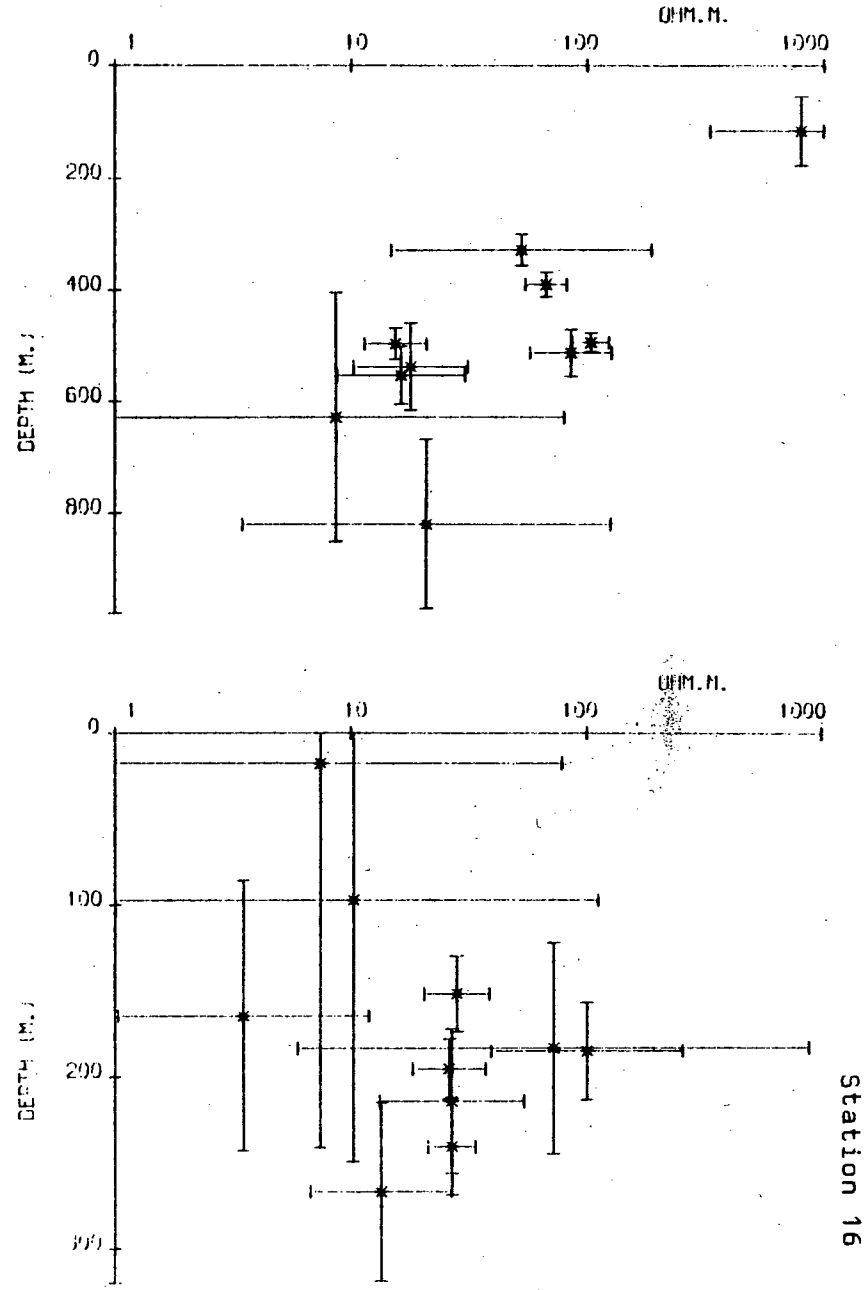

station.

At station SIN the azimuth has a constant value throughout the complete bandwidth. The switch in the values of exactly 90 degrees at WHI is attributed to the major and minor apparent resistivities being of similar magnitudes. At station EDG the azimuth in the high frequency band shows no distinct trend, while at LAM it lies in two well defined directions differing by 60 degrees.

At station LAM in the north the skew factor, defined in section 2.3(Ch2), is low particularly at long periods where it does not exceed 0.15. Such a value is less than 0.4 and consequently is indicative of 'weak two-dimensionality' as suggested by Swift's (1972) definition. Values greater than 0.8 constitute a large skew, while those in between are considered as indicating a medium skew. The skew is also low at EDG at short periods but high at long periods. At WHI the skew values are very high for the whole bandwidth, while at SIN they lie between 0.3 and 0.6 at short periods, decreasing to less than 0.4 at long periods.

The number of estimates averaged at each station shows a typical trend, rising from 4 estimates at 1000 seconds to over 36 at 100 seconds and only falling below that number at the last average, at 20 seconds. Similarly for the short periods the number of estimates rises from 4 at 4 Hz to 36 at 100 Hz and typically falls below that

level above 500 Hz. The only exception is station SIN where the number is less for the high frequency measurement. This is consistent with noise contamination during recording.

5.1.2 Traverse to the South

The three remaining stations SWINHOPE SHIELD (SWI), ROOKHOPE (ROO) and HILLEND (HIL) fall under this heading. The maximum apparent resistivity curves show a distinct change, throughout the complete bandwidth (see figures 5.5-5.7). The shape of the curves at the high frequency end becomes more varied assuming first a high value of over 100 ohm-m and then a low value of 10 ohm-m at approximately 10 Hz. At the long periods the ρ major curves rise by about an order of magnitude. The major phases show first a decrease from 75 degrees to about 30 degrees in the frequency range 100 Hz to 5 Hz, (with a sharp increase from 0 - 75 at the very short periods at station HIL) and then, for the long period data, a very well defined gradual fall at all stations, from 50 degrees - 20 degrees across the three decades of that frequency range.

The ρ minor curves have similar magnitude to the ρ major curves in the high frequency band becoming lower at longer periods. The phases also show very similar responses, although they are consistently less well estimated.

Figure 5.5 Station Swinhope Shield

(a)

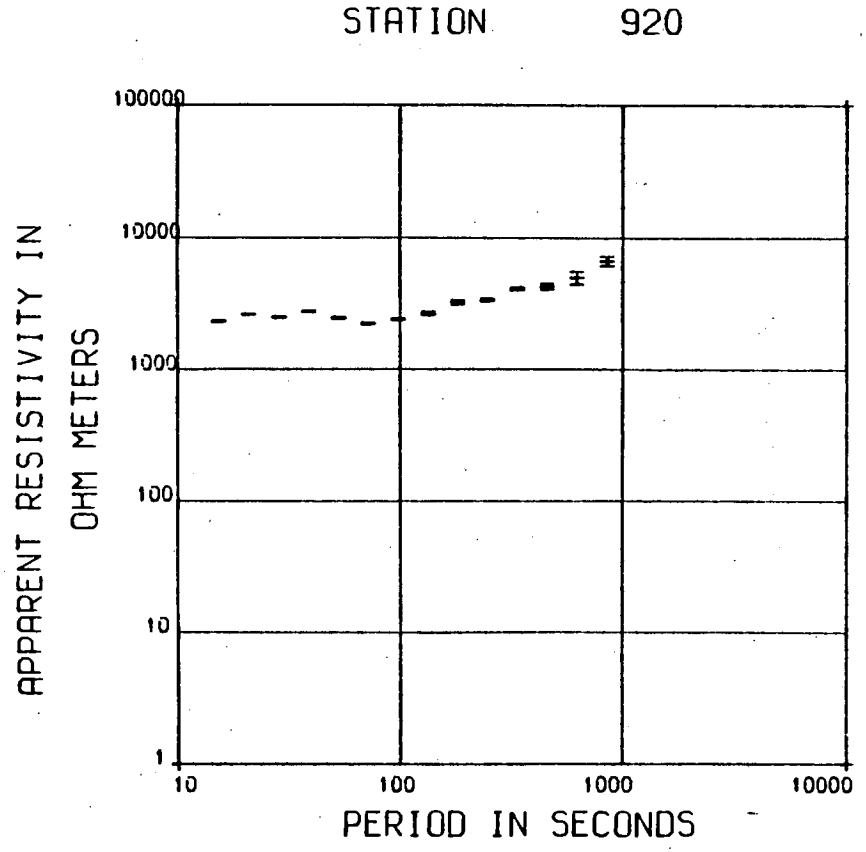

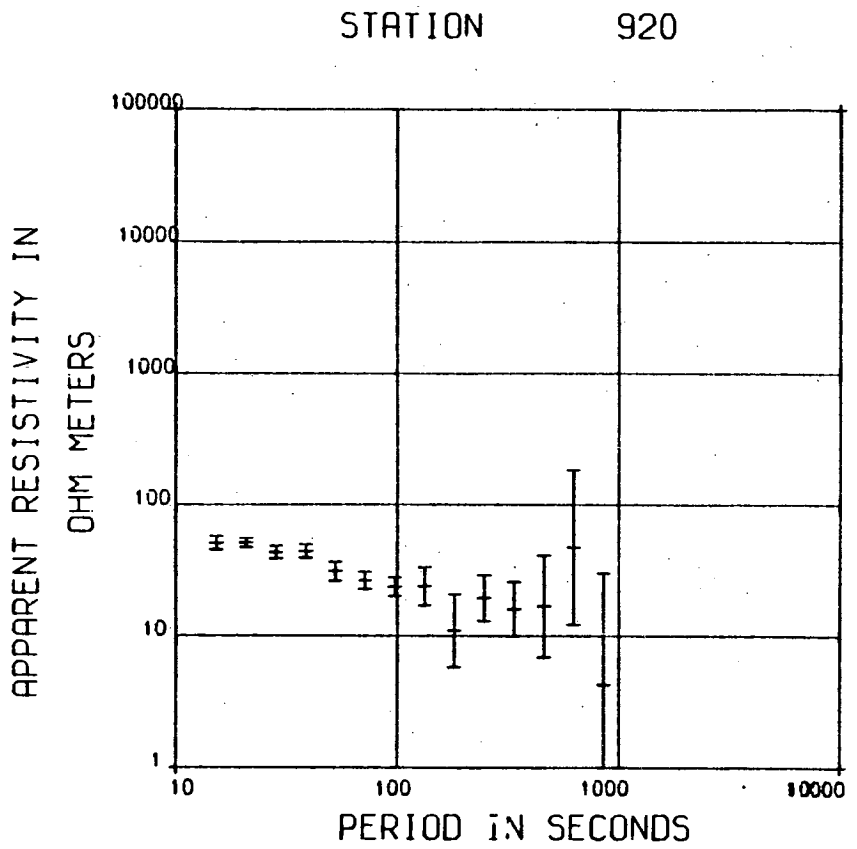

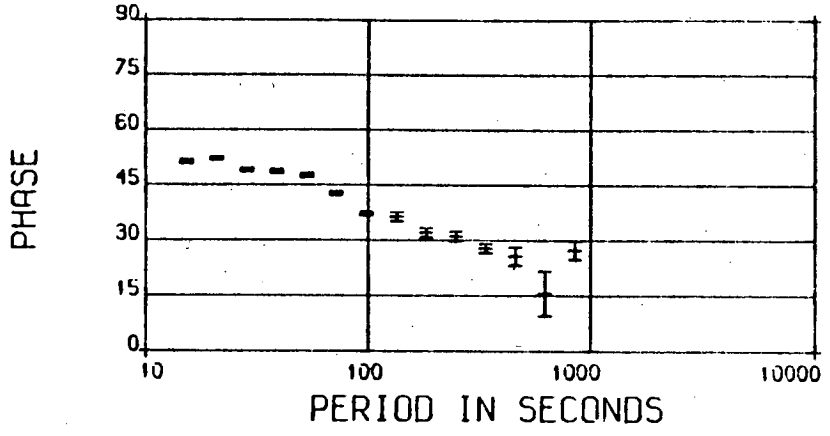

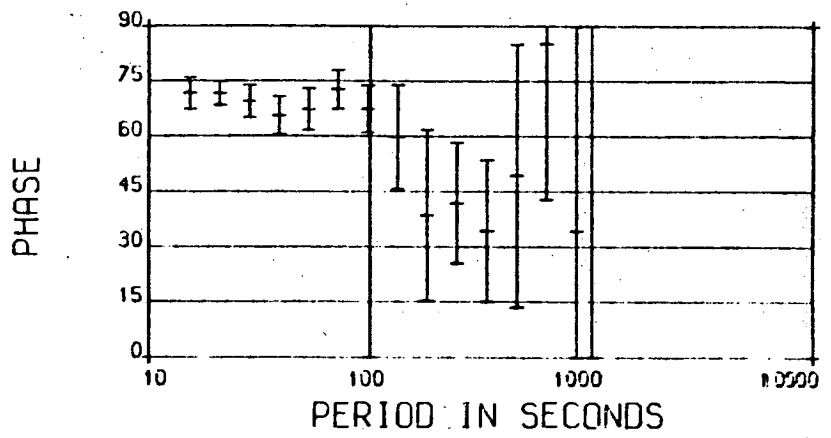

Station 920

(b)

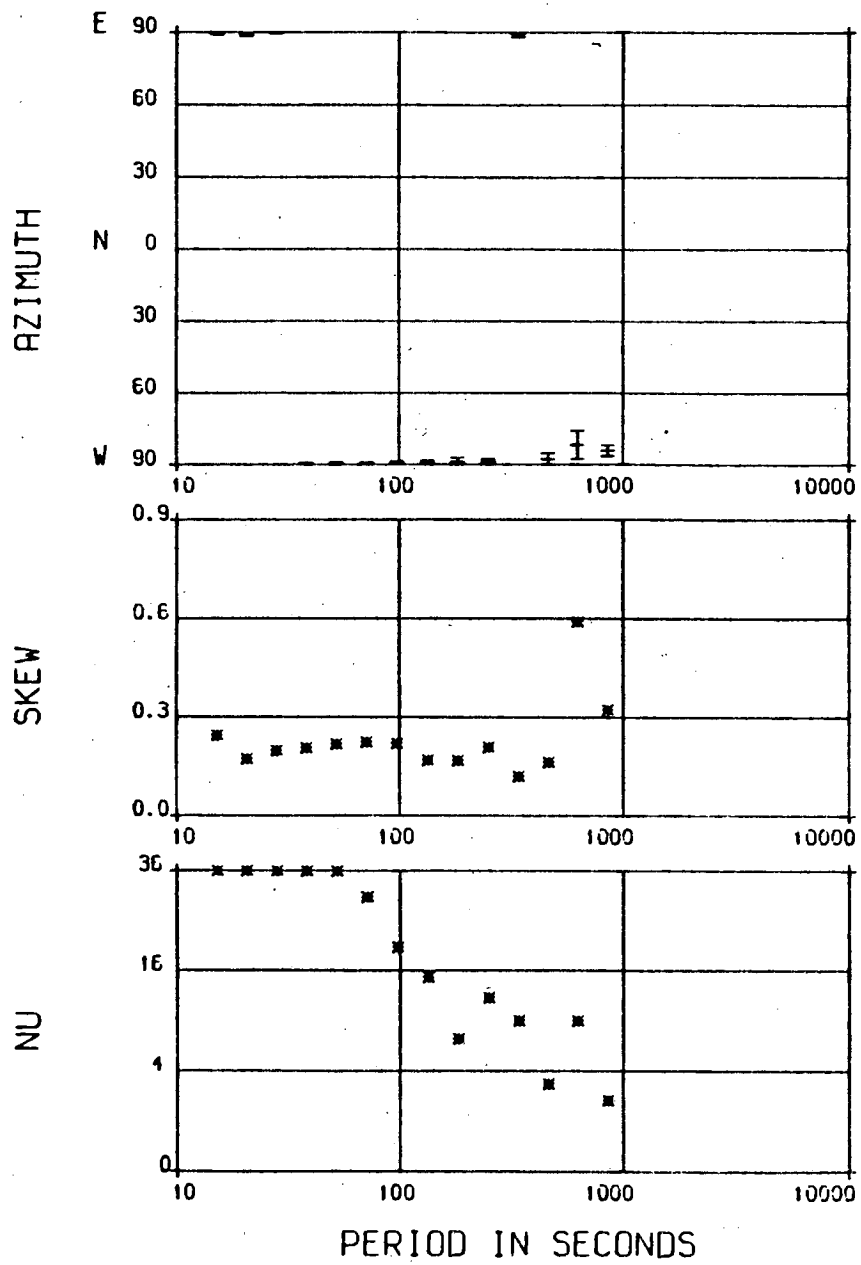
STATION 920
AZIMUTH
E 90
60
30
N 0
30
60
W 90
10
100
1000
10000
SKEW
0.9
0.6
0.3
0.0
NU
36
16
4
0
PERIOD IN SECONDS

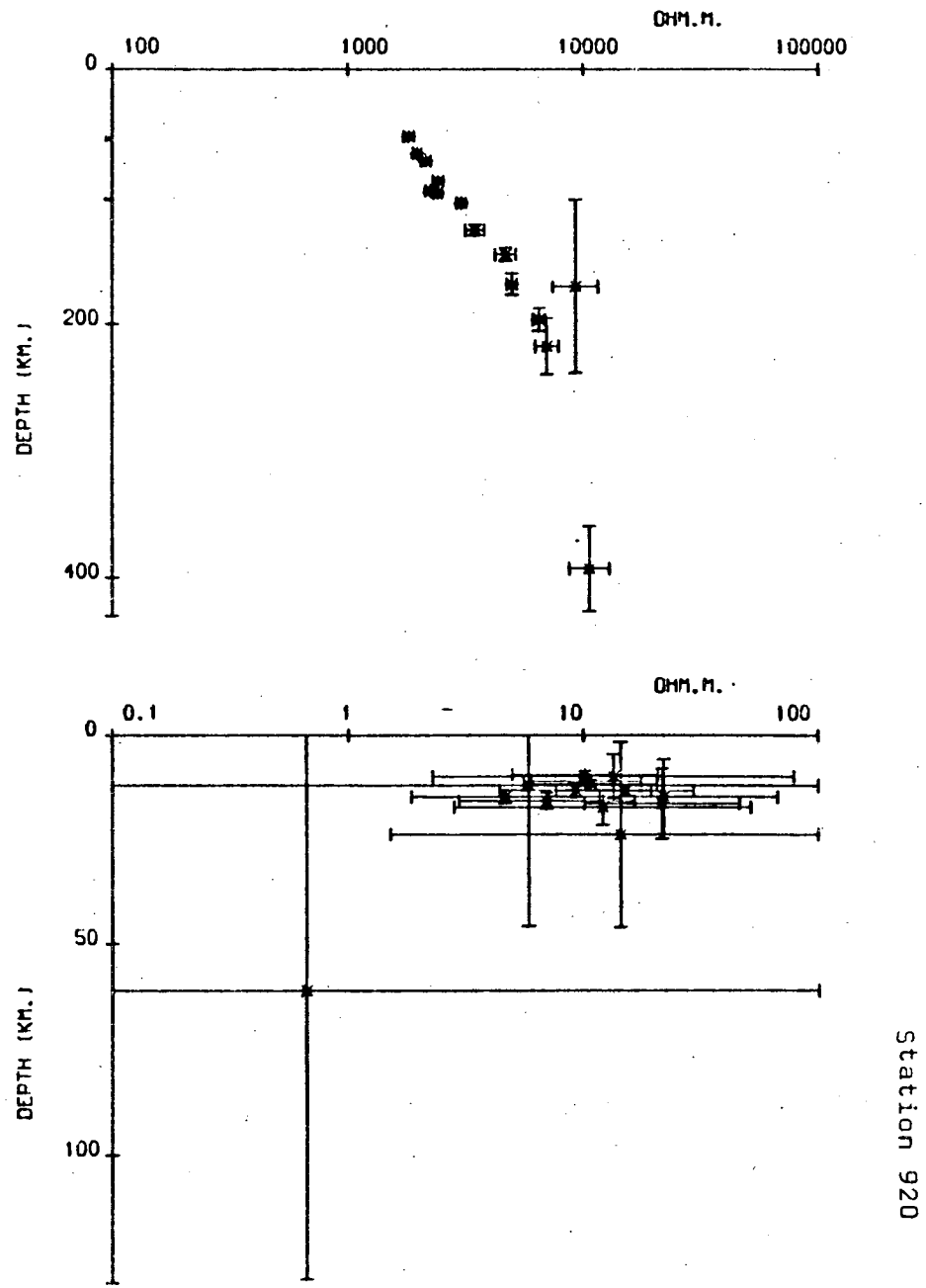
STATION 920
OHM.M.
100
1000
10000
100000
0
200
400
DEPTH (KM.)
OHM.M.
0.1
1
10
100
0
50
100
DEPTH (KM.)
Station 920

(c)

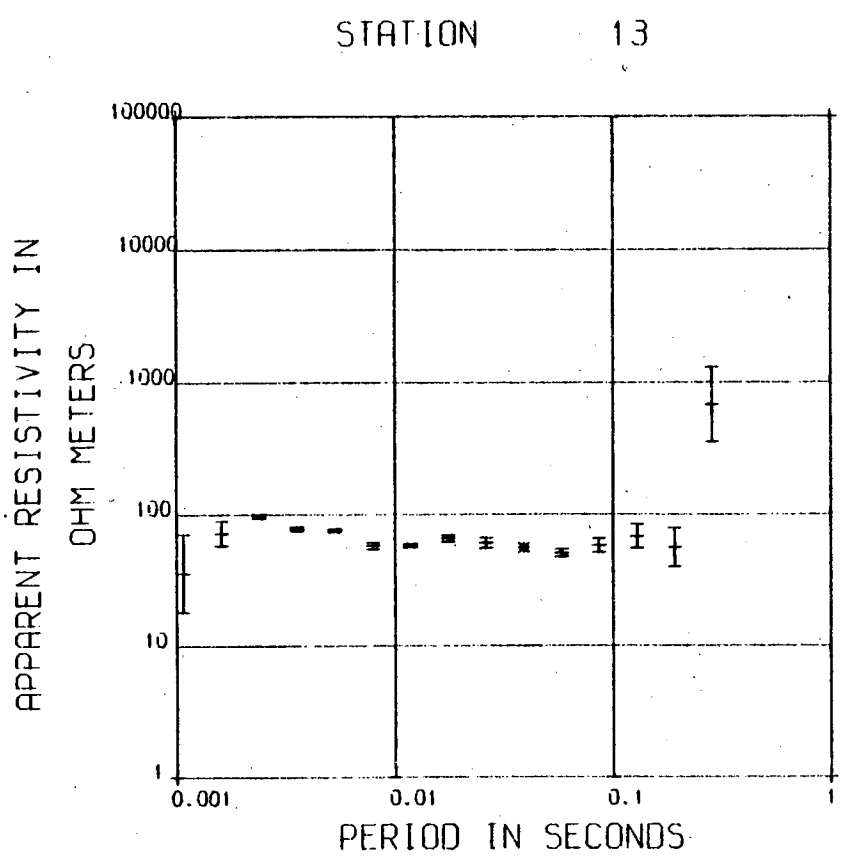
STATION 13
APPARENT RESISTIVITY IN OHM METERS
100000
10000
1000
100
10
1
0.001
0.01
0.1
1
PERIOD IN SECONDS

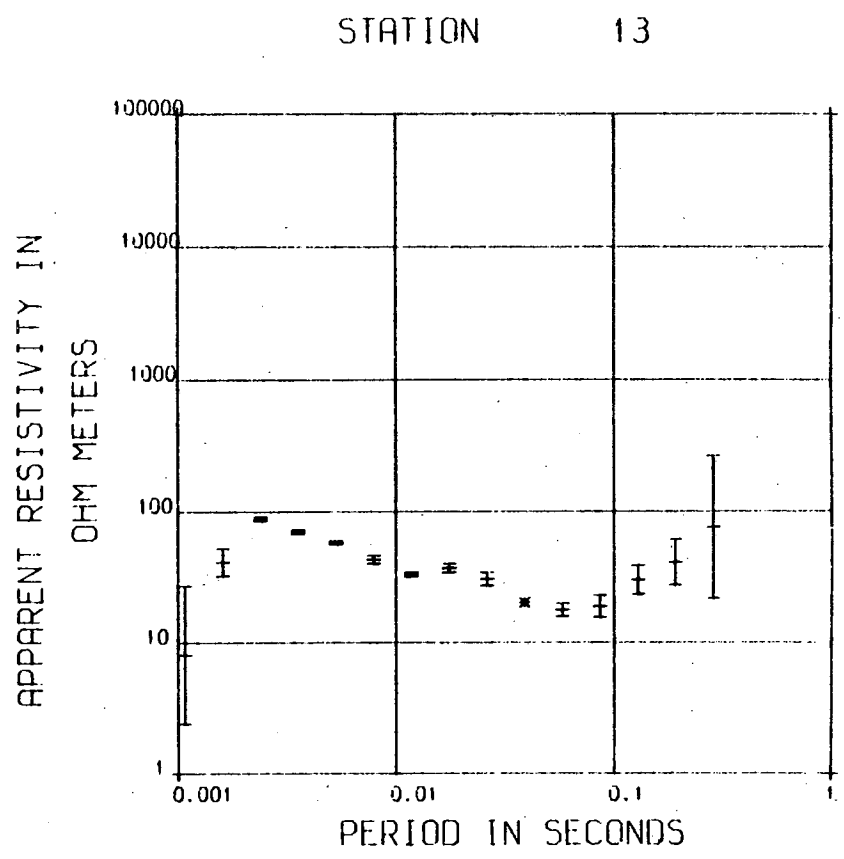
STATION 13
APPARENT RESISTIVITY IN OHM METERS
100000
10000
1000
100
10
1
0.001
0.01
0.1
1
PERIOD IN SECONDS

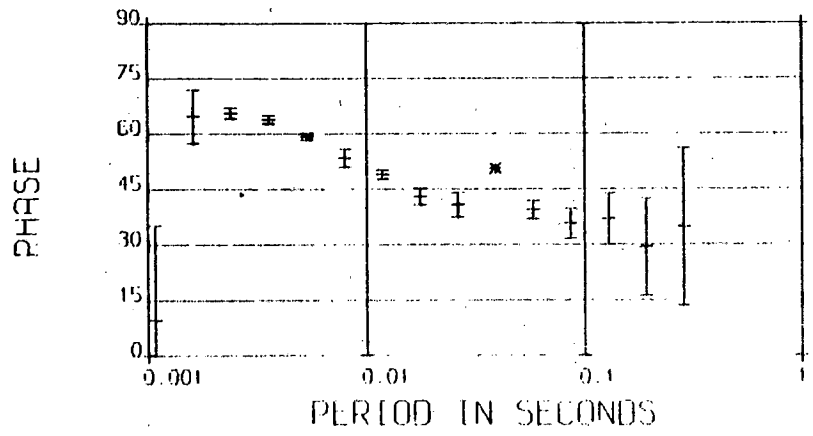
PHASE
90
75
60
45
30
15
0
0.001
0.01
0.1
1
PERIOD IN SECONDS

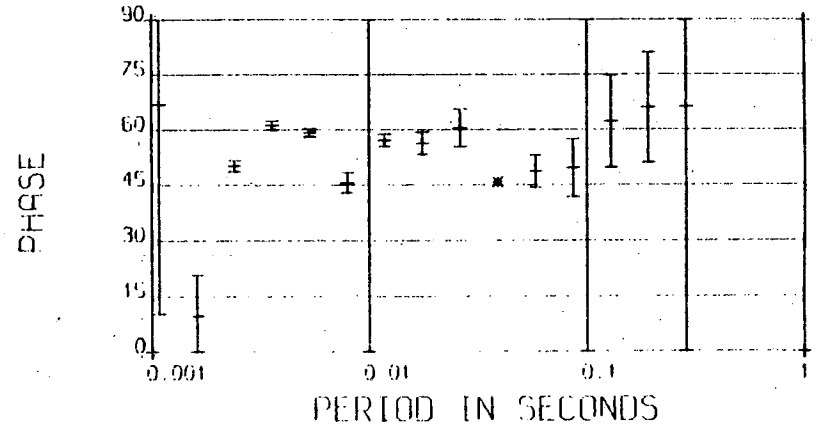
PHASE
90
75
60
45
30
15
0
0.001
0.01
0.1
1
PERIOD IN SECONDS

Station 13

(d)

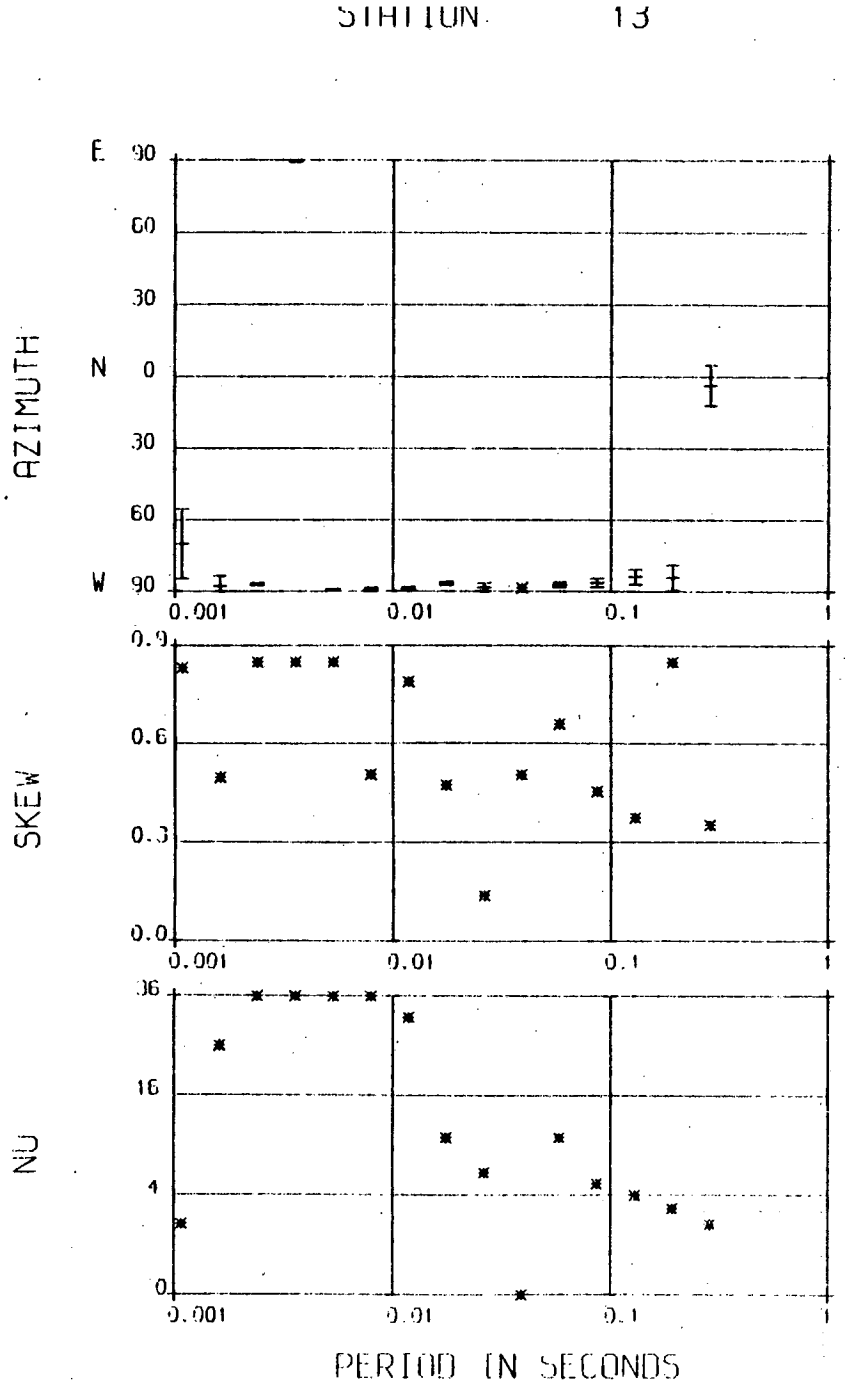
STATION 13
AZIMUTH
E 90
60
30
N 0
30
60
W 90
0.001
0.01
0.1
1
SKEW
0.9
0.6
0.3
0.0
NU
16
4
0
PERIOD IN SECONDS

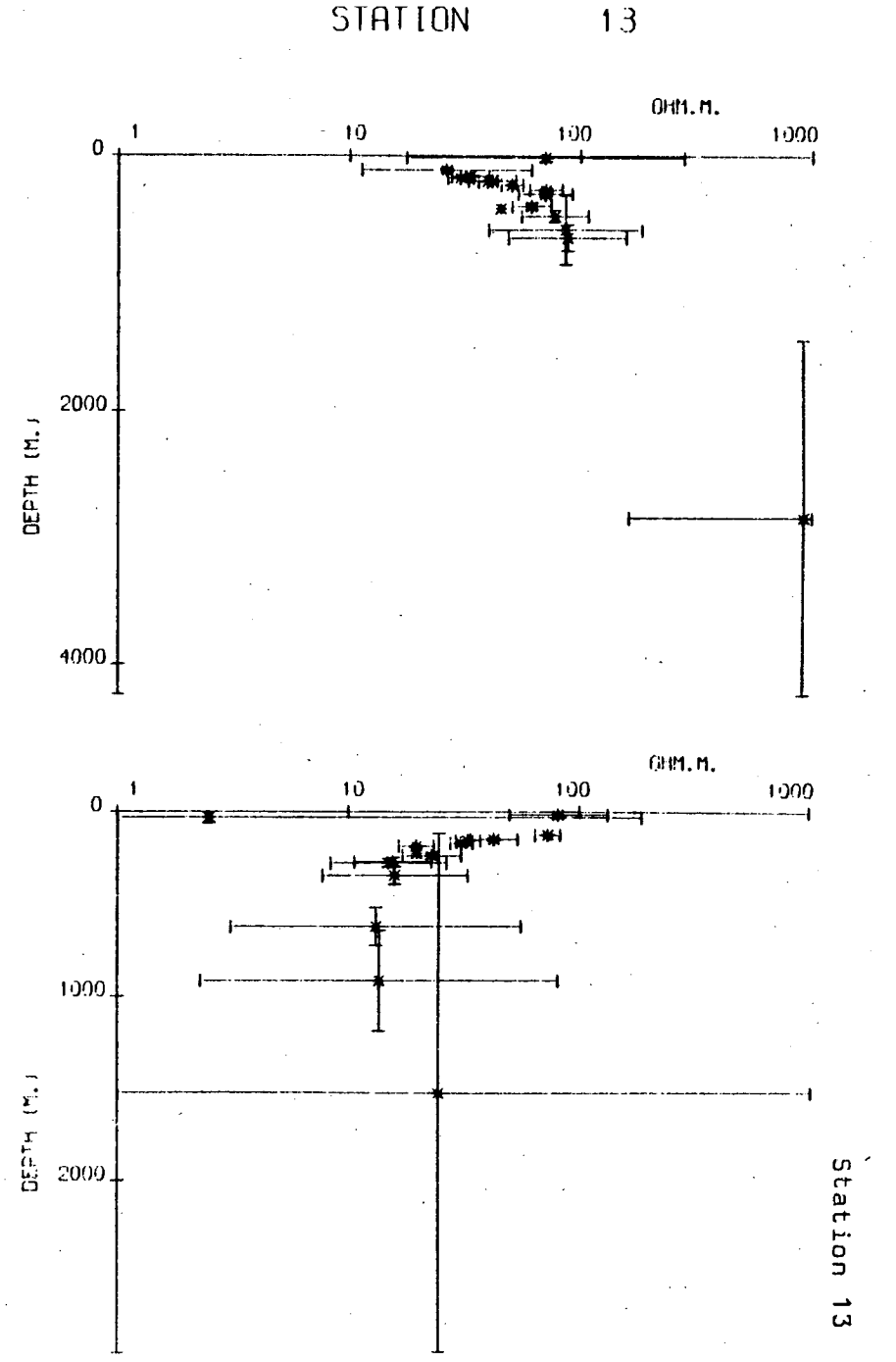
STATION 13
OHM.M.
1
10
100
1000
0
2000
4000
DEPTH (M.)
OHM.M.
1000
2000
Station 13

Figure 5.6 Station Rookhope (I)

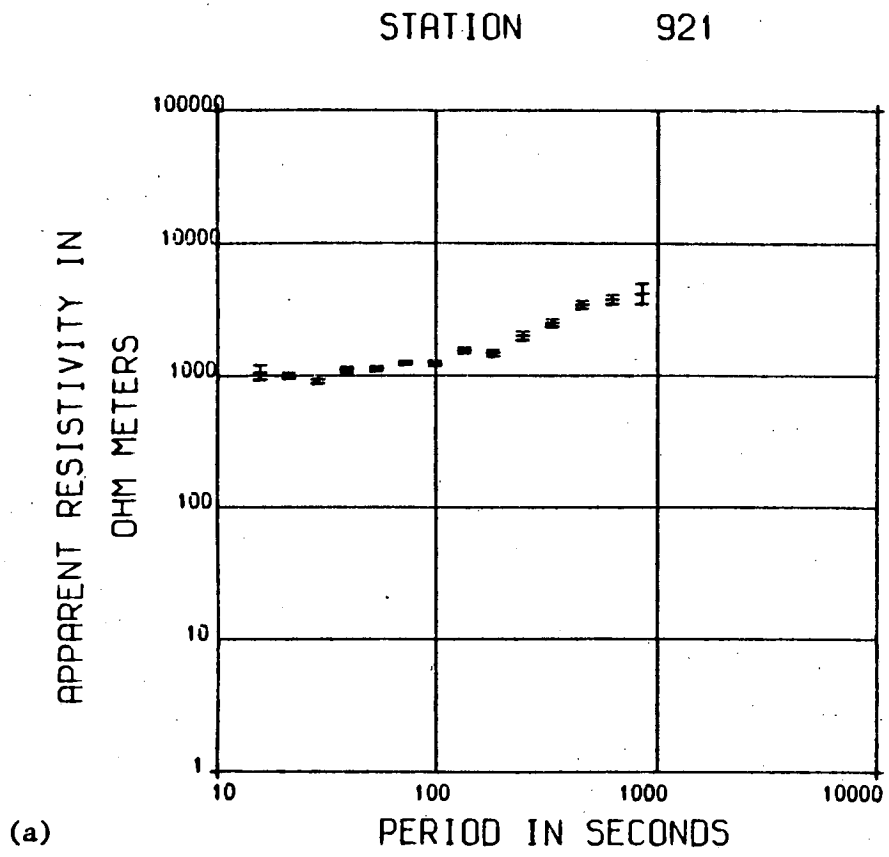
STATION 921
APPARENT RESISTIVITY IN OHM METERS
100000
10000
1000
100
10
1
10
100
1000
10000
PERIOD IN SECONDS

(a)

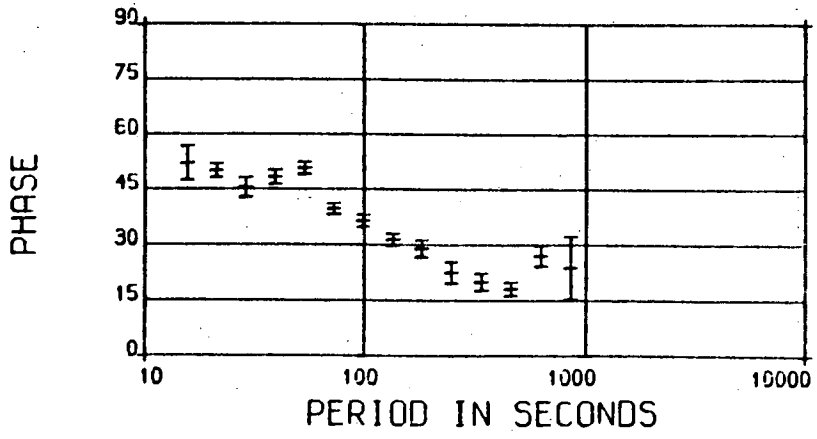
PHASE
90
75
60
45
30
15
0
10
100
1000
10000
PERIOD IN SECONDS

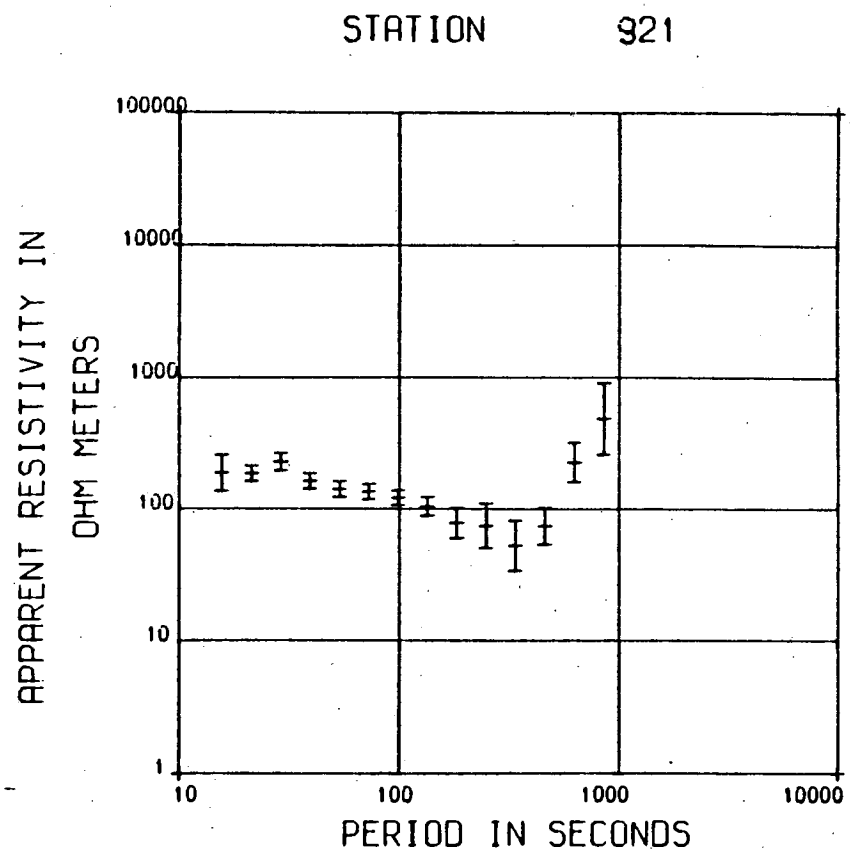
STATION 921
APPARENT RESISTIVITY IN OHM METERS
100000
10000
1000
100
10
1
10
100
1000
10000
PERIOD IN SECONDS

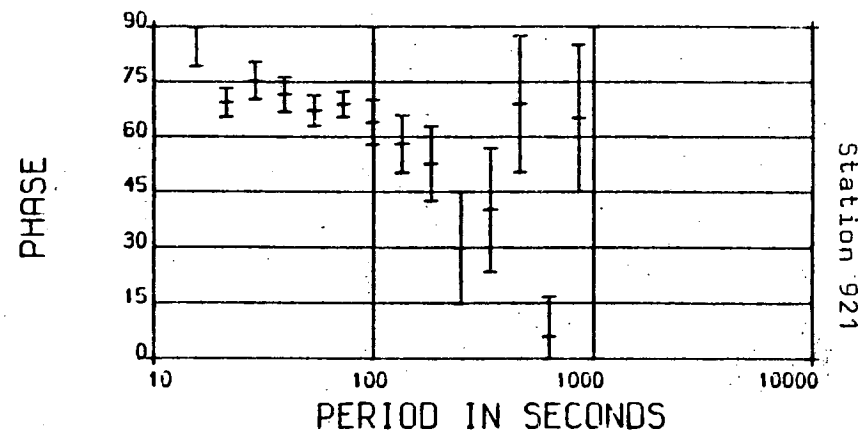
PHASE
90
75
60
45
30
15
0
10
100
1000
10000
PERIOD IN SECONDS
Station 921

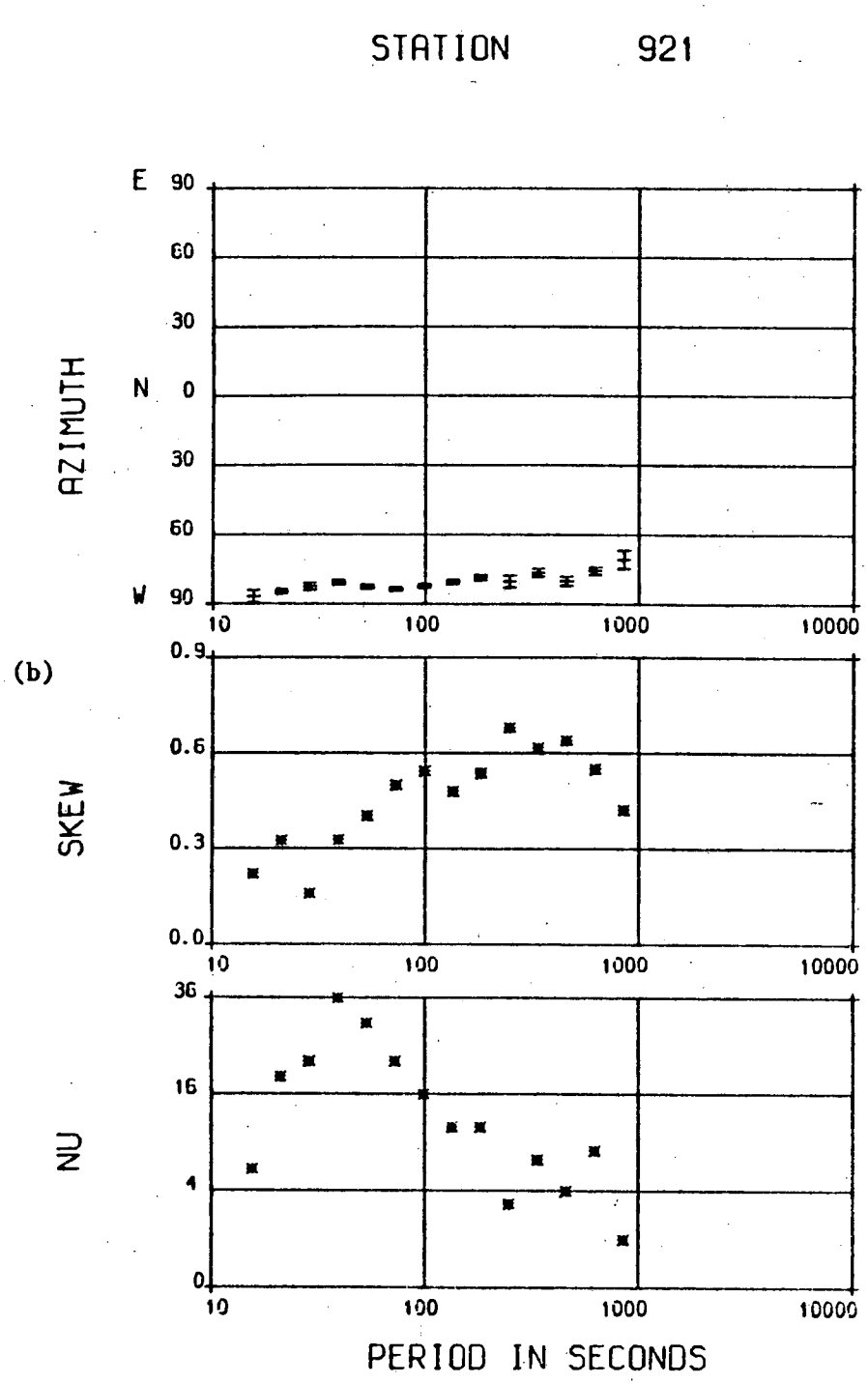
STATION 921
AZIMUTH
E 90
60
30
N 0
30
60
W 90
10
100
1000
10000
(b)
SKEW
0.9
0.6
0.3
0.0
NU
30
16
4
0
PERIOD IN SECONDS

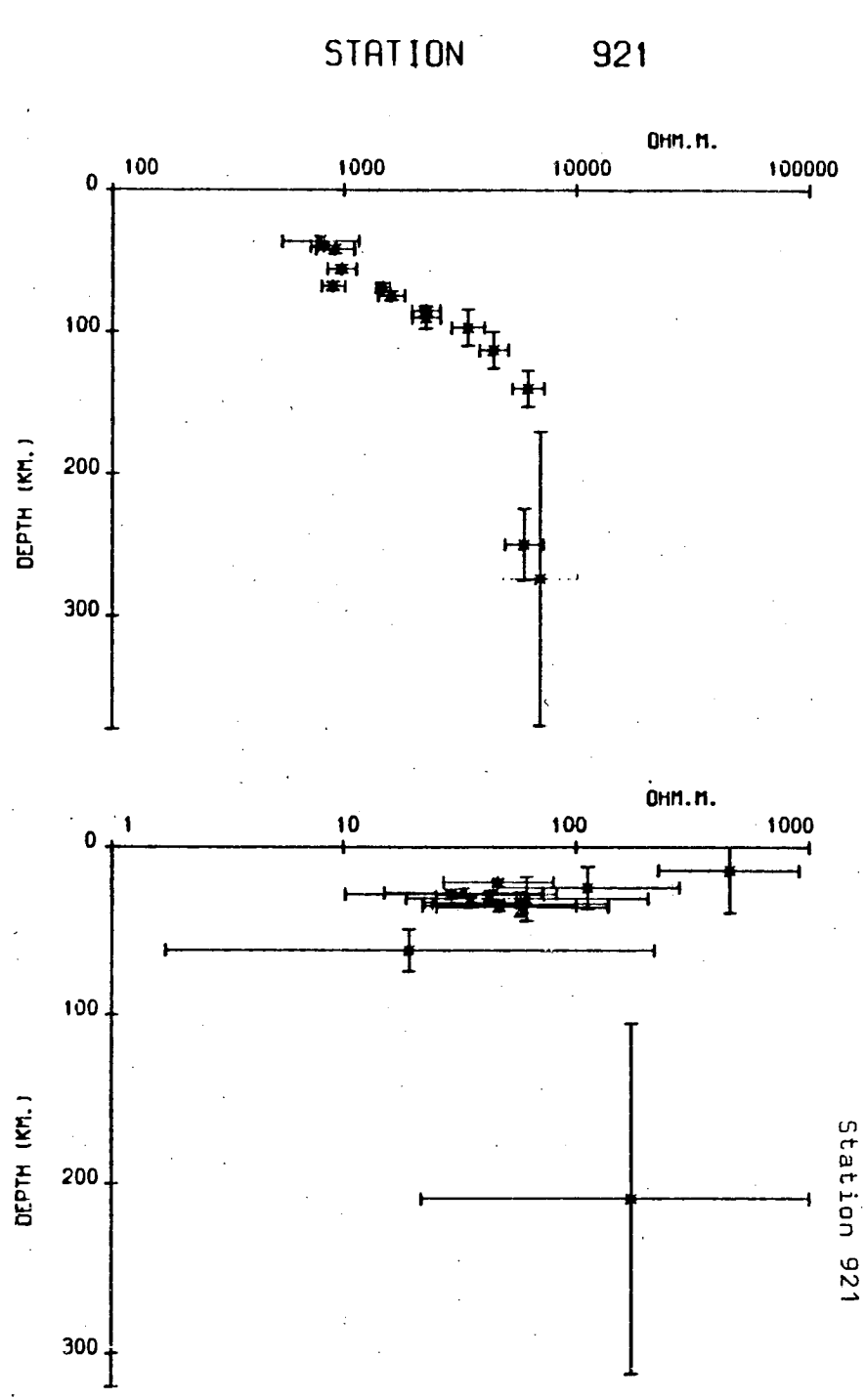
STATION 921
OHM.M.
100
1000
10000
100000
DEPTH (KM.)
0
100
200
300
OHM.M.
1
10
100
1000
Station 921

(c)

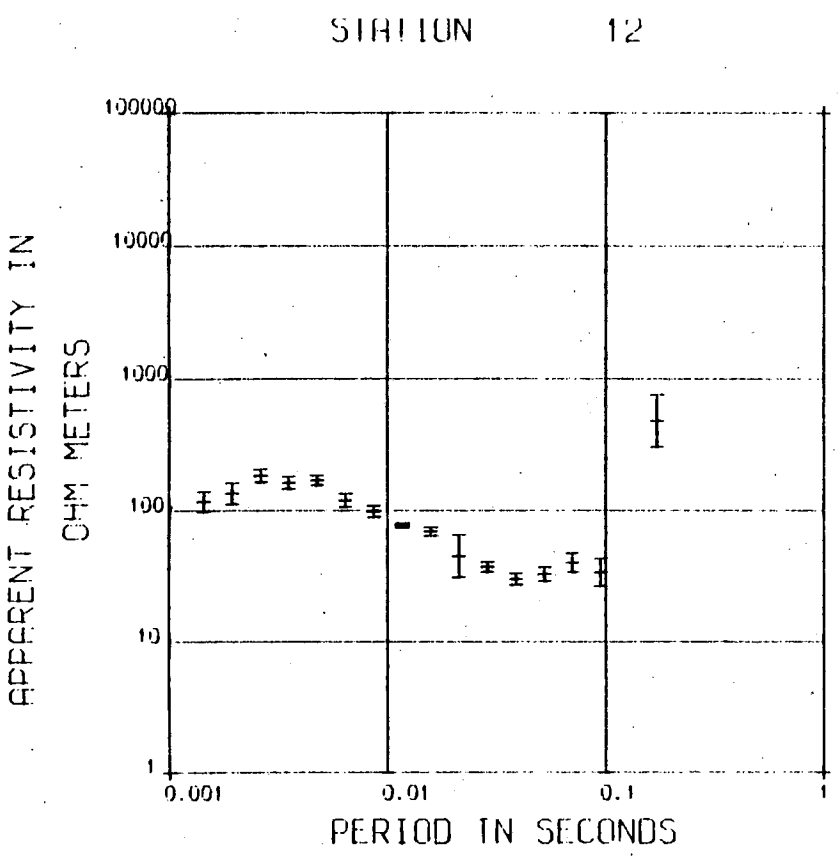
STATION 12
APPARENT RESISTIVITY IN OHM METERS
100000
10000
1000
100
10
1
0.001
0.01
0.1
1
PERIOD IN SECONDS

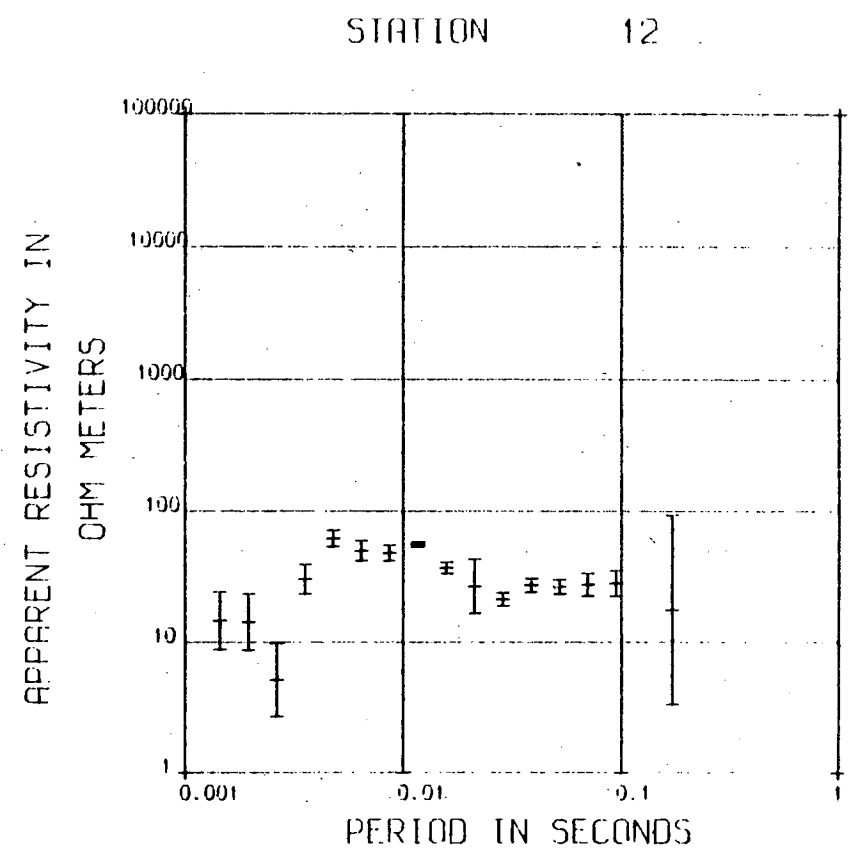
STATION 12
APPARENT RESISTIVITY IN OHM METERS
100000
10000
1000
100
10
1
0.001
0.01
0.1
1
PERIOD IN SECONDS

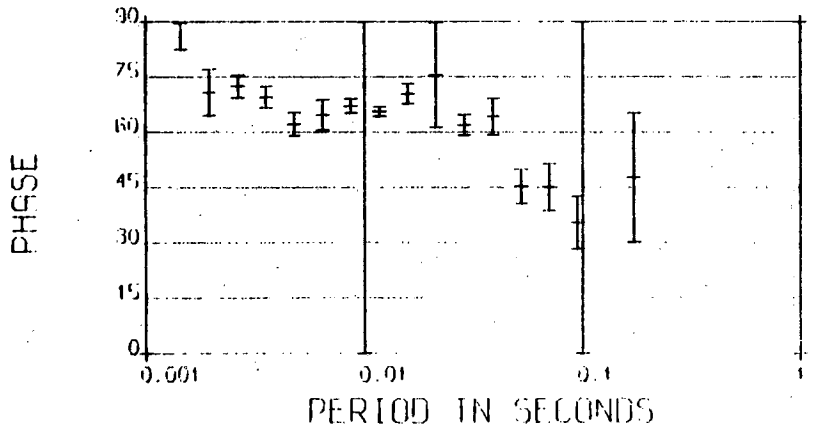
PHASE
90
75
60
45
30
15
0
0.001
0.01
0.1
1
PERIOD IN SECONDS

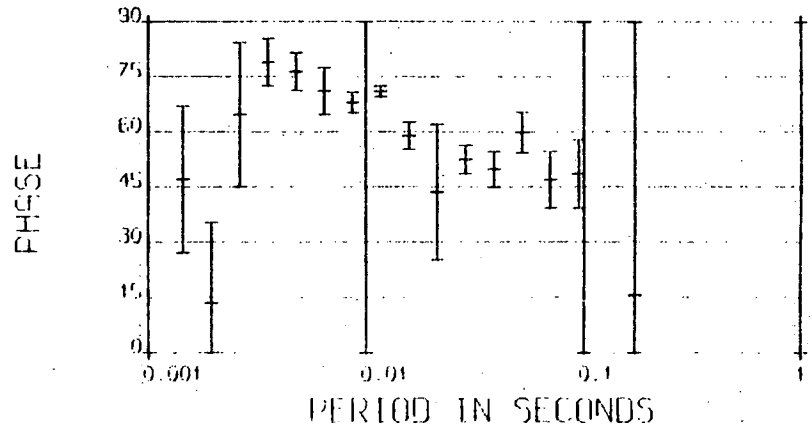
PHASE
90
75
60
45
30
15
0
0.001
0.01
0.1
1
PERIOD IN SECONDS

(d)

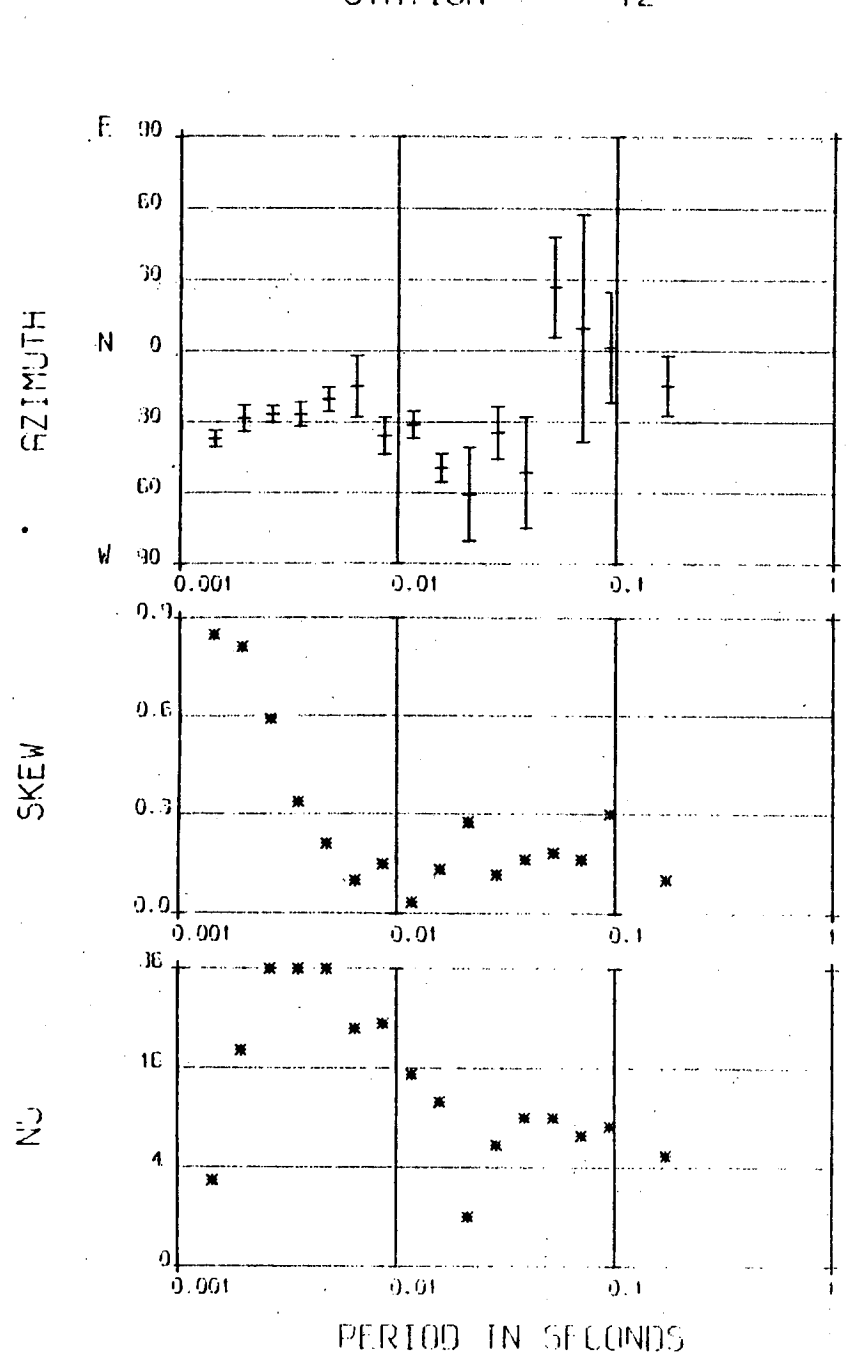
STATION 12
AZIMUTH
E 90
60
30
N 0
30
60
W 90
0.001
0.01
0.1
1
SKEW
0.9
0.6
0.3
0.0
NO
30
10
4
0
PERIOD IN SECONDS

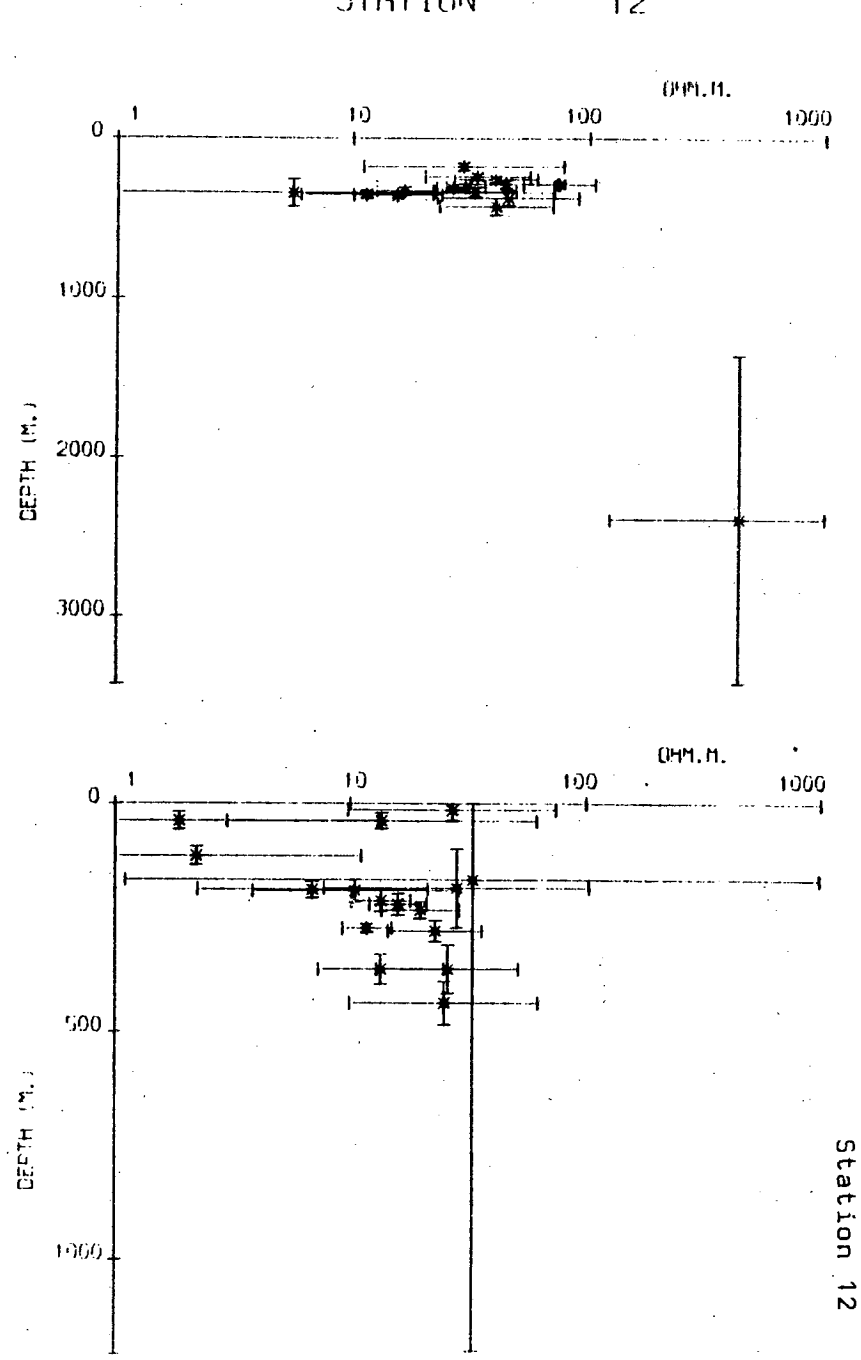
STATION 12
OHM.M.
1
10
100
1000
0
1000
2000
3000
DEPTH (M.)
OHM.M.
1
10
100
1000
0
500
1000
DEPTH (M.)
Station 12

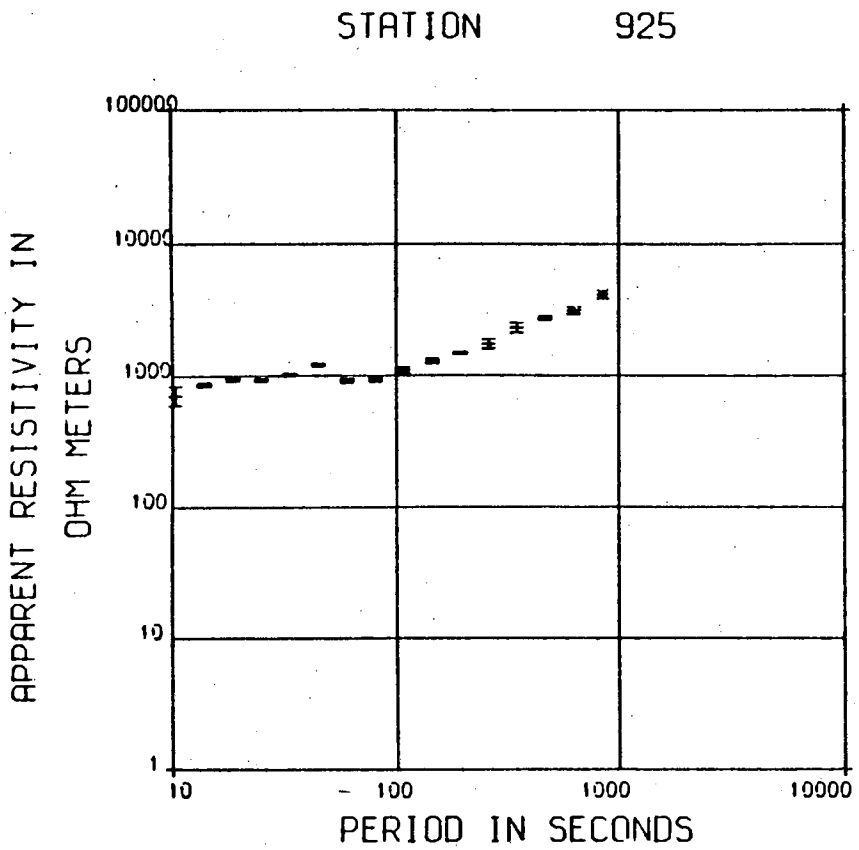

(a)

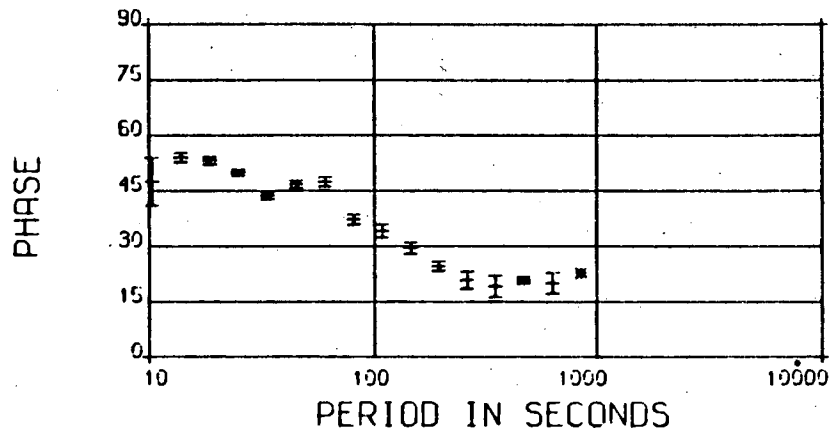

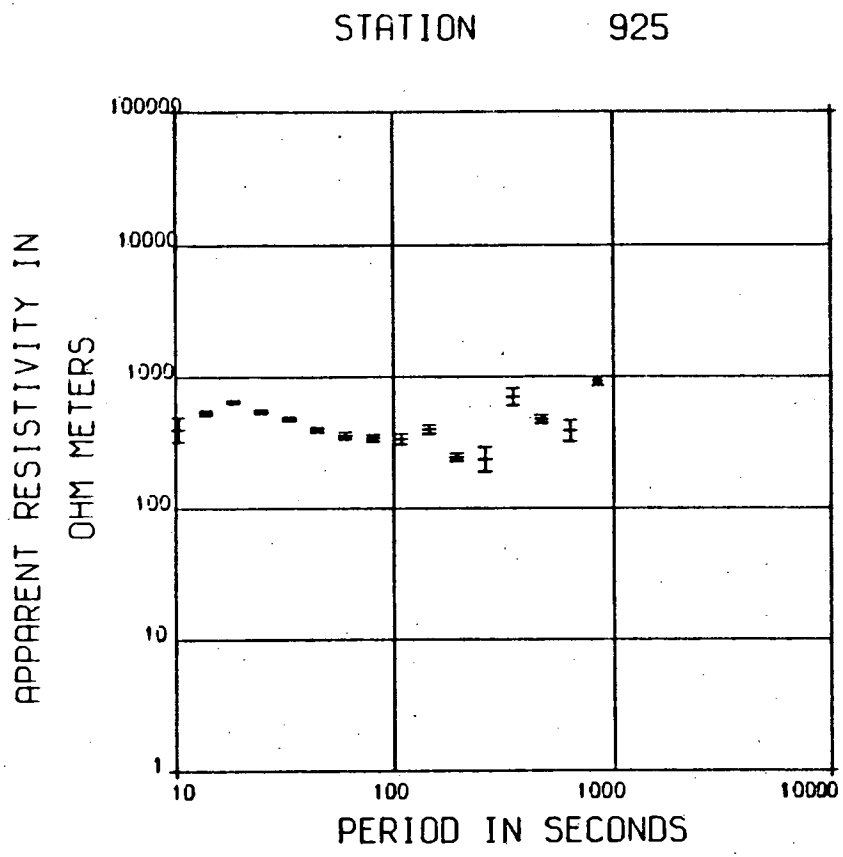

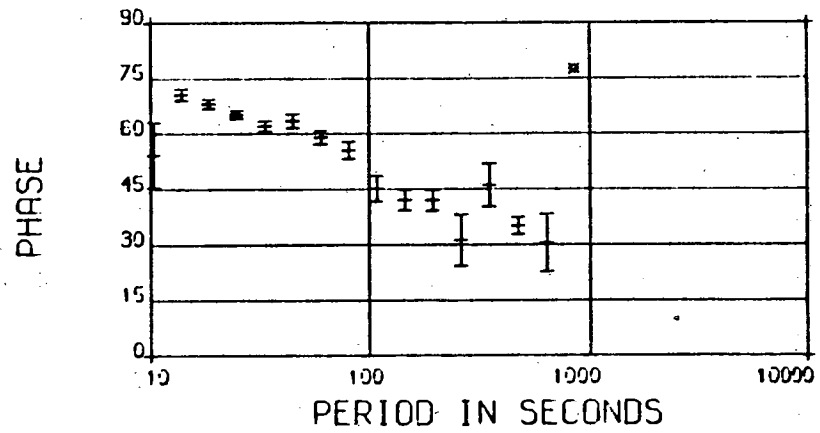

Station 925

(b)

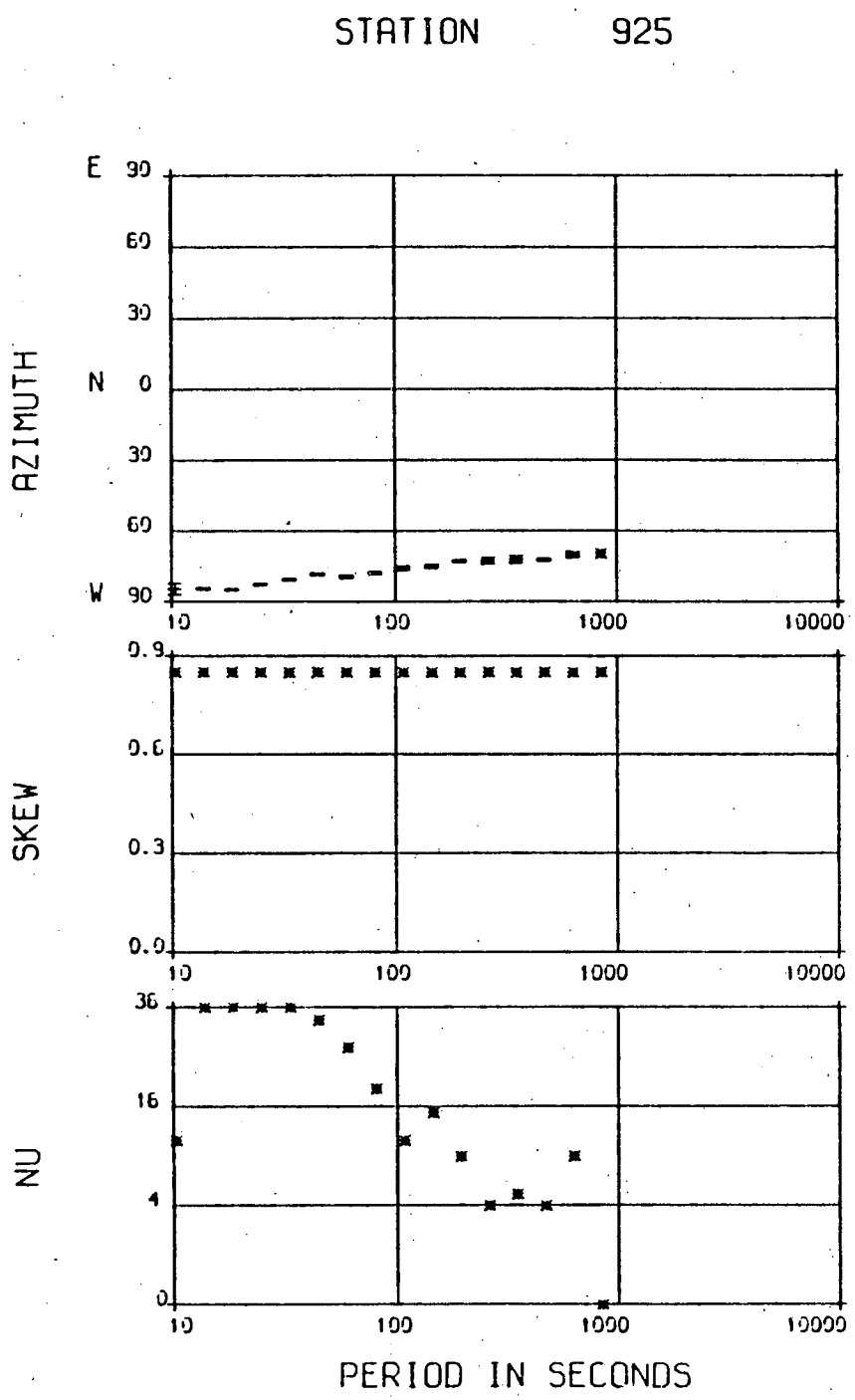
STATION 925
AZIMUTH
E 90
60
30
N 0
30
60
W 90
10
100
1000
10000
SKEW
0.9
0.6
0.3
0.0
NU
36
16
4
0
PERIOD IN SECONDS

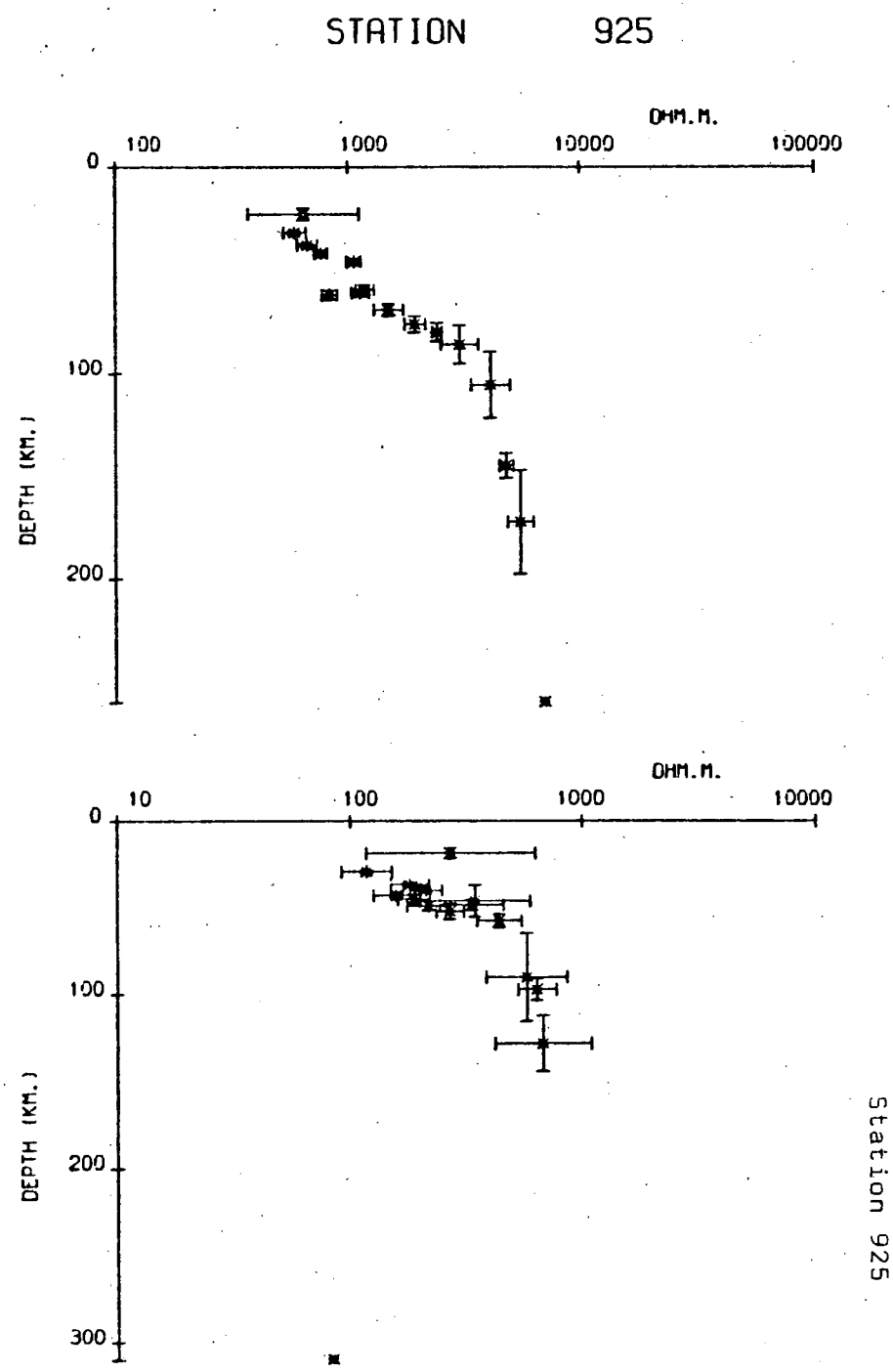
STATION 925
OHM.M.
100
1000
10000
100000
0
100
200
DEPTH (KM.)
OHM.M.
10
100
1000
10000
0
100
200
300
DEPTH (KM.)
Station 925

(c)

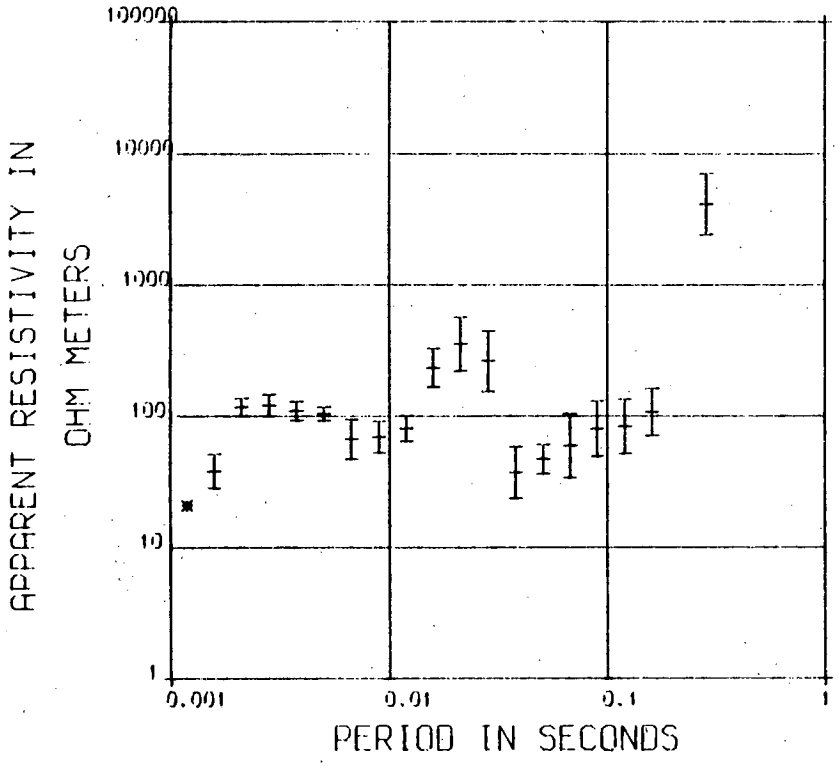
STATION 18
APPARENT RESISTIVITY IN OHM METERS
100000
10000
1000
100
10
1
0.001
0.01
0.1
1
PERIOD IN SECONDS

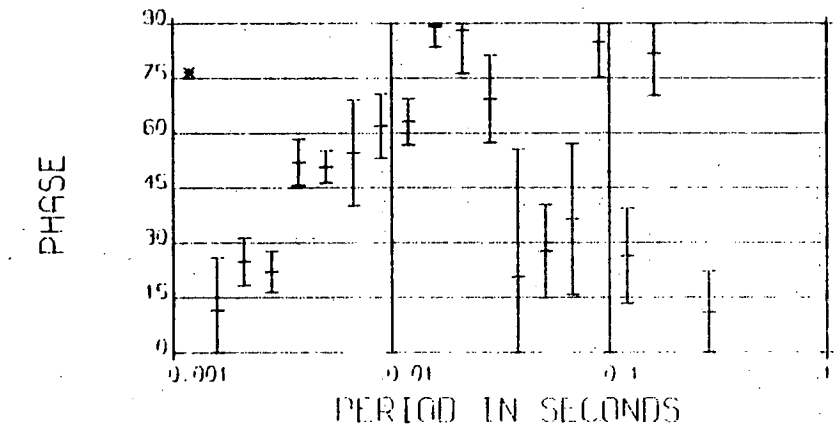
PHASE
90
75
60
45
30
15
0
0.001
0.01
0.1
1
PERIOD IN SECONDS

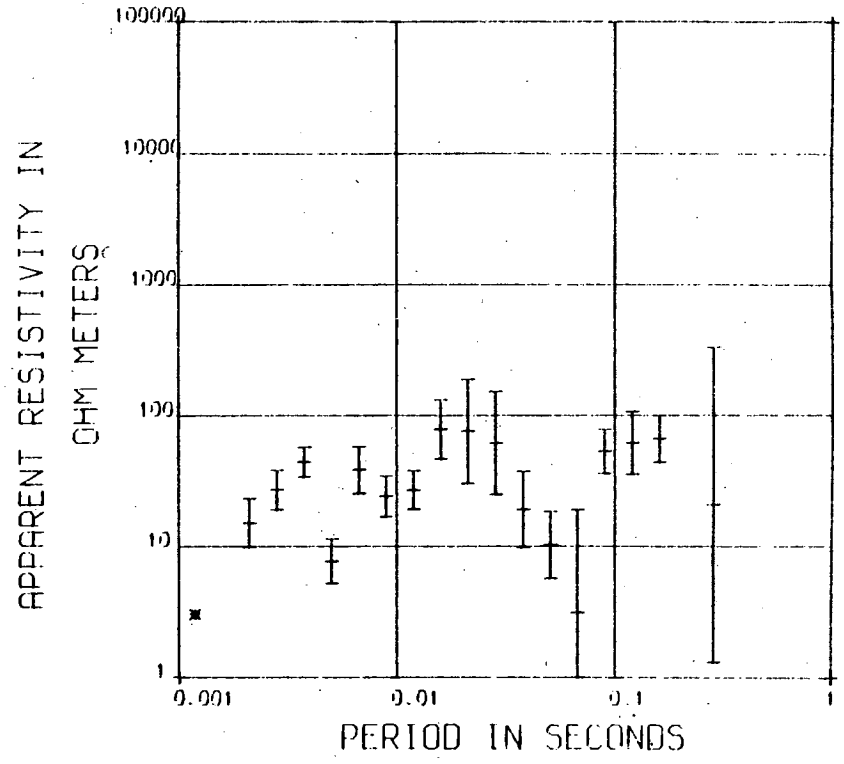
STATION 18
APPARENT RESISTIVITY IN OHM METERS
100000
10000
1000
100
10
1
0.001
0.01
0.1
1
PERIOD IN SECONDS

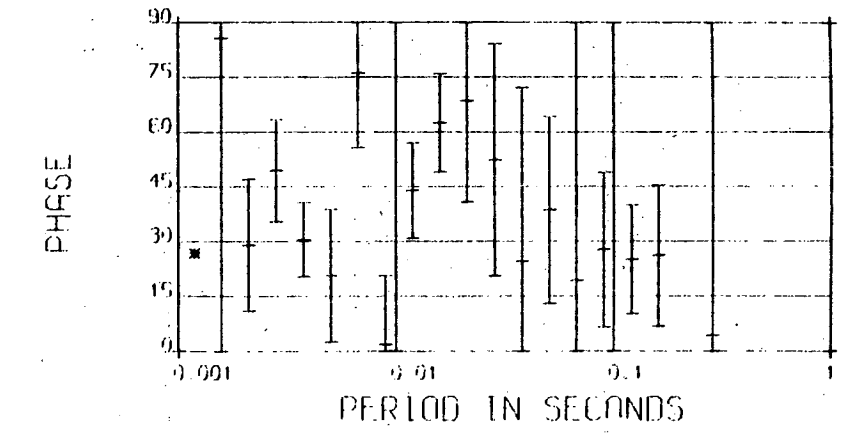
PHASE
90
75
60
45
30
15
0
0.001
0.01
0.1
1
PERIOD IN SECONDS

(d)

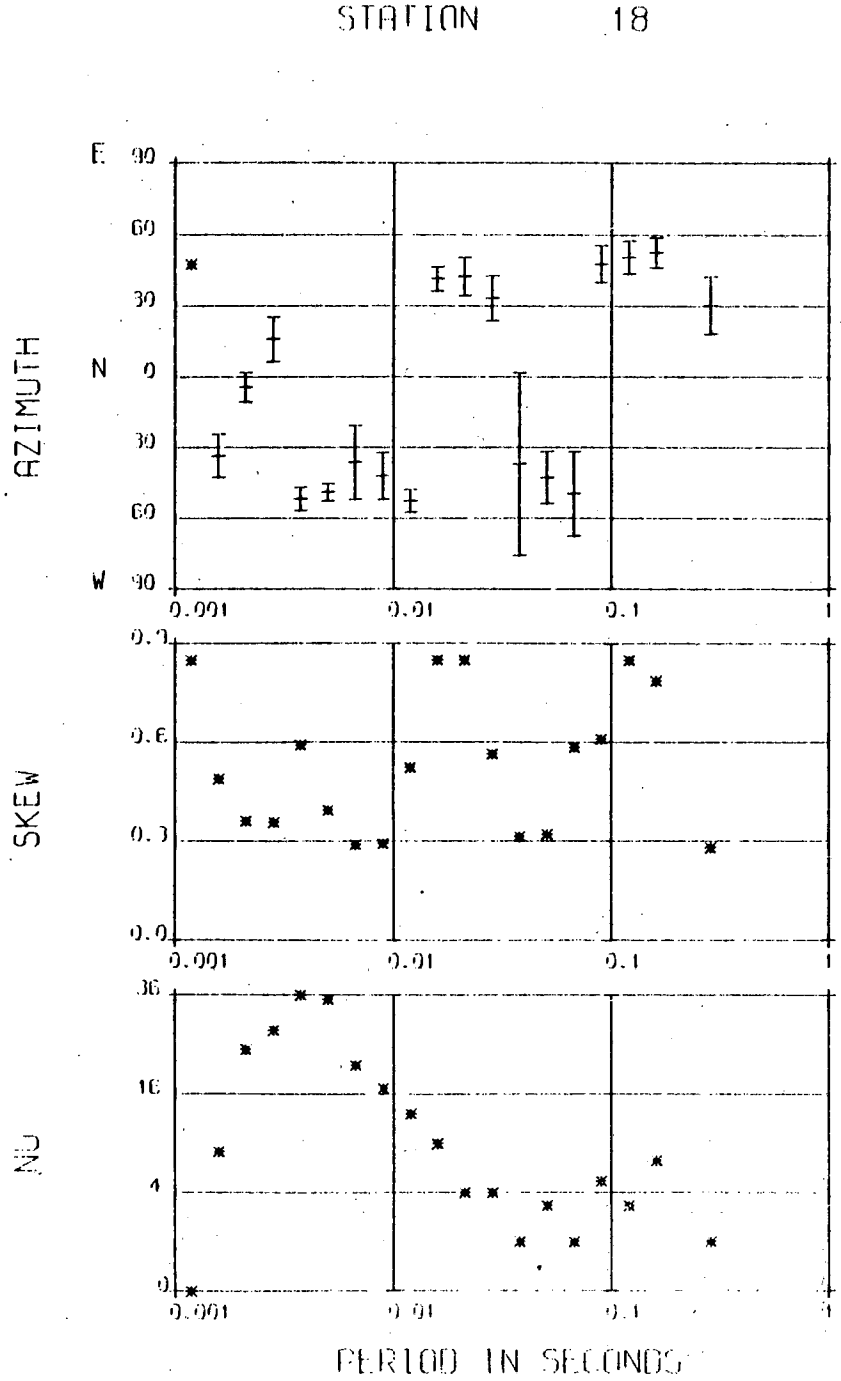
STATION 18
AZIMUTH
E 90
60
30
N 0
30
60
W 90
SKEW
0.9
0.6
0.3
0.0
NU
30
18
4
0
0.001
0.01
0.1
1
PERIOD IN SECONDS

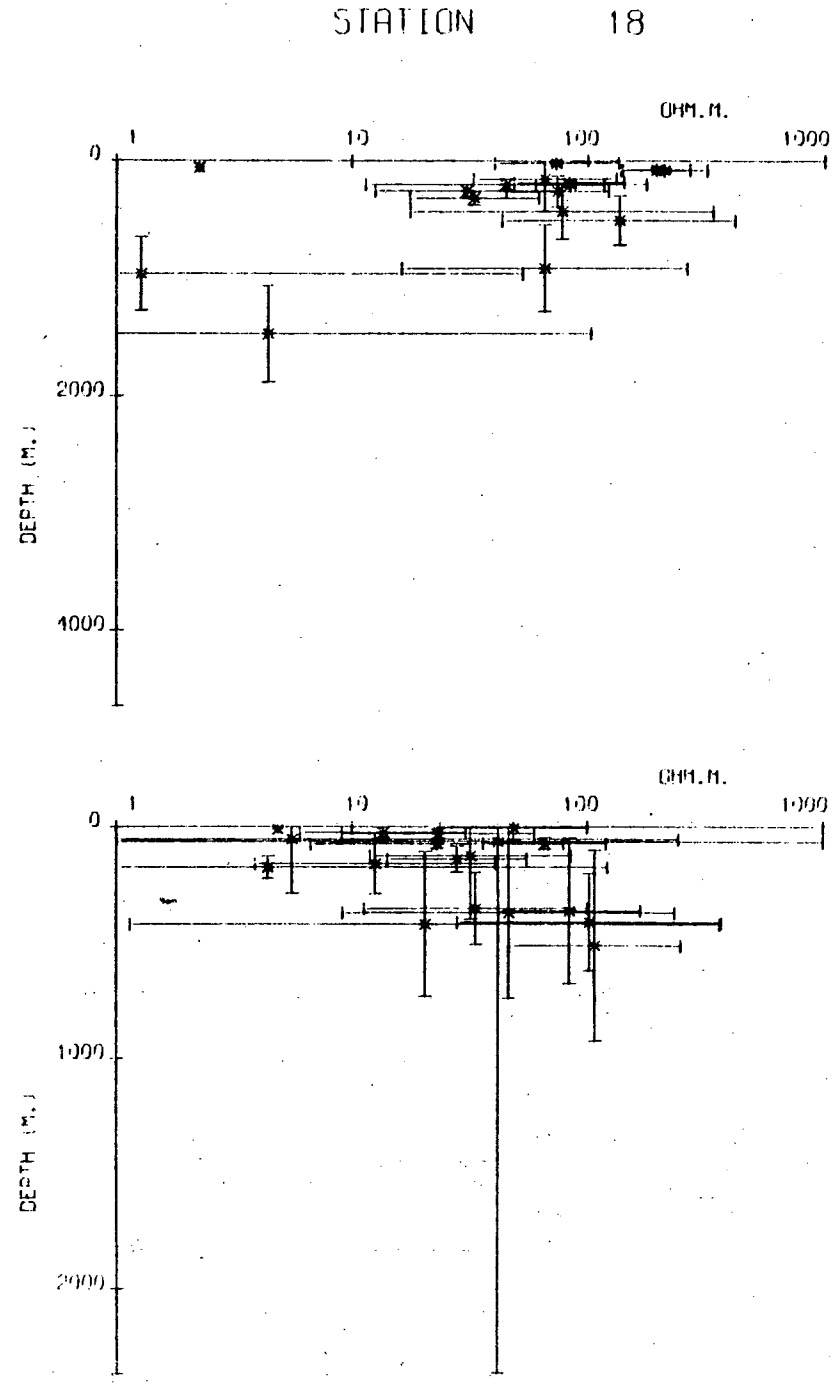
STATION 18
OHM.M.
1
10
100
1000
0
2000
4000
DEPTH (M.)
OHM.M.
1
10
100
1000
0
1000
2000
DEPTH (M.)
Station 18

At station SWI there is a striking trend in the azimuth which is aligned EW for the whole bandwidth. This direction persists for the other two stations at the long period bandwidth with only a slight clockwise rotation with increasing period. The azimuth at the high frequencies shows variation with frequency at station ROO and an apparent alignment at 45 degrees at station HIL.

AT station ROO the skew factor is generally low while at station SWI it remains high throughout the short period band. Station HIL has very high skew values particularly at long periods.

The number of estimates averaged is lower at station HIL for the high frequency band, where data display more scatter and larger error bars.

5.1.3 Magnetic results

The magnetic results for each MT site are presented as unreversed real and imaginary induction vectors and Bank's maximum and minimum induction vectors. The two sets of results, (figures 5.8-5.14) show very similar behaviour. Discussion is therefore limited to the real and imaginary vectors. The results from the two northerly stations (LAM) and (EDG) show marked differences. The magnitude of the real vector is typically less than 0.1 and certainly less than 0.2 while at the other five stations, it is greater than 0.1 and reaches 0.4. The azimuth of the real vector is well defined at the 5

Figure 5.8 MT magnetic results from station Lampert

STATION 927

INDUCTION VECTORS

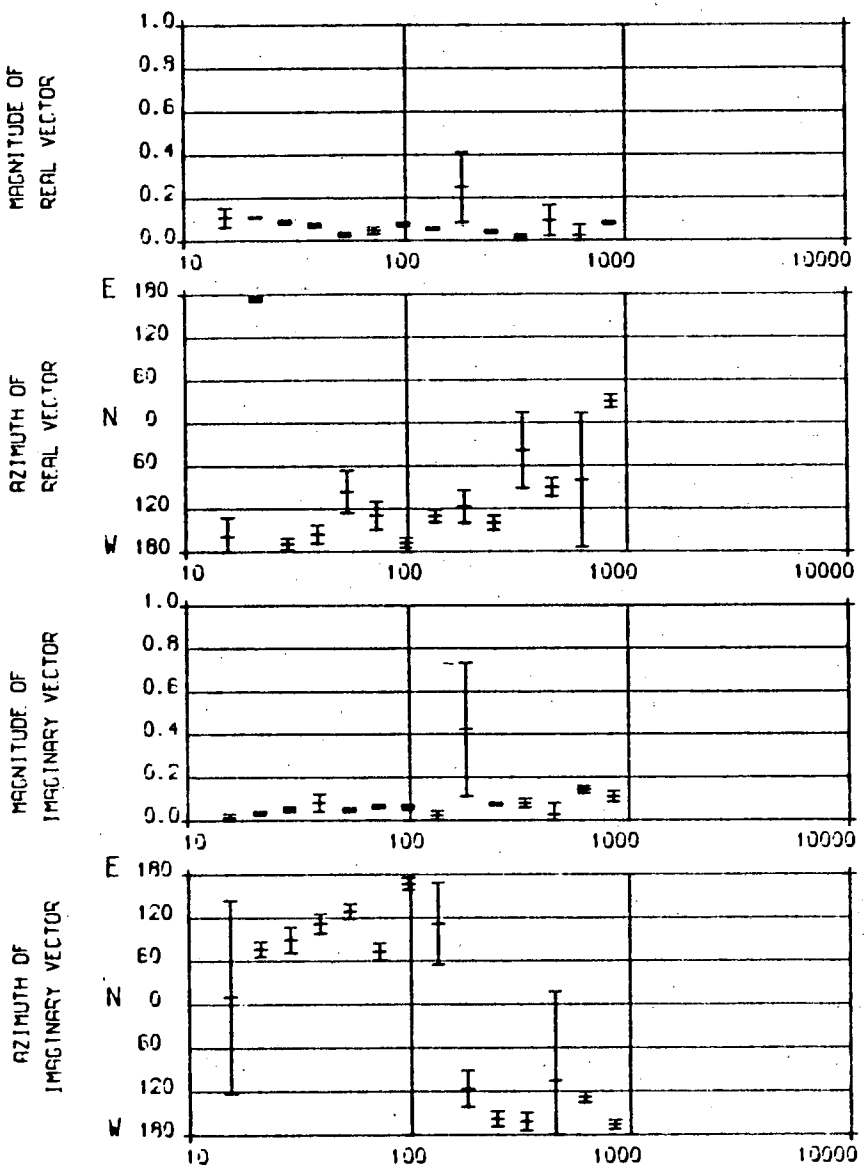

STATION 927

INDUCTION VECTORS

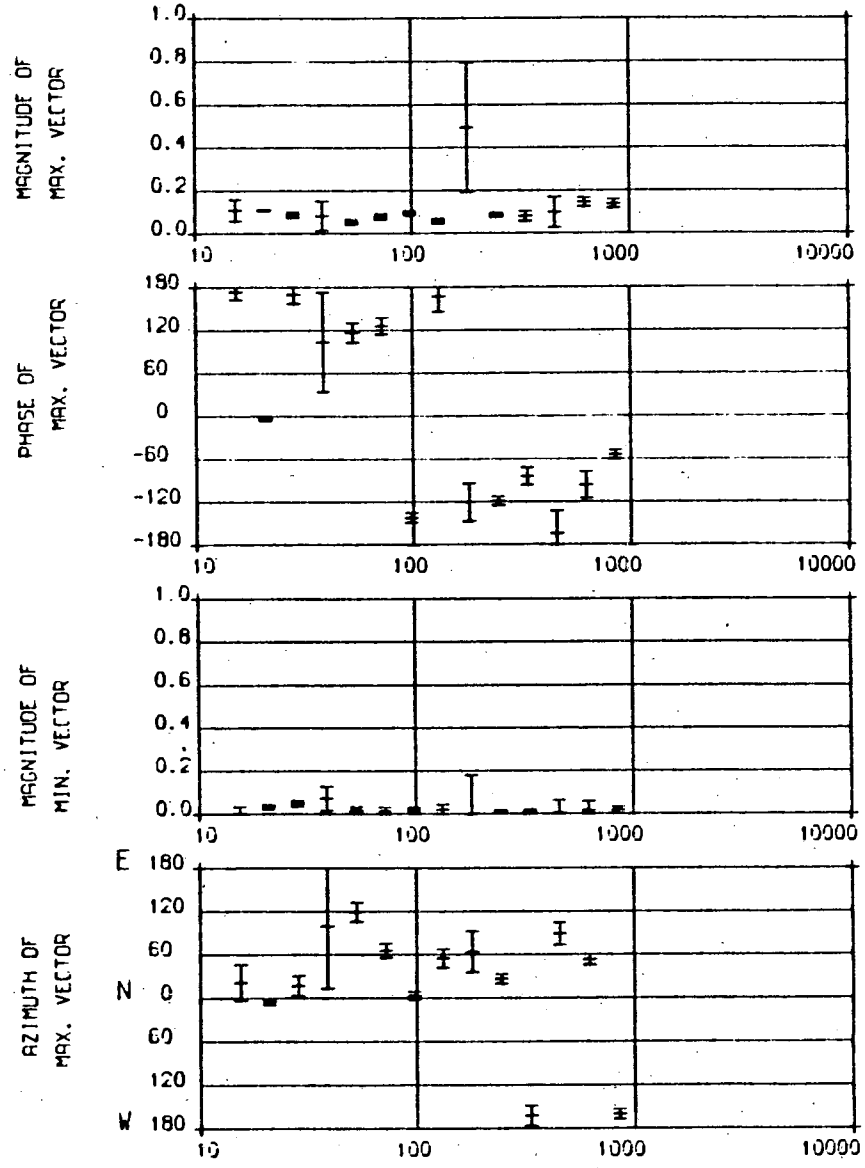

Station 927

Figure 5.9 MT magnetic results from station Edges Green

STATION 924

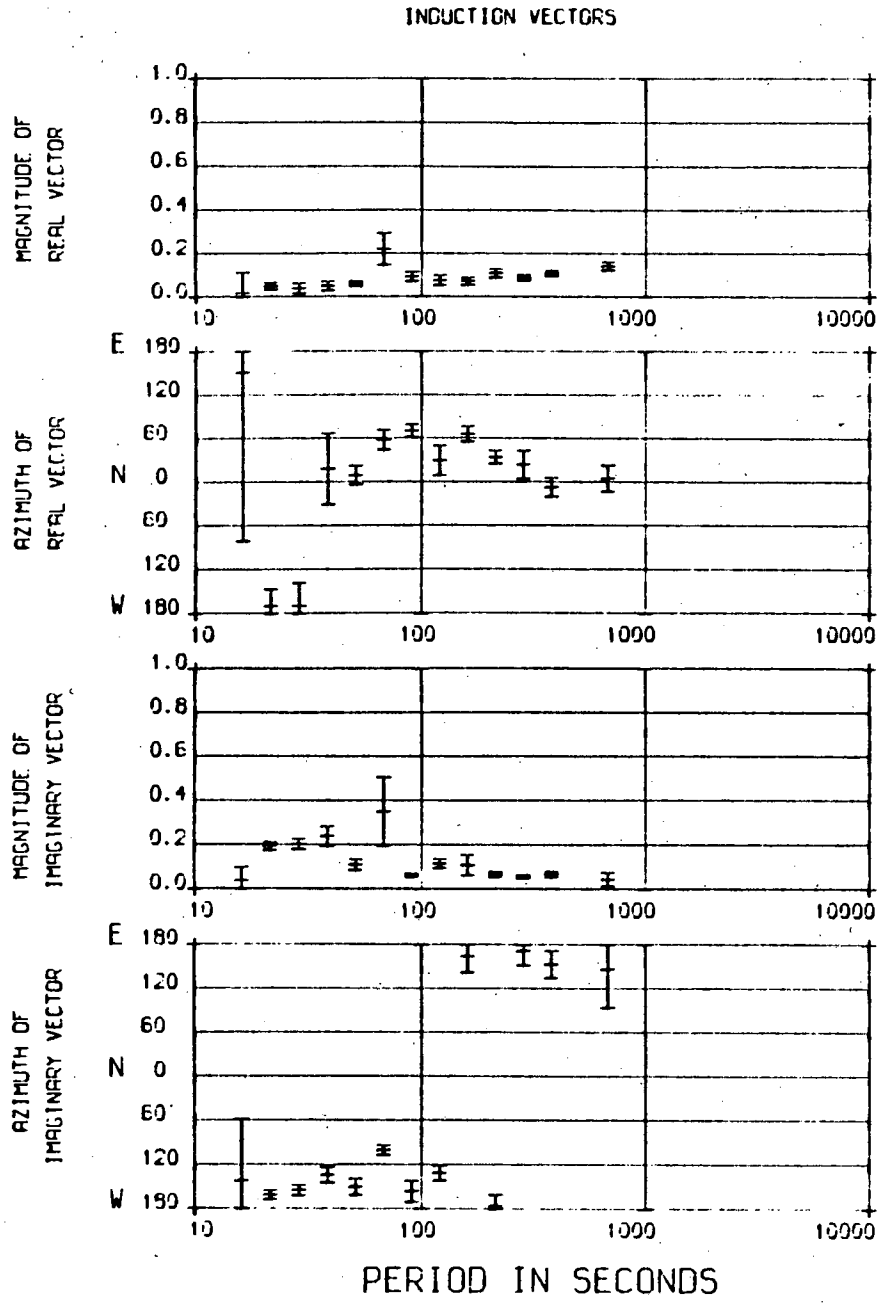

STATION 924

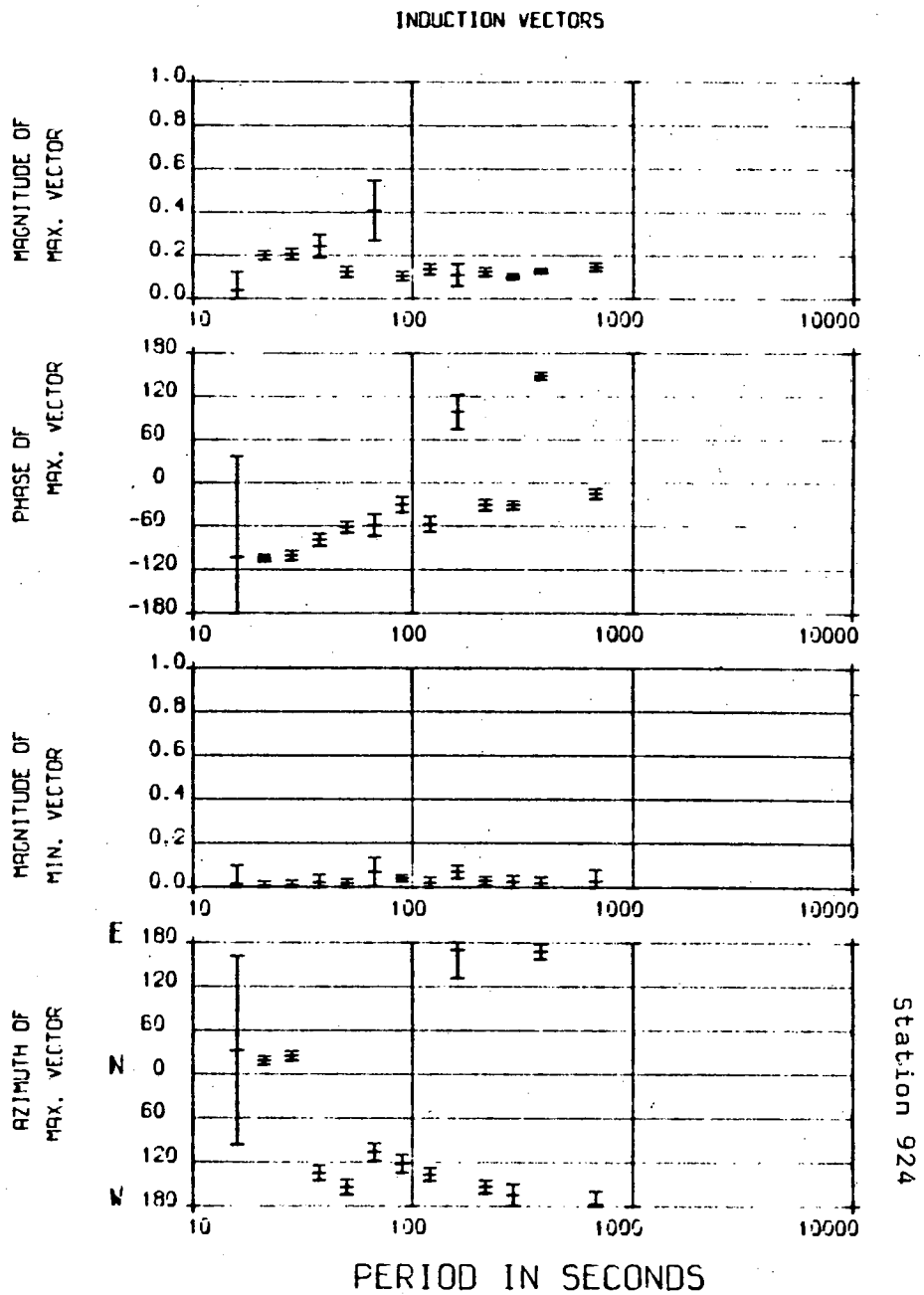

Station 924

Figure 5.10 MT magnetic results from station Whitfield

STATION 926

INDUCTION VECTORS

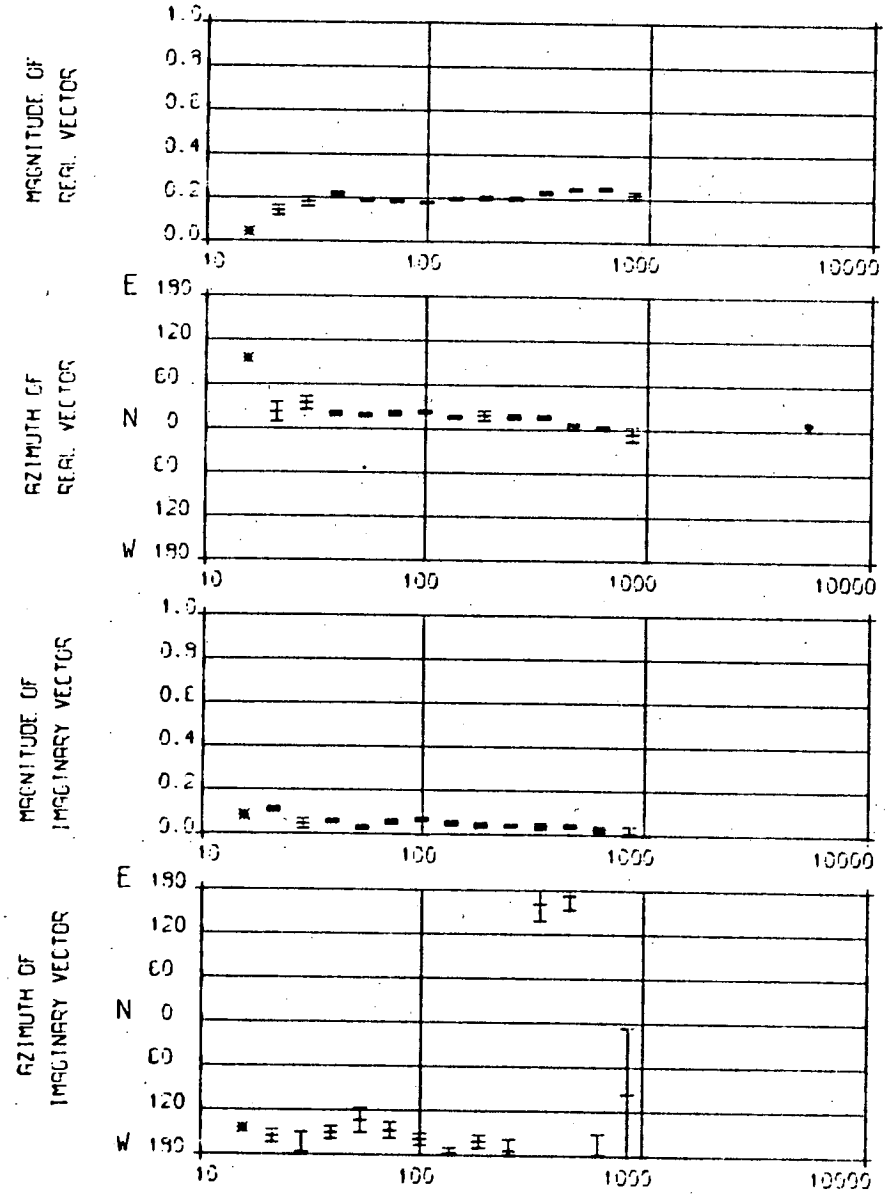

STATION 926

INDUCTION VECTORS

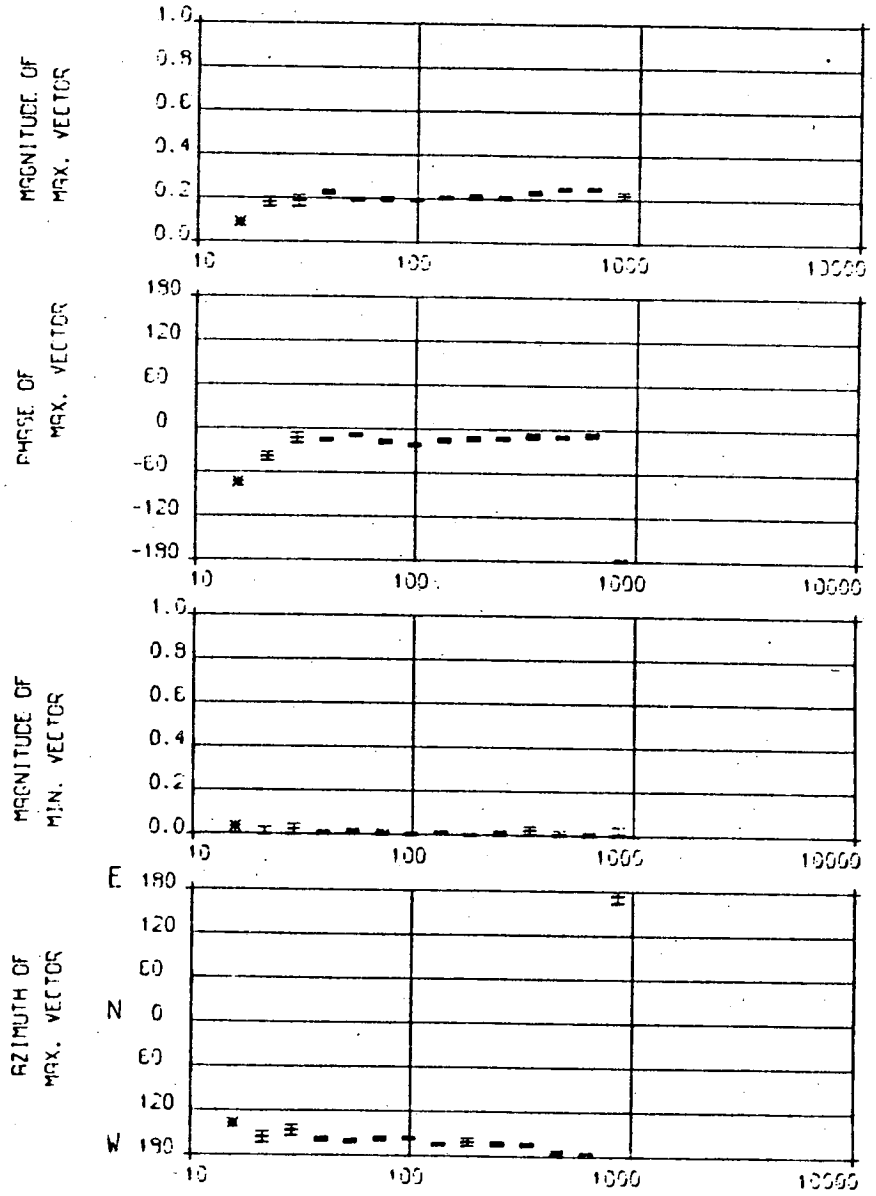

Station 926

Figure 5.11 MT magnetic results from station Sinderhope Shield

STATION 923

INDUCTION VECTORS

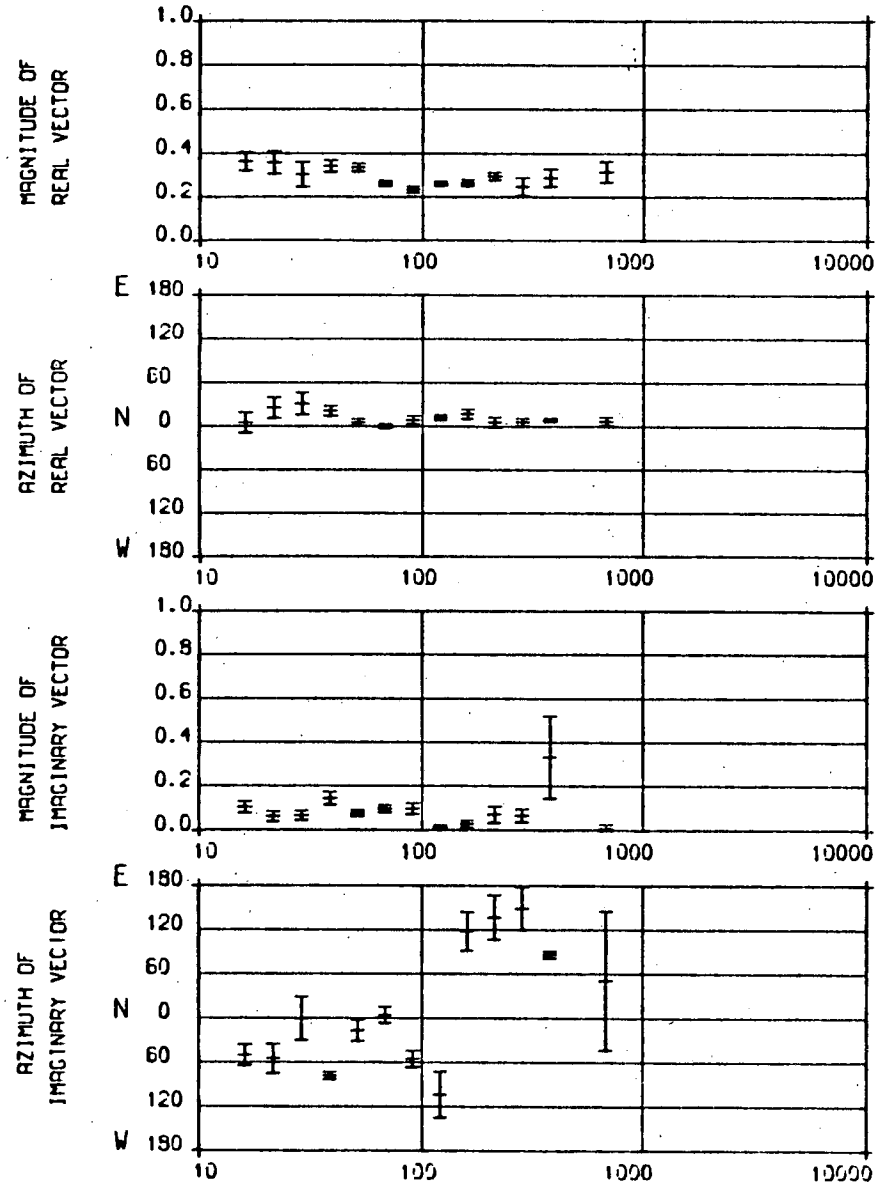

STATION 923

INDUCTION VECTORS

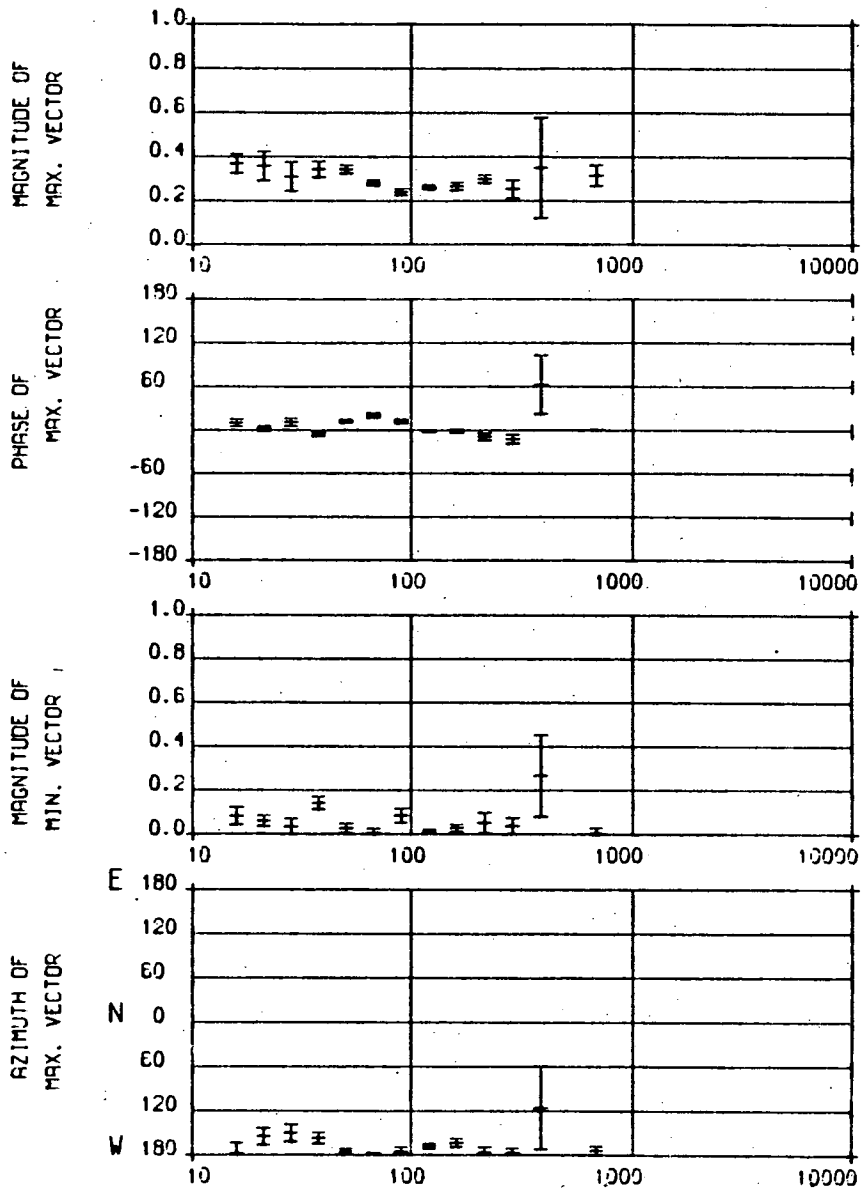

Station 923

Figure 5.12 MT magnetic results from station Swinhope Shield

STATION 920

INDUCTION VECTORS

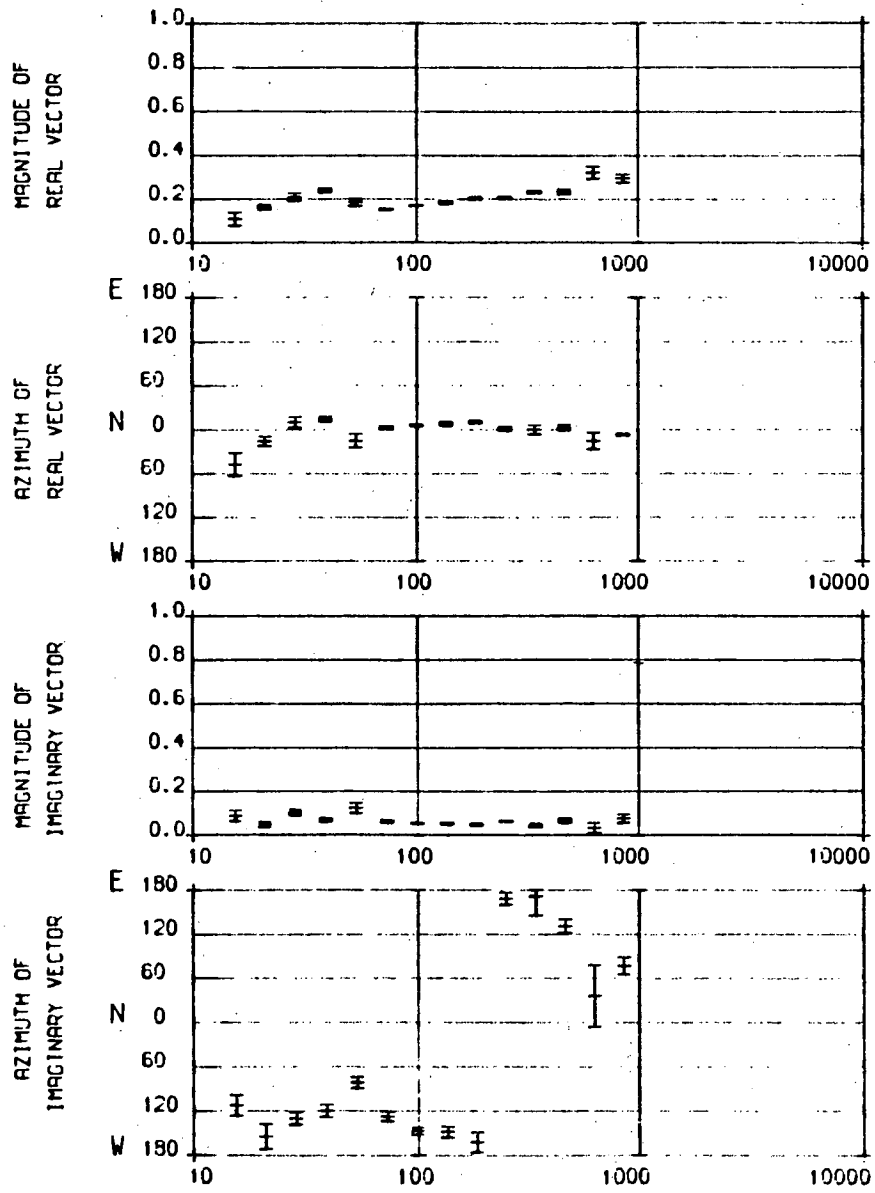

STATION 920

INDUCTION VECTORS

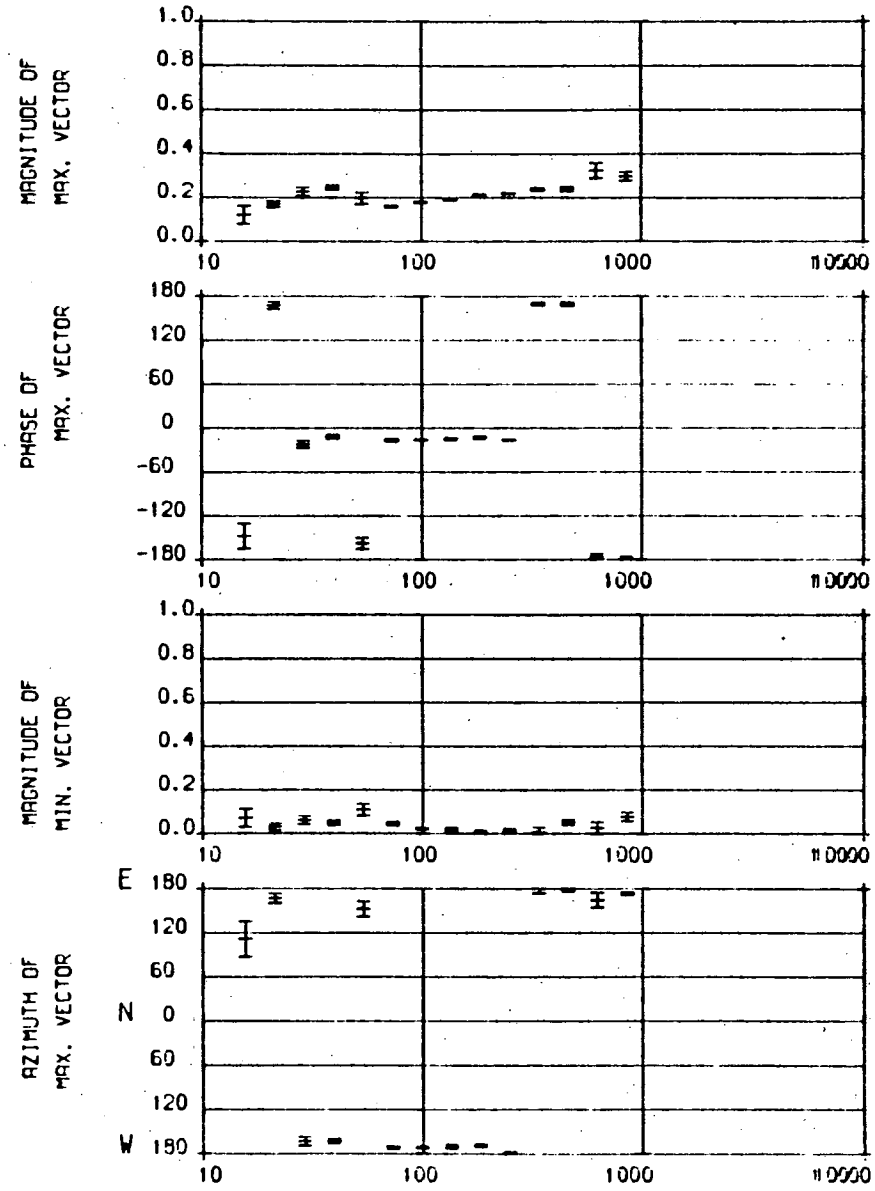

Station 920

Figure 5.13 MT magnetic results from station Rookhope

STATION 921

INDUCTION VECTORS

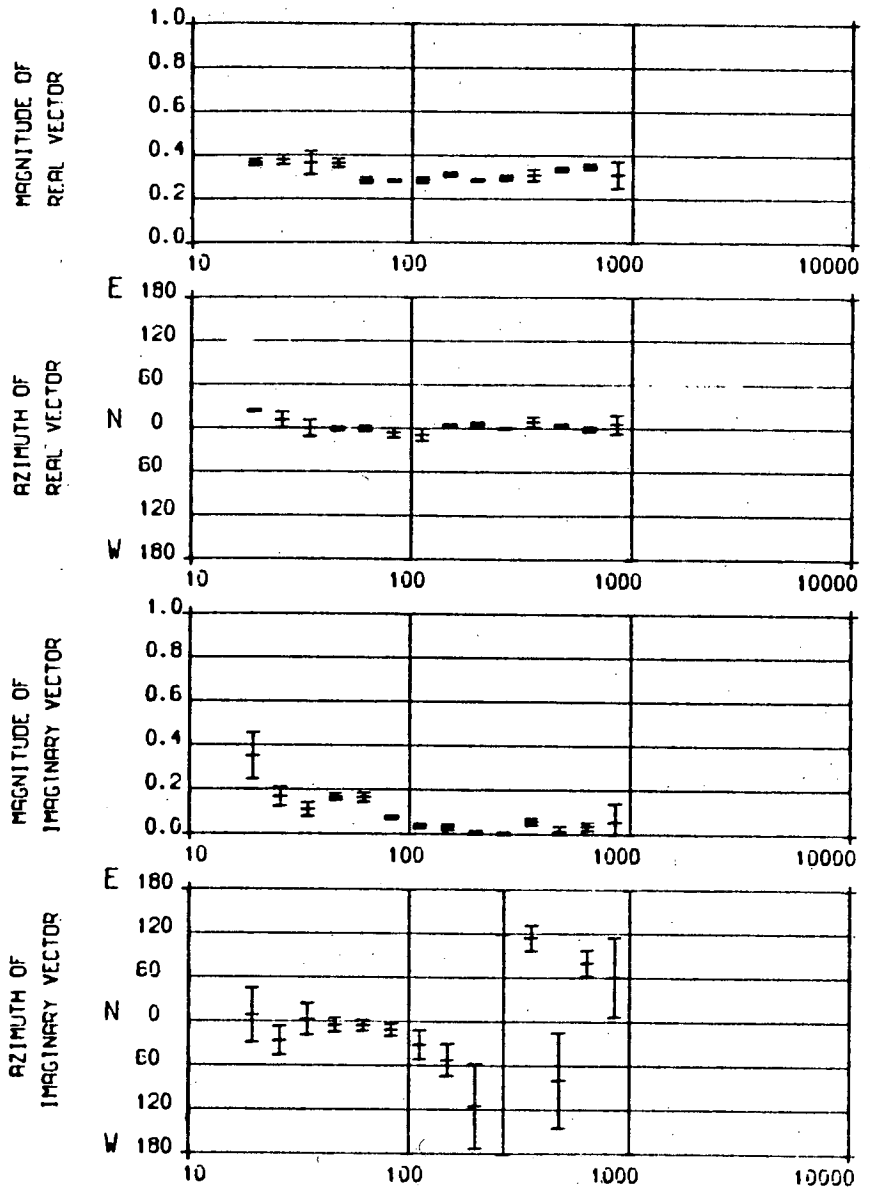

STATION 921

INDUCTION VECTORS

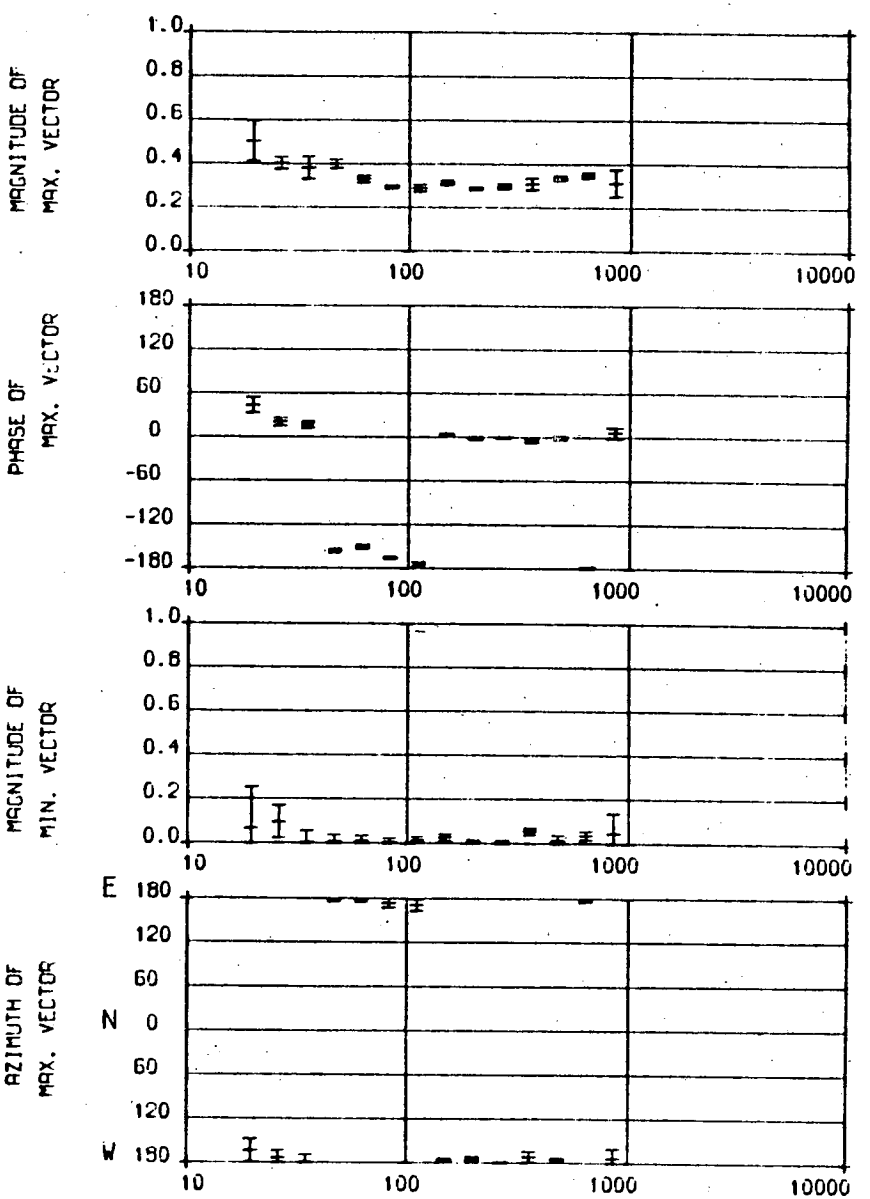

Figure 5.14 MT magnetic results from station Hill End

STATION 925

INDUCTION VECTORS

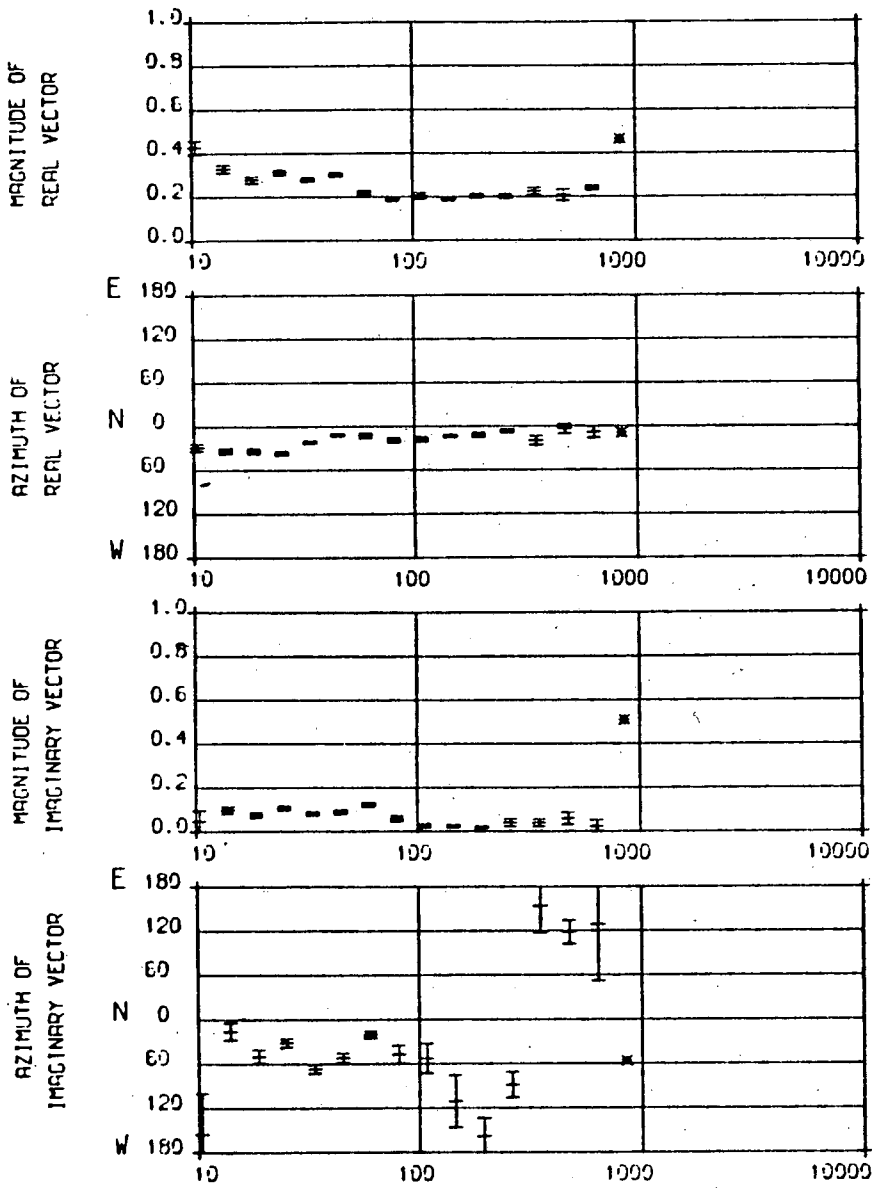

STATION 925

INDUCTION VECTORS

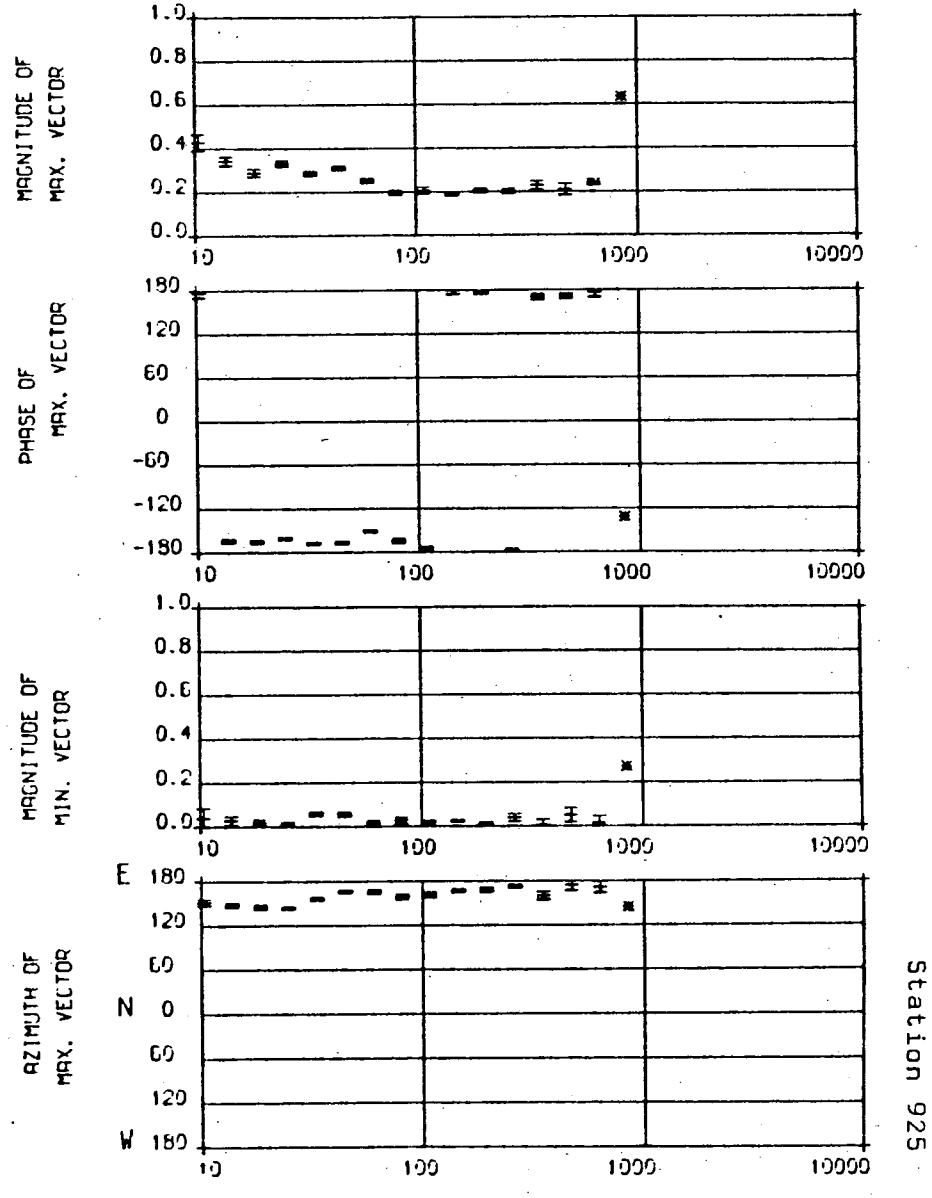

Station 925

northerly stations and is constrained to the magnetic north direction to within $\pm$ 30 degrees. For the station LAM the azimuth of the real vector lies pointing south around the 20 second period, rotating clockwise through 90 degrees for periods up to 800 seconds. At station EDG the azimuth of the real vector lies scattered around 30 degrees E of N except for periods less than 30 seconds, where it assumes a direction 180 degrees opposite.

The magnitudes of the imaginary vectors at the 5 southerly stations, are again similar, although their magnitudes are always smaller than those of the real vectors. At the two northerly stations the two vector quantities are of comparable magnitude and at station EDG the magnitude of the imaginary vector tends to exceed that of the real vector at periods less than 200 seconds.

5.2 AMT results

When a large number of observational sites forms a grid over an area, one of the most suitable representations of the data is collectively, by way of an areal display. This approach has been used successfully in the past by Hoover et al (1978) and others. Many features of the data may then be examined at a glance and without much lengthy manipulation. If, also, the responses, treated on a collective basis, can be arranged into distinct groups, within which they show similar behaviour, then the results from such a group or region can be considered - at least in the first instance - by study of those from one or more selected stations from that group.

Figure 5.15 Map showing the dimensionality indicators for the AMT stations. The 1, 2 and 3 dimensional station responses are shown by different symbols. The main profile is indicated by diamond shapes.

KEY

3 Dimensional
2 Dimensional
1 Dimensional

Anisotropy indicator
Skew values
Alignment of azimuth

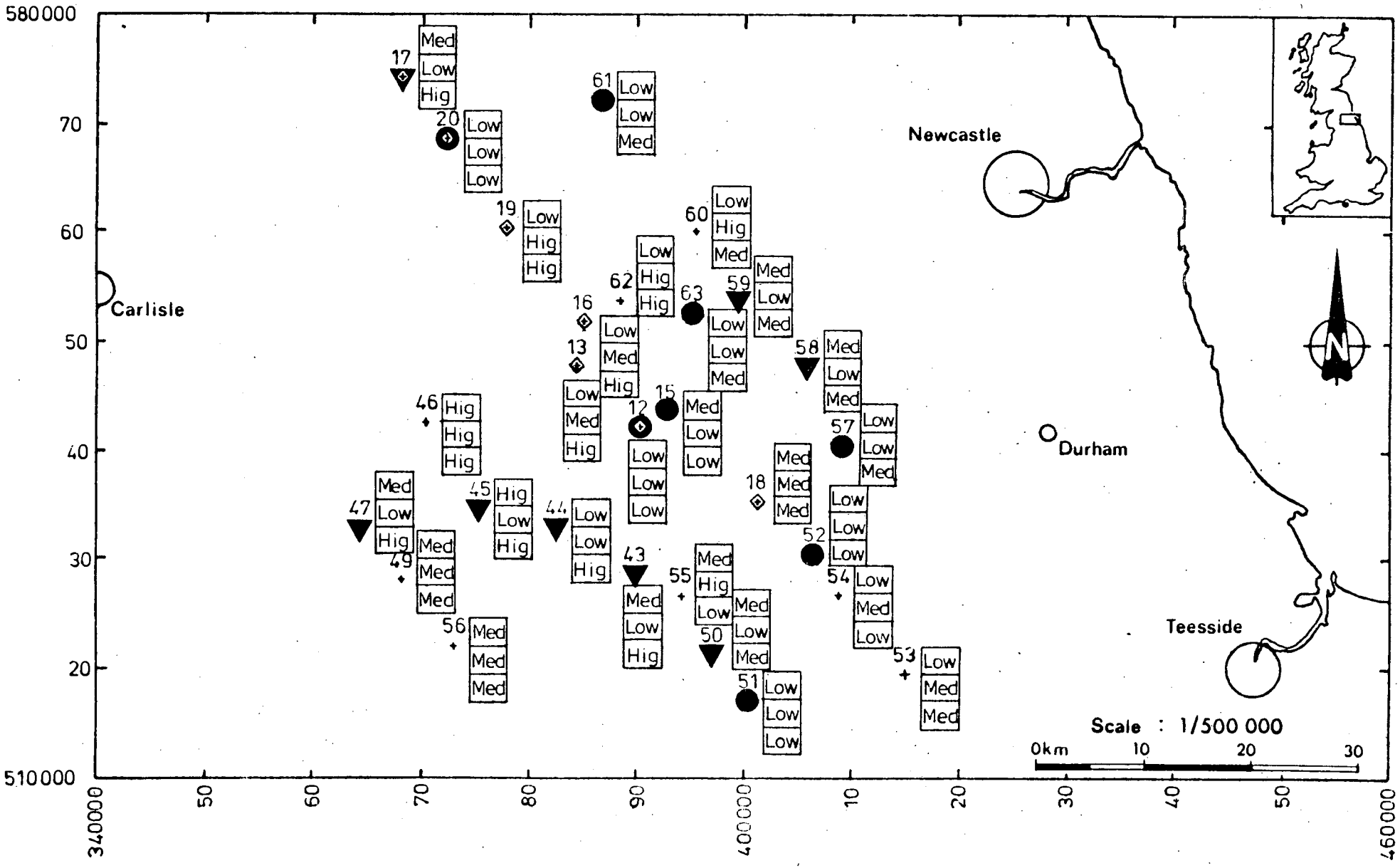
580000
70
60
50
40
30
20
510000
340000
50
60
70
80
90
400000
10
20
30
40
50
460000
Newcastle
Carlisle
Durham
Teesside
Scale : 1/500 000
0km 10 20 30
N
17 Med Low Hig
20 Low Low Low
19 Low Hig Hig
61 Low Low Med
60 Low Hig Med
62 Low Hig
16 Low Med Hig
13 Low Med Hig
63 Low Low Med
59 Med Low Med
58 Med Low Med
46 Hig Hig Hig
12 Low Low Low
15 Med Low Low
57 Low Low Med
47 Med Low Hig
45 Hig Low Hig
44 Low Low Hig
18 Med Med Med
49 Med Med Med
43 Med Low Hig
55 Med Hig Low
52 Low Low Low
54 Low Med Low
56 Med Med Med
50 Med Low Med
53 Low Med Med
51 Low Low Low

The approach of selecting representative stations is additionally advantageous, if multi-dimensional station results, defined according to criteria listed below, are present in the array. These cannot be interpreted with confidence using such one-dimensional inversion schemes, as that adopted in this study. In such cases, if it is possible to choose stations with one-dimensional responses as representative, a preliminary model for the region can be derived with more confidence when the one-dimensional inversion algorithm is used.

The tests which were applied, to determine whether a station was one-, two- or three-dimensional are standard and are summarised below.

1. If, for each set of station results, the rotated major and minor apparent resistivity curves show the same properties, in both the amplitude and the general structure, the station can be said to be one-dimensional. Normally, a ratio of 10 or less, between the mean ρ curves can be accepted as satisfying this condition.

2. A low skew parameter (zero in the absence of noise) is another essential requirement of the one-dimensionality of the station data.

3. If the azimuthal rotation values are scattered, and have large error bars, the data can be said to be

Figure 5.16 Presentation of selected AMT apparent resistivity and phase curves against period. Four main groups are highlighted, labeled (a) - (d). The station results from the stations within each group display important similarities, which differentiate the stations from different groups. The position of the grouped stations is shown in figure 5.17.

Figure 5.16 (A)

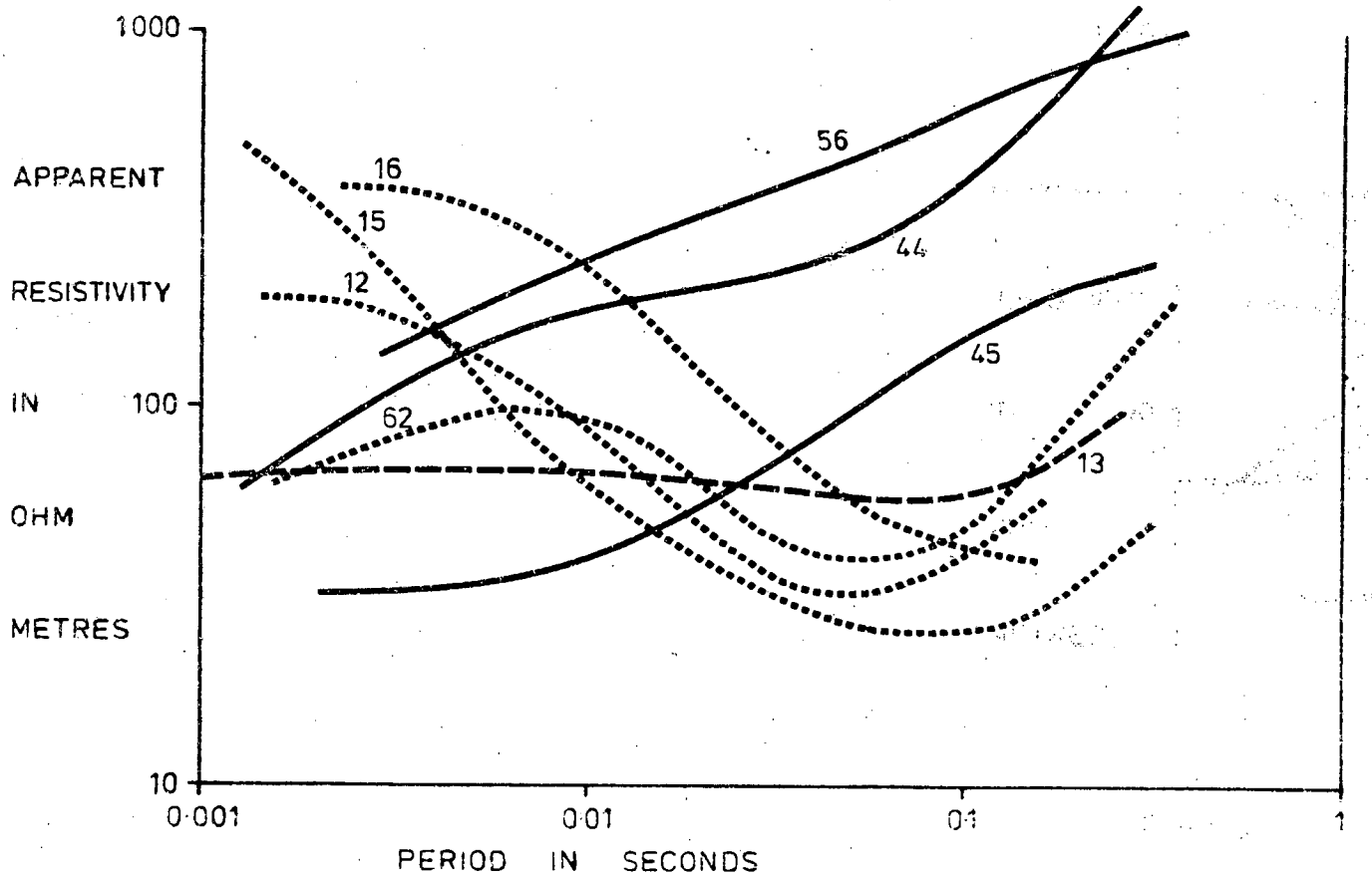
1000
100
10
APPARENT
RESISTIVITY
IN
OHM
METRES
16
15
12
62
56
44
45
13
0·001
0·01
0·1
1
PERIOD IN SECONDS

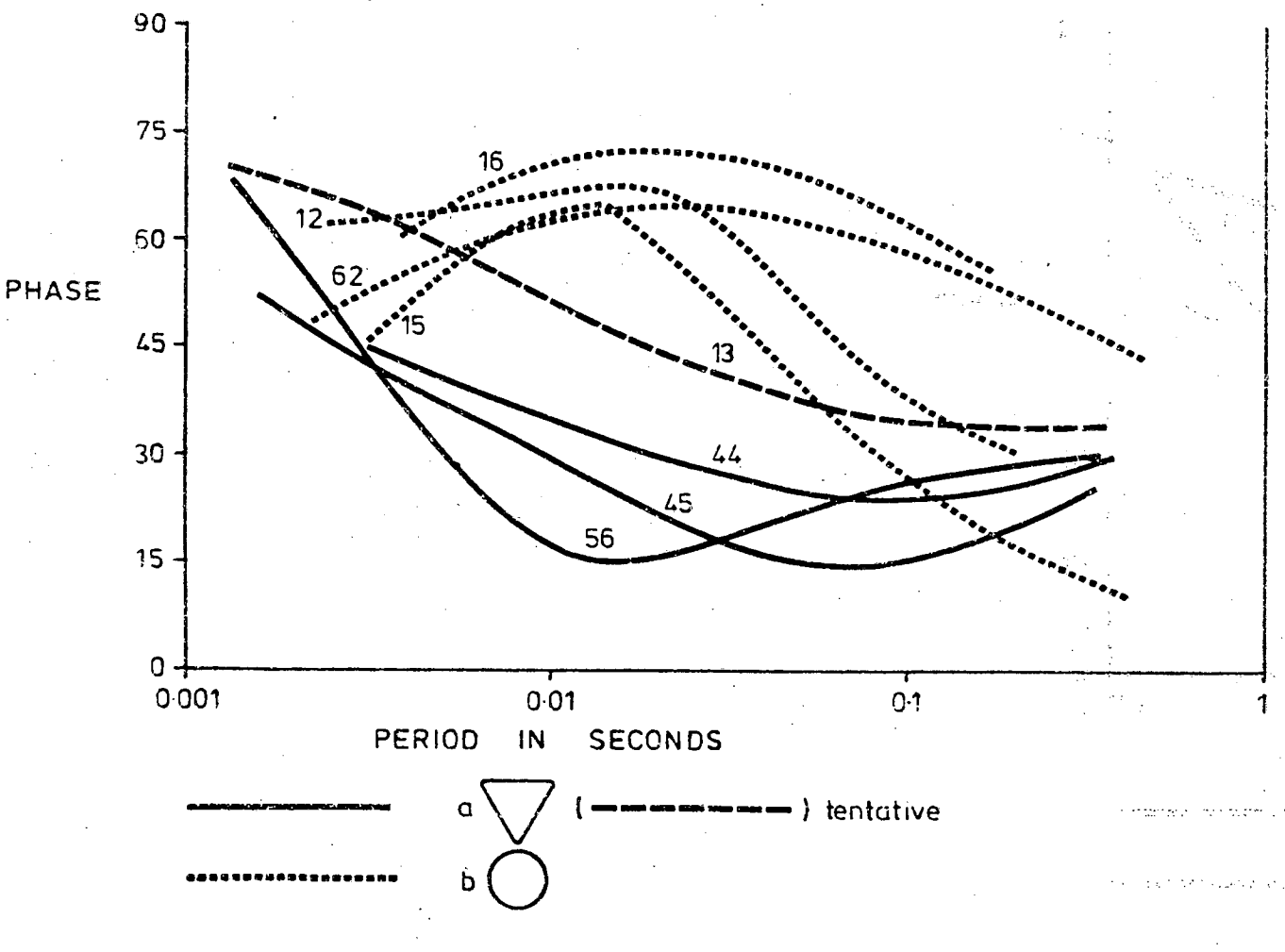
90
75
60
45
30
15
0
PHASE
16
12
62
15
13
44
45
56
0·001
0·01
0·1
1
PERIOD IN SECONDS
a
b
( ) tentative

Figure 5.16 (B)

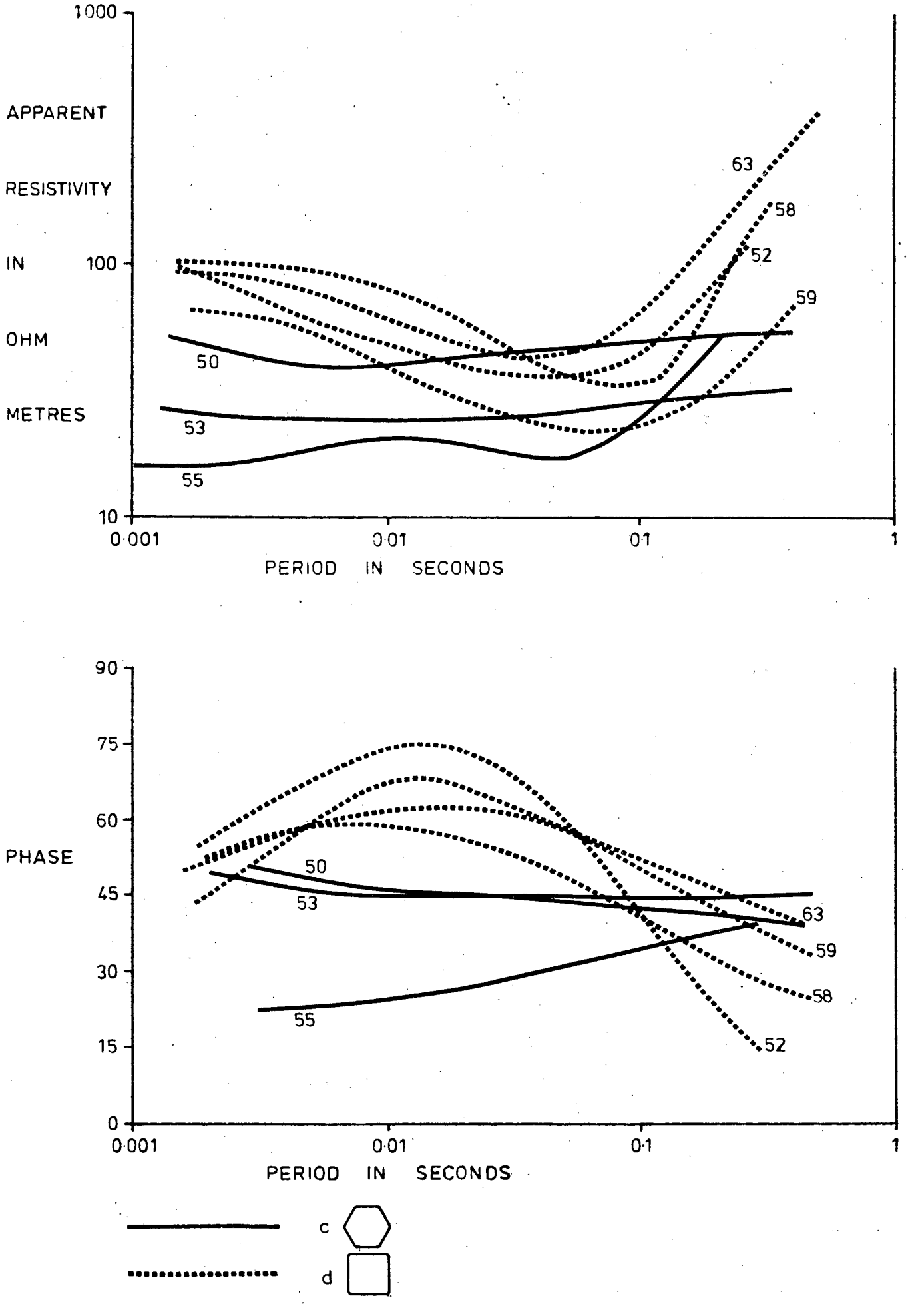
1000
APPARENT
RESISTIVITY
IN
100
OHM
METRES
10
63
58
52
59
50
53
55
0·001
0·01
0·1
1
PERIOD IN SECONDS
90
75
60
PHASE
45
30
15
0
50
53
63
59
58
55
52
0·001
0·01
0·1
1
PERIOD IN SECONDS
c
d

one-dimensional, with additional confidence.

The last criterion is, in practice, difficult to define, as the difference between scattered and unscattered data is subjective.

All results of the AMT soundings were examined for the dimensionality indicators. The observed distribution, based on the three criteria above, is shown in figure 5.15. The complete results in each figure (a) and (b) of the data , were examined for common features between stations, noting particularly the shape of the apparent resistivity and phase mean curves. These curves, as they are often referred to, were used to represent the data in the subsequent discussion. The conductivity structure, implied from these curves, as the number of layers, the resistivity values of the suggested layers and the depth to the intermediate conductor, was also noted. The first approximation resistivity - depth plots were also consulted, to support the presentation of results.

The results presented in figure 5.16 show the apparent resistivity and phase mean curves for 4 selected groups of stations. Within these groups of stations, results were observed to display similar behaviour. The station designation number, shown against each curve in figure 5.16, corresponds to the station number in figure 5.17. Each group of stations is marked by a different symbol. These curves were plotted together, to show their similarity within each group (a) to (d).

Figure 5.17 Map showing the location of stations within each of the 4 groups presented in figure 5.16. The results from these stations are discussed in the text. They showed similar behaviour within each group marked by the symbols : 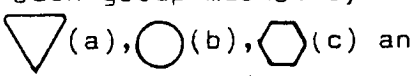 (a), (b), (c) and  (d).

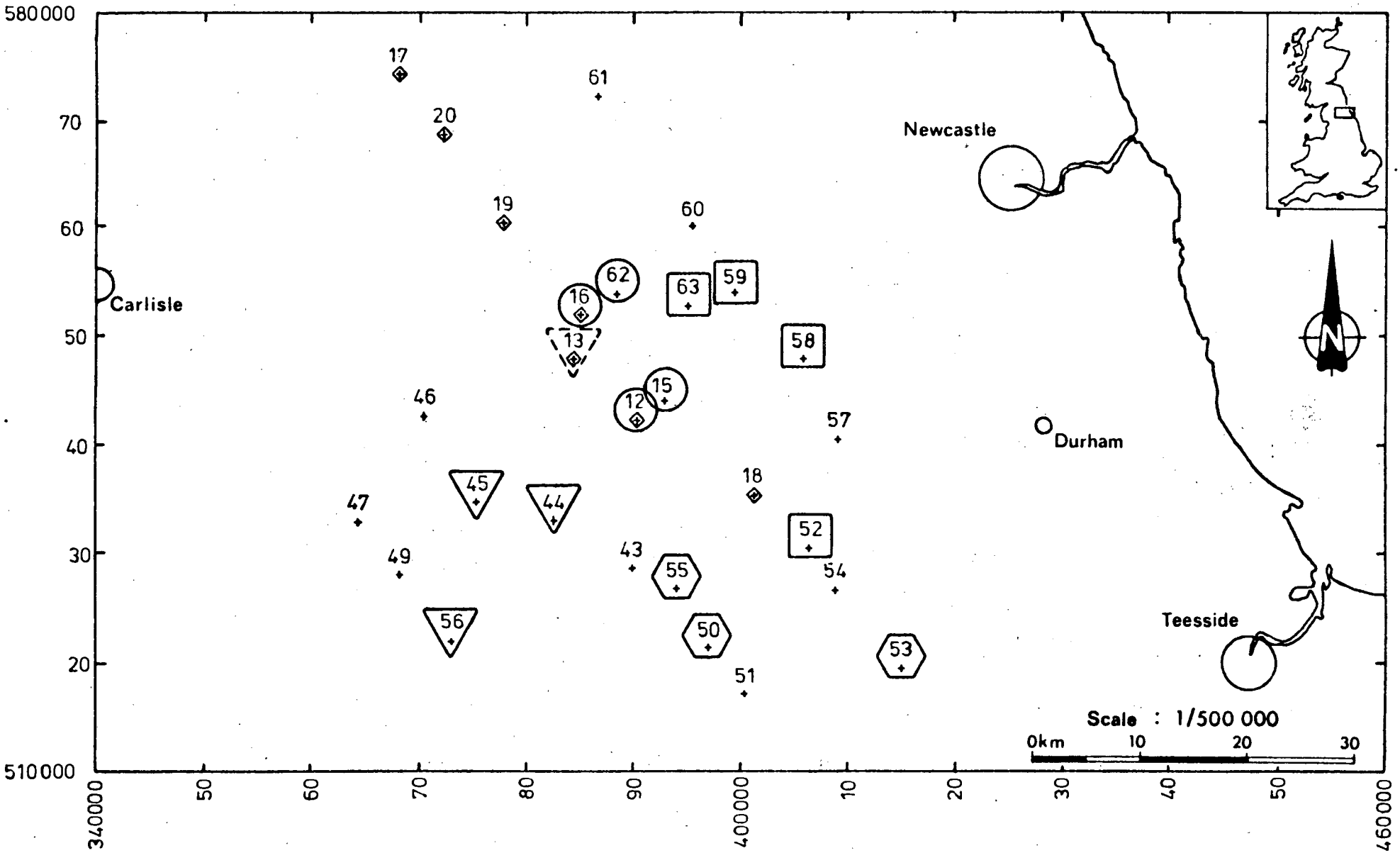
580000
70
60
50
40
30
20
510000
340000
50
60
70
80
90
400000
10
20
30
40
50
460000
17
61
20
19
60
62
63
59
16
13
58
15
12
46
57
Carlisle
Newcastle
Durham
18
45
44
47
52
43
55
49
54
56
50
53
51
Teesside
N
Scale : 1/500 000
0km 10 20 30

Figure 5.17

Group (a). The most distinctive response curves were observed at the stations 44, 45 and 56. (Triangle symbol) The results were well defined, especially at station number 44 and 45. The results indicate a conductivity structure of increasing resistivity with depth, but a deep and narrow intermediate conductor is shown by the inflection in the data at 0.06 seconds.

Group (b). Stations 12,15 and 16 are in this group. (Circles) They are distinguished by a prominent resistor-conductor -resistor three layer structure. The resistivity contrast between the layers is large and the intermediate conductor is well defined and shallow. The station 62 could be included in this group. The curves plotted in figure 5.16, representing this group of stations are clearly different to those plotted for the group (a).

Group (c). The cluster of stations 50, 53 and 55, noted by hexagon symbols in the figure 5.17, show an almost 'flat' response of the major apparent resistivity mean curve. From this curve, the implied conductivity structure is of a generally conducting medium, with no major interfaces. The station 13, which shows a similar structure, is located further to the north of this group and is tentatively included in group (a), with the stations of which it shares certain features. A similar 'flat' response of the apparent resistivity curve is registered by the 3 stations 17,20 and 60 to the north of the area.

Figures 5.18 - 5.21 Selected AMT station results from 4 distinctive groups.

Figure 5.18 Station 44

STATION 44

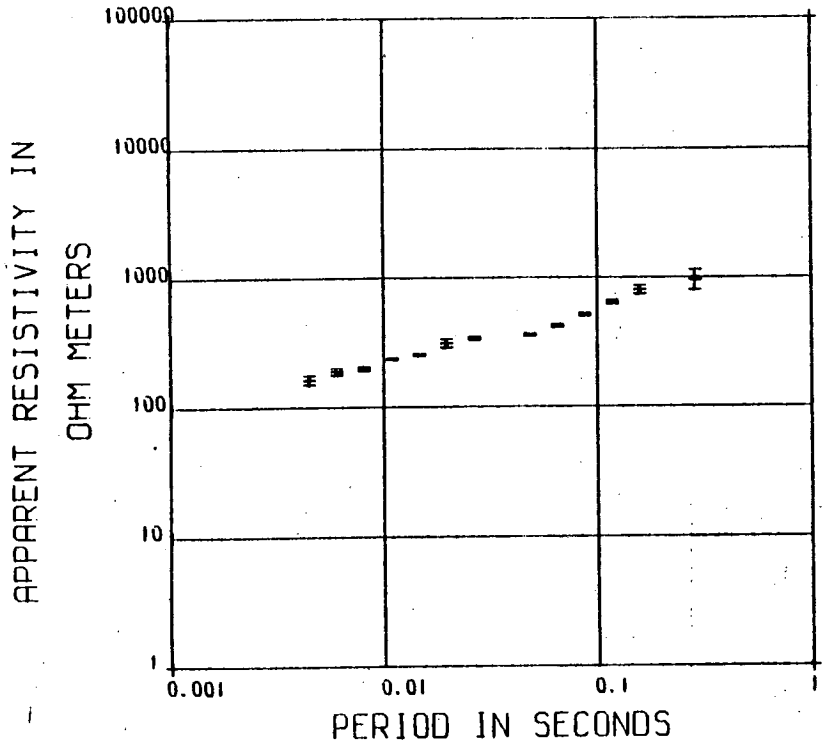

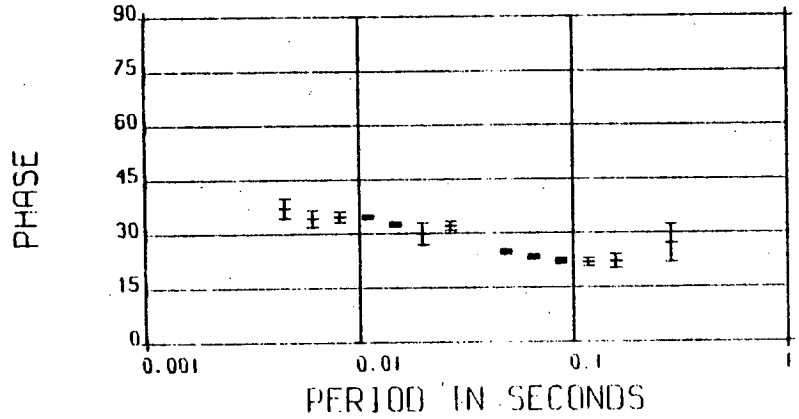

STATION 44

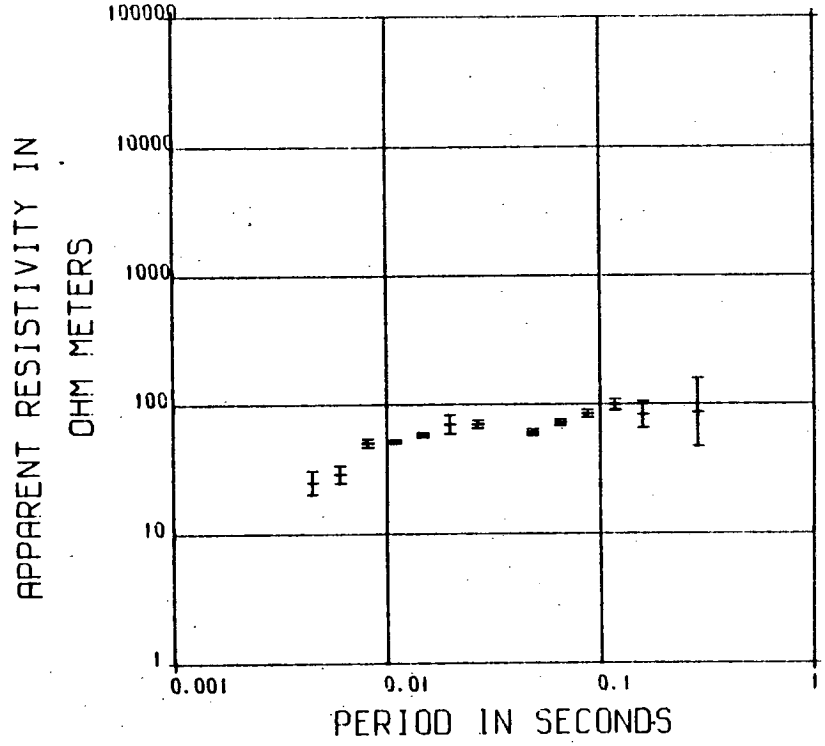

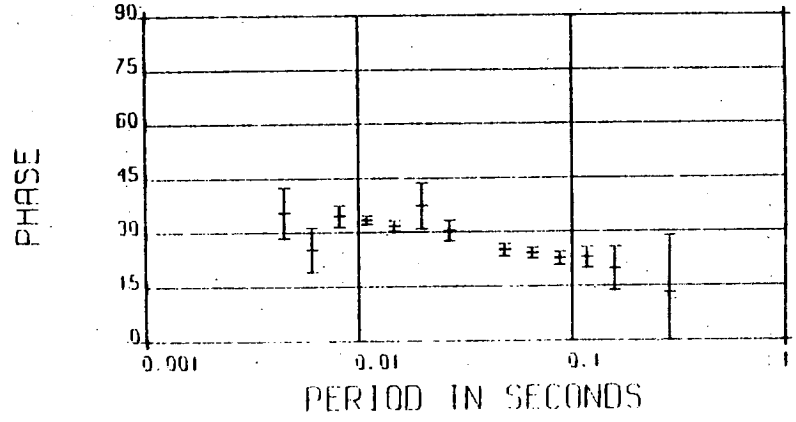

Station 44

STATION 44

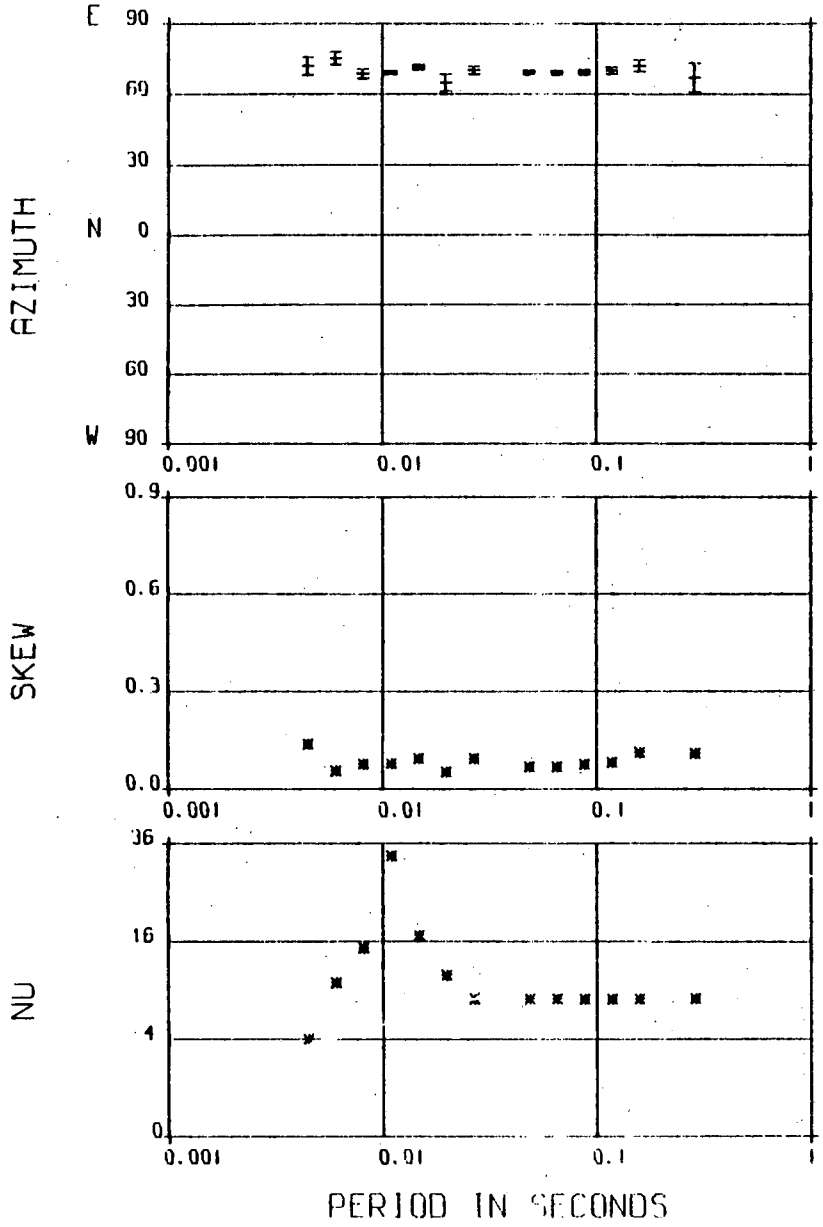

STATION 44

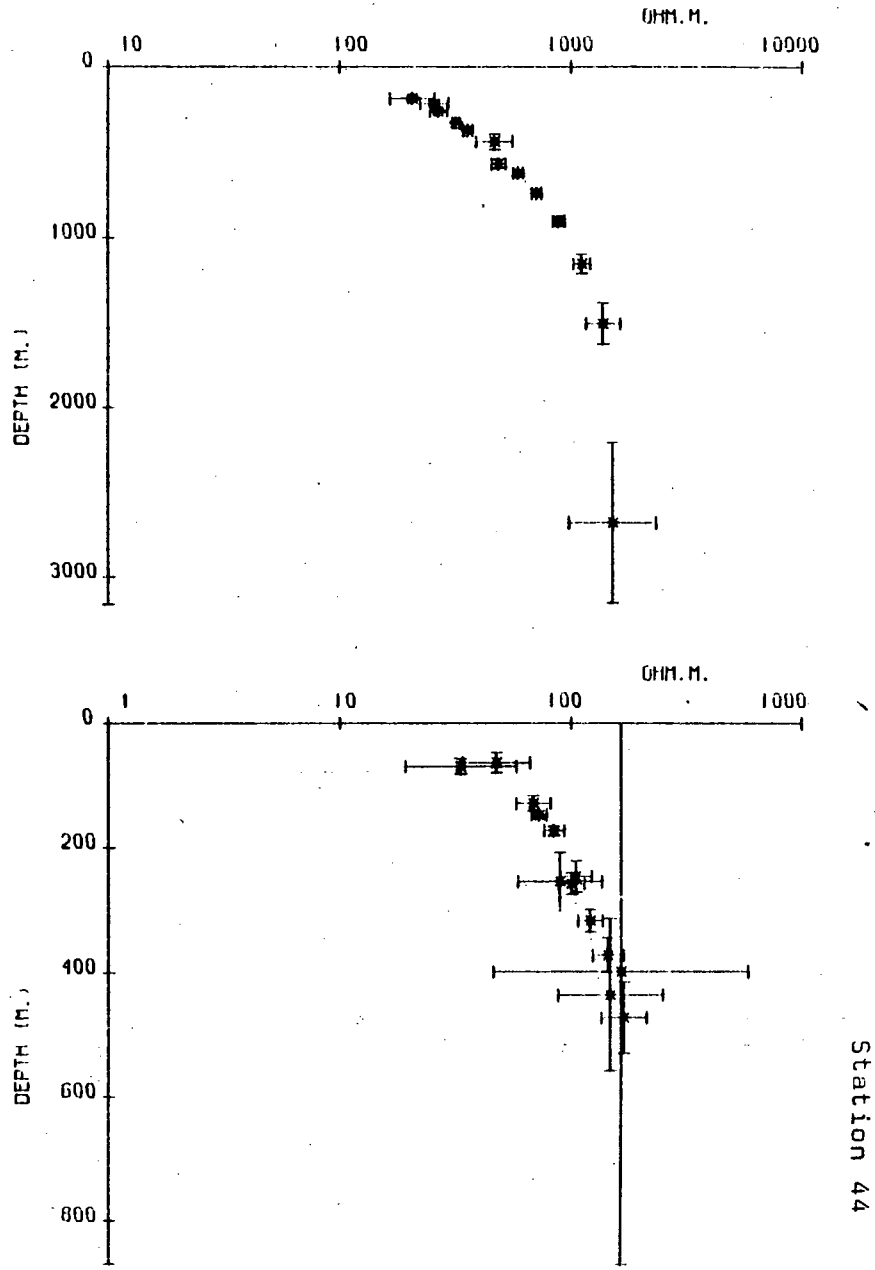

Station 44

Group (d). The final group of stations which has been distinguished in figure 5.17, contains the stations numbered 52,58,59 and 63. The results from stations numbered 18,19 and 57 display a similar, but a less well defined structure. The 4 clearly defined stations in this group bear the square symbol. The important feature of the results from stations in this group, is the well defined large and rather deep intermediate conductor. The implied first and third layers are again resistive, as in group (b), and there is an indication that the third layer is highly resistive. This is shown most clearly by the structure of the data from station 52, of between 0.1 and 1 second period.

The results from stations 47 and 49, to the west of the area, indicate the presence of a major intermediate resistor. No other stations in figure 5.17 displayed a similar result.

5.3 Discussion of selected AMT results

The full results of station number 44, 15, 50 and 52, representing an example of the results from each of the groups (a), (b), (c) and (d) above, were chosen for discussion in this section.

5.3.1 Station number 44

The station results from this station are shown in figure 5.18. They show apparent resistivity magnitudes exceeding 200 ohm-m and 50 ohm-m for the major and minor curves respectively. The major curve reaches 1000 ohm-m

Figure 5.19 Station 15

STATION 15

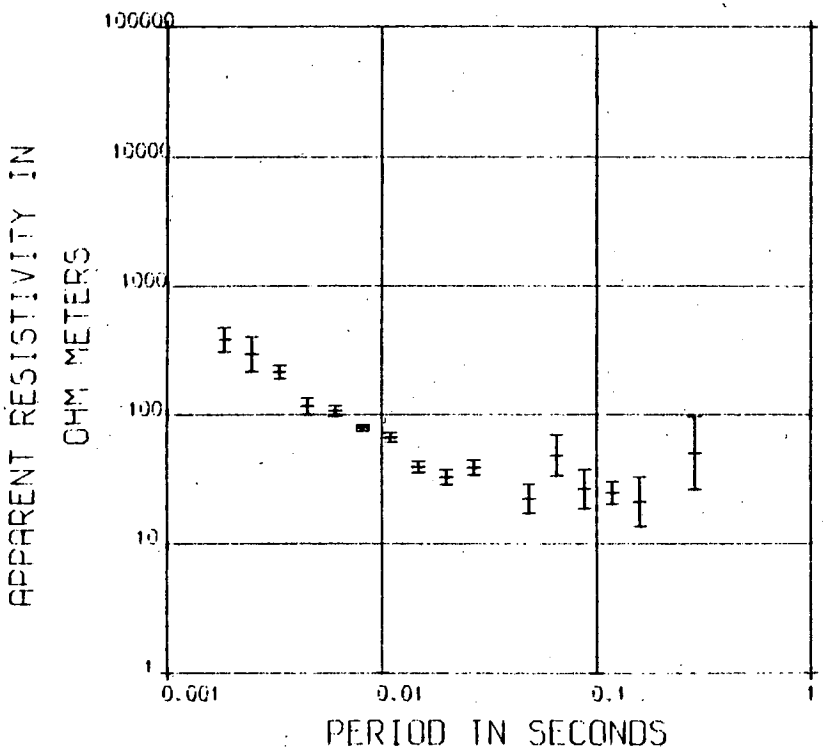

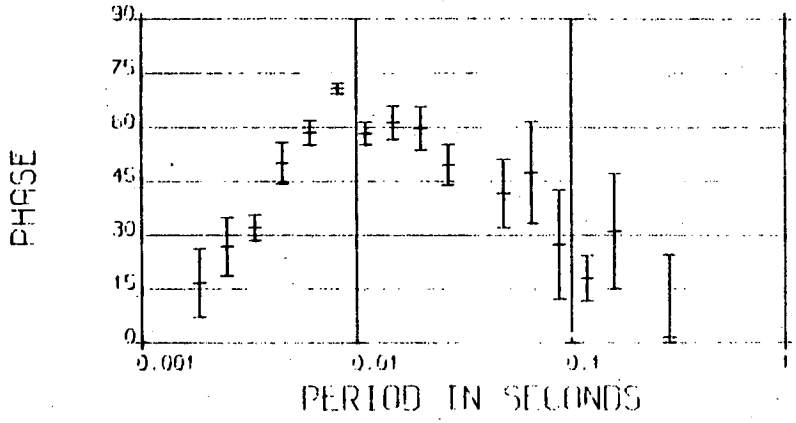

STATION 15

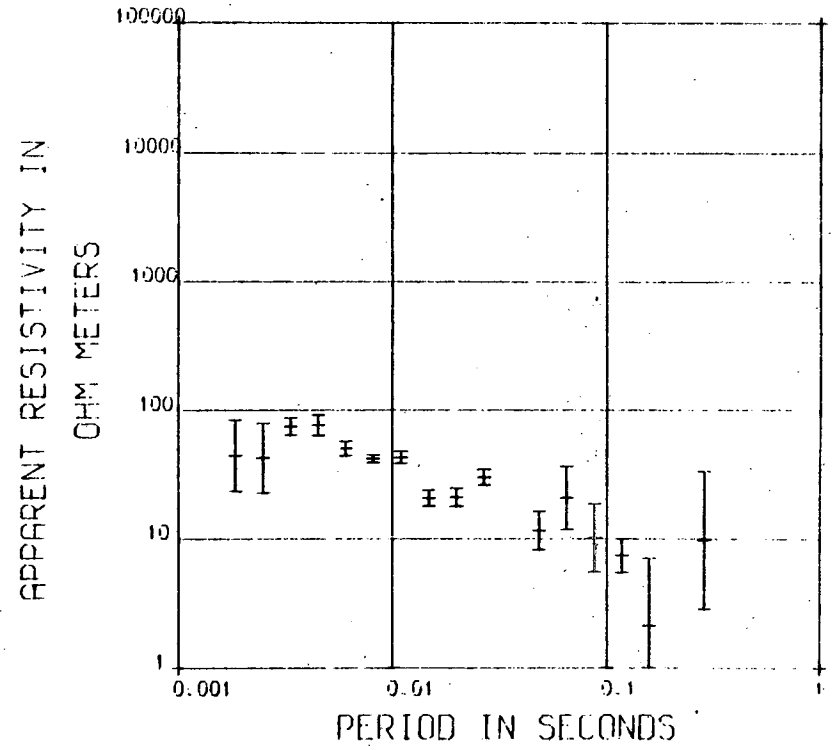

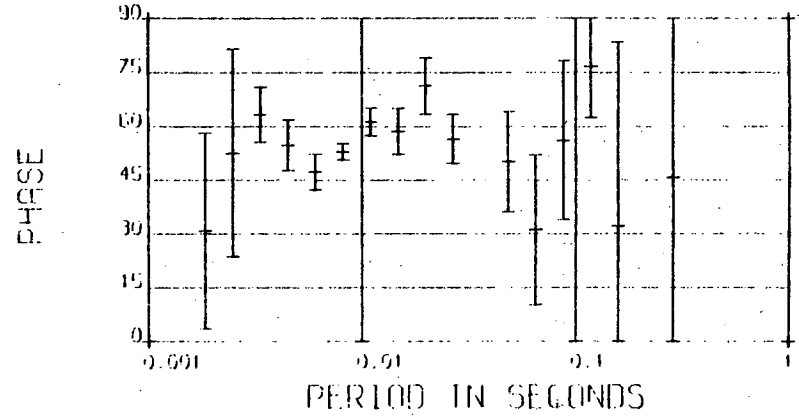

Station 15

STATION 15

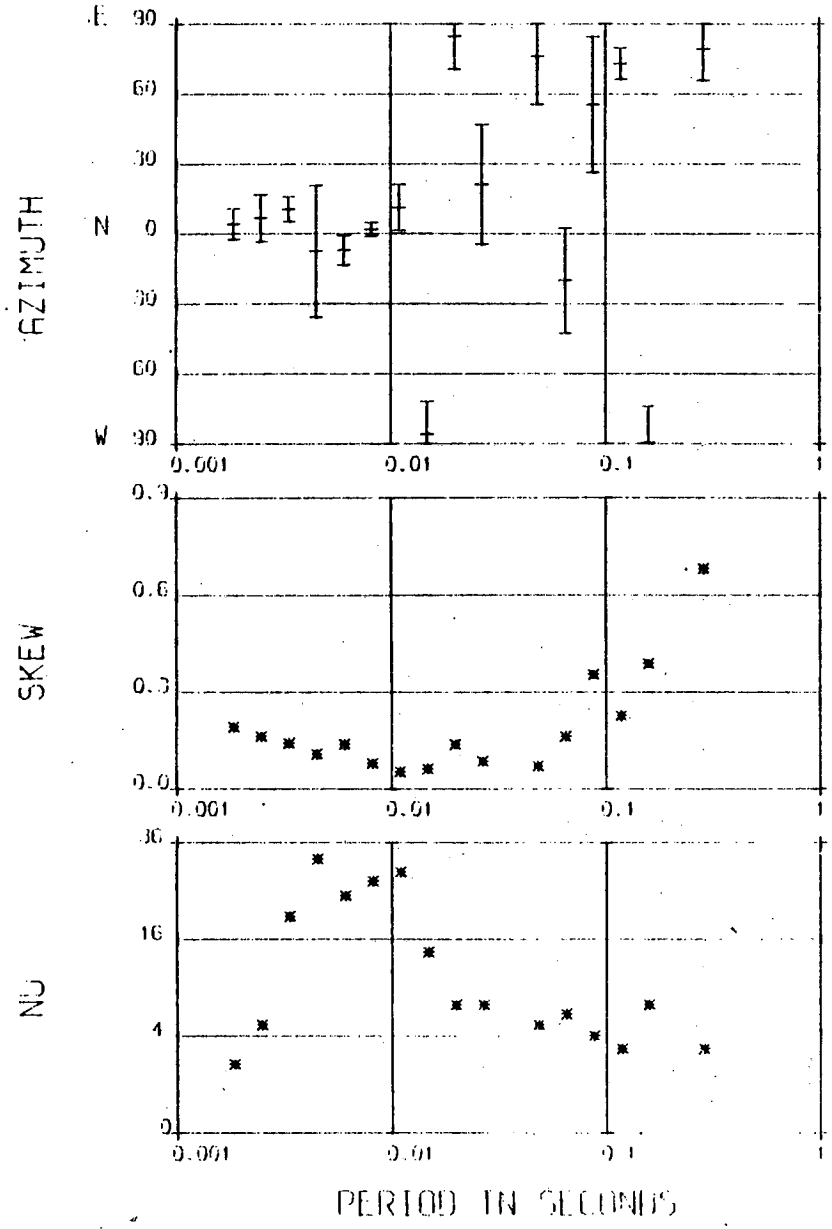

STATION 15

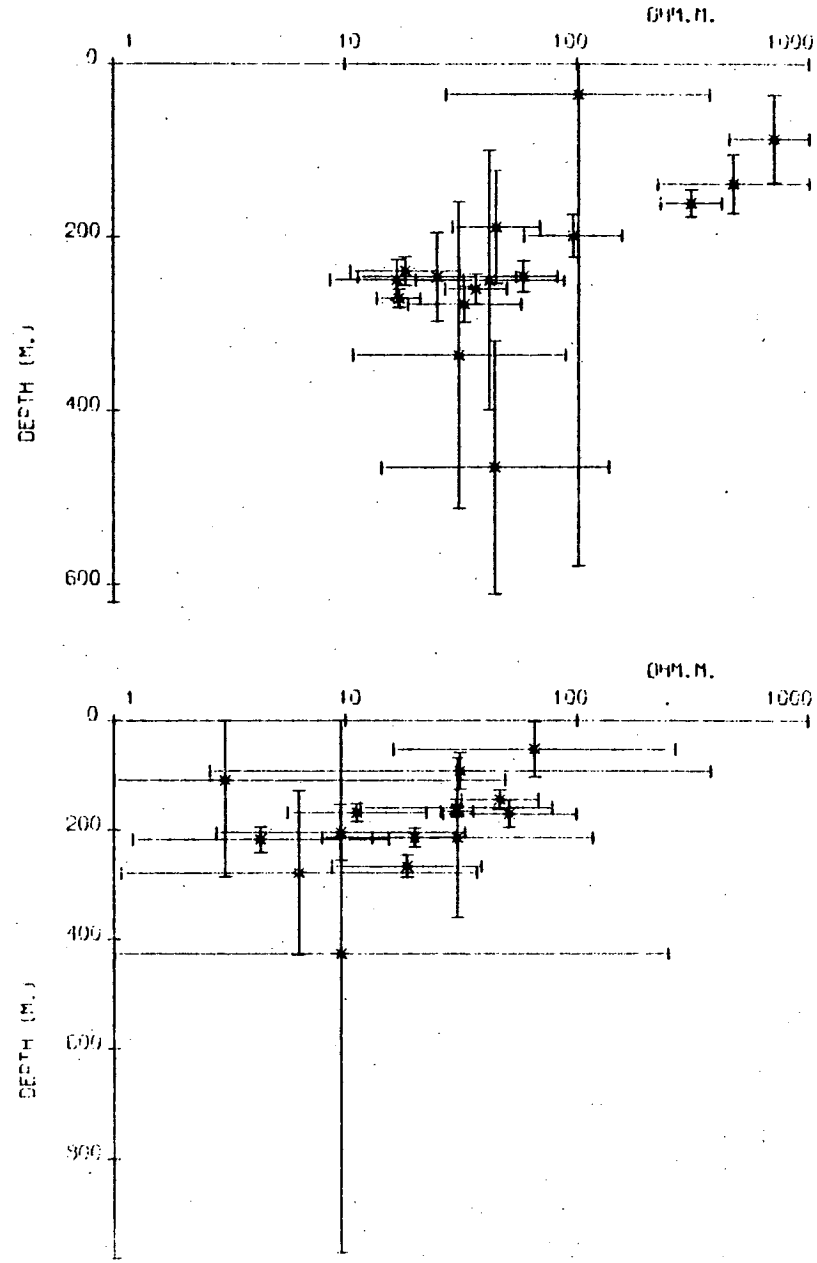

Station 15

at the lowest frequencies. The other stations in this group show complex behaviour, having medium to high skew factors. The skew values shown in the results of this station are very low, not exceeding 0.15. The data are 'mildly' isotropic, being neither isotropic or anisotropic. The azimuth of the major impedance values, shows a well defined preferred direction of 70 degrees E of N, suggesting the existence of a prominent two-dimensional structure. Some of these features are displayed in the results from stations 43 and 46 which otherwise appear not to fit in the category of this station.

5.3.2 Station number 15

This station was located near to the broadband station 12. The discussion of these two stations, Rookhope II and Rookhope I, is presented in chapter 6. The dimensionality indicators, shown in figure 5.15 indicate a one-dimensional structure at this station. The values of the skew parameter are below 0.4, except at the longest period estimate. The azimuth of rotation does not display any preferred alignment throughout the shown period band. The apparent resistivity mean curves show a pronounced fall, from the shortest period estimates, to a period of 0.1 seconds. This distincive shape indicates, that a large and shallow intermediate conductor is located at this station. Above 0.1 seconds the data indicate a transition into a resistive third layer, although this is not clearly shown by the small number of estimates accepted at this station. The major apparent resistivity phase mean curve does, however,

Figure 5.20 Station 50

STATION 50

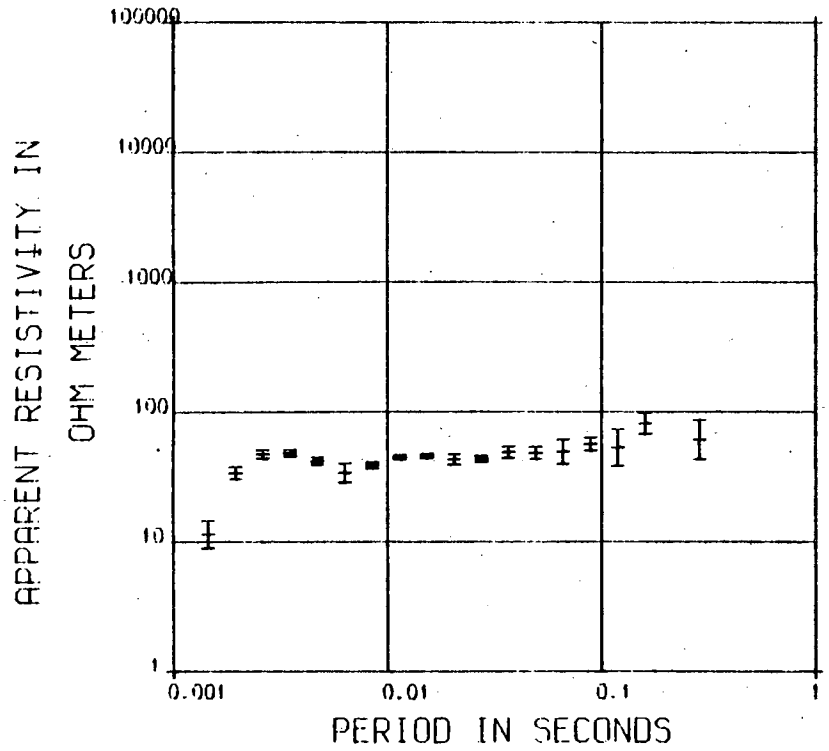

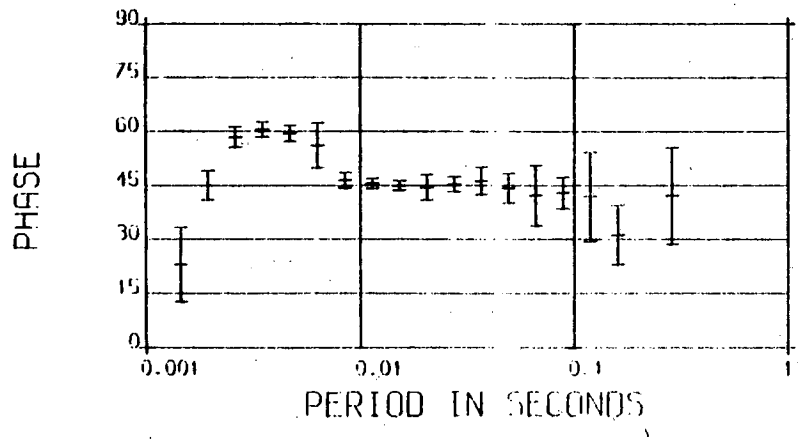

STATION 50

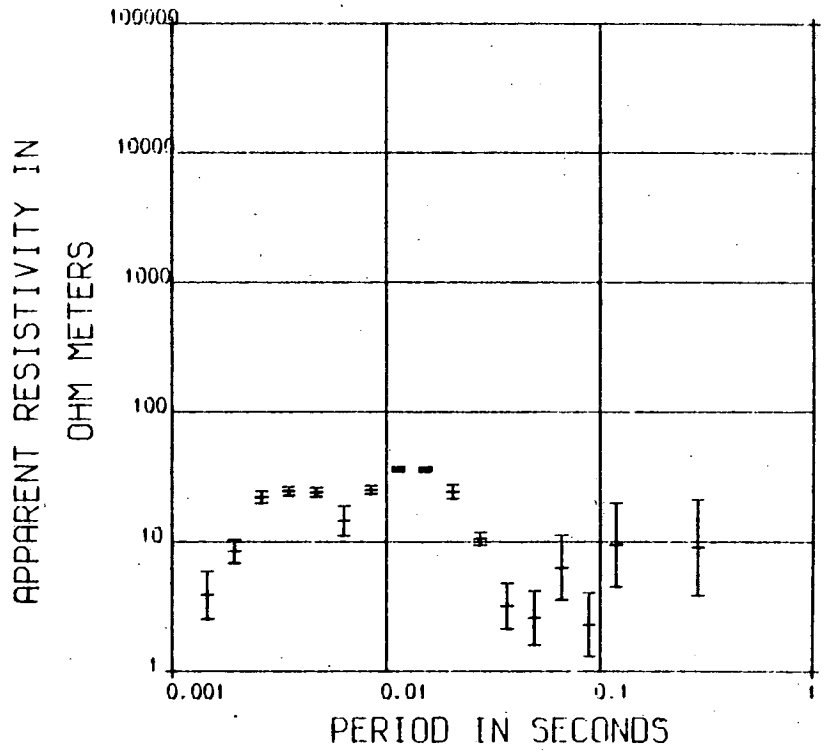

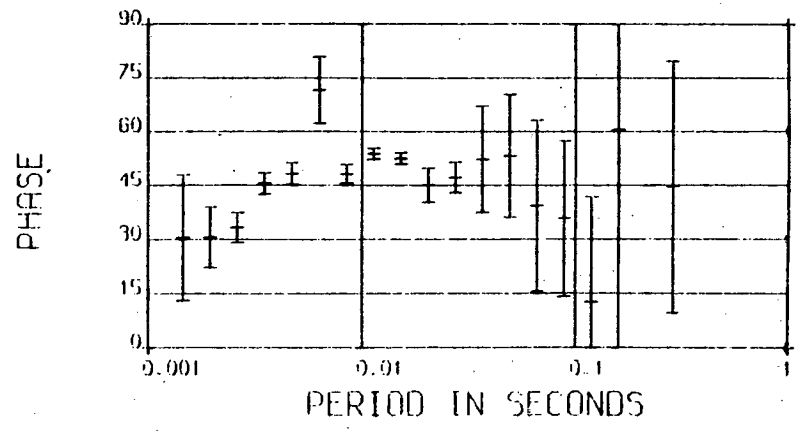

Station 50

STATION 50

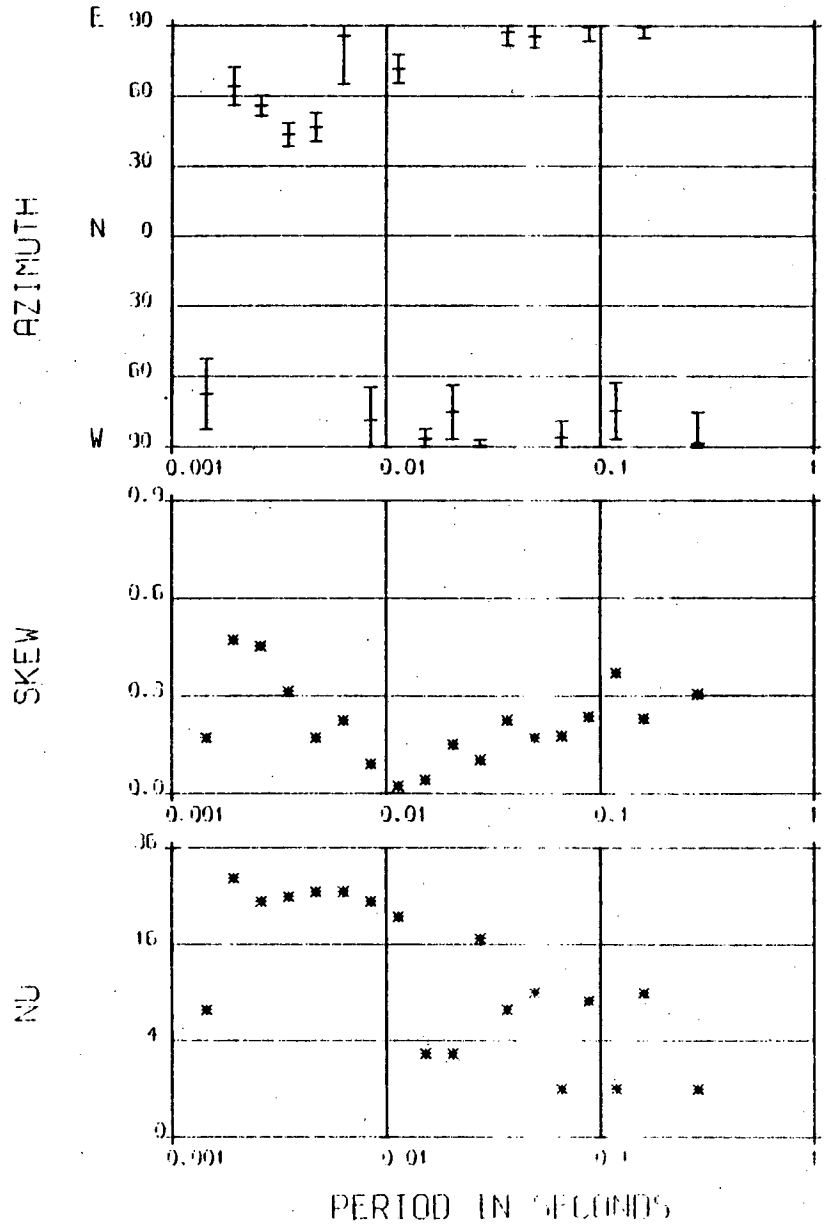

STATION 50

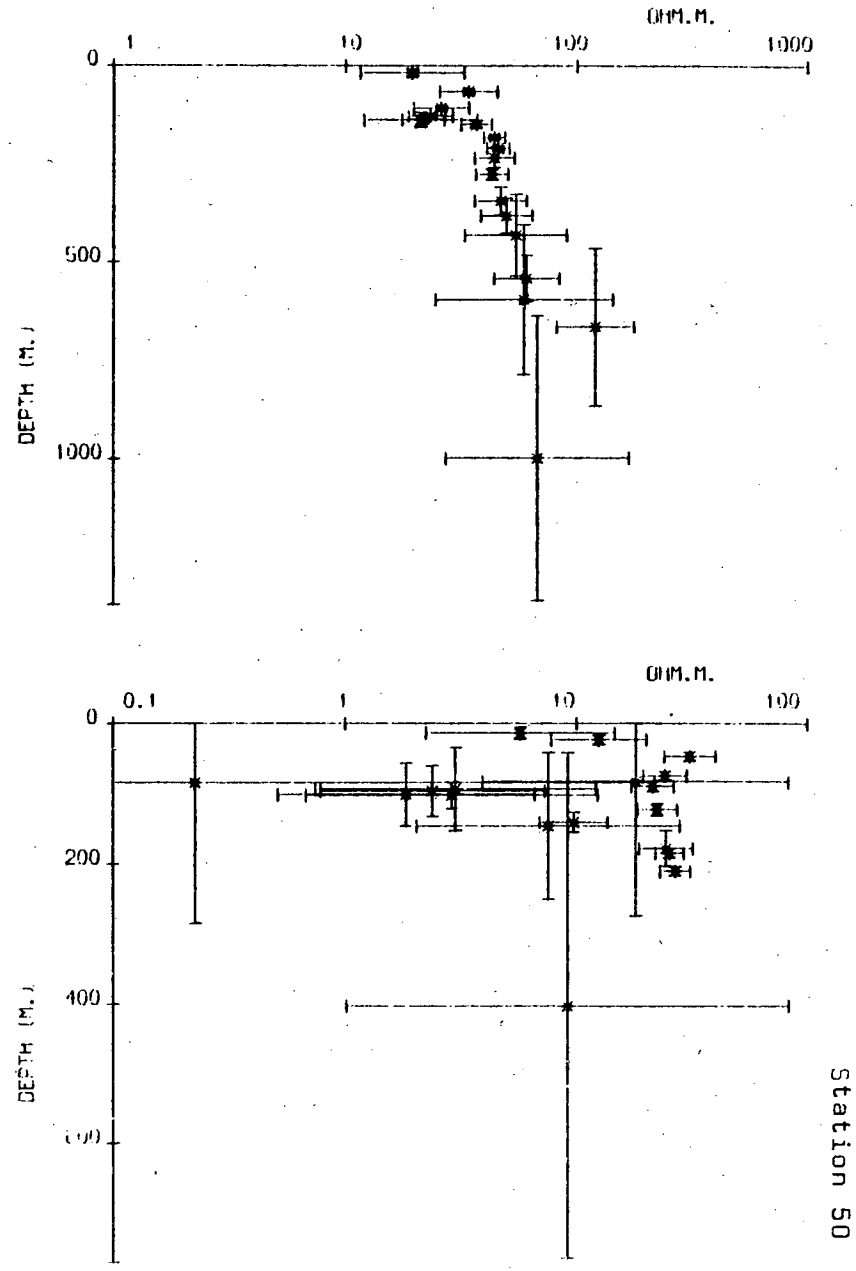

Station 50

show a clear transition from a conductor to a resistor, by the sharp fall, across the 45 degree line, from 75 degrees to 0 degrees, over the period range 0.01 seconds to 0.4 seconds. The results from station 15 are shown in figure 5.19.

5.3.3 Station number 50

The results from station number 50, shown fully in figure 5.20, display low values of resistivity, in both major and minor apparent resistivity mean curves. The respective magnitude of the curves lies mostly below 20 ohm-m and 5 ohm-m over the complete period range. The dimensionality indicators show, that this station displays two-dimensional behaviour, although the other stations in this group all display medium or high skew factors and medium to high anisotropy. (See figure 5.15) The phase of the major apparent resistivity data is steady, at 45 degrees. It does not show the fall with decreasing frequency, found in results from most other stations in the survey. The azimuth of rotation of the major impedance shows an E - W orientation, for frequencies up to 125 Hz. There appears to be a tendency towards one-dimensionality at the shortest periods, a note supported by the relative isotropy of the apparent resistivity results at these periods.

5.3.4 Station number 52

The apparent resistivity mean curves, from station 52 are characterised by first, a prominent lowering of the resistivity values at approximately 0.09 seconds, followed by a sharp rise in the values at longer periods.

STATION 52

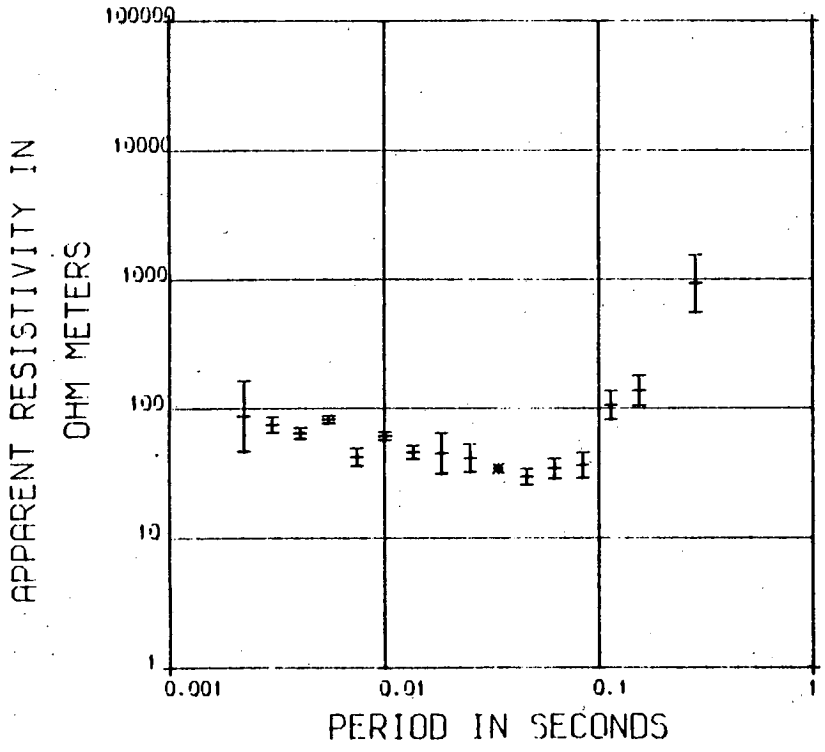

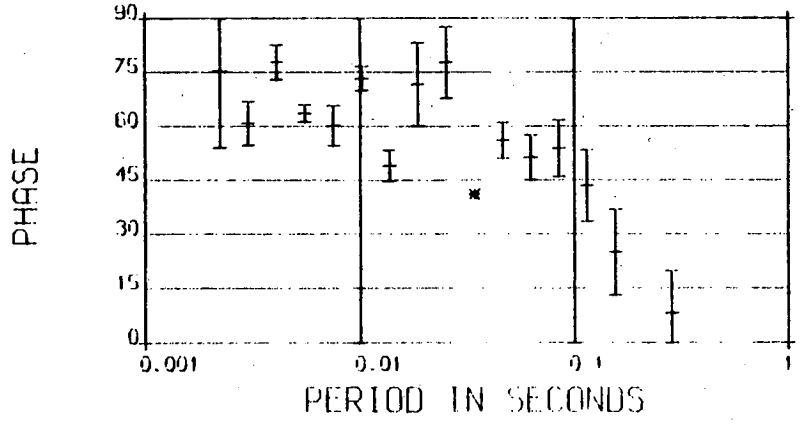

STATION 52

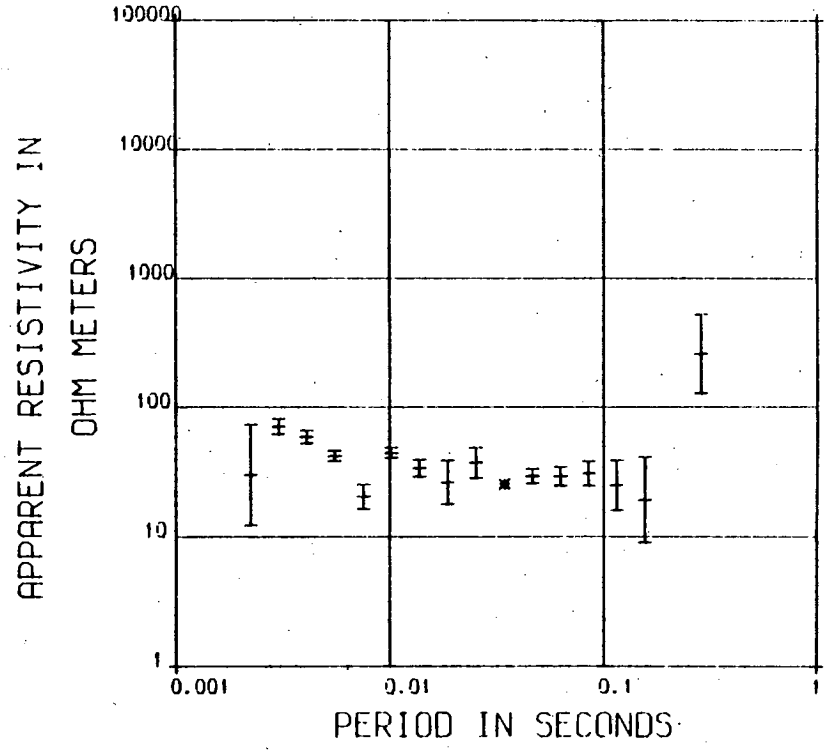

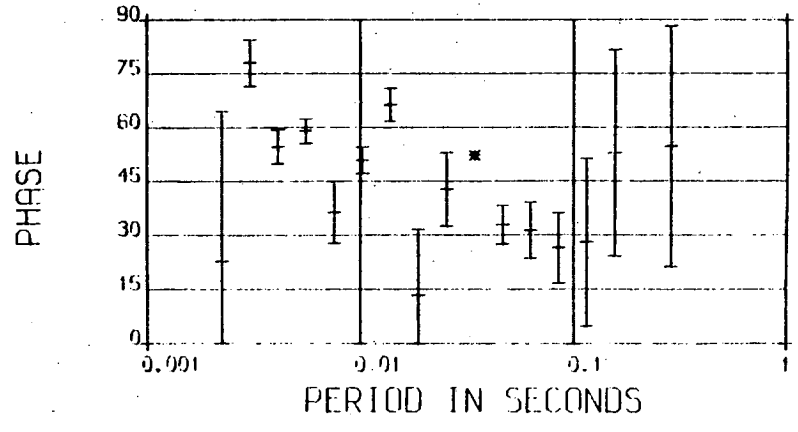

Station 52

STATION 52

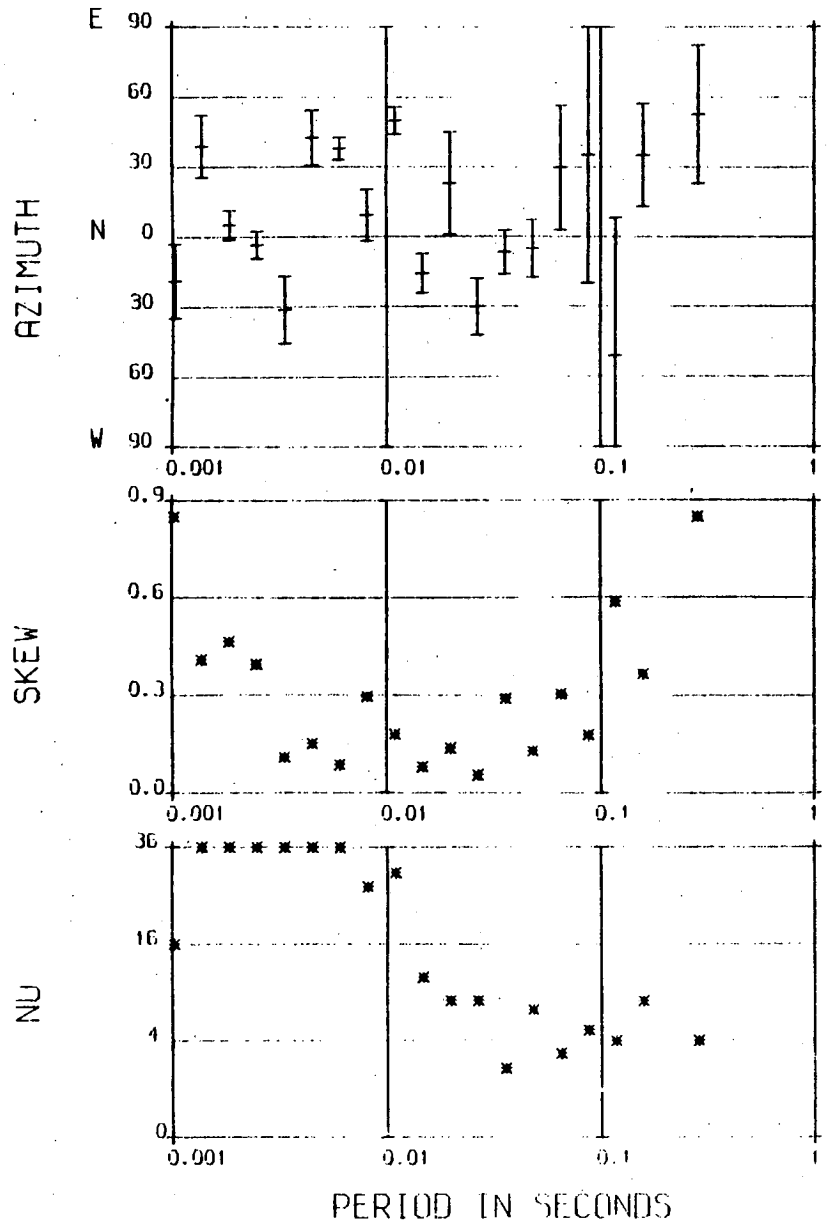

STATION 52

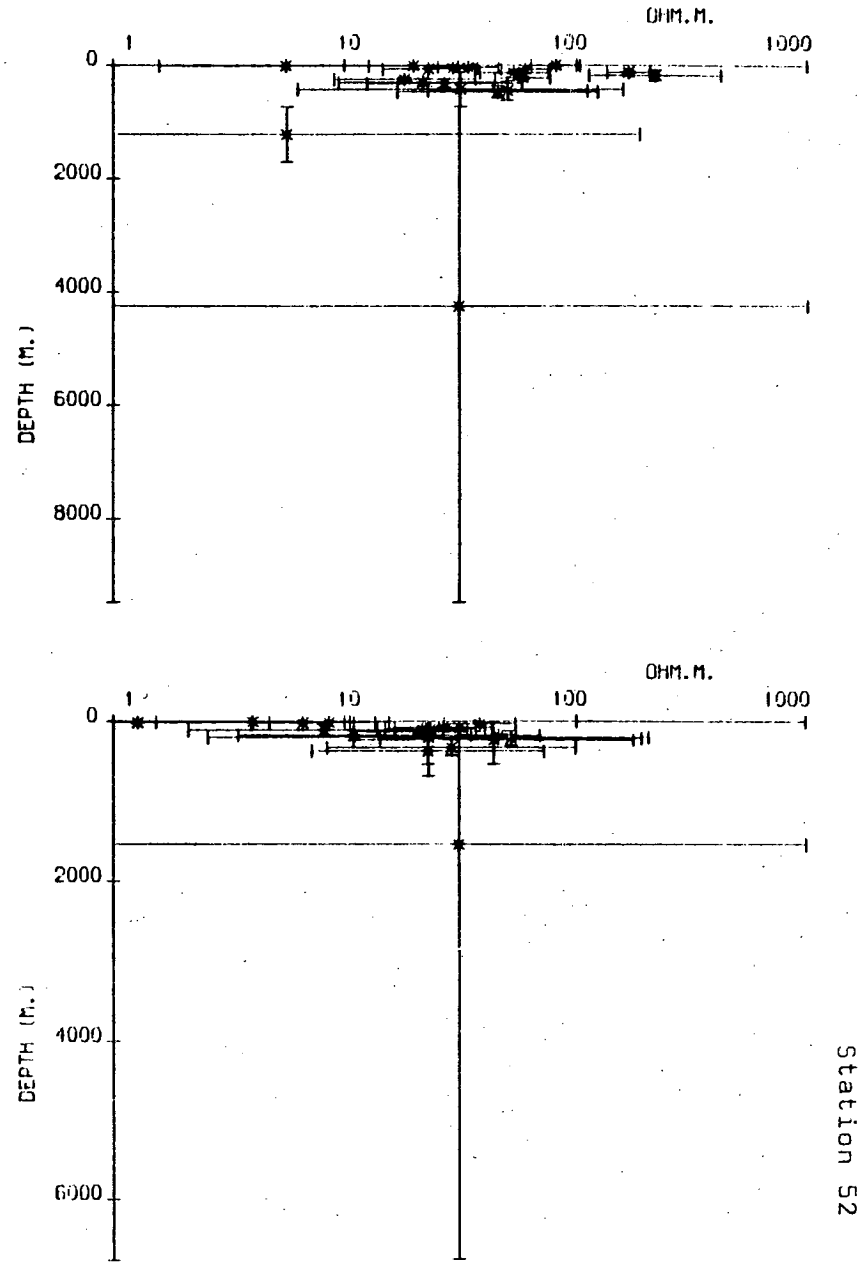

Station 52

This behaviour is typical of results from stations within group (d), but differs from the results obtained at stations in group (b), by occuring at slighly longer periods. The data from station 52 are isotropic, the skew factor shows low values, typically less than 0.5 and the azimuth parameter shows no dependence on frequency. This is summarised in figure 5.15. The implication is that of a one-dimensional structure. The results from this station are presented in full in figure 5.21. The same response was observed at many of the stations which form group (d). Major differences, particularly in the structure of the apparent resistivity and phase curves were present, however, at a number of the stations in this group, which cover a large part of the survey area.

5.4 Summary

Selected results of the AMT station coverage were presented, as representative examples of each of 4 distinctive groups of stations. Within these groups, station results showed important similarities. All AMT station results, collected during this work, have been compiled, for easy reference, in numerical order, in Appendix II.

It was noted that, at approximately 40 % of the sites, where AMT recordings were made in this study, a three-dimensional response behaviour was detected.

The results from the sites where both AMT and MT recordings were performed, have been presented and described

together. This had allowed an inspection to be made, of the behaviour of all the parameters, from long period variations of the order of 1000 seconds, to quite short period variations of 1000 c/s, with only the exception of 2 decades from 10 seconds to 10 Hz. Therefore, while changes in, for example, the azimuth of rotation of the impedance tensor were observed between the short and the long period bands, it was not possible to establish a continuous trend.

CHAPTER 6

INTERPRETATION AND CONCLUSIONS

A one-dimensional inversion algorithm of the Monte-Carlo type, described by Jones (1977), has been applied to the inversion of long period MT data by Jones and Hutton (1979), Mbipom (1980) and Ingham (1981). The observed frequency bandwidth was usually small, of the order of 3 decades, and the typical penetration depths were large, generally in excess of 20 km. The results showed that at such depths the conductivity fluctuations were restrained enough to warrant a fixed layer modelling approach with a small number of layers. Often a 2 or 3 layer representation with a constant $\frac{1}{2}$ space conductivity rendered sufficient complexity to produce a satisfactory fit to the data.

In this study a different modelling approach was found necessary to benefit fully from the extended observational bandwidth. The two main reasons for this change were:-

(a) the observation frequency spectrum spanned 6 decades and,

(b) the resolution of the more varied, shallower structure had been much improved.

6.1 The modified modelling approach

The following approach was developed and applied to the modelling of both the broadband data and the limited band AMT data.

(1) Firstly, the number of layers was selected as high as was necessary to satisfy the observed inflections in the ρ_a and ϕ data. It was observed that modelling, using more layers than was necessary, could produce an equally good (or slightly better) fit of the data. Modelling using less layers revealed, on the other hand, serious deviations of the inverted response from the observed data and their associated error bars.

(2) The model layer resistivity and depth values were allowed, wherever possible, to converge unrestrained. The selected models were free of bias due to preconceived ideas, other than the number of layers.

(3) Depending on the quality of the data and the ability of the model to converge satisfactorily, the apparent resistivity amplitude data, phase data or both were modelled at each station.

(4) Data points, clearly in error, were removed before modelling. If, as in some cases, data were difficult to model as in (2) above, a starting model was derived

by a separate computer-assisted master curve fitting procedure.

(5) The actual inversion of the data was undertaken using a version of Jones's (1977) computer programme modified and compiled by Dawes (1980).

6.1.1 Monte-Carlo method of inversion

The method of generating random n layer models from a file of random numbers was essentially unchanged. The parameters of any model were obtained from the relationship

$$\rho_i' = \rho_i 10^r \qquad i = 1,2 \ldots\ldots n$$

$$h_i' = h_i 2^r \qquad i = 1,2 \ldots\ldots n-1$$

where r is a random number between 0 and ± 1 and where ρ_i and h_i are the parameters of the previous model. The parameters were constrained by selected bounds and all but the five best models were discarded. The bounds for each variable parameter were then automatically re-adjusted using the information from the best five models. The average model was constructed from the five models and was used as the starting model in the next iteration.

The quality of fit could be calculated in a number of ways ie using the method of least squares, error weighted least square and error bar only, and was noted sequentially for each model and iteration in an output file. Models with up to nine layers could be used. Layer depths or layer

resistivity values could be held constant to refine a previously derived model.

6.1.2 Examination of the derived models

The modified approach worked well. Model responses converged quickly and efficiently to the modelled data. In some cases, governed by the structure of the observed data, a tendency to produce delta-like narrow and highly conductive layers was observed. This characteristic was associated particularly with good quality data. It was repeatedly shown to be the best interpretation of the data, by making the following examination. The product of the thickness (h) and conductivity (σ) was preserved for the narrow layer. The layer resistivity contrast was then progressively reduced. This effectively increased the layer thickness and consequently reduced the delta-likeness of the inverted model. The result was that the quality of fit could never be sustained. The tests did show that, by intensifying the delta-like functions a better fit of the data could be obtained. Also shown by the tests was the fact that, unlike the thickness of the layer which was always extremely well defined with respect to its resistivity value, the position of the layer within the resistive block was less well defined.

The final models were always chosen with the least pronounced delta-like functions, the response of which

would still fall within the bounds permitted by the observed data. The derived models were therefore considered to be the most satisfactory one-dimensional interpretations of the collected data.

6.2 Inversion of station data Rookhope I

The station Rookhope I (D12 in table 3.2) was, for the following reasons, a station of special interest.

(a) Many of the geophysical surveys relating to the area had been carried out at or near the site chosen.

(b) The results of the Rookhope boring provided a particularly ideal opportunity to verify the quality of the derived MT data.

(c) The good agreement between the results observed at the neighbouring sites Rookhope I (D12) and Rookhope II (D15) provided support for the validity of the AMT soundings.

The modelling approach described in the preceding section was, therefore, first applied to the inversion of MT data from station Rookhope I.

6.2.1 Borehole comparison

The complete results of the boring made at Rookhope can be found in Dunham et al (1965). A resistivity log, obtained in two sections to a depth of 1550 ft, is

Figure 6.1 Results of the Rookhope borehole log modelled to the AMT station 12 data. Depths held fixed. Best fitting model shown for comparison.

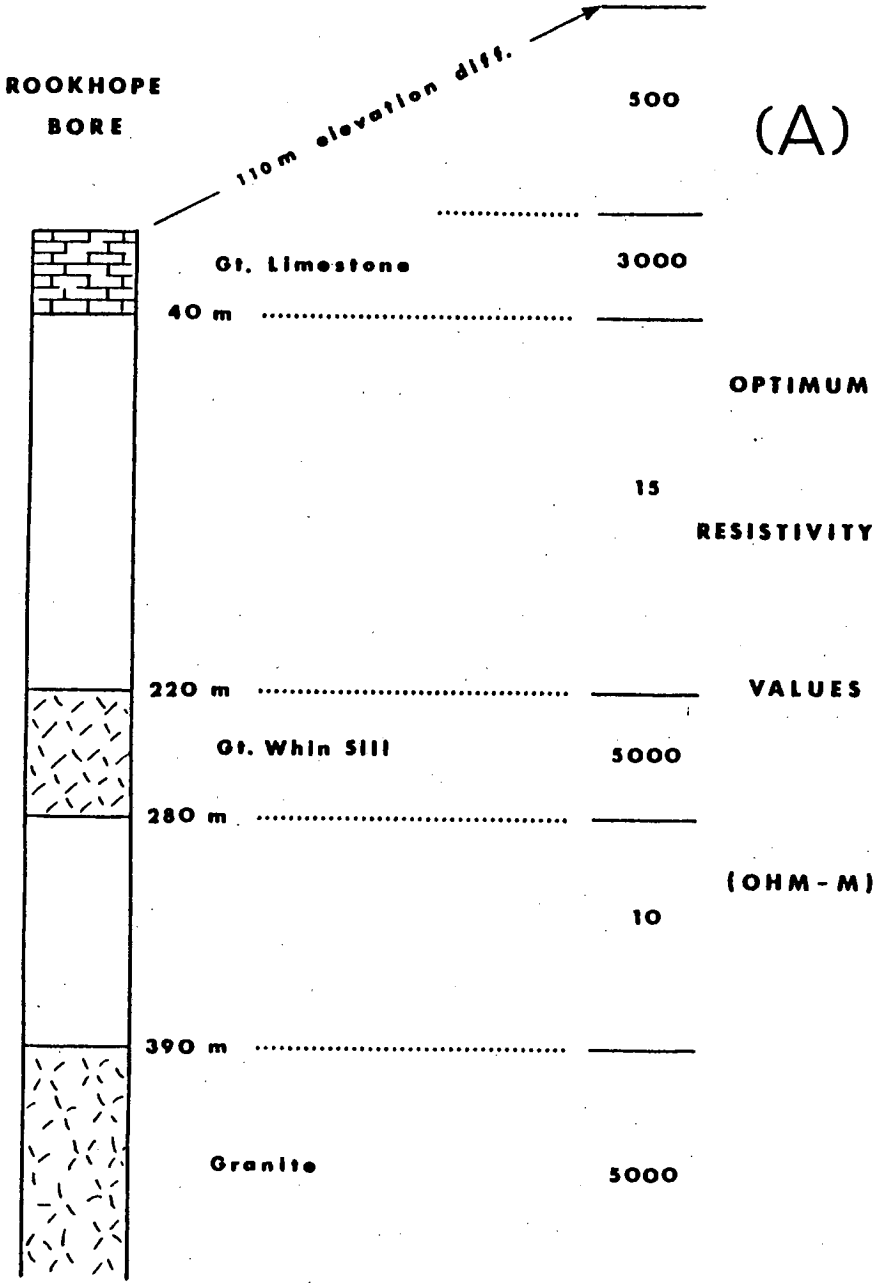
ROOKHOPE
BORE
110m elevation diff.
(A)
500
Gt. Limestone
3000
40 m
OPTIMUM
15
RESISTIVITY
220 m
VALUES
Gt. Whin Sill
5000
280 m
(OHM-M)
10
390 m
Granite
5000

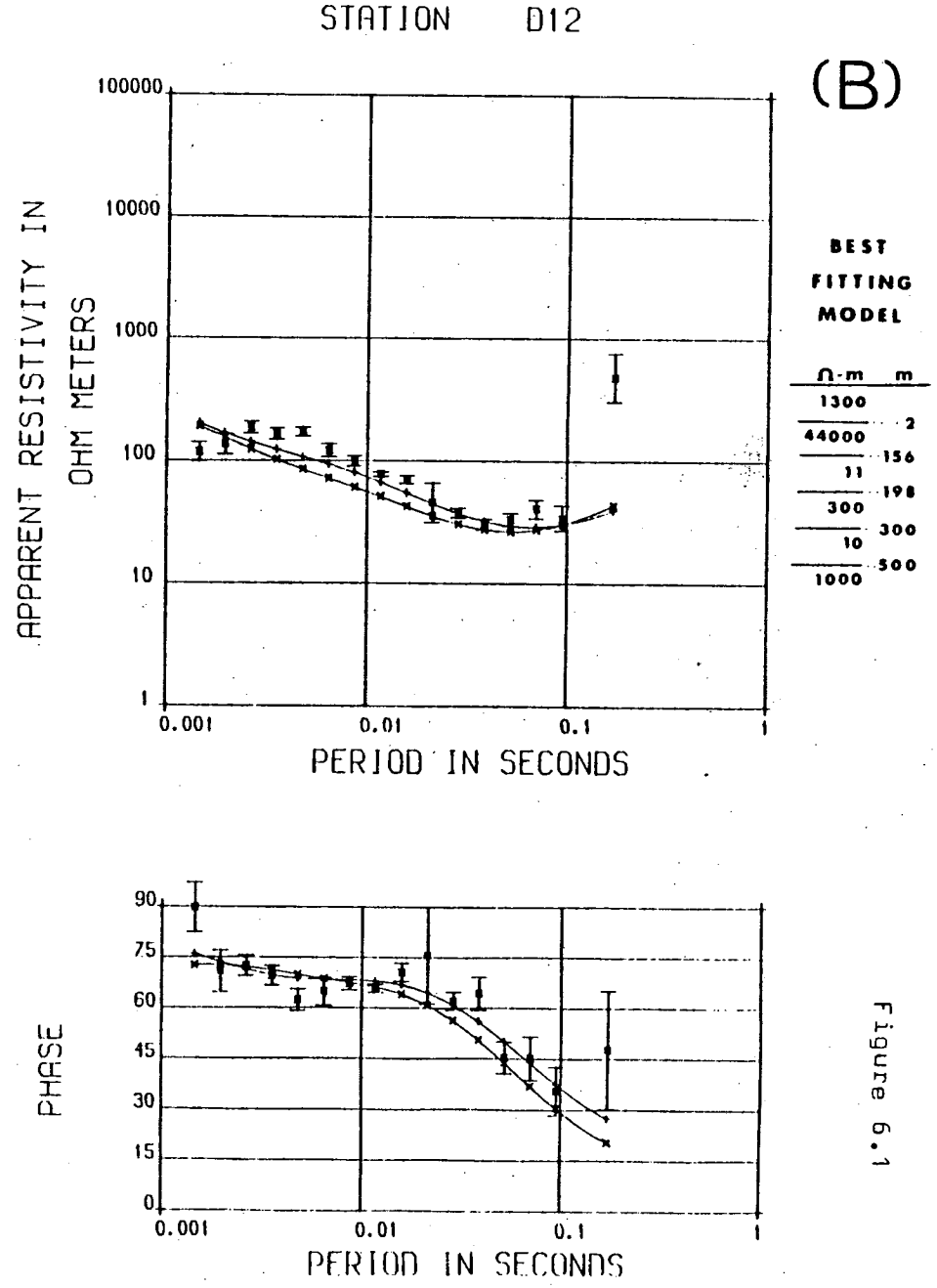
STATION D12
(B)
APPARENT RESISTIVITY IN OHM METERS
100000
10000
1000
100
10
1
0.001
0.01
0.1
1
PERIOD IN SECONDS
BEST FITTING MODEL
Ω-m m
1300
44000 2
11 156
300 198
10 300
1000 500
PHASE
90
75
60
45
30
15
0
0.001
0.01
0.1
1
PERIOD IN SECONDS

Figure 6.1

available for the borehole. However, as well as being on linear rather than on logarithmic scales, the two sections are also on different resistivity scales and consequently the exact values particularly those below 100 ohm m are difficult to read.

The summarised structure at the location of the borehole is shown in the left hand side of figure 6.1. It indicates a granite below a depth of 390 m. At this depth, the recorded values of resistivity recorded on the resistivity log show a marked increase. This, with reference to tables 2.4 and 2.5, is as we expect. In the right of figure of 6.1 are shown the ρ_a and ϕ curves obtained from AMT observations at station Rookhope I. The interpretation of these MT results, derived by applying the method described in section 6.1.1, is shown as the best fitting model. From this six layer model the depth at which a final rise in resistivity is registered is 500 m. This depth, translated to the location of the borehole by an elevation difference of 110 m is 390 m. Hence, it is likely that the transition located at 500 m derived by the inversion of the AMT data corresponds to the geophysical boundary formed by the granite and the overlying sedimentary rock.

A direct comparison between the complete borehole resistivity log and the derived MT conductivity depth profile was not possible. The resistivity log showed fluctuations which could not be easily represented in

terms of a limited number of layers. It was possible instead to locate the major resistive sections from the resistive log. These were the great Limestone, the Great Whin Sill and the Weardale granite. The exact depths of these divisions were taken from the geological borehole log and the layers were assigned average resistivities from the resistivity log. This model was used as a starting point in the modelling of the observed MT data with the interface depths held fixed and the resistivity values being allowed to vary. The results of this approach are contained in figure 6.1. In the left of the diagram is shown the simplified structure at the site of the Rookhope borehole. To the right of the structural section is shown the fixed depth model - model A - which produced the optimum fit to the AMT data. Also shown to the right of the MT response plots is the unrestrained best fitting model - model B - referred to earlier. Computed curves for models A and B are superimposed on the response estimates the crosses defining model A and the plus signs model B values.

Comparison of the two model curves and of the model and observational responses leads to the following conclusions:

(i) The computed curves for models A and B show similar trends both for ρ_a and ϕ and the agreement with the observational data is good.

(ii) The magnitudes of the resistivities of the resistive

blocks are of the right order and fall within the scatter of the values extracted from the borehole resistivity log.

(iii) The low resistivity values associated with the less resistive sandstones in the model seem to be substantially lower than the corresponding average rock resistivity values obtained in the bore.

6.2.2 Rookhope I and Rookhope II

The inversion of the broadband data from station Rookhope II (D15 in table 3.2), a station only 3 km from Rookhope I, produced the model shown in figure 6.10. The model, derived by modelling of the observed phase data, shows a distinct transition between a narrow conductor and a massive resistor located at 540 m. The resistivity of the block below this depth is very high to a depth of about 24 km. Detection of the interface at 540 m, indicated by the AMT phase data and confirmed by the long period ρ_a values strongly suggests that this transition represents, as it did in the case of station Rookhope I, the transition into the highly resistive Weardale granite. A correction to the depth to this transition is necessary for the additional elevation of 60 m above that of station Rookhope I.

6.2.3 Comparison with D.C. resistivity results

The ground resistivity mapping by Habberjam and Thanassoulas (1977) provided some results of the regional conductivity structure centered at Rookhope

To derive adequate penetration, deep D.C. resistivity mapping methods, unlike comparable MT methods, involve the use of very large electrode separations. In their approach Habberjam and Thanassoulas partially overcame this difficulty by using a technique which integrates convertional resistivity and dipole-dipole techniques up to a spacing of 4.8 km. The model, shown in the right of figure 6.2 , which has been taken from Habberjam and Thanassoulas' interpretation of the Rookhope borehole, has been modified to allow for the additional thickness of rock from the Rookhope well-head to the AMT site, Rookhope II. AMT responses have been computed for Habberjam and Thanassoulas' model and superimposed on observed responses for Rookhope II - figure 6.2 . The quality of the fit is poor both in the magnitude and form of the ρ_a and ϕ curves. Reasons for the discrepancy are not immediately clear and require further study, but it is suggested that it may arise from lateral variations of the long spread D.C. and dipole-dipole resistivity measurements. By comparison, the model chosen by Habberjam and Thanassoulas is not as easy to reconcile with either the borehole resistivity

Figure 6.2 Fit of the D.C. resistivity model (Habberjam and Thanassoulas, 1974) to the major apparent resistivity data for station 15

Figure 6.2

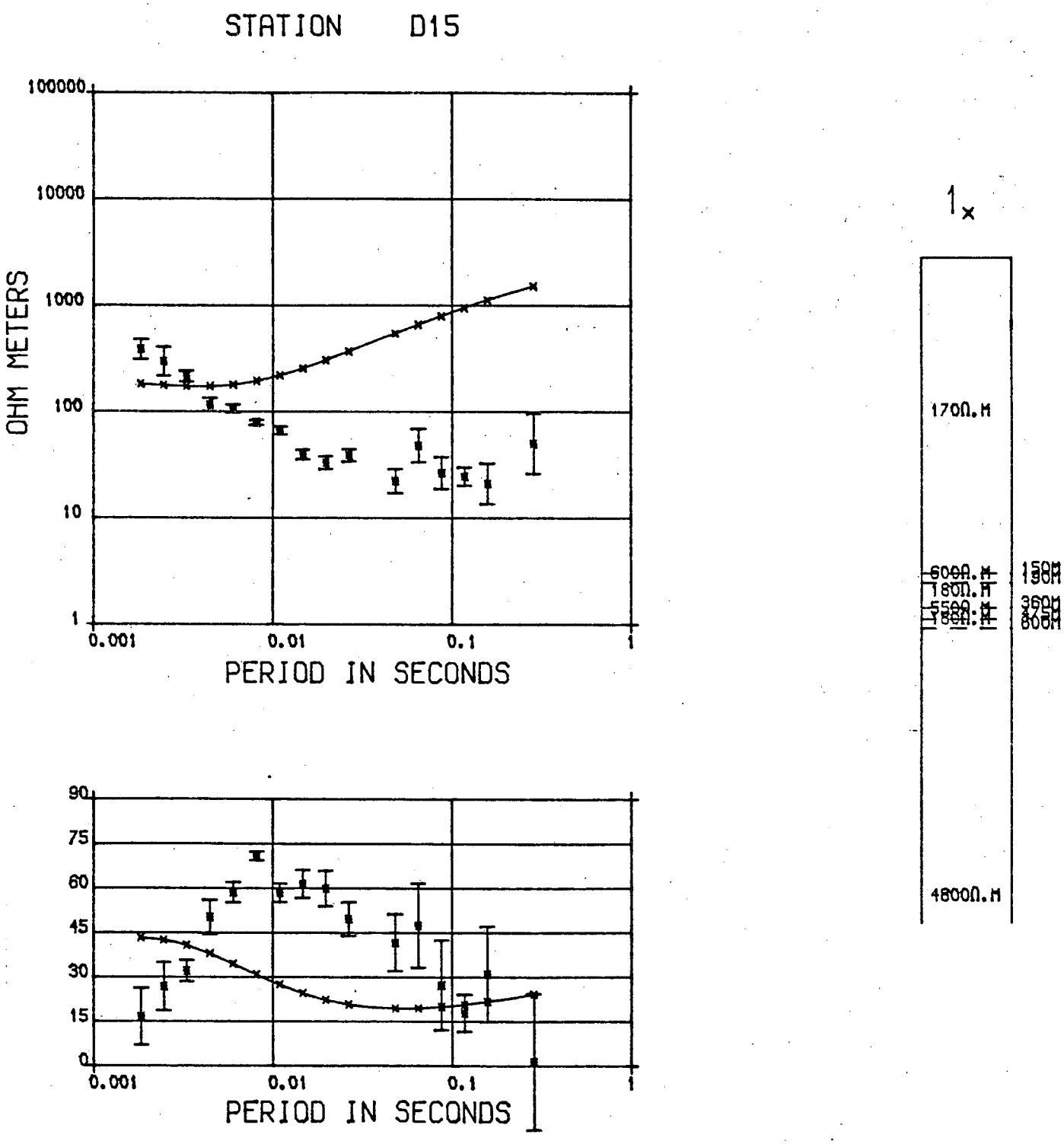
STATION D15
100000
10000
1000
100
10
1
OHM METERS
0.001
0.01
0.1
1
PERIOD IN SECONDS
90
75
60
45
30
15
0
0.001
0.01
0.1
1
PERIOD IN SECONDS
1x
170Ω.M
4800Ω.M

or the geological logs as was shown possible in the case of the derived AMT model in figure 6.1 . The AMT method thus appears to provide better layer resolution at all except the shallowest depths. It can also be applied within a time scale of about 4 man hours compared with the 70 man days required for the resistivity sounding.

6.3 Analysis of broadband data results

Both qualitative and quantitative approaches have been adopted in the interpretation of all broadband data. In the latter, the method of inversion was as that described in paragraph 6.1. The data from each of the 7 stations lying on the main profile were combined and continuous models were derived. These, as well as the plotting programmes for the broadband data, were especially adapted for this purpose by the author. The seven models from this single profile constitute the main result of the broadband data interpretation.

6.3.1 Qualitative analysis

In chapter 5 it was observed, that the azimuth of the major impedance of the long period (MT) data, was well defined and indicated an East-West direction for all the stations. This does suggest that, at depth, the structure of the Earth maintains a certain uniformity. The stations cannot however be considered to be one-dimensional, as the apparent resistivity data do not satisfy the one-dimensional requirements. The interpretation will

therefore be one-dimensional of a two-dimensional station. Reddy and Rankin (1972) showed that the conductivity variation with depth is best obtained by interpreting the E polarisation apparent resistivity (and phase) curve(s) in a one-dimensional sense.

Two-dimensional problems were studied by Wright (1970) in relation to the Rhine Graben model. He concluded that the H polarisation results corresponding to the major curves of the apparent resistivity and phase on the resistive side of the inhomogeneity, yielded a model whose interfaces were correctly estimated but whose layer resistivities were over estimated.

From the orientation of the azimuth of the rotated resistivity data, at the long periods, the stations of this study must all be considered to lie on the same side of any discontinuity, pertinent to the depths implied by these periods.

In seeming contradiction, the marked differences in the overall magnitudes of the major apparent resistivity

between the four stations to the North and the three stations to the South, suggest a marked change in the geological structure which these two groups of stations represent.

These changes are apparent in their effect on the long period data. The implication of this is, that the cause of this effect is constrained to depths shallower than those associated with the parameters of the long period data. The effect observed in the three stations to the South is that of a body resistive with respect to its counterpart in the four stations to the North. This is an oversimplification of the problem, as will eventually be shown qualitatively in the one-dimensional broadband traverse sections.

A preliminary result may be obtained by constructing a pseudo section, in which apparent resistivity values at selected periods of the observed long period data were plotted for each station. In such a representation the lateral extent of the profile is shown on the horizontal scale, while the period range is represented on a suitable vertical scale. This is commonly taken to be the log 10 of the frequency. The result is shown in figure 6.3. This is a simple representation of the basic information contained in the apparent resistivity data. It contains no additional information, other than the horizontal position of the

Figure 6.3 MT major apparent resistivity data from the main profile plotted as a pseudosection.

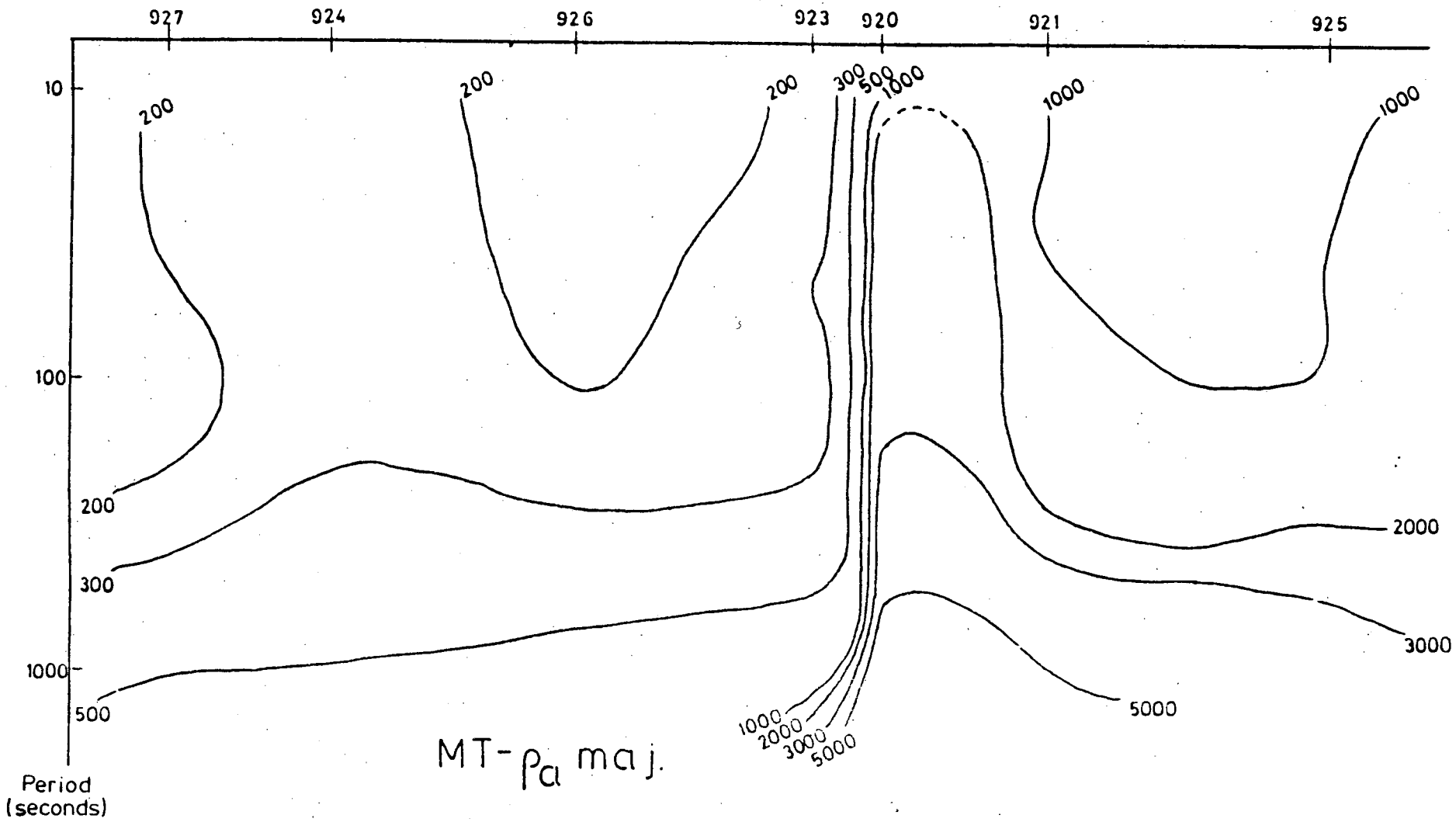
927
924
926
923
920
921
925
10
100
1000
Period
(seconds)
200
200
200
300
500
1000
1000
1000
200
300
500
2000
3000
5000
1000
2000
3000
5000
MT-ρa maj.

Figure 6.3

stations, and can be misleading in suggesting shapes which are no more than contours of the plotted resistivities. Probably the most useful feature of the plot in figure 6.3 is the enhancement of the vertical boundary between station SIN and SWI.

Plotted in figure 6.4 are the induction vector arrows for selected periods of the long period data. Periods at the centre of, and at the extremes of the available period band were chosen. In the region of stations SIN - ROO, in the centre of the traverse, the amplitudes shown are large and indicate a verical boundary in that region. The direction of the arrows also shows a reversal at the shortest periods. While at all periods to 600 sec (Beamish ,1981) the arrows are orientated in a roughly southerly direction, below 600 sec a reversal is observed in the two most northerly stations. Parkinson (1964) vectors showing this type of behaviour (Banks ,1964) indicate a current concentration below the point of reversal. This suggests a current concentration in that region. The depth of this current was shown by Summers (1981) to be constrained near the upper limit of the conducting body. The station Towhouse in Jones' (1977) study was situated in exactly that region.

Figure 6.4 Induction vector map from the seven MT stations

a. at a period of 20 sec

b. at a period of 90 sec

c. at a period of 650 sec

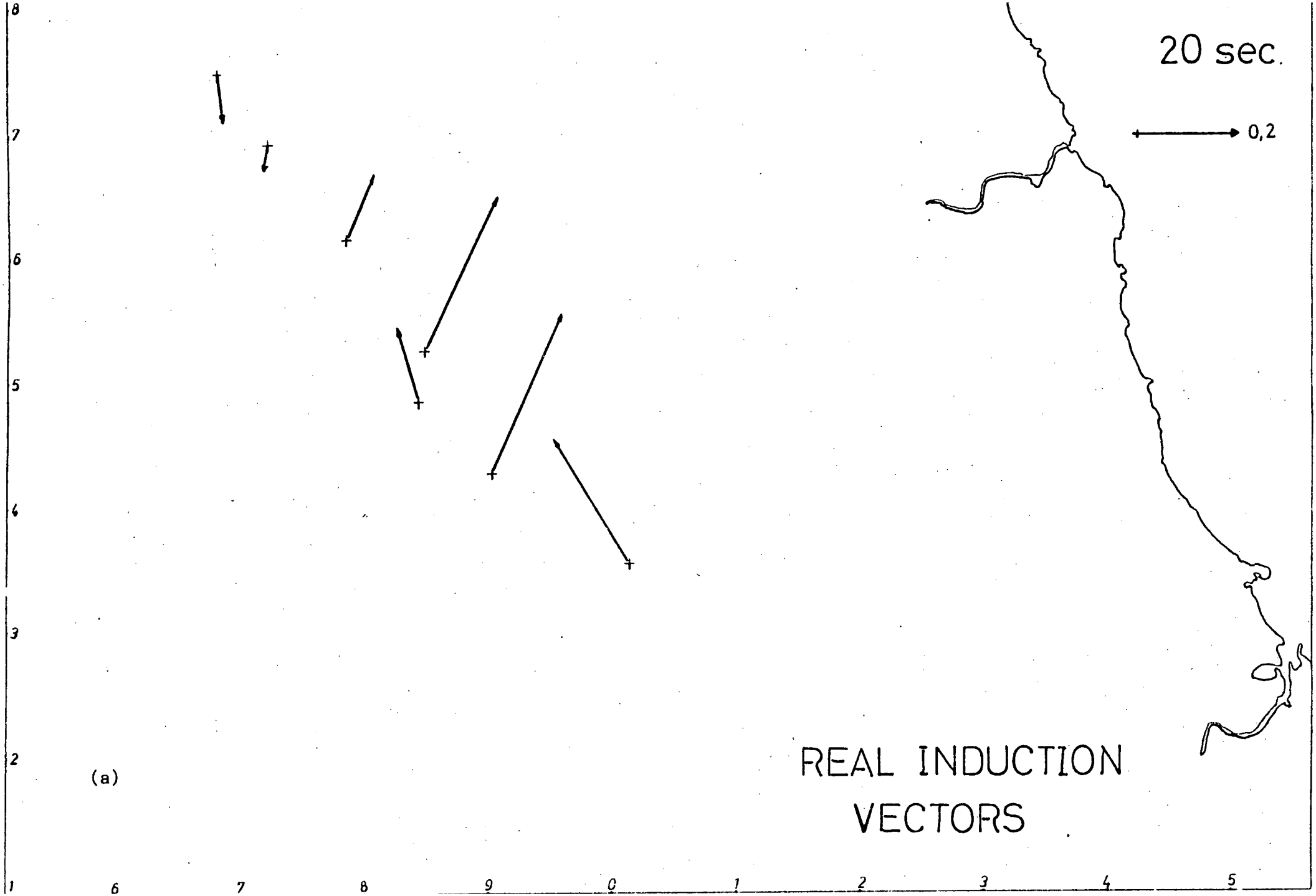

Figure 6.4 a.

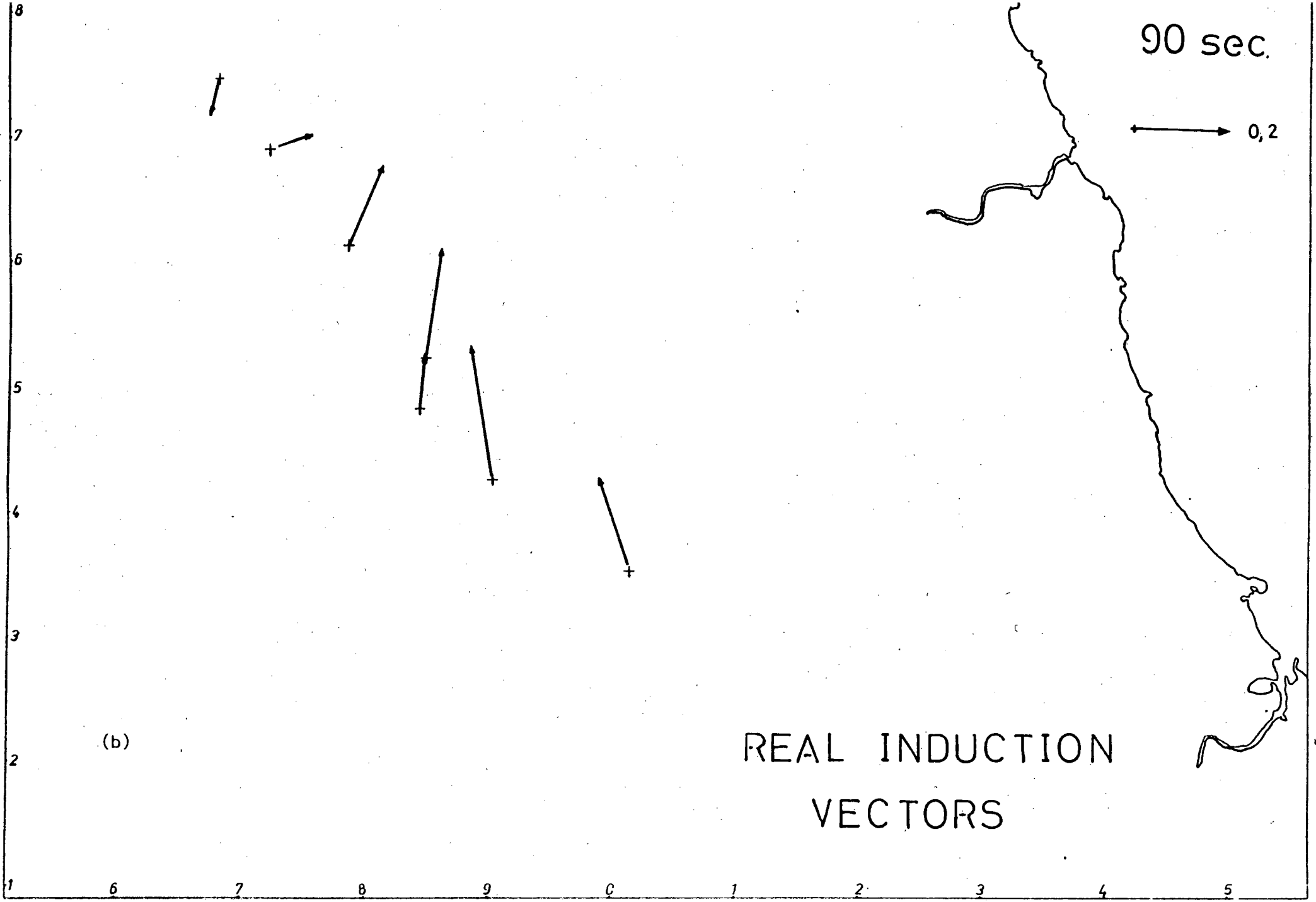

Figure 6.4 b.

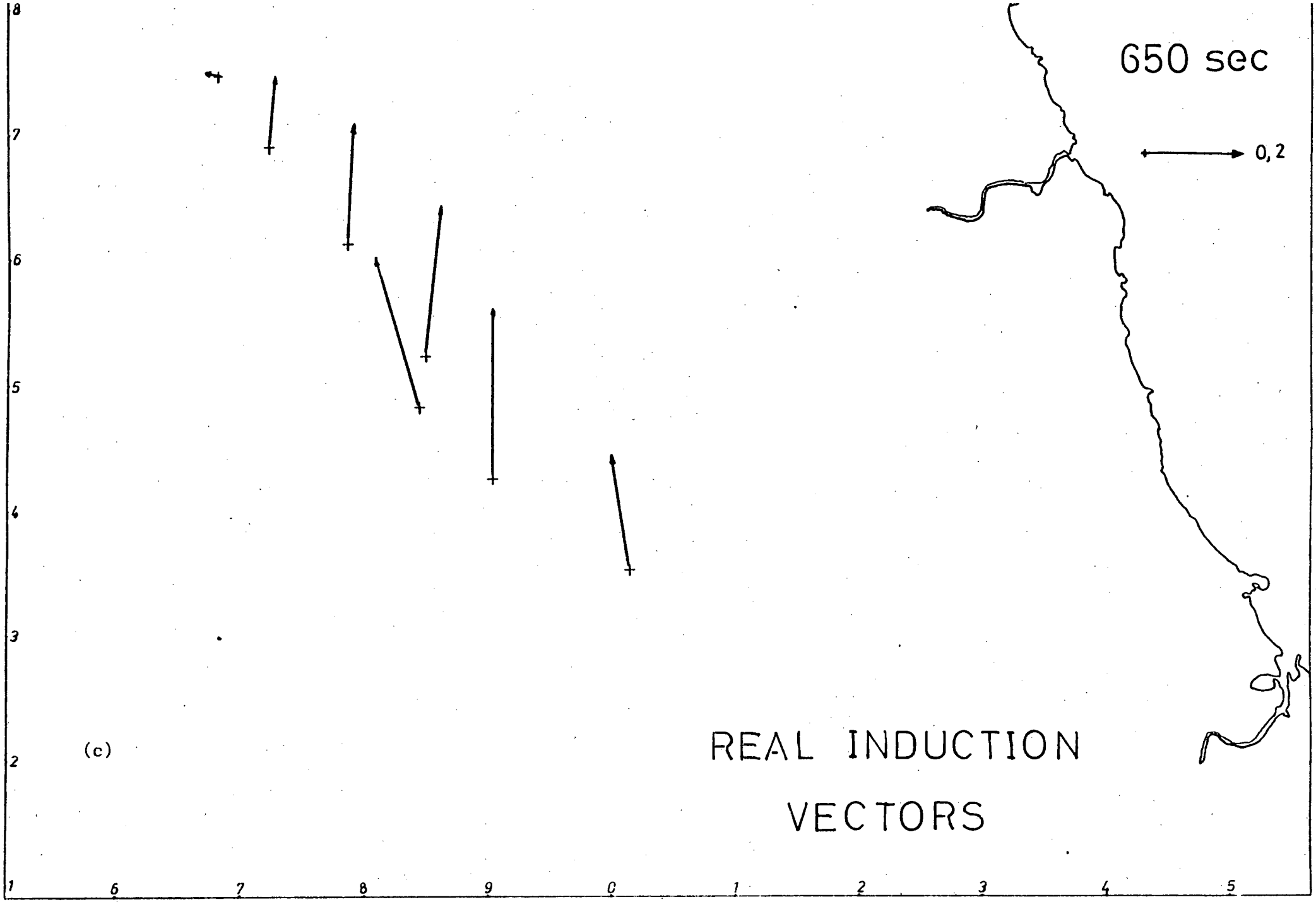

Figure 6.4 c.

The MT results alone show no one-dimensional behaviour. The data are either typically two-dimensional or by implication of the high SKEW values three-dimensional. It is possible to apply a one-dimensional inversion scheme to both two-dimensional and three-dimensional station data, but the validity of the result must be examined and understood. Consideration of the results corresponding to the distinct cases of E and H polarisation in the ideal two-dimensional example shows that the major apparent resistivities and phases are nearly always better determined.

The validity of one-dimensional interpretation of station data showing high skew factors has been briefly examined by Jones (1977). It is generally agreed that such practices can give totally misleading results and as a result have been omitted by many authors. In the present study, where interstation spacing of some 6 km corresponded to less than 1/3 of the skin depth at the shortest periods, it was considered unreasonable to disregard any station data showing three-dimensional behaviour which otherwise displayed features similar to an adjacent two-dimensional station. In all cases the appearances of the apparent resistivity amplitudes and phases were strikingly similar.

6.3.2 Inversion of the broadband data

In figures 6.5 - 6.11, the best fit models for each of the stations on the main traverse are shown, together with computed and observed response estimates. The station data are shown in order from north to south, starting with station LAM and ending with HIL in the south. The results indicate that the stations fall into 2 main groups. A group (a), of stations LAM, EDG, WHI and SIN, and a group (b) containing the stations SWI, ROO and HIL. Only two - LAM and ROO - will be discussed in detail in this section, as their results are to some extent representative of the groups (a) and (b).

The main differences in the structure of the data from the stations of the two groups are as follows.

1. The apparent resistivity values derived at station ROO, display much higher magnitudes than those from station LAM, in the period range 10 - 1000 seconds.

2. The inversion of the data from both stations, shown in the right of each figure, shows the maximum depth from which information is derived (i.e. the effective depth of penetration) to be twice as large at station ROO, as it is at station LAM.

Figure 6.5 - 6.11 Fit of best model to broadband data from the seven stations where MT and AMT measurements were made.

Figure 6.5 Broadband station Lampert

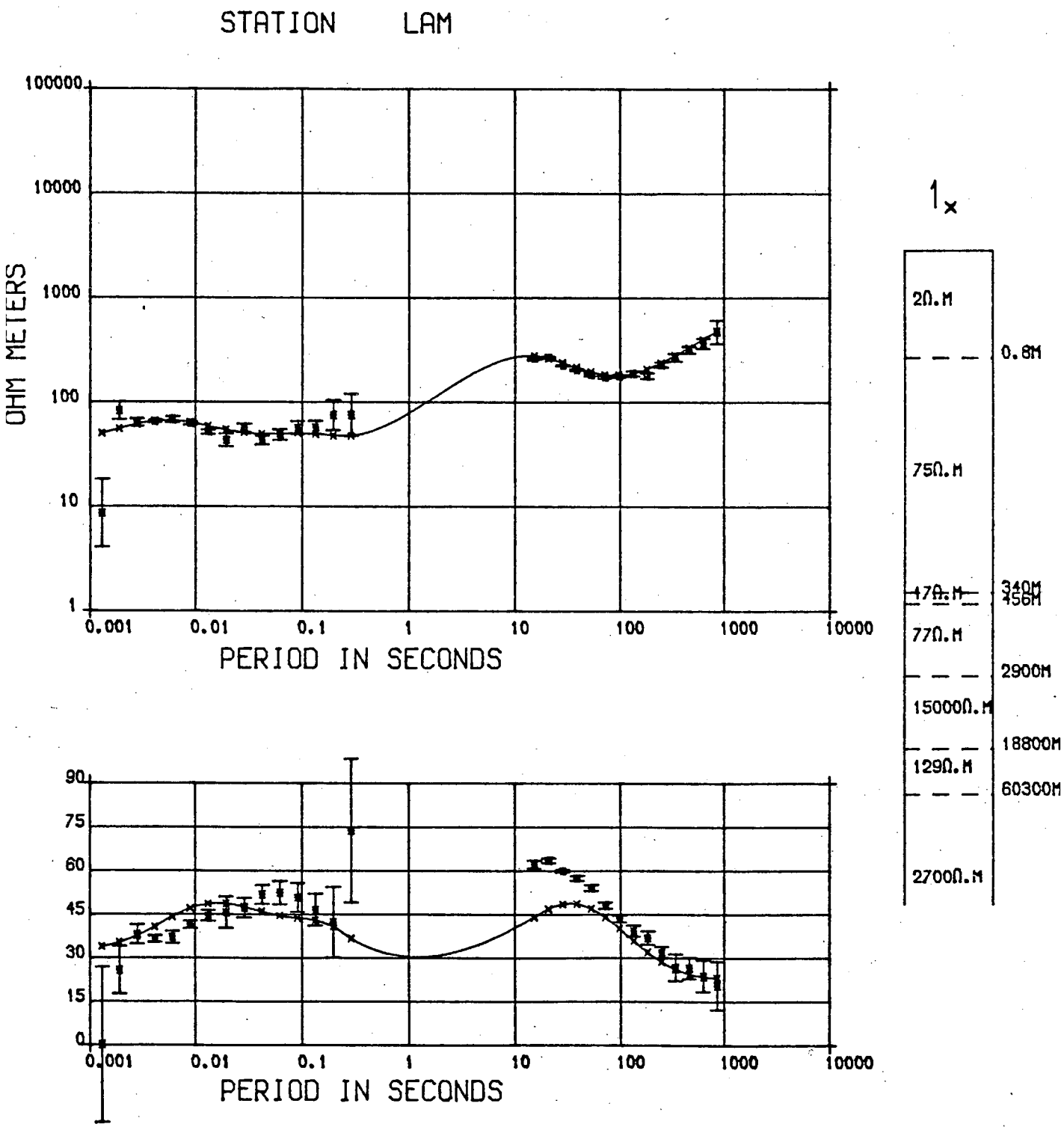
STATION LAM
OHM METERS
100000
10000
1000
100
10
1
0.001
0.01
0.1
1
10
100
1000
10000
PERIOD IN SECONDS
1x
2Ω.M
0.8M
75Ω.M
17Ω.M
340M
456M
77Ω.M
2900M
15000Ω.M
18800M
129Ω.M
60300M
2700Ω.M
90
75
60
45
30
15
0
0.001
0.01
0.1
1
10
100
1000
10000
PERIOD IN SECONDS

Figure 6.6 Broadband station Edges Green

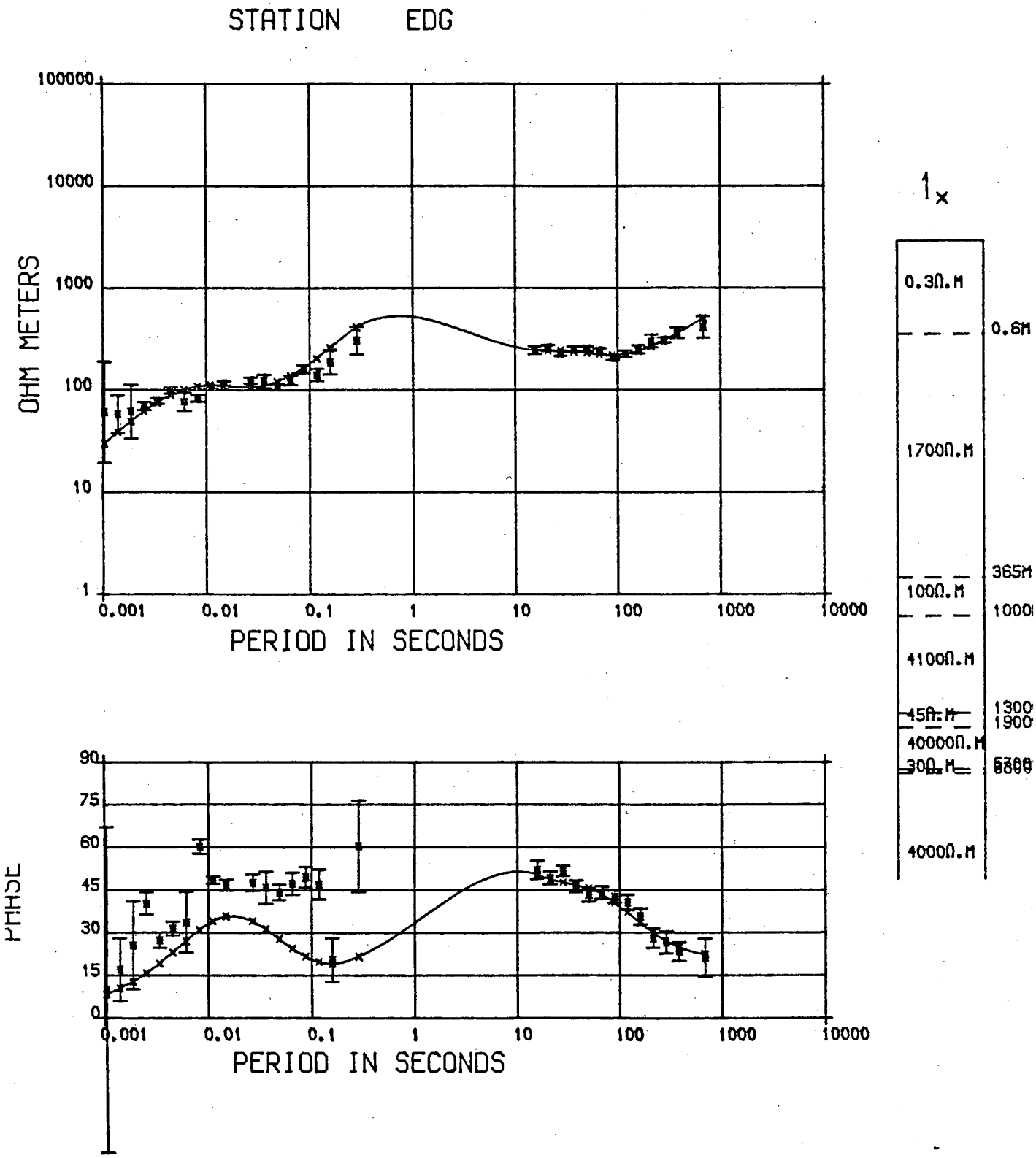
STATION EDG
OHM METERS
100000
10000
1000
100
10
1
0.001
0.01
0.1
1
10
100
1000
10000
PERIOD IN SECONDS
1x
0.3Ω.M
0.6M
1700Ω.M
365M
100Ω.M
1000
4100Ω.M
1300
1900
40000Ω.M
5700
8800
4000Ω.M
PHASE
90
75
60
45
30
15
0
0.001
0.01
0.1
1
10
100
1000
10000
PERIOD IN SECONDS

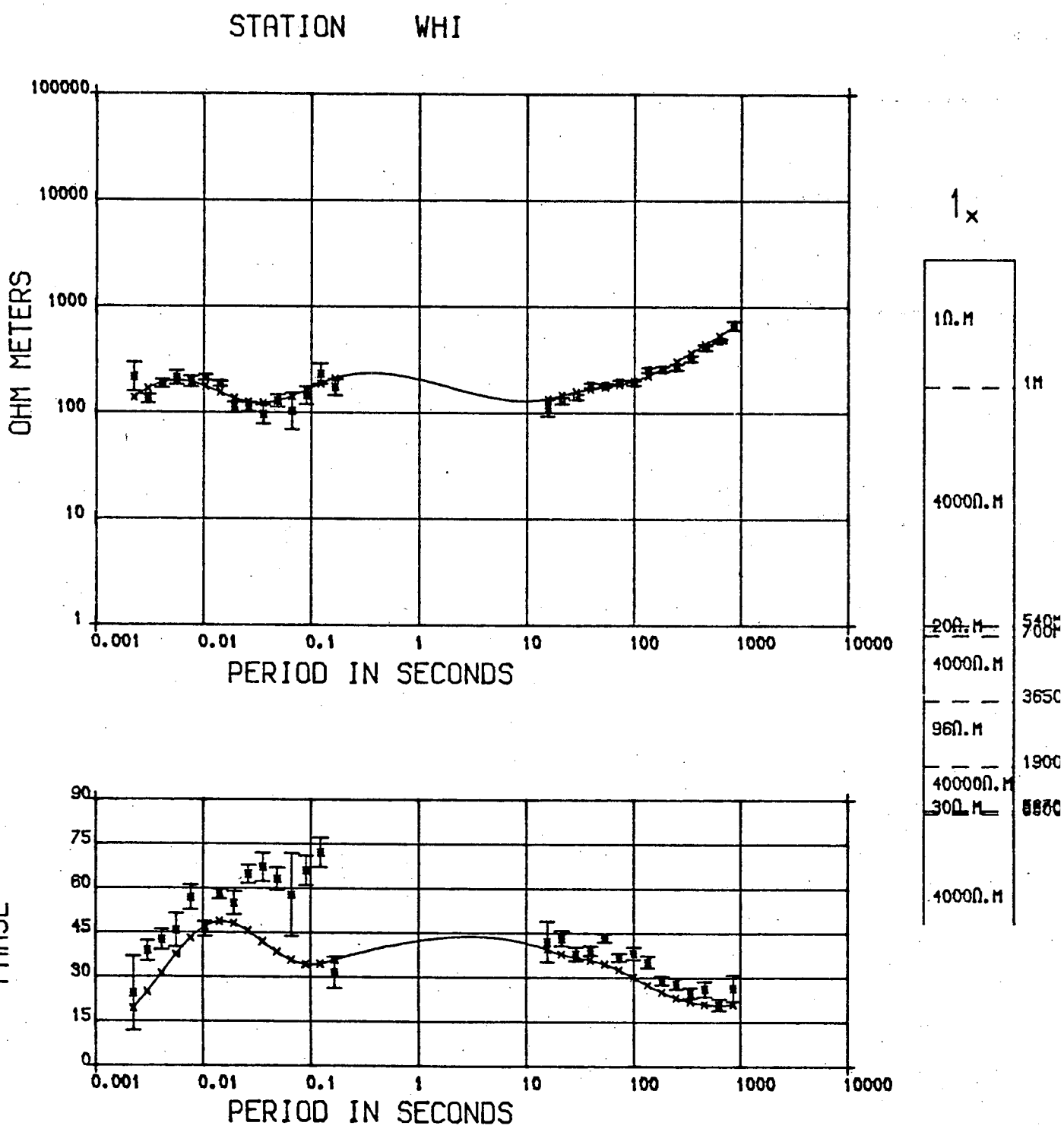
STATION WHI
OHM METERS
100000
10000
1000
100
10
1
0.001
0.01
0.1
1
10
100
1000
10000
PERIOD IN SECONDS
1x
1Ω.M
1M
4000Ω.M
20Ω.M
540
700
4000Ω.M
365
96Ω.M
190
40000Ω.M
30Ω.M
4000Ω.M
PHASE
90
75
60
45
30
15
0
0.001
0.01
0.1
1
10
100
1000
10000
PERIOD IN SECONDS

Figure 6.8 Broadband station Sinderhope Shield

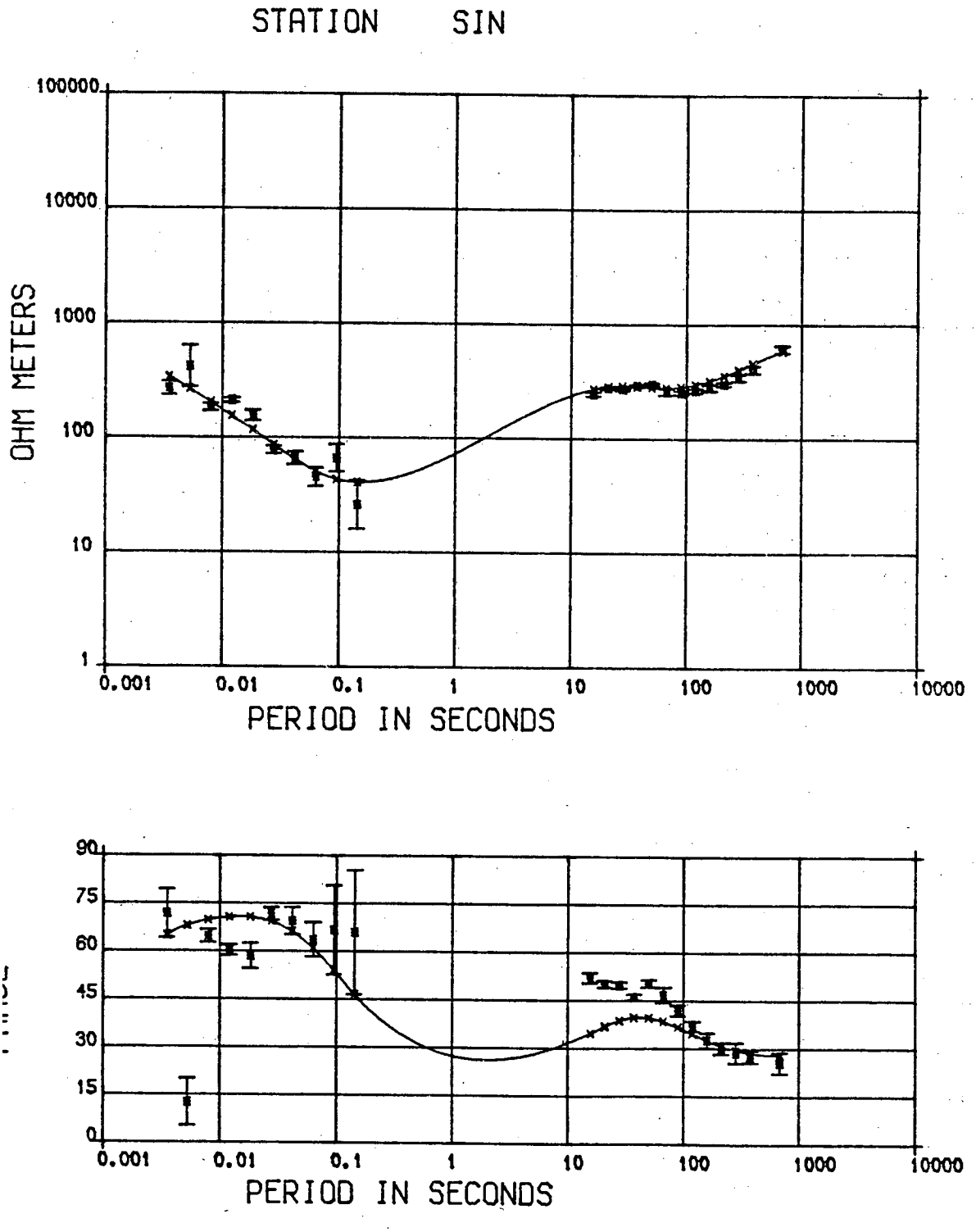
STATION SIN
OHM METERS
100000
10000
1000
100
10
1
0.001
0.01
0.1
1
10
100
1000
10000
PERIOD IN SECONDS
90
75
60
45
30
15
0
0.001
0.01
0.1
1
10
100
1000
10000
PERIOD IN SECONDS

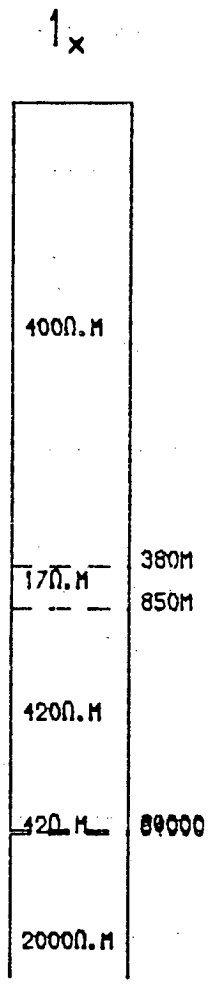
1x
400Ω.M
17Ω.M
380M
850M
420Ω.M
420Ω.M
80000
2000Ω.M

Figure 6.9 Broadband station Swinhope Shield

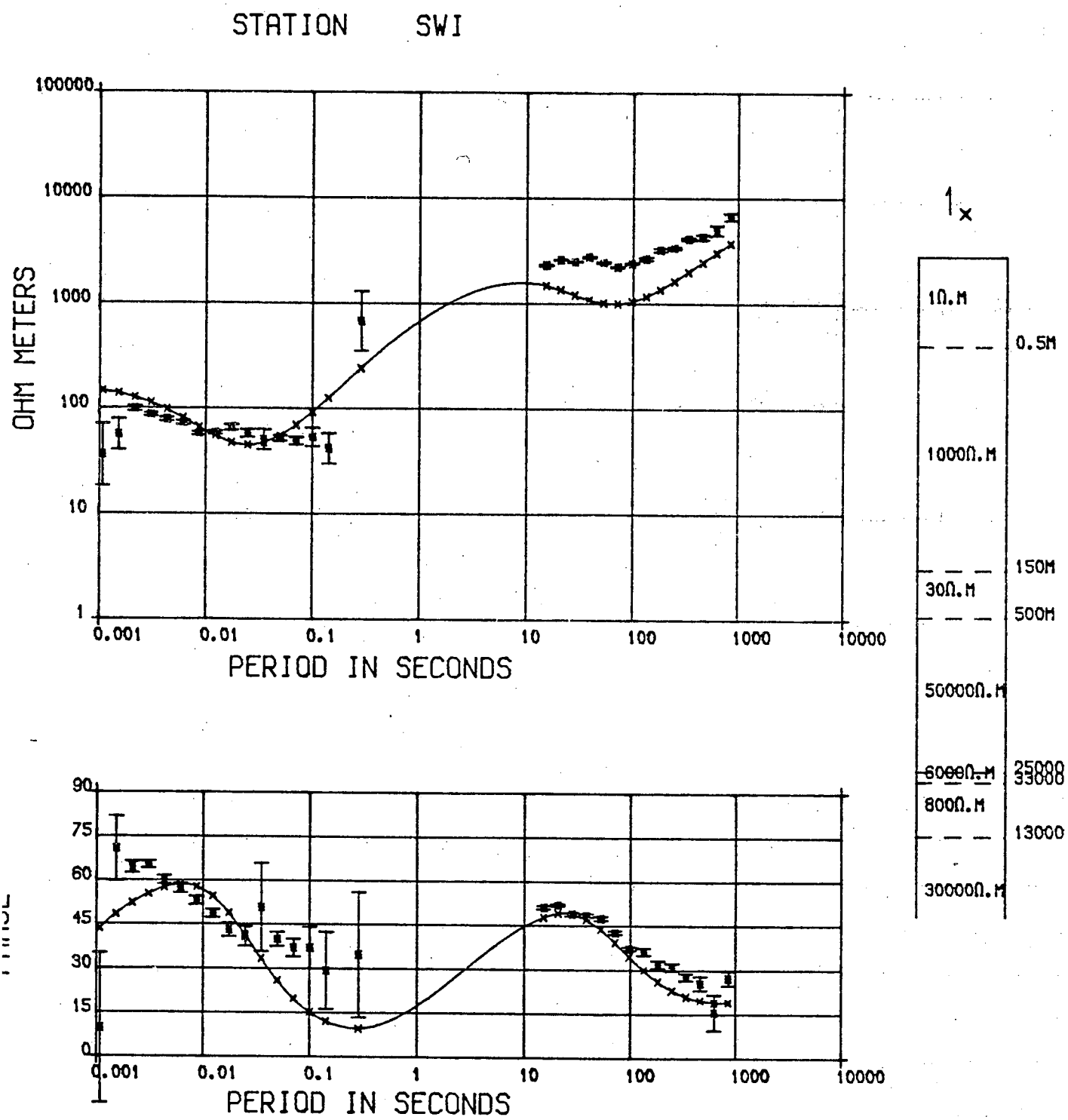
STATION SWI
OHM METERS
100000
10000
1000
100
10
1
0.001
0.01
0.1
1
10
100
1000
10000
PERIOD IN SECONDS
1x
1Ω.M
0.5M
1000Ω.M
150M
30Ω.M
500M
50000Ω.M
25000
33000
800Ω.M
13000
30000Ω.M
90
75
60
45
30
15
0
0.001
0.01
0.1
1
10
100
1000
10000
PERIOD IN SECONDS

Figure 6.10 Broadband station Rookhope

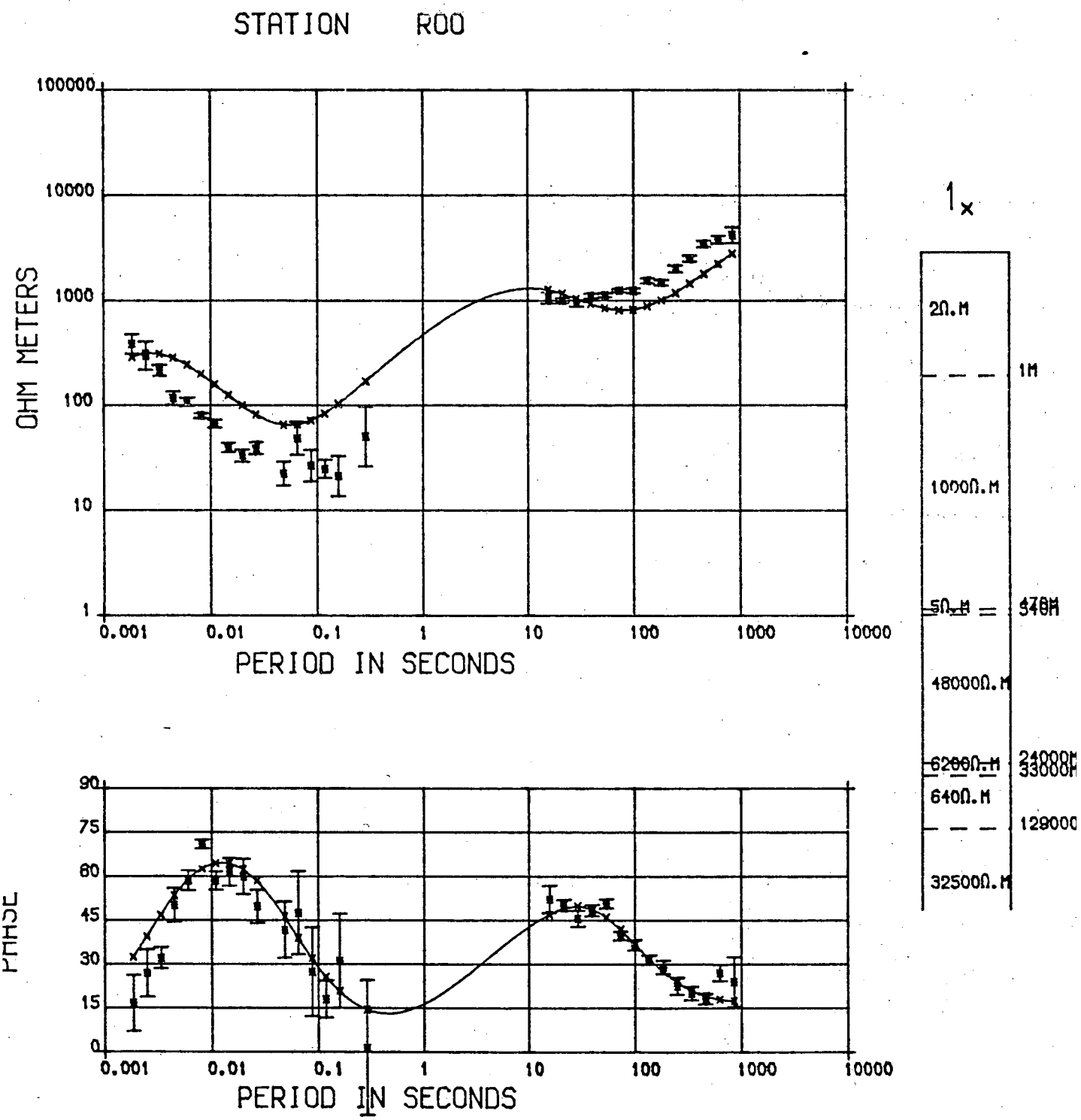
STATION R00
OHM METERS
100000
10000
1000
100
10
1
0.001
0.01
0.1
1
10
100
1000
10000
PERIOD IN SECONDS
1x
2Ω.M
1M
1000Ω.M
50Ω.M
480000Ω.M
640Ω.M
325000Ω.M
PHASE
90
75
60
45
30
15
0
PERIOD IN SECONDS

Figure 6.11 Broadband station Hill End

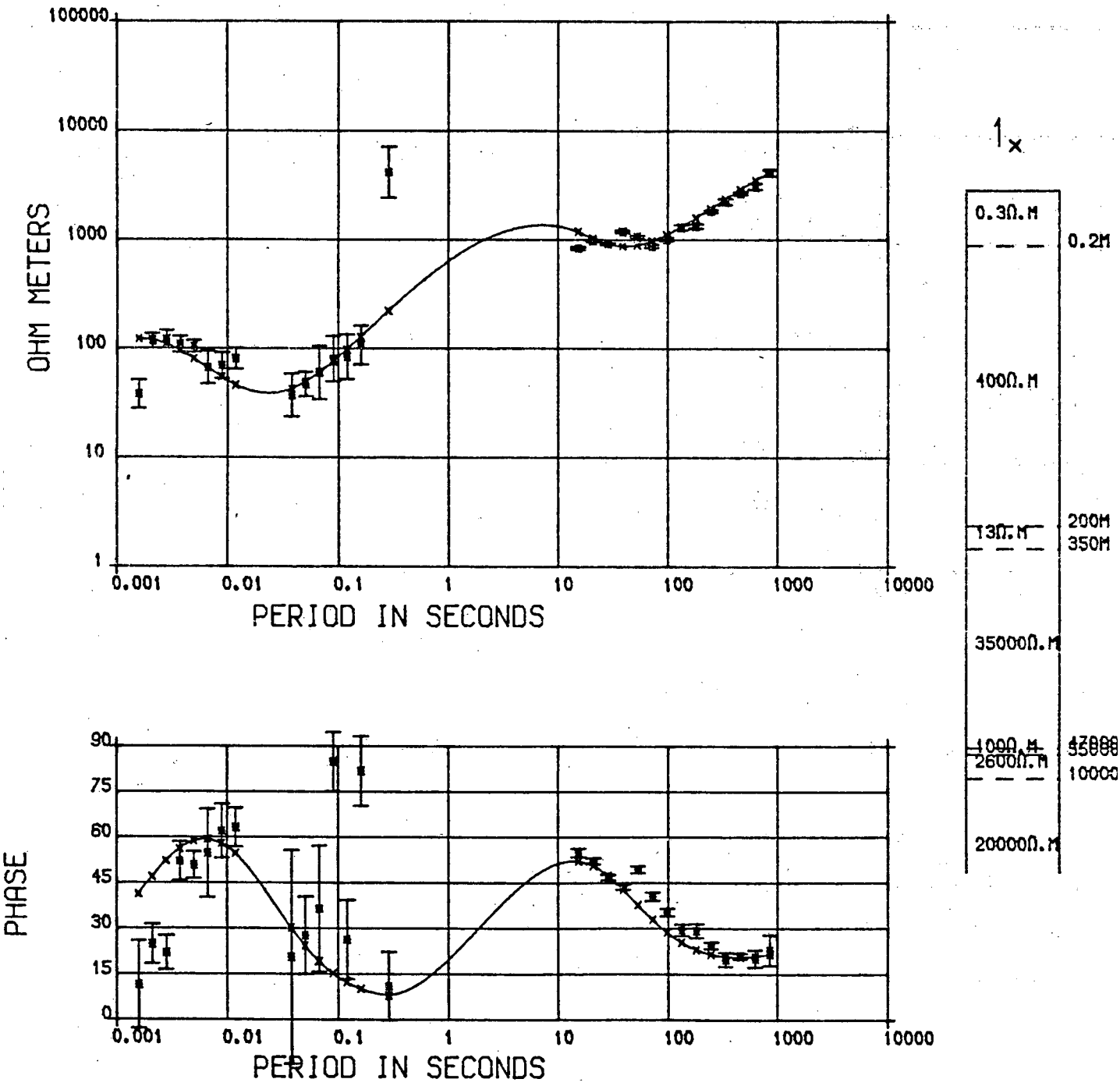
STATION HIL
OHM METERS
100000
10000
1000
100
10
1
0.001
0.01
0.1
1
10
100
1000
10000
PERIOD IN SECONDS
1x
0.3Ω.M
0.2M
400Ω.M
13Ω.M
200M
350M
350000Ω.M
1000Ω.M
2600Ω.M
10000
200000Ω.M
PHASE
90
75
60
45
30
15
0
0.001
0.01
0.1
1
10
100
1000
10000
PERIOD IN SECONDS

3. The derived model for station data ROO, is compatible with the existence of a resistive body, located below the surface at station ROO at a depth of some 500 m, and reaching to approximately 25 km. A resistive layer is also present in the upper crust at station LAM, but it is overlain by 2.9 km of conducting layers.

The models for SWI and HIL have features, which are in broad agreement with those from ROO, while those from EDG and WHI differ from that of LAM in that the highly resistive layer is present in the lower, rather than the upper crust. The model for SIN differs from all the others despite the apparent similarity of the long period MT data at SIN and at LAM and EDG.

6.3.3 The compilation of main profile models

A qualitative two-dimensional interpretation of the broadband station data can be made, by considering the one-dimensional inversion of the MT data discussed in the two previous sections, to illustrate the main regional features along the line of the traverse. The optimum parameters of the one-dimensional models for the individual stations, are summarised in figure 6.12 (A) and (B). Included in this compilation are the models obtained by Jones and Hutton (1979) for stations NEW and TOW, situated to the north of the main profile and between stations EDG and WHI of the present study, respectively.

Figure 6.12 A compilation of the broadband station models, made in two parts : (A) - surface to 1 km and (B) - shallow crust to upper mantle. The models were produced by the one-dimensional inversion scheme of Jones (1977). The derived resistivity values were averaged within major blocks to outline the main features. The resultant models were then shaded according to the key in each figure. The model from station SIN in figure (B) was not reliable, since the station was near a discontinuity, and has been omitted.

Figure 6.12 (A)

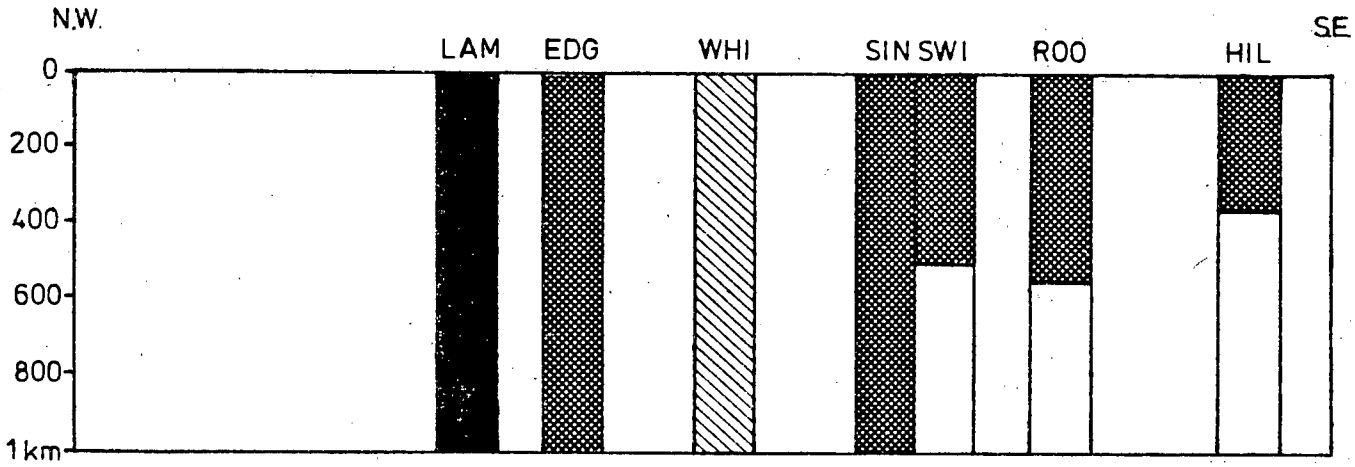

KEY

$\rho_{av.}$

< 100 Ω-m

100 - 1000 Ω-m

1000 - 10000 Ω-m

> 10000 Ω-m

VERTICAL SCALE : 1/20000 - 1cm = 200m

HORIZONTAL SCALE : 1/500 000 - 1cm = 5km

Figure 6.12 (B)

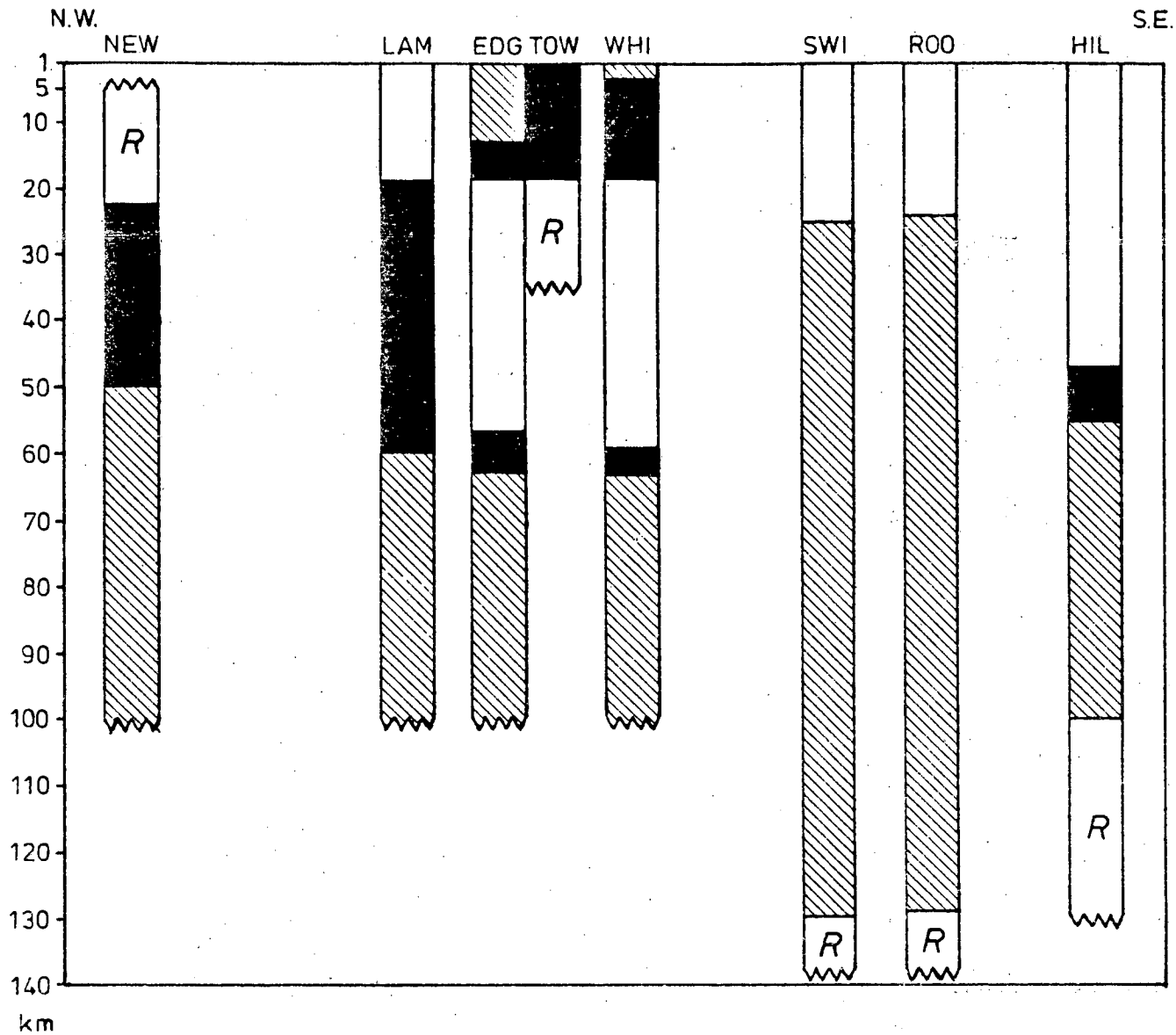

KEY

ρ av.

< 150 Ω-m

1000 - 4000 Ω-m

> 10000 Ω-m

R ≫ Neighbouring layers

VERTICAL SCALE : 1/1000000 - 1cm = 10km

HORIZONTAL SCALE : 1/500000 - 1cm = 5km

Figure 6.12 (A) shows the shallow depth part - surface to 1 km - of the models shown in figures 6.5 to 6.11. The derived resistivity values, corresponding to this depth range, were averaged over similar adjacent resistivity values within each major resistivity block, by adding the conductance value for each layer and calculating the conductance of the block. This has simplified the models. The resultant resistivity values were then shaded according to the resistivity bands shown in the key of figure 6.12 (A), so that the main common features are seen. These are

1. the very high resistance value shown at shallow depth below stations SWI and ROO, and

2. the highly conducting layers at station LAM.

The transitions between stations, particularly that between stations LAM and SWI, cannot be reasonably interpreted in detail, without additional AMT sites.

Figure 6.12 (B) shows the corresponding results of the models in figures 6.5 - 6.11 from the region of the shallow crust to the upper mantle. The resistivity values from each model have been represented by the shading, in the key of figure 6.12 (B) to stress the main common points. The three resistivity ranges shown, were adequate to represent all the observed values of resistivity. Only the two layers, comprising the intermediate section below stations SWI and ROO were averaged.

The main points and trends which can be observed from this figure are as follows.

1. The common features of stations NEW and LAM showing, particularly, the conductor in the lower crust / upper mantle. This feature was observed by Ingham, (1981) in all representative sites from the Southern Uplands.

2. The absence of this conductive layer under stations SWI and ROO

3. The transition located between stations LAM and SWI.

Since the models in figure 6.12 (A) and (B) can only give some indication of possible starting models for two-dimensional interpretation, discussion of actual resistivity and depth values can only be very tentative at this stage (Hutton and Novak, 1982, in preparation). It must also be remembered that even the one-dimensional models were attempts to fit ρ_a and/or ϕ data over 6 decades, for which no data were available for 2 of them. However, it is interesting to note that the lower crust/upper mantle conductor at LAM is in agreement with Ingham and Hutton's (1982a) 2 - D model for southern Scotland. This suggests that there is no major discontinuity in the deep structure between the Southern Uplands Fault and the south of the Northumberland Basin and that their interpretation - their figure 6

(Ingham and Hutton, 1982b) holds also for northern England. A major transition in the geo-electric structure appears to occur between EDG and SIN and this merits further study as a contribution to the tectonic history of this zone. If the existence of thin, highly conducting layers, at a depth of about 60 km in this transition region, is confirmed by two-dimensional modelling, then, at the temperatures which must exist at this depth, there is a possibility of a partial melt.

For the uppermost crustal layers between LAM and SIN, it seems reasonable to associate the good conductors with the thick sequence of sedimentary rocks of the Northumberland Basin, but the unexpectedly large thickness and conductivity of these layers in the neighbourhood of station TOW, requires confirmation and further investigation. The presence of a highly conducting layer directly above the resistive block, associated with the Weardale granite, can be interpreted as arising from hydrothermal mineralisation (Dunham, 1943).

6.4 AMT areal interpretation

The station results from the short period magnetotelluric (AMT) soundings made in grid lines across the area have been compiled in the appendix. There exist no induction vectors for these stations.

Let us first examine the features by a casual inspection of the data. Distinct differences in the rotated major apparent resistivities, as were observed in the long period (MT) data, can no longer be observed. It seems also that stations can not be grouped as readily. In the azimuth a varied response is observed. Stations such as SIN show a well defined and aligned azimuth, while stations similar to EDG show no frequency dependence at all. The station spacing is too great to map lateral variations in conductivity as was possible with the long period data.

However, a closer inspection of the data does reveal certain common features. The major rotated apparent resistivity data for station SIN as an extreme case show a distinct drop in the frequency range 80 Hz - 10 Hz. Similarly the associated phase data display a drop from around 60 deg to 15 deg for the same frequency range.

Master curves which display this behaviour are generated by a three layer model with an intermediate conductive layer.

This behaviour was observed to a varying extent in many of the station data located near the Rookhope site shown in figure 5.16.

The coverage of the area by the AMT sites allowed other qualitative interpretations to be made using an areal approach as well as the more usual single profile pseudo section approach.

One such method involved plotting, on a map of the area, the resistivity values at each station for a selected single frequency. Thus as many such maps as there are frequency bands may be constructed for each of the following parameters: rotated major, rotated minor and the mean (if it is available).

The major features, suggested by figure 6.13 are:

(a) The increasingly resistive values in the north.

(b) The highly resistive localised region reaching in from the south-west.

(c) The conductive region, shown particularly at intermediate frequencies, located in the south-east.

The nature of plots such as those shown in figures 6.13 A and B, is that the surface effects, including topography, superficial sedimentation, or the lack of it, have a direct effect on the observed values of resistivity at all frequencies. The feature (b) above can be interpreted as a lack of conductive sediments in that region, leading to the exposure of a resistive succesion. Feature (c) requires further investigation

Figure 6.13 Major apparent resistivity map at 0.09 sec period figure (A) and at 0.009 sec, figure (B).

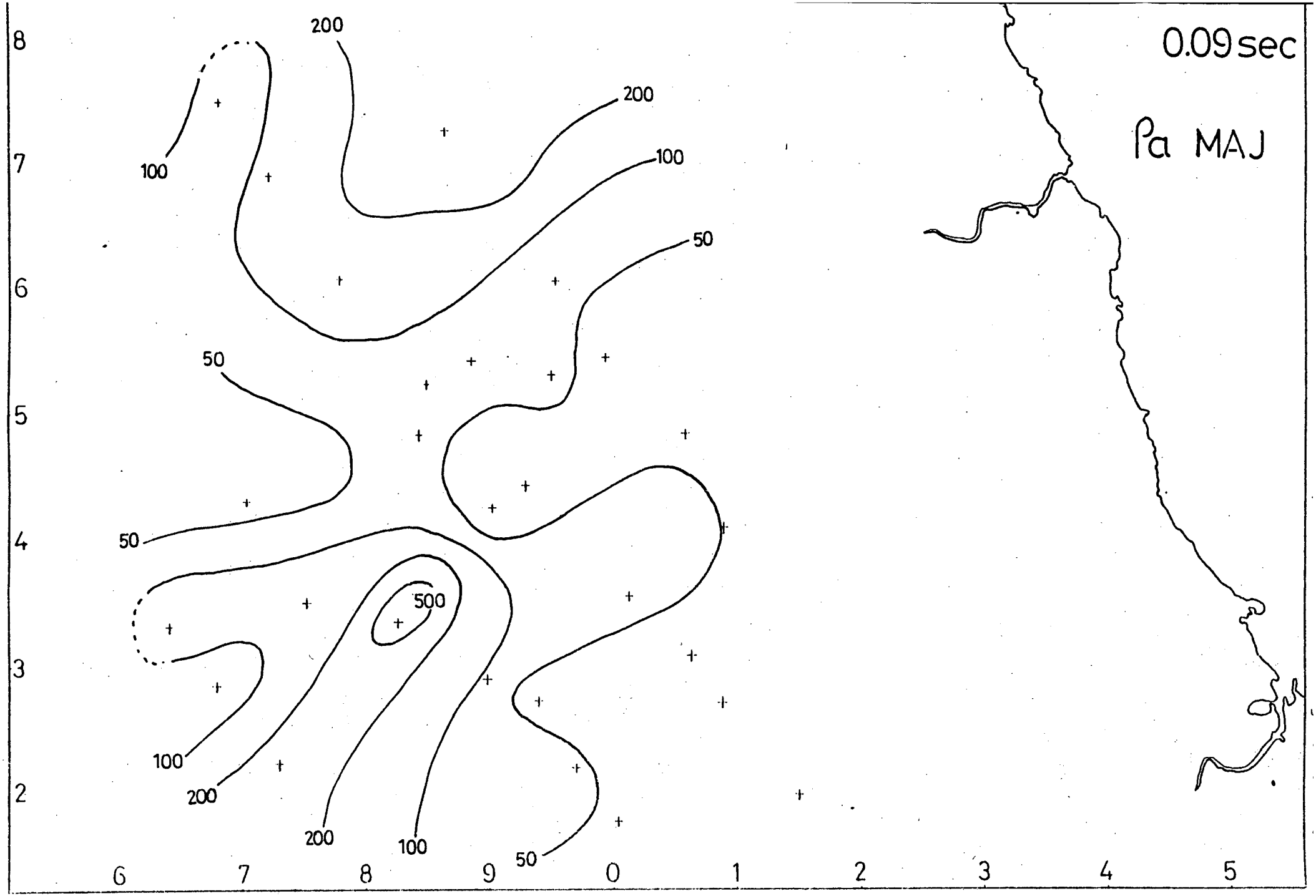
0.09 sec
Pa MAJ
200
200
100
100
50
50
50
500
100
200
200
100
50
8
7
6
5
4
3
2
6
7
8
9
0
1
2
3
4
5

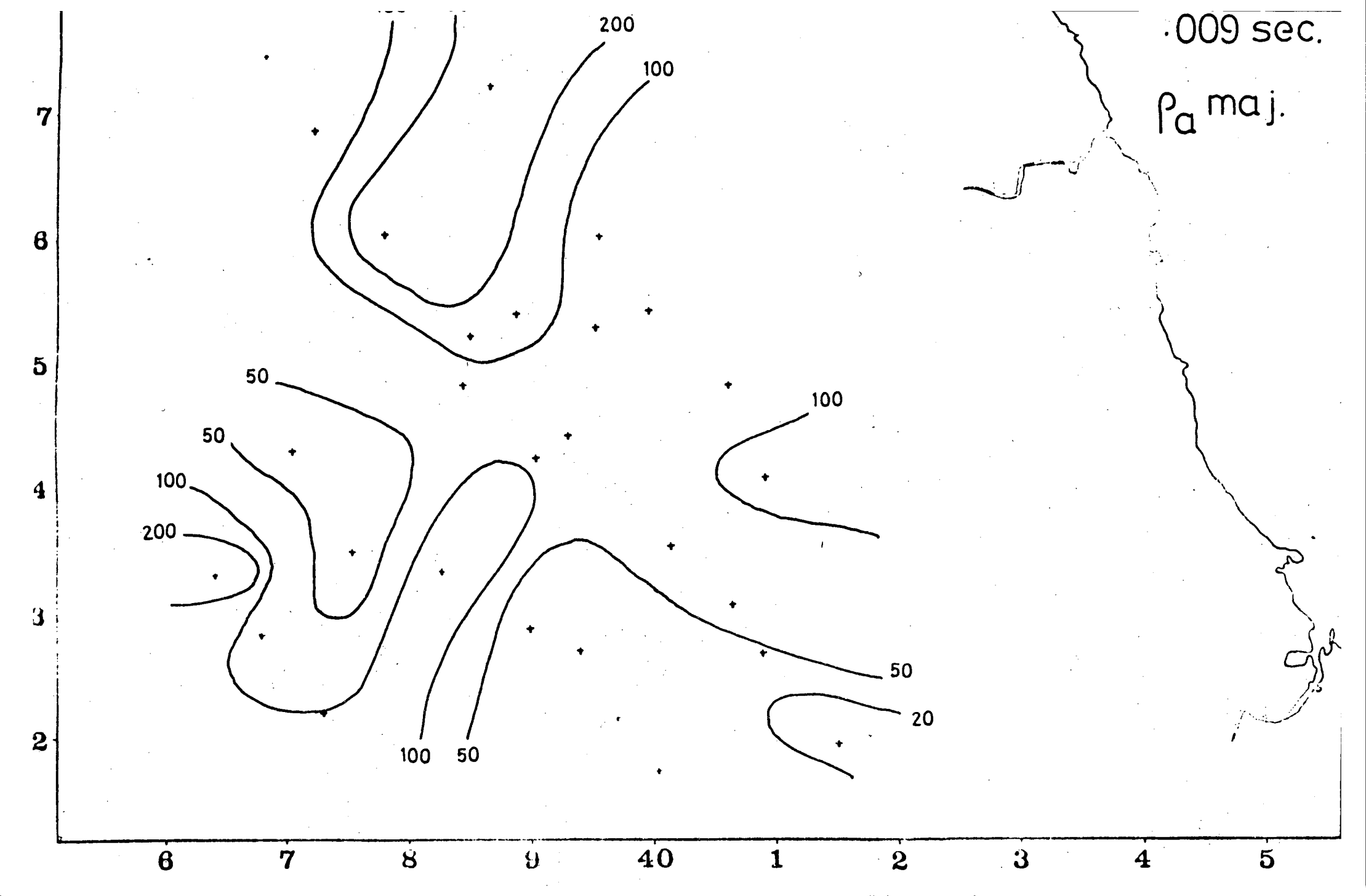
.009 sec.
ρ_a maj.
200
100
50
50
100
100
200
50
20
100
50
7
6
5
4
3
2
6
7
8
9
40
1
2
3
4
5

to examine the possibility that it is associated with increased water content, in the fractures of the Lunedale fault.

The nature of the qualitative comments, based on plots such as figure 6.13 A and B , can only be tentative in view of the data anisotropy at some stations and the large station spacing.

For a quantitative interpretation the short period station data were inverted selectively to yield suitable one-dimensional models. The Monte-Carlo method of inversion was used as described for the long period data. For station data showing a one-dimensional responses (figure 6.14) the better estimated apparent resistivity and phase data were inverted. Some station data described as two-dimensional were used to yield a mean value for the apparent resistivity and phase. It is clear that such an approach provides a more realistic approach to one-dimensional modelling of two-dimensional data. Unlike Ingham (1981) the calculation was performed to yield the mean apparent resistivities and phases separately. If the two parameters are calculated simultaneously by evaluating

$$Zmean = 1/2(Zxy - Zyx)$$

Figure 6.14 Map showing the dimensionality indicators for the AMT stations. The 1, 2 and 3 dimensional station responses are shown by different symbols. The main profile is indicated by diamond shapes.

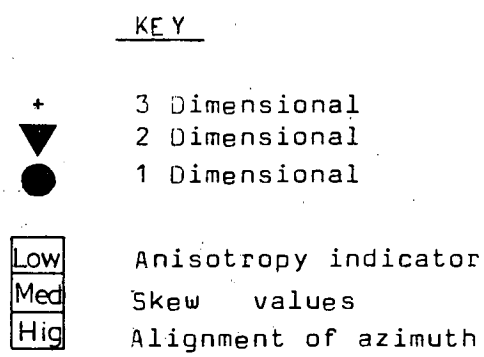

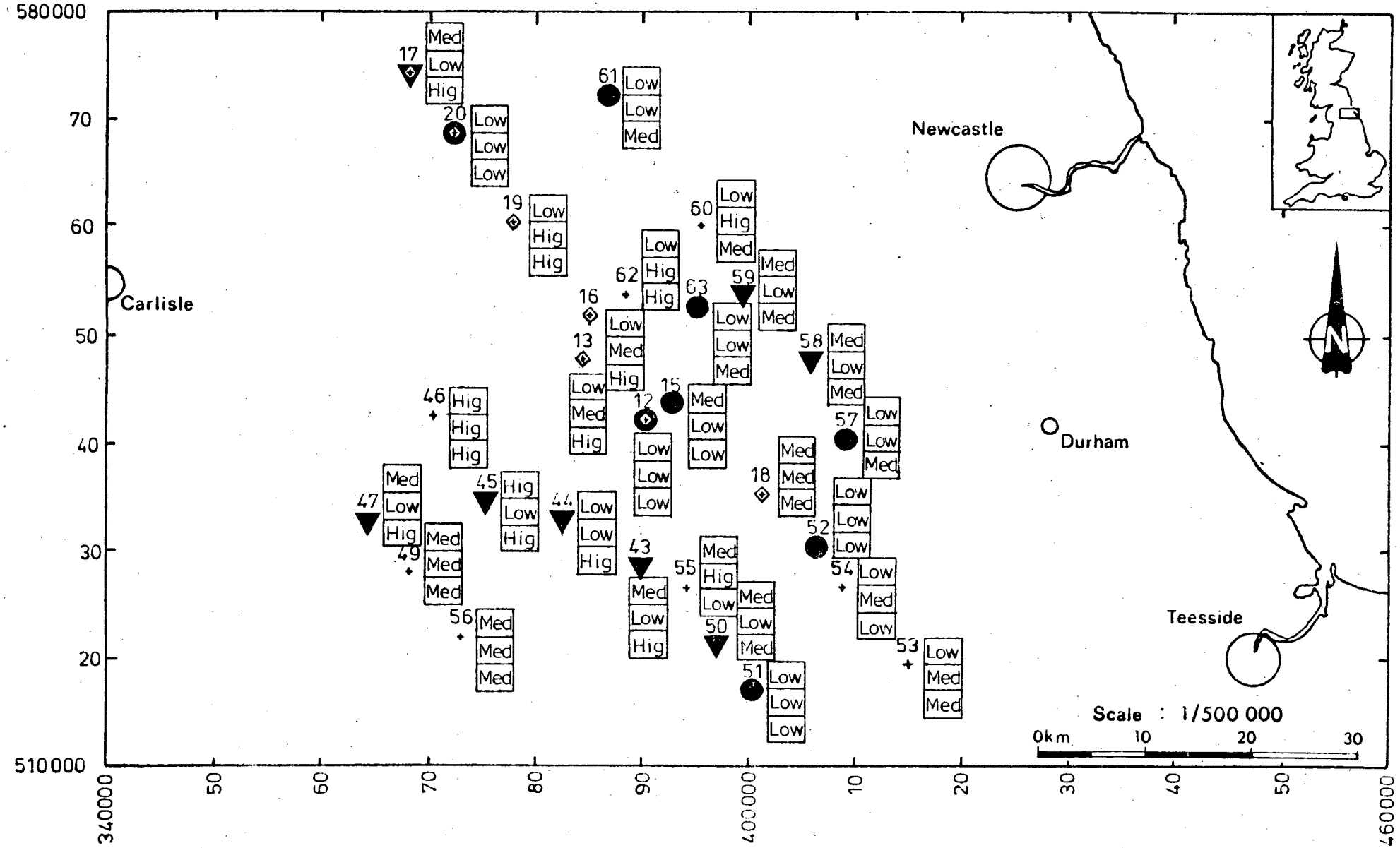
580000
70
60
50
40
30
20
510000
340000
50
60
70
80
90
400000
10
20
30
40
50
460000
Carlisle
Newcastle
Durham
Teesside
Scale : 1/500 000
0km 10 20 30
N
17 Med Low Hig
20 Low Low Low
19 Low Hig Hig
61 Low Low Med
60 Low Hig Med
62 Low Hig Hig
16 Low Med Hig
13 Low Med Hig
63 Low Low Med
59 Med Low Med
58 Med Low Med
46 Hig Hig Hig
12 Low Low Low
15 Med Low Low
57 Low Low Med
18 Med Med Med
47 Med Low Hig
45 Hig Low Hig
44 Low Low Hig
49 Med Med Med
43 Med Low Hig
55 Med Hig Low
52 Low Low Low
54 Low Med Low
56 Med Med Med
50 Med Low Med
53 Low Med Med
51 Low Low Low

where Zxy and Zyx are complex, the phase is conserved in the calculation thus:

$$\text{phase} = \text{Im}(Zmean)/\text{Re}(Zmean)$$

The magnitude may be incorrectly determined. This is possible when elements of the rotated complex impedance estimates Zxy and Zyx are of equal sign. The mean value can then assume values less than the equivalent minor resistivity value, a situation found with events of low signal strength.

The problem is resolved by evaluating the moduli of Zxy, Zyx and consequently the modulus of Zmean. The phase information, which is lost in the calculation, must be recalculated from the original impedance estimates. Using the data from station 43, as an example, the calculated mean response showed a similar type of response to the major data, but with a definite smoothing of the apparent resistivity and phase curves. As expected the magnitude of the mean curve was lower over the entire range. The models generated by inverting the curves showed a consistently similar structure to those of the rotated major data, but with slightly lower resistivity values.

The programme 'Magtel' was revised to make the input files compatible with the requirements of the Monte-Carlo modelling programme - 'Monte' - as well as the magnetotelluric curve plotting programme - 'Magtel'. The data were modelled using the sequence described in section 6.1. In general it was found that phase information was essential in obtaining a satisfactory fit. The phase showed a more exagerated response even though it was often less well estimated than the associated resistivity values. It was also a feature of the modelling that a fit of the phase data alone very often produced a well fitting resistivity curve. This was not the case in reverse. One further observation in favour of retaining phase information for modelling purposes was that phase data were able to provide information from well outside the available frequency bandwidth and certainly outside the scope of the resistivity data. This is in agreement with the theoretical relationship (Weidelt,1972) between phase and apparent resistivity, viz

$$\phi(T) \approx \pi/4 \left\{ 1 + \frac{d \log \rho_a(T)}{d \log T} \right\}$$

The station data obtained at Rookhope displayed a very definite one-dimensional behaviour. The station was therefore chosen as part of a three station profile accross the region. It would represent the response of the central region of the Alston block.

The other stations to be included in this profile were 61-Uppertown in the NE and 51-Lartington in the South. The station data at 61 showed a one-dimensional response and seemed to give better defined results than the other three stations in the Northumberland trough. It was assumed to represent the other stations in that region.

The data from station 51 was also of a one-dimensional nature. Similarly it was chosen to be representative of all the stations located in the Stainmore trough. Its position was most advanced within this trough.

The quality of fit, the associated model representation and a schematic diagram of the position of these stations with respect to the general geological features are shown in figure 6.15

The model derived from the data at station 61 is a six layer model. A five layer model is required to satisfy the observed response at station 12 and a three layer model is adequate to fit the response at station 51. The quality of fit has been achieved using the modelling approach described in section 6.1.

Figure 6.15 Results from a three station N-S traverse across the granite. The station data, best model, limit of acceptable models and position is shown for stations 61, 12 and 51

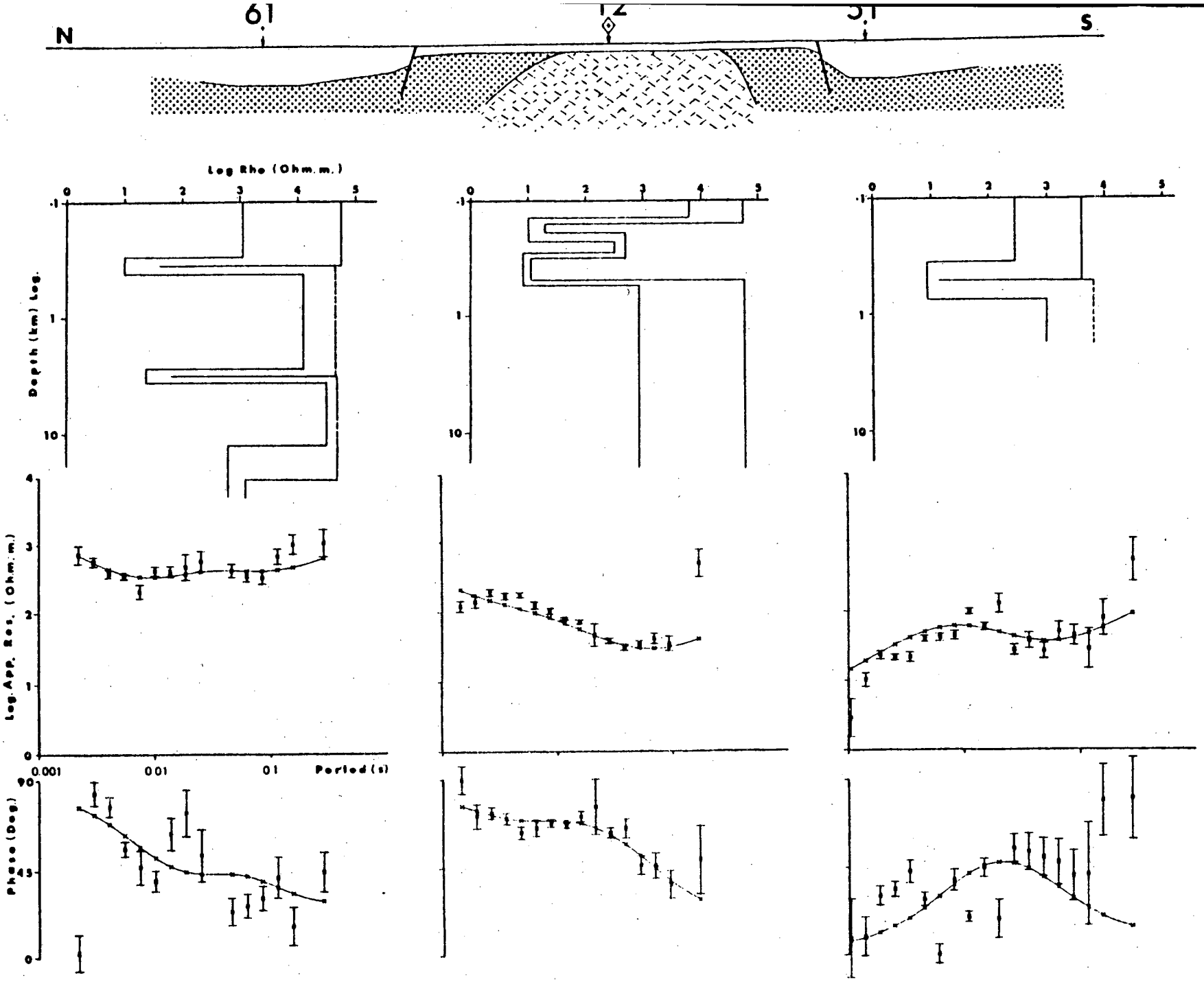
N
61
12
51
S
Log Rho (Ohm.m.)
Depth (km) Log.
Log.App. Res. (Ohm.m.)
Period (s)
0.001
001
01
Phase (Deg.)

Figure 6.15

The author sees this method to be favourable to fixed number of layers modelling, and considers the concept of over modelling, disapproved of by a number of authors, not to apply.

The idea of making a fit of the structure of the data curves is demonstrated by taking station 61 as an example. The apparent resistivity data alone could with the exception of one or two points, be fitted by a perfectly straight line - a uniform half space. Considering the phase information as well completely refutes this approach. The phase data have a definite structure and they must be modelled to be sure of a true representation.

Let us now examine the results of the three station traverse.

The model representation for each station is shown in the centre of figure 6.15 directly above the corresponding data fit. It consists of a set of curves representing a minimum and a maximum of each of the depth and resistivity parameters. This representation is an easy way to understand the bounds of the acceptable models and is a commonly used one. Typically relating to the Monte-Carlo method these curves represent the bounds of the models

acceptable at a given acceptance level. With good quality data this can be around the 95% level. Since the Monte-Carlo method had been modified and no longer selected all the models out ot the maximum of 1000 models tried, at the selected level, this representation has had to be modified also.

In the present case the maximum and minimum bounds represent the bounds of the five accepted models after a particular iteration. Obviously the more iterations one performs the lesser the spread of the bounds. In each representation the best fitting model is omitted for clarity.

Station 61 in the Northumberland trough has a best fitting model which shows three general interfaces. One at a depth of approximately 400 m , one at 2550 m and one at 14 km. The first two are typified by the presence of a 130 m thick conductor. At this site the evidence from geological and seismic (Bamford,1978) investigations suggests the presence of an interface at approximately 2.5 km associated with the base of the carboniferous trough. Also at some 14 km the lower Palaeozoic deposits meet the Pre-Caledonian basement. These depths certainly show remarkable agreement. The data suggest a six layer sequence in which the resistive layers, one, three and five take resistivity values of the order of 40,000 ohm-m This is an average value - 10000 ohm-m as well as 100000 ohm-m or more, fitting the data equally well.

The explanation of the two thin conducting layers of 40 ohm-m and 24 ohm-m resistivity is more problematic. It is suggested that they are associated with increased concentrations of meteoric water along each boundary or that they are a feature of electrical induction associated with these surfaces.

Station 12 in the centre has a five layer model response which is generally well defined. It shows a transition into a 1000 - 100000 ohm-m resistor at 540 m depth and remains resistive to depths resolved by the long period MT instrument. There is evidence for a pair of conductive layers between the transition at 540 m and the surface. The implications of this model have already been dicussed in section 6.2.

Only a proportion of the collected AMT data were inverted in the course of this work. The derived one-dimensional models were reduced to sea level and for each station model, the thickness of the conductive sediments was noted. The results, plotted in figure 6.16 show the depth in metres below sea level. The values were in most cases derived from the depth to the first resistive layer, exceeding 4000 -m resistivity and of thickness greater than 5 km. The values above sea level are shown enclosed in round brackets.

Remembering that the station spacing was too wide, in the case of the AMT measurements, and noting the assumptions involved in a one-dimensional analysis, the

Figure 6.16 Results of one-dimensional inversion of selected AMT data. The depth to a resistor > 5 km thick and > 4000 ohm-m resistivity is plotted. All results are corrected to sea level.

A shallow resistor of less than 100 m depth is marked. To the south-west a region where the values are above sea level has been outined. The values to the N-W are generally increasing.

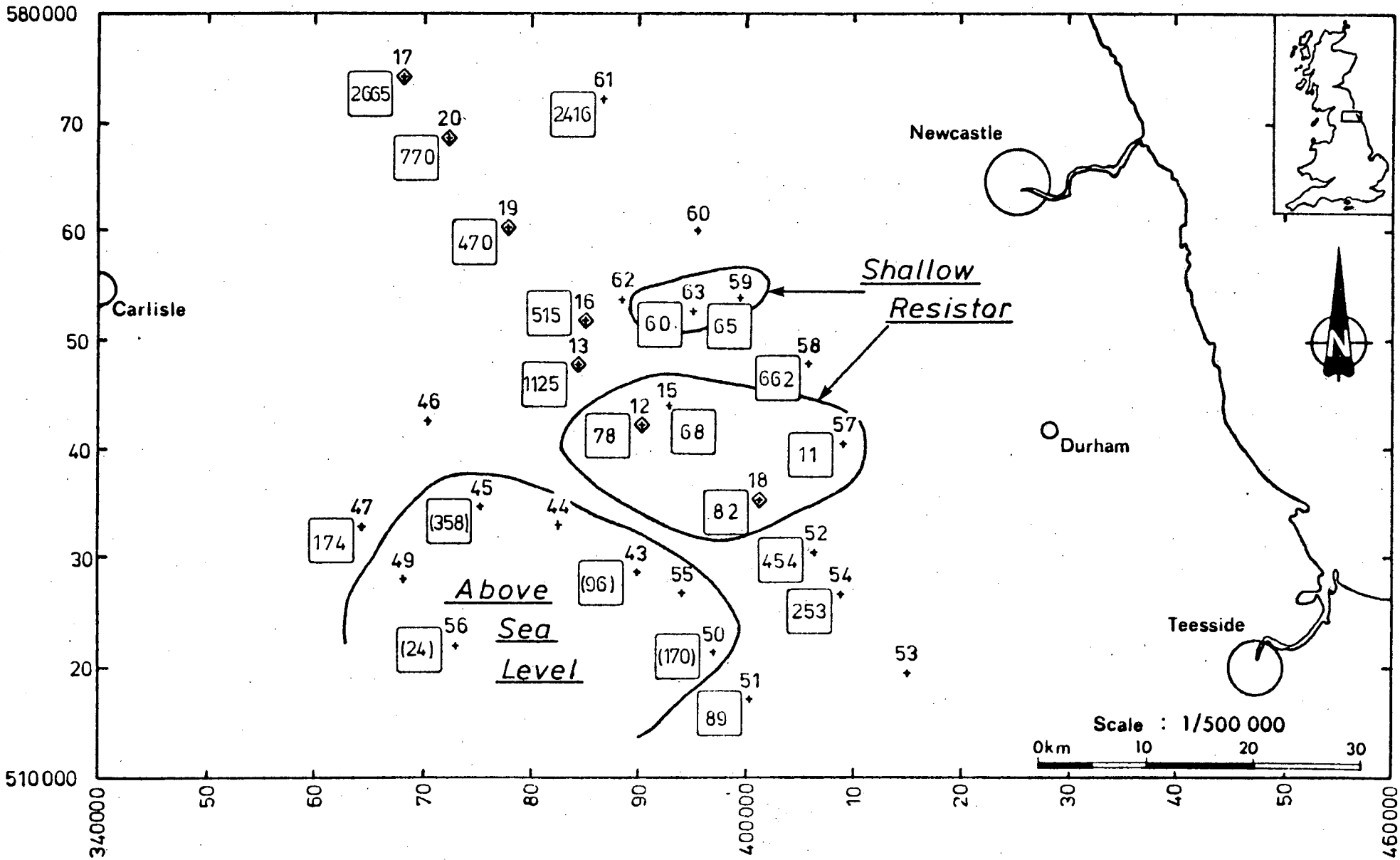
580000
70
60
50
40
30
20
510000
340000
50
60
70
80
90
400000
10
20
30
40
50
460000
Newcastle
Carlisle
Durham
Teesside
Shallow
Resistor
Above
Sea
Level
17
2665
20
770
19
470
61
2416
60
62
63
59
60
65
515
16
13
1125
58
662
46
15
12
78
68
57
11
18
82
47
174
45
(358)
44
49
43
(96)
55
52
454
54
253
56
(24)
50
(170)
53
51
89
N
Scale : 1/500 000
0km
10
20
30

data have only been outlined to show a shallow resistor at less than 100 m depth, and a separate region where the values are above sea level. To the north and south of the shallow resistor, the values increase. The extent of the area above sea level cannot be completely determined. A meaningful interpretation, based on these results, requires further closely spaced measurements to be made in the region.

6.5 Conclusions

The main contributions of this thesis can be summarised under three general headings :

(a) Development of instrumentation and computer programmes.

(b) Application of new techniques (AMT) to a field study.

(c) The results of the field study.

and are given below.

(a) Development

1. The author has assisted in the construction and testing of an audio-magnetotelluric system and has determined experimentally the corrections required for the amplitude and phase responses of the instrumentation.

2. Modifications have been made to existing computer programmes, for band averaging of response estimates, for the extended frequency range of the data and for the more efficient implementation of Jones' one-dimensional inversion programme. The advantages of applying this latter programme to phase as well as apparent resistivity estimates have been demonstrated.

(b) Application

1. For the field study, the extension of the MT technique into the AMT band and the use of an in-field mini-computer have been introduced for the first time in MT fieldwork in the U.K.

2. It has been found that the electromagnetic activity in the AMT frequency range is such, that with carefully selected events the AMT method may be used extensively and continuously. The advantage in speed of operation over other comparable probing techniques is clear, outlining the capacity of the method as a cheap, fast and easy to operate conductivity mapping and exploration tool. It has been possible to successfully measure the electric and magnetic field variations in the frequency band 1 Hz - 1 kHz in a region of the British Isles not marked for its remoteness.

(c) Results

1. A detailed study of the AMT results from two sites adjacent to the Rookhope borehole has shown that the resulting electrical models indicate a transition to a resistive layer at a depth compatible with the known depth to the granite. A conducting layer immediately above this may be associated with mineralisation.

2. A comparison of the AMT and resistivity techniques, used by Habberjam and Thanassoulas, shows that the model proposed by these authors does not satisfy the observed AMT responses. Reasons for this discrepancy require further study.

3. The station spacing of the AMT soundings over the study region was inadequate for a general interpretation of the results, but for groups of stations a preliminary interpretation has been possible e.g for a traverse across the Weardale granite from the Northumberland basin. These data are compatible with (i) the variation in depth of the sedimentary sequences of the Northumberland basin and (ii) the depths to and northerly extent of the Weardale granite as suggested by the interpretation of gravity data.

4. From the broadband MT data, it has been shown that the one-dimensional model for LAM is in agreement with previously suggested models for south Scotland.

5. These data also show that Jones' staion TOW cannot be regarded as typical of the Northumberland basin. It appears to be at the centre of a transition zone between models of the southern Scotland type and those of the Weardale granite. A major lateral variation in both crustal and

upper mantle structure is indicated in the region of EDG - SIN, both by the MT results and the magnetic transfer functions.

6. The one-dimensional models of the broadband MT data from SWI, ROO and HIL suggest a thickness of the Weardale granite of the order of 25 km.

6.6 Suggestions for future work

Two-dimensional modelling of the existing data should be undertaken using figure 6.12 as a basis for a starting model and incorporating previous results from southern Scotland.

Additional field observations over the whole study region are required to confirm some of the tentative conclusions made in this thesis. For this purpose, the soundings should cover the complete frequency range of 10^{-3} - 10^{4} secons and the station spacing reduced. This should be of the order of 1/10 to 1/2 skin depth at the longes period of each separate recording band. An area of special interest is the transition region between EDG and SIN.

To improve the response, particularly, when the instrumentation is used at the extremes of its operational bandwidth, the total bandwidth should be divided into sections. Each section should then be digitised separately at a suitably chosen frequency to avoid aliasing effects

Figure 6.17 An example of an on-line data acquisition system for use in broadband MT measurements (From Dawes, 1981)

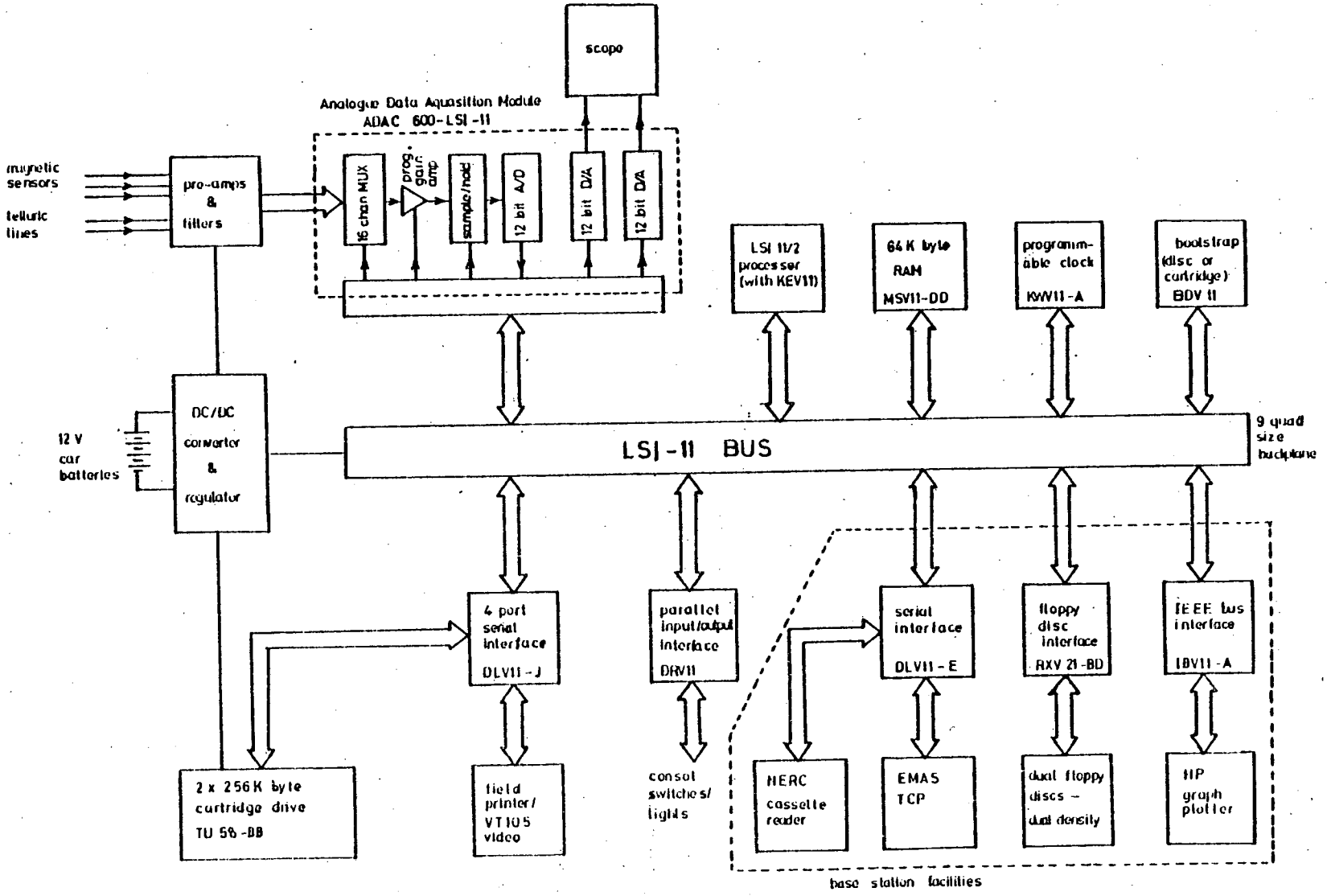
scope
Analogue Data Aquasition Module
ADAC 600-LSI-11
magnetic sensors
telluric lines
pre-amps & filters
16 chan MUX
prog. gain amp
sample/hold
12 bit A/D
12 bit D/A
12 bit D/A
LSI 11/2 processer (with KEV11)
64 K byte RAM MSV11-DD
programmable clock KWV11-A
bootstrap (disc or cartridge) BDV 11
12 V car batteries
DC/DC converter & regulator
LSI-11 BUS
9 quad size backplane
4 port serial interface DLV11-J
parallel input/output interface DRV11
serial interface DLV11-E
floppy disc interface RXV 21-BD
IEEE bus interface IBV11-A
2 x 256K byte cartridge drive TU 58-DB
field printer/ VT105 video
consol switches/ lights
NERC cassette reader
EMAS TCP
dual floppy discs - dual density
HP graph plotter
base station facilities

Figure 6.17

associated with the low fall-off characteristics of the low pass filters. Such digitising frequency must be at least four times the 3 dB cut-off point of the filter. The use of digital filtering may, in some cases, improve the quality of data, although the use of active (analogue) filters is preferred to improve the dynamic range of the natural signal, particularly when 50 Hz signals (and its harmonics) are present.

An example of an on-line acquisition and processing system is summarised in figure 6.17 after Dawes (1981). The possible use of remote reference station recording (Gamble et al, 1979) involving a precission time link to a base station should be considered.

APPENDIX

1. Note on the input impedance of the telluric pre-amplifier

Since the completion of the practical work made in this study, the satisfactory operation of the telluric pre-amplifier used for the AMT measurements has been questioned, since the input impedance of the input passive-filter network - figure 2.6 - is relatively low. This will introduce errors in the amplitude and phase responses when the electrode contact resistance is high. As was indicated in the text, page 82, no correction was used for the amplitude response between 6 and 600 Hz, since laboratory tests had shown that with low input impedance, a maximum variation of 3 % occured within this range. For the phase, however, corrections for the response, assuming low input impedance, were made, as stated on page 83.

From laboratory tests and numerical computations now undartaken with variable input impedances, it has been found that corrections are now required for the amplitude response and a small additional correction to the phase response. These are given in the appended tables. They show that in the range 6 - 600 Hz for a typical observed contact resistances of 1000 ohms the amplitude response should be increased by about 6 % throughout the range and the phase by a maximum of 1.3 degrees at the highest frequency.

In these tables A_i and Φ_i are the amplitude and phase responses for an input impedance of i ohms. Tables A give the computed responses over the frequency range 1 - 1995 Hz and tables B a summary of the values appropriate to this study.

Contact resistance 100 ohms

f(Hz)	A_o	A_{100}	$A_o - A_{100}$	Φ_o	Φ_{100}	$\Phi_o - \Phi_{100}$
1.00	0.6857	0.6835	0.0021	46.7	46.5	0.2
1.26	0.7644	0.7614	0.0030	40.1	39.9	0.2
1.58	0.8306	0.8268	0.0038	33.7	33.6	0.2
2.00	0.8825	0.8779	0.0046	27.9	27.8	0.2
2.51	0.9207	0.9155	0.0052	22.8	22.7	0.1
3.16	0.9475	0.9419	0.0056	18.5	18.3	0.1
3.98	0.9657	0.9597	0.0060	14.8	14.7	0.1
5.01	0.9777	0.9715	0.0062	11.8	11.7	0.1
6.31	0.9855	0.9792	0.0063	9.4	9.3	0.1
7.94	0.9906	0.9841	0.0064	7.4	7.3	0.1
10.00	0.9938	0.9873	0.0065	5.8	5.7	0.0
12.59	0.9958	0.9893	0.0065	4.5	4.4	0.0
15.85	0.9971	0.9905	0.0066	3.4	3.4	0.0
19.95	0.9979	0.9913	0.0066	2.5	2.5	0.0
25.12	0.9984	0.9918	0.0066	1.7	1.7	0.0
31.62	0.9987	0.9921	0.0066	1.1	1.1	0.0
39.81	0.9989	0.9923	0.0066	0.5	0.4	0.0
50.12	0.9989	0.9923	0.0066	-0.1	-0.1	0.0
63.10	0.9989	0.9923	0.0066	-0.7	-0.7	0.0
79.43	0.9988	0.9921	0.0066	-1.3	-1.4	0.0
100.00	0.9985	0.9919	0.0066	-2.1	-2.1	0.0
125.89	0.9981	0.9915	0.0066	-2.9	-2.9	0.0
158.49	0.9974	0.9907	0.0066	-3.8	-3.9	0.0
199.53	0.9962	0.9896	0.0066	-5.0	-5.0	0.0
251.19	0.9945	0.9878	0.0067	-6.4	-6.5	0.1
316.23	0.9916	0.9849	0.0067	-8.2	-8.3	0.1
398.10	0.9872	0.9805	0.0068	-10.4	-10.5	0.1
501.18	0.9803	0.9735	0.0068	-13.1	-13.2	0.1
630.95	0.9697	0.9628	0.0070	-16.4	-16.6	0.1
794.32	0.9535	0.9464	0.0071	-20.5	-20.7	0.2
1000.00	0.9294	0.9221	0.0073	-25.5	-25.7	0.2
1258.92	0.8946	0.8870	0.0076	-31.4	-31.7	0.2
1584.88	0.8465	0.8386	0.0079	-38.4	-38.7	0.3
1995.25	0.7835	0.7754	0.0081	-46.3	-46.6	0.3

f(Hz)	$\frac{A_o - A_{100}}{A_o}$ %	$\Phi_o - \Phi_{100}$ degrees
6.31	0.6	0.1
63.10	0.6	0.0
630.95	0.7	0.1

Contact resistance 200 ohms

(A)

f(Hz)	A_o	A_{200}	$A_o - A_{200}$	Φ_o	Φ_{200}	$\Phi_o - \Phi_{200}$
1.00	0.6857	0.6814	0.0043	46.7	46.3	0.4
1.26	0.7644	0.7584	0.0059	40.1	39.7	0.4
1.58	0.8306	0.8230	0.0076	33.7	33.4	0.4
2.00	0.8825	0.8734	0.0091	27.9	27.6	0.3
2.51	0.9207	0.9104	0.0103	22.8	22.5	0.3
3.16	0.9475	0.9363	0.0112	18.5	18.2	0.2
3.98	0.9657	0.9538	0.0119	14.8	14.6	0.2
5.01	0.9777	0.9654	0.0123	11.8	11.7	0.2
6.31	0.9855	0.9729	0.0126	9.4	9.2	0.1
7.94	0.9906	0.9778	0.0128	7.4	7.3	0.1
10.00	0.9938	0.9808	0.0129	5.8	5.7	0.1
12.59	0.9958	0.9828	0.0130	4.5	4.4	0.1
15.85	0.9971	0.9840	0.0130	3.4	3.3	0.1
19.95	0.9979	0.9848	0.0131	2.5	2.5	0.0
25.12	0.9984	0.9853	0.0131	1.7	1.7	0.0
31.62	0.9987	0.9856	0.0131	1.1	1.0	0.0
39.81	0.9989	0.9857	0.0131	0.5	0.4	0.0
50.12	0.9989	0.9858	0.0131	-0.1	-0.2	0.0
63.10	0.9989	0.9858	0.0131	-0.7	-0.8	0.0
79.43	0.9988	0.9856	0.0131	-1.3	-1.4	0.0
100.00	0.9985	0.9854	0.0131	-2.1	-2.1	0.1
125.89	0.9981	0.9849	0.0132	-2.9	-2.9	0.1
158.49	0.9974	0.9842	0.0132	-3.8	-3.9	0.1
199.53	0.9962	0.9830	0.0132	-5.0	-5.1	0.1
251.19	0.9945	0.9812	0.0132	-6.4	-6.5	0.1
316.23	0.9916	0.9783	0.0133	-8.2	-8.3	0.1
398.10	0.9872	0.9738	0.0134	-10.4	-10.5	0.2
501.18	0.9803	0.9668	0.0136	-13.1	-13.3	0.2
630.95	0.9697	0.9559	0.0138	-16.4	-16.7	0.3
794.32	0.9535	0.9394	0.0141	-20.5	-20.9	0.3
1000.00	0.9294	0.9149	0.0146	-25.5	-25.9	0.4
1258.92	0.8946	0.8795	0.0151	-31.4	-31.9	0.5
1584.88	0.8465	0.8308	0.0156	-38.4	-38.9	0.6
1995.25	0.7835	0.7675	0.0160	-46.3	-46.9	0.6

3)

f(Hz)	$\frac{A_o - A_{200}}{A_o}$ %	$\Phi_o - \Phi_{200}$ degrees
6.31	1.3	0.1
63.10	1.3	0.0
630.95	1.4	0.3

Contact resistance 500 ohms

f(Hz)	A_o	A_{500}	$A_o - A_{500}$	ϕ_o	ϕ_{500}	$\phi_o - \phi_{500}$
1.00	0.6857	0.6750	0.0107	46.7	45.7	0.9
1.26	0.7644	0.7497	0.0147	40.1	39.1	0.9
1.58	0.8306	0.8118	0.0188	33.7	32.9	0.9
2.00	0.8825	0.8601	0.0224	27.9	27.2	0.8
2.51	0.9207	0.8953	0.0254	22.8	22.2	0.7
3.16	0.9475	0.9199	0.0276	18.5	17.9	0.6
3.98	0.9657	0.9365	0.0291	14.8	14.3	0.5
5.01	0.9777	0.9475	0.0302	11.8	11.4	0.4
6.31	0.9855	0.9546	0.0309	9.4	9.1	0.3
7.94	0.9906	0.9592	0.0314	7.4	7.1	0.3
10.00	0.9938	0.9621	0.0317	5.8	5.6	0.2
12.59	0.9958	0.9639	0.0319	4.5	4.3	0.2
15.85	0.9971	0.9651	0.0320	3.4	3.3	0.1
19.95	0.9979	0.9658	0.0321	2.5	2.4	0.1
25.12	0.9984	0.9663	0.0321	1.7	1.6	0.1
31.62	0.9987	0.9666	0.0321	1.1	1.0	0.1
39.81	0.9989	0.9667	0.0322	0.5	0.4	0.1
50.12	0.9989	0.9667	0.0322	-0.1	-0.2	0.1
63.10	0.9989	0.9667	0.0322	-0.7	-0.8	0.1
79.43	0.9988	0.9665	0.0322	-1.3	-1.5	0.1
100.00	0.9985	0.9663	0.0322	-2.1	-2.2	0.1
125.89	0.9981	0.9658	0.0323	-2.9	-3.0	0.2
158.49	0.9974	0.9651	0.0323	-3.8	-4.0	0.2
199.53	0.9962	0.9639	0.0324	-5.0	-5.2	0.2
251.19	0.9945	0.9620	0.0325	-6.4	-6.7	0.3
316.23	0.9916	0.9590	0.0326	-8.2	-8.5	0.4
398.10	0.9872	0.9543	0.0329	-10.4	-10.8	0.5
501.18	0.9803	0.9471	0.0333	-13.1	-13.6	0.6
630.95	0.9697	0.9359	0.0339	-16.4	-17.1	0.7
794.32	0.9535	0.9189	0.0347	-20.5	-21.3	0.8
1000.00	0.9294	0.8937	0.0357	-25.5	-26.5	1.0
1258.92	0.8946	0.8577	0.0370	-31.4	-32.6	1.2
1584.88	0.8465	0.8083	0.0382	-38.4	-39.7	1.3
1995.25	0.7835	0.7446	0.0389	-46.3	-47.8	1.5

E)

f(Hz)	$\frac{A_o - A_{500}}{A_o}$ %	$\phi_o - \phi_{500}$ degrees
6.31	3.1	0.3
63.10	3.2	0.1
630.95	3.5	0.7

Contact resistance 1000 ohms

f(Hz)	A_o	A_{1000}	$A_o - A_{1000}$	ϕ_o	ϕ_{1000}	$\phi_o - \phi_{1000}$
1.00	0.6857	0.6645	0.0212	46.7	44.8	1.8
1.26	0.7644	0.7353	0.0290	40.1	38.3	1.8
1.58	0.8306	0.7937	0.0369	33.7	32.1	1.7
2.00	0.8825	0.8386	0.0438	27.9	26.4	1.5
2.51	0.9207	0.8712	0.0495	22.8	21.5	1.3
3.16	0.9475	0.8938	0.0537	18.5	17.4	1.1
3.98	0.9657	0.9090	0.0566	14.8	13.9	0.9
5.01	0.9777	0.9191	0.0586	11.8	11.1	0.7
6.31	0.9855	0.9255	0.0600	9.4	8.8	0.6
7.94	0.9906	0.9297	0.0609	7.4	6.9	0.5
10.00	0.9938	0.9324	0.0614	5.8	5.4	0.4
12.59	0.9958	0.9340	0.0618	4.5	4.2	0.3
15.85	0.9971	0.9351	0.0620	3.4	3.1	0.3
19.95	0.9979	0.9358	0.0621	2.5	2.3	0.2
25.12	0.9984	0.9362	0.0622	1.7	1.5	0.2
31.62	0.9987	0.9364	0.0623	1.1	0.9	0.2
39.81	0.9989	0.9365	0.0623	0.5	0.3	0.2
50.12	0.9989	0.9366	0.0624	-0.1	-0.3	0.2
63.10	0.9989	0.9365	0.0624	-0.7	-0.9	0.2
79.43	0.9988	0.9363	0.0624	-1.3	-1.6	0.2
100.00	0.9985	0.9360	0.0625	-2.1	-2.3	0.3
125.89	0.9981	0.9356	0.0625	-2.9	-3.2	0.3
158.49	0.9974	0.9348	0.0626	-3.8	-4.2	0.4
199.53	0.9962	0.9335	0.0627	-5.0	-5.5	0.5
251.19	0.9945	0.9315	0.0629	-6.4	-7.0	0.6
316.23	0.9916	0.9284	0.0633	-8.2	-8.9	0.7
398.10	0.9872	0.9235	0.0637	-10.4	-11.2	0.9
501.18	0.9803	0.9159	0.0645	-13.1	-14.2	1.1
630.95	0.9697	0.9042	0.0655	-16.4	-17.7	1.3
794.32	0.9535	0.8865	0.0670	-20.5	-22.1	1.6
1000.00	0.9294	0.8604	0.0690	-25.5	-27.4	1.9
1258.92	0.8946	0.8233	0.0713	-31.4	-33.7	2.3
1584.88	0.8465	0.7730	0.0734	-38.4	-41.0	2.6
1995.25	0.7835	0.7089	0.0746	-46.3	-49.1	2.8

f(Hz)	$\frac{A_o - A_{1000}}{A_o}$ %	$\phi_o - \phi_{1000}$ degrees
6.31	6.1	0.6
63.10	6.2	0.2
630.95	6.8	1.3

Contact resistance 2000 ohms

f(Hz)	A_o	A_{2000}	$A_o - A_{2000}$	Φ_o	Φ_{2000}	$\Phi_o - \Phi_{2000}$
1.00	0.6857	0.6439	0.0417	46.7	43.1	3.6
1.26	0.7644	0.7078	0.0566	40.1	36.6	3.5
1.58	0.3306	0.7594	0.0712	33.7	30.5	3.2
2.00	0.8825	0.7985	0.0840	27.9	25.1	2.9
2.51	0.9207	0.8264	0.0943	22.8	20.4	2.5
3.16	0.9475	0.8457	0.1018	18.5	16.4	2.1
3.98	0.9657	0.8585	0.1072	14.8	13.1	1.7
5.01	0.9777	0.8669	0.1108	11.8	10.4	1.4
6.31	0.9855	0.8724	0.1132	9.4	8.2	1.1
7.94	0.9906	0.8758	0.1147	7.4	6.5	0.9
10.00	0.9938	0.8781	0.1157	5.8	5.0	0.7
12.59	0.9958	0.8795	0.1163	4.5	3.9	0.6
15.85	0.9971	0.8803	0.1167	3.4	2.9	0.5
19.95	0.9979	0.8809	0.1170	2.5	2.1	0.4
25.12	0.9984	0.8812	0.1172	1.7	1.4	0.4
31.62	0.9987	0.8814	0.1173	1.1	0.7	0.4
39.81	0.9989	0.8815	0.1174	0.5	0.1	0.3
50.12	0.9989	0.8815	0.1174	-0.1	-0.5	0.4
63.10	0.9989	0.8814	0.1175	-0.7	-1.1	0.4
79.43	0.9988	0.8812	0.1175	-1.3	-1.8	0.4
100.00	0.9985	0.8809	0.1176	-2.1	-2.5	0.5
125.89	0.9981	0.8804	0.1177	-2.9	-3.4	0.6
158.49	0.9974	0.8795	0.1178	-3.8	-4.5	0.7
199.53	0.9962	0.8782	0.1181	-5.0	-5.9	0.9
251.19	0.9945	0.8760	0.1185	-6.4	-7.5	1.1
316.23	0.9916	0.8726	0.1190	-8.2	-9.5	1.3
398.10	0.9872	0.8673	0.1199	-10.4	-12.0	1.6
501.18	0.9803	0.8591	0.1212	-13.1	-15.1	2.0
630.95	0.9697	0.8466	0.1232	-16.4	-18.9	2.5
794.32	0.9535	0.8277	0.1258	-20.5	-23.5	3.0
1000.00	0.9294	0.8002	0.1292	-25.5	-29.1	3.6
1258.92	0.8946	0.7616	0.1330	-31.4	-35.6	4.2
1584.88	0.8465	0.7102	0.1362	-38.4	-43.1	4.7
1995.25	0.7835	0.6461	0.1374	-46.3	-51.4	5.1

f(Hz)	$\frac{A_o - A_{2000}}{A_o}$ %	$\Phi_o - \Phi_{2000}$ degrees
6.31	11.5	1.1
63.10	11.8	0.4
630.95	12.7	2.5

Contact resistance 5000 ohms

f(Hz)	A_o	A_{5000}	$A_o - A_{5000}$	ϕ_o	ϕ_{5000}	$\phi_o - \phi_{5000}$
1.00	0.6857	0.5867	0.0989	46.7	38.5	8.2
1.26	0.7644	0.6338	0.1306	40.1	32.2	7.8
1.58	0.8306	0.6701	0.1605	33.7	26.6	7.1
2.00	0.8825	0.6964	0.1861	27.9	21.7	6.3
2.51	0.9207	0.7147	0.2059	22.8	17.5	5.3
3.16	0.9475	0.7271	0.2204	18.5	14.0	4.4
3.98	0.9657	0.7352	0.2305	14.8	11.2	3.6
5.01	0.9777	0.7405	0.2372	11.8	8.8	3.0
6.31	0.9855	0.7438	0.2417	9.4	7.0	2.4
7.94	0.9906	0.7460	0.2446	7.4	5.4	2.0
10.00	0.9938	0.7474	0.2464	5.8	4.2	1.6
12.59	0.9958	0.7482	0.2476	4.5	3.2	1.3
15.85	0.9971	0.7488	0.2483	3.4	2.3	1.1
19.95	0.9979	0.7491	0.2488	2.5	1.6	0.9
25.12	0.9984	0.7493	0.2491	1.7	0.9	0.8
31.62	0.9987	0.7494	0.2493	1.1	0.3	0.8
39.81	0.9989	0.7494	0.2495	0.5	-0.3	0.7
50.12	0.9989	0.7494	0.2496	-0.1	-0.9	0.7
63.10	0.9989	0.7492	0.2497	-0.7	-1.5	0.8
79.43	0.9988	0.7490	0.2498	-1.3	-2.2	0.9
100.00	0.9985	0.7486	0.2499	-2.1	-3.1	1.0
125.89	0.9981	0.7480	0.2501	-2.9	-4.1	1.2
158.49	0.9974	0.7470	0.2504	-3.8	-5.3	1.5
199.53	0.9962	0.7454	0.2509	-5.0	-6.8	1.8
251.19	0.9945	0.7429	0.2516	-6.4	-8.7	2.3
316.23	0.9916	0.7390	0.2526	-8.2	-11.0	2.8
398.10	0.9872	0.7329	0.2543	-10.4	-13.8	3.5
501.18	0.9803	0.7236	0.2567	-13.1	-17.3	4.3
630.95	0.9697	0.7095	0.2602	-16.4	-21.6	5.2
794.32	0.9535	0.6888	0.2648	-20.5	-26.8	6.3
1000.00	0.9294	0.6593	0.2702	-25.5	-32.9	7.4
1258.92	0.8946	0.6192	0.2754	-31.4	-40.0	8.6
1584.88	0.8465	0.5682	0.2783	-38.4	-47.9	9.5
1995.25	0.7835	0.5076	0.2759	-46.3	-56.4	10.1

f(Hz)	$\frac{A_o - A_{5000}}{A_o}$ %	$\phi_o - \phi_{5000}$ degrees
6.31	24.5	2.4
63.10	25.0	0.8
630.95	26.8	5.2

Contact resistance 10000 ohms

f(Hz)	A_o	A_{10000}	$A_o - A_{10000}$	ϕ_o	ϕ_{10000}	$\phi_o - \phi_{10000}$
1.00	0.6857	0.5061	0.1796	46.7	32.4	14.2
1.26	0.7644	0.5353	0.2290	40.1	26.8	13.3
1.58	0.8306	0.5566	0.2739	33.7	21.8	11.9
2.00	0.8825	0.5715	0.3110	27.9	17.6	10.3
2.51	0.9207	0.5815	0.3392	22.8	14.1	8.7
3.16	0.9475	0.5881	0.3594	18.5	11.3	7.2
3.98	0.9657	0.5923	0.3733	14.8	8.9	5.9
5.01	0.9777	0.5951	0.3826	11.8	7.0	4.8
6.31	0.9855	0.5968	0.3887	9.4	5.5	3.9
7.94	0.9906	0.5979	0.3926	7.4	4.3	3.1
10.00	0.9938	0.5986	0.3951	5.8	3.2	2.6
12.59	0.9958	0.5991	0.3967	4.5	2.4	2.1
15.85	0.9971	0.5993	0.3977	3.4	1.7	1.8
19.95	0.9979	0.5995	0.3984	2.5	1.0	1.5
25.12	0.9984	0.5996	0.3988	1.7	0.4	1.3
31.62	0.9987	0.5996	0.3991	1.1	-0.1	1.2
39.81	0.9989	0.5996	0.3993	0.5	-0.7	1.2
50.12	0.9989	0.5995	0.3994	-0.1	-1.3	1.2
63.10	0.9989	0.5994	0.3995	-0.7	-2.0	1.3
79.43	0.9988	0.5991	0.3997	-1.3	-2.8	1.4
100.00	0.9985	0.5987	0.3999	-2.1	-3.7	1.7
125.89	0.9981	0.5980	0.4001	-2.9	-4.8	2.0
158.49	0.9974	0.5969	0.4005	-3.8	-6.2	2.4
199.53	0.9962	0.5952	0.4011	-5.0	-7.9	2.9
251.19	0.9945	0.5925	0.4020	-6.4	-10.0	3.6
316.23	0.9916	0.5883	0.4034	-8.2	-12.7	4.5
398.10	0.9872	0.5818	0.4054	-10.4	-15.9	5.5
501.18	0.9803	0.5720	0.4084	-13.1	-19.8	6.8
630.95	0.9697	0.5573	0.4124	-16.4	-24.6	8.2
794.32	0.9535	0.5362	0.4173	-20.5	-30.3	9.8
1000.00	0.9294	0.5072	0.4223	-25.5	-37.0	11.5
1258.92	0.8946	0.4693	0.4254	-31.4	-44.5	13.0
1584.88	0.8465	0.4232	0.4232	-38.4	-52.6	14.2
1995.25	0.7835	0.3714	0.4121	-46.3	-61.2	14.9

f(Hz)	$\frac{A_o - A_{10000}}{A_o}$ %	$\phi_o - \phi_{10000}$ degrees
6.31	39.4	3.9
63.10	40.0	1.3
630.95	42.5	8.2

2. Compilation of AMT station results

All station results from the short period AMT soundings collected during this work, are compiled here. The order is numerical and a station map is included for easy reference.

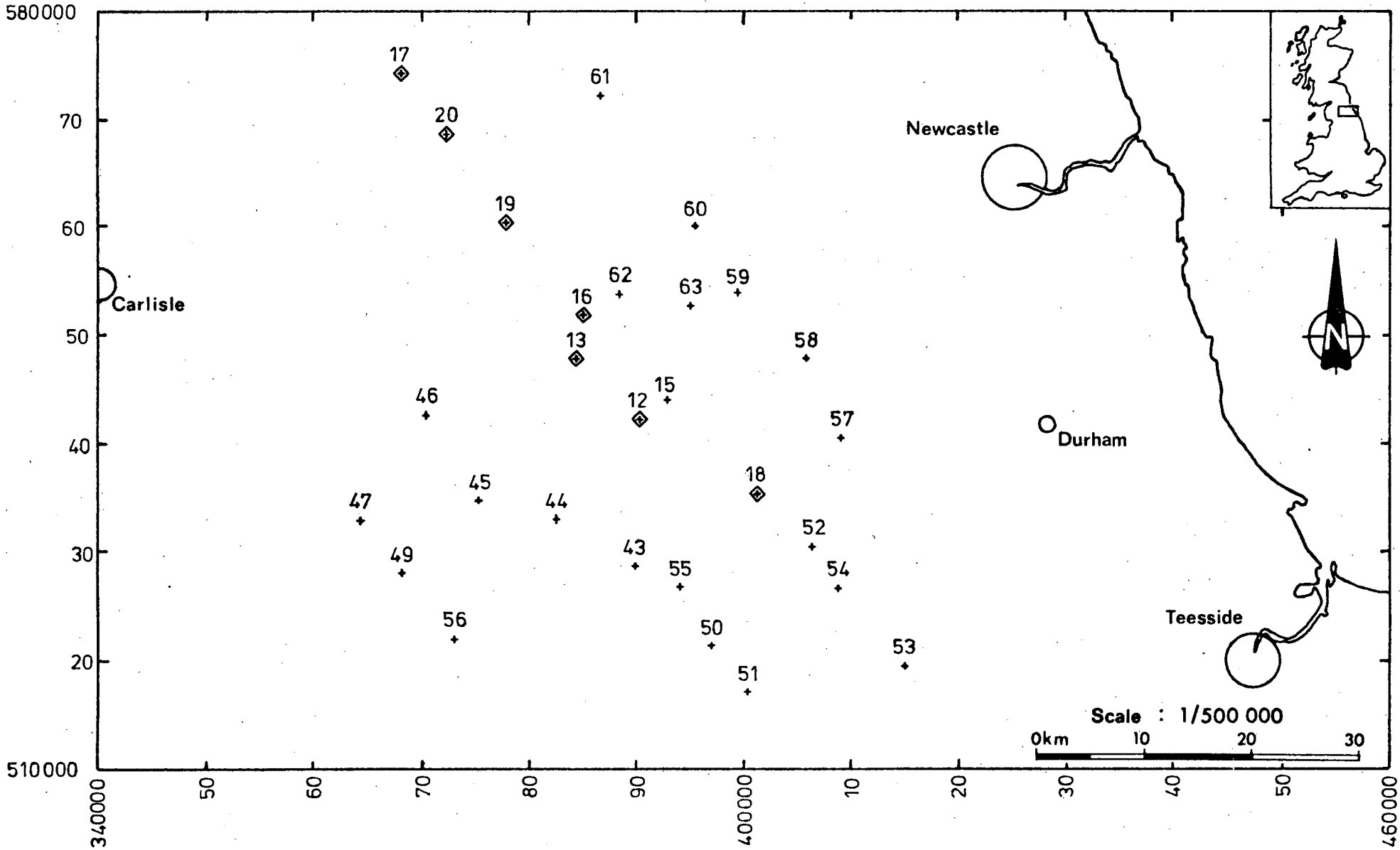
580000
70
60
50
40
30
20
510000
340000
50
60
70
80
90
400000
10
20
30
40
50
460000
17
61
20
19
60
62
63
59
16
Carlisle
13
58
46
15
12
57
Newcastle
Durham
18
45
47
44
52
43
55
54
49
56
50
53
51
Teesside
N
Scale : 1/500 000
0km
10
20
30

(c)

APPARENT RESISTIVITY IN
OHM METERS
PERIOD IN SECONDS
PHASE
PERIOD IN SECONDS

APPARENT RESISTIVITY IN
OHM METERS
PERIOD IN SECONDS
PHASE
PERIOD IN SECONDS

(c)

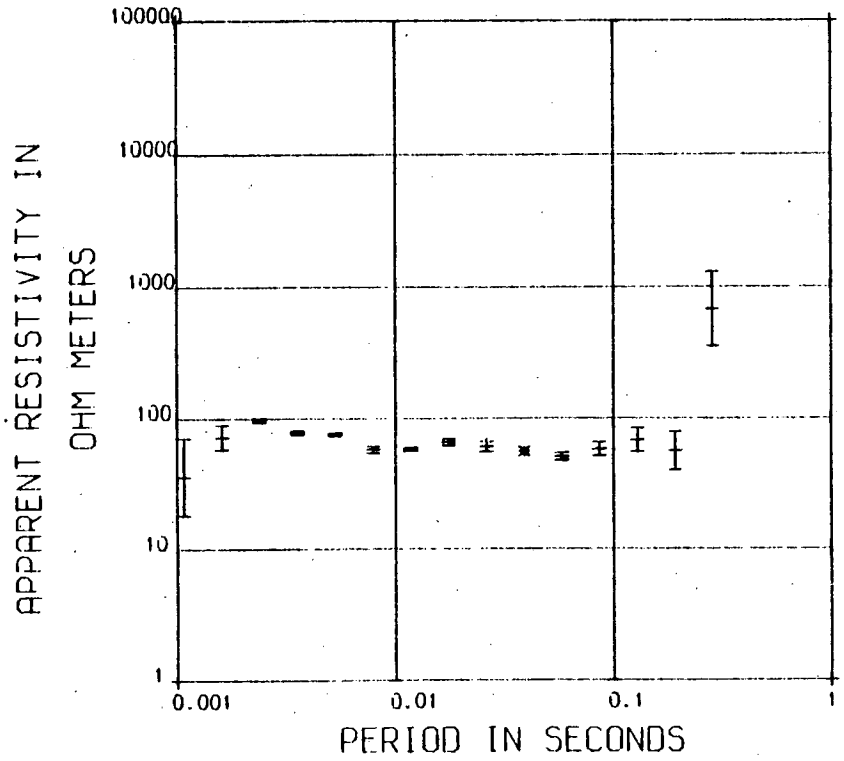
APPARENT RESISTIVITY IN
OHM METERS
100000
10000
1000
100
10
1
0.001
0.01
0.1
1
PERIOD IN SECONDS

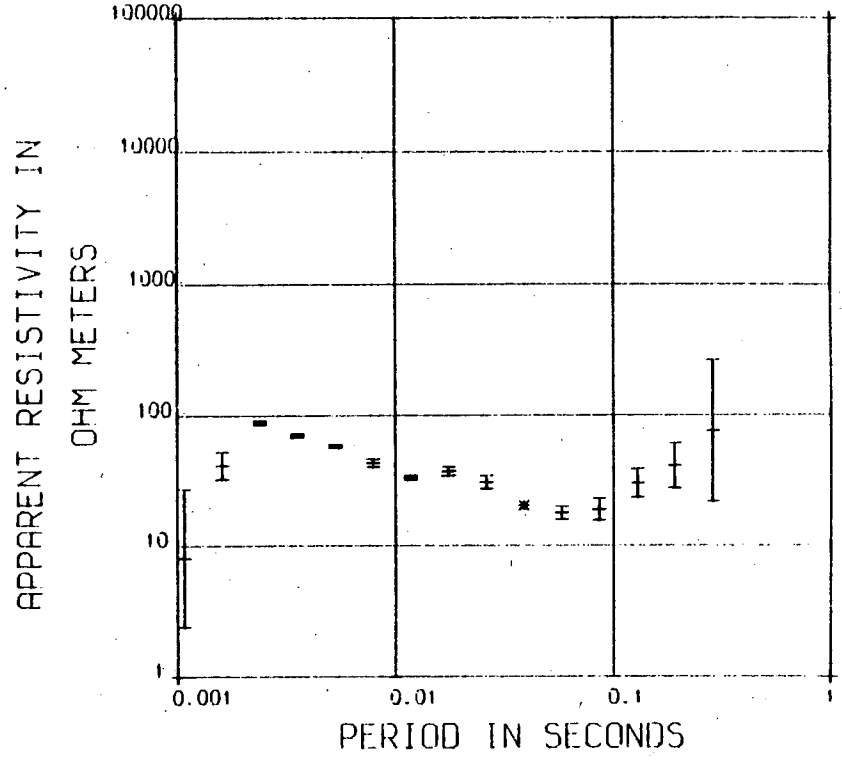
APPARENT RESISTIVITY IN
OHM METERS
100000
10000
1000
100
10
1
0.001
0.01
0.1
1
PERIOD IN SECONDS

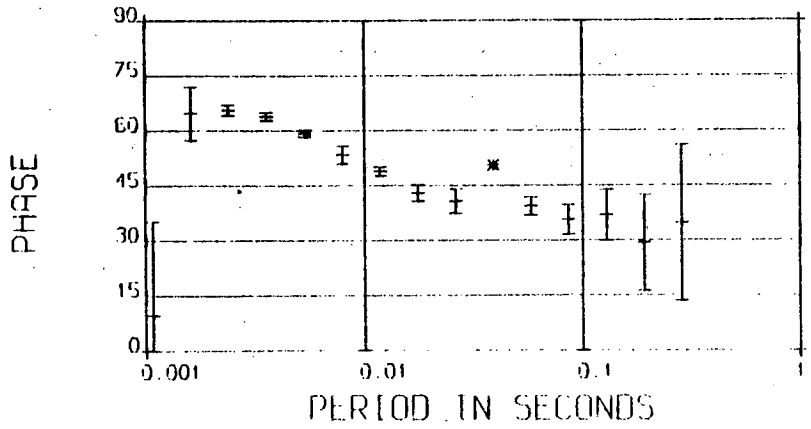
PHASE
90
75
60
45
30
15
0
0.001
0.01
0.1
1
PERIOD IN SECONDS

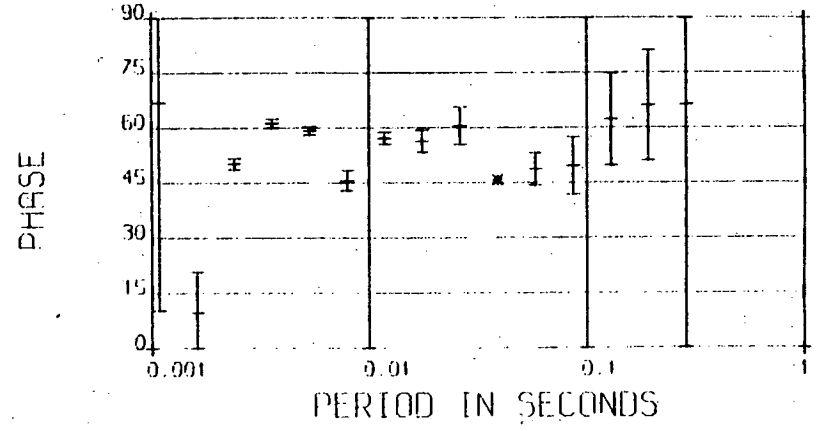
PHASE
90
75
60
45
30
15
0
0.001
0.01
0.1
1
PERIOD IN SECONDS

Station 15

STATION 15

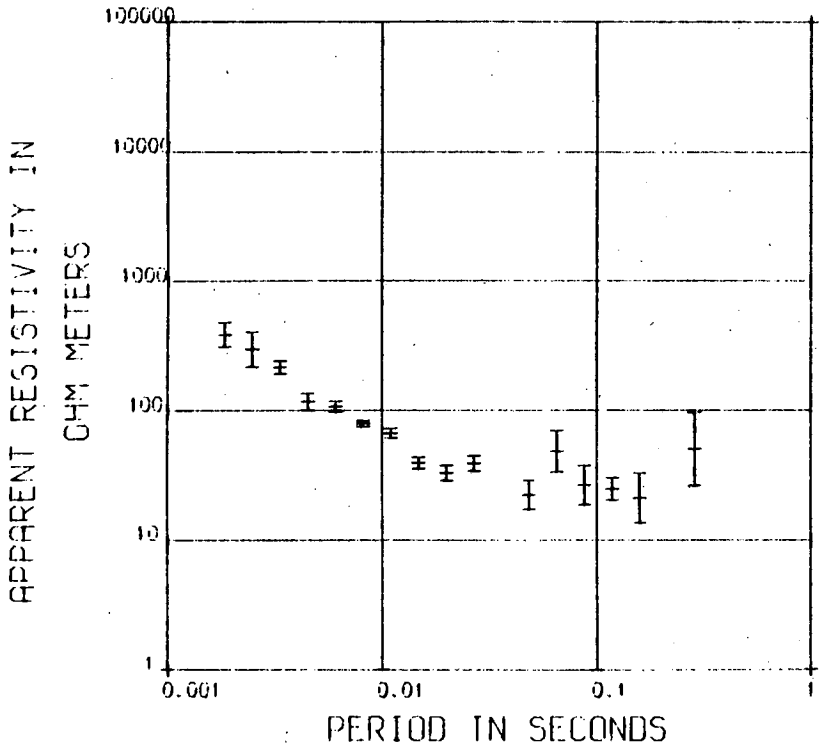

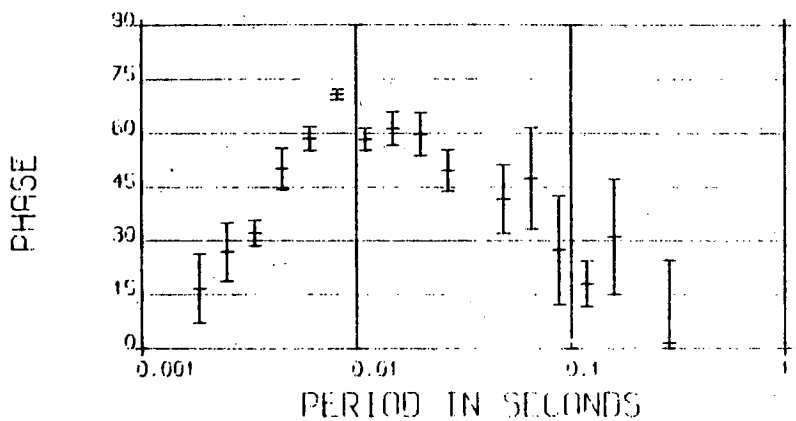

STATION 15

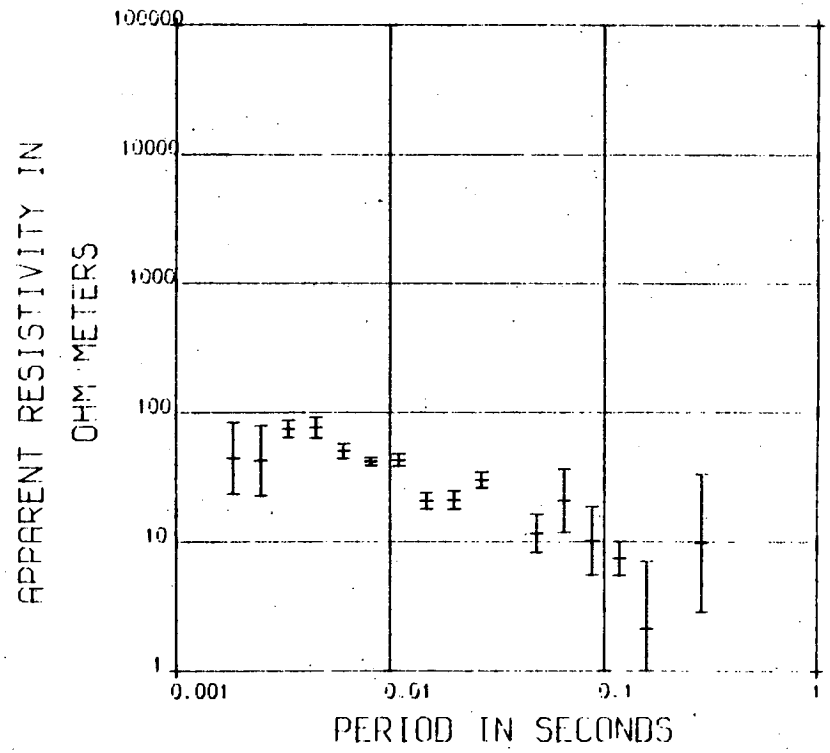

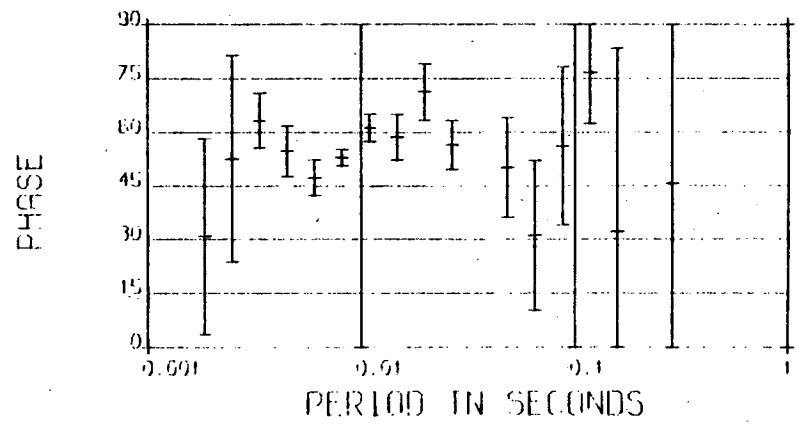

Station 15

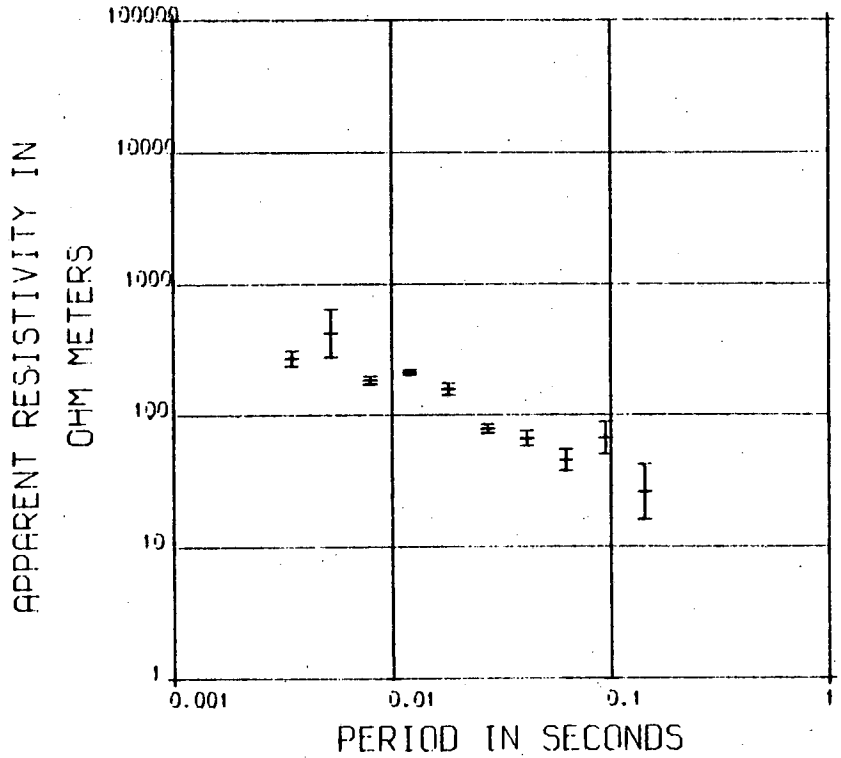
APPARENT RESISTIVITY IN
OHM METERS
100000
10000
1000
100
10
1
0.001
0.01
0.1
1
PERIOD IN SECONDS

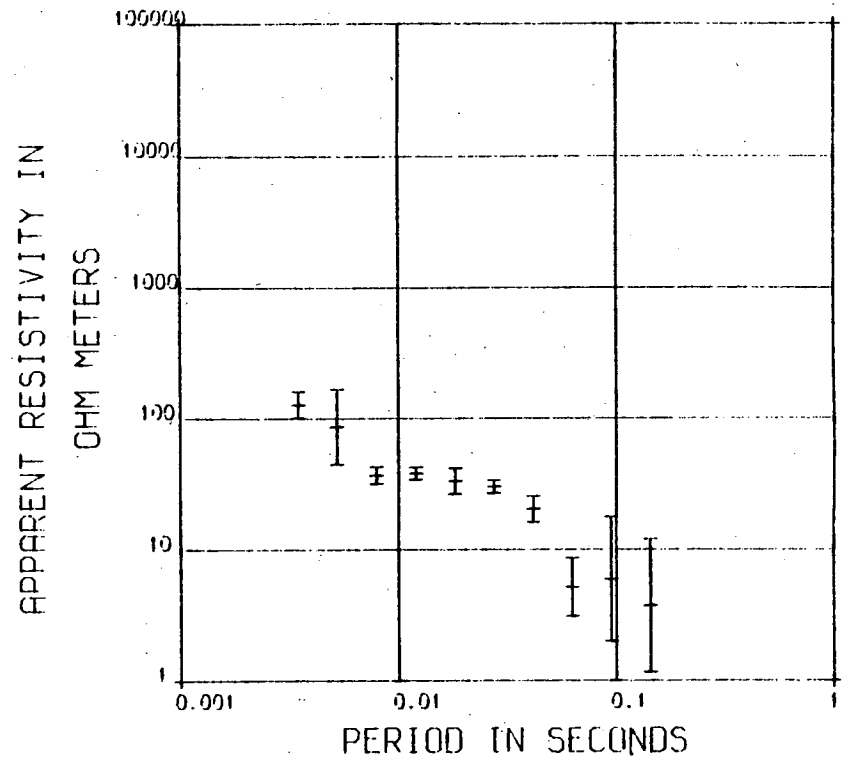
APPARENT RESISTIVITY IN
OHM METERS
100000
10000
1000
100
10
1
0.001
0.01
0.1
1
PERIOD IN SECONDS

(c)

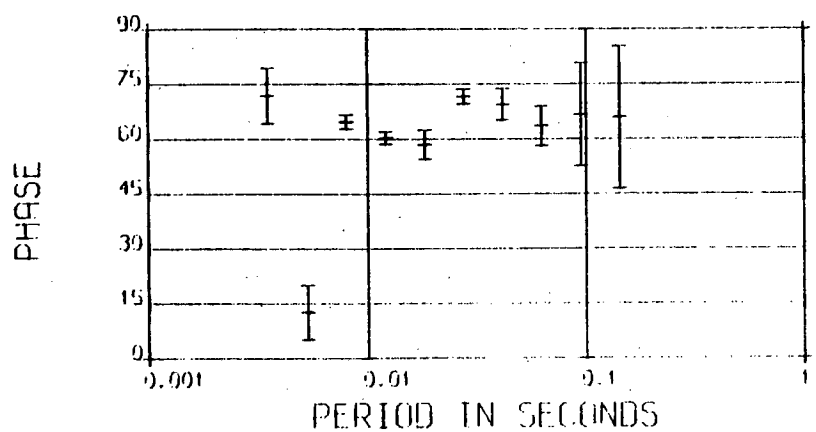
PHASE
90
75
60
45
30
15
0
0.001
0.01
0.1
1
PERIOD IN SECONDS

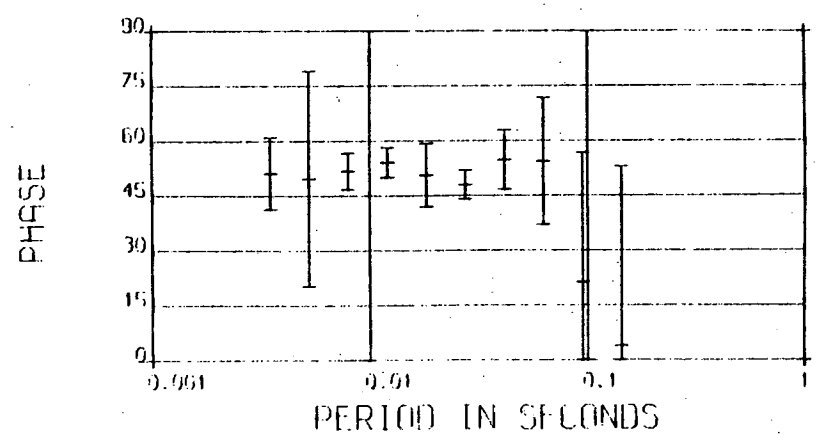
PHASE
90
75
60
45
30
15
0
0.001
0.01
0.1
1
PERIOD IN SECONDS

(c)

APPARENT RESISTIVITY IN
OHM METERS
PERIOD IN SECONDS
PHASE
PERIOD IN SECONDS

APPARENT RESISTIVITY IN
OHM METERS
PERIOD IN SECONDS
PHASE
PERIOD IN SECONDS

Station 17

(c)

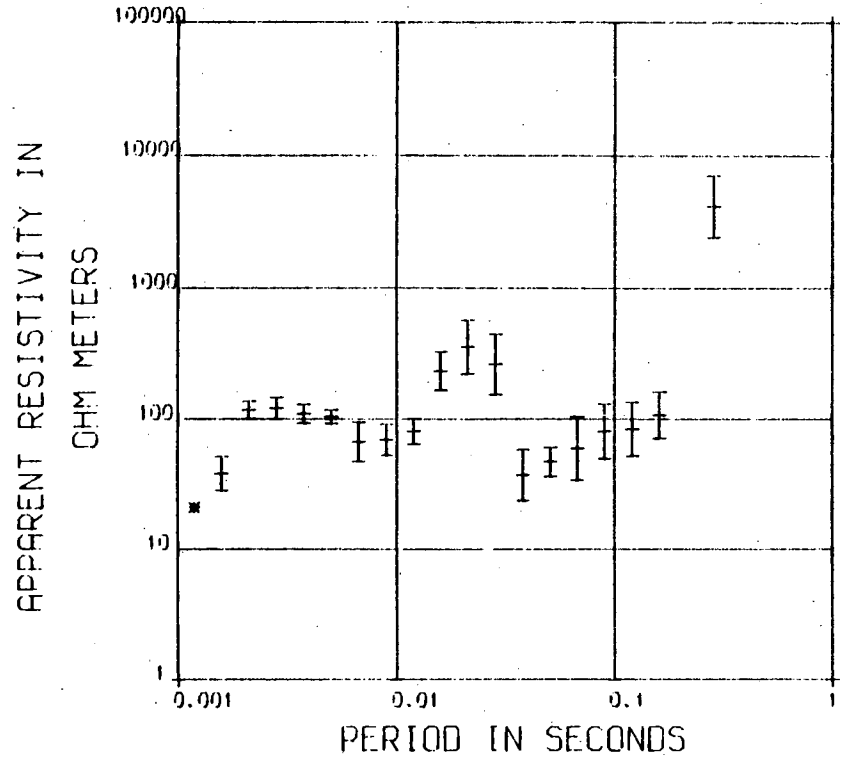
APPARENT RESISTIVITY IN
OHM METERS
100000
10000
1000
100
10
1
0.001
0.01
0.1
1
PERIOD IN SECONDS

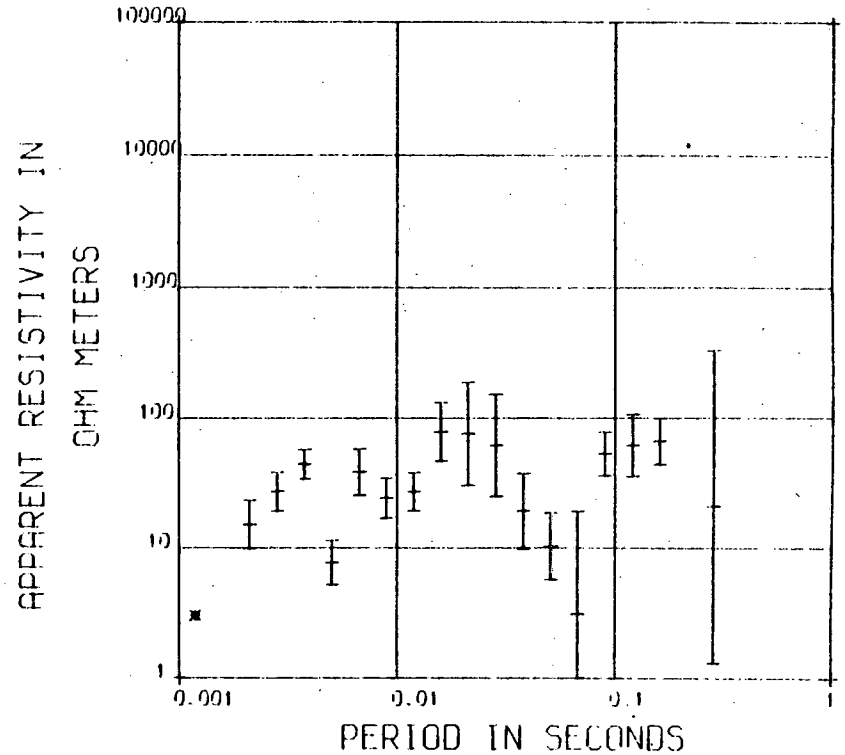
APPARENT RESISTIVITY IN
OHM METERS
100000
10000
1000
100
10
1
0.001
0.01
0.1
1
PERIOD IN SECONDS

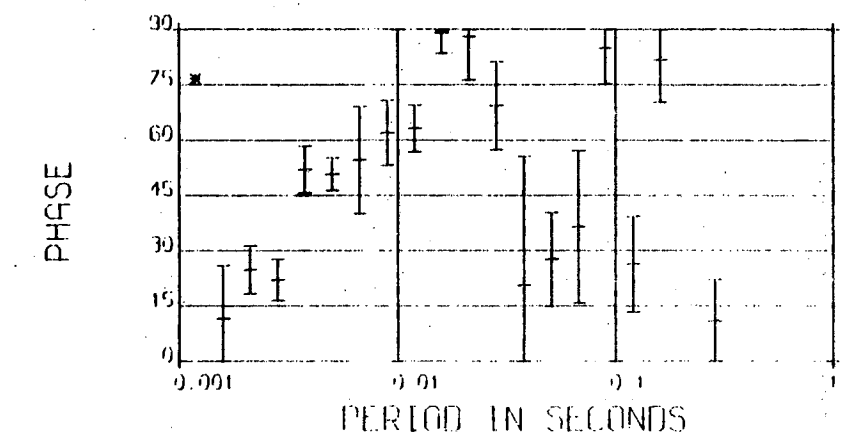
PHASE
90
75
60
45
30
15
0
0.001
0.01
0.1
1
PERIOD IN SECONDS

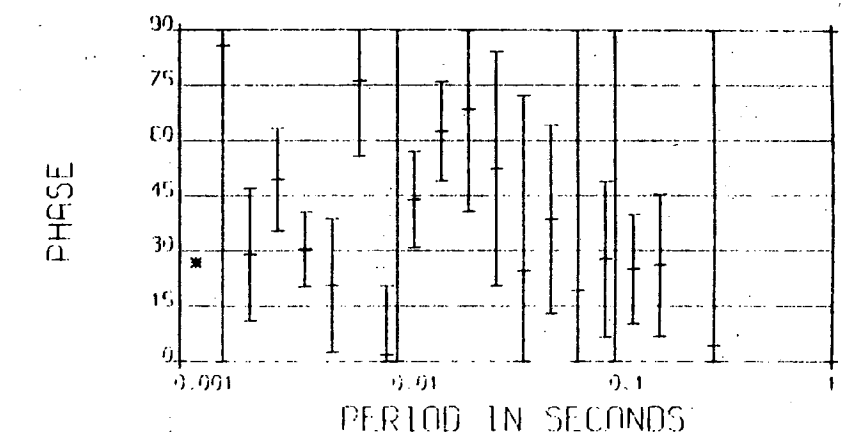
PHASE
90
75
60
45
30
15
0
0.001
0.01
0.1
1
PERIOD IN SECONDS

Station 18

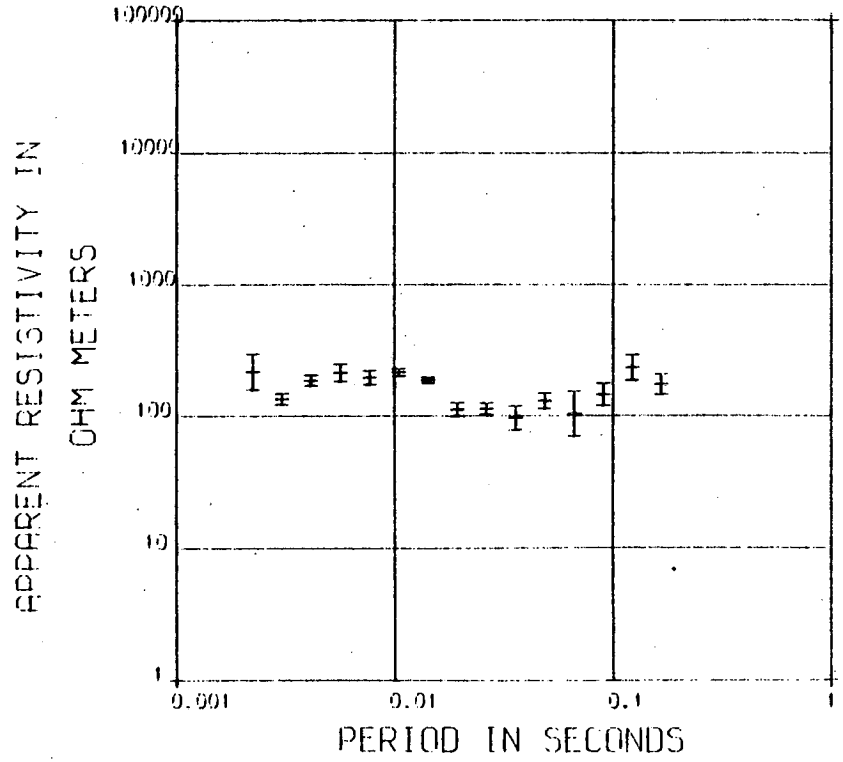
APPARENT RESISTIVITY IN
OHM METERS
100000
10000
1000
100
10
1
0.001
0.01
0.1
1
PERIOD IN SECONDS

(c)

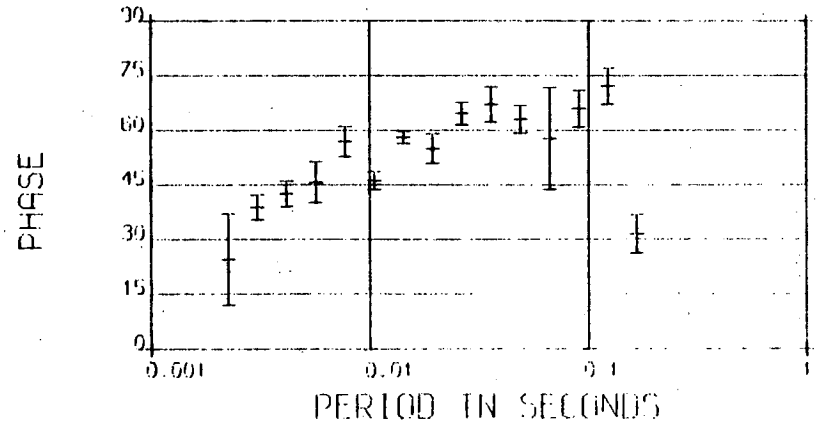
PHASE
90
75
60
45
30
15
0
0.001
0.01
0.1
1
PERIOD IN SECONDS

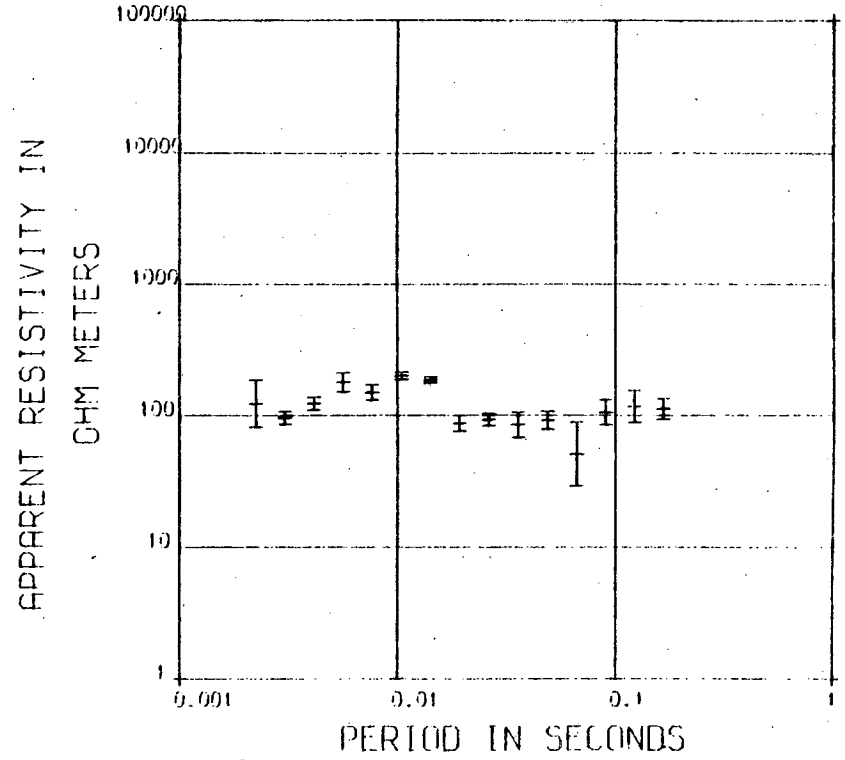
APPARENT RESISTIVITY IN
OHM METERS
100000
10000
1000
100
10
1
0.001
0.01
0.1
1
PERIOD IN SECONDS

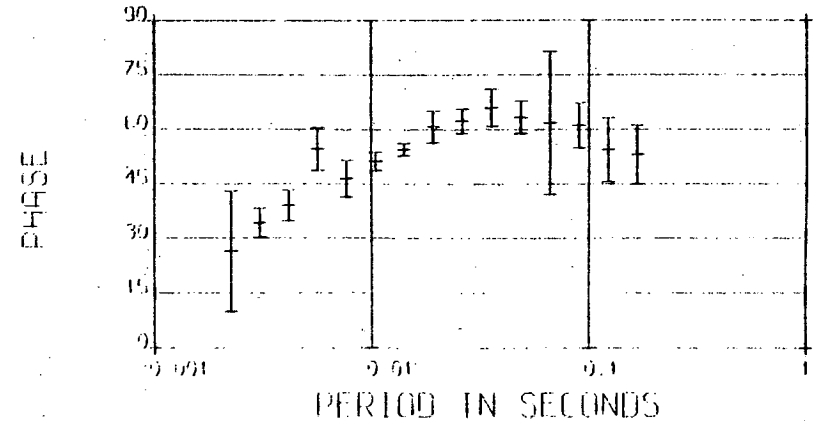
PHASE
90
75
60
45
30
15
0
0.001
0.01
0.1
1
PERIOD IN SECONDS

Station 19

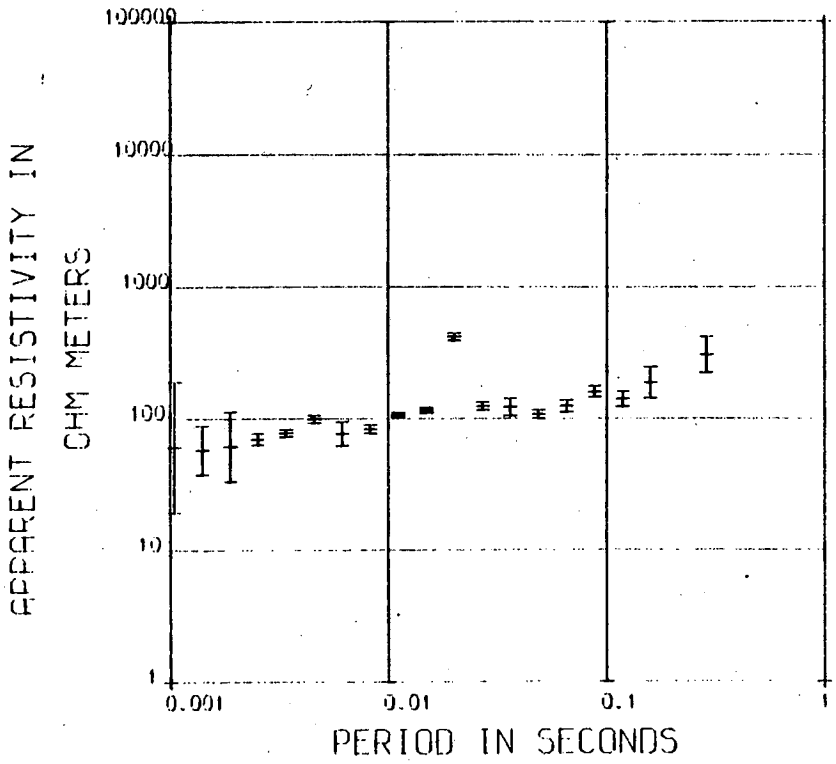
APPARENT RESISTIVITY IN
OHM METERS
100000
10000
1000
100
10
1
0.001
0.01
0.1
1
PERIOD IN SECONDS

(c)

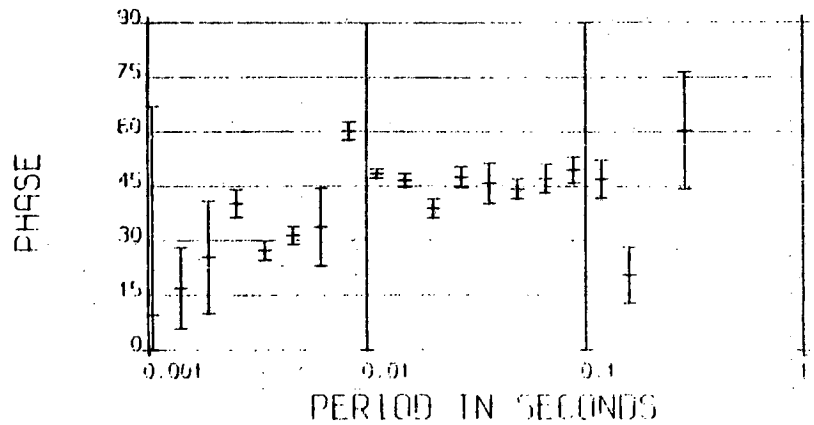
PHASE
90
75
60
45
30
15
0
0.001
0.01
0.1
1
PERIOD IN SECONDS

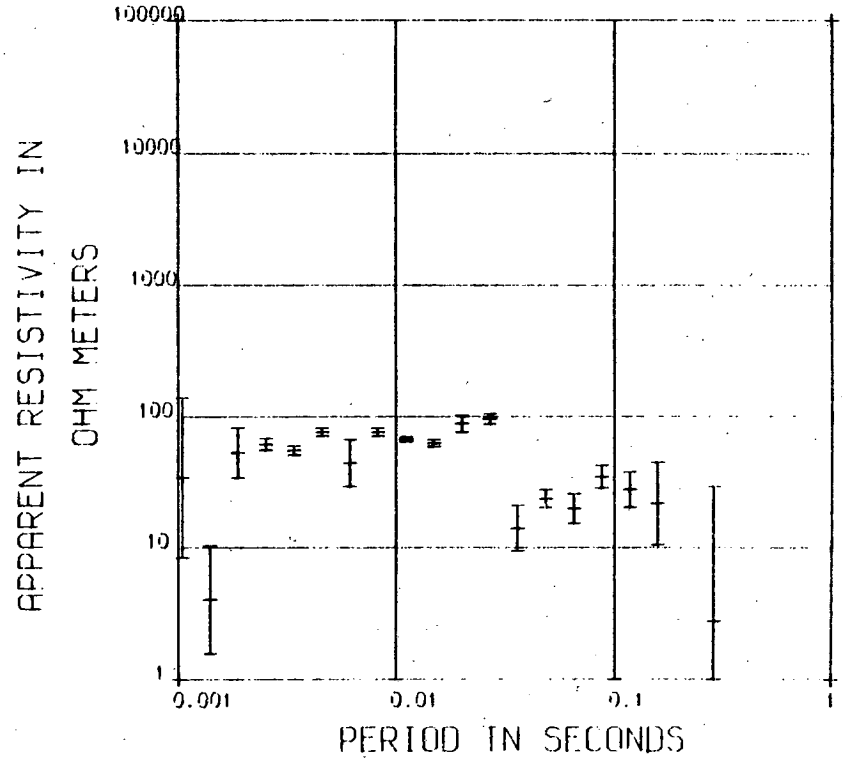
APPARENT RESISTIVITY IN
OHM METERS
100000
10000
1000
100
10
1
0.001
0.01
0.1
1
PERIOD IN SECONDS

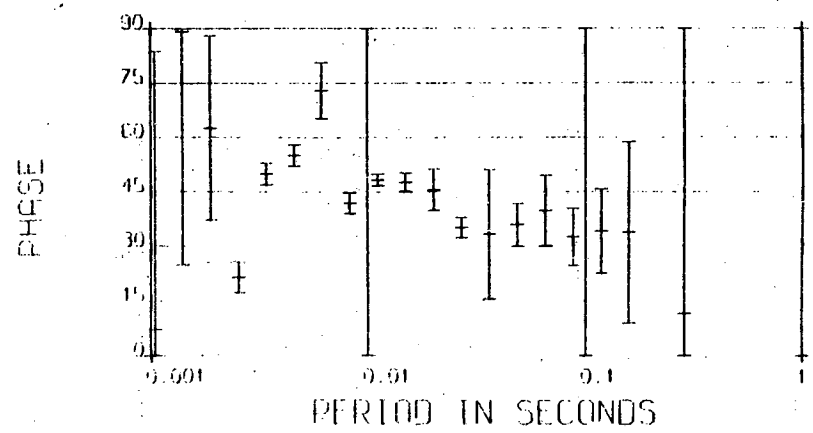
PHASE
90
75
60
45
30
15
0
0.001
0.01
0.1
1
PERIOD IN SECONDS

STATION 43

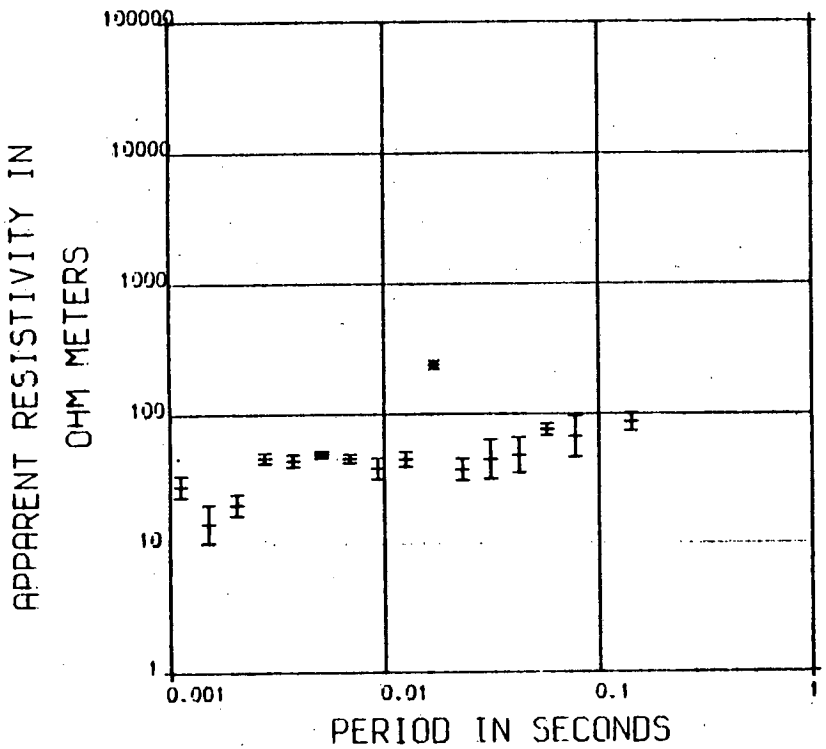

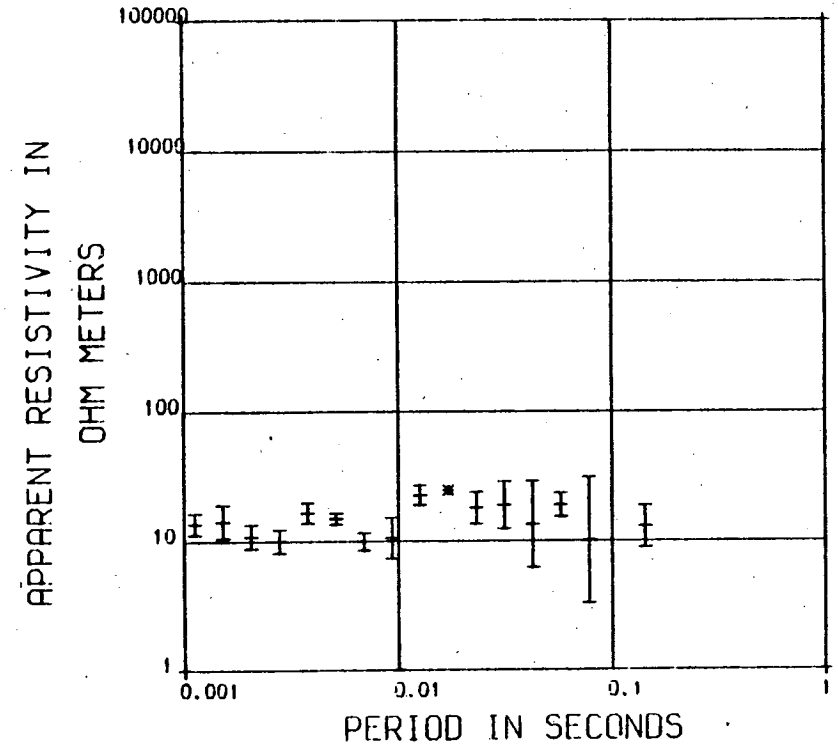

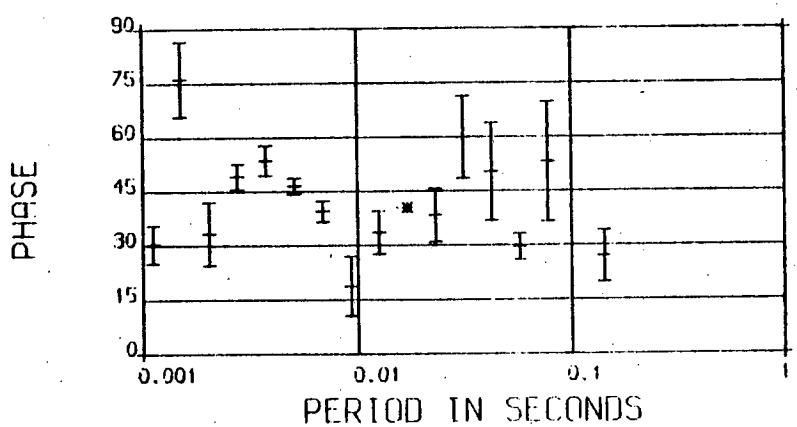

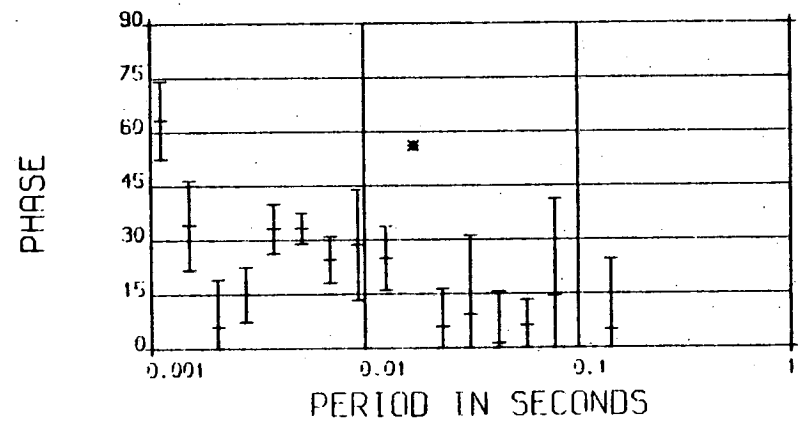

Station 43

STATION 44

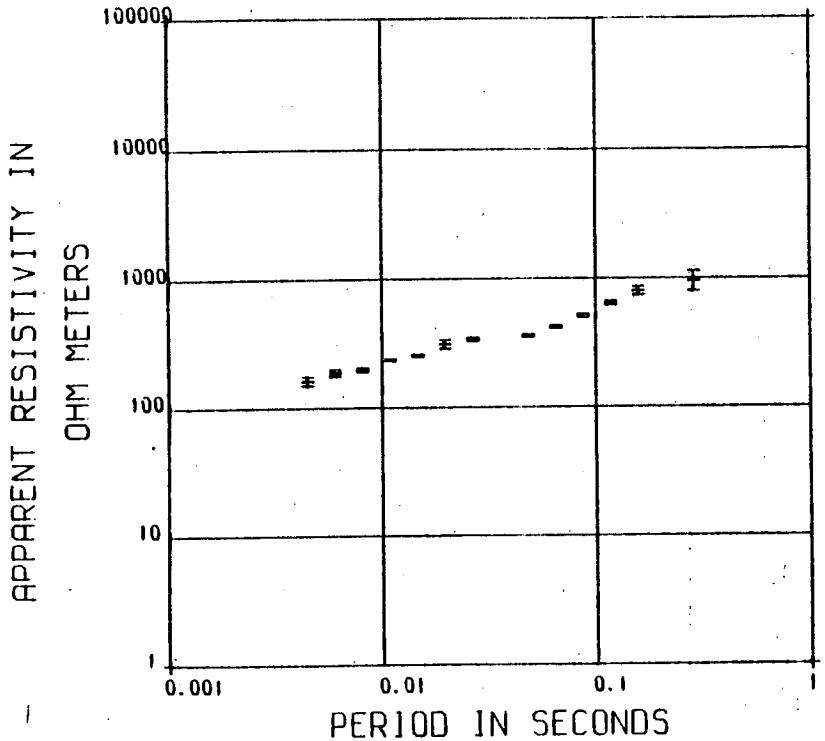

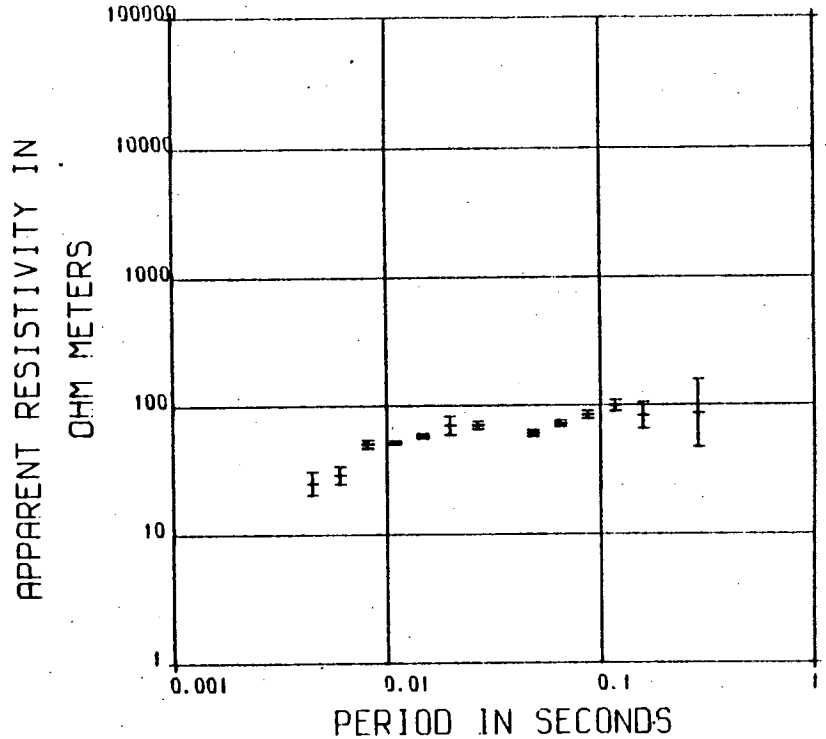

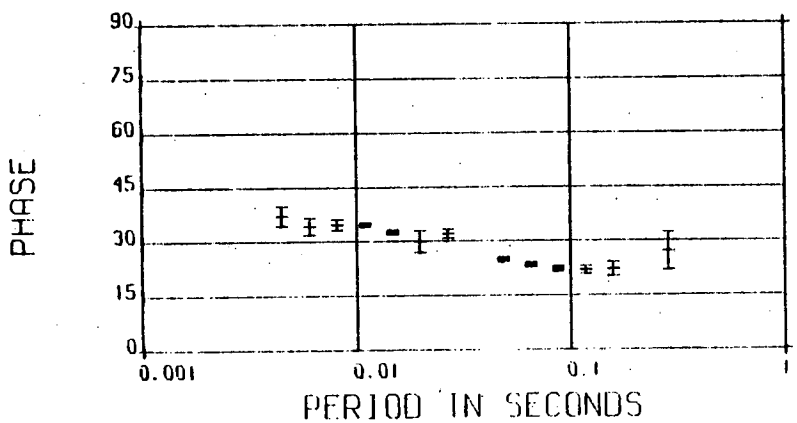

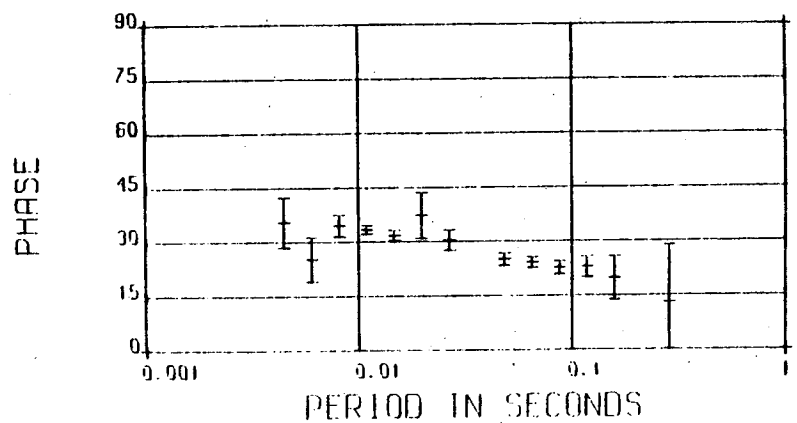

Station 44

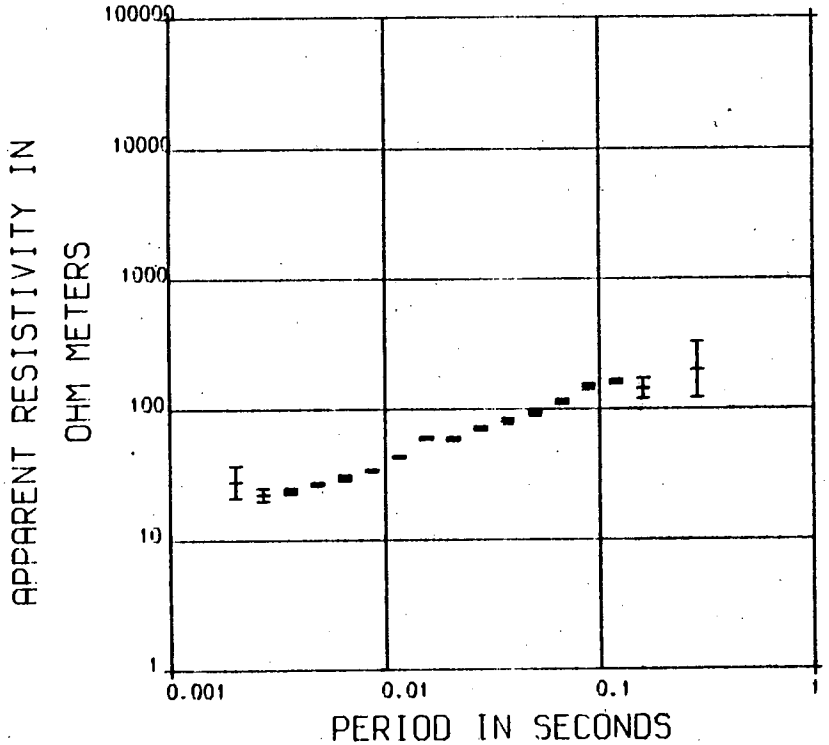
APPARENT RESISTIVITY IN
OHM METERS
100000
10000
1000
100
10
1
0.001
0.01
0.1
1
PERIOD IN SECONDS

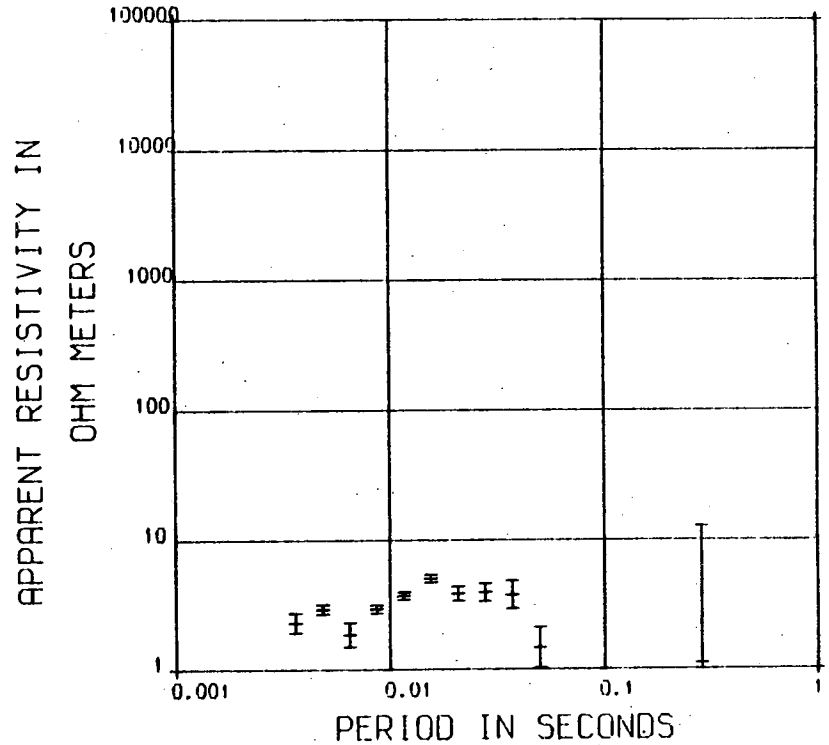
APPARENT RESISTIVITY IN
OHM METERS
100000
10000
1000
100
10
1
0.001
0.01
0.1
1
PERIOD IN SECONDS

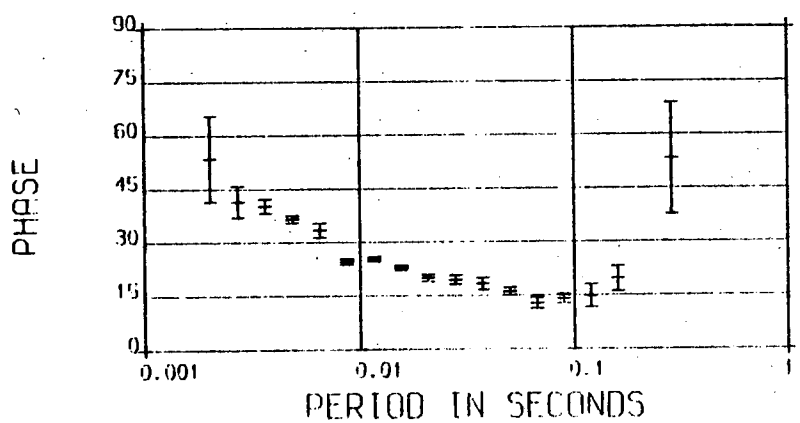
PHASE
90
75
60
45
30
15
0
0.001
0.01
0.1
1
PERIOD IN SECONDS

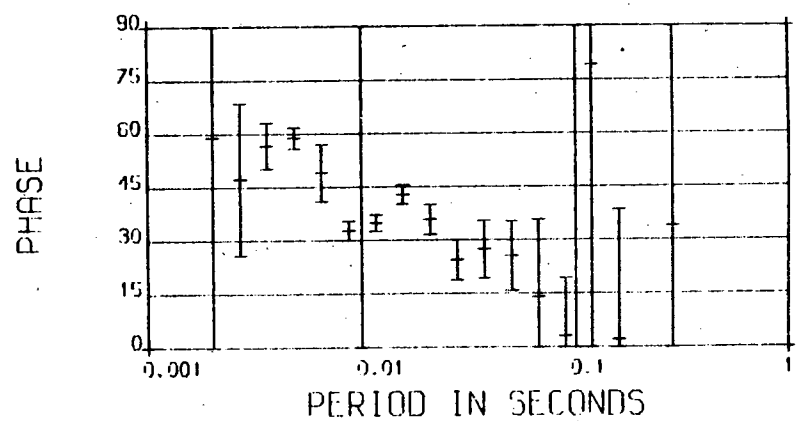
PHASE
90
75
60
45
30
15
0
0.001
0.01
0.1
1
PERIOD IN SECONDS

STATION 46

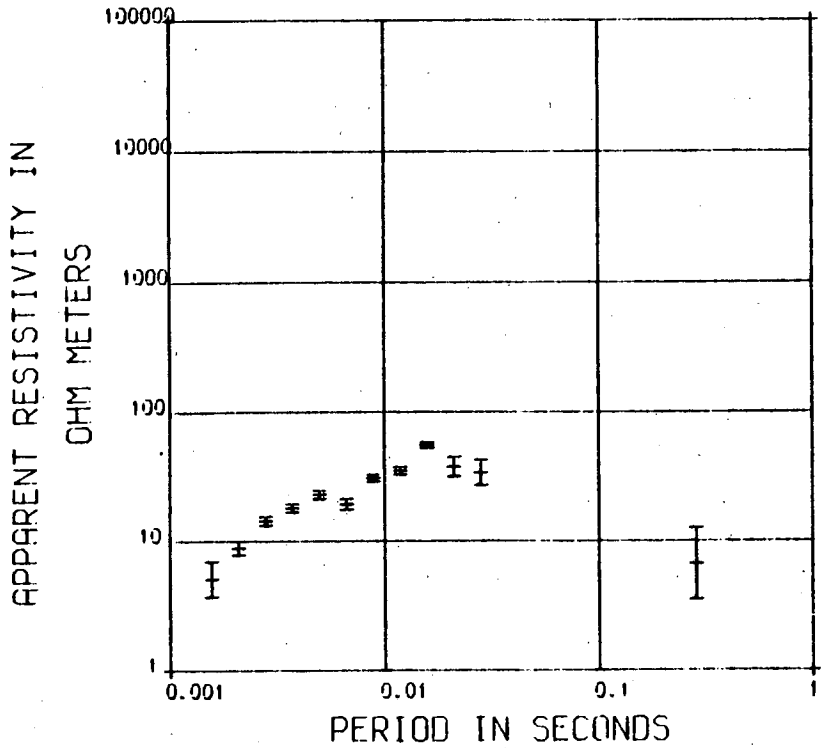

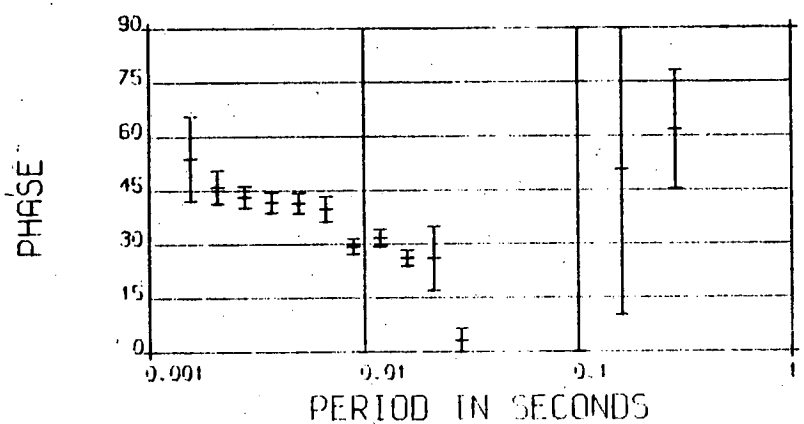

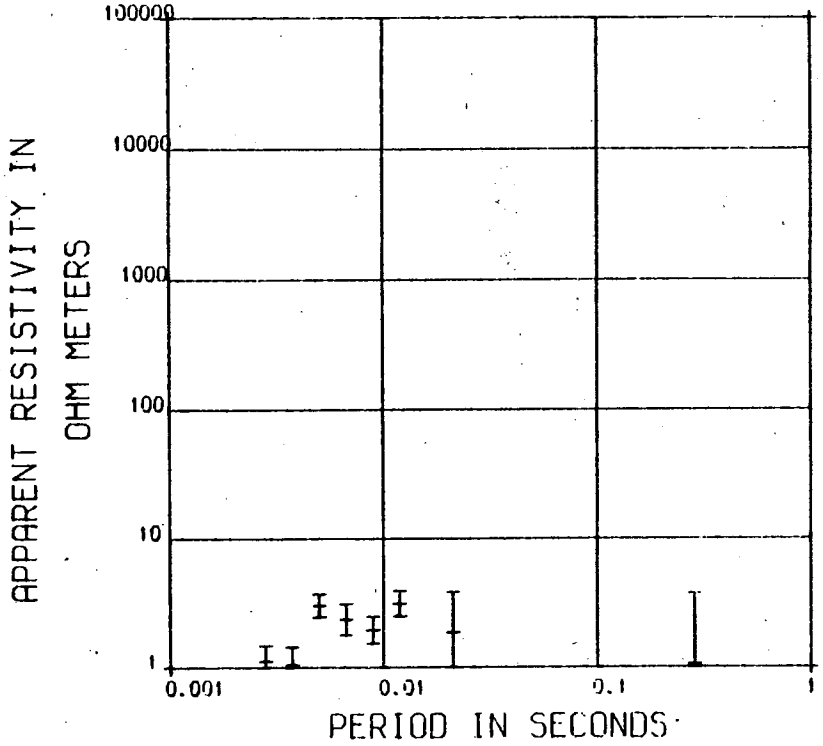

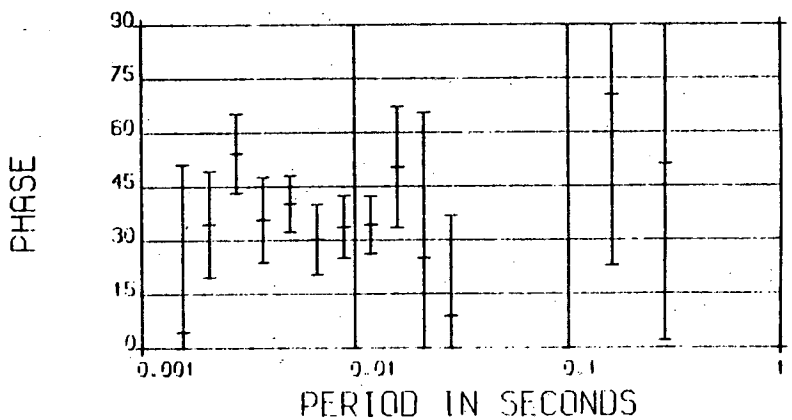

Station 46

STATION 47

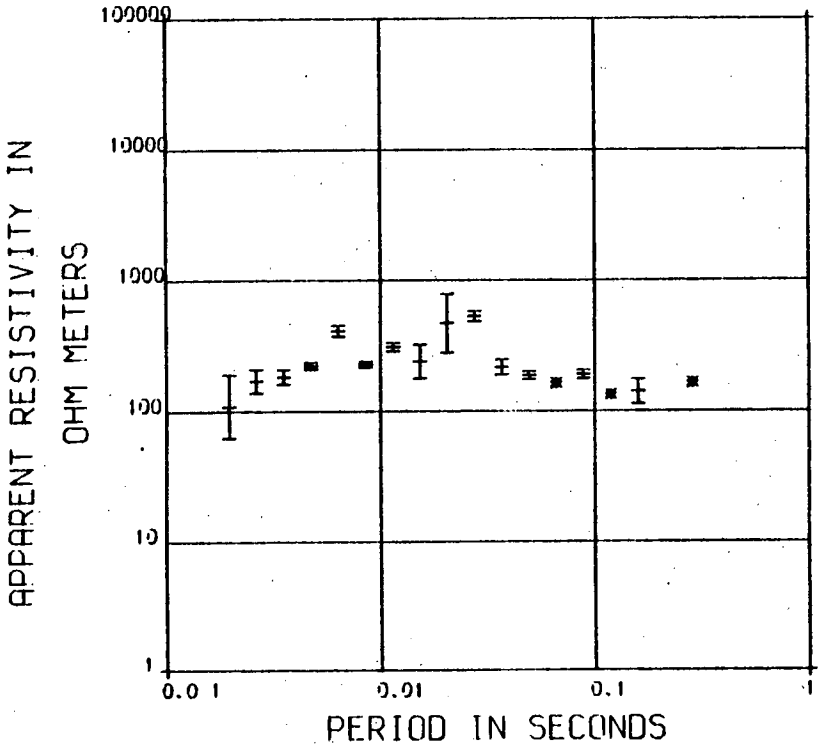

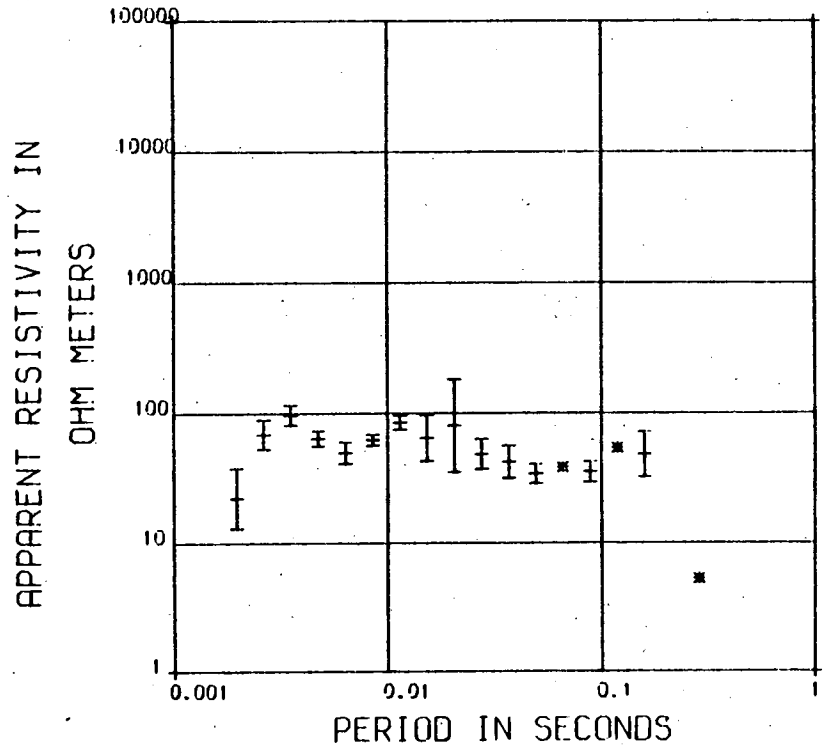

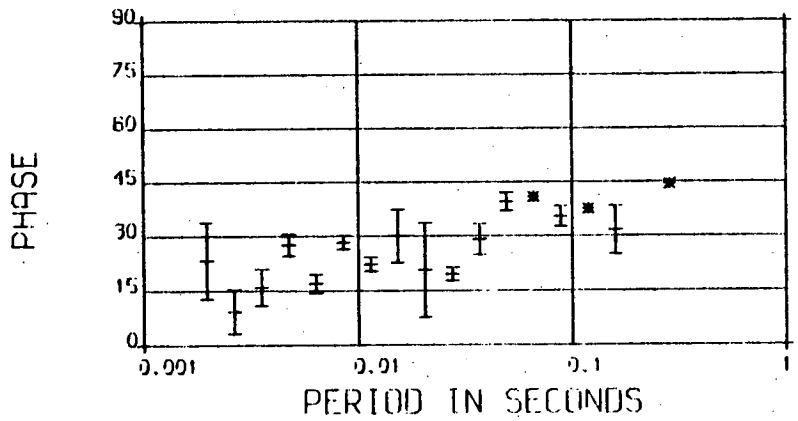

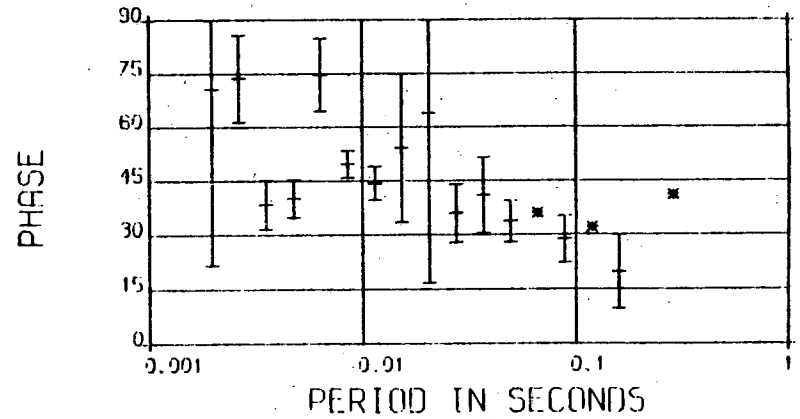

Station 47

STATION 49

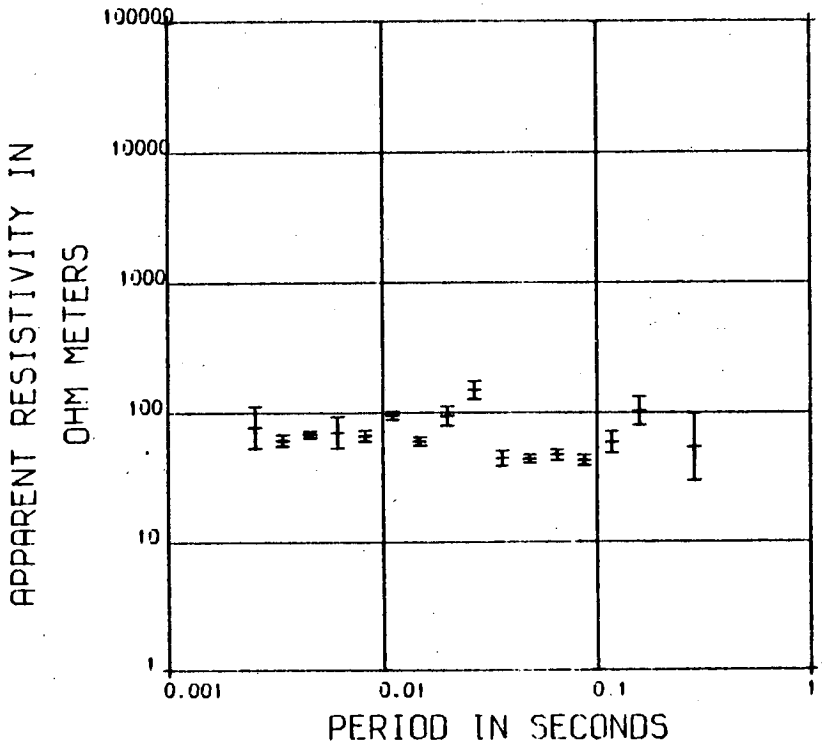

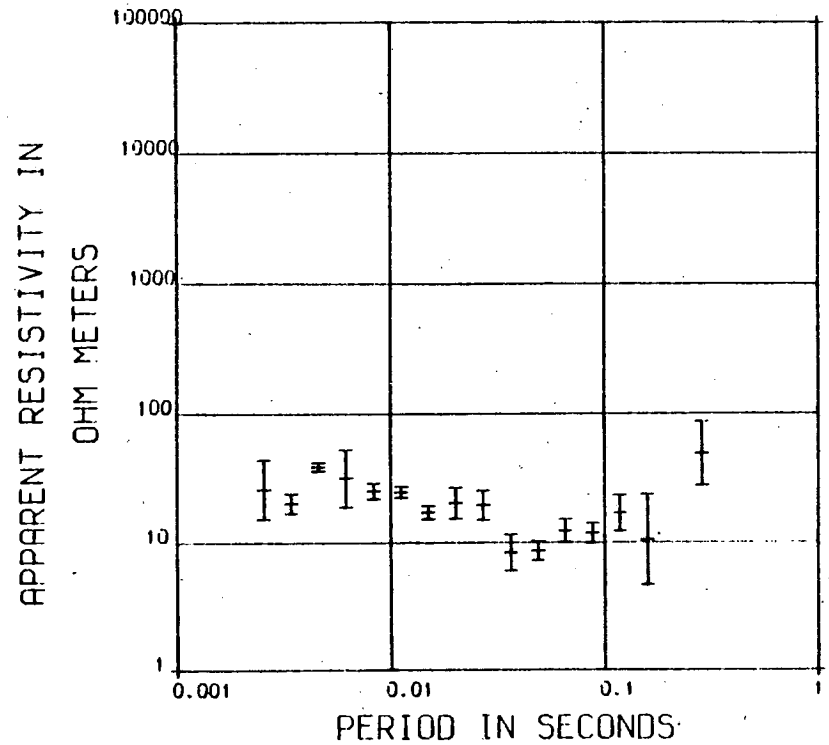

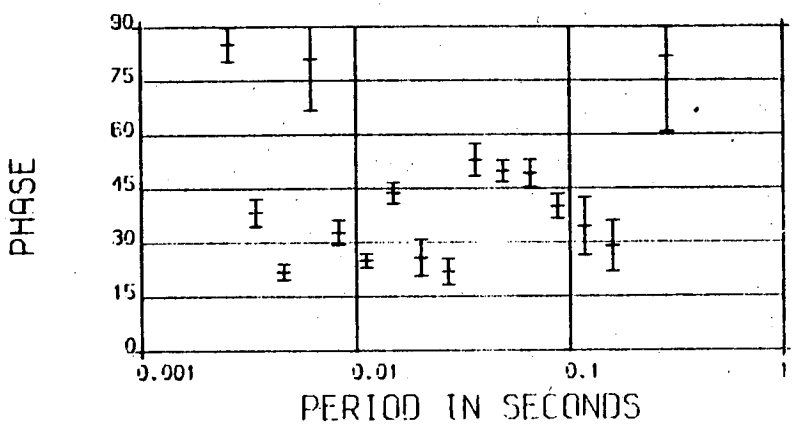

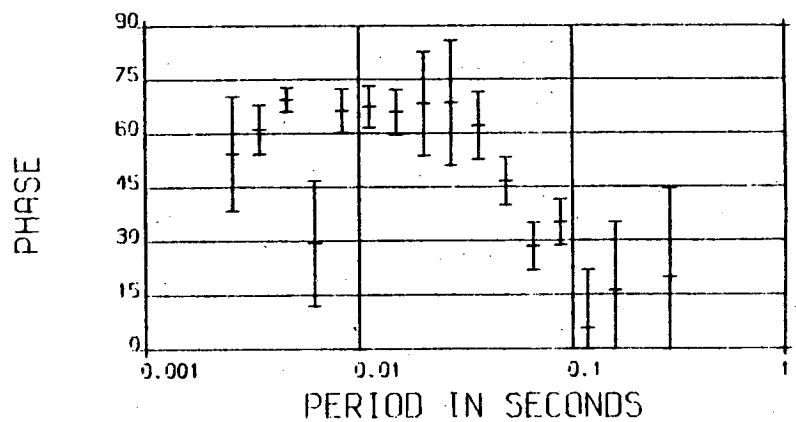

Station 49

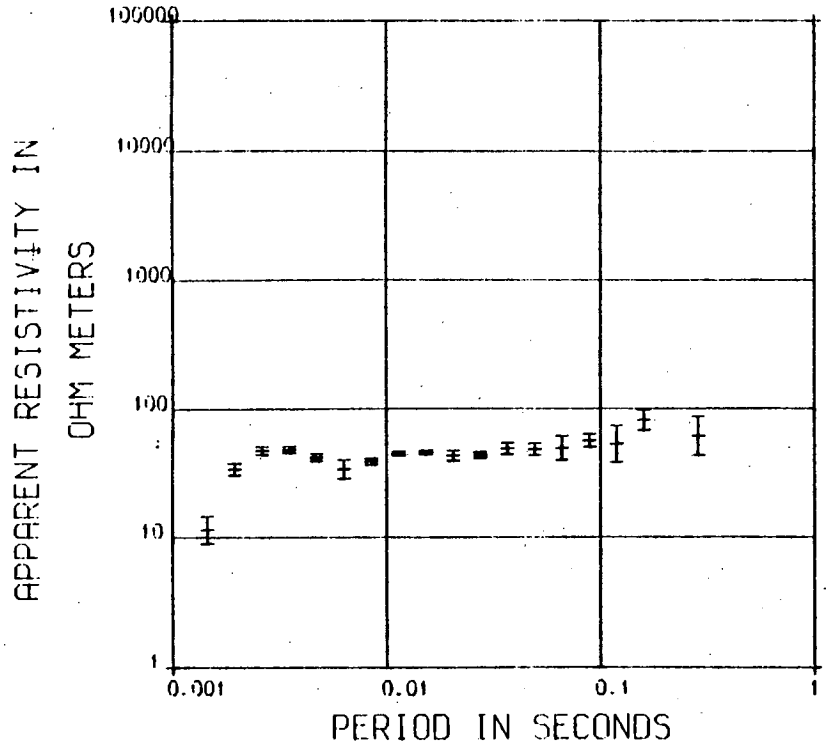
APPARENT RESISTIVITY IN
OHM METERS
100000
10000
1000
100
10
1
0.001
0.01
0.1
1
PERIOD IN SECONDS

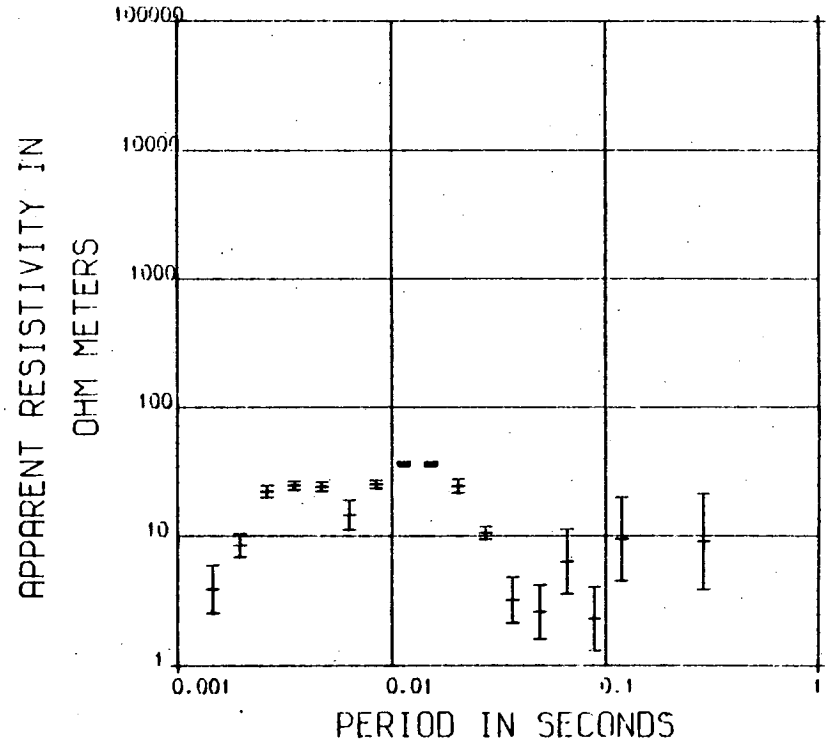
APPARENT RESISTIVITY IN
OHM METERS
100000
10000
1000
100
10
1
0.001
0.01
0.1
1
PERIOD IN SECONDS

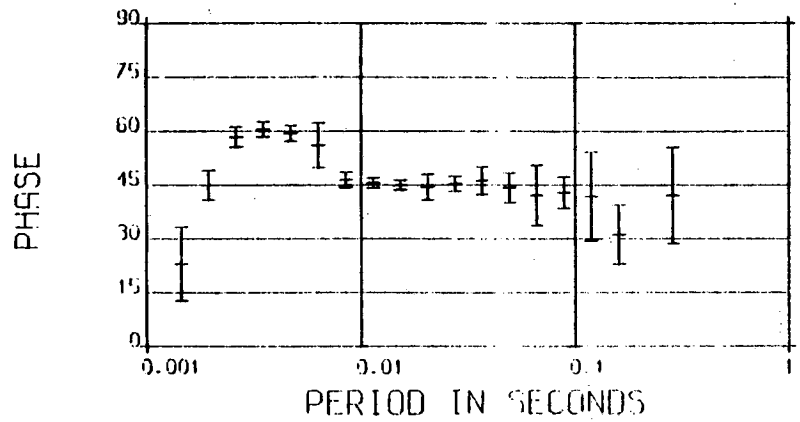
PHASE
90
75
60
45
30
15
0
0.001
0.01
0.1
1
PERIOD IN SECONDS

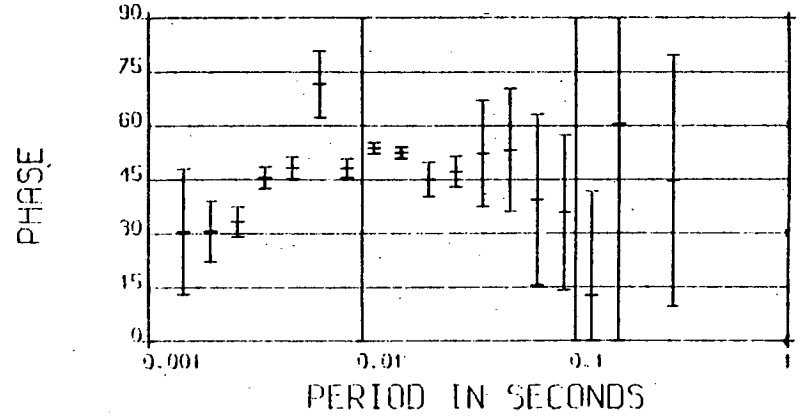
PHASE
90
75
60
45
30
15
0
0.001
0.01
0.1
1
PERIOD IN SECONDS

Station 50

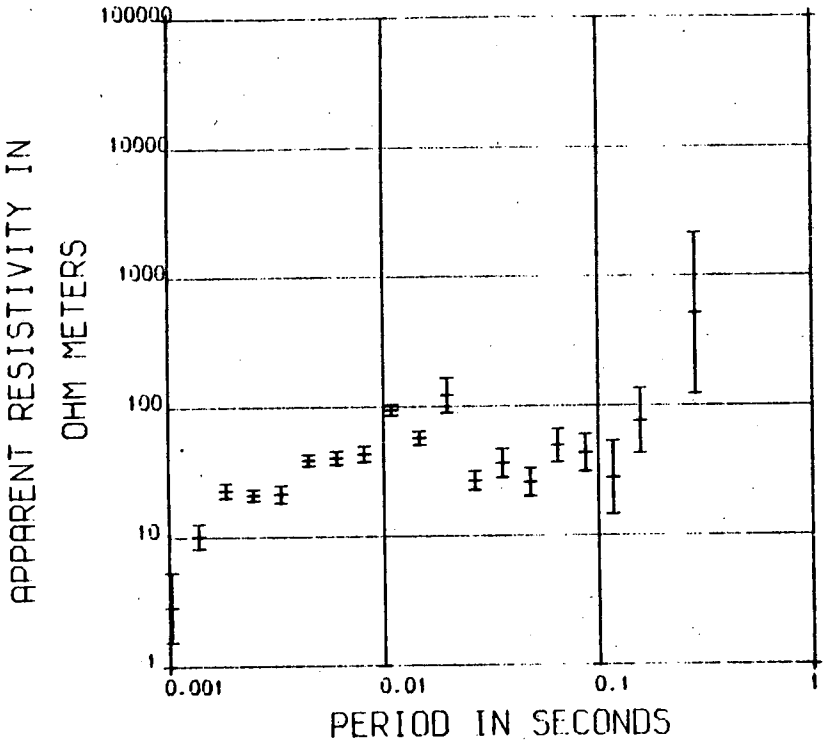
APPARENT RESISTIVITY IN
OHM METERS
100000
10000
1000
100
10
1
0.001
0.01
0.1
1
PERIOD IN SECONDS

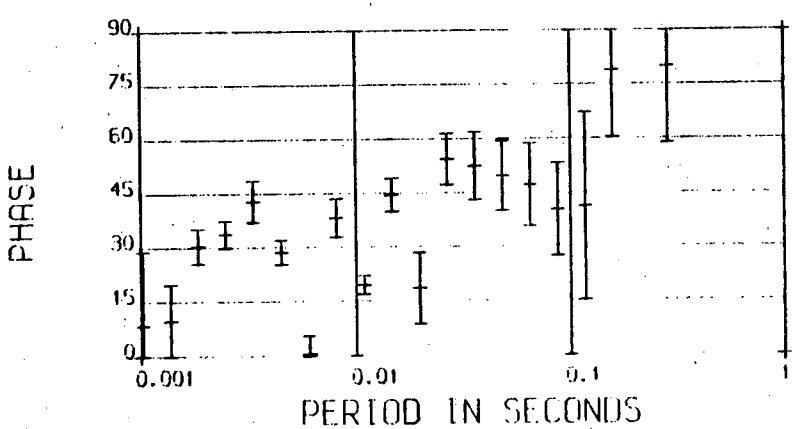
PHASE
90
75
60
45
30
15
0
0.001
0.01
0.1
1
PERIOD IN SECONDS

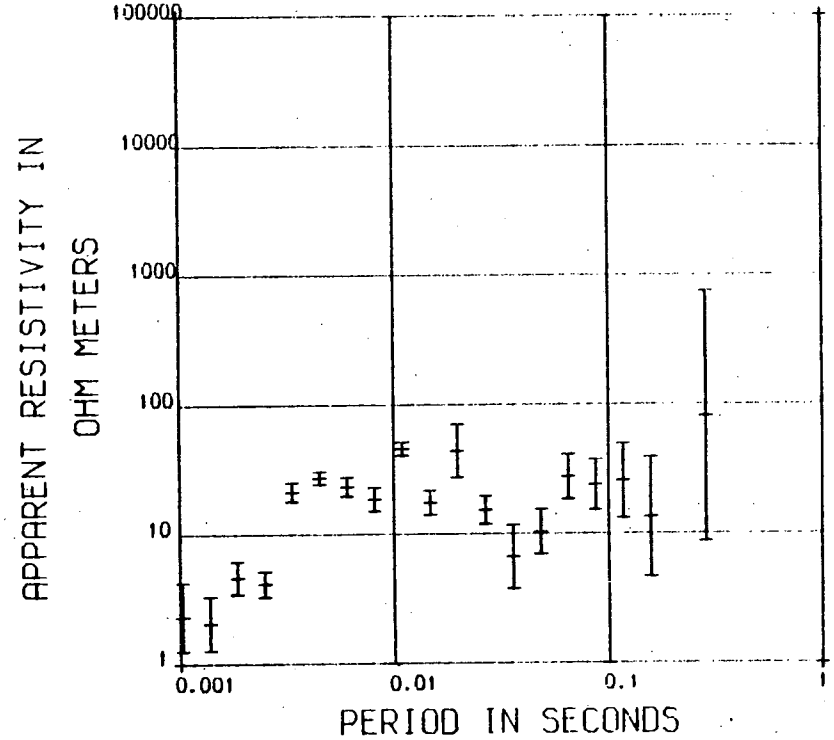
APPARENT RESISTIVITY IN
OHM METERS
100000
10000
1000
100
10
1
0.001
0.01
0.1
1
PERIOD IN SECONDS

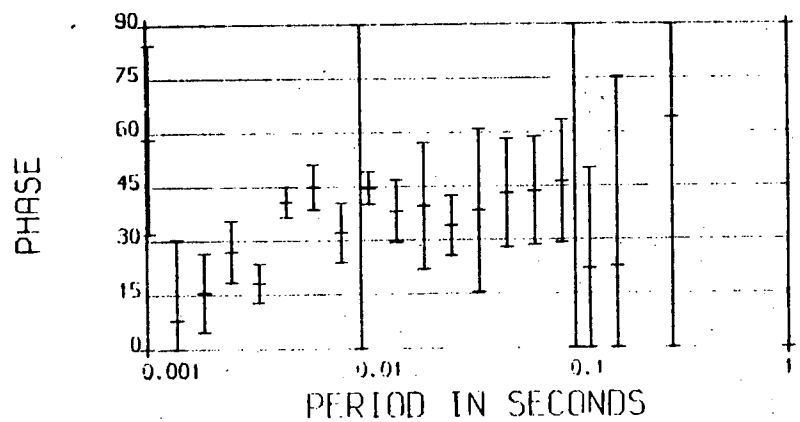
PHASE
90
75
60
45
30
15
0
0.001
0.01
0.1
1
PERIOD IN SECONDS

Station 51

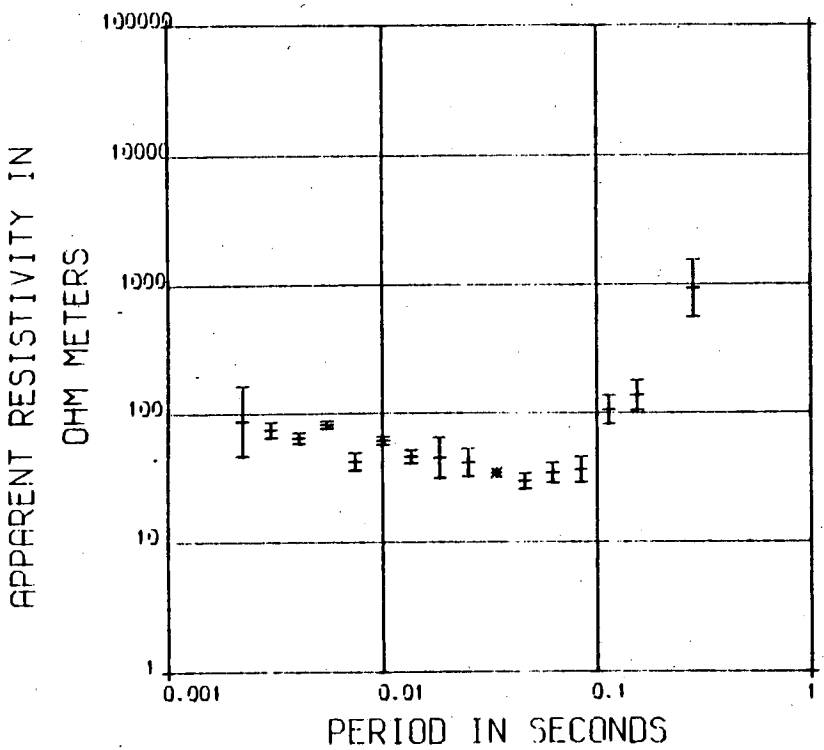
APPARENT RESISTIVITY IN
OHM METERS
100000
10000
1000
100
10
1
0.001
0.01
0.1
1
PERIOD IN SECONDS

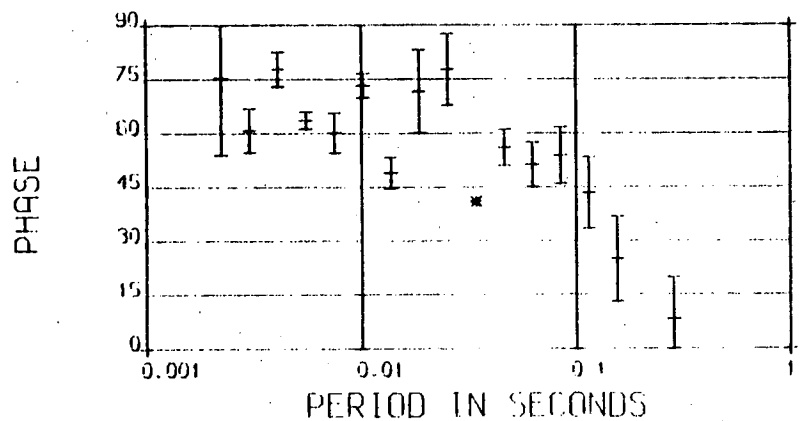
PHASE
90
75
60
45
30
15
0
0.001
0.01
0.1
1
PERIOD IN SECONDS

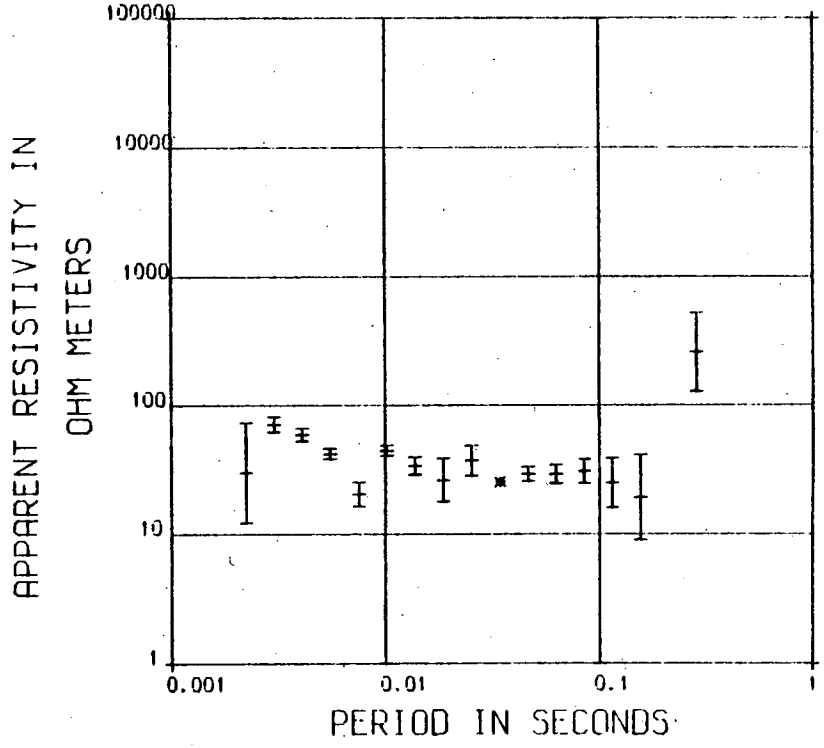
APPARENT RESISTIVITY IN
OHM METERS
100000
10000
1000
100
10
1
0.001
0.01
0.1
1
PERIOD IN SECONDS

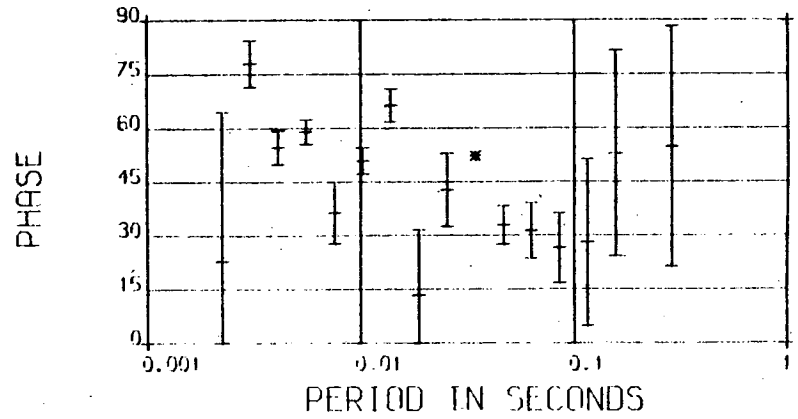
PHASE
90
75
60
45
30
15
0
0.001
0.01
0.1
1
PERIOD IN SECONDS

Station 52

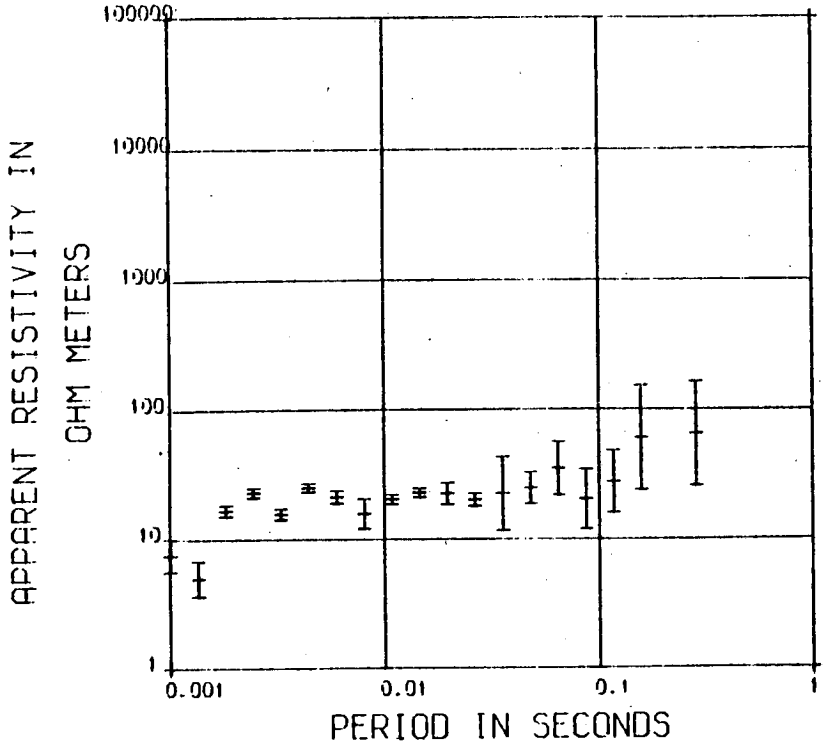
APPARENT RESISTIVITY IN
OHM METERS
100000
10000
1000
100
10
1
0.001
0.01
0.1
1
PERIOD IN SECONDS

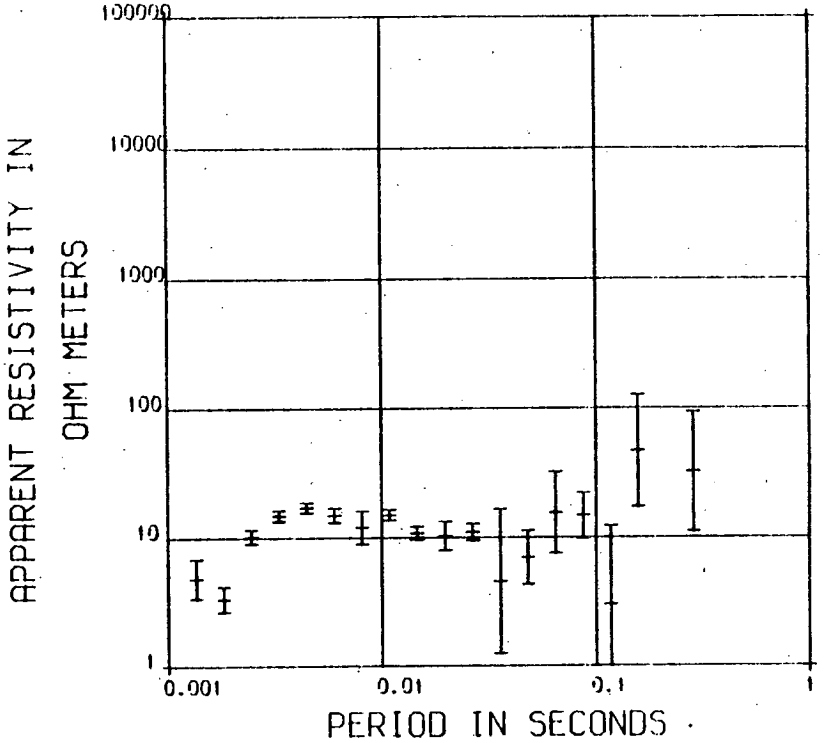
APPARENT RESISTIVITY IN
OHM METERS
100000
10000
1000
100
10
1
0.001
0.01
0.1
1
PERIOD IN SECONDS

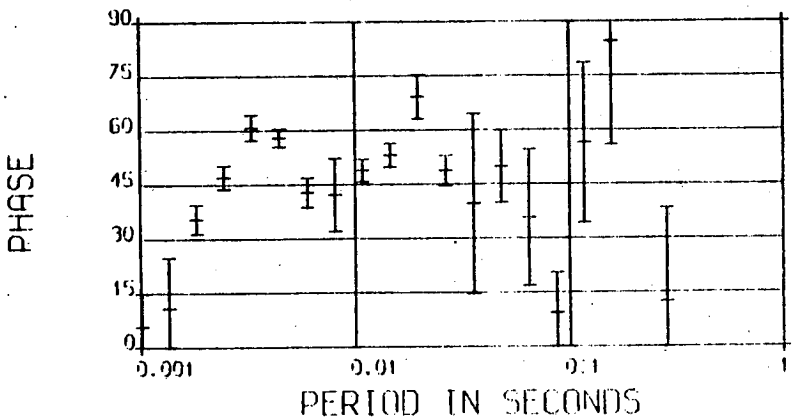
PHASE
90
75
60
45
30
15
0
0.001
0.01
0.1
1
PERIOD IN SECONDS

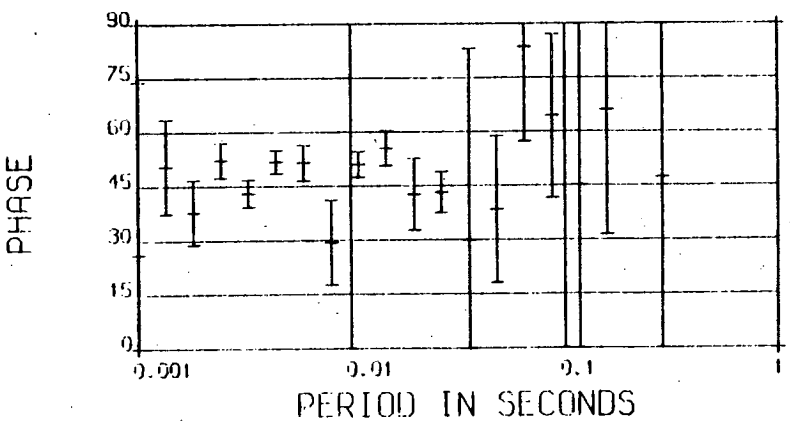
PHASE
90
75
60
45
30
15
0
0.001
0.01
0.1
1
PERIOD IN SECONDS

Station 53

PHASE
0
15
30
45
60
75
90
0.001
0.01
0.1
1
PERIOD IN SECONDS

APPARENT RESISTIVITY IN
OHM METERS
1
10
100
1000
10000
100000
0.001
0.01
0.1
1
PERIOD IN SECONDS

PHASE
0
15
30
45
60
75
90
0.001
0.01
0.1
1
PERIOD IN SECONDS

APPARENT RESISTIVITY IN
OHM METERS
1
10
100
1000
10000
100000
0.001
0.01
0.1
1
PERIOD IN SECONDS

Station 54

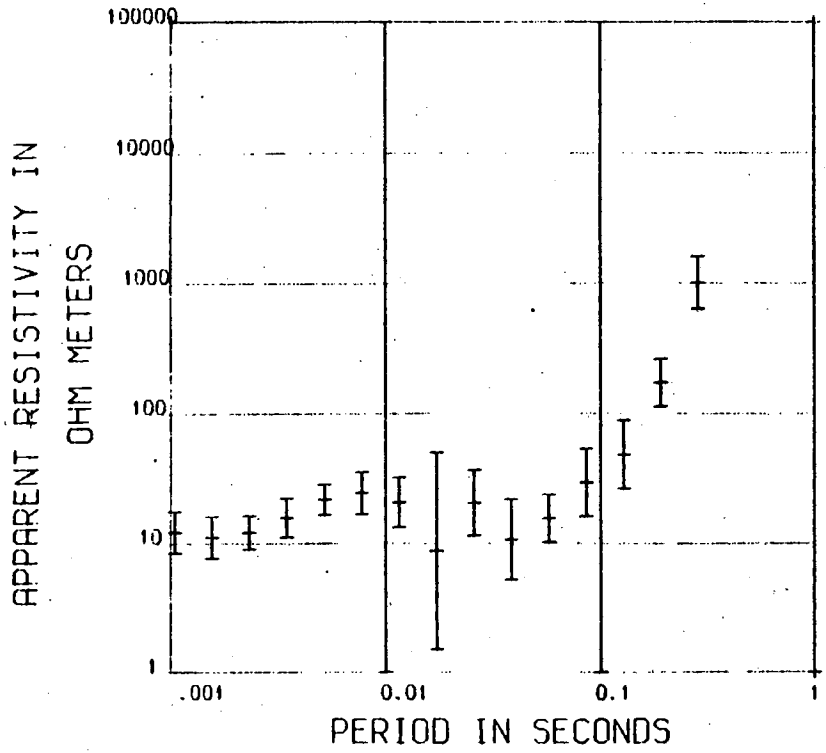
APPARENT RESISTIVITY IN
OHM METERS
100000
10000
1000
100
10
1
.001
0.01
0.1
1
PERIOD IN SECONDS

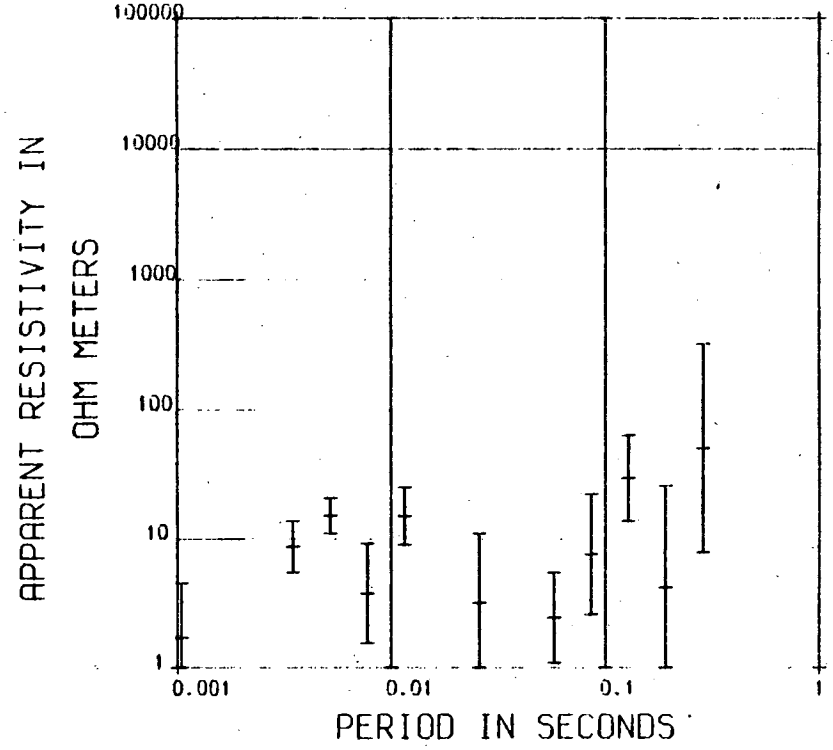
APPARENT RESISTIVITY IN
OHM METERS
100000
10000
1000
100
10
1
0.001
0.01
0.1
1
PERIOD IN SECONDS

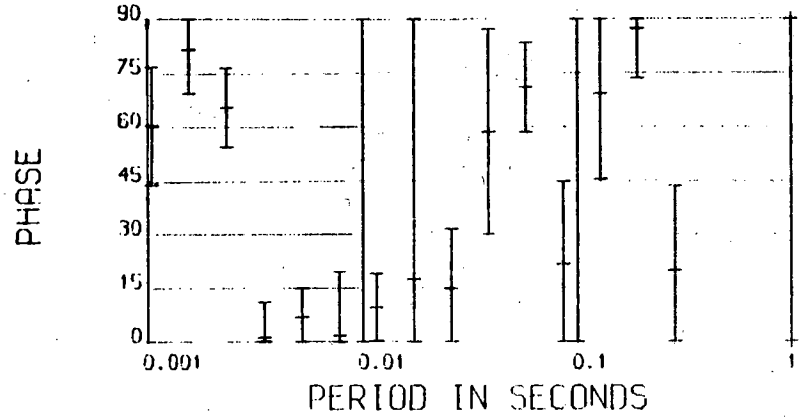
PHASE
90
75
60
45
30
15
0
0.001
0.01
0.1
1
PERIOD IN SECONDS

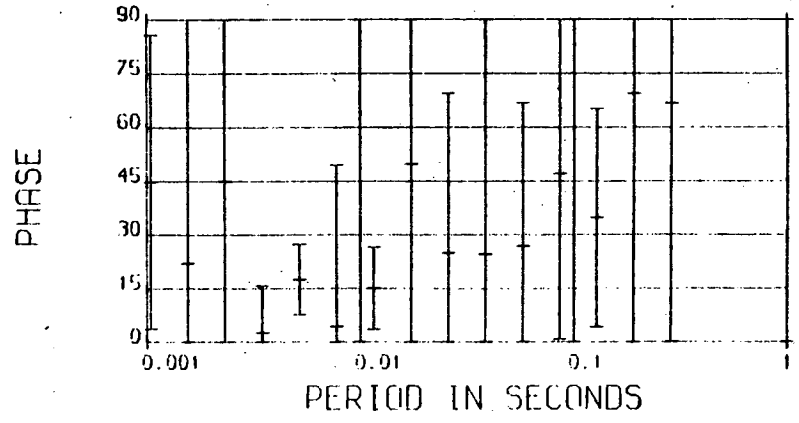
PHASE
90
75
60
45
30
15
0
0.001
0.01
0.1
1
PERIOD IN SECONDS

Station 55

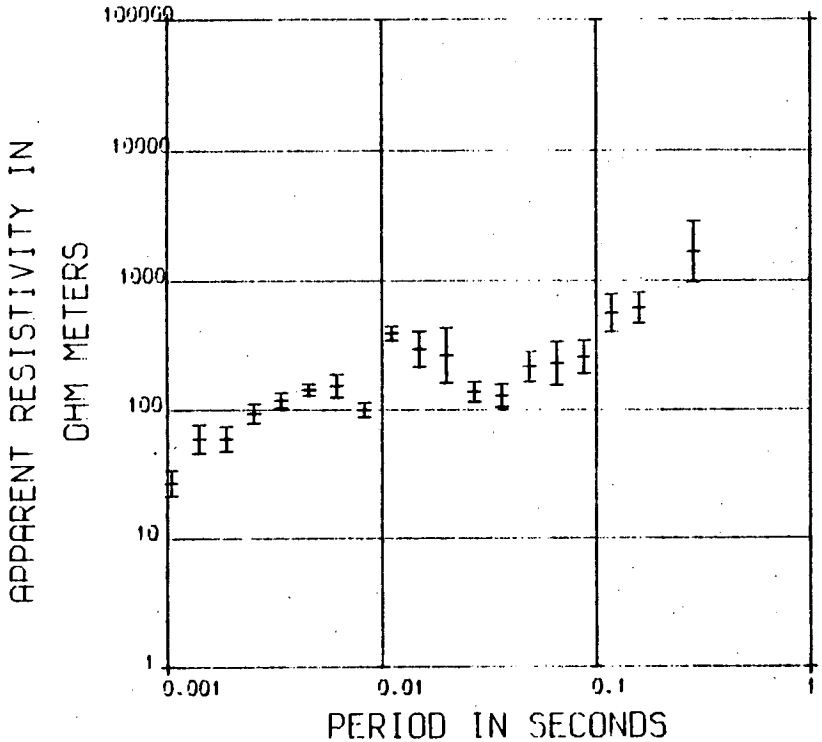
APPARENT RESISTIVITY IN
OHM METERS
100000
10000
1000
100
10
1
0.001
0.01
0.1
1
PERIOD IN SECONDS

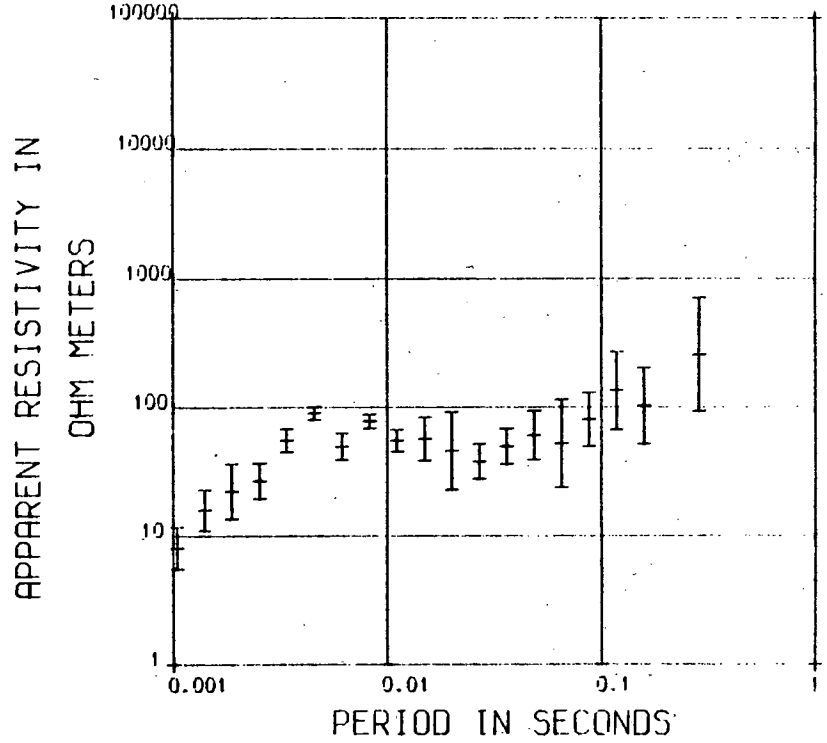
APPARENT RESISTIVITY IN
OHM METERS
100000
10000
1000
100
10
1
0.001
0.01
0.1
1
PERIOD IN SECONDS

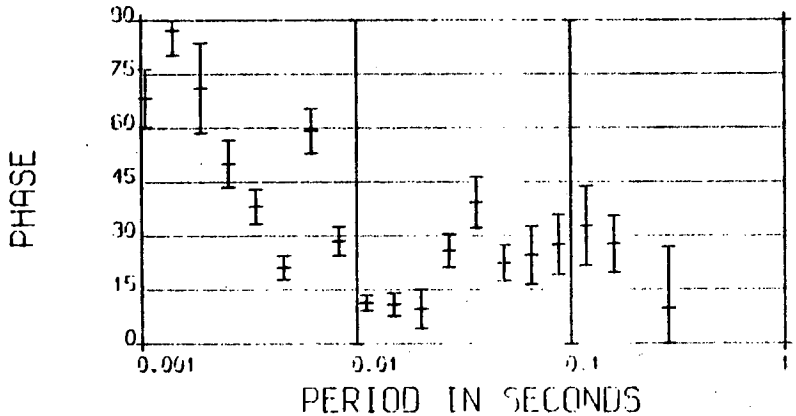
PHASE
90
75
60
45
30
15
0
0.001
0.01
0.1
1
PERIOD IN SECONDS

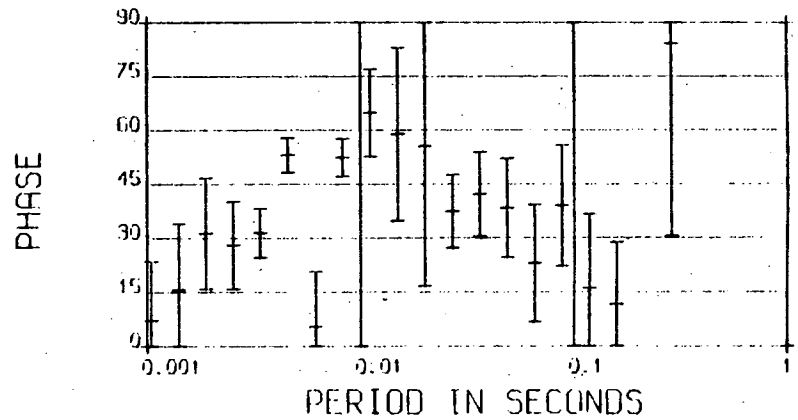
PHASE
90
75
60
45
30
15
0
0.001
0.01
0.1
1
PERIOD IN SECONDS

Station 56

STATION 57

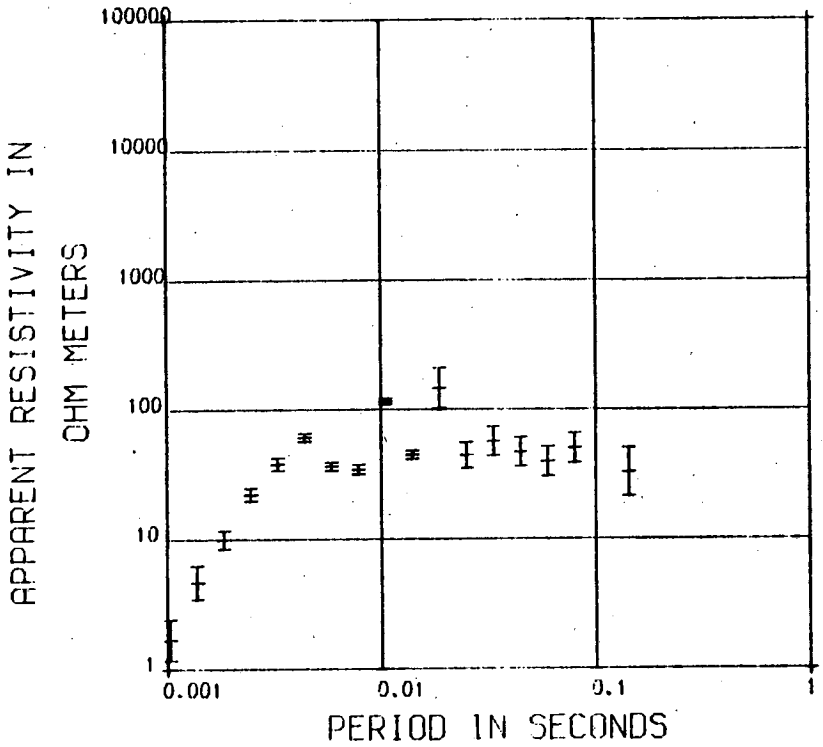
APPARENT RESISTIVITY IN
OHM METERS
100000
10000
1000
100
10
1
0.001
0.01
0.1
1
PERIOD IN SECONDS

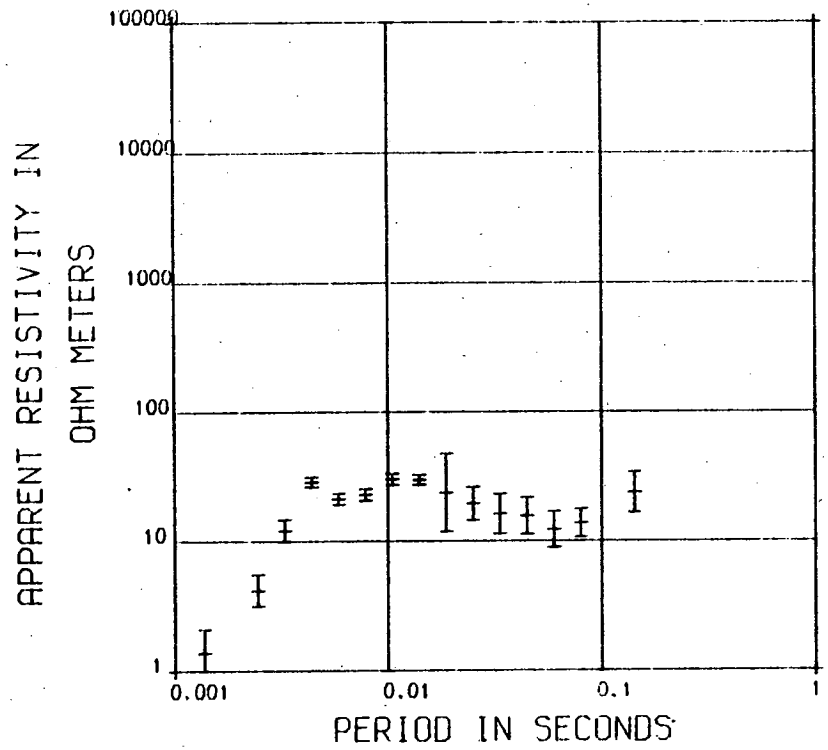
APPARENT RESISTIVITY IN
OHM METERS
100000
10000
1000
100
10
1
0.001
0.01
0.1
1
PERIOD IN SECONDS

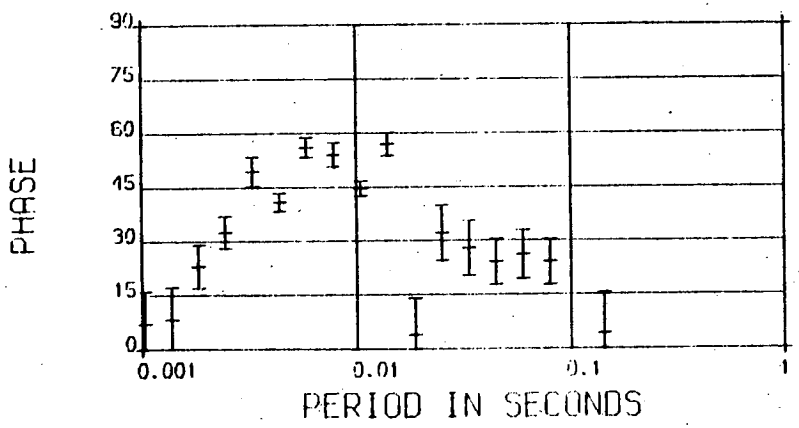
PHASE
90
75
60
45
30
15
0
0.001
0.01
0.1
1
PERIOD IN SECONDS

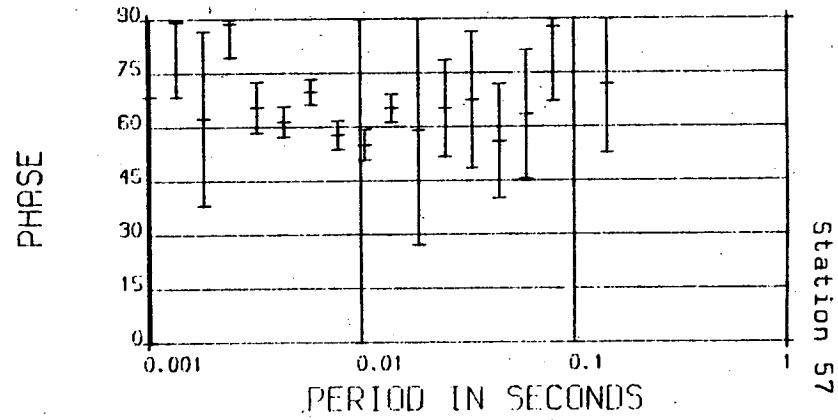
PHASE
90
75
60
45
30
15
0
0.001
0.01
0.1
1
PERIOD IN SECONDS
Station 57

STATION 58

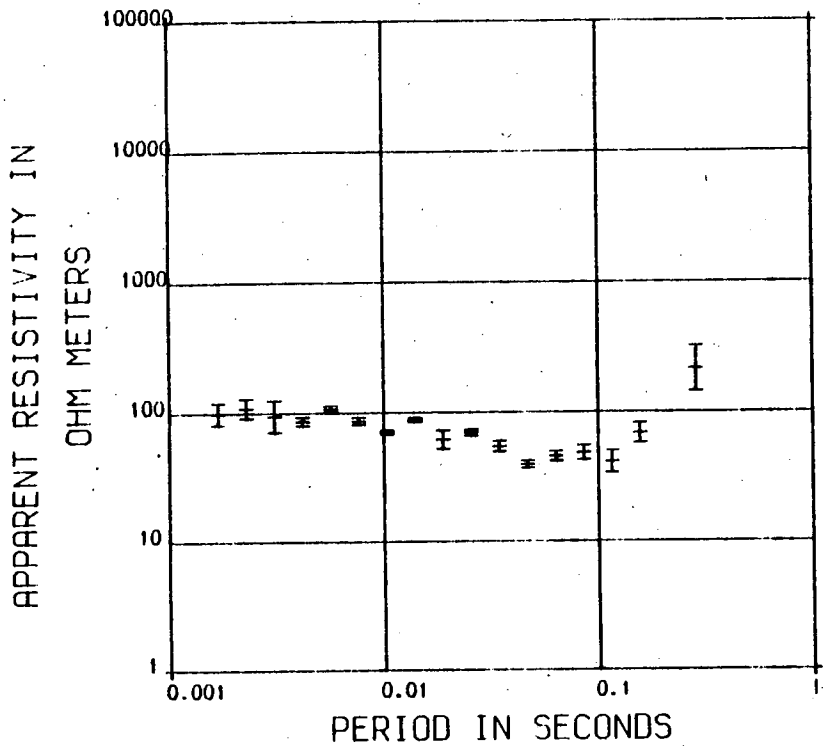

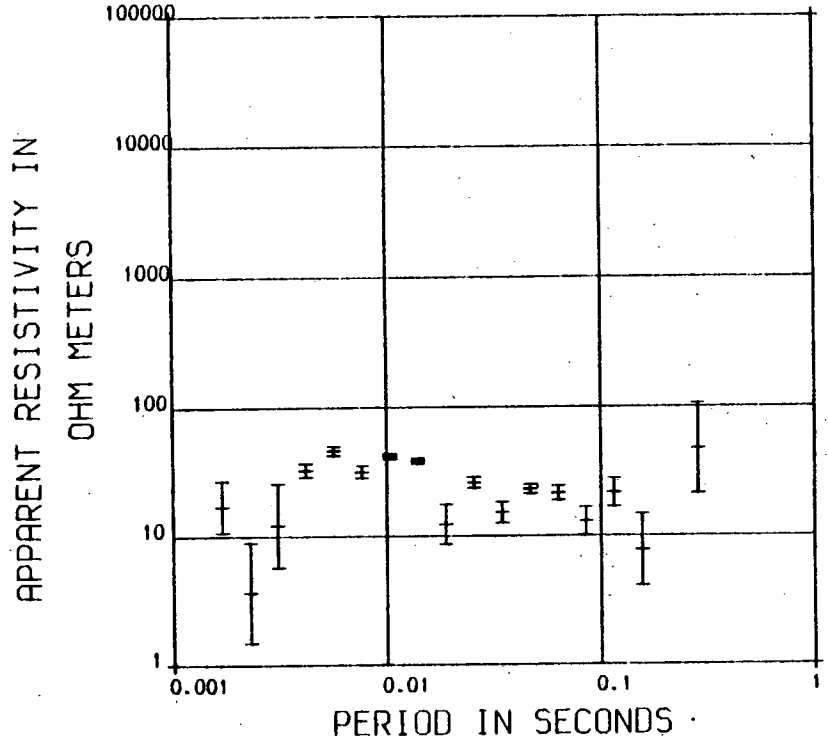

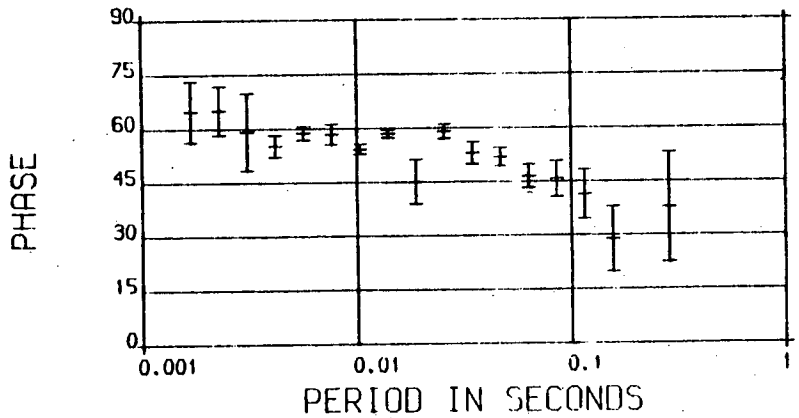

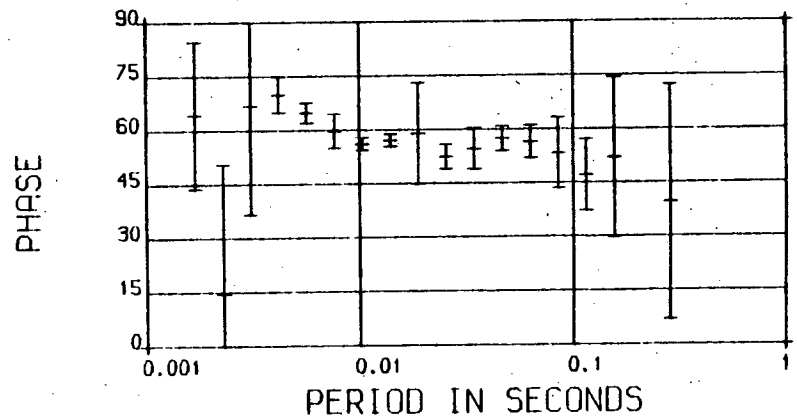

Station 58

STATION 59

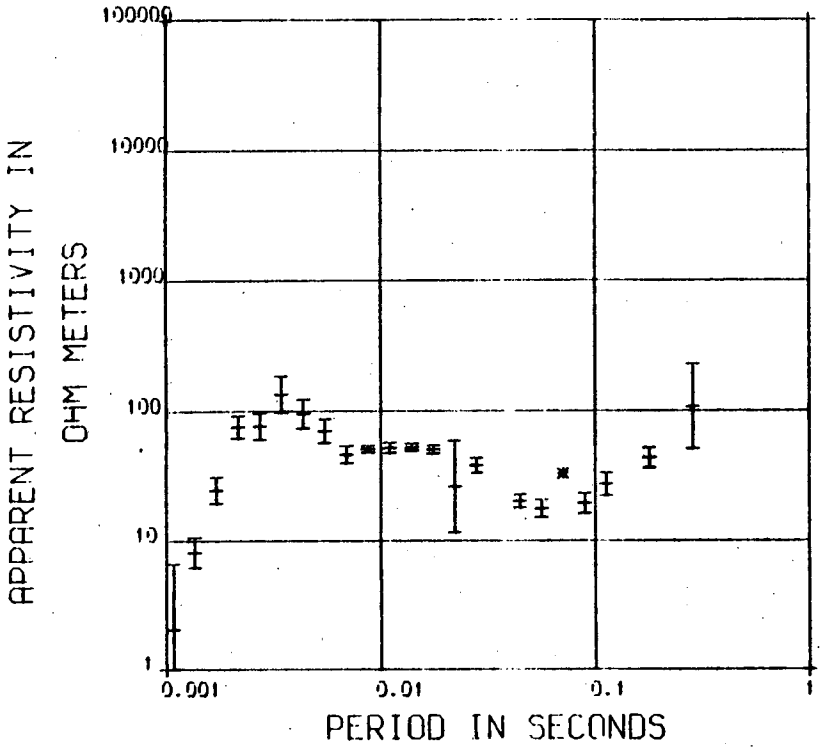

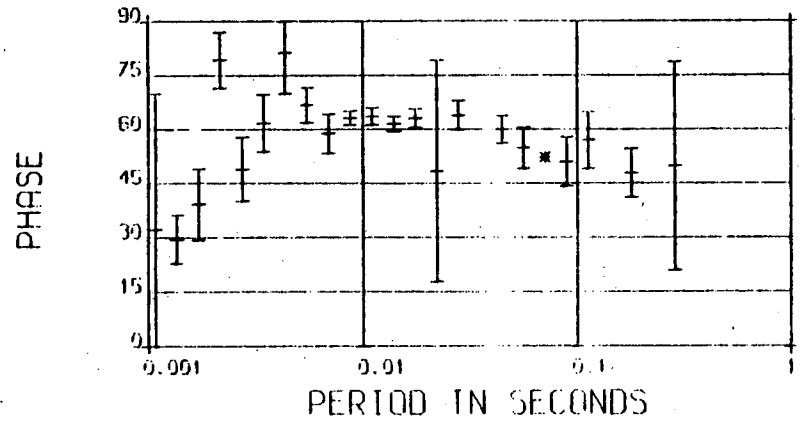

STATION 59

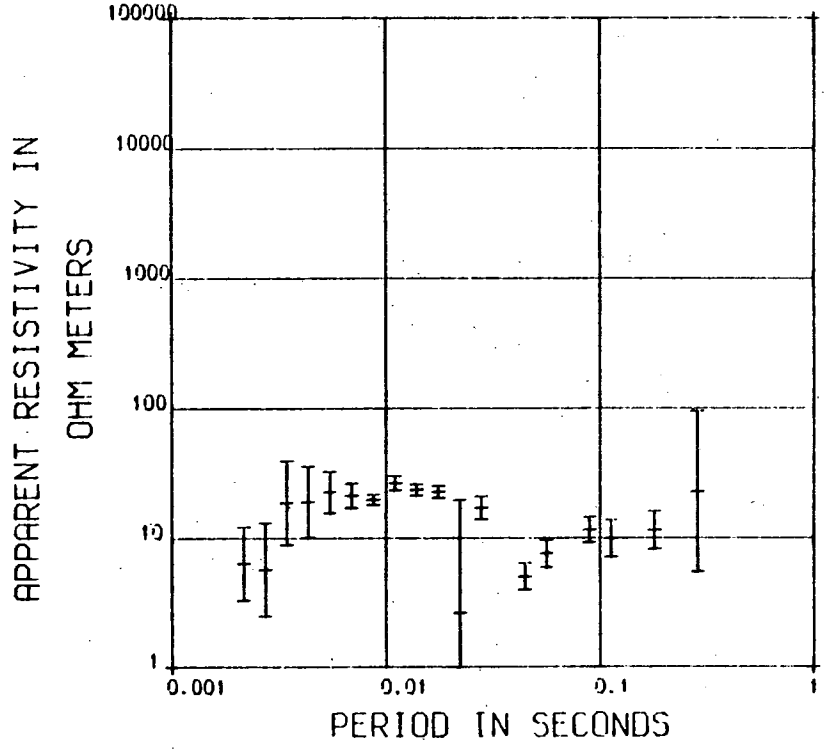

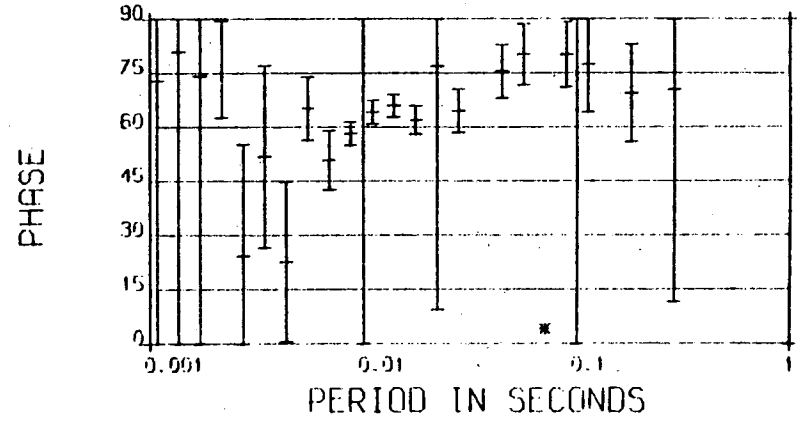

Station 59

STATION 60

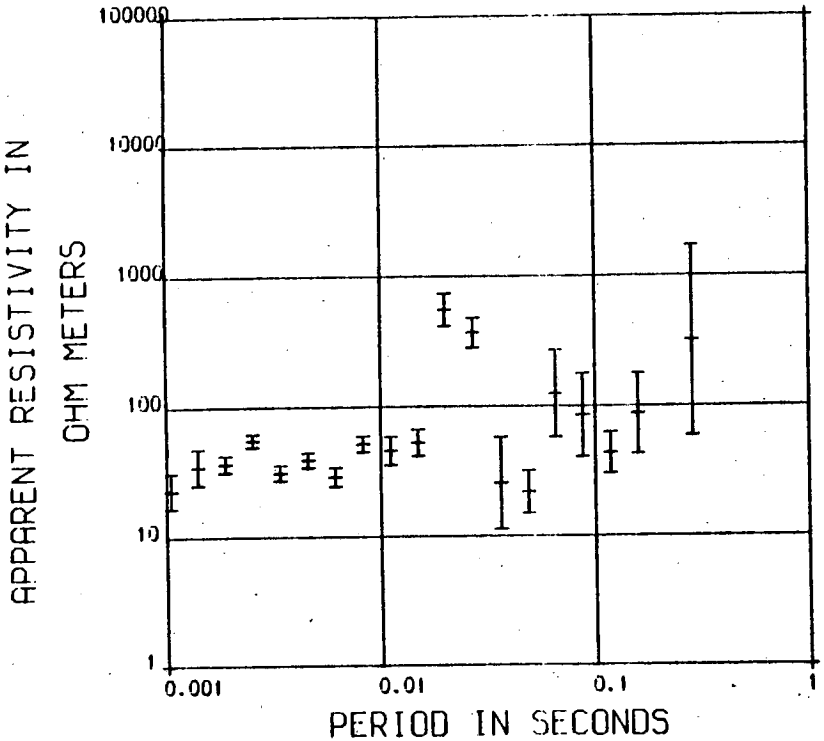
APPARENT RESISTIVITY IN
OHM METERS
100000
10000
1000
100
10
1
0.001
0.01
0.1
1
PERIOD IN SECONDS

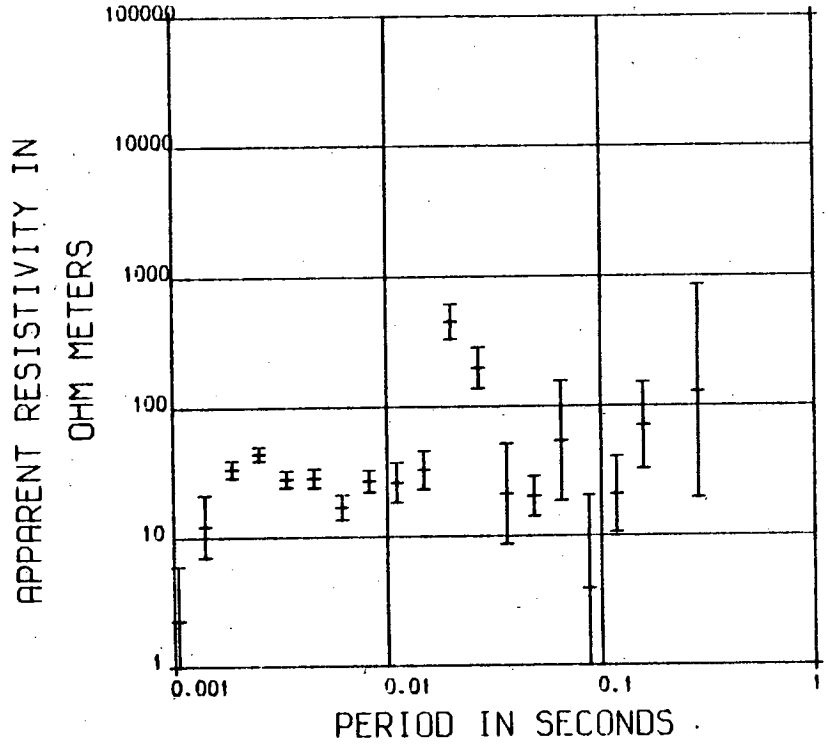
APPARENT RESISTIVITY IN
OHM METERS
100000
10000
1000
100
10
1
0.001
0.01
0.1
1
PERIOD IN SECONDS

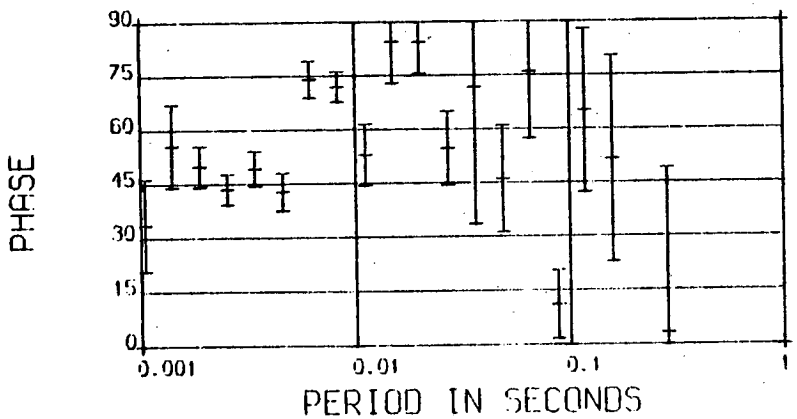
PHASE
90
75
60
45
30
15
0
0.001
0.01
0.1
1
PERIOD IN SECONDS

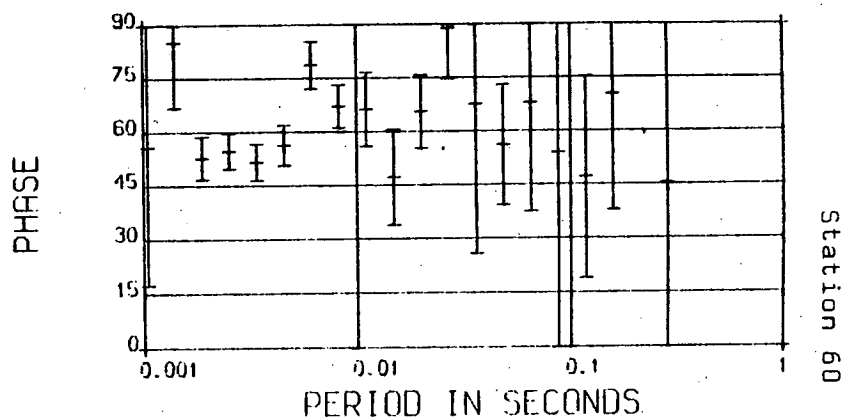
PHASE
90
75
60
45
30
15
0
0.001
0.01
0.1
1
PERIOD IN SECONDS
Station 60

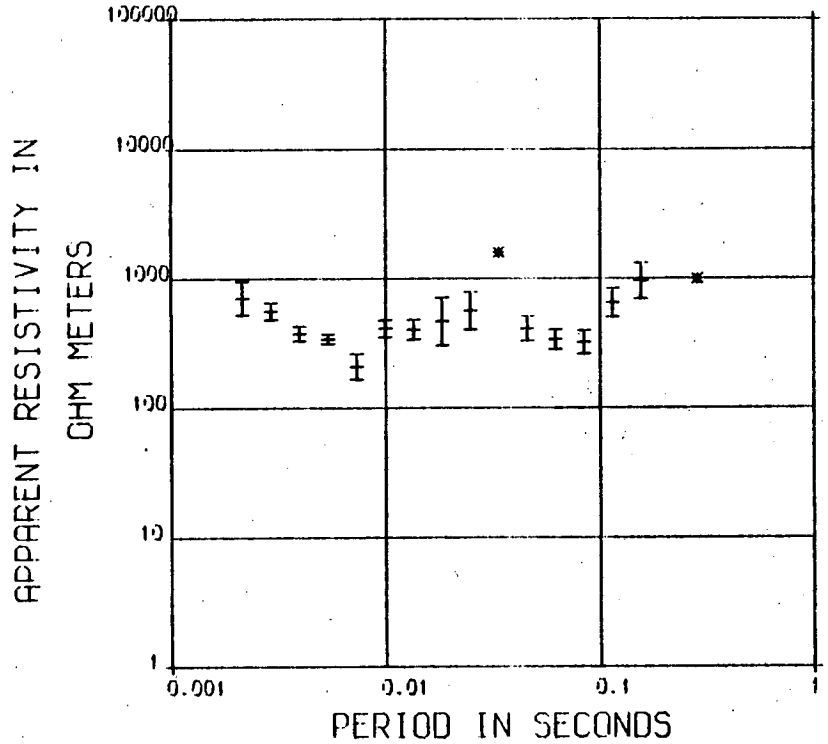
APPARENT RESISTIVITY IN
OHM METERS
100000
10000
1000
100
10
1
0.001
0.01
0.1
1
PERIOD IN SECONDS

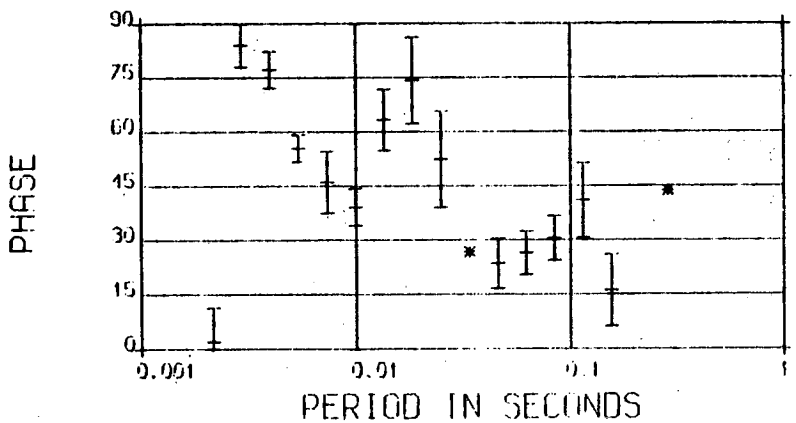
PHASE
90
75
60
45
30
15
0
0.001
0.01
0.1
1
PERIOD IN SECONDS

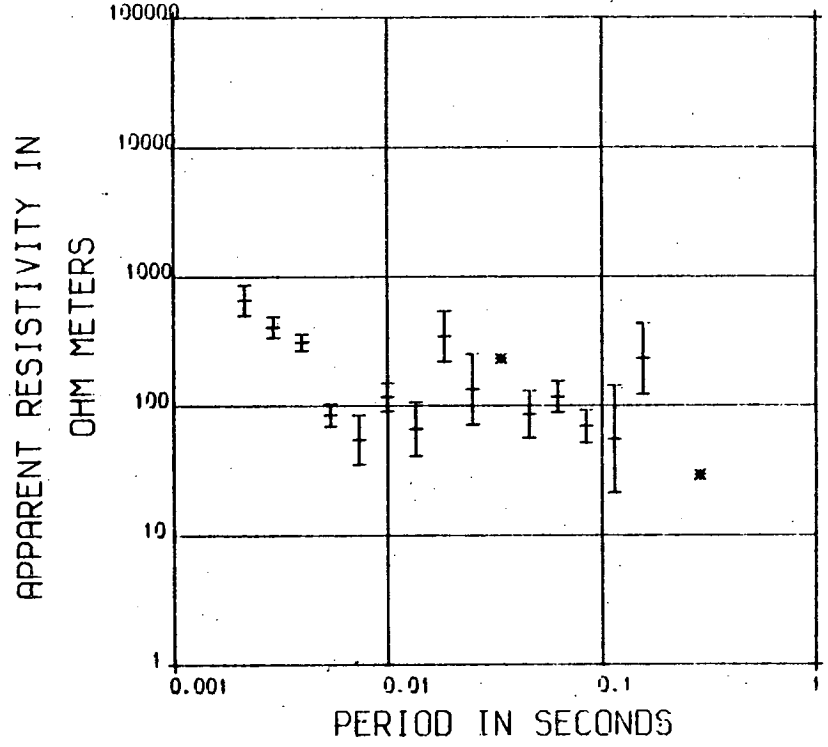
APPARENT RESISTIVITY IN
OHM METERS
100000
10000
1000
100
10
1
0.001
0.01
0.1
1
PERIOD IN SECONDS

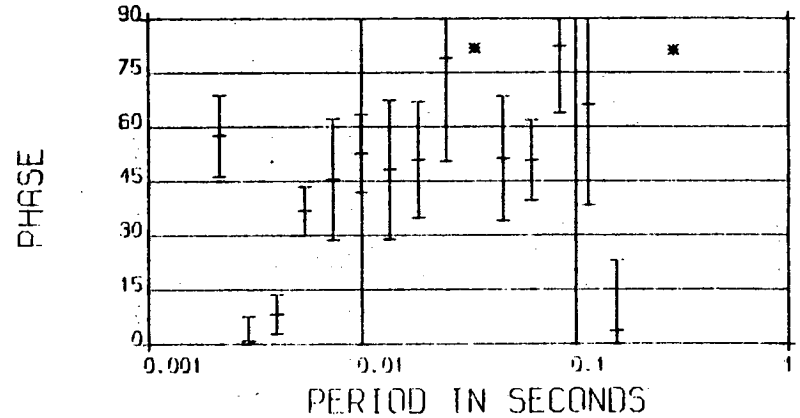
PHASE
90
75
60
45
30
15
0
0.001
0.01
0.1
1
PERIOD IN SECONDS

Station 61

STATION 62

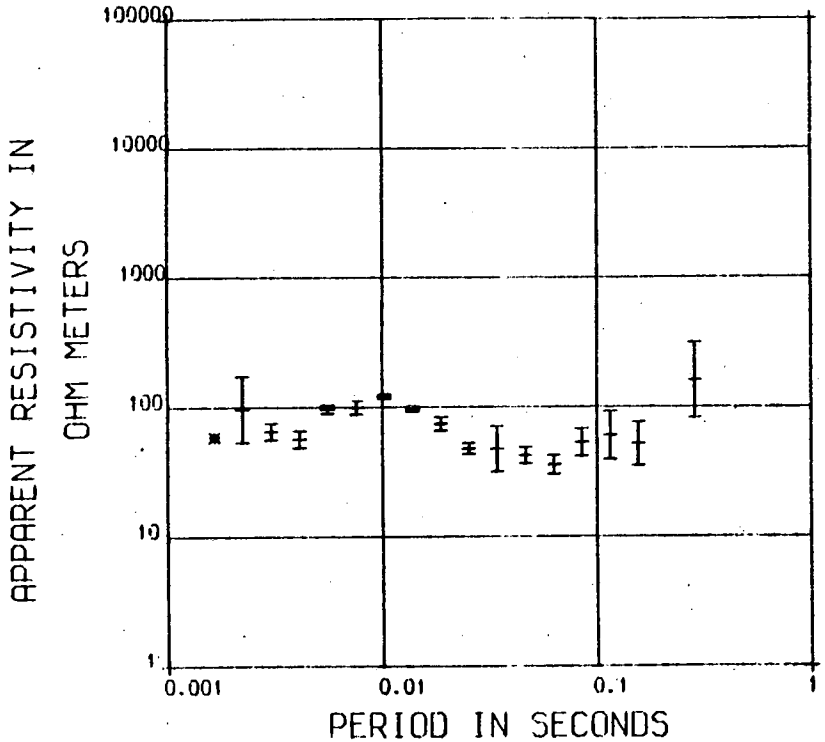

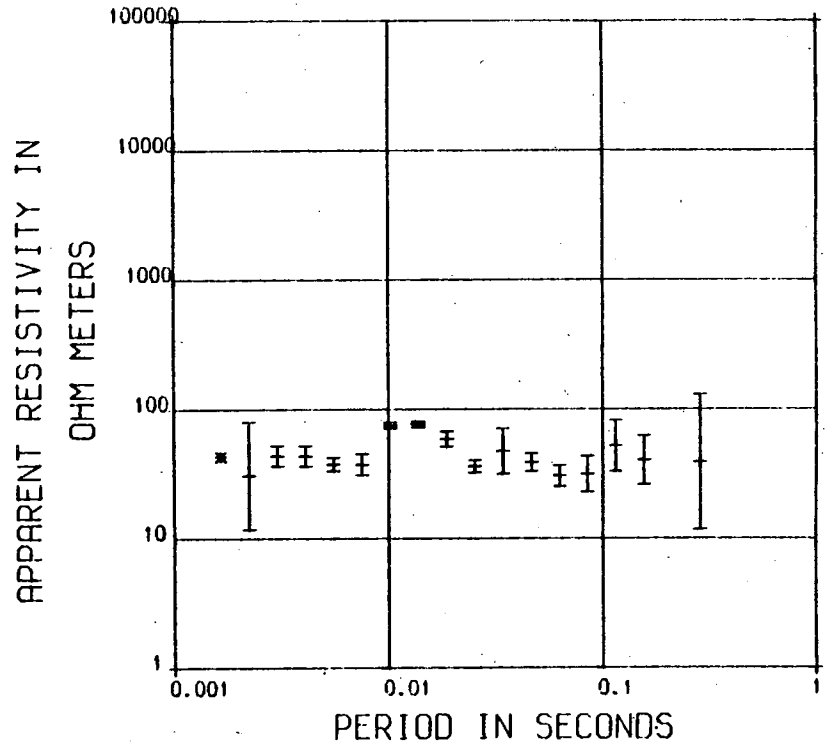

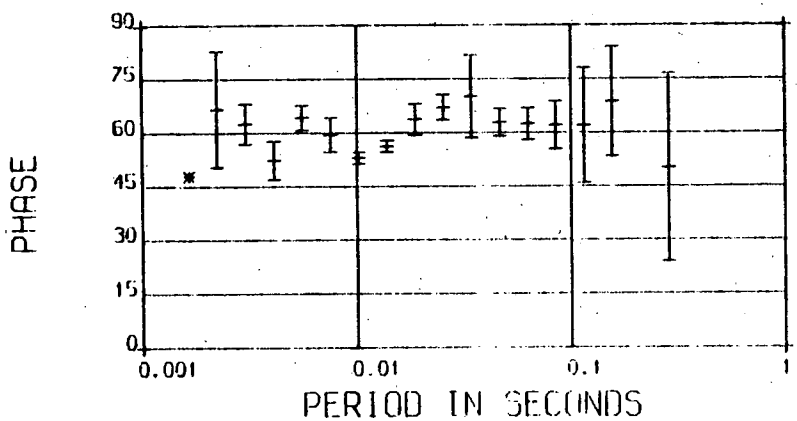

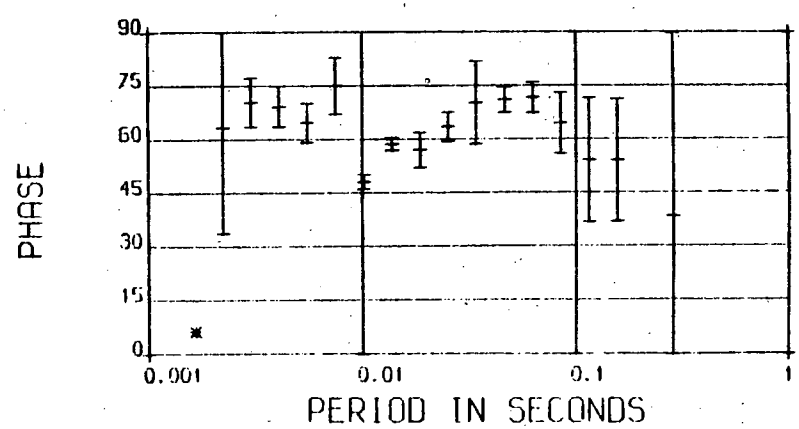

Station 62

STATION 63

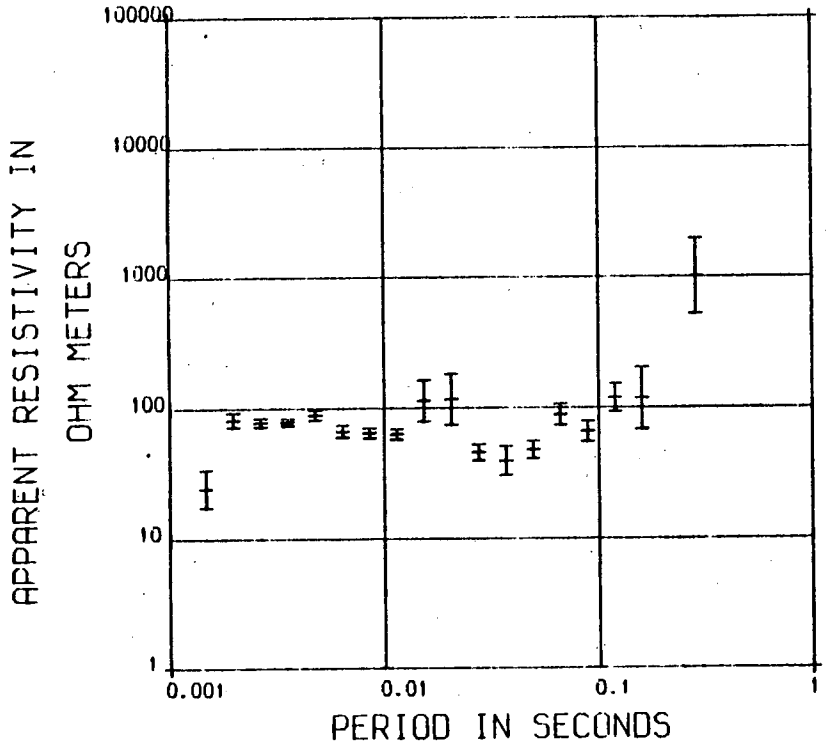

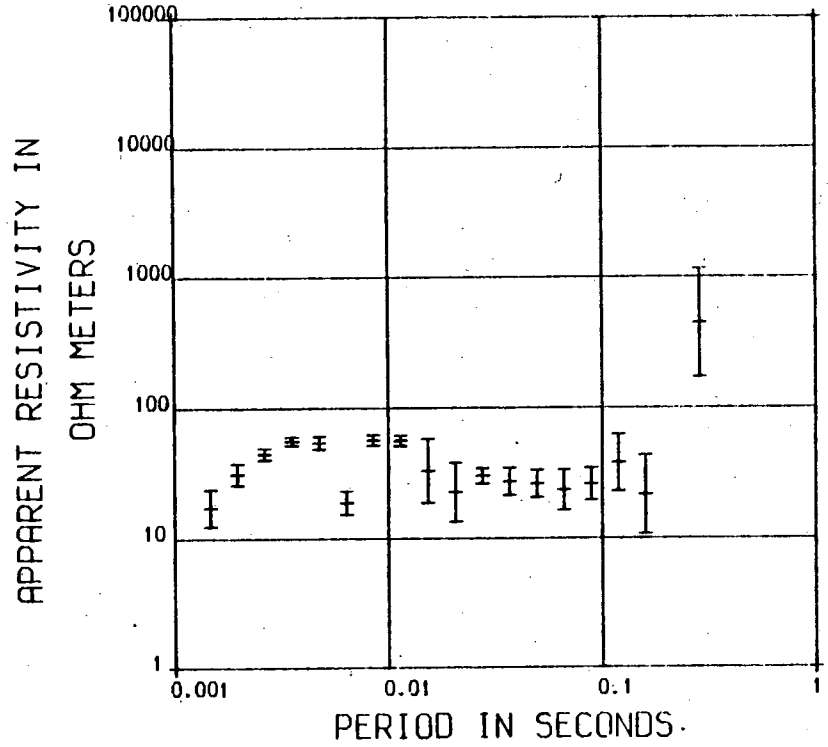

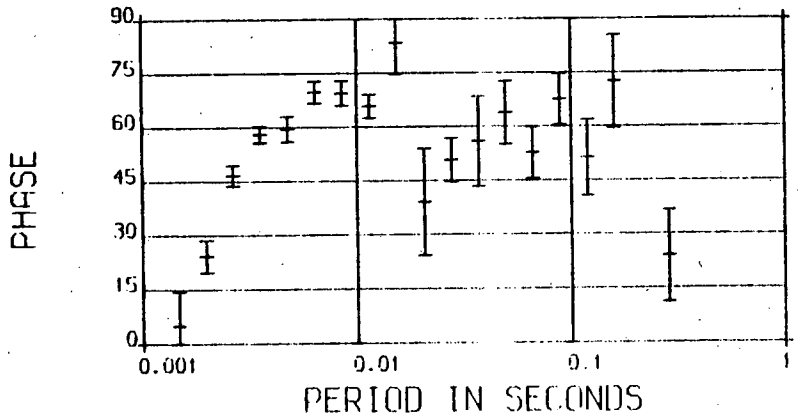

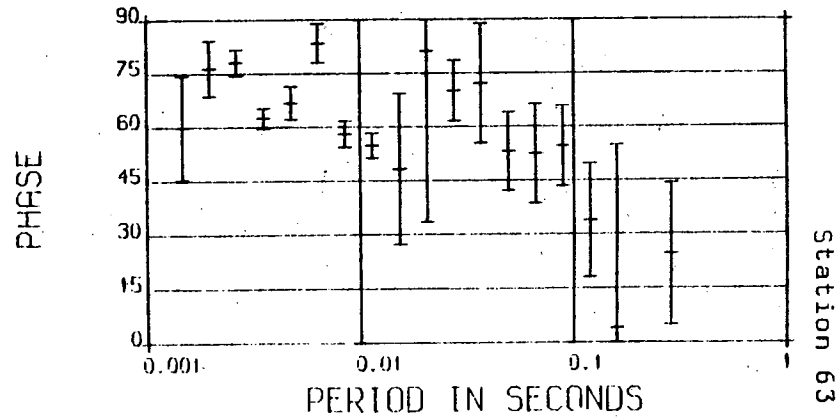

Station 63

(d)

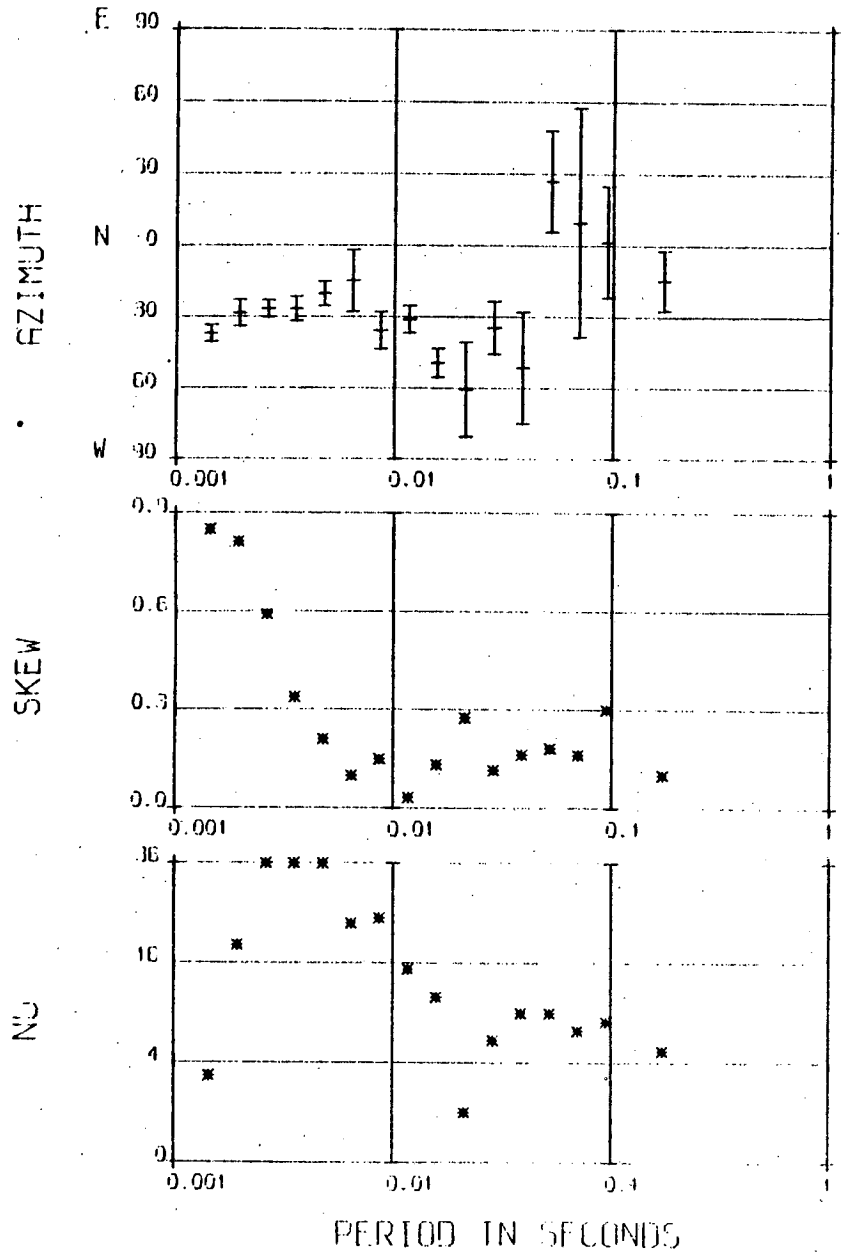
AZIMUTH
E 90
60
30
N 0
30
60
W 90
0.001
0.01
0.1
1
SKEW
0.9
0.6
0.3
0.0
NU
16
10
4
0
PERIOD IN SECONDS

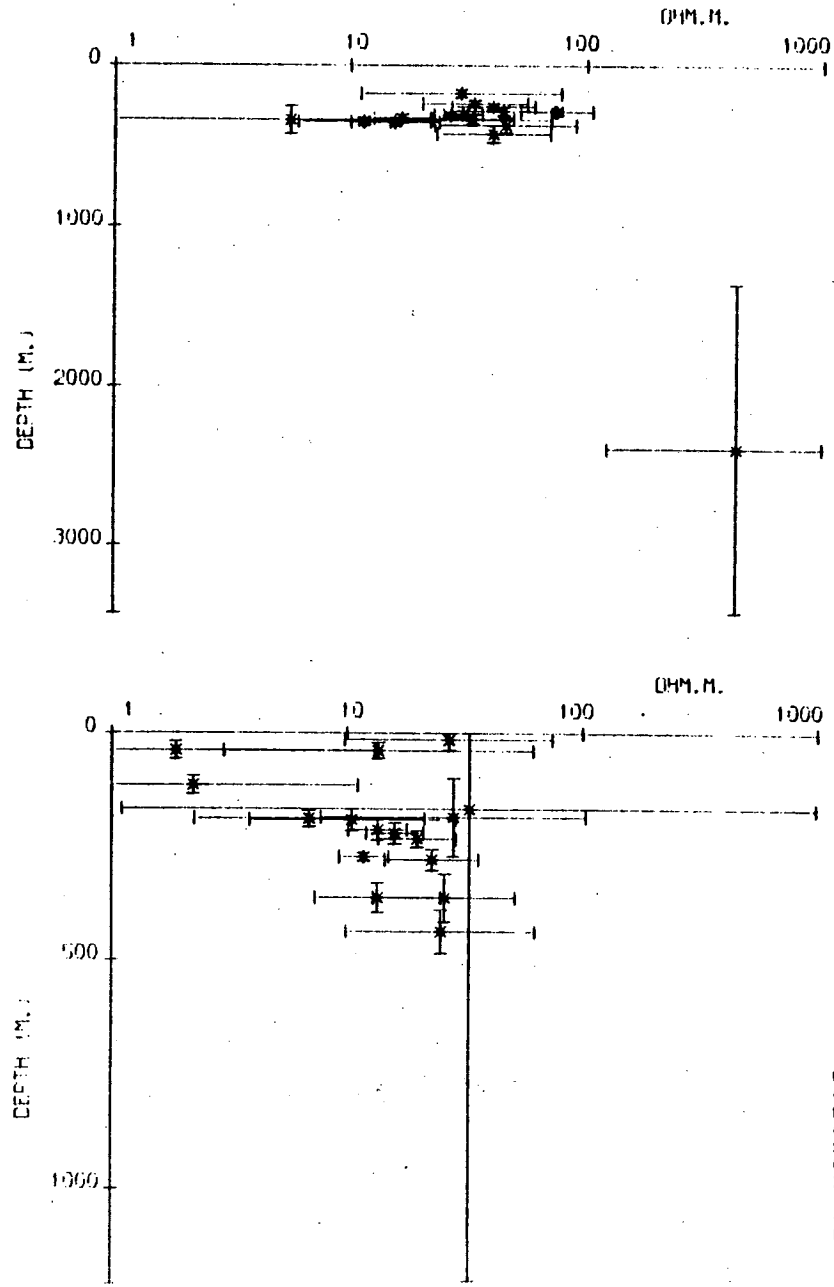
OHM.M.
1
10
100
1000
0
1000
2000
3000
DEPTH (M.)
OHM.M.
1
10
100
1000
0
500
1000
DEPTH (M.)
Station 12

(d)

STATION 15

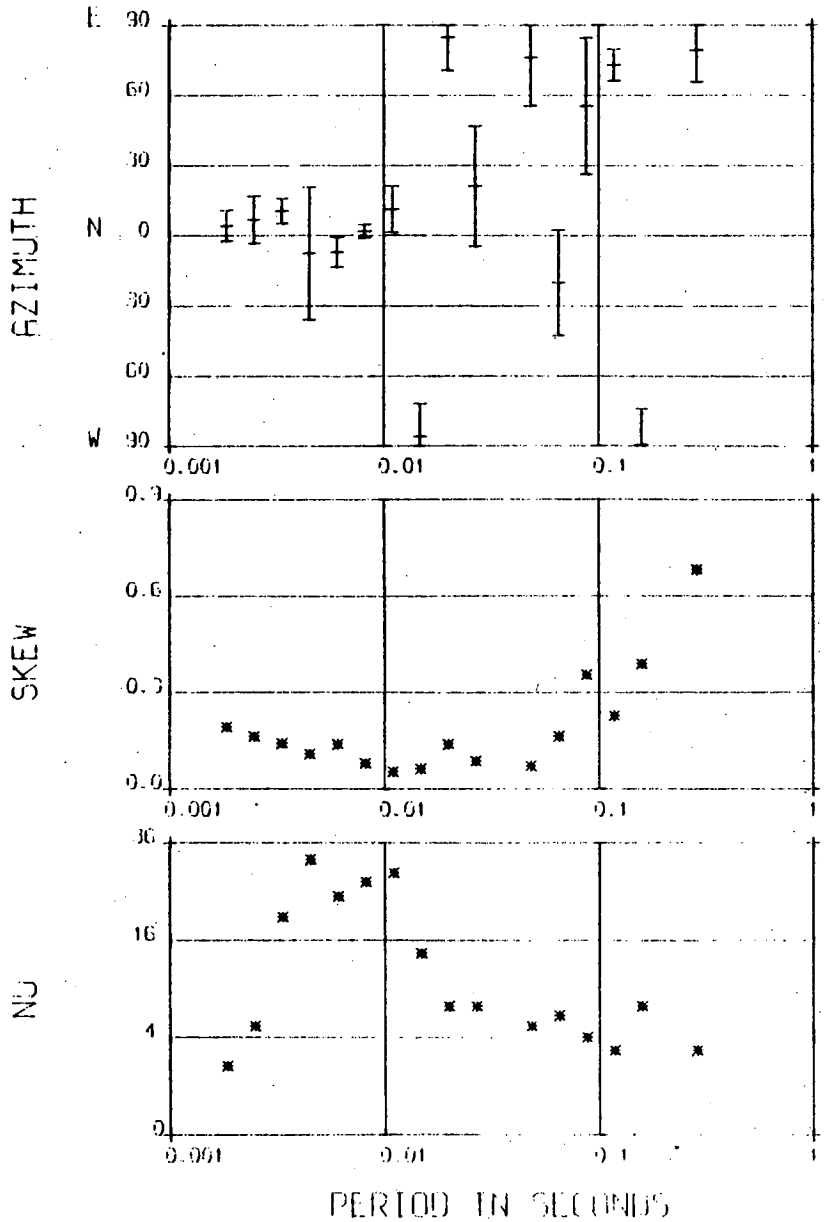

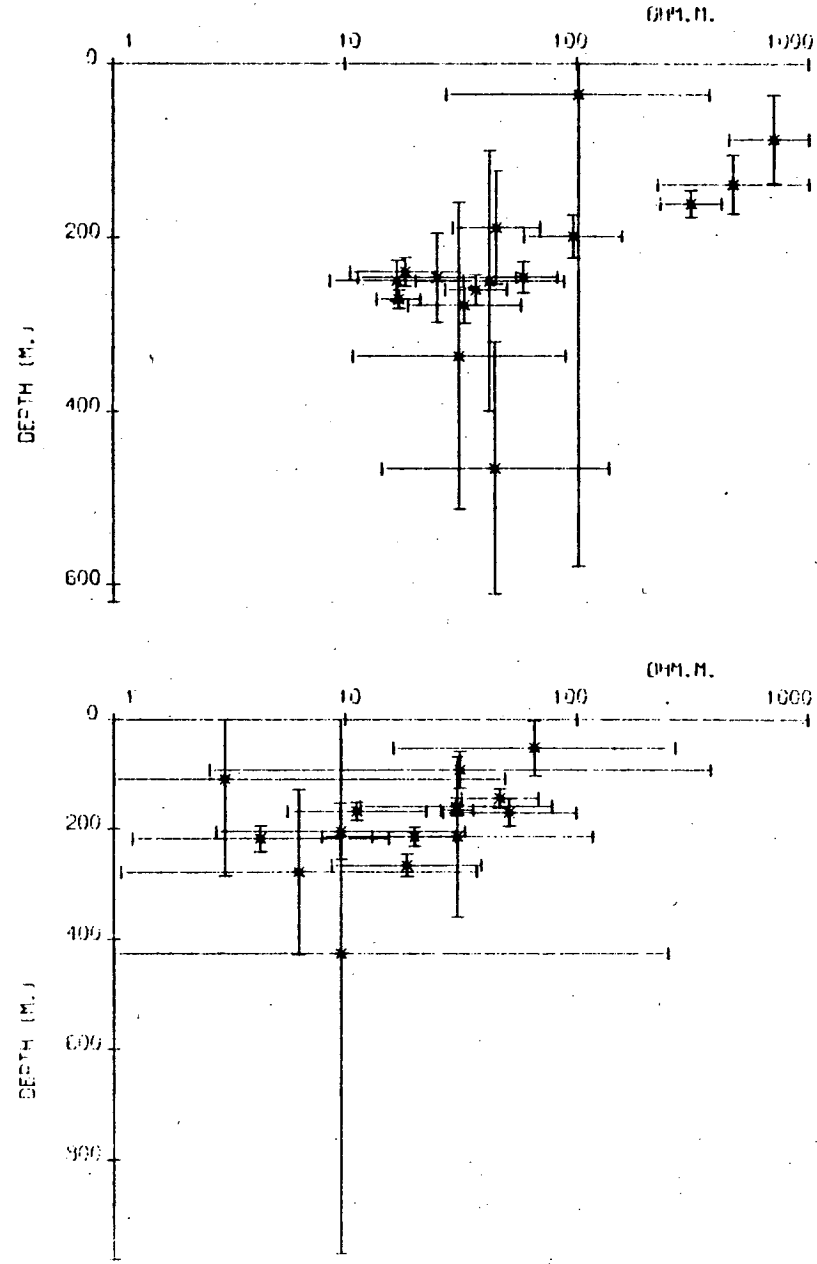

Station 15

(d)

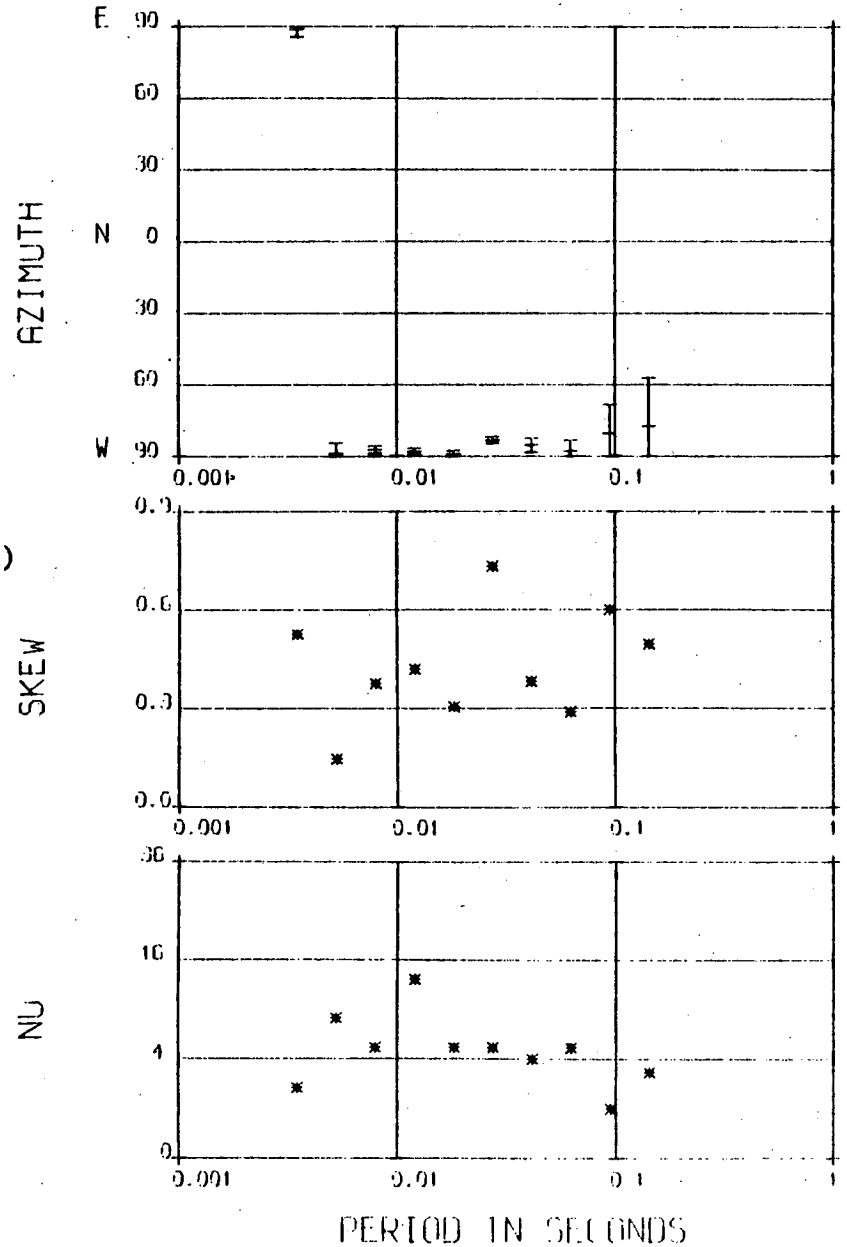
AZIMUTH
E
90
60
30
N
0
30
60
W
90
0.001
0.01
0.1
1
SKEW
0.9
0.6
0.3
0.0
NU
30
10
4
0
PERIOD IN SECONDS

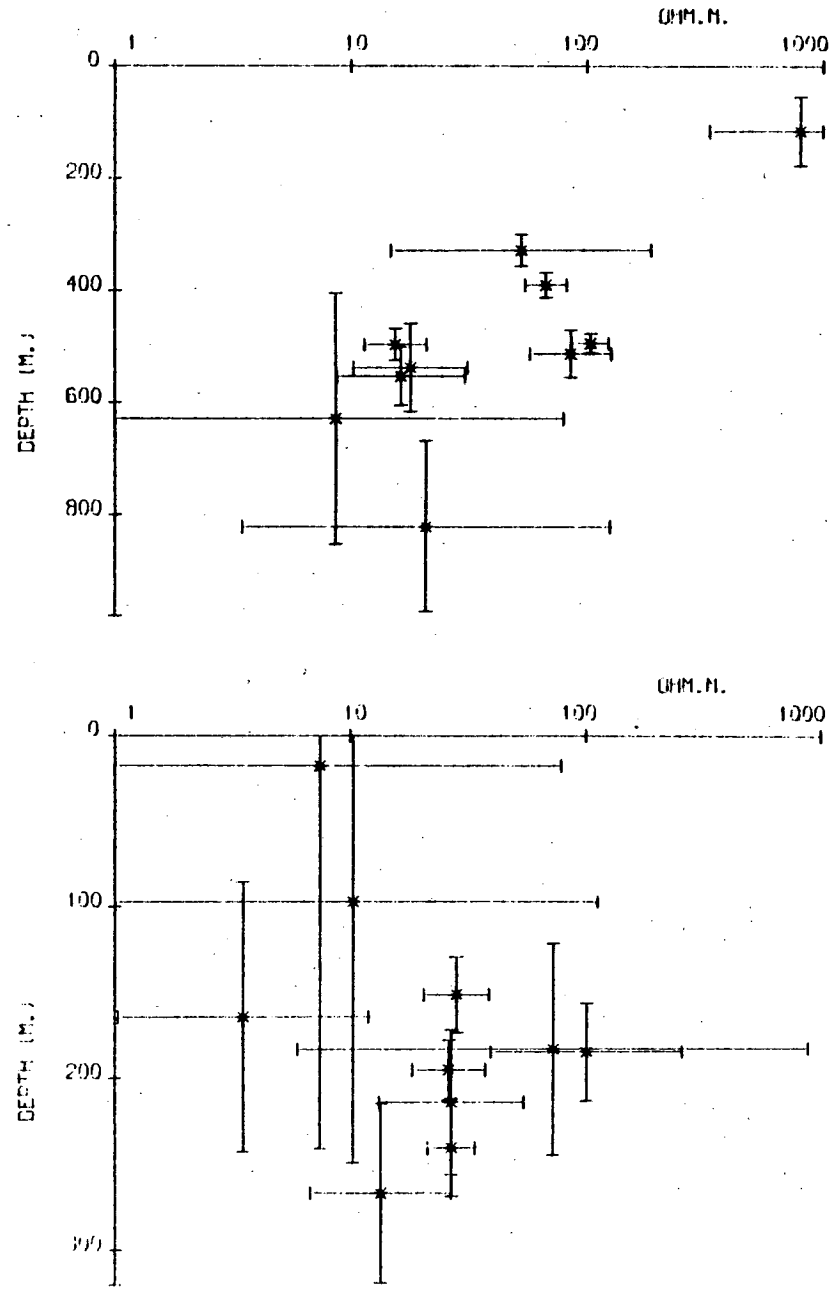
OHM.M.
1
10
100
1000
0
200
400
600
800
DEPTH (M.)
OHM.M.
1
10
100
1000
0
100
200
DEPTH (M.)

Station 16

(d)

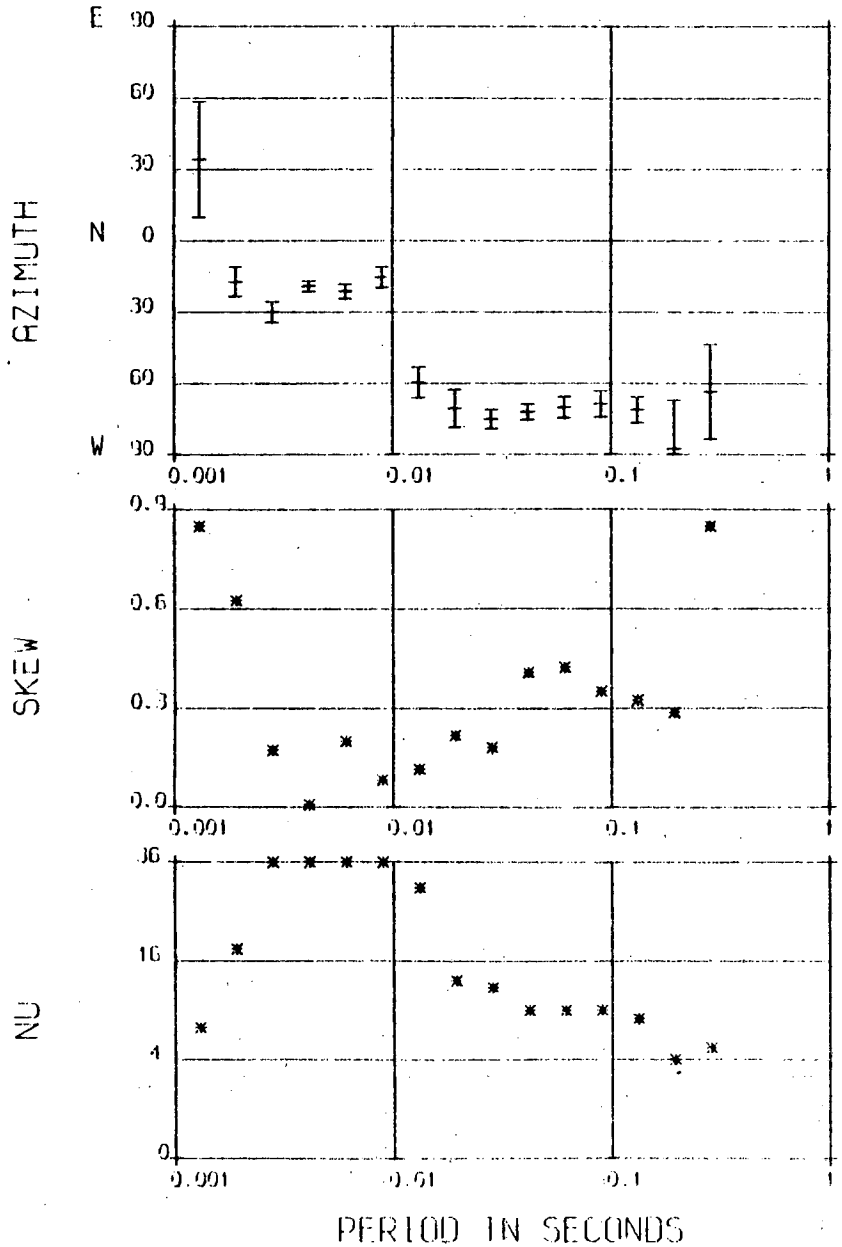
AZIMUTH
E 90
60
30
N 0
30
60
W 90
0.001
0.01
0.1
1
SKEW
0.9
0.6
0.3
0.0
NU
16
12
8
4
0
PERIOD IN SECONDS

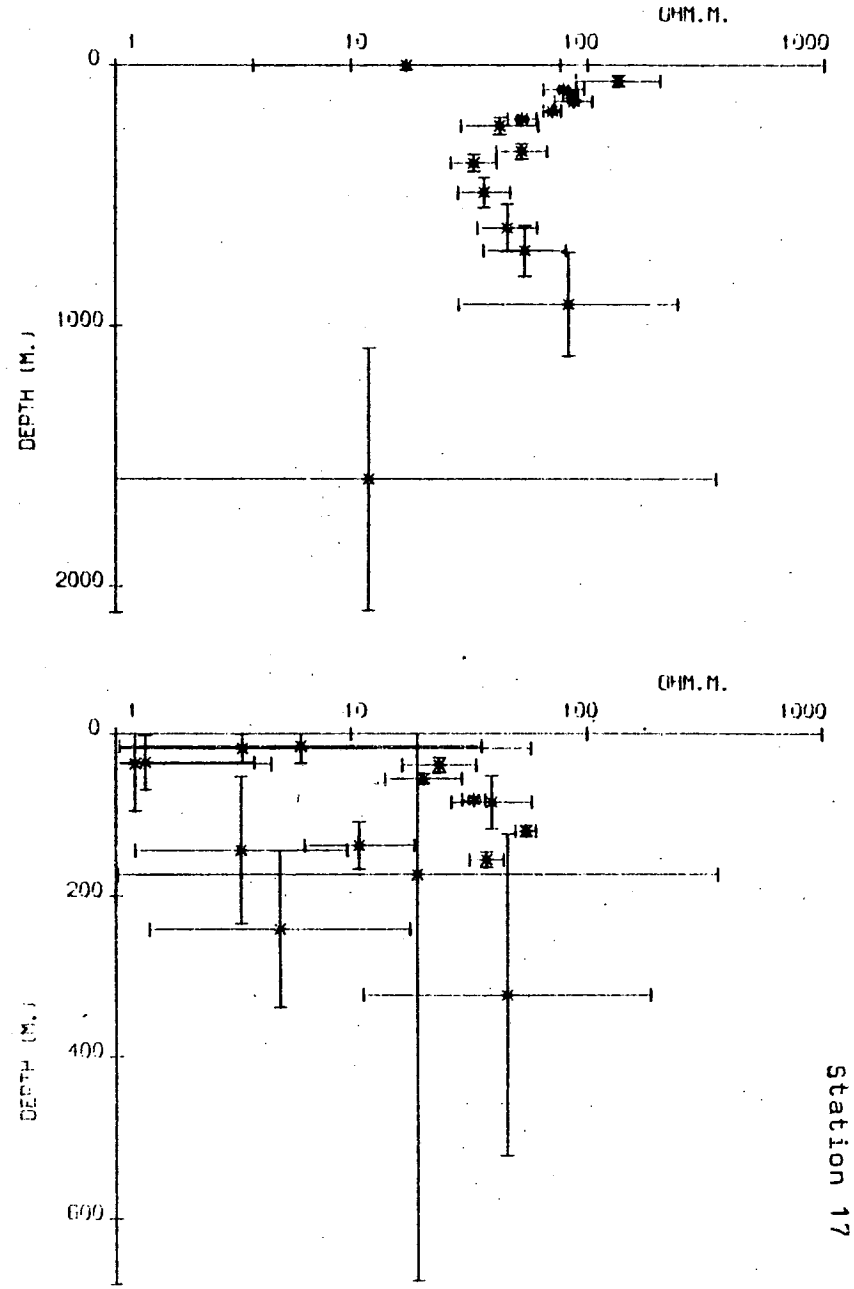
OHM.M.
1
10
100
1000
0
1000
2000
DEPTH (M.)
OHM.M.
0
200
400
600
Station 17

(d)
AZIMUTH
SKEW
NU
PERIOD IN SECONDS
DEPTH (M.)
OHM.M.
Station 18

(d)

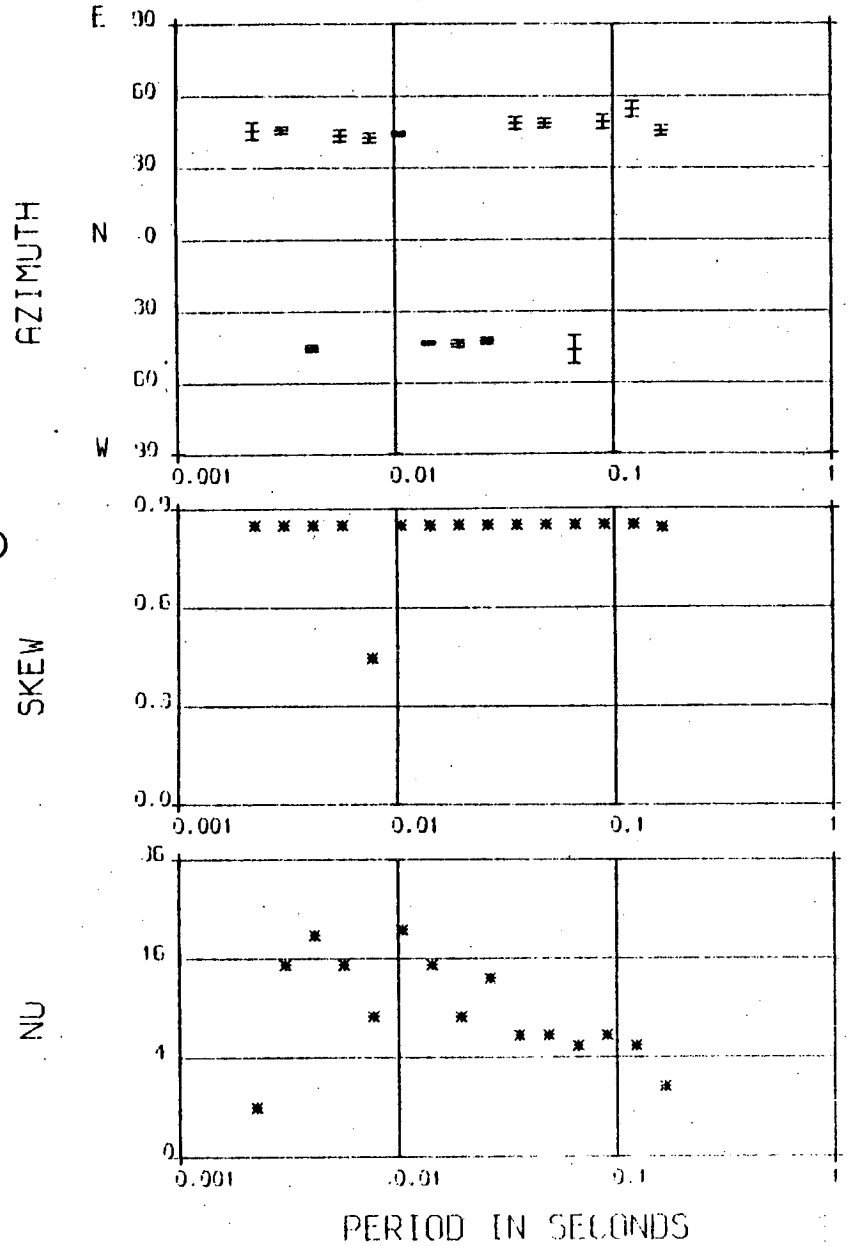
AZIMUTH
E 90
60
30
N 0
30
60
W 90
0.001
0.01
0.1
1
SKEW
0.9
0.6
0.3
0.0
NU
16
4
0
PERIOD IN SECONDS

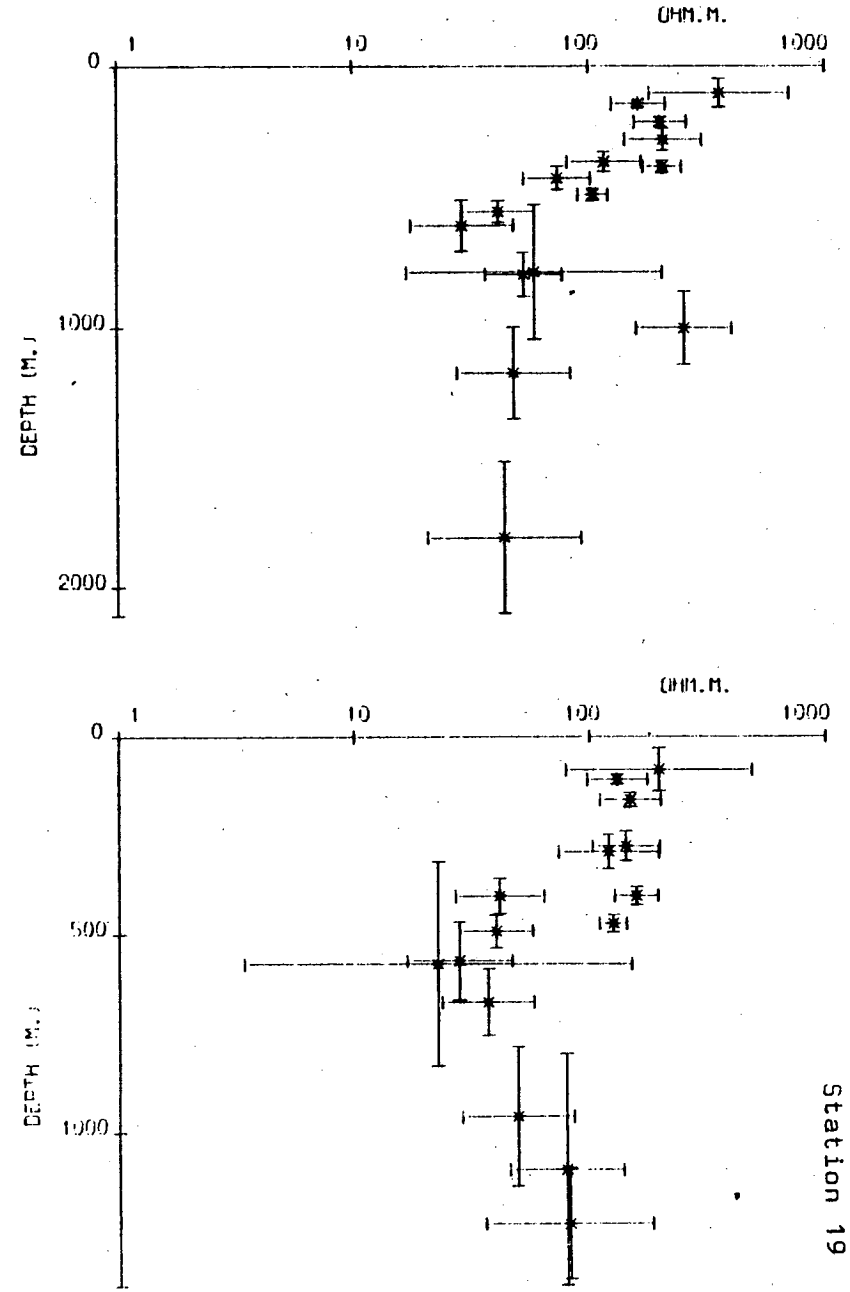
OHM.M.
1
10
100
1000
0
1000
2000
DEPTH (M.)
OHM.M.
500
1000
Station 19

(d)
AZIMUTH
SKEW
NU
PERIOD IN SECONDS
DEPTH (M.)
OHM.M.
Station 20

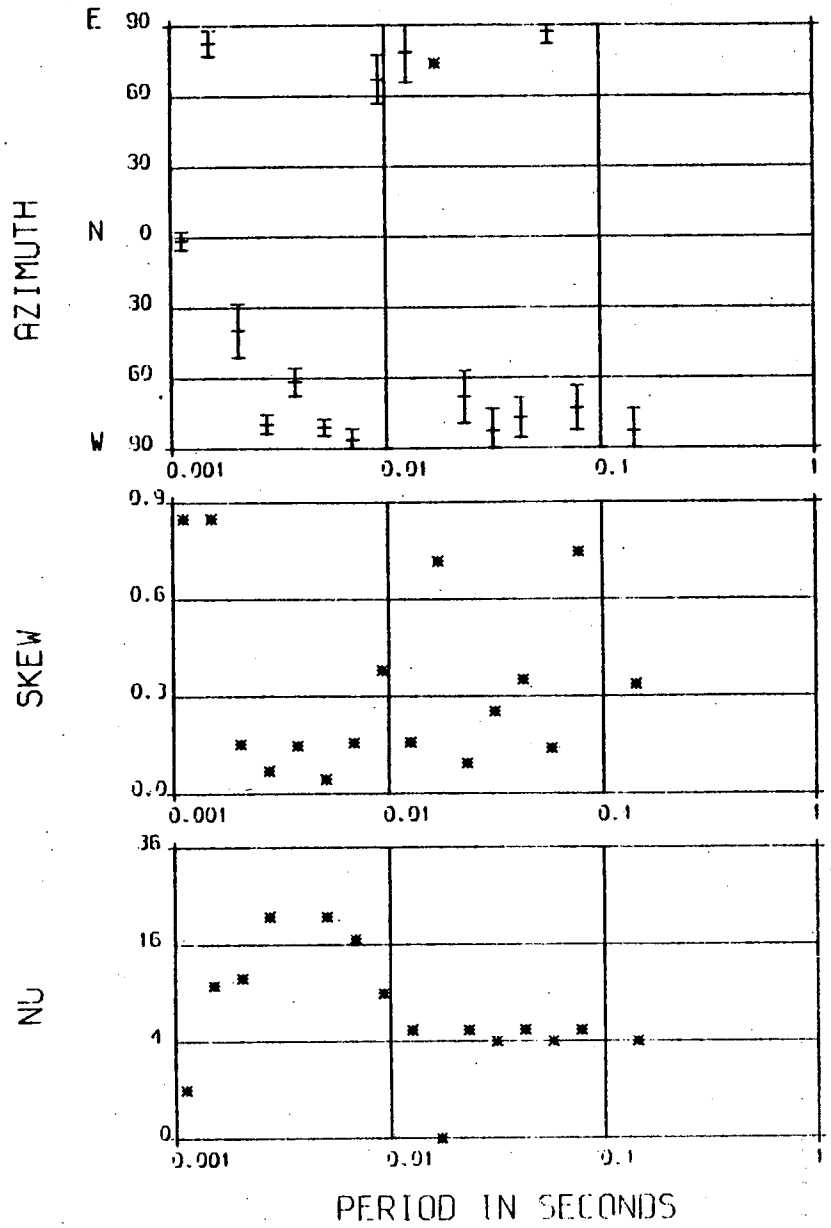
AZIMUTH
E 90
60
30
N 0
30
60
W 90
0.001
0.01
0.1
1
SKEW
0.9
0.6
0.3
0.0
NU
36
16
4
0
PERIOD IN SECONDS

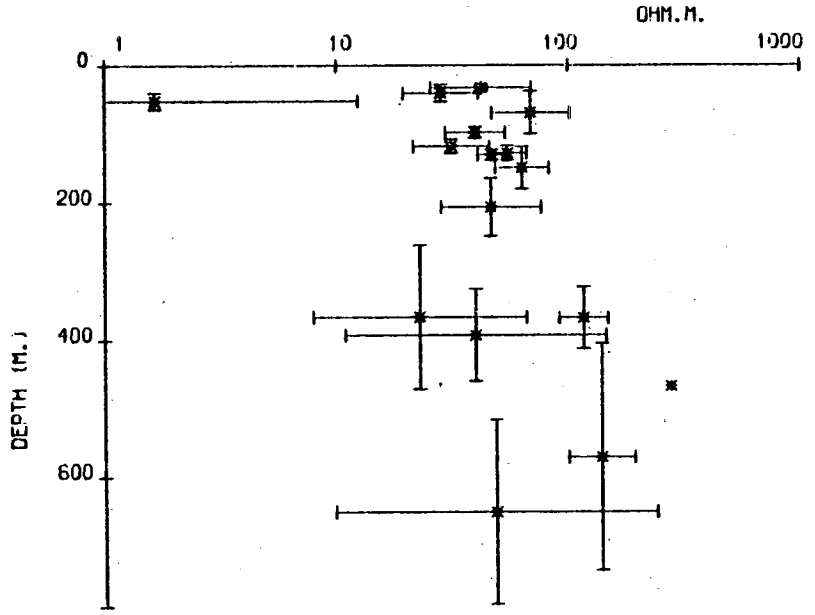
OHM.M.
1
10
100
1000
0
200
400
600
DEPTH (M.)

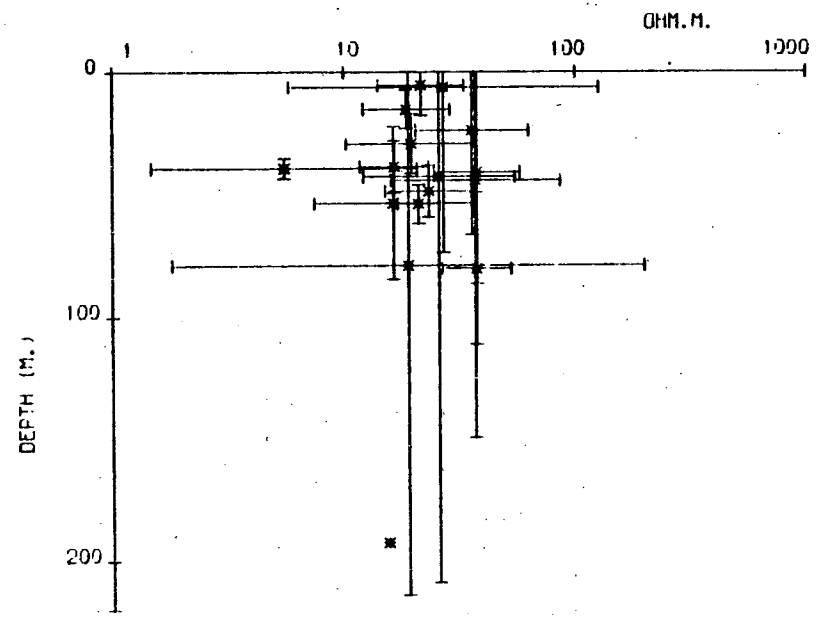
OHM.M.
1
10
100
1000
0
100
200
DEPTH (M.)

Station 43

STATION 44

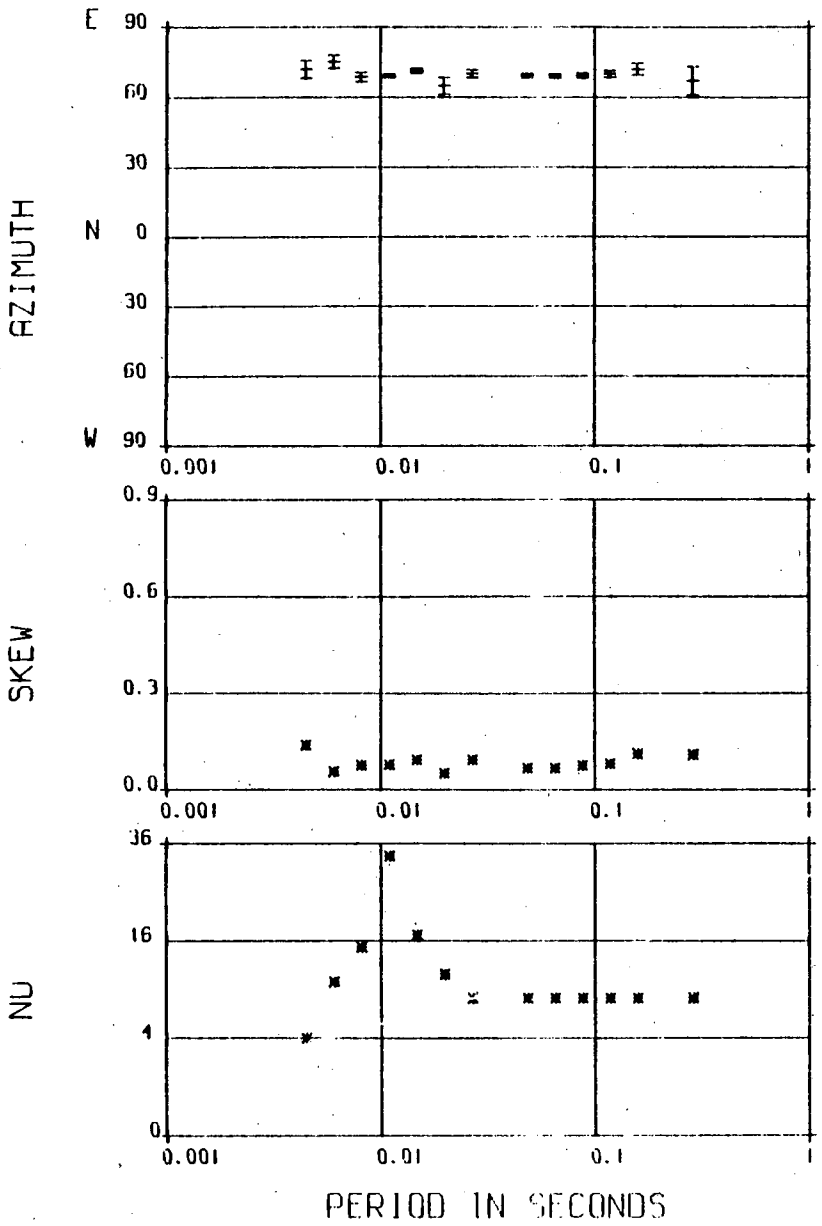

STATION 44

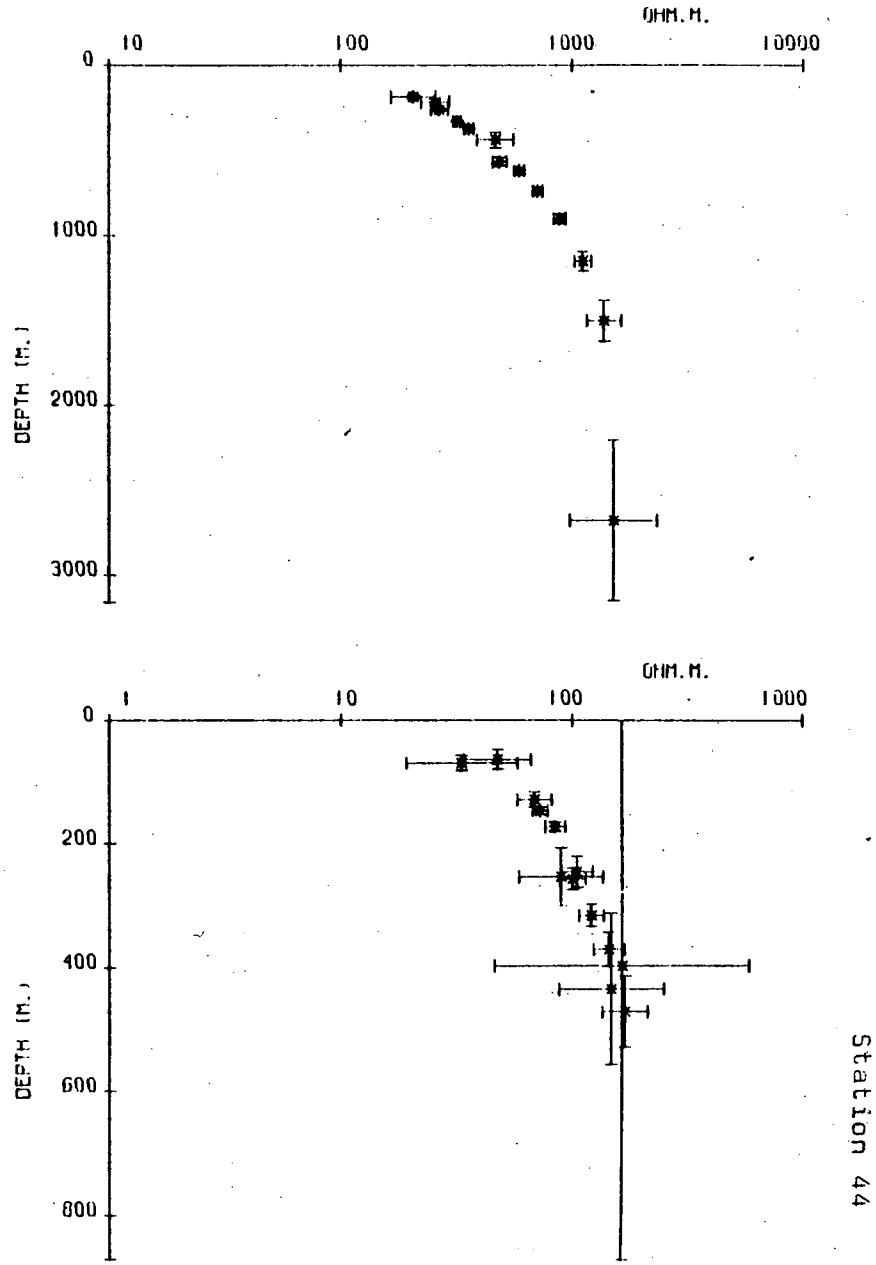

STATION 45

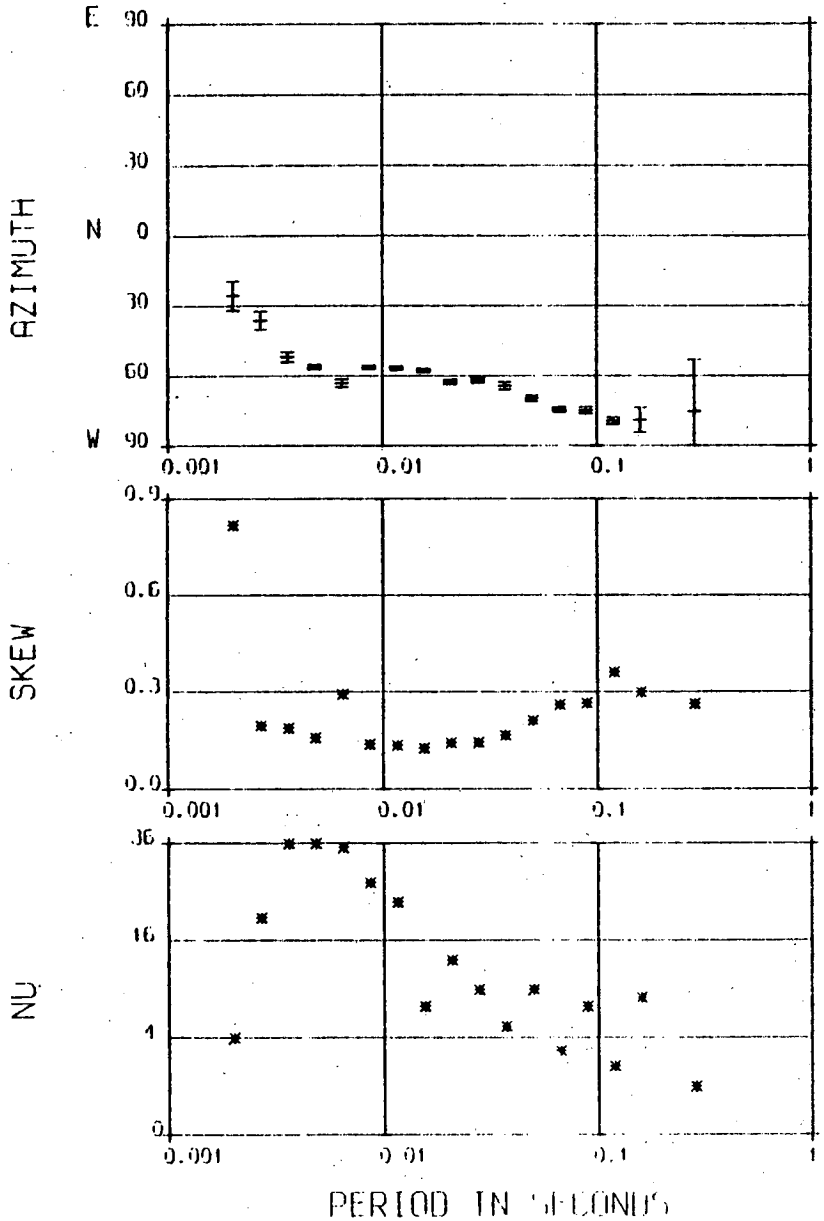

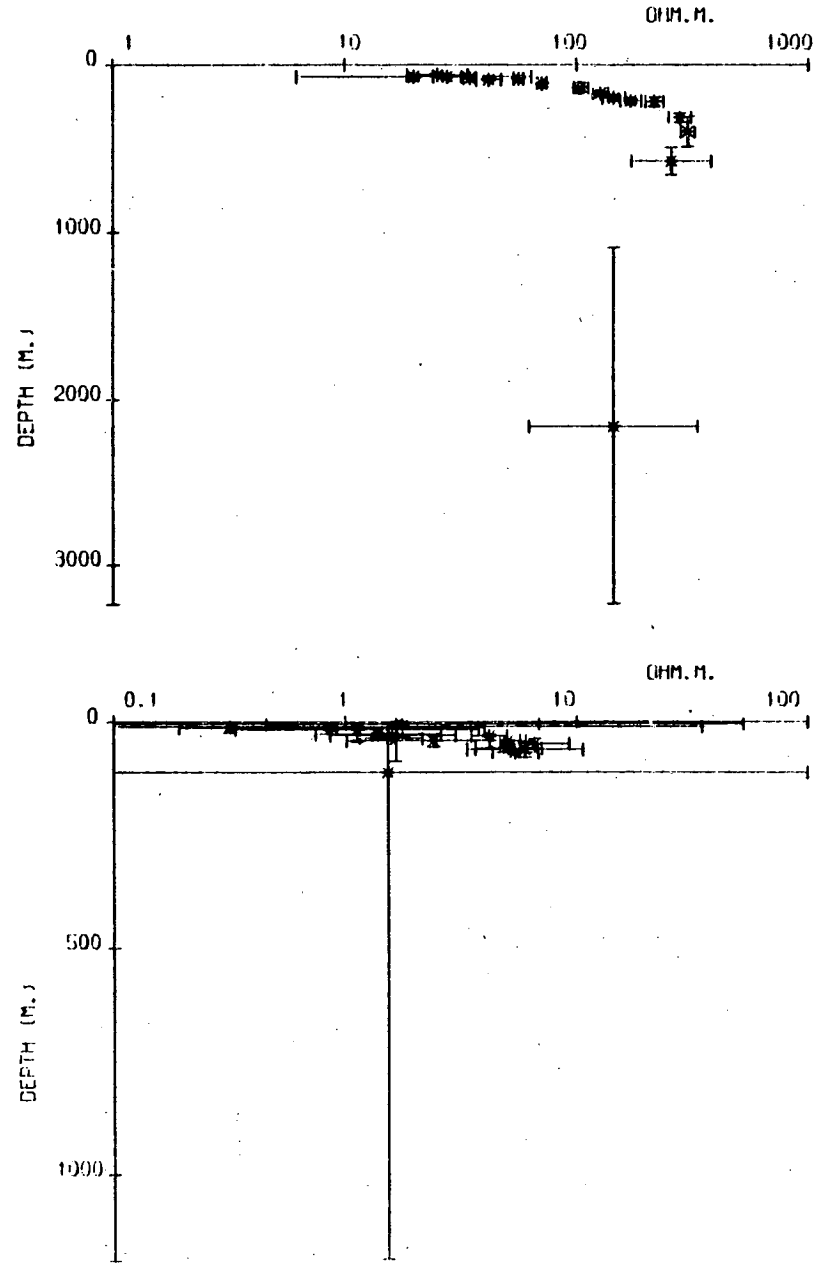

Station 45

STATION 46

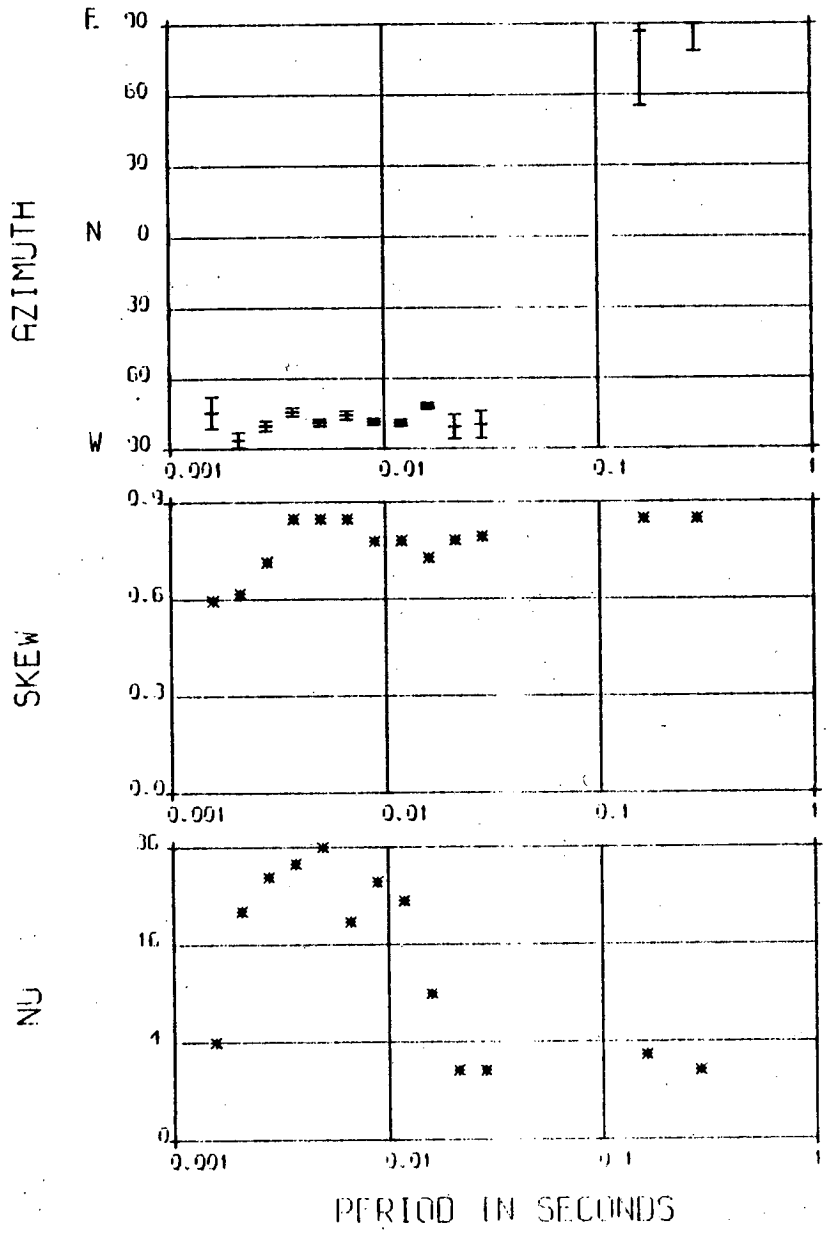

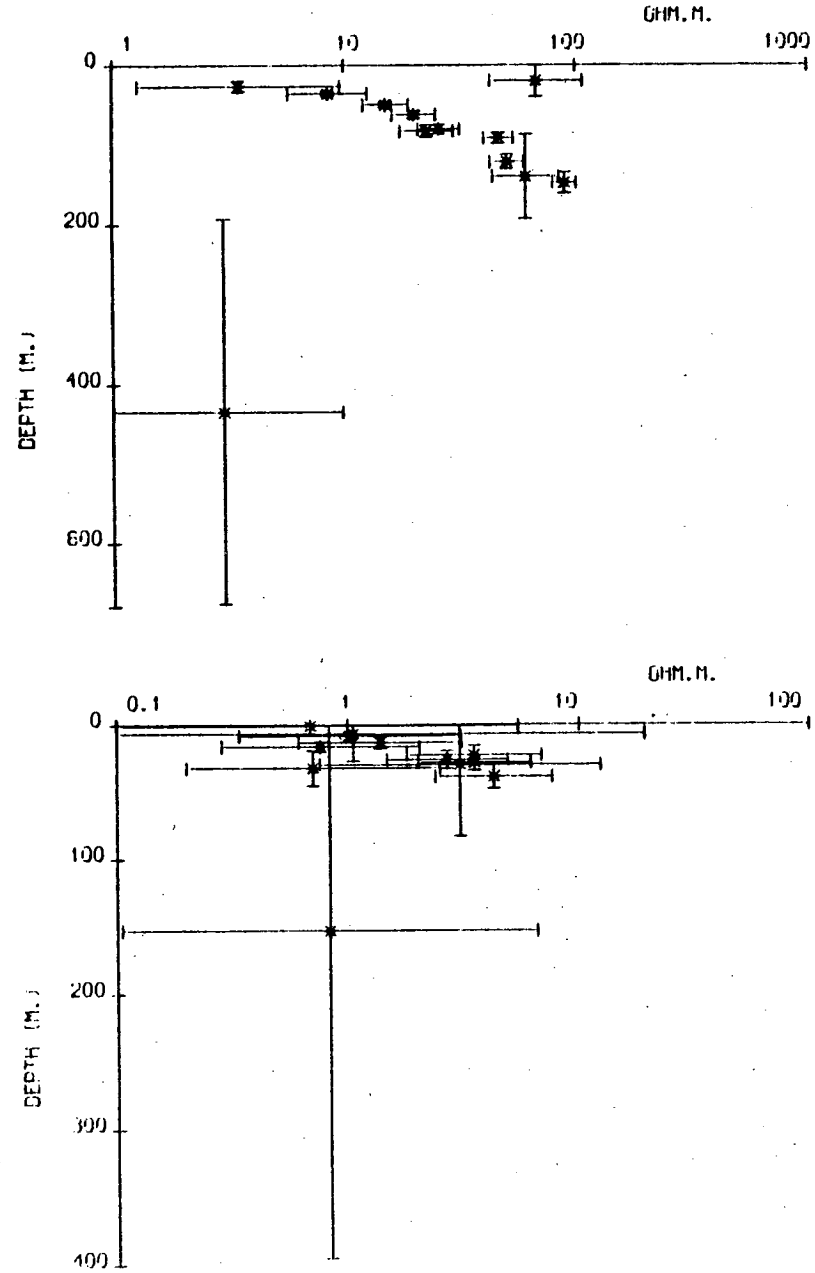

Station 46

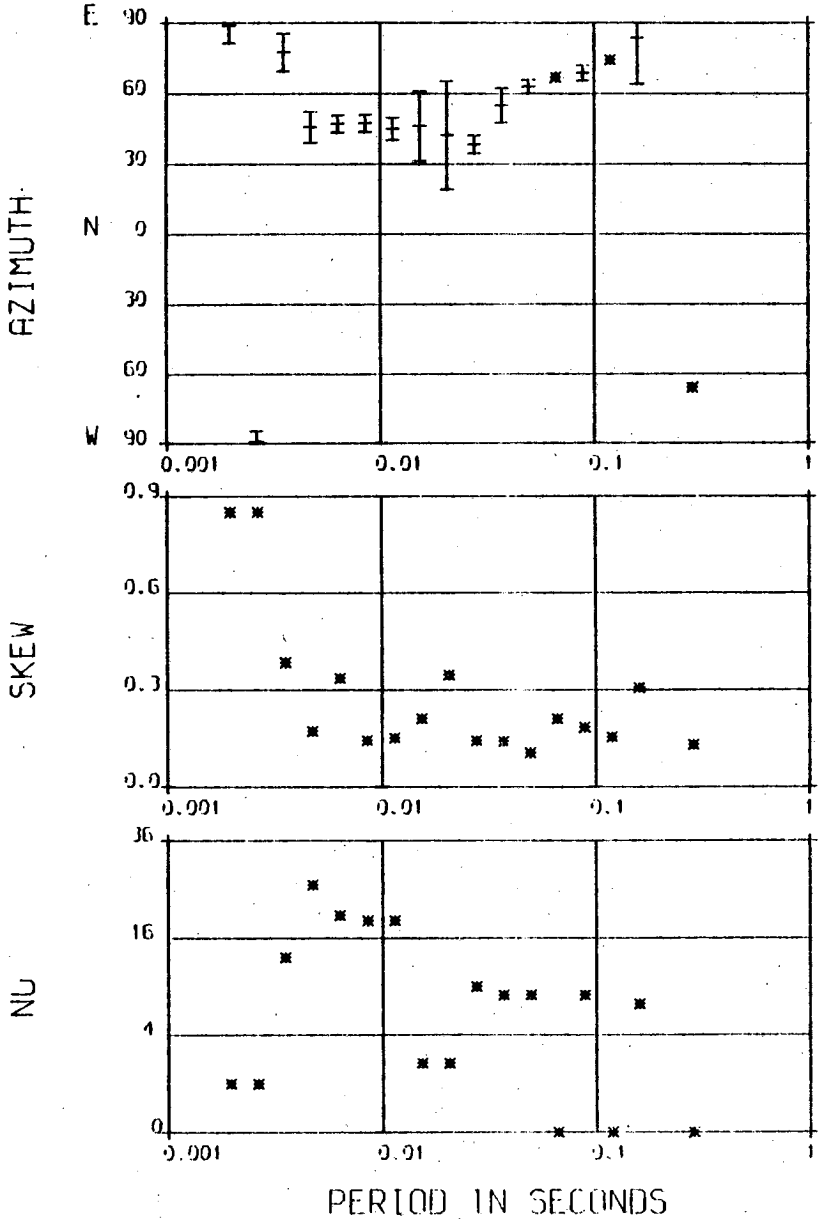
AZIMUTH
E 90
60
30
N 0
30
60
W 90
0.001
0.01
0.1
1
SKEW
0.9
0.6
0.3
0.0
NU
16
4
0
PERIOD IN SECONDS

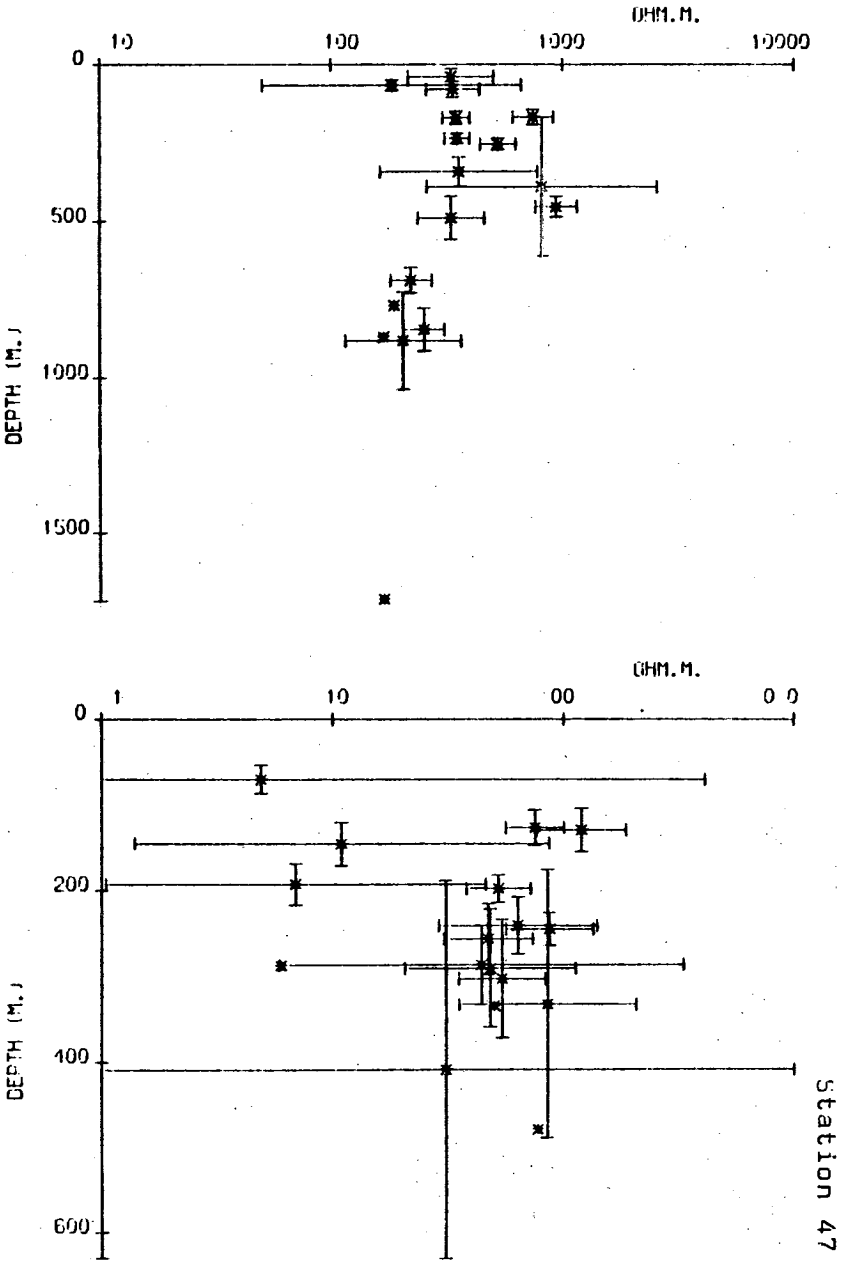
OHM.M.
10
100
1000
10000
0
500
1000
1500
DEPTH (M.)
OHM.M.
1
10
00
0 0
0
200
400
600
DEPTH (M.)
Station 47

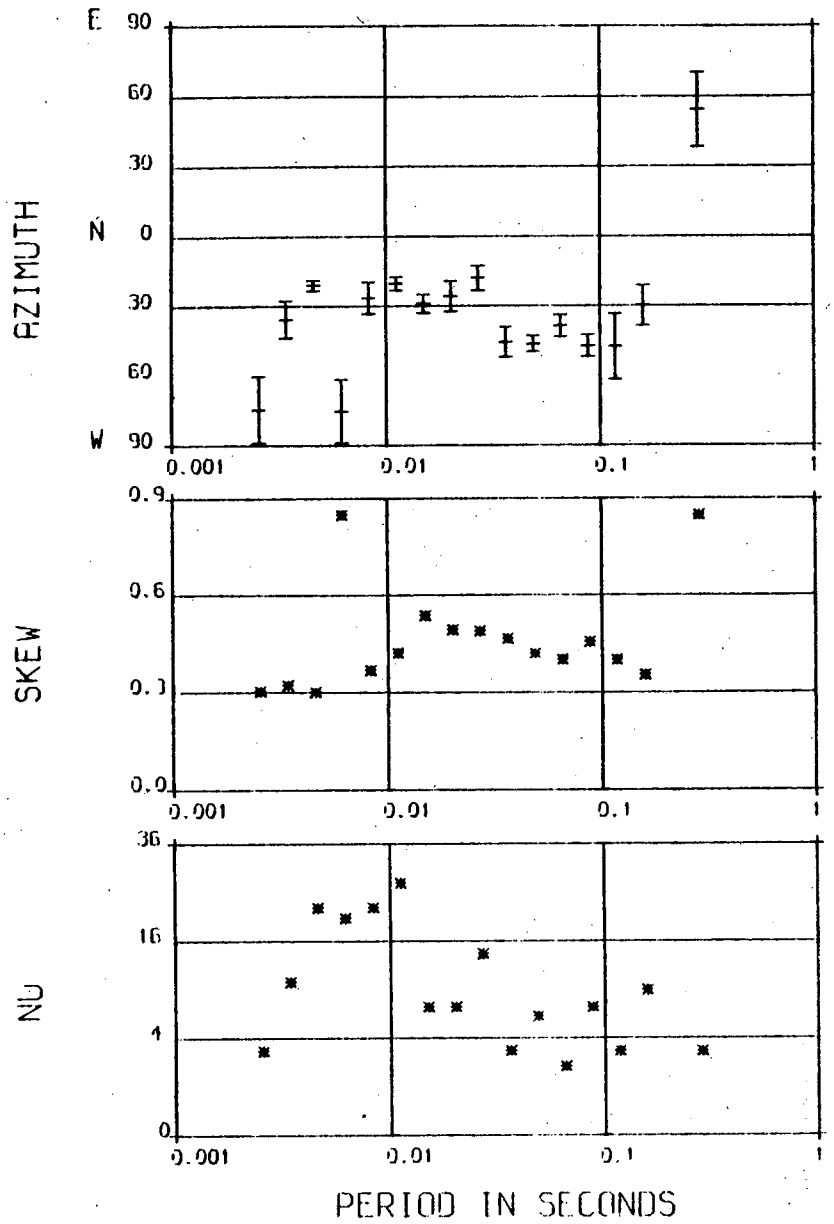
AZIMUTH
E 90
60
30
N 0
30
60
W 90
0.001
0.01
0.1
1
SKEW
0.9
0.6
0.3
0.0
NU
36
16
4
0
PERIOD IN SECONDS

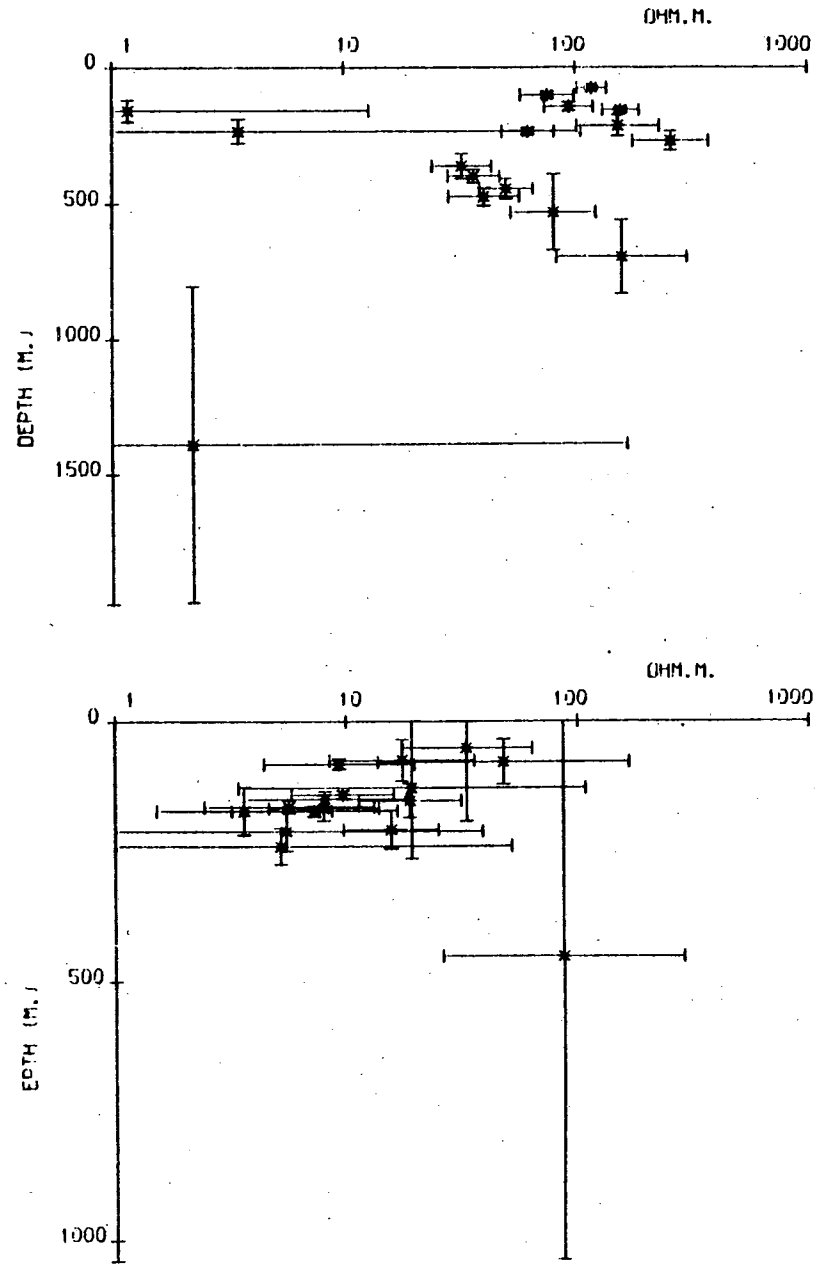
OHM.M.
1
10
100
1000
0
500
1000
1500
DEPTH (M.)
OHM.M.
500
1000

Station 49

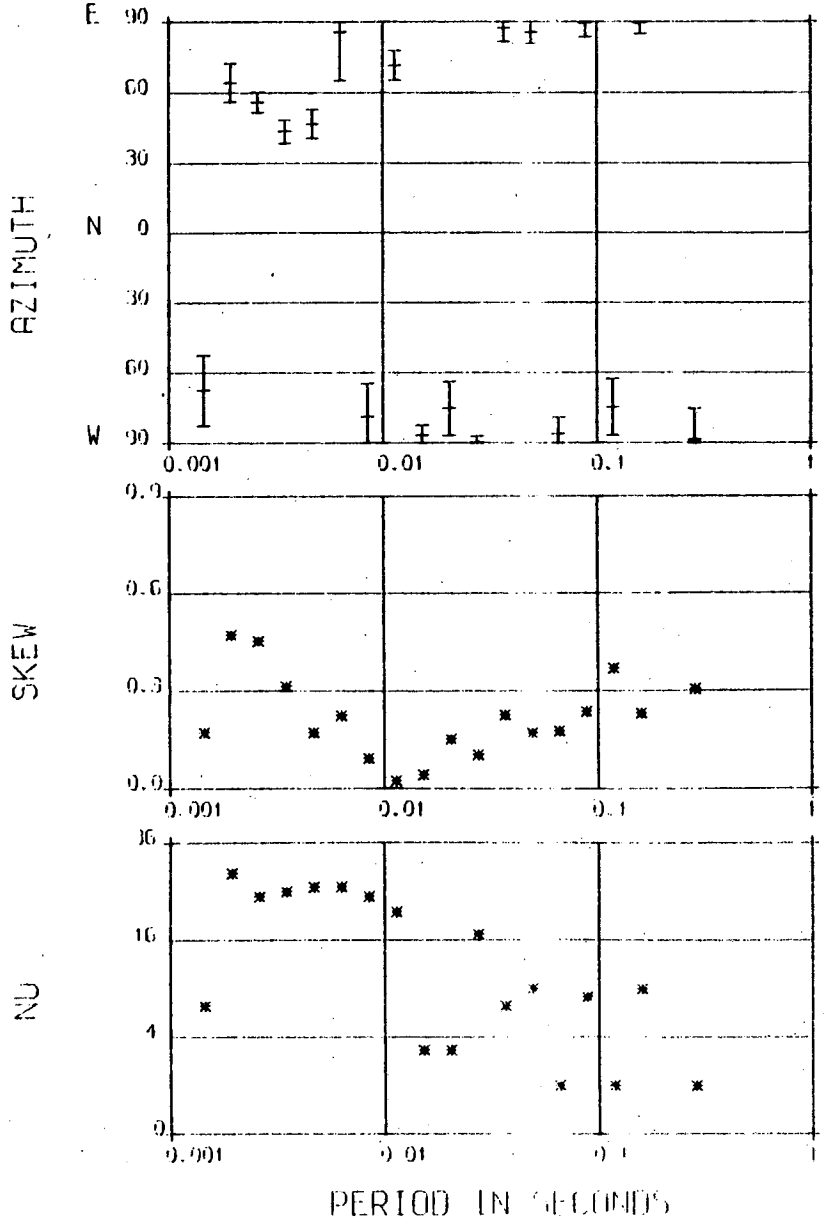
AZIMUTH
E 90
60
30
N 0
30
60
W 90
0.001
0.01
0.1
1
SKEW
0.9
0.6
0.3
0.0
NU
16
10
4
0
PERIOD IN SECONDS

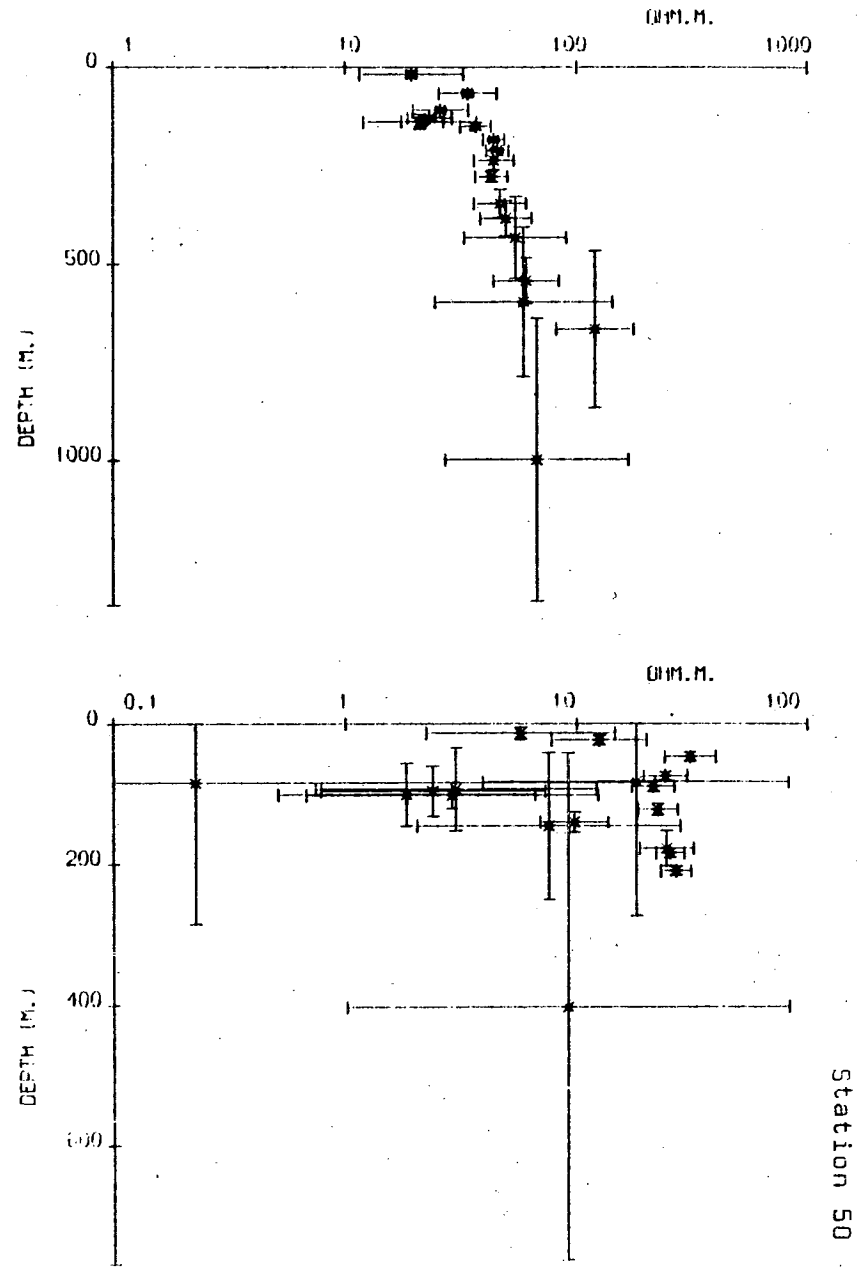
DIM.M.
1
10
100
1000
0
500
1000
DEPTH (M.)
DIM.M.
0.1
1
10
100
0
200
400
600
DEPTH (M.)

Station 50

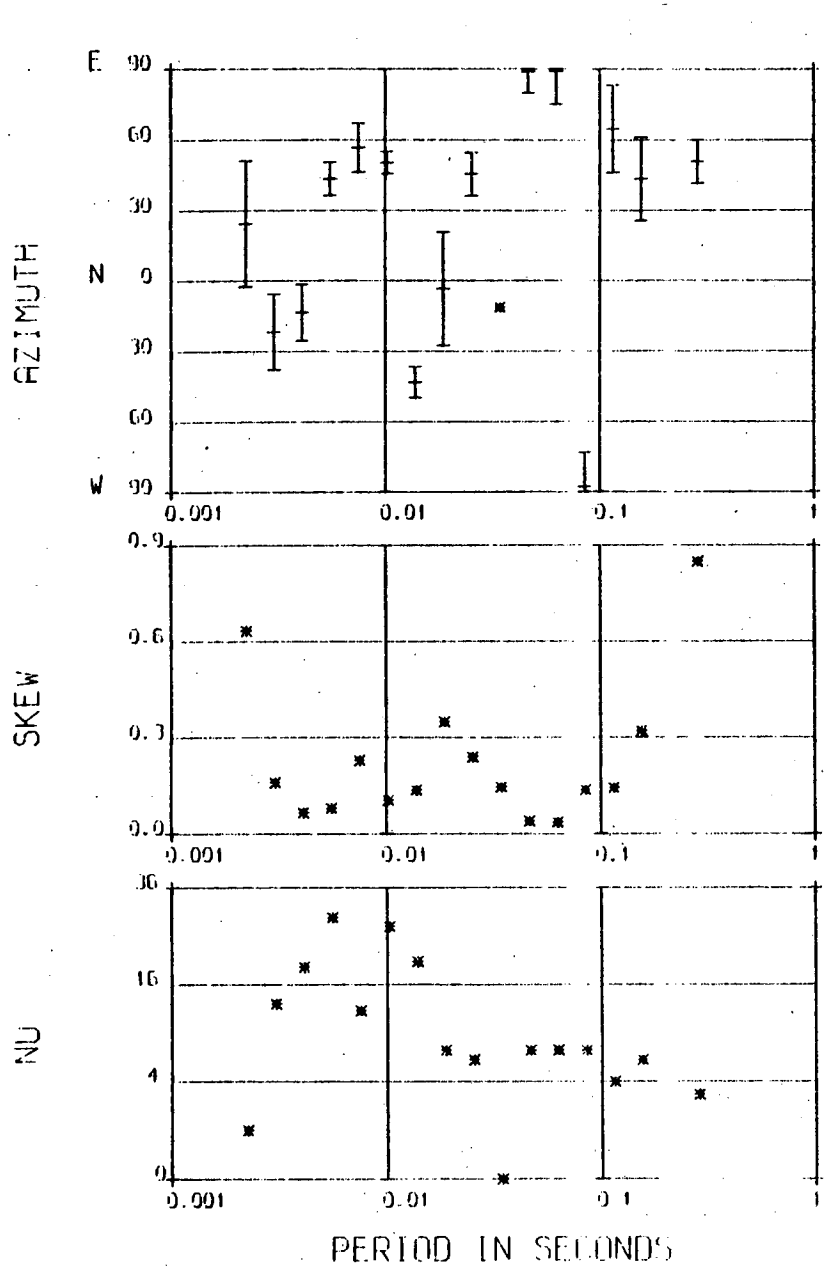
AZIMUTH
E
90
60
30
N
0
30
60
W
90
0.001
0.01
0.1
1
SKEW
0.9
0.6
0.3
0.0
NU
32
16
4
0
PERIOD IN SECONDS

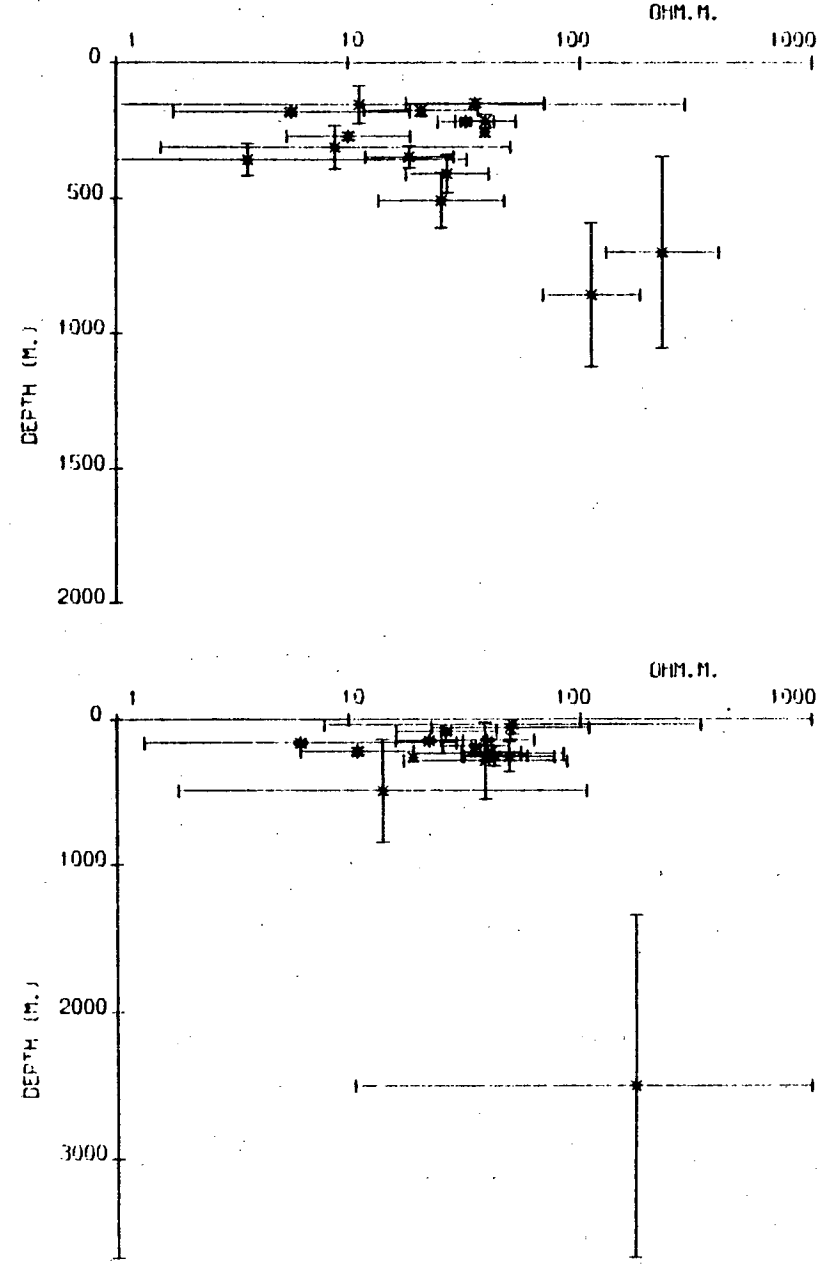
OHM.M.
1
10
100
1000
0
500
1000
1500
2000
DEPTH (M.)
OHM.M.
1
10
100
1000
0
1000
2000
3000
DEPTH (M.)

Station 51

STATION 52

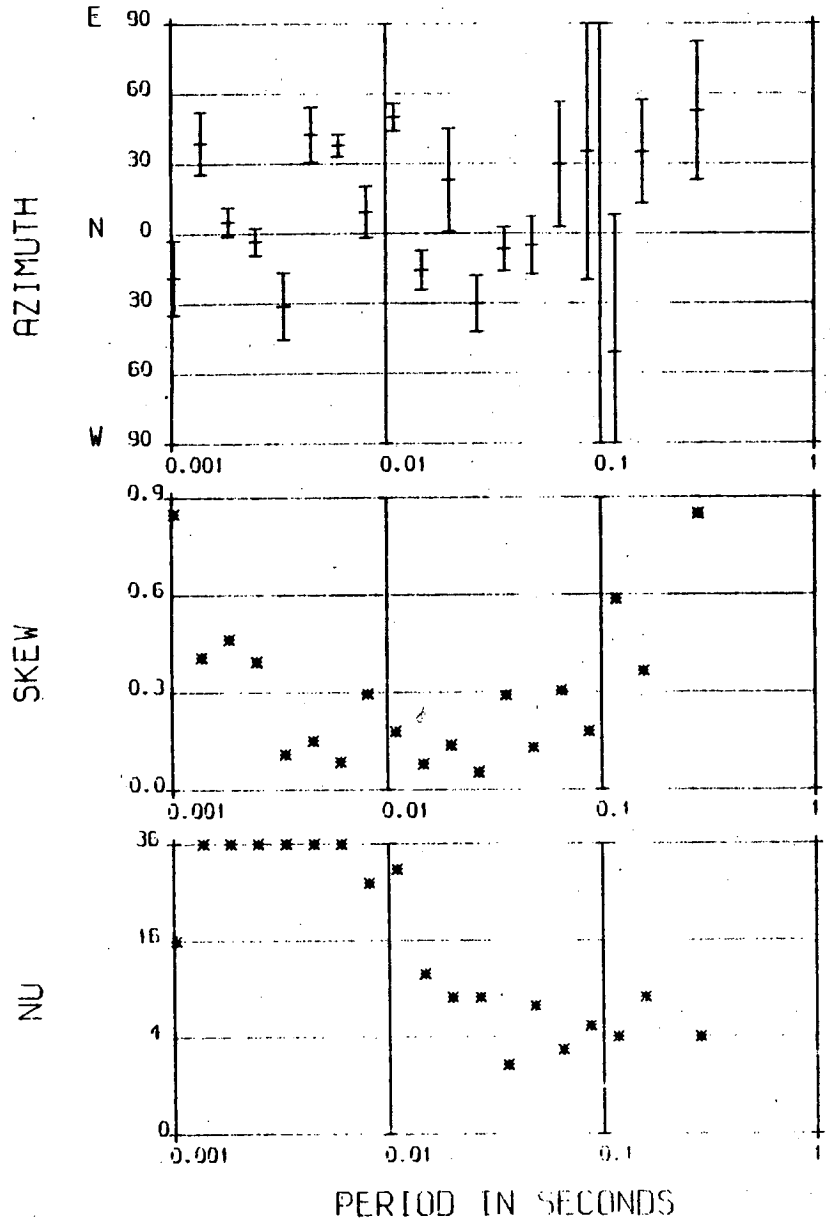
AZIMUTH
E 90
60
30
N 0
30
60
W 90
0.001
0.01
0.1
1
SKEW
0.9
0.6
0.3
0.0
NU
36
16
4
0
PERIOD IN SECONDS

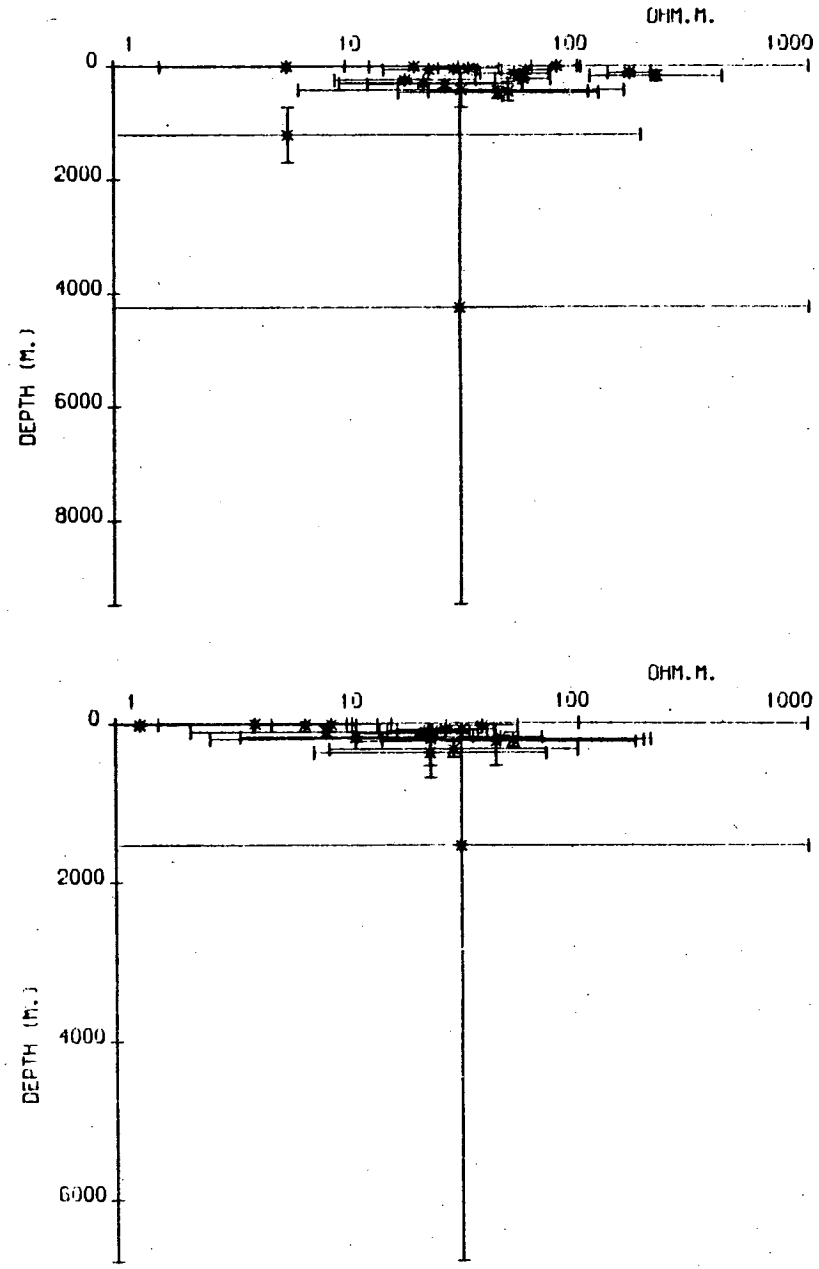
OHM.M.
1
10
100
1000
0
2000
4000
6000
8000
DEPTH (M.)
OHM.M.
DEPTH (M.)
Station 52

STATION 53

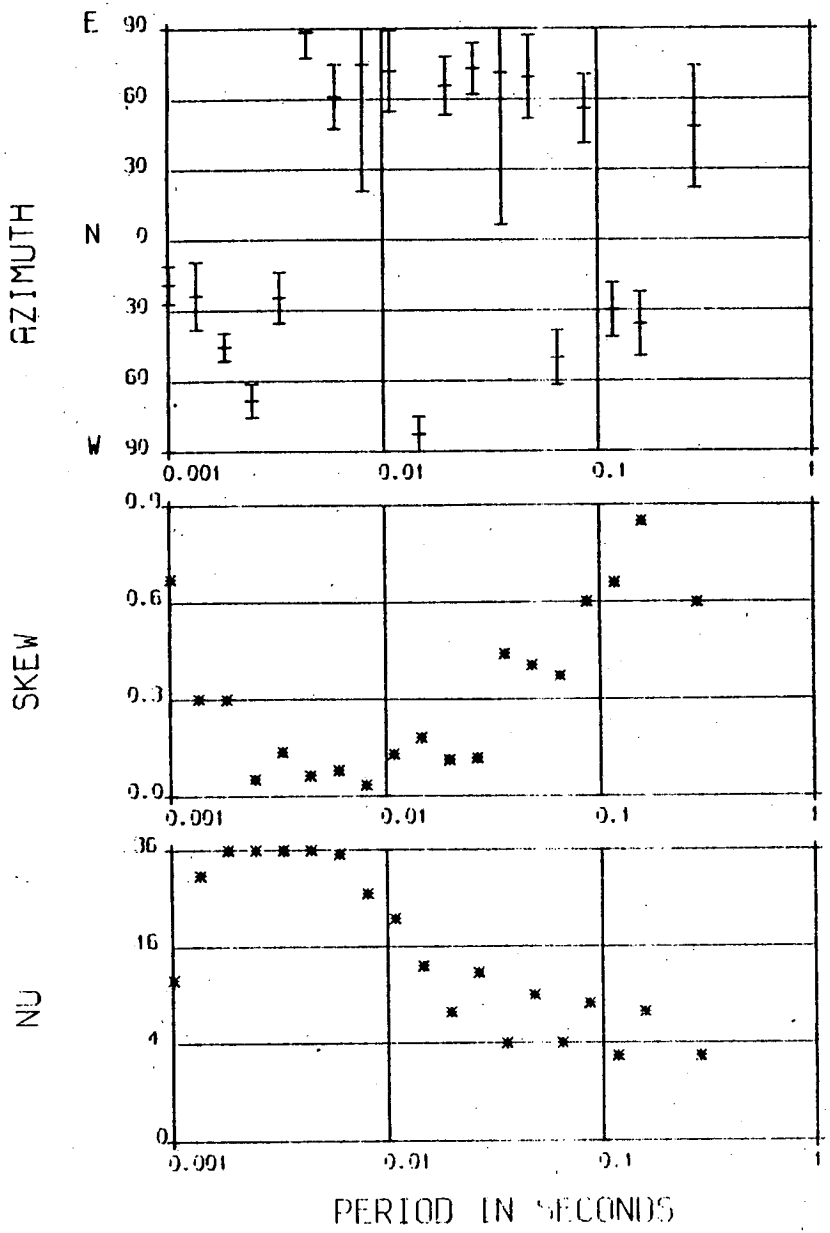

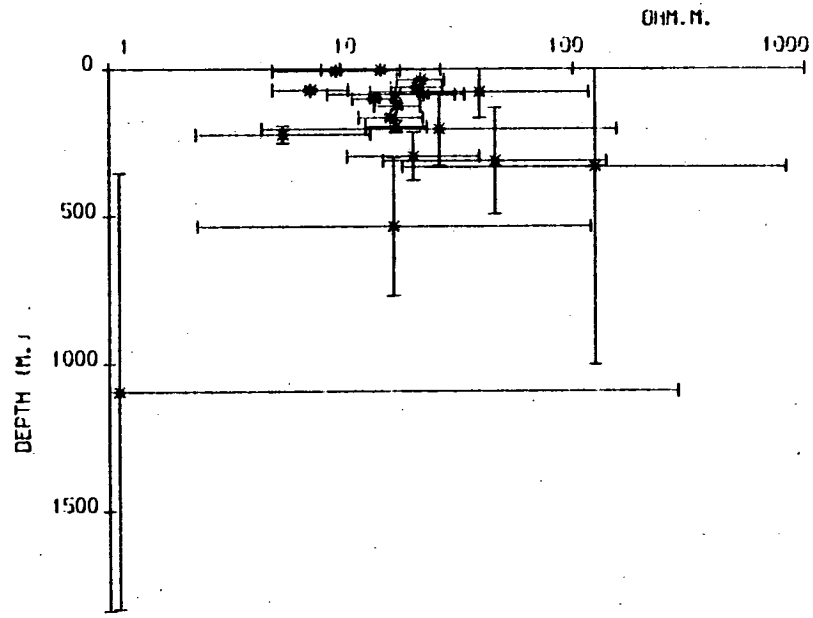

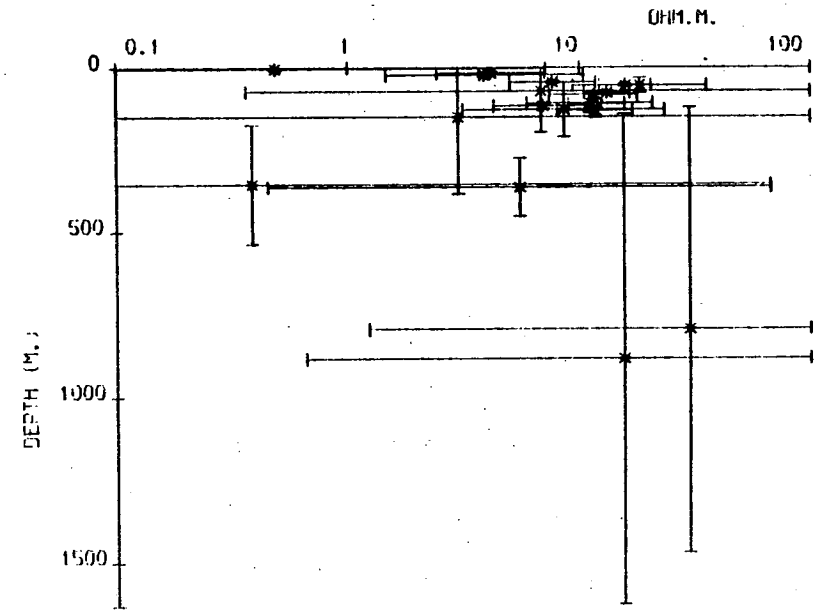

Station 53

STATION 54

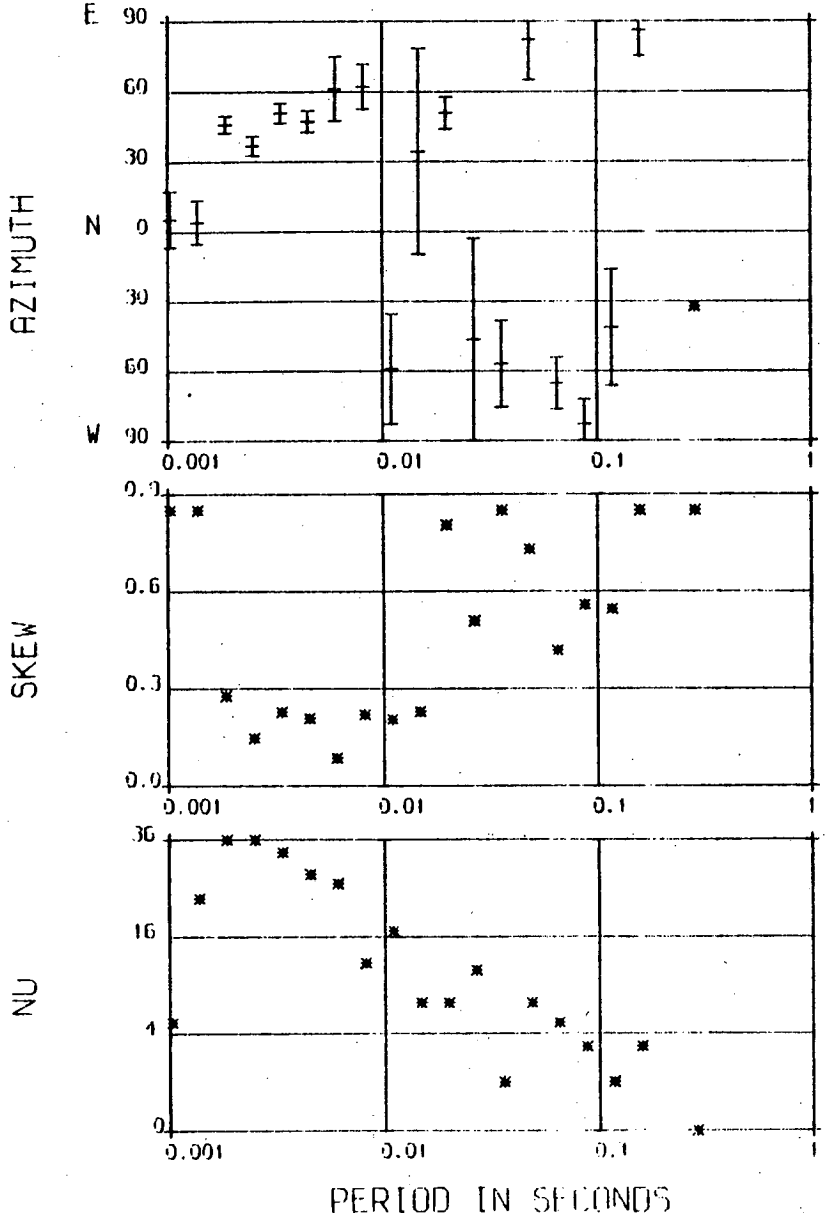

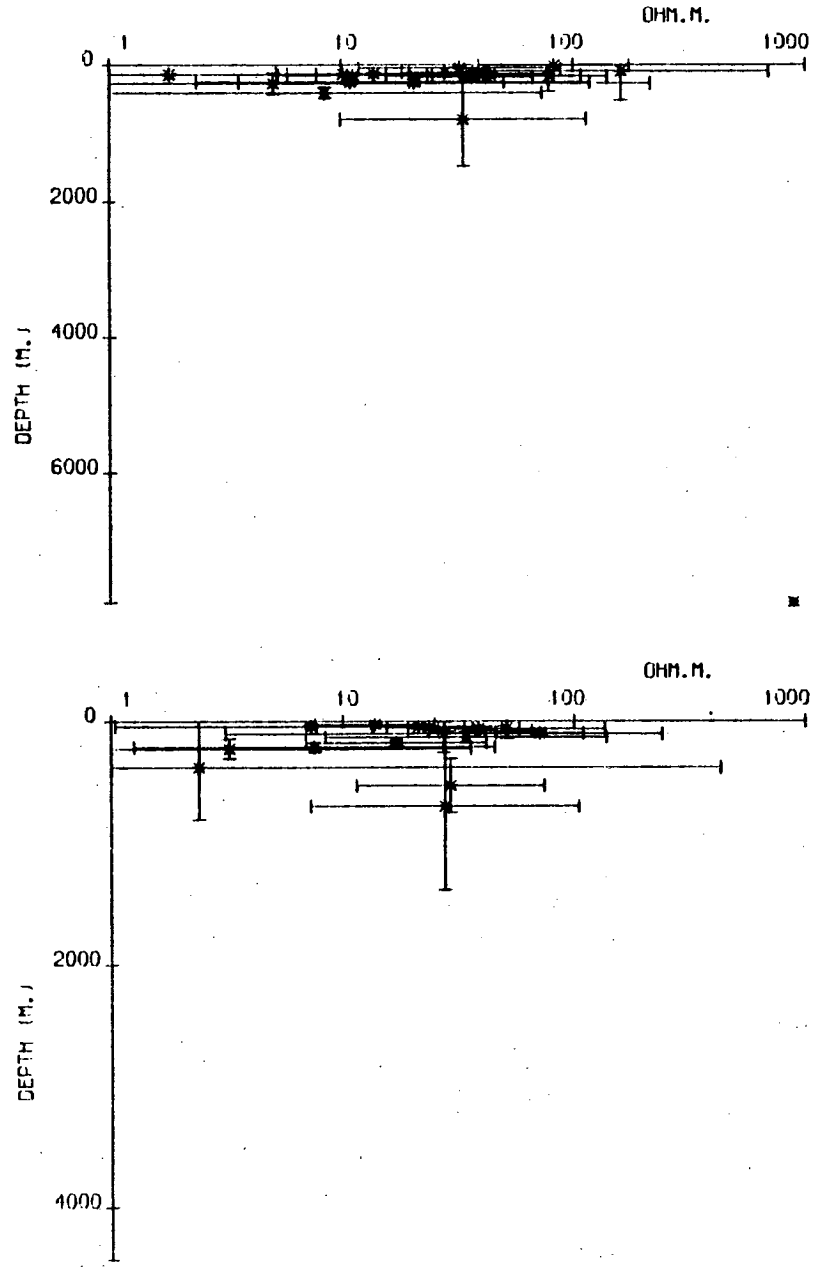

Station 54

STATION 55

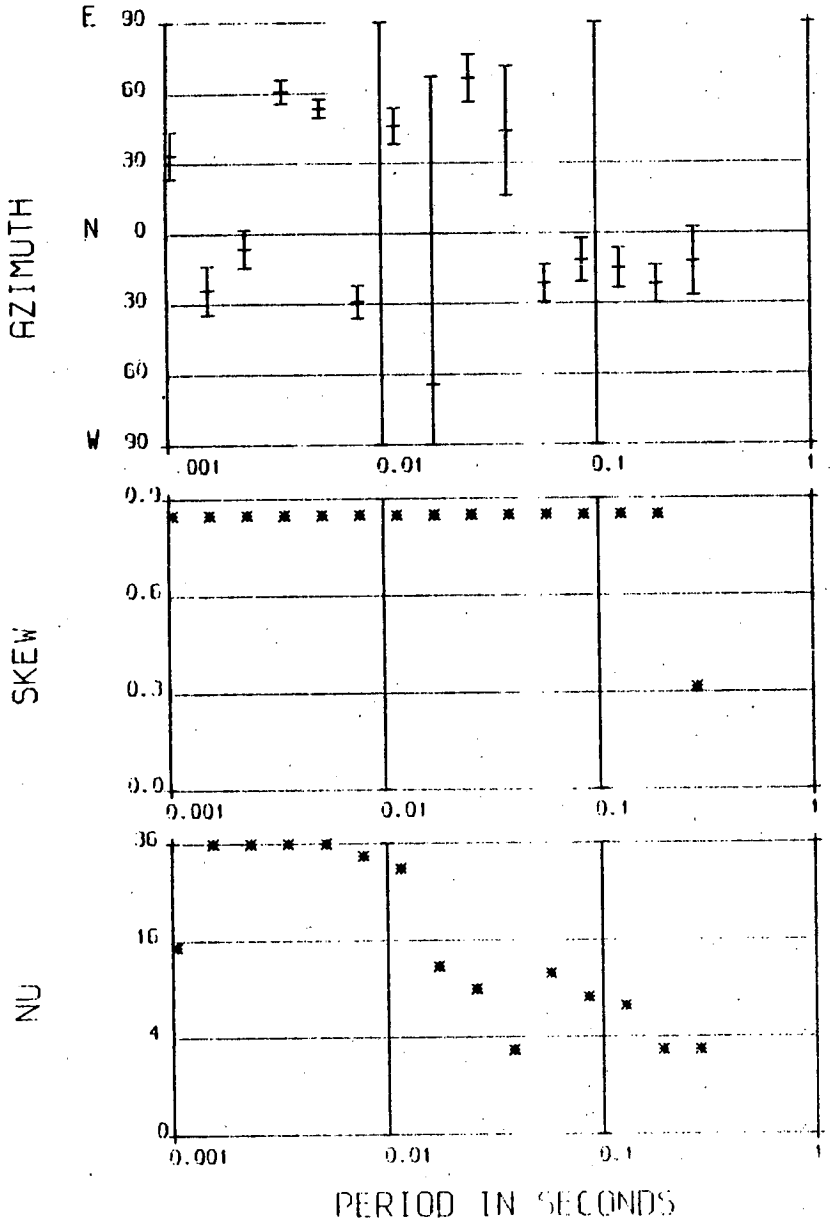

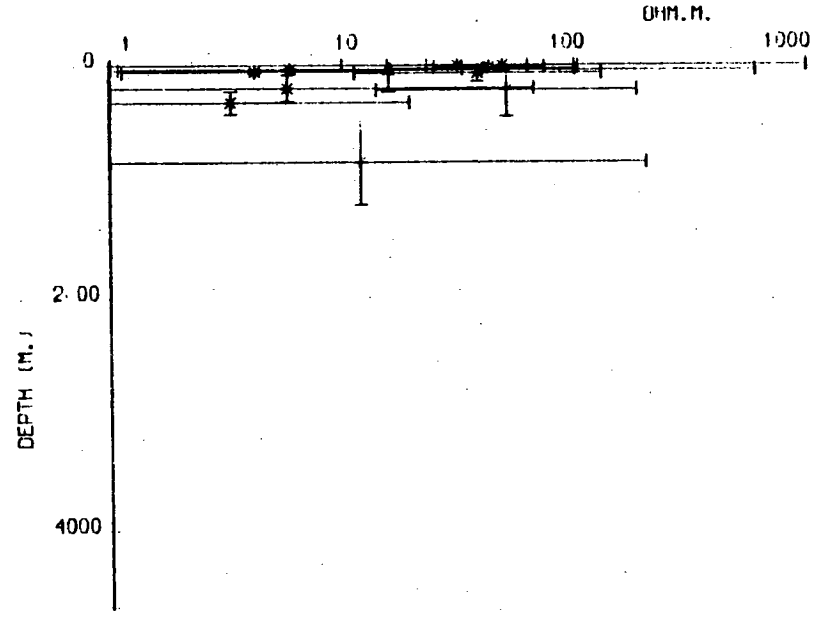

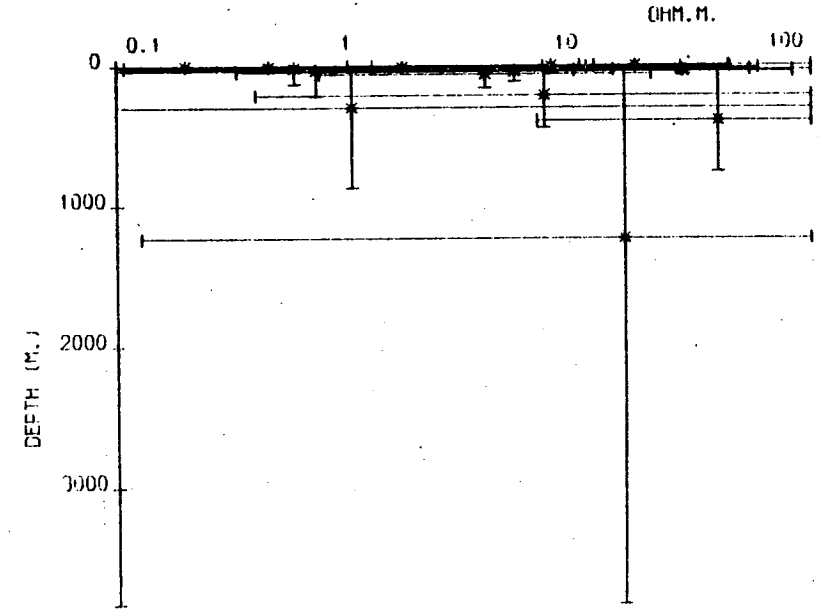

Station 55

STATION 56

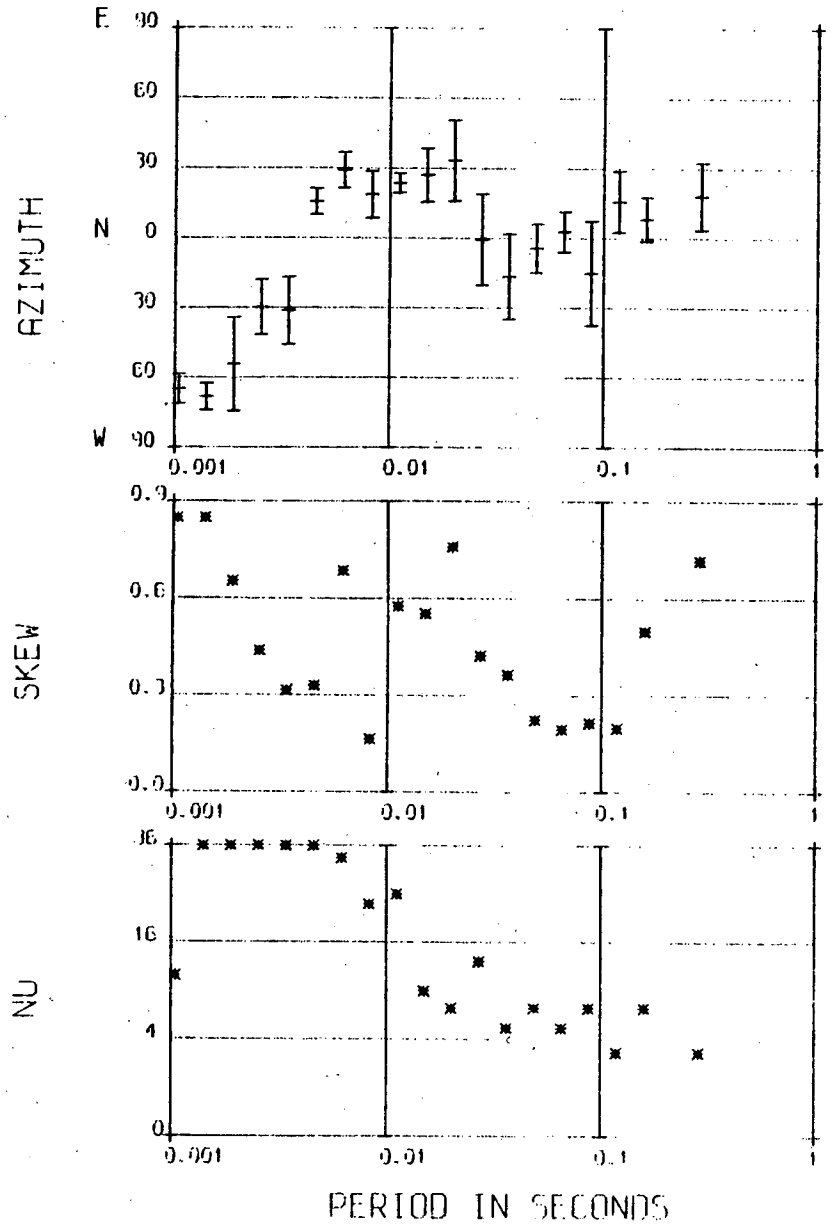

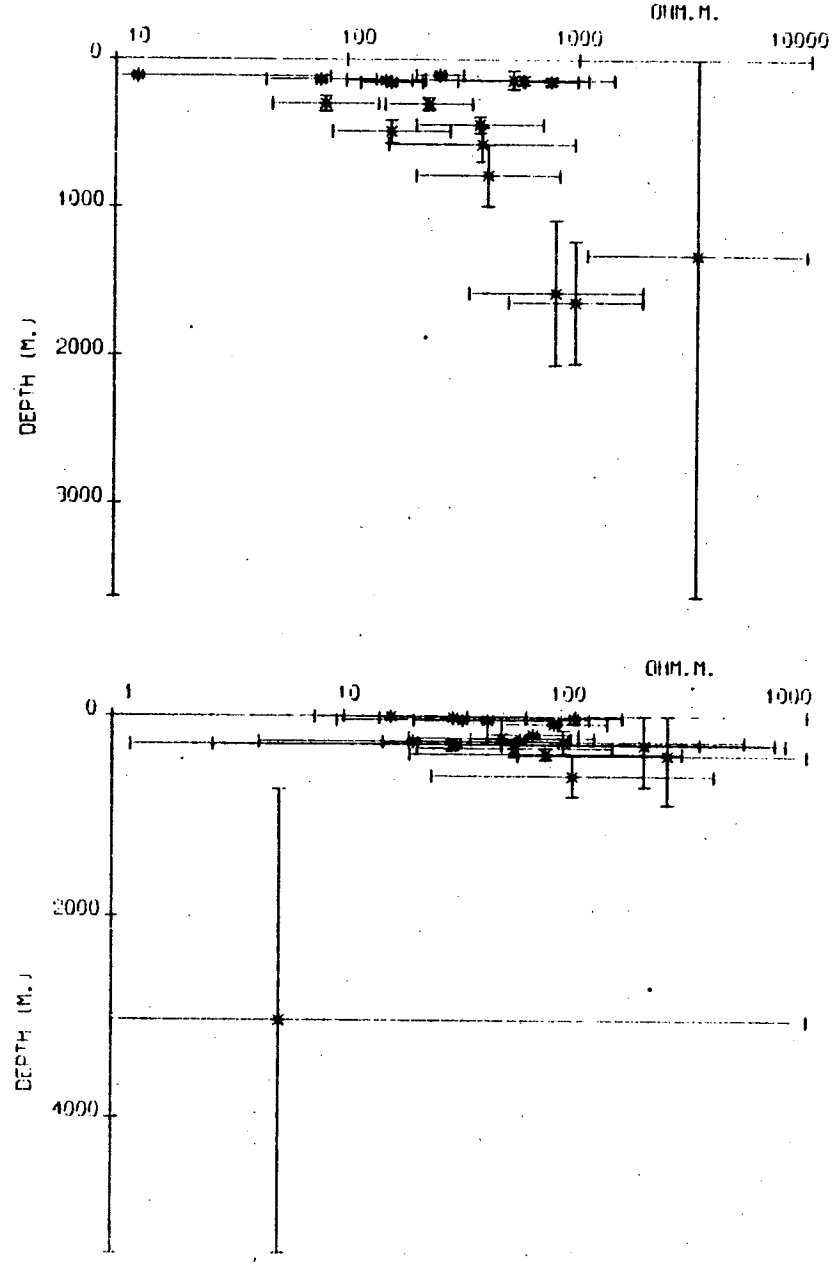

Station 56

STATION 57

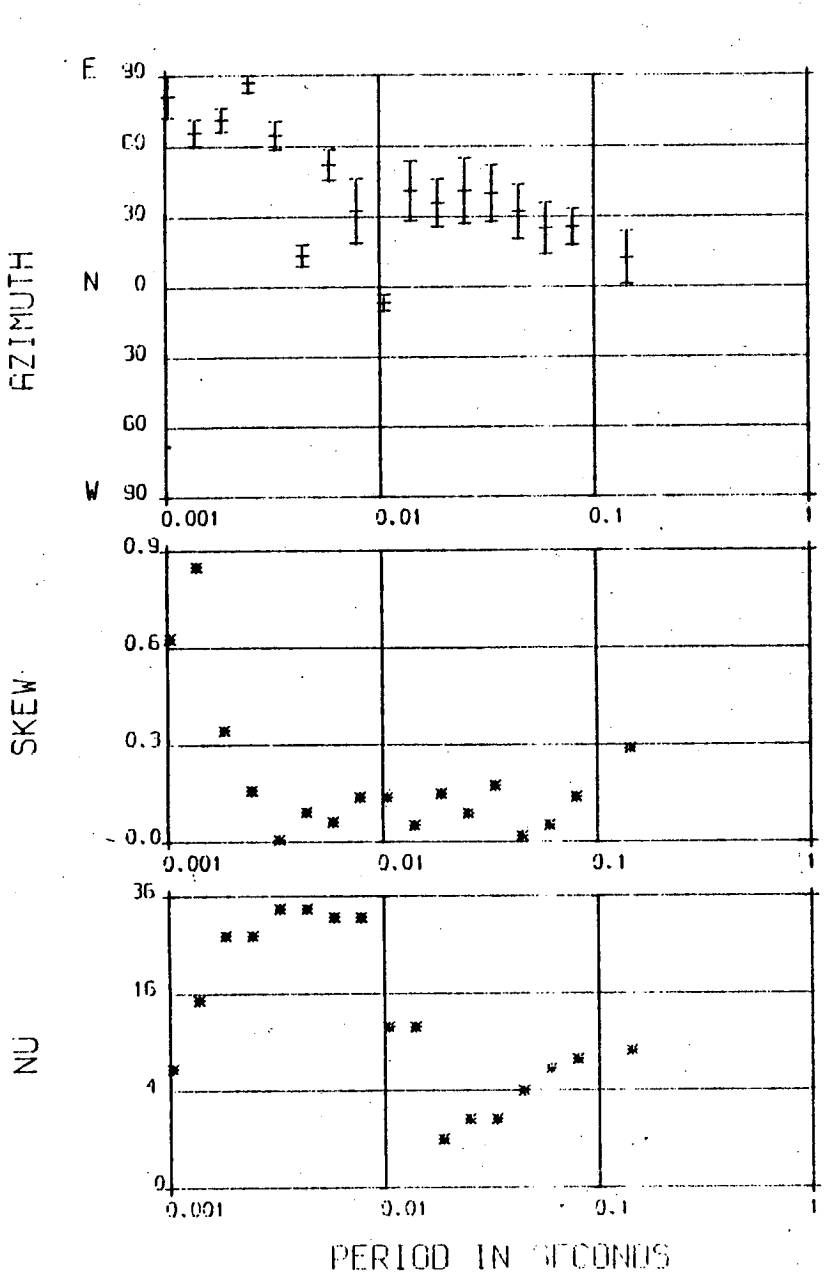

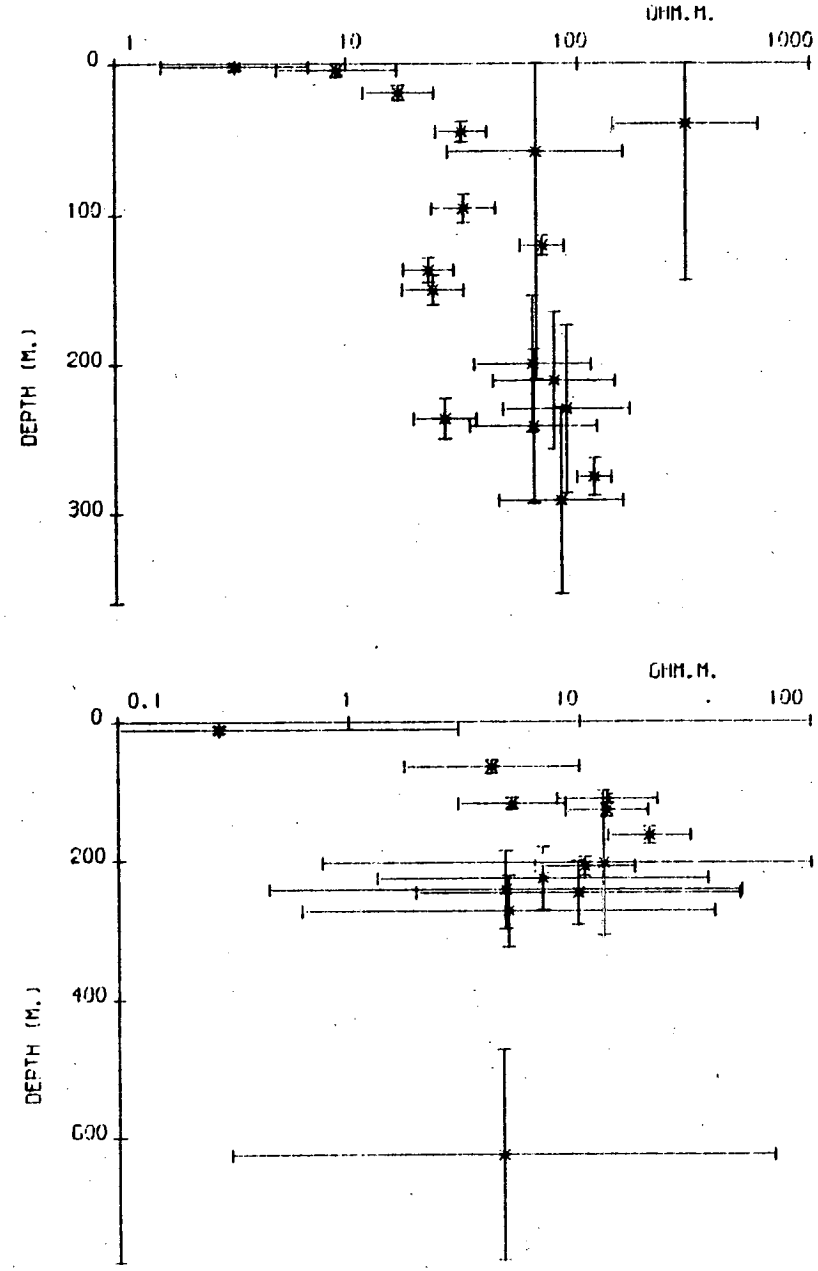

Station 57

STATION 58

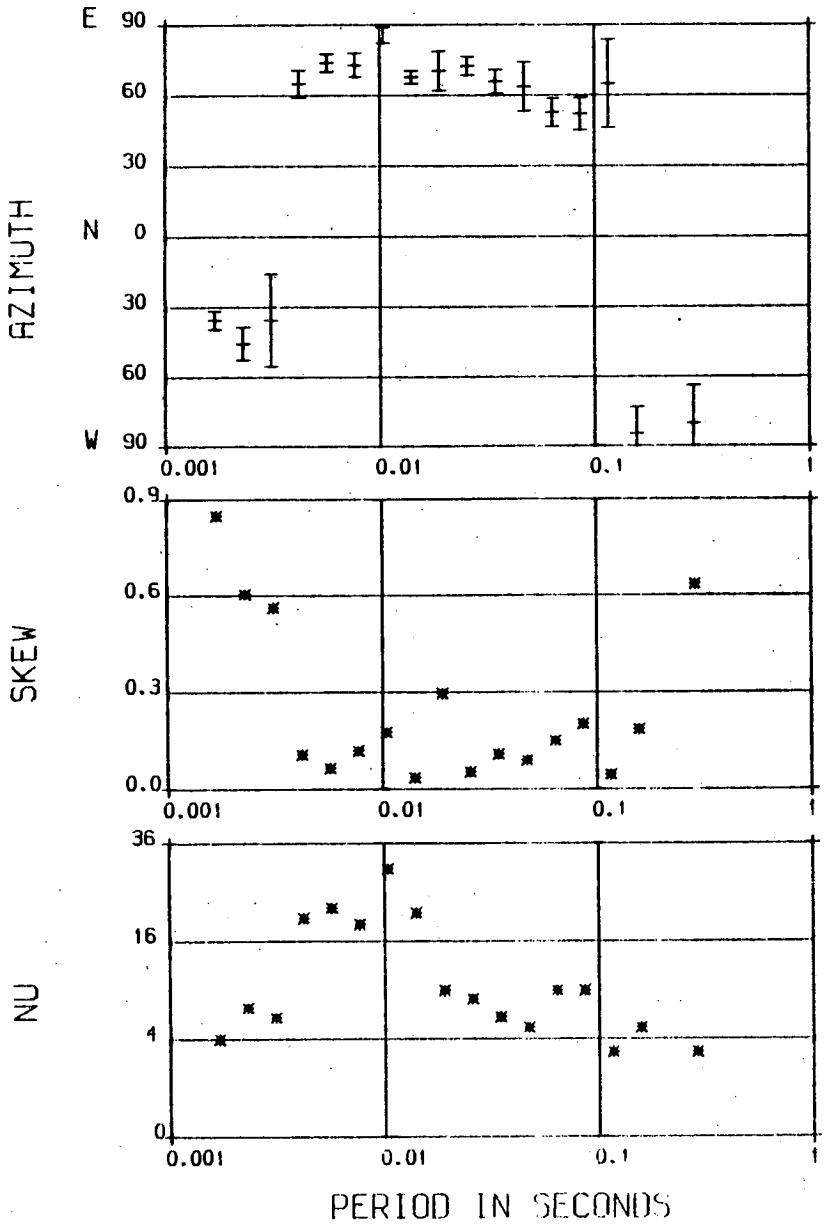

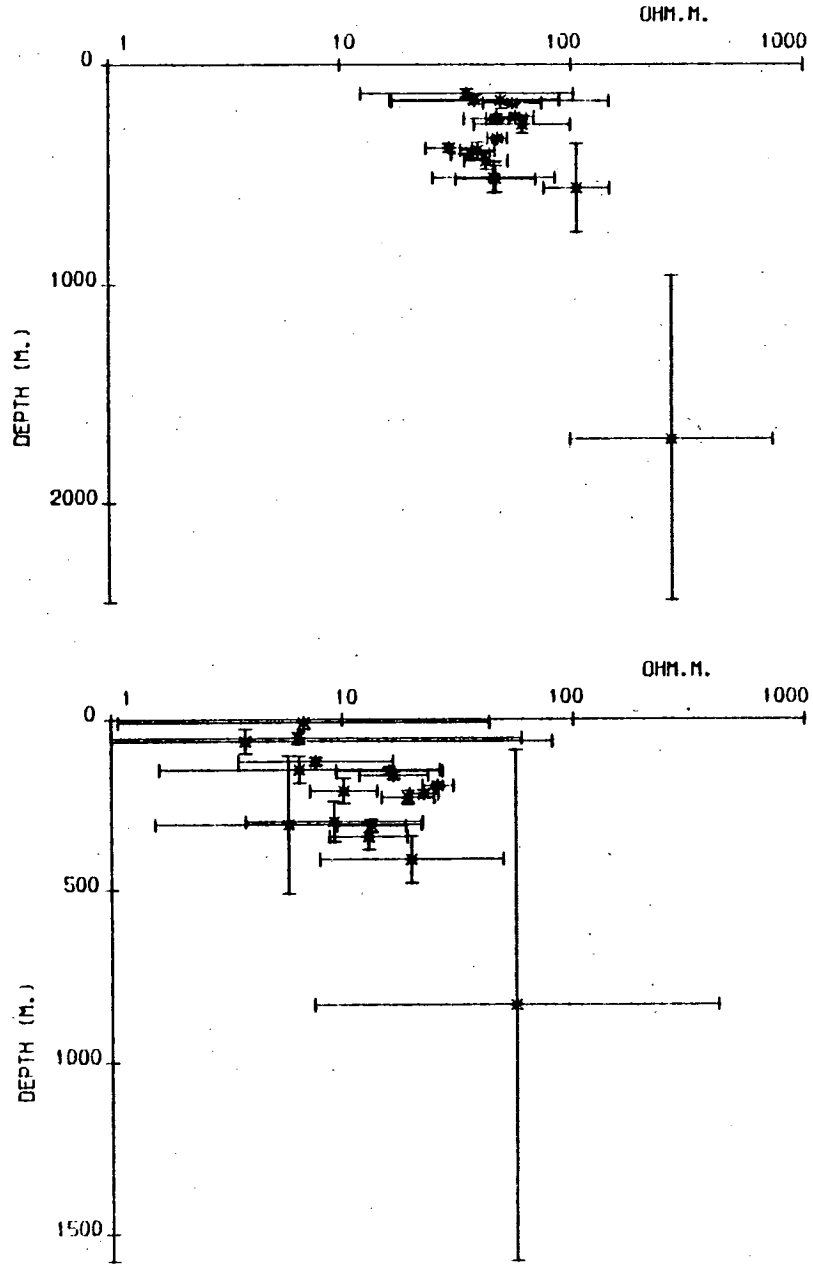

Station 58

STATION 59

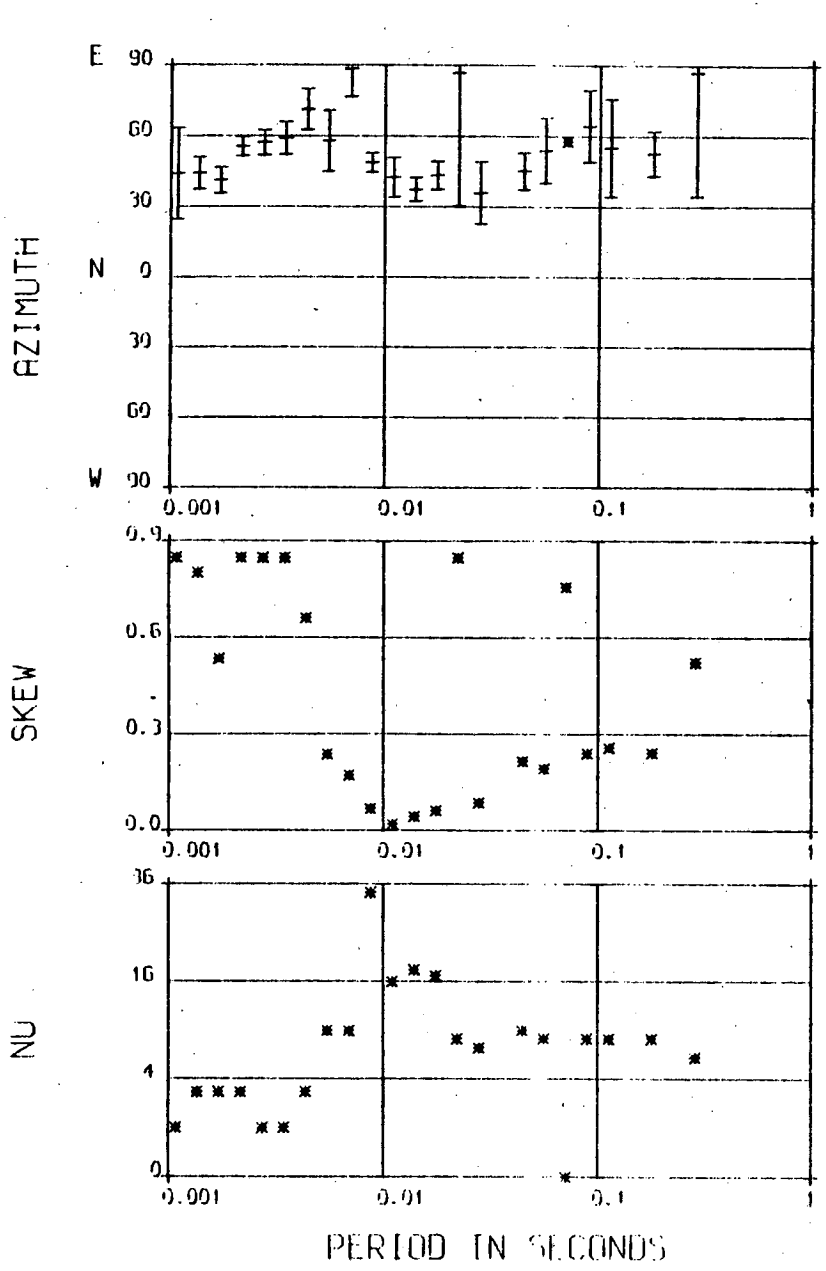

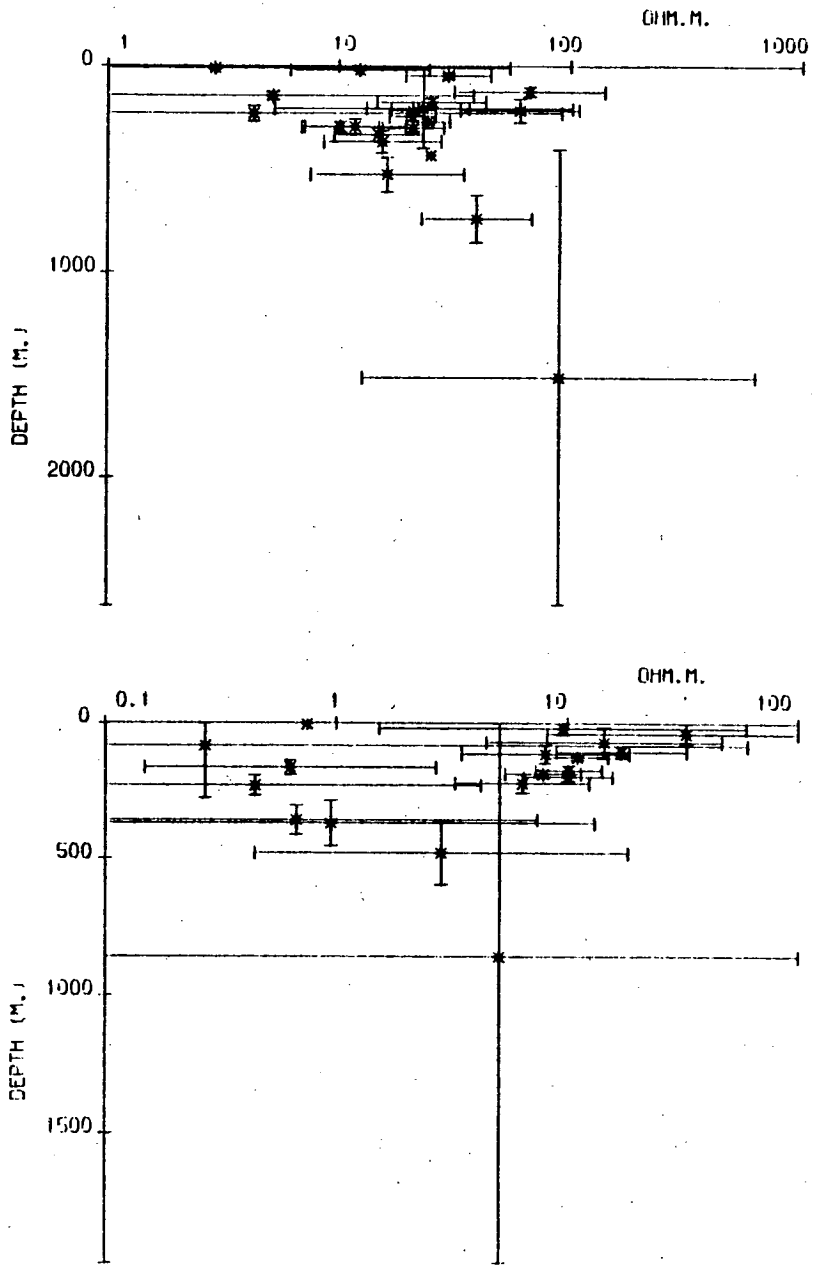

Station 59

STATION 60

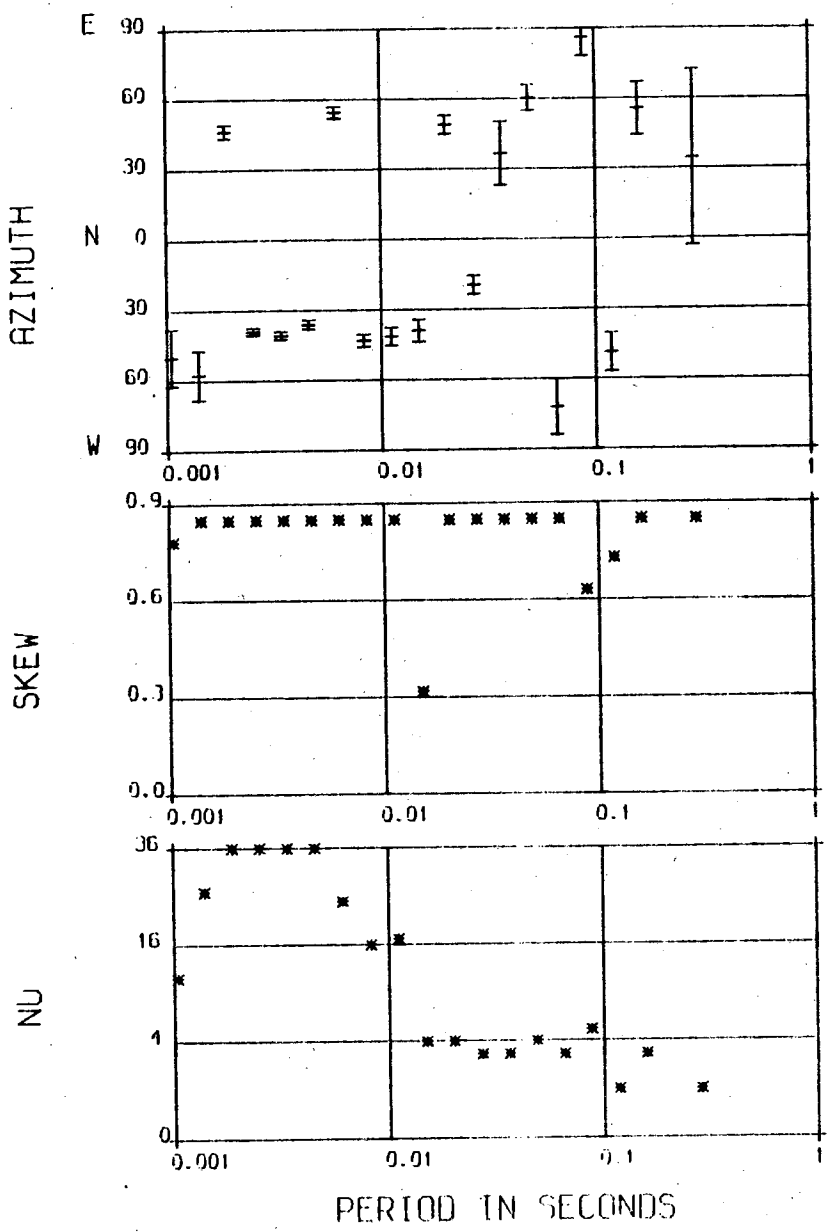

STATION 60

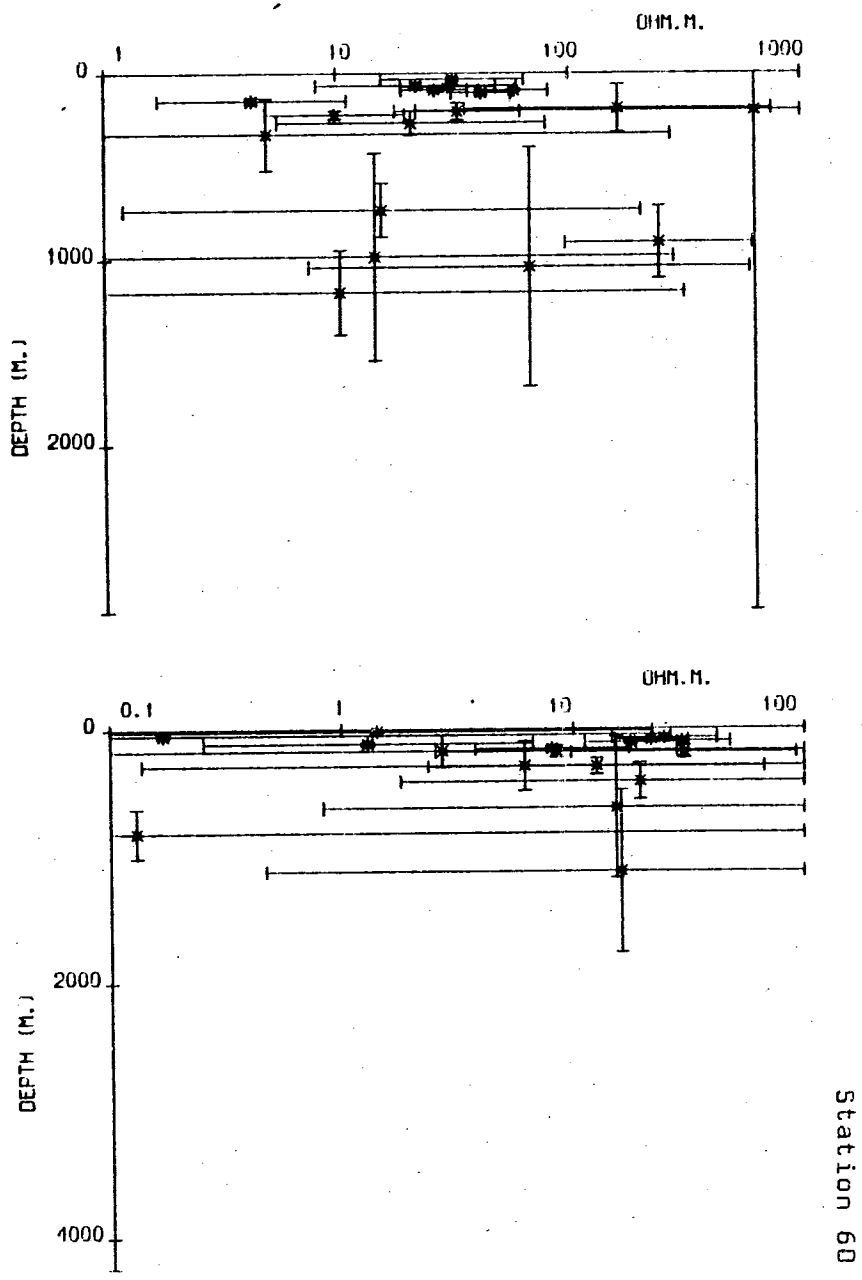

Station 60

STATION 61

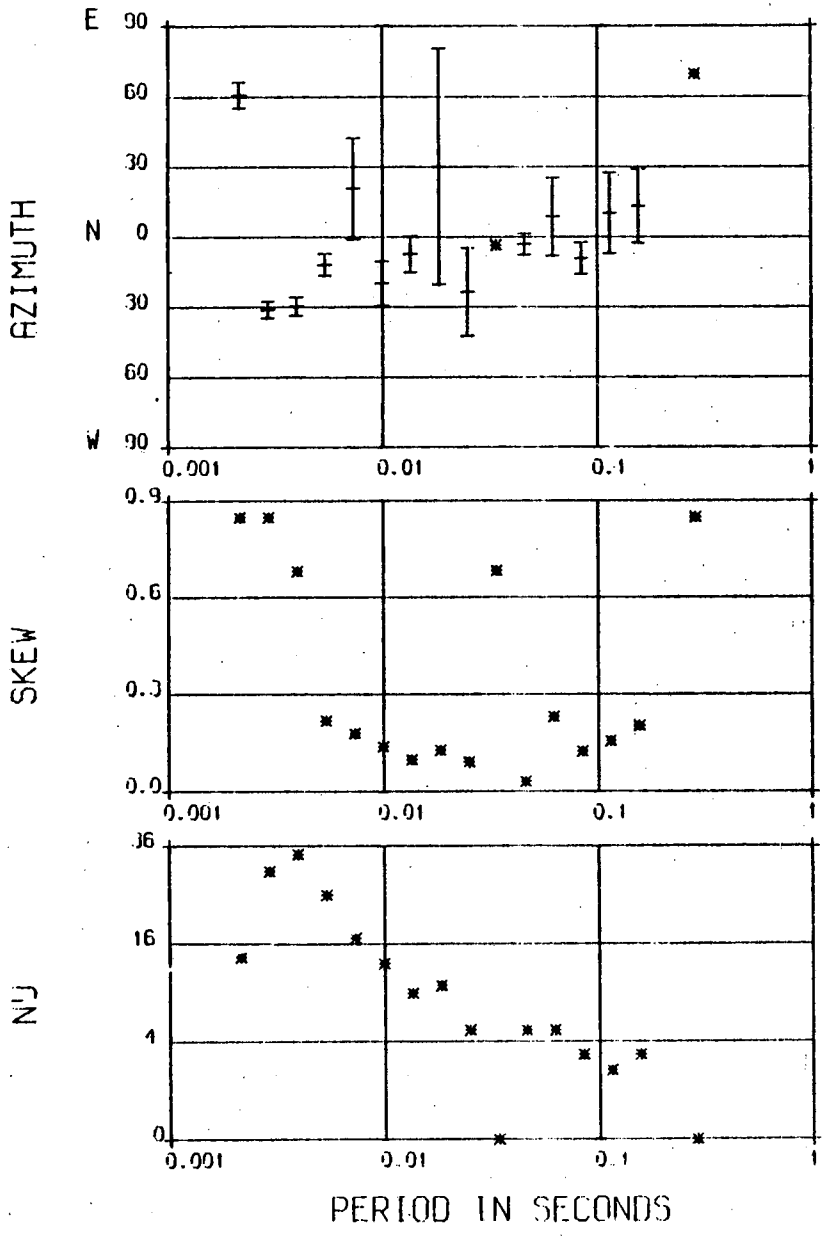
AZIMUTH
E 90
60
30
N 0
30
60
W 90
0.001
0.01
0.1
1
SKEW
0.9
0.6
0.3
0.0
NU
16
4
0
PERIOD IN SECONDS

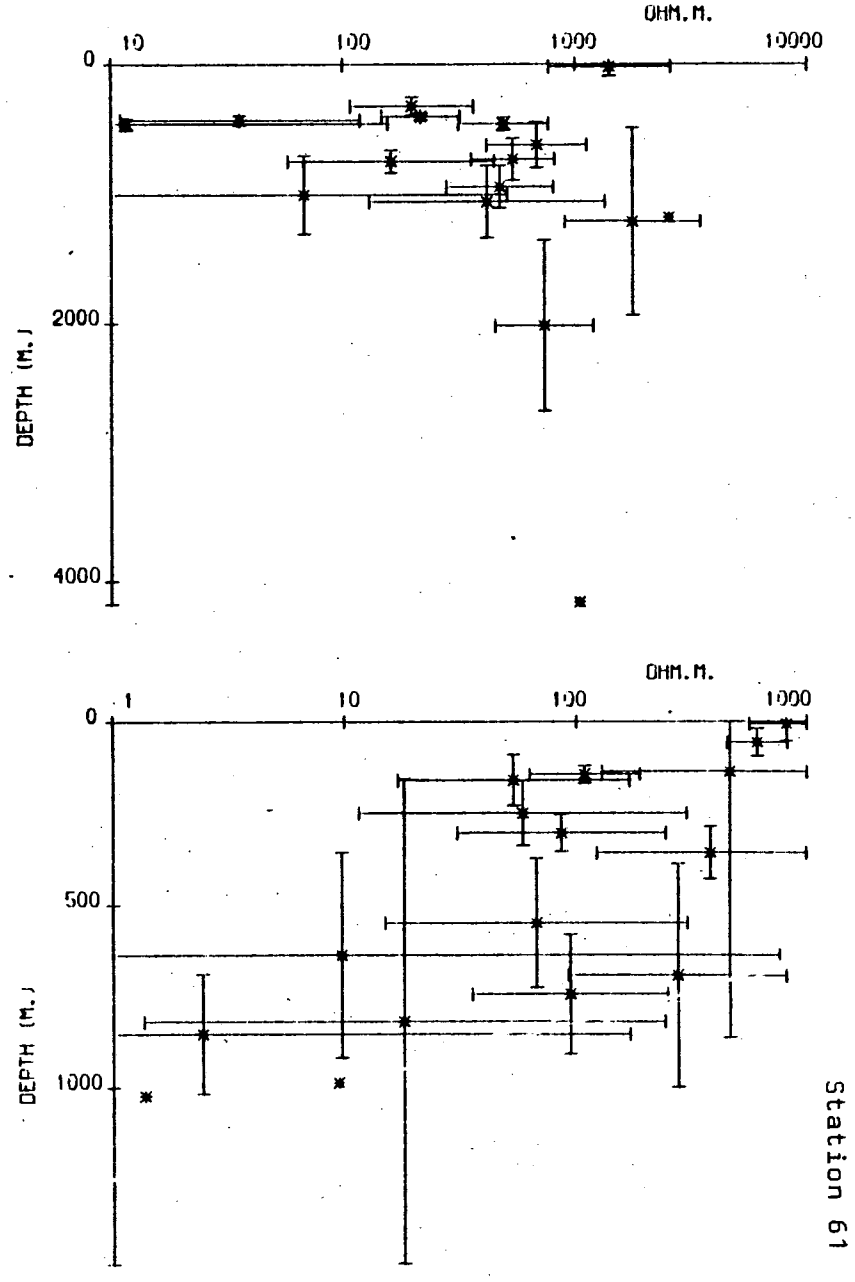
OHM.M.
10
100
1000
10000
0
2000
4000
DEPTH (M.)
OHM.M.
1
10
100
1000
0
500
1000
DEPTH (M.)
Station 61

STATION 62

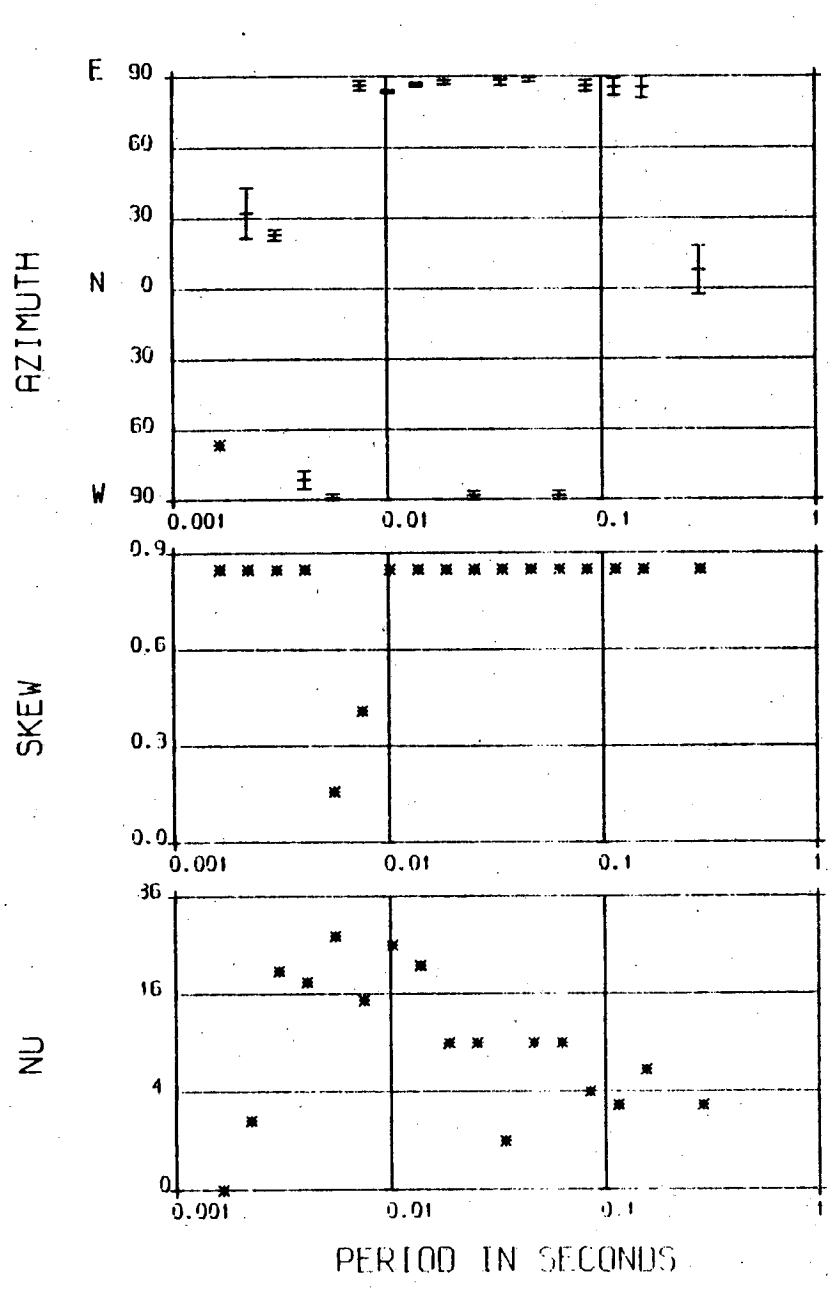

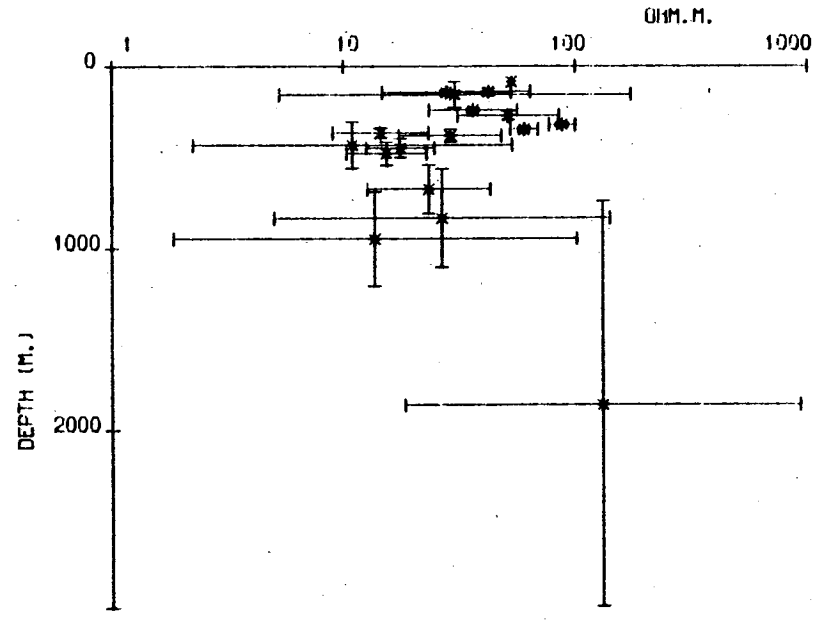

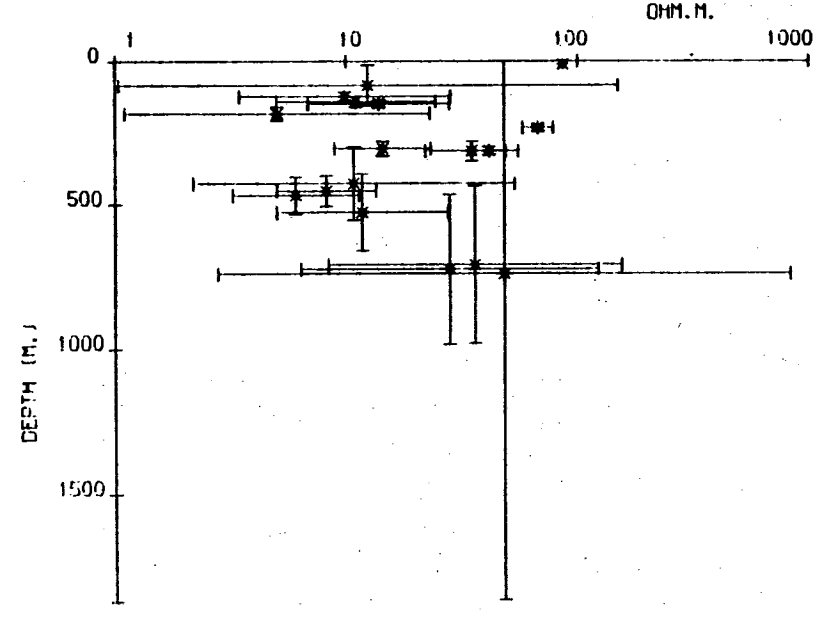

Station 62

STATION 63

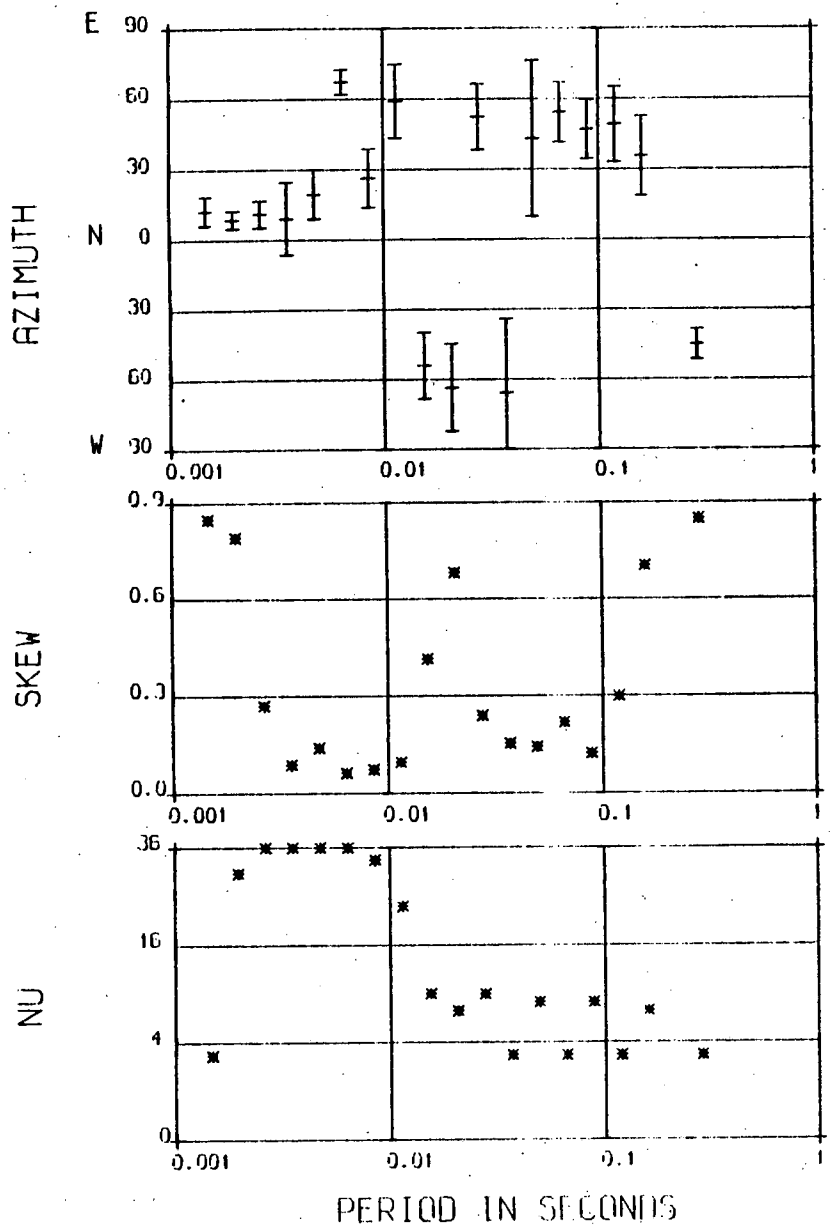

STATION 63

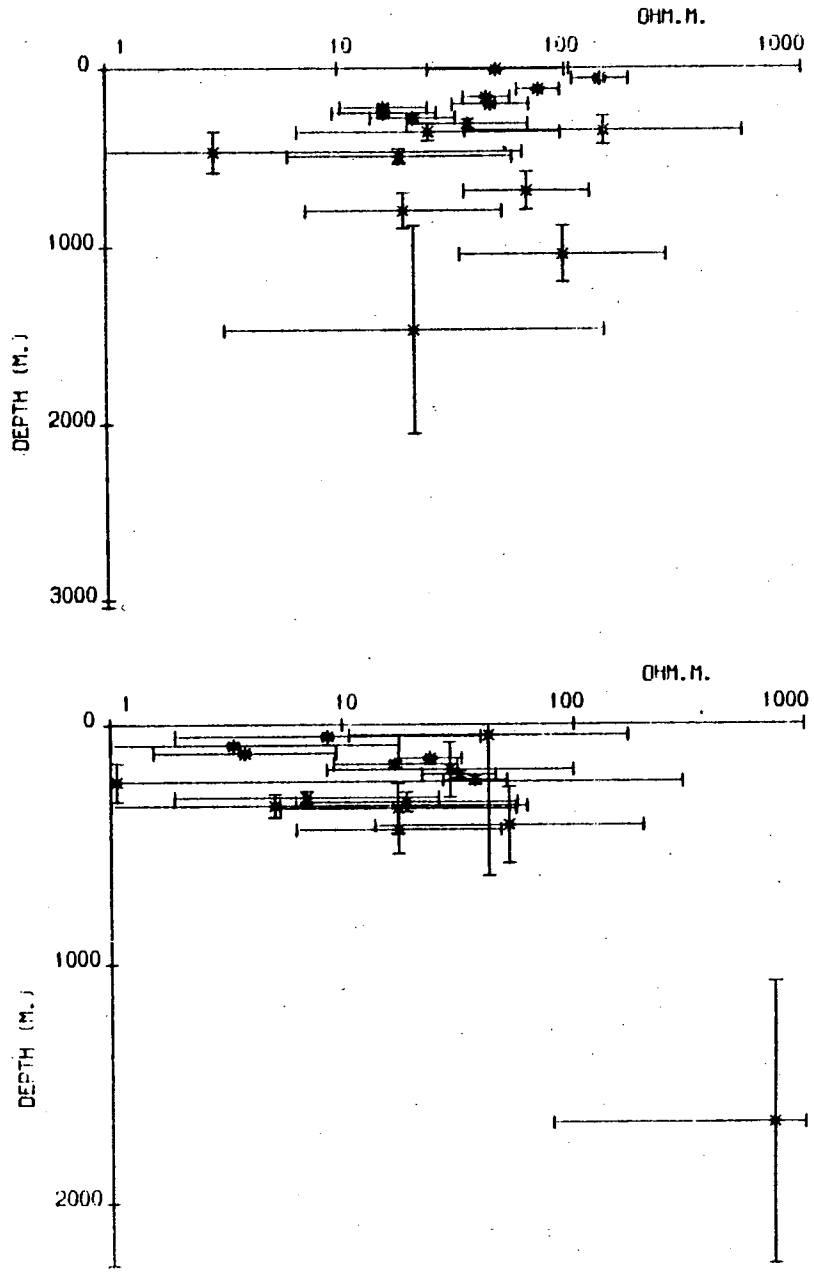

Station 63

REFERENCES

Airy, G.B., 1868. Comparison of magnetic disturbances recorded by the self-registering magnetometers at the Royal Observatory, Greenwich with magnetic disturbances deduced from the corresponding terrestrial galvanic currents recorded by the self registering galvanometer of the Royal Observatory. Phil. Trans. Roy. Soc. Lond., v. 158, 465.

Ander, M.E., 1981. AMT/MT study of the Jemez Lineament, New Mexico. Paper presented at 4th I.A.G.A. Sci. Ass., Edinburgh, Scotland.

Archie, G.E., 1942. The electrical resistivity log as an aid in determining some reservoir characteristics. Trans. A.I.M.E., v.146, 54-62.

Ashour, A.A., 1973. Theoretical models for electromagnetic induction in the oceans. Phys. Earth Plan. Int., v. 7, 303-312.

Bamford, D., Nunn, K., Prodehl, C. and Jacob, B., 1978. Lispb - IV: Crustal structure of northern Britain. Geoph. J. R. Astr. Soc., v. 54, 43-60.

Banks, R.J., 1969. Geomagnetic variations and the electrical conductivity of the upper mantle. Geoph. J. R. Astr. Soc., v. 17, 457-487.

Banks, R.J., 1973. Data processing and interpretation in geomagnetic deep sounding. Phys. Earth Planet. Int., v. 7, 1-10.

Banks, R.J., 1979. Current developments in audio-frequency magnetotelluric and controlled-source electromagnetic souding. Report to the N.E.R.C.

Banks, R.J. and Ottey, P., 1974. Geomagnetic deep souding in and around the Kenya Rift Valley. Geoph. J. R. Astr. Soc., v. 36, 321-335.

Beamish, D., 1976. A geomagnetic deep sounding array study of East Africa. Ph. D. thesis, Univ.Lancaster, U.K.

Beamish, D., 1979. Source field effects on transfer functions at mid-latitudes. Geoph. J. R. Astr. Soc., v. 58, 117-134.

Beamish, D., 1981. Magnetometers across a granite. Paper presented at 4th I.A.G.A. Sci. Ass., Edinburgh, Scotland.

Beamish, D., 1982. The time-dependence of electromagnetic response functions. Geoph. Surv., v. 4, 405-434.

Bendat, J.S. and Piersol, A.G., 1971. Random data: Analysis and measurement procedures., Wiley-Interscience, N.Y.

Benderitter, Y., Hérisson, C., Korhonen, H. and Pernu, T., 1978. Magneto-telluric experiments in northern Finland. Geoph. Prosp., v. 26, 562-571.

Bennett, D.J. and Lilley, F.E.M., 1972. Horizontal polarisation in array studies of anomalous geomagnetic variations. Nature, Physical Science, v. 237, 8-9.

Berktold, A., Kemmerle, K., Dawes, G.J.K., Hutton, V.R.S., McGavigan, T., Finzi, E., Norinelli, A., Spitz, S., Zaja, A. and Mosnier, J., 1981. Comparative electromagnetic studies in the geothermal field of Travale, Tuscany. Paper presented at 4th I.A.G.A. Sci. Ass., Edinburgh, Scotland.

Berktold, A., Kemmerle, K. and Neurieder, P., 1980. Investigation of a geothermal anomaly in S.W. Germany by different geophysical methods. Paper presented at 5th Workshop El. Ind. Earth Moon, Istanbul.

Berktold, A., Kemmerle, K. and Neurieder, P., 1980. Magneto-telluric measurements and geomagnetic depth sounding in the area of the Urach geothermal anomaly. Proc. E. C. Geoth. Energy Res. Reidel Publishing Co., 911-920.

Bobrov, V.N., 1971. Five component field electromagnetic variation station. Geomag. Aeronom., v. 11, 432-435.

Bott, M.H.P., and Masson-Smith, D., 1957(a). The geological interpretation of a gravity survey of the Alston block and the Durham coalfield. Q. J. Geol. Soc., v. 113, 93-117.

Bott, M.H.P., and Masson-Smith, D., 1957(b). Interpretation of a vertical field magnetic survey in the north-east England. Q. J. Geol. Soc., v. 113, 119-129.

Bott, M.H.P., and Johnson, G.A.L., 1968. Temperature measurements in the Woodland borehole. Bull. Geol. Surv. G. B., v. 28, 37.

Bott, M.H.P., Johnson, G.A.L., Mansfield, J. and Wheilden, J., 1972. Terrestrial heatflow in north-east England. Geoph. J. R. Astr. Soc., v. 27, 277-288.

Brace, W.F., 1971. Resistivity of saturated crustal rocks to 40 km based on laboratory measurements. A.G.U. Monogr., v. 14, 243-255.

Brace, W.F., Orange, A.S. and Madden, T.R., 1965. The effect of pressure on the electrical resistivity of water-saturated crystaline rocks. J. Geoph. Res., v. 70, 5669-5678.

Brewitt-Taylor, C.R. and Weaver, J.T., 1976. On the finite difference solution of two-dimensional induction problems. Geoph. J. R. Astr. Soc., v. 47, 375-396.

Brown, G.C., Cassidy, J., Oxburgh, E.R., Plant, J., Sabine, P.A. and Watson, J.V., 1980. Basement heatflow and metaliferous mineralisation in England and Wales. Nature, v. 288, 657-659.

Cagniard, L., 1953. Basic theory of the magnetotelluric method of geophysical prospecting. Geophysics, v. 18, 605-635.

Cantwell, I., 1960. Detection and analysis of low-frequency magnetotelluric signals. Ph.D. thesis, M.I.T., 171.

Clarke, J., Goubau, W.M. and Ketcher, M.B., 1976. Tunnel junction D.C. Squid : Fabrication, operation and performance. J. Low Temp. Phys., v. 25, 99-144.

Cooley, J.W. and Tukey, J.W., 1965. An algorithm for the machine calculations of complex Fourier Series. Mathematics of computations, v. 19, 297-307.

Dawes, G.J.K., 1980. Computer Programme Library. Internal publication, Department of Geophysics, Univ. Edin.

Dawes, G.J.K., 1981. An automatic wide-band magnetotelluric data acquisition system. Paper presented at 4th I.A.G.A. Sci. Ass., Edinburgh, Scotland.

D'Erceville, I. and Kunetz, E., 1962. The effect of a fault on the Earth's natural electromagnetic field. Geoph., v. 27, 651-665.

Dodson, M.H. and Moorbath, S., 1961. Isotopic ages of the Weardale granite. Nature, v. 190. 900.

Dosso, H.W., 1966. A plane wave analogue modelfor studying electromagnetic variations. Can. J. Phys., v. 44, 67-80.

Dosso, H.W., 1973. A review of analogue model studies of the coast effect. Phys. Earth Planet. Int., v. 7, 294-302.

Duba, A., 1976. Are laboratory electrical conductivity data relevant to the Earth? Acta Geodaet. Geoph. Mont., Acad. Sci. Hung., v. 11, 485-495.

Dunham, K.C., 1931. Mineral deposits of the Northern Pennines. Proc. Geol. Soc., v. 13, 274-281.

Dunham, K.C., 1948. Geology of the Northern Pennine Orefield. Memo. Geol. Surv. G. B. H.M.S.O.

Dunham, K.C., Bott, M.H.P., Johnson, G.A.L. and Hodge, B.L., 1961. Granite beneath the Northern Pennines. Nature, v. 190, 899-900.

Dunham, K.C., Dunham, A.C., Hodge, B.C. and Johnson, G.A.L., 1965. Granite beneath Viséan sediments with mineralisation at Rookhope, northern Pennines. Q.J. Geol. Soc. Lond., v. 121, 383-417.

Eastwood, T., 1953. Northern England. British regional geology handbook. 3rd edition, Her Majesty's Stationery Office.

Edwards, R.N., 1976. Electrical methods for the study of regional crustal conductivity anomalies. Acta Geodaet. Geoph. Mont., Acad. Sci. Hung., v. 11, 399-425.

Edwards, R.N., 1980. A grounded vertical long wire source system for plane wave magnetotelluric analog modeling. Geophysics, v. 45, 1523-1529

Edwards, R.N. and Greenhouse, J.P., 1975. Geomagnetic variations in the Eastern United States : evidence for a highly conducting lower crust? Science, v. 188, 726-728.

Everett, J.E. and Hyndman, R.D., 1967. Magnetotelluric investigations in south-western Australia. Phys. Earth Planet. Int., v. 1, 49-54.

Filloux, J.H., 1973. Techniques and instrumentation for study of natural electromagnetic induction at sea. Phys. Earth Planet. Int., v. 7, 323-338.

Fischer, G., 1980. Review of magnetotelluric observational techniques on land. Paper presented at 5th Workshop El. Ind. Earth Moon, Istanbul.

Fischer, G., 1982. Magnetotelluric observational techniques on land. Geoph. Surv., v. 4, 373-393.

Fischer, G. and Le Quang, B.V., 1980. One dimensional MT inversion : A simple analytic scheme. Paper presented at 5th Workshop El. Ind. Earth Moon, Istanbul.

Fischer, G., Schnegg, P.A., Dawes, G.J.K. and Hutton, V.R.S., 1981. A preliminary AMT survey of the Travale geothermal field, Tuscany, Italy. Paper presented at 4th I.A.G.A. Sci. Ass., Edinburgh, Scotland.

Fitch, F.J. and Miller, J.A., 1965. Age of the Weardale granite. Nature, v. 208, 743-745.

Fournier, H.G., 1966. Essai d'on historique des connaissances magnetotelluriquer. Note 17, Institt. de Physique du Globe, Universite de Paris.

Frischknecht, F.C., 1971. Electromagnetic scale modeling in Electromagnetic probing in geophysics. J. R. Wait, Ed., Golden Press, Boulder.

Gamble, T.D., Goubau, W.M. and Clarke, J., 1979. Magnetotellurics with a remote magnetic reference. Geophysics, v. 44, 53-68.

Goldstein, M.A. and Strangway, D.W., 1975. Audio/frequency magnetotellurics with a grounded electric dipole source. Geophysics, v. 40, 669-683.

Goldstein, N.E., Norris, R.A. and Wilt, M.J., 1978. Assessment of surface geophysical methods in geothermal exploration, and recommendations for future research. L.B.L. Report, 6815.

Goubau, W.M., Gamble, T.D. and Clarke, J., 1978. Magnetotelluric data analysis : removal of bias. Geophysics, v. 43, 1157-1169.

Gough, D.I. and Reitzel, J.S., 1967. A portable 3-component magnetic variometer. J. Geomag. Geoelect., v. 19, 203-215.

Gregori, G.P. and Lanzerotti, L.J., 1980. Geomagnetic depth sounding by induction arrow representation : a review. To appear in Rev. Geoph. Space Phys.

Grillot, L.R., 1975. Calculation of the magnetotelluric tensor impedance : analysis of band-limited MT signal pairs. Geophysics, v. 40, 790-797.

Habberjam, G.M. and Thanassoulas, C., 1979. A deep resistivity sounding at Rookhope, Northern England. Trans. Roy. Soc., Edinburgh.

Harris, F.J., 1978. In the use of windows for harmonic analysis with the discrete Fourier transform. Proc. I.E.E.E., v. 66, 51-83.

Hermance, J.F., 1973. Processing of magnetotelluric data. Phys. Earth Plan. Int., v. 7, 349-364.

Hermance, J.F. and Grillot, L.R., 1970. Correlation of magnetotelluric, seismic and temperature data from Southwest Iceland. J. Geoph. Res., v. 75, 6582-6591.

Hewson-Browne, R.C. and Kendall, P.C., 1976. Magnetotelluric modelling and inversion in three-dimensions. Acta Geodaet. Geoph. Mont., Arad. Sci. Hung., v. 11, 427-446.

Hobbs, B.A., 1980. Model finding for the one dimensional magnetotelluric problem using inverse theory. Paper presented at 5th Workshop El. Ind. Earth Moon, Istanbul.

Holland, J.G. and Lambert, R.S.J., 1970. Trans. Nat. Hist. Soc. Northumb., v. 41, 103-123.

Hoover, D.B., Frischknecht, F.C. and Tippens, C.L., 1976. Audiomagnetotelluric sounding as a reconnaissance exploration technique in Long Valley, CA. J. Geophy. Res., v. 81, 801-809.

Hoover, D.B., Long, C.L. and Senterfit, R.M., 1978. Some results from audiomagnetotelluric investigations in geothermal areas. Geophysics, v. 43, 1501-1514.

Hospers, J. and Willmore, P.L., 1953. Gravity measurements in Durham and Northumberland. Geological Mag., v. 90, 117-126.

Hutton, V.R.S., 1976. Induction studies in rifts and other active regions. Acta Geodaet. Geoph. Mont., Acad. Sci. Hung., v. 11, 347-376.

Ingham, M.R. and Hutton, V.R.S., 1982a.Geophys. J. Roy. Astr. Soc., v. 69, 579-594.

Ingham, M.R. and Hutton, V.R.S., 1982b. Geophys. J. Roy. Astr. Soc., v. 69, 595-606.

Ingham, M.R., 1981. Lateral variations of the electrical conductivity structure across south Scotland. Ph.D. thesis, Univ. Edinburgh, U.K.

Jolivet, J., 1966. Ph.D. thesis, University of Paris, France.

Jones, A.G., 1977. Geomagnetic induction studies in southern Scotland. Ph.D. thesis, Univ. Edinburgh, U.K.

Jones, A.G. and Hutton, V.R.S., 1979a. A multi-station magnetotelluric study in southern Scotland - I. Fieldwork, data analysis and results. Geophys. J. R. Astr. Soc., v. 56, 329-349.

Jones, A.G. and Hutton, V.R.S., 1979b. A multi-station magnetotelluric study in southern Scotland - II. Monte-Carlo inversion of the data and its geophysical and tectonic implications. Geophys. J. R. Astr. Soc., v. 56, 351-368.

Jones, F.W., 1973. Induction in laterally non-uniform conductors : theory and numerical models. Phys. Earth Planet. Int., v. 7, 282-293.

Jones, F.W. and Pascoe, L.J., 1971. A general computer programme to determine the perturbation of alternating electric currents in a two-dimensional model of a region of uniform conductivity with an embedded inhomogeneity. Geoph. J. R. Astr. Soc., v. 24, 3-30.

Jones, F.W. and Pascoe, L.J., 1972. The perturbation of alternating geomagnetic fields by three dimensional conductivity inhomogeneities. Geoph. J. R. Astr. Soc., v. 27, 479-485.

Jones, F.W. and Price, A.T., 1970. The perturbations of alternating geomagnetic fields by conductivity anomalies. Geoph. J. R. Astr. Soc., v. 20, 317-334.

Jones, F.W. and Vozoff, K., 1978. The calculation of magnetotelluric quantities for three-dimensional conductivity inhomogeneities. Geophysics, v. 43, 1167-1175.

Jupp, D.L.P., 1978. Estimation of the magnetotelluric impedance functions. Phys. Earth Planet. Int., v. 17, 75-82.

Jupp, D.L.B. and Vozoff, K., 1977. Two-dimensional magnetotelluric inversion. Geoph. J. R. Astr. Soc., v. 5, 333-352.

Kahle, A.B., Ball, R.H. and Cain, J.C., 1969. Prediction of geomagnetic secular change confirmed. Nature, v. 223, 165.

Kao, D.W. and Rankin, D., 1977. Enhancement of signal to noise ration in magnetotelluric data. Geophysics, v. 42, 103-110.

Kao, D.W. and Rankin, D., 1980. Magnetotelluric response on inhomogeneous layered earth. Geophysics, v. 45, 1793-1802.

Keller, G.V., 1971. Electrical studies of the crust and upper mantle. A.G.U. Monogr., v. 14, 107-126.

Keller, G.V., 1980. Geophysics of geothermal areas : state of the art and future development. Paper presented at Erice, Italy.

Keller, G.V. and Frischknecht, F.C., 1966. Electrical methods in geophysical prospecting. Pergamon Press, New York.

Koziar, A. and Strangway, D.W., 1978. Shallow crustal sounding in the Superior province by audio frequency magnetotellurics. Can. J. Earth Sci., v. 15, 1701.

Lahiri, B.N. and Price, A.T., 1939. Electromagnetic induction in non uniform conductors, and the determination of the conductivity of the Earth from terrestial magnetic variations. Phil. Trans. Roy. Soc. Lond. Ser. A., v. 237, 509-540.

Leary, P. and Phiney, R.A., 1974. A magnetotelluric traverse across the Yellowstone region. A.G.U. Geoph. Res. Letters 1., v. 6, 265-268.

Lienert, B.R., 1980. The effect of source field polarisation on estimates of the magnetotelluric impedance tensor. Geophysics, v. 45, 1803-1812.

Lilley, F.E.M., 1974. Analysis of the geomagnetic induction tensor. Phys. Earth Planet. Int., v. 8, 301-316.

Long, C.L. and Kaufmann, H.E., 1980. Reconnaisance geophysics of a known geothermal resource area, Weiser, Idaho and Vale, Oregon. Geophysics, v. 45, 312-322.

Lorrain, P. and Corson, D., 1970. Electromagnetic fields and waves. 2nd ed. W. H. Freeman & Co., San Francisco.

Losecke, W., 1980. A magnetotelluric equipment designed for in-field data processing and remote reference measurements. Paper presented at 5th Workshop El. Ind. Earth Moon, Istanbul.

MacGregor, M. and MacGregor, A.G., 1948. British regional geology handbook. 2nd edition. Her Majesty's Stationery Office.

Marianiuk, J., 1977. Photoelectric converter for recording the geomagnetic field elements : construction and principles of operation. Publ. Inst. Geoph. Polish Aca. Sci., v. 114, 57.

Matsushita, S., 1974. The geomagnetic field of external origin as observed at the earth's surface : Ionospheric sources. E.O.S., v. 55, 591-593.

Mbipom, E.W., 1980. Geoelectric studies of the crust and upper mantle in northern Scotland. Ph.D. thesis, University of Edinburgh, U.K.

McDonald, K.L., 1957. Penetration of the geomagnetic secular field through a mantle with variable conductivity. J. Geoph. Res., v. 62, 117.

Mills, D.A.C., Hull, J.H. and Ramsbottom, W.H.C., 1968. The Geological Survey borehole at Woodland, Co. Durham. (1962). Bull. Geol. Surv. G.B., v. 28, 1-34.

Mosnier, J., 1980. Induction in the earth's crust : observational methods on land and sea. Paper presented at 5th Workshop El. Ind. Earth Moon, Istanbul.

Nienaber, W., Dosso, H.W., Law, L.K., Jones, F.W. and Ramaswamy, V., 1976. An analog model study of electromagnetic induction for island-continent ocean channels. Phys. Earth Planet. Int., v. 13, 169-183.

Novak, M., Dawes, G.J.K. and Hutton, V.R.S., 1980. Audio-magnetotelluric investigations in north east England. Abstract in Geoph. J. R. Astr. Soc., v. 61, 205.

Novak, M. and Hutton, V.R.S., 1981a. An broad-band magnetotelluric investigation in north-east England. Abstract in Geoph. J. R. Astr. Soc., v. 65, 257.

Novak, M. and Hutton, V.R.S., 1981b. An AMT survey in a high heat flow region underlain by a granite batholith. Paper presented at 4th I.A.G.A. Sci. Ass., Edinburgh, Scotland.

Orr, D., 1973. Magnetic pulsations within the magnetosphere - a review. J. Atm. Terr. Phys., v. 35, 1-50.

Orr, D. and Kao, D., 1980. Magnetotelluric studies in the Market Weighton area. Paper presented at 5th Workshop El. Ind. Earth Moon, Istanbul.

Parkinson, W.D., 1959. Directions of geomagnetic fluctuations. Geoph. J. R. Astr. Soc., v. 2, 1-14.

Parkinson, W.D., 1962. The influence of continents and oceans on geomagnetic variations. Geoph. J. R. Astr. Soc., v. 6, 441-449.

Parkinson, W.D., 1964. Conductivity anomalies in Australia and the coast effect. J. Geomag. Geoelect., v. 15, 222-226.

Porath, M., 1971. A review of the evidence on low-resistivity layers in the earth's crust. A.G.U. Monogr., v. 14, 127-144.

Porstendorfer, G., 1975. Principles of magnetotelluric prospecting, in Geoexploration Mono., v. 5, G. Kunetz and D.S. Parasnis, Eds., Berlin, Gebruder Borntraeger.

Price, A.T., 1950. Electromagnetic induction in a semi infinite conductor with a plane boundary. Quart. J. Mech. Appl. Maths., v. 3, 385-410.

Price, A.T., 1962. The theory of magnetotelluric methods when the source field is considered. J. Geoph. Res., v. 67, 1907-1918.

Price, A.T., 1973. The theory of geomagnetic induction. Phys. Earth Planet. Int., v. 7, 227-233.

Pridmore, D.F., 1978. Three-dimensional modeling of electric and electromagnetic data using the finite-element method. Ph.D. thesis, University of Utah, Salt Lake City.

Reddy, I.K., Phillips, R.J., Whitcomb, J.H., Cole, D.M. and Taylor, R.A., 1976. Monitoring of time-dependent electrical resistivity by magnetotellurics. J. Geomag. Geoelect., v. 28, 165-178.

Richardson, S.W. and Oxburgh, E.R., 1978. Heatflow, radiogenic heat production and crustal temperatures in England and Wales. J. Geol. Soc. Lond., v. 135, 323-337.

Rikitake, T., 1950. Bull. Earthq. Res. Int., Tokyo University, v. 28, 45-219.

Rikitake, T., 1966. Electromagnetism and the earth's interior. Elsevier, Amsterdam.

Rikitake, T., 1973. Global electrical conductivity of the earth. Phys. Earth Planet. Int., v. 7, 245-250.

Risk, G.F., MacDonald, W.J.P. and Dawson, G.B., 1970. D.C. resistivity surveys of the Broadlands geothermal region, New Zealand. Geothermics, v. 2, 287-294.

Rooney, D., 1976. Magnetotelluric measurements across the Kenyan Rift Valley. Ph.D. thesis, Univ. of Edinburgh, U.K.

Schmucker, V., 1964. Anomalies of geomagnetic variations in the south western United States. J. Geomag. Geoelect., v. 15, 193-221.

Schmucker, V., 1970. Anomalies of geomagnetic variations in the south western United States. Bull. Scripps Inst. Ocean., Univ. Calif., v. 13, 165.

Schnegg, P.A. and Fischer, G., 1979. On-line determination of the apparent resistivities in audio magnetotelluric measurements. Paper presented at 17th I.U.G.G. Gen. Ass., Canberra.

Schnegg, P.A. and Fischer, G., 1980. On-line determination of apparent resistivities in audio-magnetotelluric (AMT) soundings. In press.

Schuster, A., 1889. The diurnal variation of terrestrial magnetism. Phil. Trans. Roy. Soc. Lond. Ser. A., v. 180, 467-518.

Serson, P.H., 1973. Instrumentation for induction studies on land. Phys. Earth Planet. Int., v. 7, 313-322.

Shankland, T.J., 1975. Electrical conduction in rocks and minerals : parameters for interpretation. Phys. Earth Planet. Int., v. 10, 209-219.

Sims, W.E., Bostick, F.X. Jr. and Smith, H.W., 1971. The estimation of magnetotelluric impedance tensor elements from measured data. Geophysics, v. 36, 938-942.

Srivastava, S.P., 1965. Method of interpretation of magneto-telluric data when source field is considered. J. Geoph. Res., v. 70, 945-954.

Stanley, W.D., Boehl, J.E., Bostick, F.X. and Smith, H.W., 1977. Geothermal significance of magnetotelluric sounding in the eastern Snake River Plain - Yellowstone Region. J. Geoph. Res., v. 82, 2501-2514.

Stegena, L., Horváth, F. and Ádám, A., 1971. Spreading investigated by magnetotelluric anisotropy. Nature, v. 18, 442.

Stegena, L., 1976. Electric conductivity structure and geothermal reservoirs. Acta Geodaet. Geoph. Mont., Acad. Sci. Hung., v. 11, 377-397.

Sternberg, B.K., 1979. Electrical resistivity structure of the crust in the southern extension of the Canadian Shield - layered earth models. J. Geoph. Res., v. 84, 212.

Strangway, D.W., 1980. Geophysical methods and toxic waste disposal. Geoscience Canada, v. 7, 30-32.

Strangway, D.W., Swift, C.M. and Holmer, R.C., 1973. The application of audiomagnetotellurics (AMT) to mineral exploration. Geophysics, v. 38, 1159-1175.

Summers, D., 1981. Interpreting the magnetic field associated with two-dimensional induction anomalies. Geoph. J. R. Astr. Soc., v. 65, 535-552.

Swift, C.M. Jr., 1967. A magnetotelluric investigation of an electrical conductivity anomaly in the south western U.S. Ph.D. thesis, M.I.T., 211.

Telford, W.M., Geldart, L.P., Sheriff, R.E. and Keys, D.A., 1976. Applied Geophysics. Cambridge University Press, Cambridge.

Telford, W.M., 1977. The characteristics of audio and sub-audio telluric signals. Geophysics Prosp., v. 25, 321.

Tikhonov, A.V., 1950. Determination of the electrical characteristics of the deep strata of the earth's crust. Dokl. Akad. Nauk., v. 73, 295-297.

Ting, S.C. and Hohman, G.W., 1978. Three-dimensional magnetotelluric modeling. Presented at 48th Annual International S.E.G. Meeting, Nov. 1 1978, San Francisco.

Trigg, D.F., Serson, P.H. and Camfield, P.A., 1971. Publ. Earth Phys. Branch, v. 41, 66.

Valiant, M.J., 1976. N.E.R.C. Geologger technical handbook, I.G.S. Magnetic Observatory, Hartland.

Valiant, M.J., 1979. Assessment of commercially available magneto-telluric equipment. A report to the N.E.R.C.

Vozoff, K., 1972. The magnetotelluric method in the exploration of sedimentary basins. Geophysics, v. 37, 98-141.

Wait, J.R., 1954. On the relationship between telluric currents and the earth's magnetic field. Geophysics, v. 19, 281-289.

Wait, J.R., 1962. Electromagnetic waves in stratified media. Oxford, Pergamon press.

Weaver, J.T., 1973. Induction in a layered plane earth by uniform and non-uniform source fields. Phys. Earth Planet. Int., v. 7, 266-281.

Weidelt, P., 1972. The inverse problem of geomagnetic induction. Zeitschrift Fur Geophysik. v. 38, 257-289.

Wienert, K.A., 1970. Notes on geomagnetic observatory and survey practice. Unesco, Belgium.

Whiteford, P.C., 1975. Assessment of the audio-magnetotelluric methods for geothermal resistivity surveying. Paper presented at the 2nd U.N. Geothermal Symposium, San Francisco.

Wright, J.A., 1970. Anisotropic apparent resistivities arising from non-homogeneous two-dimensional structures. Can. J. Earth Sci., v. 7, 527-531.

Yukutake, T., 1959. Bull. Earthq. Res. Inst., Tokyo Univ., v. 37, 13.